2019

Factors That Mediate Expression Of Unique Ggggcc Repeat Expansions In C9orf72-Associated Als/ftd.

Lindsey D. Goodman
University of Pennsylvania, lindsey@goodman.net

Factors That Mediate Expression Of Unique Ggggcc Repeat Expansions In C9orf72-Associated Als/ftd.

Abstract
Amyotrophic lateral sclerosis and frontotemporal dementia spectrum disorders (ALS/FTD) are characterized by the degeneration of motor and cortical neurons. Recently, a hexanucleotide-repeat expansion of >30 repeats was discovered within intron 1 of C9orf72, defining ~40% of familial and ~7% of sporadic ALS/FTD cases. Aberrant accumulation of G4C2-RNA and the aggregation of its repeat-associated non-AUG (RAN-) translation products occurs in diseased tissue. Herein, we developed two Drosophila models that overexpressed G4C2-repeats. Expression of >30 repeats causes degenerative effects supporting gain-of-function mechanisms are contributing to disease. To define disease mechanisms, we performed an unbiased, RNAi-based screen covering ~4000 genes (~25% of the fly genome) and identified the PAF1 complex (PAF1C), an RNAPII-transcription factor, as a suppressor of G4C2-toxicity. Loss of PAF1C reduced RNA and peptide expression from sense-G4C2 and antisense-G2C4 transgenes in Drosophila and in yeast. Importantly, components Paf1 and Leo1 were selective for expression from toxic (>30) G4C2-repeats versus inert (≤29) repeats, arguing selectivity to the disease-associated repeat expansion. Leo1 was also shown to interact with C9orf72-chromatin in C9+-patient cells. Expression of PAF1C components became upregulated in response to expression of >30 G4C2-repeats in flies, mice, patient cells, and FTD tissue, further supporting their importance in disease. Interestingly, expression from PAF1 and LEO1 in FTD tissue correlated with expression of the repeat-expansion within C9orf72, supporting that these components of PAF1C are important for expression of the repeat in disease. In addition to PAF1C, we also identified 11 translation factors that may be important for peptide production from G4C2-transcripts in a second, targeted screen. Follow-up studies revealed that eIF4B and eIF4H knockdown reduced GR-peptide levels produced from G4C2-transcripts and G4C2-toxicity in the fly, defining them as potential RAN-translation factors in C9+ disease. In summary, jumping from unbiased forward genetic screens in Drosophila, we took an interdisciplinary approach to uncover key players whose activity regulates expression of the unique G4C2-hexanucleotide repeat expansion found in C9orf72 in a subset of ALS/FTD cases. This work increases our understanding of disease mechanisms while highlighting potential therapeutic targets.

Degree Type
Dissertation

Degree Name
Doctor of Philosophy (PhD)

Graduate Group
Neuroscience

First Advisor
Nancy M. Bonini

Keywords
amyotrophic lateral sclerosis, C9orf72, Drosophila, neurodegeneration, Paf1, translation factors

FACTORS THAT MEDIATE EXPRESSION OF UNIQUE GGGGCC REPEAT EXPANSIONS IN *C9ORF72*-ASSOCIATED ALS/FTD.

Lindsey D. Goodman

A DISSERTATION

in

Neuroscience

Presented to the Faculties of the University of Pennsylvania

in

Partial Fulfillment of the Requirements for the

Degree of Doctor of Philosophy

2019

Supervisor of Dissertation

_____
Nancy M. Bonini, PhD
Florence R.C. Murray Professor of Biology

Graduate Group Chairperson

_____
Joshua I. Gold, PhD
Professor of Neuroscience

Dissertation Committee

Edward B. Lee, MD, PhD
Assistant Professor of Pathology and Laboratory Medicine

Zhaolan (Joe) Zhou, PhD
Associate Professor of Genetics,

Thomas A. Jongens, PhD
Associate Professor of Genetics

Kenneth H. Fischbeck, MD
NIH Distinguished Investigator,
NINDS/National Institute of Health

FACTORS THAT MEDIATE EXPRESSION OF UNIQUE GGGGCC REPEAT EXPANSIONS IN *C9ORF72*-ASSOCIATED ALS/FTD.

ACKNOWLEDGMENT

I am forever grateful to the multiple professors who have supported me in my journey to becoming a research scientist. This work would not have been possible without the support of my advisor, Dr. Nancy M. Bonini. I have learned so much about how to be an impactful and rigorous scientist. I cannot thank Nancy enough for everything she has done for me, including giving me the opportunity to work on a highly exploratory project. It was a unique, and dream-fulfilling, opportunity to train under such a prestigious professor while learning about fly genetics and neurodegeneration. In addition to Dr. Bonini, I would also like to thank Dr. Erik P. Sulman who gave me my first research position out of undergraduate school. I would not be where I am today without the training I received in his lab and his continued support. Last, I would like to thank my PhD committee members and the chair of my graduate program. In particular, Dr. Edward B. Lee, my committee chair, was an amazing support.

On a personal note, nobody has been more important to me than my dearest husband, Richard P. SoRelle. Words cannot convey how thankful I am to have found him in my life. His seemingly unending support of me and his drive for us to maintain a fulfilling life outside of our work will always be cherished.

Thank you to my family, friends, and lab-mates, each of whom supported me in their own unique way. Particularly, I would like to thank my in-laws, Ruth and Paul SoRelle, and husband's extended family. More, I would like to thank my parents, both of whom showed me what hard-work and cunning can achieve while giving me unique opportunities to make my dreams come true. My mother, Sheryl A. Goodman, pushed me to be independent and to define what makes me happy in life. Further, thanks to my father, Dr. John G. Goodman, Jr., without whom I likely would not have developed such a passion for research as he exposed me to science and medicine in my youth.

ABSTRACT

FACTORS THAT MEDIATE EXPRESSION OF UNIQUE GGGGCC REPEAT EXPANSIONS IN C9ORF72-ASSOCIATED ALS/FTD.

Lindsey D. Goodman

Nancy M. Bonini

Amyotrophic lateral sclerosis and frontotemporal dementia spectrum disorders (ALS/FTD) are characterized by the degeneration of motor and cortical neurons. Recently, a hexanucleotide-repeat expansion of >30 repeats was discovered within intron 1 of *C9orf72*, defining ~40% of familial and ~7% of sporadic ALS/FTD cases. Aberrant accumulation of G4C2-RNA and the aggregation of its repeat-associated non-AUG (RAN-) translation products occurs in diseased tissue. Herein, we developed two *Drosophila* models that overexpressed G4C2-repeats. Expression of >30 repeats causes degenerative effects supporting gain-of-function mechanisms are contributing to disease. To define disease mechanisms, we performed an unbiased, RNAi-based screen covering ~4000 genes (~25% of the fly genome) and identified the PAF1 complex (PAF1C), an RNAPII-transcription factor, as a suppressor of G4C2-toxicity. Loss of PAF1C reduced RNA and peptide expression from sense-G4C2 and antisense-G2C4 transgenes in *Drosophila* and in yeast. Importantly, components *Paf1* and *Leo1* were selective for expression from toxic (>30) G4C2-repeats versus inert (≤29) repeats, arguing selectivity to the disease-associated repeat expansion. Leo1 was also shown to interact with *C9orf72*-chromatin in C9+-patient cells. Expression of PAF1C components became upregulated in response to expression of >30 G4C2-repeats in flies, mice, patient cells, and FTD tissue, further supporting their importance in disease. Interestingly, expression from *PAF1* and *LEO1* in FTD tissue correlated with expression

of the repeat-expansion within *C9orf72*, supporting that these components of PAF1C are important for expression of the repeat in disease. In addition to PAF1C, we also identified 11 translation factors that may be important for peptide production from G4C2-transcripts in a second, targeted screen. Follow-up studies revealed that *eIF4B* and *eIF4H* knockdown reduced GR-peptide levels produced from G4C2-transcripts and G4C2-toxicity in the fly, defining them as potential RAN-translation factors in C9+ disease. In summary, jumping from unbiased forward genetic screens in *Drosophila*, we took an interdisciplinary approach to uncover key players whose activity regulates expression of the unique G4C2-hexanucleotide repeat expansion found in *C9orf72* in a subset of ALS/FTD cases. This work increases our understanding of disease mechanisms while highlighting potential therapeutic targets.

TABLE OF CONTENTS

LIST OF TABLES

LIST OF ILLUSTRATIONS

CHAPTER 1: A CURRENT PERSPECTIVE ON *C9ORF72*-ALS/FTD

Introduction

Amyotrophic lateral sclerosis (ALS) is the most common neurodegenerative disease primarily affecting upper and lower motor neurons within the motor cortex, brain stem and spinal cord (Al-Chalabi and Hardiman, 2013). In recent years, it has become evident that ALS exists as a spectrum disorder with frontotemporal degeneration (FTD) as these diseases share clinical and pathological features (Ji et al., 2017a). FTD is the third most common neurodegenerative disease primarily affecting frontal and temporal cortical neurons (Sieben et al., 2012). Despite a surge in investigations on ALS/FTD, successful therapeutics have yet to be developed, supporting that a greater understanding of disease mechanisms is needed.

The discovery of Tar DNA-binding protein 43 (TDP-43) inclusions as the primary pathology in ALS and ~50% of FTD drove the hypothesis that these two diseases are related (Lee et al., 2011; Neumann et al., 2006). Further evidence came as a number of mutations were found to occur in both diseases (Ito et al., 2017a; Ji et al., 2017a; Zhao et al., 2018), including a hexanucleotide repeat expansion of $(GGGGCC)_n$ (Balendra and Isaacs, 2018; Vatsavayai et al., 2019; Yuva-Aydemir et al., 2018). Termed G4C2, this mutation is associated with disease when >30 repeats are found within the first intron of *C9orf72* (DeJesus-Hernandez et al., 2011; Renton et al., 2011), located on chromosome 9p21. The maximum number of repeats is estimated to be in the thousands (Buchman et al., 2013; Dobson-Stone et al., 2013; van Blitterswijk et al., 2013; Hübers et al., 2014). The presence of G4C2 is associated with ~40% of familial ALS/FTD and ~7% of sporadic ALS/FTD, making it the most common known mutation in these diseases to date (Renton et al., 2014). Further, patients bearing the G4C2-mutation also have TDP-43 pathology, while accumulating evidence suggests that these two etiologies are

connected (Chew et al., 2015, 2019; Cooper-Knock et al., 2015a; Edbauer and Haass, 2016; Steinacker et al., 2018; Vatovec et al., 2014; Vatsavayai et al., 2016).

Currently, there are three leading hypotheses as to how G4C2 confers toxicity: a loss-of-function hypothesis centered around the reduced expression of the C9orf72 protein and two related gain-of-function hypotheses centered around the aberrant expression of the G4C2-containing intron (Balendra and Isaacs, 2018; Yuva-Aydemir et al., 2018). Bidirectional transcription of the repeat-containing intron can produce both expanded sense-G4C2 and antisense-G2C4 RNA (termed G4C2‖G2C4). Both RNA strands can accumulate to form foci in patient tissue. These foci are hypothesized to sequester RNA-binding proteins and cause a depletion of these proteins so they cannot function normally, conferring toxicity (Vatovec et al., 2014; Haeusler et al., 2016). Interestingly, these RNAs can also be translated into dipeptides, despite the absence of a canonical AUG start codon: GA and GR (sense-strand associated), PA and PR (antisense-strand associated), and GP (produced from both sense- and antisense-strands) (Ash et al., 2013; Mori et al., 2013a; Mann et al., 2013; Gendron et al., 2013; Mackenzie et al., 2013, 2015; Niblock et al., 2016). This process is termed Repeat-Associated Non-AUG (RAN-) translation and has been reported to occur in multiple repeat-expansion associated diseases (Nguyen et al., 2019; Zu et al., 2018). Notably, the resulting dipeptides can form aggregates in patients and are associated with toxicity in model systems, a common feature in neurodegeneration (Balendra and Isaacs, 2018; Soto and Estrada, 2008; Yuva-Aydemir et al., 2018).

There is accumulating evidence that the gain-of-function mechanisms associated with the aberrant expression of G4C2-RNA and its resulting dipeptides are contributing to toxicity in *C9orf72*-ALS/FTD (Balendra and Isaacs, 2018; Yuva-Aydemir et al., 2018). Significantly, this highlights potential therapeutic avenues for patients with G4C2-

expansion, focused on disrupting expression of the repeat. Recently proposed therapeutics include the use of antisense oligonucleotides (ASOs) (Donnelly et al., 2013; Jiang et al., 2016; Lagier-Tourenne et al., 2013) or small molecules (Simone et al., 2018; Su et al., 2014; Wang et al., 2018b) to disrupt foci formation by the repeat-RNA and its translation. In fact, one such ASO has entered phase I clinical trial (Biogen, 2018). While these approaches are promising, multiple variables need to be considered to improve efficacy including stability of molecules *in vivo*, their ability to cross the blood-brain barrier (e.g. ASOs cannot cross the BBB and must be directly injected into the CSF), and permeability across cell membranes (Gustincich et al., 2017; Longhena et al., 2017; Magen and Hornstein, 2014; Mathis and Le Masson, 2018; Mis et al., 2017; Riboldi et al., 2014). A limitation relevant to the C9-mutation is that current proposed molecules are unable to simultaneously target sense and antisense G4C2‖G2C4 strands, indicating that a cocktail of multiple molecules will be needed (Jiang and Cleveland, 2016; Mathis and Le Masson, 2018). This could complicate drug specificity to the mutation, resulting in increased side effects in patients. An alternative approach has been proposed upon the discovery that G4C2-transcription is sensitive to the loss of specific transcriptional machinery, including components of the DSIF and PAF1 complexes (**see Chapter 2 and** (Goodman et al., 2019a; Jiang and Cleveland, 2016; Kramer et al., 2016). Pharmacological inhibition of unessential subunits from these complexes could inhibit expression from the G4C2‖G2C4-DNA and downstream toxicity, offering an alternative (or additional) therapeutic target. Overall, this work highlights potential mechanisms that can simultaneously disrupt expression of potentially toxic RNA and dipeptides produced from both strands of the repeat within *C9orf72*. Herein, I discuss limitations to current gain-of-function models, unique features of G4C2 DNA/RNA, and potential mechanisms underlying the expression of this distinct repeat expansion.

Clinical and pathological features of *C9orf72*-ALS/FTD

Amyotrophic lateral sclerosis (ALS, also known as Lou Gehrig's disease and motor neuron disease, MND) results from the progressive loss of upper and lower motor neurons in the motor cortex, brain stem and spinal cord of patients (Al-Chalabi and Hardiman, 2013; Logroscino and Piccininni, 2019). The loss of these neurons causes weakness, spasticity, paralysis, and death, usually within 2-5 years of onset. ALS is the most common motor-neuron disease, affecting ~2-5 in 100,000 individuals (annually). Frontotemporal dementia (FTD), defined pathologically as frontotemporal lobar degeneration (FTLD), is also progressive, with neurodegeneration occurring primarily in the frontal and temporal cortices (Pottier et al., 2016; Raffaele et al., 2019; Seltman and Matthews, 2012). The most common manifestation of FTD is the behavioral variant (bvFTD), characterized by behavioral and personality changes in addition to memory loss. FTD affects ~3-15 in 100,000 individuals (annually), while the risk for FTD is higher among individuals 45-64 years old (Knopman and Roberts, 2011; Pottier et al., 2016). The average lifespan for FTD patients varies between ~5 and ~10 years after disease onset. As mentioned, ALS and FTD represent two extremes of one spectrum disorder. Clinical presentation in patients can fall between these two diagnoses, resulting in both motor and cognitive deficits and a diagnosis of ALS/FTD. Interestingly, different families carrying the same disease-associated mutation or individuals from the same afflicted family can present with ALS only, FTD only, or ALS/FTD symptoms, potentially the result of environmental and genetic modifiers (van Blitterswijk et al., 2014a, 2014b; Renton et al., 2011). Currently, there are no effective disease modifiers for ALS/FTD and therapies are centered around alleviating symptoms. Approved treatments include riluzole (a glutamate antagonist; treats glutamate-sensitivity of motor neurons), edaravone (an antioxidant; antagonizes oxidative stress pathways), and Nuedexta (a drug cocktail

including dextromethorphan, an NMDA receptor antagonist, and quinidine, an inhibitor of Na+/K+ ATPase activity), while other potential drugs have been proposed and/or are being tested (Prasad et al., 2019; Smith et al., 2017).

While there are multiple mutations associated with ALS/FTD, a common theme is that there are disruptions in RNA-based pathways (Zhao et al., 2018). In particular, TDP-43, an RNA-binding protein encoded by the *TARDBP* gene, is the primary component of ubiquitinated inclusions in ALS and a subset of FTD (Neumann et al., 2006). Further, a mutation of a hexanucleotide repeat expansion within *C9orf72* has been identified as the most common mutation known to date. The percentage of reported familial ALS/FTD patients harboring this mutation varies between ~25% and ~60%, with a higher frequency seen in European populations (van Blitterswijk et al., 2012; DeJesus-Hernandez et al., 2011; Gijselinck et al., 2012, 2017; Renton et al., 2011). Non-familial ALS/FTD, termed sporadic ALS/FTD, can also present with this mutation at a ~5-10% frequency. Recently, a number of studies have shown that TDP-43 inclusion formation and the aberrant expression of the hexanucleotide repeat expansions in *C9orf72* are related (Cooper-Knock et al., 2015a; Davidson et al., 2014; Edbauer and Haass, 2016; Saberi et al., 2018). Importantly, TDP-43 pathology may be induced by the expression of the hexanucleotide repeat (Chew et al., 2015, 2019; Solomon et al. 2018).

The G4C2 expansion within *C9orf72* is located between non-coding exons, 1a and 1b, placing it within the first intron of variants 1 and 3 and within the promotor of variant 2 **(Fig. 1-1A)** (Gendron and Petrucelli, 2017; Xiao et al., 2016). The *C9orf72* gene can produce two protein isoforms: C9orf72-Long (produced from mRNA variants 2 and 3) and C9orf72-Short (produced from mRNA variant 1) **(Fig. 1-1B)**. Investigations into the protein encoded by *C9orf72* have revealed that it contains a DENN (Differentially Expressed in Neoplastic versus Normal cells) domain, which is a common feature of

GTP-GDP exchange factors (GEFs) for Rab GTPases (Zhang et al., 2012; Levine et al., 2013). Consistently, C9orf72 interacts with a number of Rabs in cultured neurons and mediates endosomal trafficking and autophagy (Chitiprolu et al., 2018; Farg et al., 2014; Frick et al., 2018; Ho et al., 2019; Sellier et al., 2016; Shi et al., 2018; Webster et al., 2016a).

Overall, *C9orf72* expression is significantly downregulated in ALS/FTD cases harboring the G4C2-expansion (van Blitterswijk et al., 2015; DeJesus-Hernandez et al., 2011; Frick et al., 2018; Renton et al., 2011; Viodé et al., 2018; Xiao et al., 2015). All three variants can be downregulated, while variants 1 and 2 show the most robust decrease (Balendra and Isaacs, 2018; van Blitterswijk et al., 2015). On the protein level, two studies have shown that C9orf72-Long is downregulated in the frontal cortex of C9+ ALS/FTD patients (Waite et al., 2014; Xiao et al., 2015). Potential disease mechanisms associated with *C9orf72* haploinsufficiency are a focus of current investigations (Vatsavayai et al., 2019; Webster et al., 2016b; Xiao et al., 2016). However, the extent to which *C9orf72* downregulation contributes to disease is currently unclear. Mouse models with disrupted murine *C9orf72* expression do not show phenotypes expected in neurodegeneration but rather autoimmune defects (Lagier-Tourenne et al., 2013; Koppers et al., 2015; Atanasio et al., 2016; O'Rourke et al., 2016; Sudria-Lopez et al., 2016; Ji et al., 2017b). In contrast, zebrafish and *C. elegan* models lacking endogenous *C9orf72* orthologues develop motor dysfunction (Ciura et al., 2013; Therrien et al., 2013), potentially the result of deficits during development (Ho et al., 2019; Yeh et al., 2018). Importantly, in C9+ patients, an upstream CpG island is methylated, shutting down the *C9orf72* gene and effectively the aberrant expression of the G4C2-RNA (Xi et al., 2013; Liu et al., 2014; Xi et al., 2014; Belzil et al., 2014; Russ et al., 2015; McMillan et al., 2015). This mechanism is believed to be neuroprotective as increased methylation

reduces RNA foci formation, dipeptide aggregation and neuron loss in patient brains (Liu et al., 2014; Russ et al., 2015; McMillan et al., 2015). However, if the *C9orf72* gene product was essential for maintaining neuron health, this would be an unexpected response to the G4C2-mutation within *C9orf72* as it would also disrupt C9orf72-function. That said, a recent study suggested that depleted C9orf72 protein may play a synergistic role with dipeptide-associated toxicity in disease (Shi et al, 2018).

Under normal conditions, intron 1 of *C9orf72* is spliced out of nascent *C9orf72* transcripts and immediately degraded. Evidence suggests that the presence of the repeat expansion disrupts this process through unknown mechanisms and the stable G4C2-RNA remains present. Notably, this RNA could exist in a number of forms, including: intronic RNA (Vatovec et al., 2014; Haeusler et al., 2016; Tran et al., 2015), *C9orf72*-mRNA transcripts retaining the intron (Niblock et al., 2016), and aborted *C9orf72*-RNA transcripts (van Blitterswijk et al., 2015; Haeusler et al., 2014) **(Fig. 1-1C)**. Both sense G4C2 and antisense G2C4 RNA foci form throughout the nervous system in patients, and are predominantly nuclear (DeJesus-Hernandez et al., 2011; Gendron et al., 2013; Renton et al., 2011; Vatsavayai et al., 2019; Zu et al., 2013). Foci formation is not specific to neurons as they have been reported in glia and non-neuronal cells, albeit at lower relative frequencies (Gendron et al., 2013; Mizielinska et al., 2013; Zu et al., 2013). Investigations into RNA-binding proteins that interact with G4C2-RNA have revealed a number of candidates, some of which were further shown to co-localize with RNA foci in patients, including: ADARB2, SRSFs (1 and 2), ALYREF, hnRNPs (A1, A3, H, and K), Pur-α, nucleolin (Česnik et al., 2019; Kumar et al., 2017).

G4C2‖G2C4 RNA can undergo RAN-translation through currently undefined mechanisms (discussed later), producing five dipeptides (DPR): GA, GR, GP, PA, PR **(Fig. 1-1D)** (Ash et al., 2013; Gendron et al., 2013; Mori et al., 2013b, 2013a). These

DPR form aggregates in patient neurons but rarely in glia (Vatsavayai et al., 2019). In patients, DPR aggregates stain positive for p62 (an autophagic marker), predominantly stain negative for TDP-43, and are more frequent in the cytoplasm (Mann et al., 2013; Saberi et al., 2018; Vatsavayai et al., 2019). Rare, diffuse DPR staining has also been reported in patient neurons, arguing that associations with disease do not require visible aggregation (Gendron et al., 2013; Mackenzie et al., 2015; Saberi et al., 2018; Schludi et al., 2015). Further, soluble GP can be found in patient cerebral spinal fluid (CSF) and blood (Gendron et al., 2017; Lehmer et al., 2017).

Overall, sense-strand associated aggregates – GA, GR, and GP_s – are more abundant than antisense-strand associated aggregates – PA, PR, GP_{AS}. Of these, GA aggregates are most prominent (Mackenzie et al., 2015; Schludi et al., 2015). Currently, GP_S and GP_{AS} produced from the separate RNA stands are considered similar, while translation of GP_S extends beyond the repeat to produce a unique C-terminal fragment that is not present in GP_{AS} (Mori et al., 2013b; Zu et al., 2013). This fragment could alter stability or toxicity associated with GP_S versus GP_{AS}. Unique C-terminal fragments are also found in the other reading frames for GA, GR, PA, and PR.

Investigations into DPR-associated toxicity in model systems have revealed that expression of specific DPRs (expressed from non-G4C2 transcripts) may contribute to disease: GA, GR, and PR have been associated with toxicity in multiple model systems while GR and PR cause consistent, strong degenerative effects across systems (Balendra and Isaacs, 2018; Yuva-Aydemir et al., 2018). In patients, targeted investigations have shown colocalization of DPR aggregates with specific proteins, suggesting mechanistic disruptions to related endogenous pathways may contribute to toxicity: GA has been reported to interact with Drosha, Unc119, HR23B (May et al., 2014; Porta et al., 2015; Zhang et al., 2016b); GR has been reported to interact with

eIF3B (also called eIF3η), STAU2, and multiple ribosomal proteins, including S6, S25, L19, L21, L36A (Hartmann et al., 2018; Zhang et al., 2018). Despite these findings and the observation that DPR aggregation predominantly occurs in neurons (versus glia), potential positive correlations between DPR expression and disease still need to be defined. Since the discovery of the repeat expansion in *C9orf72*-ALS/FTD, multiple studies have reported that the frequency of DPR aggregates does not correlate with degenerating tissue or clinical symptoms (i.e. age-of-onset, disease progression, disease severity) (Babić Leko et al., 2019; Vatsavayai et al., 2019). Only recently have two compelling studies described positive correlations between GR, but not the other DPRs, and diseased tissue (Saberi et al., 2018; Sakae et al., 2018). Overall, it is evident that additional, systematic investigations are needed, while consideration of multiple factors may help clarify results (i.e. disease stage, soluble versus insoluble DPR).

Current gain-of-function G4C2 models

Current investigations into disease mechanisms underlying the G4C2-expansion in ALS/FTD have relied on model systems expressing sense G4C2-repeat RNA. Antisense G2C4-RNA models showing degenerative effects have been limited (Swinnen et al., 2018). These models have highlighted a large number of potential cellular mechanisms that may be disrupted in C9+ patients by the aberrant expression of G4C2-RNA and its dipeptide products (Balendra and Isaacs, 2018; Batra and Lee, 2017; Yuva-Aydemir et al., 2018). Here, I will discuss pertinent information in regard to current gain-of-function models and highlight areas requiring further investigation to elucidate gain-of-function disease mechanisms.

In patients, G4C2-expansions of >30 repeats are associated with ALS/FTD, while healthy individuals can maintain short, inert repeats of < 25 within *C9orf72*. Consistent

with human data, expression of < 25 G4C2 repeats does not produce degenerative effects in mice, zebrafish, *Drosophila*, and *C. elegans* (Balendra and Isaacs, 2018; Batra and Lee, 2017; Yuva-Aydemir et al., 2018). Positive correlations between repeat-length and repeat-expression level with toxicity are consistent among models, despite no correlation in repeat-length and clinical symptoms currently reported in patients with C9+ disease. Investigations into intermediate (25-30) repeats in patients have reported associations with neuropsychiatric symptoms and potentially other movement disorders (Bourinaris and Houlden, 2018; Ng and Tan, 2017). In support of shorter repeat expansions being moderately toxic in neurons, expression of a (G4C2)29 transgene in *Drosophila* showed mild degenerative effects (**see Chapter 2 and** (Goodman et al., 2019a)). Further, BAC-mice expressing (G4C2)29/36 from a human *C9orf72*-gene show toxic effects (Liu et al., 2016).

A major on-going debate relevant to gain-of-function disease mechanisms in *C9orf72*-ALS/FTD is whether the RNA is contributing to toxicity or if dipeptides are driving gain-of-function disease mechanisms. Based on data from model systems, it is evident that the expression of specific dipeptides – GA, GR, and PR – from RNA transcripts lacking the G4C2-repeat sequence can cause degenerative effects across multiple species (Balendra and Isaacs, 2018; Yuva-Aydemir et al., 2018). However, given the lack of strong correlative data in patients for DPR-expression and clinical symptoms, whether the DPR are the major contributor to gain-of-function disease mechanisms in humans is unclear. In contrast to DPR, the G4C2-RNA could potentially contribute to toxicity through the sequestration of RNA binding proteins (RBPs). In fact, disruptions in RNA-metabolism is a common theme in neurodegeneration (Conlon and Manley, 2017; Ito et al., 2017b). In particular, mutations in RBPs is a reoccurring feature of ALS/FTD (Zhao et al., 2018).

As one can appreciate, it is technically difficult to separate G4C2-RNA associated toxicity from toxicity caused by DPR produced from these RNA transcripts. Compelling investigations have depended on the use of G4C2-RNA transcripts containing translation stop codons between every 12 repeats of a G4C2-expansion, termed “RNA-only” models (Mizielinska et al., 2013). In *Drosophila*, no appreciable DPR or degenerative effects are observed with the expression of these RNA-only transcripts, despite the RNA forming similar secondary structures as those formed by a pure G4C2-expansion, the formation of RNA foci, and the colocalization of Glorund (fly orthologue to hnRNPH) with 15% of these foci (Mizielinska et al., 2013; Moens et al., 2018). In contrast, these same transgenes disrupted axon morphology in zebrafish, suggesting that RNA-only transcripts can be toxic in vertebrates, particularly during neurodevelopment (Swinnen et al., 2018). Overall, the full effects of adding interruptions between the G4C2-repeats is unclear as such interruptions within the repeat-expansion could alter transient versus stable interactions with RBPs. Further, investigations into the impact of stress on potential RNA-toxicity needs to be evaluated. Remarkably, recent studies have found that RAN-translation is upregulated during stress arguing that even these RNA-only models may produce toxic DPR under different conditions (Cheng et al., 2018; Green et al., 2017; Sonobe et al., 2018).

A considerable factor of most, current gain-of-function models for *C9orf72* is that the G4C2-transcript produced is processed into mRNA, containing a 5’ m^7G cap and a 3’ polyadenylated (poly(A)) tail. As mentioned earlier, the G4C2-RNA within patients could exist in several forms: intronic RNA (Vatovec et al., 2014; Haeusler et al., 2016; Tran et al., 2015), truncated *C9orf72* transcripts (van Blitterswijk et al., 2015; Haeusler et al., 2014), and *C9orf72* transcripts retaining the intron/repeat (Niblock et al., 2016). Of these, only the latter would be predicted to be fully processed to include a 5’ cap and a 3’

poly(A) tail. Validating current models, *C9orf72*-transcripts retaining the G4C2-expansion have been reported in patient samples and shown to be shuttled into the cytoplasm, where they can undergo RAN-translation to produce toxic DPR (Green et al., 2017; Hautbergue et al., 2017; Niblock et al., 2016; Tabet et al., 2018; Tran et al., 2015; Westergard et al., 2019). However, as this only represents one potential form of the G4C2-RNA in patients, further investigations into the potential contribution of the additional forms of G4C2-RNA in disease are needed.

To our knowledge, only two studies have actively investigated potential toxicity associated with G4C2-intronic RNA with conflicting results. One investigation expressed a truncated *C9orf72*-mutant transgene in *Drosophila* (Tran et al., 2015). Researchers confirmed that the G4C2-repeat was properly spliced from the *C9orf72*-mutant transgene but, curiously, it failed to induce toxicity or cause appreciable expression of one of the DPRs – GP – at normal temperatures. In contrast, Wen and colleagues argued that G4C2-intronic RNA could be toxic *ex vivo* in neurons (Wen et al., 2014). These researchers smartly developed a G4C2-reporter construct that placed the repeat within an intron flanked by truncated GFP-exons. Only when the repeat-containing intron was properly spliced was the GFP-transcript complete and GFP fluorescence could be observed in cells. Importantly, GFP-expressing cortical and motor neurons, but not hippocampal neurons, contained G4C2 RNA foci and demonstrated progressive, dose-dependent cell death. Consistent with Tran and colleagues' fly data, the G4C2-intronic RNA failed to express appreciable amounts of DPR (Tran et al.; 2015). While further analysis is needed to confirm that no DPR was present and that all G4C2-containing transcripts were indeed properly spliced from the chimeric transgene, this study presented compelling data in support of the idea that the G4C2-intronic RNA could be toxic in mammalian neurons relevant to disease.

To date, only two of five mouse models developed to express either truncated or full-length *C9orf72*-mutant transgenes cause neurodegeneration (Batra and Lee, 2017). While differences in these results could be due to several factors, including the genetic background of the animals and expression level of the transgenes, I note that these studies did not investigate if the G4C2-repeat was properly spliced from the *C9orf72*-mutant transgene *in vivo*. Thus, another variable may be differences in the splicing efficiency between the mouse models. Overall, further investigations are needed to rule out potential toxicity associated with G4C2-RNA lacking a 5' cap and 3' poly(A) tail, while considering multiple variables relevant to patients (i.e. impact of stress, effects of age, tissue-specificity).

In summary, while dramatic advances have been made in a relatively short amount of time since the discovery of the G4C2-expansion in ALS/FTD, vital areas of research remain to be elucidated before we can fully understand disease mechanisms. That said, current gain-of-function models have proven to be valuable and have highlighted numerous pathways that are worth further investigation in C9+ disease. Perturbed endogenous pathways that may be disrupted in C9+ disease by the aberrant expression of the G4C2-RNA and/or its dipeptide products currently include: gene expression (Cooper-Knock et al., 2015b; Prudencio et al., 2015, 2017), mRNA processing (Conlon et al., 2016; Cooper-Knock et al., 2014, 2015a, 2015b; Lee et al., 2013; Prudencio et al., 2015; Yin et al., 2017), nuclear-cytoplasmic shuttling of mRNAs (Boeynaems et al., 2016; Hautbergue et al., 2017; Jovičić et al., 2015; Kramer et al., 2018; Shi et al., 2017; Zhang et al., 2015), ribosome biogenesis (Haeusler et al., 2014; Kwon et al., 2014; Lee et al., 2016; Mizielinska et al., 2017; Suzuki et al., 2018; Tao et al., 2015), translation (Hartmann et al., 2018; Kanekura et al., 2016; Rossi et al., 2015; Zhang et al., 2018), ubiquitin-proteasome system (Gupta et al., 2017; May et al., 2014),

and neuron excitability (Selvaraj et al., 2018; Xu and Xu, 2018). Further, studies have shown that multiple stress-induced pathways may be involved in cellular responses to G4C2/dipeptide expression, including: the integrated stress response (including ER stress and stress granule formation) (Cheng et al., 2018; Chew et al., 2019; Green et al., 2017; Tabet et al., 2018; Tao et al., 2015; Westergard et al., 2019; Zhang et al., 2014), heat-shock response (Mordes et al., 2018; Shaw et al., 2018), DNA damage (Farg et al., 2017; Lopez-Gonzalez et al., 2016; Walker et al., 2017). Additional investigations will begin to highlight key pathways common among models and the role these pathways play in disease.

Unique secondary structures formed by G4C2 DNA and RNA

GC-rich nucleic acid strands have the propensity to form a number of non-canonical secondary structures (Bochman et al., 2012; Kaushik et al., 2016). In particular, quadruplex and R-loop formation by GC-rich DNA/RNA can mediate disease-relevant biological processes, including: transcription, repeat-stability, DNA damage, RNA-processing, and translation (Bochman et al., 2012; Crossley et al., 2019; Kim and Jinks-Robertson, 2012; Sauer and Paeschke, 2017). To date, multiple studies have investigated G4C2‖G2C4 DNA and RNA for their abilities to form relevant structures (Kumar et al., 2016), discussed here from a biological perspective.

Typical, duplexed DNA strands preferentially form right-handed double helices (e.g. B-form DNA). In contrast, GC-rich DNA can form into unique, stable secondary structures as a result of strong interactions between the multiple guanines (G) and/or cytosines (C). *In vitro* investigations into sense G4C2-repeat DNA/RNA have shown that short (≤ 5 repeats) strands fold into chair-type G-quadruplexes that exist in equilibrium with hairpin structures **(Fig. 1-1E-F)** (Ash et al., 2013; Wang et al., 2019). G-

quadruplexes involve the formation of G-tetrads between 4 guanines – a square planar structure held together by Hoogsteen hydrogen bonds. These G-tetrads then stack on top of each other and are stabilized by cations: particularly potassium (K+) and, to a lesser extent, sodium (Na+) then lithium (Li+). In G4C2 structures, the cytosines create edgewise loops connecting the stacked G-tetrads. G-quadruplexes can take several topologies depending on the direction of the strands: parallel, antiparallel or mixed. G4C2-DNA seems to prefer an antiparallel topology (Brčić and Plavec, 2016, 2017; Haeusler et al., 2014; Šket et al., 2015; Zhou et al., 2015) and G4C2-RNA, a parallel topology (Fratta et al., 2012; Haeusler et al., 2014; Reddy et al., 2013; Su et al., 2014). These G-quadruplexes can form within one DNA/RNA strand (termed intermolecular) or between multiple strands (termed intramolecular) (Haeusler et al., 2014; Reddy et al., 2013; Šket et al., 2015; Su et al., 2014; Zhou et al., 2015). Further, G4C2-DNA and its RNA transcripts can interact to form hybrid secondary structures known as R-loops **(Fig. 1-1G)** (Diab et al., 2018; Haeusler et al., 2014; Reddy et al., 2014), which may be stabilized by quadruplex formation on the complementary strand (Zamiri et al., 2015).

While less studied, the formation of quadruplexes by antisense-G2C4 DNA/RNA is more debated (Reddy et al., 2013; Zamiri et al., 2015). Recent reports present compelling evidence that G2C4 DNA can form non-canonical quadruplex structures. Specifically, Zamiri and colleagues proposed that quadruplexes could result from unique G:C-tetrad structures under physiological conditions (Zamiri et al., 2015, 2018). Further, in acidic conditions, cytosines can become protonated, driving C:C+ interactions and the formation of quadruplex structures termed i-motifs (Kovanda et al., 2015; Zamiri et al., 2018). At neutral pH, these i-motifs exist in equilibrium with hairpins (Zamiri et al., 2018). Last, antisense G2C4 DNA may form e-motifs, a relatively unstudied secondary structure (Pan et al., 2018; Zhang et al., 2017b). In contrast to anti-sense DNA, G2C4

RNA may preferentially form more canonical double helices over i-motifs (Dodd et al., 2016). Further investigations into this RNA are needed to fully elucidate potential structures into which it could fold.

To date, most structural studies have depended on *in vitro* data currently limited to investigating short (typically ≤ 8) repeats. A number of factors could contribute to complexity of G4C2-structures *in vivo*, including the number of repeats (Zhou et al., 2015), pH of tissue (Brčić and Plavec, 2018; Zamiri et al., 2018), and modification of G4C2‖G2C4 strands (Baral et al., 2013; Mukherjee et al., 2019). In particular, G4C2-repeat expansions are methylated in patients (Bauer, 2016; Xi et al., 2015) and methylation of G4C2‖G2C4 DNA has been shown to impact resulting structures *in vitro* (Zamiri et al., 2015). Further, as the repeats are expanded to >30 in patients, the impact of large stretches of G4C2-repeats on structure formation has yet to be defined. One hypothesis is that expanded G4C2‖G2C4-repeats could form multiple, small quadruplex structures in a row (Zamiri et al., 2015). Alternatively, few, very large, compact G-quadruplexes could form (Abu-Ghazalah and Macgregor, 2009; Pedroso et al., 2007). Further, more complex structures could form from a combination of G-quadruplexes and hairpins arranging along the same strand (Palumbo et al., 2009).

G-quadruplexes, hairpins, and R-loops are reported to form *in vivo* based on direct and indirect evidence (Armas et al., 2016; Simone et al., 2015; Vanoosthuyse, 2018). However, with the exception of one study showing that R-loops can form in a C9+ mouse model (Esanov et al., 2017), data supporting the formation of G4C2‖G2C4 secondary structures in disease are primarily correlative. Specifically, one study showed that the RNA-binding protein nucleolin (NCL) preferentially binds G4C2-associated G-quadruplexes *in vitro* and may co-localize with G4C2-RNA foci in C9+ patient-derived tissues (Haeusler et al., 2014). Another compelling study identified small molecules that

bind G4C2-associated G-quadruplexes *in vitro* and further showed that these molecules could reduce RNA-foci formation, DPR production, and toxicity in patient-derived iPS neurons (*ex vivo*) and in (G4C2)36-expressing *Drosophila* (*in vivo*) (Simone et al., 2018). A recent study defined a small molecule capable of binding the unique hairpin structure of G4C2-RNA (Wang et al., 2019). Exposing (G4C2)66-transfected cells to this molecule disrupted G4C2-foci formation and RBP interactions *ex vivo*. Overall, data are consistent with the formation of unique quadruplexes, hairpins, and R-loops by G4C2‖G2C4 RNA in disease, while more direct *ex vivo* and *in vivo* studies are needed to fully define their role and expand investigations to include G4C2‖G2C4 DNA.

Role of G-quadruplexes and R-loops in general transcription

To better understand transcription of expanded G4C2‖G2C4 DNA, one must first understand the impact of GC-rich DNA under normal conditions on RNA polymerase II- (RNAPII-) driven transcription.

RNAPII-transcription has been well studied for decades. Overall, RNAPII activity is mediated by a number of factors that can act at multiple stages of transcription in metazoans: initiation, promoter:proximal pausing , elongation, or termination (Jonkers and Lis, 2015; Luse, 2013). Different genes require different factors that can act at one or multiple stages (Hartzog and Fu, 2013; Luo et al., 2012; Soutourina, 2017; Van Oss et al., 2017). Throughout the process, duplexed DNA must locally unwind, exposing the individual strands to transcriptional machinery. However, this leaves the ssDNA, particularly if it is GC-rich, vulnerable to forming secondary structures including quadruplexes, hairpins, or R-loops (Duquette et al., 2004; Wu and Brosh, 2010; Zhang et al., 2013; Zheng et al., 2013). These structures would need to be resolved, likely by transcription activators and helicases, for RNAPII to be able to move along the gene

(Armas et al., 2016; Brázda et al., 2014; Mendoza et al., 2016). Elongating RNAPII seems to be particularly sensitive to issues when transcribing GC-rich DNA, evidenced by high GC-content causing reduced RNAPII-elongation rates (Jonkers et al., 2014; Veloso et al., 2014). Fittingly, there is an array of accessory factors available to help RNAPII during elongation (Jonkers and Lis, 2015). These factors can directly stimulate RNAPII interactions with DNA and can recruit additional transcriptional machinery required to locally open up the chromatin (Izban and Luse, 1992).

Data indicate that secondary structures formed by GC-rich DNA can have both positive and negative effects on RNAPII-driven transcription. G-quadruplexes are found throughout the human genome in more than 300,000 genes (Chambers et al., 2015; Kudlicki, 2016; Lam et al., 2013). They tend to be located within regulatory gene regions: promoters, 5'UTR, 3'UTR, and telomeres. Supporting their regulatory role, the presence of a G-quadruplex within the genome of a species may be evolutionarily conserved (Capra et al., 2010; Nakken et al., 2009). While there are increasing examples of gene regulation by G-quadruplex formation, *c-MYC* is particularly well studied (Sauer and Paeschke, 2017). This proto-oncogene has a G-quadruplex within its promoter that can be stabilized with small molecules, causing reduced *c-MYC* expression by blocking transcription factors (Brooks and Hurley, 2010; Brown et al., 2011). Multiple examples of G-quadruplex formation within introns show that they can mediate alternative splicing of genes (Marcel et al., 2011; Verma and Das, 2018). Moreover, their formation within the first intron of *TOP1* has been proposed to inhibit RNAPII-transcription (Reinhold et al., 2010), suggesting that multiple mechanisms may be disrupted when G-quadruplexes aberrantly form within the gene-body. Overall, it is hypothesized that the formation of quadruplexes on template ssDNA would inhibit transcription by blocking RNAPII and/or transcription factors (Agarwal et al., 2014; Armas et al., 2016; Bochman et al., 2012;

Miglietta et al., 2016). Their formation on non-template ssDNA could similarly block transcription but also could promote transcription by maintaining the open DNA.

In addition to G-quadruplexes, R-loops also regulate RNAPII-transcription. These DNA:RNA hybrids are proposed to facilitate transcription through multiple mechanisms, including the protection of ssDNA from methylation and recruitment of transcription factors (Crossley et al., 2019). Increasing numbers of studies support that R-loop formation by GC-rich DNA/RNA occurs during transcription and that their accumulation can disrupt polymerase activity *in vitro* and *in vivo* (Belotserkovskii et al., 2010; Duquette et al., 2004; Kim and Jinks-Robertson, 2012; Zamft et al., 2012). In support of a high requirement for RNAPII to resolve these structures for successful transcription, a number of RNA-binding and accessory proteins have been identified that are proposed to resolve or prevent R-loop formation (Crossley et al., 2019). One of the earliest examples is the THO/TREX complex. Loss of THO/TREX components causes R-loops to accumulate and a reduction in RNAPII elongation rates (Domínguez-Sánchez et al., 2011; Huertas and Aguilera, 2003; Kim and Jinks-Robertson, 2012). In addition, the oncogenes *BRCA1* and *BRCA2* have been shown to prevent R-loop accumulation and thus promote RNAPII-driven transcription (Shivji et al., 2018; Zhang et al., 2017a). Of importance, BRCA2 recruits Paf1 (discussed later) to promoter:proximal gene sites and overexpression of *Paf1* can rescue deficits caused by *BRCA2* loss by resolving accumulated R-loops (Shivji et al., 2018), suggesting that BRCA1/2 is not directly acting on R-loops but rather recruits factors to resolve these hybrids. Overall, the accumulation of R-loops can stall transcription, cause DNA breaks, and has been linked to multiple diseases (Crossley et al., 2019; Richard and Manley, 2017).

Generally, due to the complexity of transcribing GC-rich DNA and the ability for individual sequences to form unique secondary structures, it is likely that there are a

number of factors available to resolve these DNA/RNA structures within cells (e.g. senataxin) (Grunseich et al., 2018).

Transcription of G4C2‖G2C4 repeat expansions

Regardless of whether the G4C2-repeat RNA is contributing to toxicity or if DPR-induced toxicity is the primary contributor to gain-of-function disease mechanisms, a potential therapeutic approach would be to inhibit the transcription of the repeat expansion. This would prevent expression of both RNA and DPR simultaneously. Given the unique secondary structures formed by G4C2‖G2C4-DNA, it is reasonable to hypothesize that these structures could be targeted by small molecules to inhibit transcription (Brown et al., 2011; Sun et al., 2019). However, multiple molecules would be needed to simultaneously target unique structures formed by sense-G4C2 and antisense-G2C4 strands. Alternatively, pharmacological (e.g. drugs, small molecules, antisense oligonucleotides) inhibition of endogenous machinery required to help RNAPII during transcription of GC-rich DNA would prevent expression of both G4C2‖G2C4 strands concurrently. Herein I will discuss complexes found to regulate G4C2‖G2C4 transcription in disease – the DSIF and PAF1 complexes – and potential mechanisms.

The DSIF complex: Spt4 and Spt5

The DRB-sensitivity-inducing factor (DSIF) complex was recently shown to modulate expression from expanded G4C2‖G2C4 DNA (Kramer et al., 2016). This highly conserved complex is comprised of two subunits, Spt4 and Spt5, which form a heterodimer (Hartzog and Fu, 2013). Originally described as an RNAPII-activating complex in yeast, DSIF has since been implicated in multiple steps of RNAPII transcription, including: promoter:proximal pausing, elongation, and RNA

processing/termination (Jonkers and Lis, 2015; Yamaguchi et al., 2013). It can have both positive and negative impacts on transcription as DSIF interacts with the Negative Elongation Factor (NELF) during RNAPII-promoter:proximal pausing. Phosphorylation of Spt5 by the positive elongation factor-b (P-TEFb) causes DSIF to release NELF and become a positive transcription factor. RNAPII is also phosphorylated by P-TEFb, further driving its interactions with phospho-DSIF and other elongation factors (like PAF1C, discussed below) while promoting the transition into elongation. During elongation, the DSIF complex helps to promote RNAPII-stability on template ssDNA with successful transcription of GC-rich DNA being particularly sensitive to its loss in yeast (Rondón et al., 2003).

The involvement of DSIF in the transcription of repeat-expansions in disease was originally described in CAG-expansion models for Huntington's disease (HD) (Cheng et al., 2015; Liu et al., 2012). Polyglutamine diseases are known to result from CAG-repeat expansions of >30 repeats (Krzyzosiak et al., 2012). Notably, expanded CAG-repeats can form similar secondary structures to G4C2-repeats, including hairpins and R-loops (Ciesiolka et al., 2017; Freudenreich, 2018; Krzyzosiak et al., 2012; Reddy et al., 2014). Cheng and colleagues found that depletion of the DSIF component, Spt4, reduced RNA/protein expression and toxicity associated with (CAG)81+ in yeast and cultured neurons (Liu et al., 2012). Mechanistic studies in yeast revealed that Spt4 deletion caused reduced RNAPII occupancy downstream of a (CAG)99-expansion when the CAG was inserted into a reporter gene. This effect was not seen with an inert, (CAG)29-repeat, arguing repeat-length specificity. Further investigations showed that 50% downregulation of SUPT4H (mammalian Spt4) in two HD-mouse model expressing expanded (CAG)115+ repeats could reduce RNA/protein expression from transgenes *in vivo* (Cheng et al., 2015). Importantly, in one of these mouse models that expressed the

mutant, this reduced expression was associated with reduced neurodegenerative effects caused by the mutant-*Htt*-*Q115*+. Overall, these data supported DSIF as a transcriptional-regulator of expanded CAG-repeats in human disease.

Kramer and colleagues took a multi-disciplinary approach to extend the discovery of DSIF as a transcriptional regulator of expanded CAG-repeats to G4C2-repeats in *C9orf72*-disease (Kramer et al., 2016). Using gain-of-function yeast, worm, and fly models that expressed (G4C2)49+ repeats, investigators found that depletion of Spt4 orthologues could suppress RNA expression and toxicity of expanded G4C2-transgenes. Using (G4C2)66- and (G2C4)66-expressing yeast, the effects of Spt4 deletion was shown to impact both repeat-transcripts produced bidirectionally from the *C9orf72*-mutant gene in patients. In addition, the effects of Spt4 were dose-dependent as upregulation of SUPT4H1 (ortholog to Spt4) in *C. elegans* caused significant increases in G4C2-RNA levels and toxicity. Findings from transgenic models were further translated to C9+ disease situations. Downregulation of both DSIF components, Spt4 and Spt5, in C9+ patient-derived cells caused reduced expression of repeat-associated *C9orf72* transcripts, sense-G4C2 and antisense-G2C4 RNA foci formation as well as GP-levels. Finally, positive correlations between SUPT4H1 (mammalian Spt4) and SUPT5H (mammalian Spt5) expression and expression of the repeat were defined using post-mortem tissue from C9+ ALS/FTD patients. Since this initial paper, we have validated Spt4 of the DSIF complex as a transcriptional regulator of G4C2-repeat DNA in flies (**see Chapter 2** and (Goodman et al., 2019a)). However, our data showed that Spt4 loss impacted RNA expression from inert (G4C2)8- and (G4C2)29-repeats in addition to toxic, (G4C2)49-repeats, arguing that further investigations are needed to validate selectivity of DSIF towards expanded G4C2-repeats in higher organisms.

Overall, there is accumulating evidence that the DSIF complex is important for regulating GC-rich DNA expression, and this effect is particularly impactful in repeat-expansion diseases. Arguing that this complex may globally affect repeat-associated diseases, a recent study further defined DSIF in mediating RNA-expression from GGCCTG-repeat expansions in spinocerebellar ataxia type 36 (SCA36) (Furuta et al., 2019). However, the global impact of downregulating this complex in higher organisms needs further investigation (**see Chapter 2 and** (Goodman et al., 2019a; Naguib et al., 2019).

The PAF1 complex: Paf1, Leo1, CDC73, Ctr9, and Rtf1

Similar to DSIF, the Polymerase II Associating Factor 1 complex (PAF1C) was first defined as a RNAPII-transcriptional regulator in *S. cerevisiae* (Van Oss et al., 2017). The core components of PAF1C are highly conserved, including: Paf1, Leo1, CDC73, Ctr9 and Rtf1. Metazoan PAF1C can also include a multifunctional protein, WDR61 (Zhu et al., 2005). Since PAF1C's discovery, accumulating evidence supports conserved roles in regulating RNAPII-transcription at multiple stages, including: initiation, promoter:proximal pausing, elongation, and RNA processing/termination. During the transition of poised to elongating RNAPII, PAF1C displaces NELF upon p-TEFb-mediated phosphorylation of DSIF. In yeast, studies have shown that PAF1C recruitment is dependent on Spt5 interactions with Rtf1. However, in metazoans this requirement for Spt5 may not be conserved. Importantly, metazoan Rtf1 is not tightly associated with PAF1C (Adelman et al, 2006; Cao et al., 2015; Mbogning et al., 2013). Further, Leo1, CDC73, and a Paf1:Ctr9 subcomplex have all been shown to recruit the remaining PAF1C components to RNAPII, independently of DSIF (Amrich et al., 2012; Dermody and Buratowski, 2010; Qiu et al., 2012; Xie et al., 2018). After PAF1C recruitment, structural data shows that

PAF1C directly interacts with elongating RNAPII, stimulating its activity (Kim et al., 2010; Xu et al., 2017; Chu et al., 2013; Vos et al., 2018). PAF1C can also recruit chromatin remodeling factors that promote active transcription (Van Oss et al., 2017). Interestingly, only expression from a subset of genes is impacted by PAF1C loss, suggesting that it selectively regulates RNAPII-transcription versus having a global impact. Further, like DSIF, RNAPII-transcription of GC-rich DNA is particularly susceptible to PAF1C loss (Rondón et al., 2004).

In addition to DSIF, evidence shows that PAF1C may also be important for promoting RNAPII-transcription of G4C2‖G2C4-repeat expansions in C9+ ALS/FTD. We identified the components of the PAF1 complex as disease modifiers through a large-scale RNAi-based screen encompassing ~25% of the fly genome (**see Chapter 2** and (Goodman et al., 2019a)). Reduced expression of core PAF1C components reduced RNA and dipeptide expression from multiple toxic (G4C2)30+ transgenes in the fly and caused concomitant reductions in degenerative effects. Of interest, RNA expression from inert, short (G4C2)<30 transgenes was unaltered by depletion of two PAF1C components – Paf1 and Leo1 (which form a heterodimer within the PAF1 complex (Chu et al., 2013) – arguing selectivity for toxic G4C2-repeat expansions. In contrast, downregulation of the other PAF1C components and Spt4 of DSIF similarly impacted RNA levels produced from all G4C2-transgenes tested: (G4C2)8, (G4C2)29, and (G4C2)49. Continued investigations in yeast expressing sense-(G4C2)66 and antisense-(G2C4)66 transgenes revealed that deletion of PAF1C components, Leo1 and CDC73, could impact expression from both products of the mutant *C9orf72* gene. Further mechanistic investigation in C9+ derived patient cells revealed that Leo1 protein bound the *C9orf72*-intron 1 immediately 3' of the G4C2 expansion. Last, in post-mortem cortical tissue derived from C9+ FTD patients, we found that the expression of Paf1 and Leo1,

but not CDC73, positively correlated with the expression of *C9orf72* transcripts containing the G4C2-repeat expansion, supporting their role in the expression of the repeat in disease. This correlation was not seen in FTD cases lacking the G4C2-repeat or healthy controls, supporting that it was the direct result of the repeat versus PAF1C regulating the normal gene.

Overall, this work provides strong evidence that PAF1C is a transcriptional regulator of expanded G4C2‖G2C4-DNA in *C9orf72*-disease. In particular, components Paf1 and Leo1 seem to be selective for expanded G4C2-DNA of >30 repeats in the fly, a finding that is substantiated by correlation data in C9+ FTD tissue.

Current model for G4C2‖G2C4-repeat transcription

Current data from multiple model systems and patient samples support that DSIF and PAF1 complexes are important for regulating RNAPII-transcription of G4C2‖G2C4-repeat DNA in C9+ situations (**see Chapter 2 and** (Goodman et al., 2019a; Kramer et al., 2016)). Assuming that both complexes work cooperatively to promote RNAPII-transcription along G4C2‖G2C4-repeats, this suggests a model where the PAF1C and DSIF complexes interact with RNAPII during transcription elongation (**Fig. 1-2**). Moreover, of all the components of these two complexes, only the Paf1:Leo1 heterodimer shows specificity to disease-associated repeat expansions in metazoans (**see Chapter 2** and (Goodman et al., 2019a)). Additionally, chromatin immunoprecipitation (ChIP) assays confirmed Leo1 binding to *C9orf72* chromatin, immediately 3' of the repeat in C9+-derived patient cells, supporting the hypothesis that the Paf1:Leo1 heterodimer functions during elongation versus other stages of transcription. This suggests a model wherein Paf1:Leo1 downregulation reduces RNAPII occupancy along the expanded G4C2‖G2C4 DNA in C9+ disease.

Recent cryo-EM studies investigated the structure of poised versus elongating RNAPII and its binding partners in humans (Vos et al., 2018, 2018). Vos and colleagues found that DSIF was bound to RNAPII at both stages, while PAF1C was only bound to elongating-RNAPII. The specificity of PAF1C function to elongating RNAPII is further reflected by ChIP and ChIP-sequencing studies looking at binding patterns of DSIF and PAF1C components along genes (Chen et al., 2009; Mayer et al., 2010; Qiu et al., 2006; Van Oss et al., 2016). Overall, Spt4/Spt5 binding is enriched at promoter:proximal regions and at the 3' end of genes. In contrast, PAF1C binding is relatively low at these sites and high within the gene body. Whether this binding pattern is the same for mutated *C9orf72* gene in C9+ disease needs to be determined, but this argues that the DSIF and PAF1 complexes may be acting at different stages of its transcription.

A surprising feature we identified in *C9orf72*-associated disease is that PAF1C components become upregulated in response to expression of toxic (G4C2)30+ repeats but not inert (G4C2)<8 repeats in flies, mice, and patient-derived cells (**see Chapter 2 and** (Goodman et al., 2019a)). This is not the effect of toxicity as expression of another, related disease gene, TDP-43, did not induce PAF1C upregulation. Supporting our fly data that Paf1 and Leo1 play a particularly important role in mediating RNAPII-transcription of >30 G4C2‖G2C4 repeats, these two components were found to be upregulated in C9+ FTD patient tissue but not in C9- FTD tissue or in healthy tissue. In contrast, CDC73 was not upregulated, depletion of this PAF1C component similarly impacted G4C2-RNA levels from multiple G4C2-transgenes: (G4C2)8, (G4C2)29 and (G4C2)49 (**see Chapter 2 and** (Goodman et al., 2019a)). Based on these findings, I hypothesize that a feed-forward loop exists in C9+ disease wherein the G4C2-repeat expansion sequesters the PAF1C components, resulting in the cells upregulating these genes to compensate for their depletion at other genes **(Fig. 1-2)**.

Additional mechanistic insights

As mentioned, G4C2‖G2C4-repeat DNA can form multiple secondary structures that may disrupt RNAPII-transcription. Investigations into whether DSIF and/or PAF1C activity is needed to help resolve these structures would add additional mechanistic insights into C9+ disease.

Of particular significance, DSIF has been shown to mediate transcription from G4C2- and CAG- repeat expansions while both can form hairpins and R-loops (Ciesiolka et al., 2017; Freudenreich, 2018; Krzyzosiak et al., 2012; Lin and Wilson, 2011; Reddy et al., 2014). More, there are accumulating data showing that R-loop formation is an important feature of mutated *C9orf72* (van Blitterswijk et al., 2015; Esanov et al., 2017; Haeusler et al., 2014; Reddy et al., 2014). Thus, it is tempting to hypothesize that DSIF promotes G4C2‖G2C4 transcription by resolving these structures. Currently, little data supports the idea that DSIF directly interacts with GC-rich R-loops with the exception of one study (Wang et al., 2018a). Further, DSIF can act on A-rich R-loops (Blythe et al., 2016; Liu et al., 2012). DSIF may recruit factors important for mediating these secondary structures, such as Spt6 (Nojima et al., 2018) and PAF1C (discussed below). It needs to be determined if DSIF can act directly on G4C2‖G2C4 DNA/RNA or if it primarily functions by recruiting transcription factors that can act on this DNA/RNA.

In contrast to DSIF, PAF1C could play a more direct role in helping to resolve G-quadruplexes and R-loops along G4C2‖G2C4 DNA/RNA (Hershman et al., 2008). Accumulating evidence supports that PAF1C regulates pathways involving these secondary structures. In particular, multiple studies have shown that PAF1C components can mediate R-loop formation in cells to promote transcription (Landsverk et al., 2019; Shivji et al., 2018; Wahba et al., 2011; Wang et al., 2018a). Further, components Paf1 and Ctr9 have been shown to regulate telomere repeat containing

RNA (TERRA), which is GC-rich and prone to R-loop and G-quadruplex formation (Neidle, 2010; Rodrigues and Lydall, 2018; Toubiana and Selig, 2018). PAF1C has also been shown to mediate *c-MYC* expression, a well-characterized proto-oncogene that involves a regulatory G-quadruplex within its promoter (Gerlach et al., 2017; Sauer and Paeschke, 2017; Zhi et al., 2015). Ultimately, unbiased approaches have shown that PAF1C components can directly interact with G-quadruplexes, including those formed by G4C2-RNA (*in vitro*) (Gadaleta and Noguchi, 2017; Gómez Ramos, 2017; Haeusler et al., 2014; Lambert et al., 2005; Wanzek, 2016).

While directed investigations are needed, these data implicate the secondary structures formed by G4C2‖G2C4-repeat DNA as potential variables mediating interactions with PAF1C and, potentially, DSIF. PAF1C may act directly on these nucleotides and/or may recruit additional factors meant to resolve these structures, such as the THO/TREX complex (Dermody and Buratowski, 2010; Domínguez-Sánchez et al., 2011; Kim and Jinks-Robertson, 2012). Additional investigations into PAF1C as a transcriptional regulator of other repeat-expansions, such as CAG-repeats (Krzyzosiak et al., 2012), would further define it as a global disease modifier.

Translation of G4C2‖G2C4 repeat expansions

As mentioned, G4C2‖G2C4-repeat RNA can undergo a process termed Repeat-Associated Non-AUG (RAN-) translation to produce five dipeptides (DPR): GA, GR, GP, PA, PR (**Fig. 1-1D**). As specific dipeptides seem to be particularly toxic in model systems (Balendra and Isaacs, 2018; Freibaum and Taylor, 2017), an alternative therapeutic approach could be to target translation of repeat-containing RNA to disrupt their expression. In fact, a number of small molecules have been proposed that interact with G-quadruplex and hairpin structures formed by G4C2-RNA (Simone et al., 2018; Su

et al., 2014; Wang et al., 2019). *Ex vivo* and *in vivo* data show that these molecules can reduce RNA foci formation, dipeptide levels and G4C2-induced toxicity. Herein, I will discuss current literature on G4C2‖G2C4 RAN-translation.

Canonical versus non-canonical translation

Canonical translation is well studied and involves multiple stages: initiation, elongation, and termination (Marygold et al., 2017; Shatsky et al., 2018; Sonenberg and Hinnebusch, 2009). Of these, initiation seems to be highly regulated and requires a large number of translation factors, termed eukaryotic initiation factors (eIFs). Translation initiation involves the formation of two main complexes, a ternary complex and a preinitiation complex (PIC). eIF5-mediates the ternary complex formation between the eIF2 complex (subunits: eIF2α, eIF2β, eIF2γ) and initiator methionine-transfer ribonucleic acid (Met-tRNA$_i$). This complex then forms the PIC with the 40S ribosome and eIFs: eIF1, eIF1A, eIF5, eIF3 (a large, multi-subunit complex); this process is mediated by multiple translation factors including eIF2A. For translation to initiate, another complex, the eIF4F complex (subunits: eIF4E, eIF4G, eIF4A), recognizes the 5' m^{7}G cap on a template mRNA. Specifically, eIF4E recognizes the cap, recruits the scaffold protein eIF4G, which then recruits eIF4A, an RNA helicase. It is the helicase activity of eIF4A that unwinds secondary structures formed by the mRNA, while this activity is significantly stimulated by one of two RNA-binding proteins, eIF4B and eIF4H. The exposed mRNA then interacts with the PIC and the 48S scanning complex forms. Scanning of the mRNA continues 5' to 3' until a start codon is identified. This triggers the 48S scanning complex to release many of the eIFs and bind the 60S ribosome, forming the elongating 80S ribosome (subunits: 40S and 60S ribosomes). The transition into elongation is further stimulated by eIF5B (and potentially eIF5). During elongation, a

relatively small number of eukaryotic elongation factors (eEFs) associate with the 80S ribosome to aid in productive translation.

Interestingly, non-canonical forms of translation have been described to occur under multiple normal and disease-associated contexts (Godet et al., 2019; Leppek et al., 2018; Shatsky et al., 2018; Terenin et al., 2017), of which internal ribosome entry-site (IRES-) translation is the most studied. The pathway underlying IRES-translation varies dramatically between situations. In many cases, IRES-translation is cap-independent and circumvents canonical translation initiation steps. A common theme is that translation initiation requires a minimal PIC complex, which includes only a small number of specific translation factors and the 40S ribosome. Further, secondary structure formation within the 5' untranslated-region (UTR) of RNA templates plays an important role in the recruitment of translation initiation machinery (Leppek et al., 2018).

Like IRES-translation, disease-associated RAN-translation also seems to depend on secondary structures and/or unique features within the 5' UTR. The first paper describing mechanisms underlying RAN-translation looked at peptide formation from expanded CAG‖CTG-repeats associated with spinocerebellar ataxia type 8 (SCA8) and myotonic dystrophy type 1 (DM1) (Zu et al., 2011). Zu and colleagues found that peptide formation was repeat-length dependent, with increasing numbers of repeats causing more peptide to be expressed. Interestingly, translation required the formation of a hairpin structure; in contrast to (CAG)100+ repeats, (CAA)100+ repeats did not form hairpins nor undergo translation. Other studies on CGG-repeat expansions associated with fragile X-associated tremor ataxia syndrome (FXTAS) utilizing *Drosophila* and tissue-culture models showed that RAN-translation could initiate upstream of the repeat in a 5' UTR region containing a non-canonical CUG start codon (Kearse et al., 2016; Todd et al., 2013).

Properties of G4C2-RNA that may influence RAN-translation

While mechanisms underlying G4C2-associated RAN-translation are relatively undefined, recent studies have begun to uncover potential variables. Drawing parallels between CGG- and G4C2-associated RAN-translation, Todd and colleagues used a novel *ex vivo* reporter system to show that G4C2-RAN translation requires the cap-recognizing factor, eIF4E, and, subsequently, eIF4A (Green et al., 2017). The dependence of G4C2-RAN translation on eIF4E and eIF4A was validated by another research group using an independent *ex vivo* model (Tabet et al., 2018), Moreover, this group showed that eIF4G, the scaffold protein between eIF4E and eIF4A, was required. To date, multiple studies have demonstrated that G4C2-RAN translation is promoted by the presence of a near-cognate start codon within the GA-reading frame, a CUG (Green et al., 2017; Sonobe et al., 2018; Tabet et al., 2018). This CUG is found in the G4C2-RNA transcript, upstream of the G4C2-repeat within the intronic RNA (sequence derived from intron 1 of *C9orf72* and found upstream of G4C2-repeats in patients). Frame-shifting is predicted to cause the production of the multiple dipeptides from a single G4C2-RNA strand when translation is initiated at this CUG (Tabet et al., 2018).

In addition to studies showing the dependence of G4C2-RAN translation on cap-recognizing eIF4F complex components – eIF4E, eIF4G, and eIF4A – translation may also be promoted by stress responses expected to inhibit cap-dependent translation (Cheng et al., 2018; Green et al., 2017; Tabet et al., 2018; Westergard et al., 2019). During neuronal stress, the integrated stress response (ISR) is triggered, resulting in eIF2α phosphorylation and activation of pathways hypothesized to protect the cell during conflict, such as stress granule formation, which sequesters cap-dependent translation machinery (Moon et al., 2018). Under these stress conditions, cap-independent translation can persist, allowing for the expression of proteins that help protect the cell

(e.g. Heat-shock proteins) (Godet et al., 2019; Shatsky et al., 2018). Interestingly, multiple studies have shown that triggering ISR can stimulate dipeptide production from expanded G4C2-RNA (Cheng et al., 2018; Green et al., 2017; Sonobe et al., 2018; Westergard et al., 2019). Further, translation of G4C2-RNA can occur independent of a 5' cap (Cheng et al., 2018). Suggesting a feed-forward loop, G4C2-expression can trigger ISR, potentially the result of GR-induced mechanisms (Hartmann et al., 2018; Tao et al., 2015; Zhang et al., 2018).

Overall, a considerable variable when discussing G4C2-RAN translation is that the G4C2-RNA may exist in multiple forms in patients (**see Fig. 1-1C**): a properly spliced intron (Vatovec et al., 2014; Haeusler et al., 2016; Tran et al., 2015), aborted transcripts (van Blitterswijk et al., 2015; Haeusler et al., 2014), or a retained intron (Niblock et al., 2016). Each of these forms of RNA may undergo different RAN-translation mechanisms. Given that RAN-translation can persist when cap-dependent translation is inhibited (via eIF2α phosphorylation) this suggests that there could be multiple pathways driving dipeptide production. Speculatively, one pathway may require the 5' m^7G cap, predicted to impact G4C2-RNA still retained within the *C9orf72*-transcript. Another pathway may initiate in a cap-independent manner, predicted to impact G4C2-RNA that is within a properly spliced intron or aborted *C9orf72*-transcript. Pertaining to the intron retention model, one study suggested that if the G4C2-containing intron was retained in *C9orf72*-transcripts then RAN-translation may be significantly downregulated or inhibited by upstream sequences found within exon 1a of the *C9orf72* gene (Tabet et al., 2018). In conflict, two other groups argued that G4C2-RAN translation persisted when the repeat was retained within *C9orf72*-transcripts (Hautbergue et al., 2017; Westergard et al., 2019). Further, RAN translation can persist in the presence of a properly spliced intron containing the G4C2-repeat expansion (Cheng et al., 2018; Tran et al., 2015). When the

G4C2-RNA existed in this form, its translation was promoted by ISR (Cheng et al., 2018).

While I note that conflicting data may be technical not biological (different G4C2-models will differ in construct design, cell type, and expression level of constructs), these studies have offered the first pieces of valuable mechanistic insights into G4C2-RAN translation. Current data suggest that G4C2-RAN translation may involve multiple pathways and may vary between cell types (Westergard et al., 2019). With speculation, the process might begin with cap-dependent mechanisms but then, as cells become stressed, RAN translation could be promoted by ISR-dependent mechanisms, driving disease progression. Further investigations will help to confirm and define these pathways while shedding light on relevant C9+ disease mechanisms.

Potential G4C2-RAN translation factors and mechanisms

While continued investigations into mechanisms underlying G4C2‖G2C4-RAN translation are underway, a short-list of translation factors have been proposed that may mediate this process. As mentioned, multiple studies have implicated the eIF4F complex as an important player (Cheng et al., 2018; Green et al., 2017; Tabet et al., 2018). Depletion or inhibition of the subunits of eIF4F – eIF4E, eIF4G, eIF4A – causes reduced GA, GP, and GR production from G4C2-transcripts in *ex vivo* models. Also, eIF2A has been proposed to be important for GA-production from G4C2-RNA transcripts, as its downregulation in cells could reduce GA-dipeptide levels (Sonobe et al., 2018). Last, eIF2α has been proposed by multiple groups to promote ISR and cause an increase in GA, GP, and GR production, although the pathway underlying this effect needs elucidation (Cheng et al., 2018; Green et al., 2017; Sonobe et al., 2018). In non-G4C2

disease, eIF3F, a component of the eIF3 complex, has also been proposed to mediate CAG‖CTG-RAN translation (Ayhan et al., 2018).

In order to shed light on translation factors that may be involved in the production of toxic-GR dipeptide in C9+ ALS/FTD, we took an unbiased, *in vivo* approach (**see Chapter 3,** (Goodman et al., 2019b)). We developed a fly model that expressed the intronic RNA sequence found immediately upstream of a toxic (G4C2)44-repeat. The intronic RNA sequence was derived from the 114 bp sequence found 5' of G4C2-repeats within intron 1 of *C9orf72* in patients. Further, a GFP tag was inserted immediately 3' of the G4C2-repeats in the GR-reading frame, effectively labeling any GR-dipeptides produced from the repeats with this fluorescent marker. We chose to focus on GR as its expression, independent of a G4C2-repeat RNA, is particularly toxic in model systems, including *Drosophila* (Freibaum et al., 2015; Mizielinska et al., 2014). No canonical start codons were found within the construct, while the near-cognate CUG start codon was present in the GA-reading frame, thus mimicking C9+ ALS/FTD. By expressing this transgene specifically within the fly eye, we could rapidly screen for genes that impacted GR-dipeptide levels produced from the (G4C2)44. Comparisons could then be made between GR-levels and toxicity.

Using established loss-of-function mutant or RNAi lines and this new, more patient-relevant (G4C2)44 fly model (described above), we screened 48 of 56 (86%) known translation factors in the fly for their ability to alter GR-GFP production and G4C2-induced toxicity (Marygold et al., 2017). This screen included factors involved in multiple stages of translation: initiation, elongation, and termination. After control experiments ruled out nonspecific effects and factors that were likely acting downstream of toxic GR-production, 11 candidate RAN-translation factors were identified: *eIF4B*, *eIF4H*, *eIF5B*, *eIF5*, *eIF2β*, *eIF3D1*, *eIF3I*, and multiple orthologues to eIF4E (*E3*, *E4*, *E5*, *E7*).

Intriguingly, most of the factors identified act with, or are orthologues to, already proposed RAN-translation factors: eIF4F components and eIF2α (**Fig. 1-3**). eIF4B and eIF4H became the focus of further investigations as these two proteins have non-redundant roles in stimulating eIF4A-helicase activity (Rogers et al., 2001; Rozovsky et al., 2008; Nielsen et al., 2011; Sun et al., 2012; Harms et al., 2014; García-García et al., 2015; Vaysse et al., 2015; Sen et al., 2016). These two factors behaved in a manner consistent with them acting as G4C2-RAN translation factors. Their depletion reduced G4C2-toxicity, reduced GR-levels produced from G4C2-RNA, did not alter G4C2-RNA levels, did not reduce toxicity caused by GR-dipeptides. Pertinent to disease, eIF4B and eIF4H contain an RNA recognition motif and were previously shown to interact with G4C2-RNA (Cooper-Knock et al., 2014; Haeusler et al., 2014; Satoh et al., 2014). Further, we found that eIF4H, but not eIF4B, was downregulated in C9+ derived cells. In post-mortem C9+ ALS/FTD tissue, *eIF4H* downregulation was also observed compared to C9- ALS/FTD and healthy tissue, arguing that *eIF4H* downregulation was a response to the presence of the G4C2 expansion within *C9orf72*.

The importance of eIF4B/H-mediated activation of eIF4A in G4C2-RAN translation is further supported by the observation that G4C2-RNA can form unique secondary structures (Brázda et al., 2014; Nishida et al., 2017; Simone et al., 2015). G-quadruplexes and hairpins formed by GC-rich RNA can inhibit translation (Fay et al., 2017; Maizels, 2015; Wang et al., 2018b). Notably, eIF4A was previously shown to promote translation from RNA transcripts predicted to form G-quadruplexes, presumably by resolving these secondary structures (Wolfe et al., 2014). Fittingly, stabilizing G4C2-RNA quadruplexes/hairpins with small molecules can inhibit dipeptide production and downstream toxic effects (Simone et al., 2018; Su et al., 2014; Wang et al., 2019); this indicates that resolving these structures would be needed to allow translation to occur.

Interestingly, eIF4A's ability to unwind longer, more structured 5' UTRs on transcripts is significantly strengthened by eIF4B or eIF4H (Rozovsky et al., 2008; Sun et al., 2012; Vaysse et al., 2015; Sen et al., 2016). Unwound RNA can then interact with ribosomes and the 43S scanning complex (Sharma et al., 2015; Spirin, 2009; Walker et al., 2013). Overall, these data support a model whereby eIF4A is recruited to G4C2-RNA, potentially by eIF4E/G (**Fig. 1-3D**). Then, with the help of eIF4B/H, eIF4A is able to unwind the secondary structures formed by G4C2-RNA, thus allowing PIC to interact with the RNA template and promoting scanning by the 48S scanning complex until reaching a start translation start site, potentially the near cognate CUG in the GA reading frame (Green et al., 2016; Tabet et al., 2018). Alternatively, the GR-dipeptides could be formed by unknown mechanisms during this scanning process.

Overall, our unbiased approach highlighted additional factors that may be important for G4C2-associated RAN-translation in the fly. Further investigations are needed to validate their involvement in disease mechanisms. Notably, of the 48 translation factors screened, only downregulation of a subset impacted GR-production from G4C2-transcripts. This argues that, like with IRES translation, RAN translation can circumvent canonical translation steps and may utilize only a small number of translation factors.

Thesis work

The following chapters describe our detailed investigations into PAF1C and eIF4B/H, factors that mediate expression from unique G4C2-repeat expansions (>30 repeats) found within *C9orf72* in a subset of ALS/FTD cases. When I began this project, the discovery of the G4C2-repeat expansion was relatively new and no disease mechanisms were known (DeJesus-Hernandez et al., 2011; Renton et al., 2011). The goal of my

thesis work was to define potential disease mechanisms associated with gain-of-function toxicity in C9+ ALS/FTD. By using the powerful genetic tool, *Drosophila melanogaster*, I could test for genetic modifiers of G4C2-associated toxicity in an unbiased manner (Bilen and Bonini, 2007; Jung et al., 2011; Lessing and Bonini, 2008; Li et al., 2008). Overall, I hypothesized that proteins or complexes could be identified that were particularly important in C9+ disease by using this approach. Follow-up, interdisciplinary studies would then allow me to define potential mechanisms associated with identified genes-of-interest. Specifically, the lab was well positioned to perform studies in flies, yeast, mice, patient-derived cells, and/or post-mortem patient tissue, allowing me to define how these genes functioned in the context of human C9+ disease (Elden et al., 2010; Kim et al., 2014).

Drawing parallels with other known repeat-expansions associated with neurodegenerative diseases (Krzyzosiak et al., 2012; Nguyen et al., 2019), Dr. Bonini had developed a novel fly model expressing an expanded, pure G4C2 repeat (**see Fig. 2-1a**). These constructs lacked any known start codons or additional sequences from human *C9orf72*. The goal was to develop a control line expressing inert (G4C2)12 and a disease line expressing (G4C2)48. Overall, in the (G4C2)48 cohort, expression of these repeats could cause degenerative effects, supporting that gain-of-function mechanisms were contributing to toxicity in C9+ ALS/FTD (Balendra and Isaacs, 2018; Batra and Lee, 2017; Yuva-Aydemir et al., 2018). Interestingly, not all fly lines developed showed this effect and, as a whole, they needed extensive, comprehensive characterization. My early work characterized these flies, defining the exact number of G4C2-repeats inserted into the genome of each line (**see Fig. 2-1b**), which lines expressed transgenes at similar levels (**see Fig. 2-1c**), showing that (G4C2)49 expression in all tissues was toxic (data not shown), and defining progressive degenerative effects of expressing (G4C2)n

in neurons (**see Fig. 2-3**; data not shown). This work allowed me to master applicable techniques that resulted in my first publication from the lab (Yu et al., 2015). Due to instability of the G4C2-repeat expansion during molecular cloning, we found that the (G4C2)48 cohort expressed an array of repeat lengths, a finding that we then used to our advantage. Notably, fly lines that had degenerative effects expressed ≥ 29 repeats (**see Fig. 2-1d**), showing that toxicity was dependent on the repeat length.

While the lab had performed targeted, small-scale screens for specific pathways on (G4C2)49 flies, I wanted to define disease mechanisms from an impartial perspective. With Dr. Bonini's input, I developed an unbiased approach to define genes that were able to alter (G4C2)49-induced toxicity in the fly eye (**see Fig. 2-1e**). By using established shRNA fly lines, I tested for effects of downregulating individual genes on toxicity in flies expressing (G4C2)49 within their optic system. In total, ~4000 genes were tested (~25% of the fly genome). To accomplish this seemingly daunting task, I developed an efficient protocol for determining effects and defined 119 genes that could modify (G4C2)49-toxicity, while ruling out lines that had unspecific effects (**see Appendix 4**). Gene-ontology term analyses allowed me to define components, processes, or functions that were enriched among these genes, highlighting the PAF1 complex (PAF1C) as a suppressor of G4C2-toxicity when depleted (**see Fig. 2-1g-h**).

Spt4, one of the components of the DSIF complex (Hartzog and Fu, 2013), was among the 119 (G4C2)49 modifiers, and a collaboration with Dr. Aaron Gitler's laboratory at Stanford University further defined it as a transcriptional regulator of G4C2‖G2C4-repeat expansions in C9+ ALS/FTD (Kramer et al., 2016). As components of PAF1C were enriched in our screen and PAF1C is known to interact with the DSIF complex, I hypothesized that PAF1C could also be acting on RNAPII during transcription of (G4C2)49. Like DSIF, PAF1C is a transcription factor important for stabilizing

elongating RNAPII, particularly along GC-rich DNA (Rondón et al., 2004; Van Oss et al., 2017). This hypothesis was tested in flies, yeast, mice, patient-derived cells, and post-mortem patient tissue. Importantly, fly data revealed that PAF1C components, Paf1 and Leo1, selectively impacted expression from toxic G4C2-DNA (> 30) versus inert G4C2-DNA (≤ 29), unlike other PAf1C components and Spt4. Overall, this argued that these components may be of special importance in C9+ disease. The accumulation of data supporting that PAF1C plays a role in expression of expanded G4C2‖G2C4-repeat DNA was the basis for my primary research manuscript, “Toxic expanded GGGGCC repeat transcription is mediated by the PAF1 complex in C9orf72-associated FTD” (**see Chapter 2** and (Goodman et al., 2019a)).

While we had focused on PAF1C in post-screen studies, I also noted that a select list of translation factors was enriched among the 119 (G4C2)49-modifers (**see Fig. 2-2c**). This observation led to the development of a second G4C2 fly model meant to test for RAN-translation of toxic GR-dipeptides (**see Fig. 3-1**). This model contained a 5’ leader sequence (the 114 bp sequence found immediately upstream of the repeat in intron 1 of *C9orf72* in patients) upstream of the repeat expansion, placing the repeat in a more patient-relevant context. This sequence is hypothesized to be important for RAN-translation (Kearse et al., 2016; Todd et al., 2013). To aid in experimentation, the GR-dipeptide was tagged with a fluorescent marker, GFP. To test for translation factors that may be involved in G4C2-RAN translation, I developed a novel approach to allow for the rapid screening of genes that altered GR-GFP levels and toxicity in the fly (**see Fig. 3-2A**). This work defined 11 candidate translation factors of 48 genes tested whose loss resulted in reduced GR-GFP levels and (G4C2)44-toxicity *in vivo*. Ensuing investigations focused on two factors, eIF4B and eIF4H, as these had previously been reported to interact with G4C2-RNA and they function with eIF4A, a previously reported G4C2-RAN

translation factor (Cooper-Knock et al., 2014; Haeusler et al., 2014; Marygold et al., 2017; Satoh et al., 2014; Shatsky et al., 2018; Sonenberg and Hinnebusch, 2009). Using flies, patient-derived cells, and post-mortem patient tissue, evidence that eIF4B and eIF4H play a role in C9+ ALS/FTD resulted in the publication, "*eIF4B* and *eIF4H* mediate GR production from expanded G4C2 in a *Drosophila* model for *C9orf72*-associated ALS." (**see Chapter 3** and (Goodman et al., 2019b)).

While the direct results of my thesis work centered around defining factors important for the expression of G4C2‖G2C4-repeat expansions in C9+ ALS/FTD, other pathways were also tested in our G4C2-fly models. Notably, in collaboration with Dr. Kevin Eggan's laboratory at Harvard University, we found that stress-genes were upregulated in C9+ ALS/FTD patient tissue, likely the result of the repeat expansion being expressed as gene orthologues were also upregulated (G4C2)49- and (GR)100-expressing flies (Mordes et al., 2018). In another study with co-first author Dr. Amit Berson in the Bonini lab, we found that the mRNA-export factor, *ALYREF*, may also regulate expression from expanded G4C2-repeats while showing overlapping effects with a TDP-43 fly model (Berson et al., 2019).

Concluding remarks

In C9+ ALS/FTD, there is a rapid surge in studies defining disease mechanisms associated with the G4C2-repeat expansion in *C9orf72*. Breakthroughs in the field have centered around gain-of-function disease mechanisms associated with the aberrant expression of G4C2‖G2C4-RNA and its dipeptide products. In particular, data in *Drosophila* showing that the dipeptide products, particularly GR and PR, could cause degenerative effects independent of a G4C2-RNA transcript promoted the idea that these dipeptides may be a key contributor to disease (Mizielinska et al., 2014). A key

breakthrough in the field was made using a mouse model which overexpressed >30 G4C2-repeats (Chew et al., 2015, 2019). Along with multiple progressive, neurodegenerative phenotypes, expression of the G4C2-repeat expansion induced TDP-43 cytoplasmic aggregates in the mouse brain, introducing the first mechanistic link between G4C2-repeat expression and TDP-43 pathology, a hallmark of ALS/FTD (Cooper-Knock et al., 2015a; Edbauer and Haass, 2016; Steinacker et al., 2018; Vatovec et al., 2014; Vatsavayai et al., 2016). In addition to this work, a number of groups have performed unbiased screens in simple systems, such as my own, to define pathways perturbed by expression of G4C2-repeats and/or its dipeptide products (Boeynaems et al., 2016; Freibaum et al., 2015; Jovičić et al., 2015; Kramer et al., 2018; Zhang et al., 2015). This work has generated a new and large focus on perturbed nuclear-cytoplasmic shuttling in disease (Zhang et al., 2016a). Evidence from *ex vivo*, *in vivo* and patient-derived samples shows this essential process to be disrupted in C9+ ALS/FTD. Last, multiple groups have defined proteins that can interact with G4C2-RNA and/or its dipeptide products, while disruptions to their normal function(s) may be contributing to C9+ disease (Balendra and Isaacs, 2018; Yuva-Aydemir et al., 2018).

Currently, there seems to be a complex number of pathways underlying disease mechanisms associated with the aberrant expression of expanded G4C2‖G2C4-DNA. However, as investigations are pursued, key pathways will become more evident while, hopefully, highlighting effective therapeutic targets.

Chapter 1: Figures and Legends

Figure 1-1

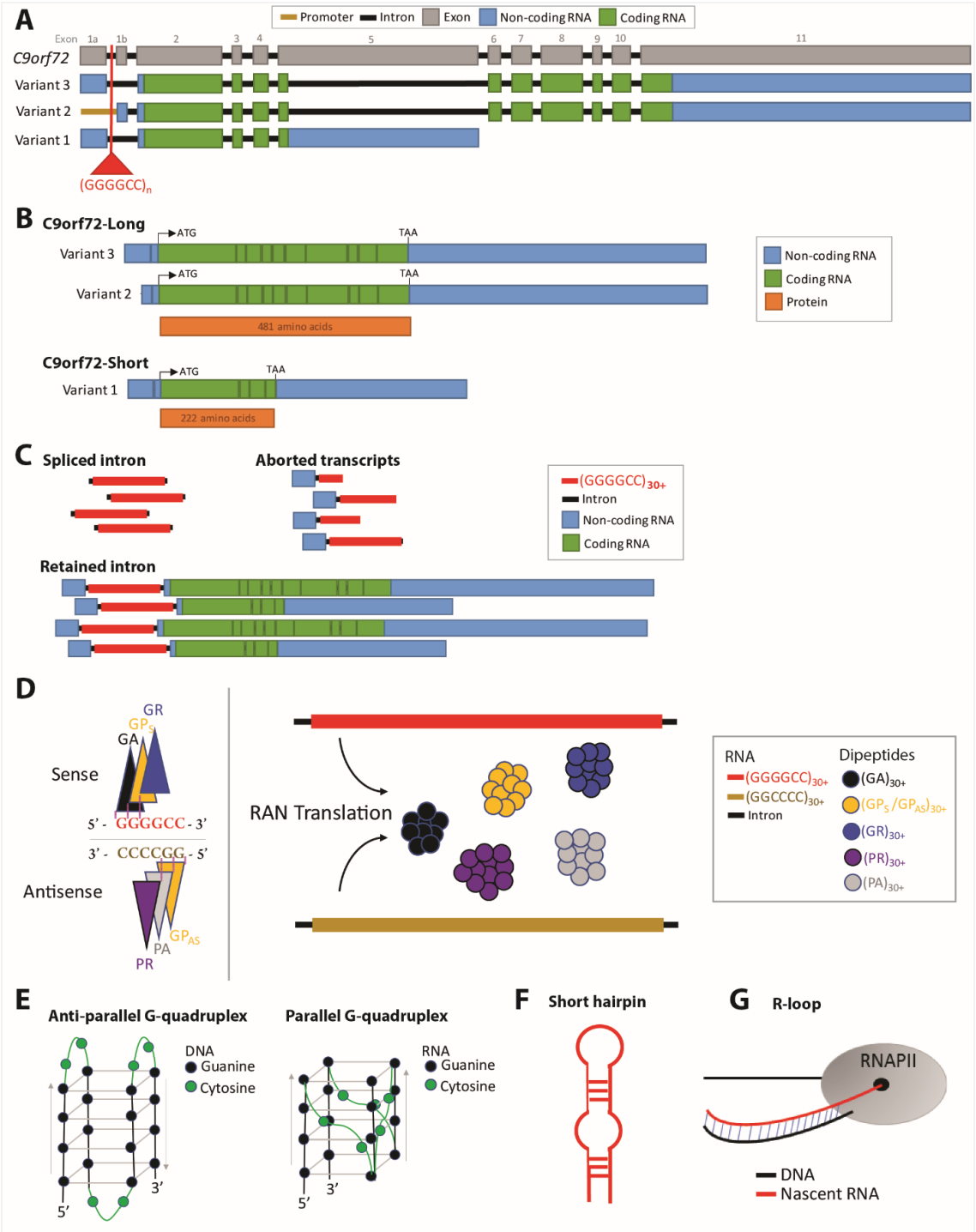

Figure 1-1: C9orf72-associated ALS/FTD.

A. A hexanucleotide expansion of >30 (G4C2)n repeats is found within the *C9orf72* gene in ~40% of familial ALS/FTD cases and ~7% of sporadic ALS/FTD cases. Three mRNA variants are produced from *C9orf72,* while the repeat expansion is found within intron 1 of mRNA Variants 1 and 3. For mRNA Variant 2, it is in the promoter. **B.** Two protein products are made from *C9orf72*, C9orf72-long and C9orf72 short. mRNA Variants 2 and 3 code for C9orf72-Long and mRNA Variant 1 codes C9orf72-Short. **C.** Three RNA products could be produced from mutant *C9orf72*, each carrying the G4C2-exansion in different contexts. Only RNA produced based on the "retained intron" hypothesis would be predicted to include a 5' m^7G-cap and a 3' polyadenylated tail. **D.** Repeat-associated Non-AUG (RAN-) translation occurs in C9+ ALS/FTD, producing 5 dipeptide products from the sense-G4C2 and antisense-G2C4 repeat RNA. The reading frame determined with dipeptide is produced while frameshifting could occur. All five dipeptides can form insoluble aggregates in diseased tissue. **E.** (G4C2)4 DNA and RNA can form chair-type G-quadruplex secondary structures *in vitro*. DNA prefers an anti-parallel confirmation and RNA prefers a parallel confirmation. How these structures look *in vivo* and with >30 G4C2 repeats still needs to be investigated. **F.** G-quadruplex structures formed by G4C2 D/RNA can coexist with another secondary structure, a short hairpin. These structures have been implicated in RAN-translation when found in repeat-containing RNA. **G.** During RNAPII-driven transcription of G4C2-DNA, unique DNA:RNA hybrids known as R-loops can form between the ssDNA and nascent RNA. R-loops can promote transcription while their accumulation can inhibit RNAPII, cause genomic instability, and cause DNA damage.

Figure 1-2

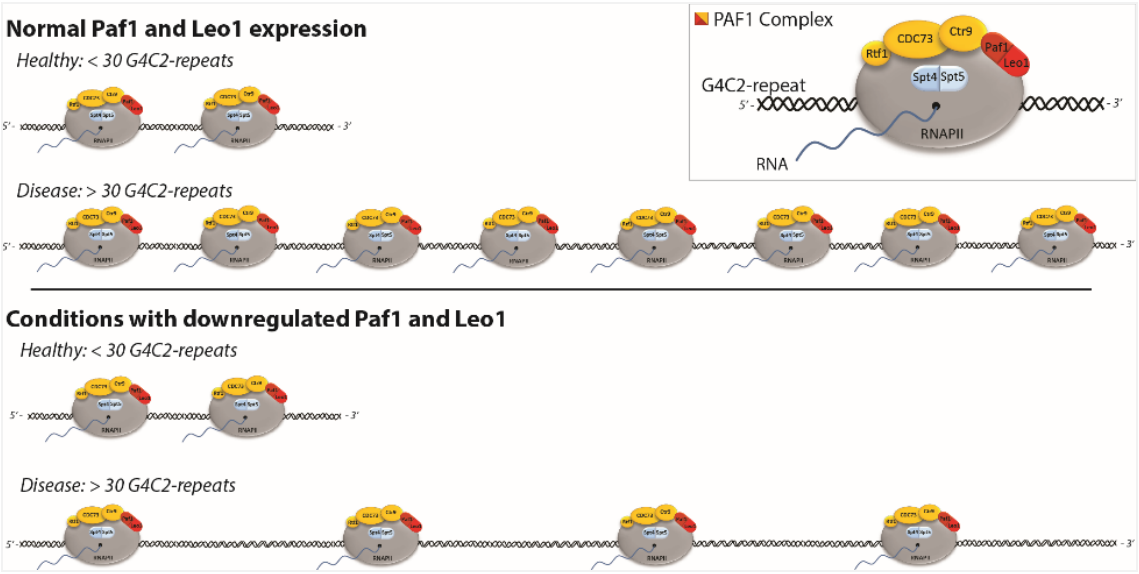

Figure 1-2: A model for G4C2llG2C4 transcription.

Transcription elongation factors, DSIF (Spt4/5) and PAF1C (Paf1/ Leo1/ CDC73/ Ctr9/ Rtf1), are recruited to, and important for, elongating RNAPII at G4C2-repeats. In flies, PAF1C components Paf1 and Leo1 (which form a heterodimer within PAF1C) seem most important for this transcription, showing specificity to >30 G4C2 repeats. Our data show that PAF1C components are upregulated in response to the expression of >30 G4C2 repeats in flies, in mice, and in patient-derived cells. Further, hPAF1 and hLEO1 are upregulated in patient tissue, in contrast to hCDC73, potentially the result of an increased requirement for them within the cell. I hypothesize that transcription of the expanded G4C2 DNA requires PAF1C along with RNAPII, for elongation through the repeat expansion while we show that PAF1C is bound to *C9orf72* through the repeat. DSIF may be important for recruiting PAF1C to the G4C2-repeat expansion, while additional mechanistic studies are needed.

Figure 1-3

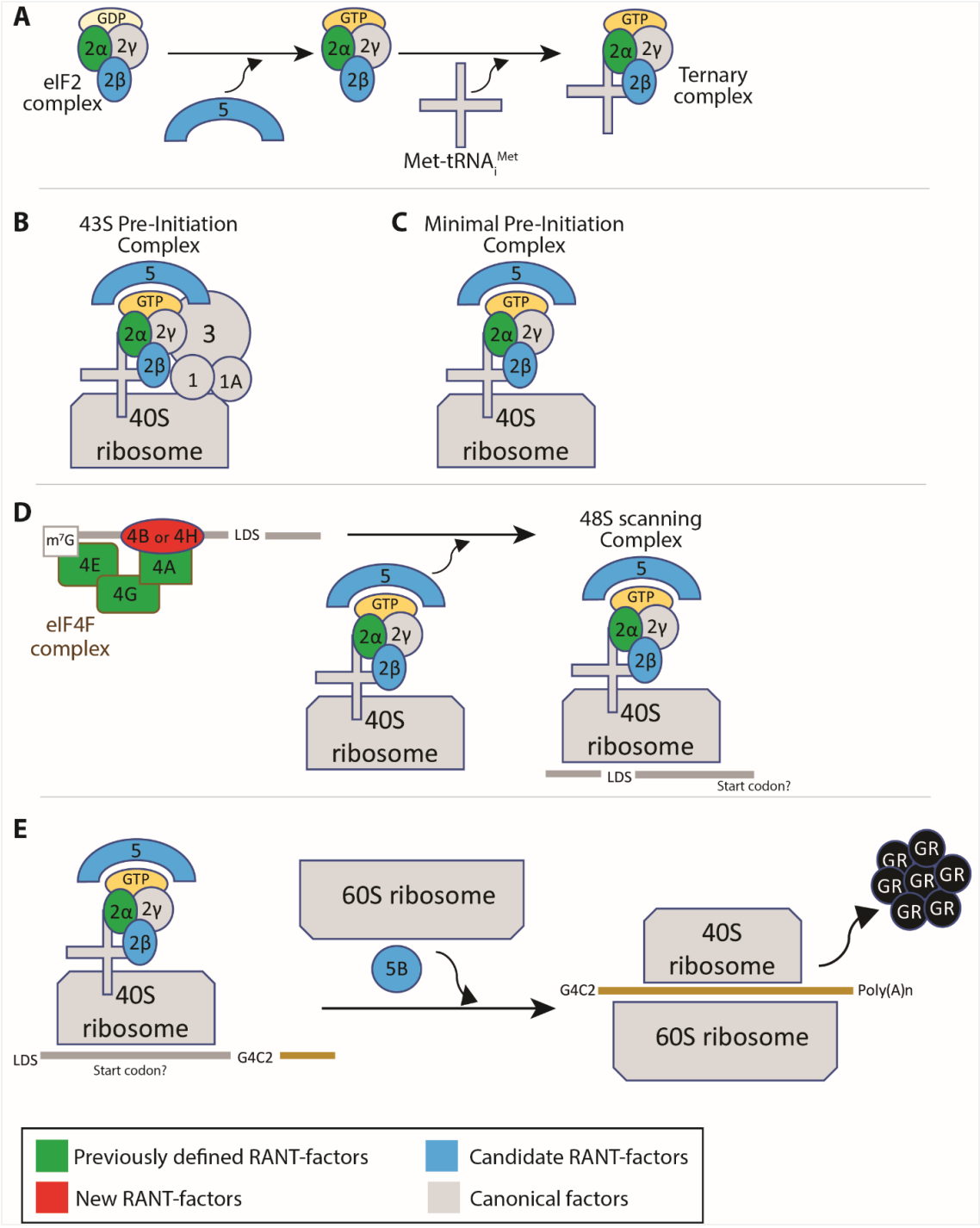
A
GDP
2α 2γ
2β
eIF2 complex
5
GTP
2α 2γ
2β
Met-tRNA$_i^{Met}$
GTP
2α 2γ
2β
Ternary complex
B
43S Pre-Initiation Complex
5
GTP
2α 2γ
2β
3
1
1A
40S ribosome
C
Minimal Pre-Initiation Complex
5
GTP
2α 2γ
2β
40S ribosome
D
m^{7}G
4B or 4H
LDS
4E
4A
4G
eIF4F complex
5
GTP
2α 2γ
2β
40S ribosome
48S scanning Complex
5
GTP
2α 2γ
2β
40S ribosome
LDS
Start codon?
E
5
GTP
2α 2γ
2β
40S ribosome
LDS
Start codon?
G4C2
60S ribosome
5B
40S ribosome
G4C2
Poly(A)n
60S ribosome
GR
Previously defined RANT-factors
Candidate RANT-factors
New RANT-factors
Canonical factors

Figure 1-3: A potential model for G4C2 RAN-translation of GR-dipeptides.

Here I draw comparisons between canonical translation and RAN-translation based on current literature and known functions of translation factors. Note that mechanisms underlying RAN-translation are still relatively unknown. **A.** In normal translation and potentially in RAN-translation, ternary complex formation requires eIF5-mediated exchange of GDP to GTP on eIF2 complex (includes eIFs 2α, 2β, 2γ). eIF2α is highly regulated during stress and is reported to mediate G4C2 translation (Cheng et al., 2018; Green et al., 2017). eIF2β and eIF5 were identified as modifiers in this study. **B.** In normal translation, the formation of the 43S pre-initiation complex (PIC) involves the joining of a number of factors, including Ternary complex (formed in A) and eIFs 1, 1A, 3, and 5. **C.** A minimal PIC complex may potentially mediate RAN-translation (Akulich et al., 2016; Leppek et al., 2018; Shatsky et al., 2018; Terenin et al., 2017). **D.** mRNA transcripts are recognized by the eIF4F complex, includes eIFs 4E, 4G, 4A; all of which have been defined as G4C2 translation factors arguing that G4C2 RAN-translation is cap-dependent (Cheng et al., 2018; Tabet et al., 2018). eIF4E recognizes the 5-prime m^7G cap on mRNAs (Browning and Bailey-Serres, 2015; Sonenberg and Hinnebusch, 2009; Spilka et al., 2013); notably, 4 of 6 eIF4E components were identified in our screen. eIF4A is recruited by eIF4E to mRNA transcripts (via the scaffold protein eIF4G). mRNA is then unwound by eIF4A, an activity that is significantly promoted by eIF4B or eIF4H, identified herein (Rogers et al., 2001; Rozovsky et al., 2008; Sun et al., 2012; García-García et al., 2015; Vaysse et al., 2015). This action allows for the formation of the 48S scanning complex. **E.** In canonical translation, the 48S scanning complex moves down a transcript until identifying an AUG start codon. A CUG codon in the LDS sequence upstream of G4C2 may function as a start codon in the GA-reading frame (Green et al., 2017; Tabet et al., 2018). Frame-shifting could allow for translation of the

GR and GP from this codon. Candidate RAN translation factors eIF5B and potentially eIF5, mediate ribosome scanning, start codon recognition, and translation activation (Browning and Bailey-Serres, 2015; Lin et al., 2018; Pisareva and Pisarev, 2014). *(This model was published in* (Goodman et al., 2019b)*)*

Bibliography

Abu-Ghazalah, R., and Macgregor, R.B. (2009). Structural polymorphism of the four-repeat Oxytricha nova telomeric DNA sequences. Biophys. Chem. *141*, 180–185.

Adelman, K., Wei, W., Ardehali, M.B., Werner, J., Zhu, B., Reinberg, D., and Lis, J.T. (2006). Drosophila Paf1 Modulates Chromatin Structure at Actively Transcribed Genes. Mol Cell Biol *26*, 250–260.

Agarwal, T., Roy, S., Kumar, S., Chakraborty, T.K., and Maiti, S. (2014). In the Sense of Transcription Regulation by G-Quadruplexes: Asymmetric Effects in Sense and Antisense Strands. Biochemistry *53*, 3711–3718.

Akulich, K.A., Andreev, D.E., Terenin, I.M., Smirnova, V.V., Anisimova, A.S., Makeeva, D.S., Arkhipova, V.I., Stolboushkina, E.A., Garber, M.B., Prokofjeva, M.M., et al. (2016). Four translation initiation pathways employed by the leaderless mRNA in eukaryotes. Sci. Rep. *6*, 37905.

Al-Chalabi, A., and Hardiman, O. (2013). The epidemiology of ALS: a conspiracy of genes, environment and time. Nat. Rev. Neurol. *9*, 617.

Amrich, C.G., Davis, C.P., Rogal, W.P., Shirra, M.K., Heroux, A., Gardner, R.G., Arndt, K.M., and VanDemark, A.P. (2012). Cdc73 Subunit of Paf1 Complex Contains C-terminal Ras-like Domain That Promotes Association of Paf1 Complex with Chromatin. J. Biol. Chem. *287*, 10863–10875.

Armas, P., David, A., and Calcaterra, N.B. (2016). Transcriptional control by G-quadruplexes: In vivo roles and perspectives for specific intervention. Transcription *8*, 21–25.

Ash, P.E.A., Bieniek, K.F., Gendron, T.F., Caulfield, T., Lin, W.-L., DeJesus-Hernandez, M., van Blitterswijk, M.M., Jansen-West, K., Paul, J.W., Rademakers, R., et al. (2013). Unconventional translation of C9ORF72 GGGGCC expansion generates insoluble polypeptides specific to c9FTD/ALS. Neuron *77*, 639–646.

Atanasio, A., Decman, V., White, D., Ramos, M., Ikiz, B., Lee, H.-C., Siao, C.-J., Brydges, S., LaRosa, E., Bai, Y., et al. (2016). C9orf72 ablation causes immune dysregulation characterized by leukocyte expansion, autoantibody production, and glomerulonephropathy in mice. Sci. Rep. *6*.

Ayhan, F., Perez, B.A., Shorrock, H.K., Zu, T., Banez-Coronel, M., Reid, T., Furuya, H., Clark, H.B., Troncoso, J.C., Ross, C.A., et al. (2018). SCA8 RAN polySer protein preferentially accumulates in white matter regions and is regulated by eIF3F. EMBO J. *37*, e99023.

Babić Leko, M., Župunski, V., Kirincich, J., Smilović, D., Hortobágyi, T., Hof, P.R., and Šimić, G. (2019). Molecular Mechanisms of Neurodegeneration Related to C9orf72 Hexanucleotide Repeat Expansion.

Balendra, R., and Isaacs, A.M. (2018). C9orf72 -mediated ALS and FTD: multiple pathways to disease. Nat. Rev. Neurol. *14*, 544.

Baral, A., Kumar, P., Pathak, R., and Chowdhury, S. (2013). Emerging trends in G-quadruplex biology – role in epigenetic and evolutionary events. Mol. Biosyst. *9*, 1568–1575.

Batra, R., and Lee, C.W. (2017). Mouse Models of C9orf72 Hexanucleotide Repeat Expansion in Amyotrophic Lateral Sclerosis/ Frontotemporal Dementia. Front. Cell. Neurosci. *11*.

Bauer, P.O. (2016). Methylation of C9orf72 expansion reduces RNA foci formation and dipeptide-repeat proteins expression in cells. Neurosci. Lett. *612*, 204–209.

Belotserkovskii, B.P., Liu, R., Tornaletti, S., Krasilnikova, M.M., Mirkin, S.M., and Hanawalt, P.C. (2010). Mechanisms and implications of transcription blockage by guanine-rich DNA sequences. Proc. Natl. Acad. Sci. U. S. A. *107*, 12816–12821.

Belzil, V.V., Bauer, P.O., Gendron, T.F., Murray, M.E., Dickson, D., and Petrucelli, L. (2014). Characterization of DNA hypermethylation in the cerebellum of c9FTD/ALS patients. Brain Res. *1584*, 15–21.

Berson, A.*, Goodman, L.D.*, Sartoris, A.N., Otte, C.G., Aykit, J.A., Lee, V.M.-Y., Trojanowski, J.Q., and Bonini, N.M. (2019). Drosophila Ref1/ALYREF regulates transcription and toxicity associated with ALS/FTD disease etiologies. Acta Neuropathol. Commun. (* equal contribution)

Bilen, J., and Bonini, N.M. (2007). Genome-Wide Screen for Modifiers of Ataxin-3 Neurodegeneration in Drosophila. PLOS Genet. *3*, e177.

Biogen (2018). A Study to Assess the Safety, Tolerability, and Pharmacokinetics of BIIB078 in Adults With C9ORF72-Associated Amyotrophic Lateral Sclerosis. ClinicalTrials.gov Identifier: NCT03626012.

van Blitterswijk, M., DeJesus-Hernandez, M., and Rademakers, R. (2012). How do C9ORF72 repeat expansions cause ALS and FTD: can we learn from other non-coding repeat expansion disorders? Curr. Opin. Neurol. *25*, 689–700.

van Blitterswijk, M., DeJesus-Hernandez, M., Niemantsverdriet, E., Murray, M.E., Heckman, M.G., Diehl, N.N., Brown, P.H., Baker, M.C., Finch, N.A., Bauer, P.O., et al. (2013). Associations of repeat sizes with clinical and pathological characteristics in C9ORF72 expansion carriers (Xpansize-72): a cross-sectional cohort study. Lancet Neurol. *12*.

van Blitterswijk, M., Mullen, B., Heckman, M.G., Baker, M.C., DeJesus-Hernandez, M., Brown, P.H., Murray, M.E., Hsiung, G.-Y.R., Stewart, H., Karydas, A.M., et al. (2014a). Ataxin-2 as potential disease modifier in C9ORF72 expansion carriers. Neurobiol Aging *35*, 2421.e13-2421.e17.

van Blitterswijk, M., Mullen, B., Nicholson, A.M., Bieniek, K.F., Heckman, M.G., Baker, M.C., DeJesus-Hernandez, M., Finch, N.A., Brown, P.H., Murray, M.E., et al. (2014b). TMEM106B protects C9ORF72 expansion carriers against frontotemporal dementia. Acta Neuropathol *127*, 397–406.

van Blitterswijk, M., Gendron, T.F., Baker, M.C., DeJesus-Hernandez, M., Finch, N.A., Brown, P.H., Daughrity, L.M., Murray, M.E., Heckman, M.G., Jiang, J., et al. (2015). Novel clinical associations with specific C9ORF72 transcripts in patients with repeat expansions in C9ORF72. Acta Neuropathol. (Berl.) *130*, 863–876.

Blythe, A.J., Yazar-Klosinski, B., Webster, M.W., Chen, E., Vandevenne, M., Bendak, K., Mackay, J.P., Hartzog, G.A., and Vrielink, A. (2016). The yeast transcription elongation factor Spt4/5 is a sequence-specific RNA binding protein: Spt4/5 is an RNA-Binding Protein. Protein Sci. *25*, 1710–1721.

Bochman, M.L., Paeschke, K., and Zakian, V.A. (2012). DNA secondary structures: stability and function of G-quadruplex structures. Nat. Rev. Genet. *13*, 770–780.

Boeynaems, S., Bogaert, E., Michiels, E., Gijselinck, I., Sieben, A., Jovičić, A., De Baets, G., Scheveneels, W., Steyaert, J., Cuijt, I., et al. (2016). Drosophila screen connects nuclear transport genes to DPR pathology in c9ALS/FTD. Sci. Rep. *6*, 20877.

Bourinaris, T., and Houlden, H. (2018). C9orf72 and its Relevance in Parkinsonism and Movement Disorders: A Comprehensive Review of the Literature. Mov. Disord. Clin. Pract. *5*, 575–585.

Brázda, V., Hároníková, L., Liao, J.C.C., and Fojta, M. (2014). DNA and RNA Quadruplex-Binding Proteins. Int. J. Mol. Sci. *15*, 17493.

Brčić, J., and Plavec, J. (2016). G-quadruplex formation of oligonucleotides containing ALS and FTD related GGGGCC repeat. Front. Chem. Sci. Eng. *10*, 222–237.

Brčić, J., and Plavec, J. (2017). ALS and FTD linked GGGGCC-repeat containing DNA oligonucleotide folds into two distinct G-quadruplexes. Biochim. Biophys. Acta BBA - Gen. Subj. *1861*, 1237–1245.

Brčić, J., and Plavec, J. (2018). NMR structure of a G-quadruplex formed by four d(G4C2) repeats: insights into structural polymorphism. Nucleic Acids Res. *46*, 11605–11617.

Brooks, T.A., and Hurley, L.H. (2010). Targeting MYC Expression through G-Quadruplexes. Genes Cancer *1*, 641–649.

Brown, R.V., Danford, F.L., Gokhale, V., Hurley, L.H., and Brooks, T.A. (2011). Demonstration that Drug-targeted Down-regulation of MYC in Non-Hodgkins Lymphoma Is Directly Mediated through the Promoter G-quadruplex. J. Biol. Chem. *286*, 41018–41027.

Browning, K.S., and Bailey-Serres, J. (2015). Mechanism of Cytoplasmic mRNA Translation. Arab. Book Am. Soc. Plant Biol. *13*.

Buchman, V.L., Cooper-Knock, J., Connor-Robson, N., Higginbottom, A., Kirby, J., Razinskaya, O.D., Ninkina, N., and Shaw, P.J. (2013). Simultaneous and independent detection of C9ORF72 alleles with low and high number of GGGGCC repeats using an optimised protocol of Southern blot hybridisation. Mol. Neurodegener. *8*, 12.

Cao, Q.-F., Yamamoto, J., Isobe, T., Tateno, S., Murase, Y., Chen, Y., Handa, H., and Yamaguchi, Y. (2015). Characterization of the Human Transcription Elongation Factor Rtf1: Evidence for Nonoverlapping Functions of Rtf1 and the Paf1 Complex. Mol. Cell. Biol. *35*, 3459–3470.

Capra, J.A., Paeschke, K., Singh, M., and Zakian, V.A. (2010). G-Quadruplex DNA Sequences Are Evolutionarily Conserved and Associated with Distinct Genomic Features in Saccharomyces cerevisiae. PLOS Comput. Biol. *6*, e1000861.

Česnik, A.B., Darovic, S., Mihevc, S.P., Štalekar, M., Malnar, M., Motaln, H., Lee, Y.-B., Mazej, J., Pohleven, J., Grosch, M., et al. (2019). Nuclear RNA foci from C9ORF72 expansion mutation form paraspeckle-like bodies. J Cell Sci jcs.224303.

Chambers, V.S., Marsico, G., Boutell, J.M., Antonio, M.D., Smith, G.P., and Balasubramanian, S. (2015). High-throughput sequencing of DNA G-quadruplex structures in the human genome. Nat. Biotechnol. *33*, 877.

Chen, Y., Yamaguchi, Y., Tsugeno, Y., Yamamoto, J., Yamada, T., Nakamura, M., Hisatake, K., and Handa, H. (2009). DSIF, the Paf1 complex, and Tat-SF1 have nonredundant, cooperative roles in RNA polymerase II elongation. Genes Dev. *23*, 2765–2777.

Cheng, H.-M., Chern, Y., Chen, I.-H., Liu, C.-R., Li, S.-H., Chun, S.J., Rigo, F., Bennett, C.F., Deng, N., Feng, Y., et al. (2015). Effects on Murine Behavior and Lifespan of Selectively Decreasing Expression of Mutant Huntingtin Allele by Supt4h Knockdown. PLoS Genet. *11*.

Cheng, W., Wang, S., Mestre, A.A., Fu, C., Makarem, A., Xian, F., Hayes, L.R., Lopez-Gonzalez, R., Drenner, K., Jiang, J., et al. (2018). C9ORF72 GGGGCC repeat-associated non-AUG translation is upregulated by stress through eIF2α phosphorylation. Nat. Commun. *9*, 51.

Chew, J., Gendron, T.F., Prudencio, M., Sasaguri, H., Zhang, Y.-J., Castanedes-Casey, M., Lee, C.W., Jansen-West, K., Kurti, A., Murray, M.E., et al. (2015). C9ORF72 repeat expansions in mice cause TDP-43 pathology, neuronal loss, and behavioral deficits. Science *348*, 1151–1154.

Chew, J., Cook, C., Gendron, T.F., Jansen-West, K., del Rosso, G., Daughrity, L.M., Castanedes-Casey, M., Kurti, A., Stankowski, J.N., Disney, M.D., et al. (2019). Aberrant deposition of stress granule-resident proteins linked to C9orf72-associated TDP-43 proteinopathy. Mol. Neurodegener. *14*, 9.

Chitiprolu, M., Jagow, C., Tremblay, V., Bondy-Chorney, E., Paris, G., Savard, A., Palidwor, G., Barry, F.A., Zinman, L., Keith, J., et al. (2018). A complex of C9ORF72 and p62 uses arginine methylation to eliminate stress granules by autophagy. Nat. Commun. *9*, 2794.

Chu, X., Qin, X., Xu, H., Li, L., Wang, Z., Li, F., Xie, X., Zhou, H., Shen, Y., and Long, J. (2013). Structural insights into Paf1 complex assembly and histone binding. Nucleic Acids Res. *41*, 10619–10629.

Ciesiolka, A., Jazurek, M., Drazkowska, K., and Krzyzosiak, W.J. (2017). Structural Characteristics of Simple RNA Repeats Associated with Disease and their Deleterious Protein Interactions. Front. Cell. Neurosci. *11*.

Ciura, S., Lattante, S., Le Ber, I., Latouche, M., Tostivint, H., Brice, A., and Kabashi, E. (2013). Loss of function of C9orf72 causes motor deficits in a zebrafish model of amyotrophic lateral sclerosis. Ann. Neurol. *74*, 180–187.

Conlon, E.G., and Manley, J.L. (2017). RNA-binding proteins in neurodegeneration: mechanisms in aggregate. Genes Dev. *31*, 1509–1528.

Conlon, E.G., Lu, L., Sharma, A., Yamazaki, T., Tang, T., Shneider, N.A., and Manley, J.L. (2016). The C9ORF72 GGGGCC expansion forms RNA G-quadruplex inclusions and sequesters hnRNP H to disrupt splicing in ALS brains. ELife *5*, e17820.

Cooper-Knock, J., Walsh, M.J., Higginbottom, A., Robin Highley, J., Dickman, M.J., Edbauer, D., Ince, P.G., Wharton, S.B., Wilson, S.A., Kirby, J., et al. (2014). Sequestration of multiple RNA recognition motif-containing proteins by C9orf72 repeat expansions. Brain *137*, 2040–2051.

Cooper-Knock, J., Higginbottom, A., Stopford, M.J., Highley, J.R., Ince, P.G., Wharton, S.B., Pickering-Brown, S., Kirby, J., Hautbergue, G.M., and Shaw, P.J. (2015a). Antisense RNA foci in the motor neurons of C9ORF72-ALS patients are associated with TDP-43 proteinopathy. Acta Neuropathol. (Berl.) *130*, 63–75.

Cooper-Knock, J., Bury, J.J., Heath, P.R., Wyles, M., Higginbottom, A., Gelsthorpe, C., Highley, J.R., Hautbergue, G., Rattray, M., Kirby, J., et al. (2015b). C9ORF72 GGGGCC Expanded Repeats Produce Splicing Dysregulation which Correlates with Disease Severity in Amyotrophic Lateral Sclerosis. PLoS ONE *10*.

Crossley, M.P., Bocek, M., and Cimprich, K.A. (2019). R-Loops as Cellular Regulators and Genomic Threats. Mol. Cell *73*, 398–411.

Davidson, Y.S., Barker, H., Robinson, A.C., Thompson, J.C., Harris, J., Troakes, C., Smith, B., Al-Saraj, S., Shaw, C., Rollinson, S., et al. (2014). Brain distribution of dipeptide repeat proteins in frontotemporal lobar degeneration and motor neurone disease associated with expansions in C9ORF72. Acta Neuropathol Commun *2*.

DeJesus-Hernandez, M., Mackenzie, I.R., Boeve, B.F., Boxer, A.L., Baker, M., Rutherford, N.J., Nicholson, A.M., Finch, N.A., Gilmer, H.F., Adamson, J., et al. (2011). Expanded GGGGCC hexanucleotide repeat in non-coding region of C9ORF72 causes chromosome 9p-linked frontotemporal dementia and amyotrophic lateral sclerosis. Neuron *72*, 245–256.

Dermody, J.L., and Buratowski, S. (2010). Leo1 Subunit of the Yeast Paf1 Complex Binds RNA and Contributes to Complex Recruitment. J. Biol. Chem. *285*, 33671–33679.

Diab, M.A., Mor-Shaked, H., Cohen, E., Cohen-Hadad, Y., Ram, O., Epsztejn-Litman, S., and Eiges, R. (2018). The G-rich Repeats in FMR1 and C9orf72 Loci Are Hotspots for Local Unpairing of DNA. Genetics *210*, 1239–1252.

Dobson-Stone, C., Hallupp, M., Loy, C.T., Thompson, E.M., Haan, E., Sue, C.M., Panegyres, P.K., Razquin, C., Seijo-Martínez, M., Rene, R., et al. (2013). C9ORF72 Repeat Expansion in Australian and Spanish Frontotemporal Dementia Patients. PLOS ONE *8*, e56899.

Dodd, D.W., Tomchick, D.R., Corey, D.R., and Gagnon, K.T. (2016). Pathogenic C9ORF72 Antisense Repeat RNA Forms a Double Helix with Tandem C:C Mismatches. Biochemistry *55*, 1283–1286.

Domínguez-Sánchez, M.S., Barroso, S., Gómez-González, B., Luna, R., and Aguilera, A. (2011). Genome Instability and Transcription Elongation Impairment in Human Cells Depleted of THO/TREX. PLOS Genet. *7*, e1002386.

Donnelly, C.J., Zhang, P.-W., Pham, J.T., Heusler, A.R., Mistry, N.A., Vidensky, S., Daley, E.L., Poth, E.M., Hoover, B., Fines, D.M., et al. (2013). RNA Toxicity from the ALS/FTD C9ORF72 Expansion Is Mitigated by Antisense Intervention. Neuron *80*, 415–428.

Drillon, G., Audit, B., Argoul, F., and Arneodo, A. (2016). Evidence of selection for an accessible nucleosomal array in human. BMC Genomics *17*, 526.

Duquette, M.L., Handa, P., Vincent, J.A., Taylor, A.F., and Maizels, N. (2004). Intracellular transcription of G-rich DNAs induces formation of G-loops, novel structures containing G4 DNA. Genes Dev. *18*, 1618–1629.

Edbauer, D., and Haass, C. (2016). An amyloid-like cascade hypothesis for C9orf72 ALS/FTD. Curr. Opin. Neurobiol. *36*, 99–106.

Elden, A.C., Kim, H.-J., Hart, M.P., Chen-Plotkin, A.S., Johnson, B.S., Fang, X., Armakola, M., Geser, F., Greene, R., Lu, M.M., et al. (2010). Ataxin-2 intermediate-length polyglutamine expansions are associated with increased risk for ALS. Nature *466*, 1069–1075.

Esanov, R., Cabrera, G.T., Andrade, N.S., Gendron, T.F., Brown, R.H., Benatar, M., Wahlestedt, C., Mueller, C., and Zeier, Z. (2017). A C9ORF72 BAC mouse model recapitulates key epigenetic perturbations of ALS/FTD. Mol. Neurodegener. *12*, 46.

Farg, M.A., Sundaramoorthy, V., Sultana, J.M., Yang, S., Atkinson, R.A.K., Levina, V., Halloran, M.A., Gleeson, P.A., Blair, I.P., Soo, K.Y., et al. (2014). C9ORF72, implicated in amytrophic lateral sclerosis and frontotemporal dementia, regulates endosomal trafficking. Hum. Mol. Genet. *23*, 3579–3595.

Farg, M.A., Konopka, A., Soo, K.Y., Ito, D., and Atkin, J.D. (2017). The DNA damage response (DDR) is induced by the C9orf72 repeat expansion in amyotrophic lateral sclerosis. Hum. Mol. Genet. *26*, 2882–2896.

Fay, M.M., Lyons, S.M., and Ivanov, P. (2017). RNA G-quadruplexes in biology: principles and molecular mechanisms. J. Mol. Biol. *429*, 2127–2147.

Fratta, P., Mizielinska, S., Nicoll, A.J., Zloh, M., Fisher, E.M.C., Parkinson, G., and Isaacs, A.M. (2012). C9orf72 hexanucleotide repeat associated with amyotrophic lateral sclerosis and frontotemporal dementia forms RNA G-quadruplexes. Sci. Rep. *2*.

Freibaum, B.D., and Taylor, J.P. (2017). The Role of Dipeptide Repeats in C9ORF72-Related ALS-FTD. Front. Mol. Neurosci. *10*.

Freibaum, B.D., Lu, Y., Lopez-Gonzalez, R., Kim, N.C., Almeida, S., Lee, K.-H., Badders, N., Valentine, M., Miller, B.L., Wong, P.C., et al. (2015). GGGGCC repeat expansion in C9ORF72 compromises nucleocytoplasmic transport. Nature *525*, 129–133.

Freudenreich, C.H. (2018). R-loops: targets for nuclease cleavage and repeat instability. Curr. Genet. 1–6.

Frick, P., Sellier, C., Mackenzie, I.R.A., Cheng, C.-Y., Tahraoui-Bories, J., Martinat, C., Pasterkamp, R.J., Prudlo, J., Edbauer, D., Oulad-Abdelghani, M., et al. (2018). Novel antibodies reveal presynaptic localization of C9orf72 protein and reduced protein levels in C9orf72 mutation carriers. Acta Neuropathol. Commun. *6*, 72.

Furuta, N., Tsukagoshi, S., Hirayanagi, K., and Ikeda, Y. (2019). Suppression of the yeast elongation factor Spt4 ortholog reduces expanded SCA36 GGCCUG repeat aggregation and cytotoxicity. Brain Res.

Gadaleta, M.C., and Noguchi, E. (2017). Regulation of DNA Replication through Natural Impediments in the Eukaryotic Genome. Genes *8*.

García-García, C., Frieda, K.L., Feoktistova, K., Fraser, C.S., and Block, S.M. (2015). Factor-dependent processivity in human eIF4A DEAD-box helicase. Science *348*, 1486–1488.

Gendron, T.F., and Petrucelli, L. (2017). Disease Mechanisms of C9ORF72 Repeat Expansions. Cold Spring Harb. Perspect. Med.

Gendron, T.F., Bieniek, K.F., Zhang, Y.-J., Jansen-West, K., Ash, P.E.A., Caulfield, T., Daughrity, L., Dunmore, J.H., Castanedes-Casey, M., Chew, J., et al. (2013). Antisense transcripts of the expanded C9ORF72 hexanucleotide repeat form nuclear RNA foci and undergo repeat-associated non-ATG translation in c9FTD/ALS. Acta Neuropathol. (Berl.) *126*, 829–844.

Gendron, T.F., Chew, J., Stankowski, J.N., Hayes, L.R., Zhang, Y.-J., Prudencio, M., Carlomagno, Y., Daughrity, L.M., Jansen-West, K., Perkerson, E.A., et al. (2017). Poly(GP) proteins are a useful pharmacodynamic marker for C9ORF72-associated amyotrophic lateral sclerosis. Sci. Transl. Med. *9*, eaai7866.

Gerlach, J.M., Furrer, M., Gallant, M., Birkel, D., Baluapuri, A., Wolf, E., and Gallant, P. (2017). PAF1 complex component Leo1 helps recruit Drosophila Myc to promoters. Proc. Natl. Acad. Sci. *114*, E9224–E9232.

Gijselinck, I., Van Langenhove, T., van der Zee, J., Sleegers, K., Philtjens, S., Kleinberger, G., Janssens, J., Bettens, K., Van Cauwenberghe, C., Pereson, S., et al. (2012). A C9orf72 promoter repeat expansion in a Flanders-Belgian cohort with disorders of the frontotemporal lobar degeneration-amyotrophic lateral sclerosis spectrum: a gene identification study. Lancet Neurol. *11*, 54–65.

Gijselinck, I., Cruts, M., and Van Broeckhoven, C. (2017). The Genetics of C9orf72 Expansions. Cold Spring Harb. Perspect. Med.

Godet, A.-C., David, F., Hantelys, F., Tatin, F., Lacazette, E., Garmy-Susini, B., and Prats, A.-C. (2019). IRES Trans-Acting Factors, Key Actors of the Stress Response. Int. J. Mol. Sci. *20*, 924.

Gómez Ramos, L.M. (2017). Structure, Function, and Drug Targeting: Ribosome Expansion Segments. Georgia Institute of Technology.

Goodman, L.D., Prudencio, M., Kramer, N.J., Martinez-Ramirez, L.F., Srinivasan, A.R., Lan, M., Parisi, M.J., Zhu, Y., Chew, J., Cook, C.N., et al. (2019a). Expanded GGGGCC repeat transcription is mediated by the PAF1 complex in C9orf72-associated FTD. Nat. Neurosci.

Goodman, L.D., Prudencio, M., Srinivasan, A.R., Rifai, O.M., Lee, V.M.-Y., Petrucelli, L., and Bonini, N.M. (2019b). eIF4B and eIF4H mediate GR production from expanded G4C2 in a Drosophila model for C9orf72-associated ALS. Acta Neuropathol. Commun.

Green, K.M., Linsalata, A.E., and Todd, P.K. (2016). RAN translation—what makes it run? Brain Res. *1647*, 30–42.

Green, K.M., Glineburg, M.R., Kearse, M.G., Flores, B.N., Linsalata, A.E., Fedak, S.J., Goldstrohm, A.C., Barmada, S.J., and Todd, P.K. (2017). RAN translation at C9orf72-associated repeat expansions is selectively enhanced by the integrated stress response. Nat. Commun. *8*.

Grunseich, C., Wang, I.X., Watts, J.A., Burdick, J.T., Guber, R.D., Zhu, Z., Bruzel, A., Lanman, T., Chen, K., Schindler, A.B., et al. (2018). Senataxin Mutation Reveals How R-Loops Promote Transcription by Blocking DNA Methylation at Gene Promoters. Molecular Cell *69*, 426-437.e7.

Guo, Q., Lehmer, C., Martínez-Sánchez, A., Rudack, T., Beck, F., Hartmann, H., Pérez-Berlanga, M., Frottin, F., Hipp, M.S., Hartl, F.U., et al. (2018). In Situ Structure of Neuronal C9orf72 Poly-GA Aggregates Reveals Proteasome Recruitment. Cell *172*, 696-705.e12.

Gupta, R., Lan, M., Mojsilovic-Petrovic, J., Choi, W.H., Safren, N., Barmada, S., Lee, M.J., and Kalb, R. (2017). The Proline/Arginine Dipeptide from Hexanucleotide Repeat Expanded C9ORF72 Inhibits the Proteasome. ENeuro *4*.

Gustincich, S., Zucchelli, S., and Mallamaci, A. (2017). The Yin and Yang of nucleic acid-based therapy in the brain. Progress in Neurobiology *155*, 194–211.

Haeusler, A.R., Donnelly, C.J., Periz, G., Simko, E.A.J., Shaw, P.G., Kim, M.-S., Maragakis, N.J., Troncoso, J.C., Pandey, A., Sattler, R., et al. (2014). C9orf72 Nucleotide Repeat Structures Initiate Molecular Cascades of Disease. Nature *507*, 195–200.

Haeusler, A.R., Donnelly, C.J., and Rothstein, J.D. (2016). The expanding biology of the C9orf72 nucleotide repeat expansion in neurodegenerative disease. Nat. Rev. Neurosci. *17*, 383–395.

Hamperl, S., and Cimprich, K.A. (2016). Conflict Resolution in the Genome: How Transcription and Replication Make It Work. Cell *167*, 1455–1467.

Harms, U., Andreou, A.Z., Gubaev, A., and Klostermeier, D. (2014). eIF4B, eIF4G and RNA regulate eIF4A activity in translation initiation by modulating the eIF4A conformational cycle. Nucleic Acids Res. *42*, 7911–7922.

Hartmann, H., Hornburg, D., Czuppa, M., Bader, J., Michaelsen, M., Farny, D., Arzberger, T., Mann, M., Meissner, F., and Edbauer, D. (2018). Proteomics and C9orf72 neuropathology identify ribosomes as poly-GR/PR interactors driving toxicity. Life Sci. Alliance *1*, e201800070.

Hartzog, G.A., and Fu, J. (2013). The Spt4-Spt5 complex: a multi-faceted regulator of transcription elongation. Biochim. Biophys. Acta *1829*, 105.

Hautbergue, G.M., Castelli, L.M., Ferraiuolo, L., Sanchez-Martinez, A., Cooper-Knock, J., Higginbottom, A., Lin, Y.-H., Bauer, C.S., Dodd, J.E., Myszczynska, M.A., et al. (2017). SRSF1-dependent nuclear export inhibition of C9ORF72 repeat transcripts prevents neurodegeneration and associated motor deficits. Nat. Commun. *8*.

Hershman, S.G., Chen, Q., Lee, J.Y., Kozak, M.L., Yue, P., Wang, L.-S., and Johnson, F.B. (2008). Genomic distribution and functional analyses of potential G-quadruplex-forming sequences in Saccharomyces cerevisiae. Nucleic Acids Res. *36*, 144–156.

Ho, W.Y., Tai, Y.K., Chang, J.-C., Liang, J., Tyan, S.-H., Chen, S., Guan, J.-L., Zhou, H., Shen, H.-M., Koo, E., et al. (2019). The ALS-FTD-linked gene product, C9orf72, regulates neuronal morphogenesis via autophagy. Autophagy *0*, 1–16.

Hübers, A., Marroquin, N., Schmoll, B., Vielhaber, S., Just, M., Mayer, B., Högel, J., Dorst, J., Mertens, T., Just, W., et al. (2014). Polymerase chain reaction and Southern blot-based analysis of the C9orf72 hexanucleotide repeat in different motor neuron diseases. Neurobiol. Aging *35*, 1214.e1-6.

Huertas, P., and Aguilera, A. (2003). Cotranscriptionally Formed DNA:RNA Hybrids Mediate Transcription Elongation Impairment and Transcription-Associated Recombination. Mol. Cell *12*, 711–721.

Ito, D., Hatano, M., and Suzuki, N. (2017a). RNA binding proteins and the pathological cascade in ALS/FTD neurodegeneration. Sci. Transl. Med. *9*, eaah5436.

Ito, D., Hatano, M., and Suzuki, N. (2017b). RNA binding proteins and the pathological cascade in ALS/FTD neurodegeneration. Sci. Transl. Med. *9*, eaah5436.

Izban, M.G., and Luse, D.S. (1992). Factor-stimulated RNA polymerase II transcribes at physiological elongation rates on naked DNA but very poorly on chromatin templates. J. Biol. Chem. *267*, 13647–13655.

Ji, A.-L., Zhang, X., Chen, W.-W., and Huang, W.-J. (2017a). Genetics insight into the amyotrophic lateral sclerosis/frontotemporal dementia spectrum. J. Med. Genet. *54*, 145–154.

Ji, Y.J., Ugolino, J., Brady, N.R., Hamacher-Brady, A., and Wang, J. (2017b). Systemic deregulation of autophagy upon loss of ALS- and FTD-linked C9orf72. Autophagy *13*, 1254–1255.

Jiang, J., and Cleveland, D.W. (2016). Bidirectional Transcriptional Inhibition as Therapy for ALS/FTD Caused by Repeat Expansion in C9orf72. Neuron *92*, 1160–1163.

Jiang, J., Zhu, Q., Gendron, T.F., Saberi, S., McAlonis-Downes, M., Seelman, A., Stauffer, J.E., Jafar-nejad, P., Drenner, K., Schulte, D., et al. (2016). Gain of toxicity from ALS/FTD-linked repeat expansions in C9ORF72 is alleviated by antisense oligonucleotides targeting GGGGCC-containing RNAs. Neuron *90*, 535–550.

Jonkers, I., and Lis, J.T. (2015). Getting up to speed with transcription elongation by RNA polymerase II. Nat. Rev. Mol. Cell Biol. *16*, 167–177.

Jonkers, I., Kwak, H., and Lis, J.T. (2014). Genome-wide dynamics of Pol II elongation and its interplay with promoter proximal pausing, chromatin, and exons. ELife *3*.

Jovičić, A., Mertens, J., Boeynaems, S., Bogaert, E., Chai, N., Yamada, S.B., Paul, J.W., Sun, S., Herdy, J.R., Bieri, G., et al. (2015). Modifiers of C9orf72 DPR toxicity implicate nucleocytoplasmic transport impairments in c9FTD/ALS. Nat. Neurosci. *18*, 1226–1229.

Jung, J., Jaarsveld, M.T.M. van, Shieh, S.-Y., Xu, K., and Bonini, N.M. (2011). Defining Genetic Factors That Modulate Intergenerational CAG Repeat Instability in Drosophila melanogaster. Genetics *187*, 61–71.

Kanekura, K., Yagi, T., Cammack, A.J., Mahadevan, J., Kuroda, M., Harms, M.B., Miller, T.M., and Urano, F. (2016). Poly-dipeptides encoded by the C9ORF72 repeats block global protein translation. Hum. Mol. Genet. *25*, 1803–1813.

Kaushik, M., Kaushik, S., Roy, K., Singh, A., Mahendru, S., Kumar, M., Chaudhary, S., Ahmed, S., and Kukreti, S. (2016). A bouquet of DNA structures: Emerging diversity. Biochem. Biophys. Rep. *5*, 388.

Kearse, M.G., Green, K.M., Krans, A., Rodriguez, C.M., Linsalata, A.E., Goldstrohm, A.C., and Todd, P.K. (2016). CGG Repeat-Associated Non-AUG Translation Utilizes a Cap-Dependent Scanning Mechanism of Initiation to Produce Toxic Proteins. Mol. Cell *62*, 314–322.

Kim, N., and Jinks-Robertson, S. (2012). Transcription as a source of genome instability. Nat. Rev. Genet. *13*, 204–214.

Kim, H.-J., Raphael, A.R., LaDow, E.S., McGurk, L., Weber, R., Trojanowski, J.Q., Lee, V.M.-Y., Finkbeiner, S., Gitler, A.D., and Bonini, N.M. (2014). Therapeutic modulation of eIF2α-phosphorylation rescues TDP-43 toxicity in amyotrophic lateral sclerosis disease models. Nat. Genet. *46*, 152–160.

Kim, J., Guermah, M., and Roeder, R.G. (2010). The Human PAF1 Complex Acts in Chromatin Transcription Elongation Both Independently and Cooperatively with SII/TFIIS. Cell *140*, 491–503.

Knopman, D.S., and Roberts, R.O. (2011). Estimating the Number of Persons with Frontotemporal Lobar Degeneration in the US Population. J. Mol. Neurosci. MN *45*, 330.

Koppers, M., Blokhuis, A.M., Westeneng, H., Terpstra, M.L., Zundel, C.A.C., Vieira de Sá, R., Schellevis, R.D., Waite, A.J., Blake, D.J., Veldink, J.H., et al. (2015). C9orf72 ablation in mice does not cause motor neuron degeneration or motor deficits. Ann. Neurol. *78*, 426–438.

Kovanda, A., Zalar, M., Šket, P., Plavec, J., and Rogelj, B. (2015). Anti-sense DNA d(GGCCCC)n expansions in C9ORF72 form i-motifs and protonated hairpins. Sci. Rep. *5*.

Kramer, N.J., Carlomagno, Y., Zhang, Y.-J., Almeida, S., Cook, C.N., Gendron, T.F., Prudencio, M., Van Blitterswijk, M., Belzil, V., Couthouis, J., et al. (2016). Spt4 selectively regulates the expression of C9orf72 sense and antisense mutant transcripts associated with c9FTD/ALS. Science *353*, 708–712.

Kramer, N.J., Haney, M.S., Morgens, D.W., Jovičić, A., Couthouis, J., Li, A., Ousey, J., Ma, R., Bieri, G., Tsui, C.K., et al. (2018). CRISPR–Cas9 screens in human cells and primary neurons identify modifiers of C9ORF72 dipeptide-repeat-protein toxicity. Nat. Genet. 1.

Krzyzosiak, W.J., Sobczak, K., Wojciechowska, M., Fiszer, A., Mykowska, A., and Kozlowski, P. (2012). Triplet repeat RNA structure and its role as pathogenic agent and therapeutic target. Nucleic Acids Res. *40*, 11–26.

Kudlicki, A.S. (2016). G-Quadruplexes Involving Both Strands of Genomic DNA Are Highly Abundant and Colocalize with Functional Sites in the Human Genome. PLoS ONE *11*.

Kumar, V., kashav, T., Islam, A., Ahmad, F., and Hassan, M.I. (2016). Structural insight into C9orf72 hexanucleotide repeat expansions: Towards new therapeutic targets in FTD-ALS. Neurochem. Int. *100*, 11–20.

Kumar, V., Hasan, G.M., and Hassan, M.I. (2017). Unraveling the Role of RNA Mediated Toxicity of C9orf72 Repeats in C9-FTD/ALS. Front. Neurosci. *11*.

Kwon, I., Xiang, S., Kato, M., Wu, L., Theodoropoulos, P., Wang, T., Kim, J., Yun, J., Xie, Y., and McKnight, S.L. (2014). Poly-dipeptides encoded by the C9orf72 repeats bind nucleoli, impede RNA biogenesis, and kill cells. Science *345*, 1139–1145.

Lagier-Tourenne, C., Baughn, M., Rigo, F., Sun, S., Liu, P., Li, H.-R., Jiang, J., Watt, A.T., Chun, S., Katz, M., et al. (2013). Targeted degradation of sense and antisense C9orf72 RNA foci as therapy for ALS and frontotemporal degeneration. Proc. Natl. Acad. Sci. U. S. A. *110*, E4530–E4539.

Lam, E.Y.N., Beraldi, D., Tannahill, D., and Balasubramanian, S. (2013). G-quadruplex structures are stable and detectable in human genomic DNA. Nat. Commun. *4*, 1796.

Lambert, S., Watson, A., Sheedy, D.M., Martin, B., and Carr, A.M. (2005). Gross Chromosomal Rearrangements and Elevated Recombination at an Inducible Site-Specific Replication Fork Barrier. Cell *121*, 689–702.

Landsverk, H.B., Sandquist, L.E., Sridhara, S.C., Rødland, G.E., Sabino, J.C., de Almeida, S.F., Grallert, B., Trinkle-Mulcahy, L., and Syljuåsen, R.G. (2019). Regulation of ATR activity via the RNA polymerase II associated factors CDC73 and PNUTS-PP1. Nucleic Acids Res. *47*, 1797–1813.

Lee, E.B., Lee, V.M.-Y., and Trojanowski, J.Q. (2011). Gains or losses: molecular mechanisms of TDP43-mediated neurodegeneration. Nat. Rev. Neurosci. *13*, 38–50.

Lee, K.-H., Zhang, P., Kim, H.J., Mitrea, D.M., Sarkar, M., Freibaum, B.D., Cika, J., Coughlin, M., Messing, J., Molliex, A., et al. (2016). C9orf72 Dipeptide Repeats Impair the Assembly, Dynamics, and Function of Membrane-Less Organelles. Cell *167*, 774-788.e17.

Lee, Y.-B., Chen, H.-J., Peres, J.N., Gomez-Deza, J., Attig, J., Štalekar, M., Troakes, C., Nishimura, A.L., Scotter, E.L., Vance, C., et al. (2013). Hexanucleotide Repeats in ALS/FTD Form Length-Dependent RNA Foci, Sequester RNA Binding Proteins, and Are Neurotoxic. Cell Rep. *5*, 1178–1186.

Lehmer, C., Oeckl, P., Weishaupt, J.H., Volk, A.E., Diehl-Schmid, J., Schroeter, M.L., Lauer, M., Kornhuber, J., Levin, J., Fassbender, K., et al. (2017). Poly-GP in cerebrospinal fluid links C9orf72-associated dipeptide repeat expression to the asymptomatic phase of ALS/FTD. EMBO Mol. Med. *9*, 859–868.

Leppek, K., Das, R., and Barna, M. (2018). Functional 5′ UTR mRNA structures in eukaryotic translation regulation and how to find them. Nat. Rev. Mol. Cell Biol. *19*, 158–174.

Lessing, D., and Bonini, N.M. (2008). Polyglutamine Genes Interact to Modulate the Severity and Progression of Neurodegeneration in Drosophila. PLOS Biol. *6*, e29.

Levine, T.P., Daniels, R.D., Gatta, A.T., Wong, L.H., and Hayes, M.J. (2013). The product of C9orf72, a gene strongly implicated in neurodegeneration, is structurally related to DENN Rab-GEFs. Bioinformatics *29*, 499–503.

Li, L.-B., Yu, Z., Teng, X., and Bonini, N.M. (2008). RNA toxicity is a component of ataxin-3 degeneration in Drosophila. Nature *453*, 1107.

Lin, Y., and Wilson, J.H. (2011). Transcription-induced DNA toxicity at trinucleotide repeats. Cell Cycle *10*, 611–618.

Lin, K.Y., Nag, N., Pestova, T.V., and Marintchev, A. (2018). Human eIF5 and eIF1A Compete for Binding to eIF5B. Biochemistry *57*, 5910–5920.

Liu, C.-R., Chang, C.-R., Chern, Y., Wang, T.-H., Hsieh, W.-C., Shen, W.-C., Chang, C.-Y., Chu, I.-C., Deng, N., Cohen, S.N., et al. (2012). Spt4 Is Selectively Required for Transcription of Extended Trinucleotide Repeats. Cell *148*, 690–701.

Liu, E.Y., Russ, J., Wu, K., Neal, D., Suh, E., McNally, A.G., Irwin, D.J., Van Deerlin, V.M., and Lee, E.B. (2014). C9orf72 hypermethylation protects against repeat expansion-associated pathology in ALS/FTD. Acta Neuropathol. (Berl.) *128*, 525–541.

Liu, Y., Pattamatta, A., Zu, T., Reid, T., Bardhi, O., Borchelt, D.R., Yachnis, A.T., and Ranum, L.P.W. (2016). C9orf72 BAC Mouse Model with Motor Deficits and Neurodegenerative Features of ALS/FTD. Neuron *90*, 521–534.

Logroscino, G., and Piccininni, M. (2019). Amyotrophic Lateral Sclerosis Descriptive Epidemiology: The Origin of Geographic Difference. Neuroepidemiology *52*, 93–103.

Longhena, F., Spano, P., and Bellucci, A. (2017). Targeting of Disordered Proteins by Small Molecules in Neurodegenerative Diseases. Targeting Trafficking in Drug Development 85–110.

Lopez-Gonzalez, R., Lu, Y., Gendron, T.F., Karydas, A., Tran, H., Yang, D., Petrucelli, L., Miller, B.L., Almeida, S., and Gao, F.-B. (2016). Poly(GR) in C9ORF72-Related ALS/FTD Compromises Mitochondrial Function and Increases Oxidative Stress and DNA Damage in iPSC-Derived Motor Neurons. Neuron *92*, 383–391.

Luo, Z., Lin, C., and Shilatifard, A. (2012). The super elongation complex (SEC) family in transcriptional control. Nat. Rev. Mol. Cell Biol. *13*, 543.

Luse, D.S. (2013). Promoter clearance by RNA polymerase II. Biochim. Biophys. Acta *1829*, 63.

Mackenzie, I.R., Arzberger, T., Kremmer, E., Troost, D., Lorenzl, S., Mori, K., Weng, S.-M., Haass, C., Kretzschmar, H.A., Edbauer, D., et al. (2013). Dipeptide repeat protein pathology in C9ORF72 mutation cases: clinico-pathological correlations. Acta Neuropathol. (Berl.) *126*, 859–879.

Mackenzie, I.R.A., Frick, P., Grässer, F.A., Gendron, T.F., Petrucelli, L., Cashman, N.R., Edbauer, D., Kremmer, E., Prudlo, J., Troost, D., et al. (2015). Quantitative analysis and clinico-pathological correlations of different dipeptide repeat protein pathologies in C9ORF72 mutation carriers. Acta Neuropathol. (Berl.) *130*, 845–861.

Magen, I., and Hornstein, E. (2014). Oligonucleotide-based therapy for neurodegenerative diseases. Brain Research *1584*, 116–128.

Maizels, N. (2015). G4-associated human diseases. EMBO Rep. *16*, 910–922.

Mann, D.M., Rollinson, S., Robinson, A., Bennion Callister, J., Thompson, J.C., Snowden, J.S., Gendron, T., Petrucelli, L., Masuda-Suzukake, M., Hasegawa, M., et al. (2013). Dipeptide repeat proteins are present in the p62 positive inclusions in patients with frontotemporal lobar degeneration and motor neurone disease associated with expansions in C9ORF72. Acta Neuropathol. Commun. *1*, 68.

Marcel, V., Tran, P.L.T., Sagne, C., Martel-Planche, G., Vaslin, L., Teulade-Fichou, M.-P., Hall, J., Mergny, J.-L., Hainaut, P., and Van Dyck, E. (2011). G-quadruplex structures in TP53 intron 3: role in alternative splicing and in production of p53 mRNA isoforms. Carcinogenesis *32*, 271–278.

Marygold, S.J., Attrill, H., and Lasko, P. (2017). The translation factors of Drosophila melanogaster. Fly (Austin) *11*, 65–74.

Mathis, S., and Le Masson, G. (2018). RNA-Targeted Therapies and Amyotrophic Lateral Sclerosis. Biomedicines *6*, 9.

Mis, M.S.C., Brajkovic, S., Tafuri, F., Bresolin, N., Comi, G.P., and Corti, S. (2017). Development of Therapeutics for C9ORF72 ALS/FTD-Related Disorders. Molecular Neurobiology *54*, 4466–4476.

May, S., Hornburg, D., Schludi, M.H., Arzberger, T., Rentzsch, K., Schwenk, B.M., Grässer, F.A., Mori, K., Kremmer, E., Banzhaf-Strathmann, J., et al. (2014). C9orf72 FTLD/ALS-associated Gly-Ala dipeptide repeat proteins cause neuronal toxicity and Unc119 sequestration. Acta Neuropathol. (Berl.) *128*, 485–503.

Mayer, A., Lidschreiber, M., Siebert, M., Leike, K., Söding, J., and Cramer, P. (2010). Uniform transitions of the general RNA polymerase II transcription complex. Nat. Struct. Mol. Biol. *17*, 1272.

Mbogning, J., Nagy, S., Pagé, V., Schwer, B., Shuman, S., Fisher, R.P., and Tanny, J.C. (2013). The PAF Complex and Prf1/Rtf1 Delineate Distinct Cdk9-Dependent Pathways Regulating Transcription Elongation in Fission Yeast. PLoS Genet. *9*.

McMillan, C.T., Russ, J., Wood, E.M., Irwin, D.J., Grossman, M., McCluskey, L., Elman, L., Van Deerlin, V., and Lee, E.B. (2015). C9orf72 promoter hypermethylation is neuroprotective: Neuroimaging and neuropathologic evidence. Neurology *84*, 1622–1630.

Mendoza, O., Bourdoncle, A., Boulé, J.-B., Brosh, R.M., and Mergny, J.-L. (2016). G-quadruplexes and helicases. Nucleic Acids Res. *44*, 1989–2006.

Miglietta, G., Cogoi, S., Pedersen, E.B., and Xodo, L.E. (2016). GC-elements controlling HRAS transcription form i-motif structures unfolded by heterogeneous ribonucleoprotein particle A1. Sci. Rep. *5*.

Mizielinska, S., Lashley, T., Norona, F.E., Clayton, E.L., Ridler, C.E., Fratta, P., and Isaacs, A.M. (2013). C9orf72 frontotemporal lobar degeneration is characterised by frequent neuronal sense and antisense RNA foci. Acta Neuropathol. (Berl.) *126*, 845–857.

Mizielinska, S., Grönke, S., Niccoli, T., Ridler, C.E., Clayton, E.L., Devoy, A., Moens, T., Norona, F.E., Woollacott, I.O.C., Pietrzyk, J., et al. (2014). C9orf72 repeat expansions cause neurodegeneration in Drosophila through arginine-rich proteins. Science *345*, 1192–1194.

Mizielinska, S., Ridler, C.E., Balendra, R., Thoeng, A., Woodling, N.S., Grässer, F.A., Plagnol, V., Lashley, T., Partridge, L., and Isaacs, A.M. (2017). Bidirectional nucleolar dysfunction in C9orf72 frontotemporal lobar degeneration. Acta Neuropathol. Commun. *5*, 29.

Moens, T.G., Mizielinska, S., Niccoli, T., Mitchell, J.S., Thoeng, A., Ridler, C.E., Grönke, S., Esser, J., Heslegrave, A., Zetterberg, H., et al. (2018). Sense and antisense RNA are not toxic in Drosophila models of C9orf72-associated ALS/FTD. Acta Neuropathol. (Berl.) 1–13.

Moon, S.L., Sonenberg, N., and Parker, R. (2018). Neuronal Regulation of eIF2α Function in Health and Neurological Disorders. Trends Mol. Med. *24*, 575–589.

Mordes, D.A., Prudencio, M.*, Goodman, L.D.*, Klim, J.R., Moccia, R., Limone, F., Pietilainen, O., Chowdhary, K., Dickson, D.W., Rademakers, R., et al. (2018). Dipeptide repeat proteins activate a heat shock response found in C9ORF72-ALS/FTLD patients. Acta Neuropathol. Commun. *6*. (* equal contribution)

Mori, K., Weng, S.-M., Arzberger, T., May, S., Rentzsch, K., Kremmer, E., Schmid, B., Kretzschmar, H.A., Cruts, M., Van Broeckhoven, C., et al. (2013a). The C9orf72 GGGGCC repeat is translated into aggregating dipeptide-repeat proteins in FTLD/ALS. Science *339*, 1335–1338.

Mori, K., Arzberger, T., Grässer, F.A., Gijselinck, I., May, S., Rentzsch, K., Weng, S.-M., Schludi, M.H., Zee, J. van der, Cruts, M., et al. (2013b). Bidirectional transcripts of the expanded C9orf72 hexanucleotide repeat are translated into aggregating dipeptide repeat proteins. Acta Neuropathol. (Berl.) *126*, 881–893.

Mukherjee, A.K., Sharma, S., and Chowdhury, S. (2019). Non-duplex G-Quadruplex Structures Emerge as Mediators of Epigenetic Modifications. Trends Genet. *35*, 129–144.

Naguib, A., Sandmann, T., Yi, F., Watts, R.J., Lewcock, J.W., and Dowdle, W.E. (2019). SUPT4H1 Depletion Leads to a Global Reduction in RNA. Cell Rep. *26*, 45-53.e4.

Nakken, S., Rognes, T., and Hovig, E. (2009). The disruptive positions in human G-quadruplex motifs are less polymorphic and more conserved than their neutral counterparts. Nucleic Acids Res. *37*, 5749–5756.

Neidle, S. (2010). Human telomeric G-quadruplex: The current status of telomeric G-quadruplexes as therapeutic targets in human cancer. FEBS J. *277*, 1118–1125.

Neumann, M., Sampathu, D.M., Kwong, L.K., Truax, A.C., Micsenyi, M.C., Chou, T.T., Bruce, J., Schuck, T., Grossman, M., Clark, C.M., et al. (2006). Ubiquitinated TDP-43 in Frontotemporal Lobar Degeneration and Amyotrophic Lateral Sclerosis. Science *314*, 130–133.

Ng, A.S.L., and Tan, E.-K. (2017). Intermediate C9orf72 alleles in neurological disorders: does size really matter? J. Med. Genet. *54*, 591–597.

Nguyen, L., Cleary, J.D., and Ranum, L.P.W. (2019). Repeat-Associated Non-ATG Translation: Molecular Mechanisms and Contribution to Neurological Disease. Annu. Rev. Neurosci. *42*.

Niblock, M., Smith, B.N., Lee, Y.-B., Sardone, V., Topp, S., Troakes, C., Al-Sarraj, S., Leblond, C.S., Dion, P.A., Rouleau, G.A., et al. (2016). Retention of hexanucleotide repeat-containing intron in C9orf72 mRNA: implications for the pathogenesis of ALS/FTD. Acta Neuropathol. Commun. *4*.

Nielsen, K.H., Behrens, M.A., He, Y., Oliveira, C.L.P., Sottrup Jensen, L., Hoffmann, S.V., Pedersen, J.S., and Andersen, G.R. (2011). Synergistic activation of eIF4A by eIF4B and eIF4G. Nucleic Acids Res. *39*, 2678–2689.

Nishida, K., Kuwano, Y., Nishikawa, T., Masuda, K., and Rokutan, K. (2017). RNA Binding Proteins and Genome Integrity. Int. J. Mol. Sci. *18*, 1341.

Nojima, T., Tellier, M., Foxwell, J., Ribeiro de Almeida, C., Tan-Wong, S.M., Dhir, S., Dujardin, G., Dhir, A., Murphy, S., and Proudfoot, N.J. (2018). Deregulated Expression of Mammalian lncRNA through Loss of SPT6 Induces R-Loop Formation, Replication Stress, and Cellular Senescence. Mol. Cell *72*, 970-984.e7.

O'Rourke, J.G., Bogdanik, L., Yáñez, A., Lall, D., Wolf, A.J., Muhammad, A.K.M.G., Ho, R., Carmona, S., Vit, J.P., Zarrow, J., et al. (2016). C9orf72 is required for proper macrophage and microglial function in mice. Science *351*, 1324–1329.

Palumbo, S.L., Ebbinghaus, S.W., and Hurley, L.H. (2009). Formation of a Unique End-to-End Stacked Pair of G-Quadruplexes in the hTERT Core Promoter with Implications for Inhibition of Telomerase by G-Quadruplex-Interactive Ligands. J. Am. Chem. Soc. *131*, 10878–10891.

Pan, F., Zhang, Y., Man, V.H., Roland, C., and Sagui, C. (2018). E-motif formed by extrahelical cytosine bases in DNA homoduplexes of trinucleotide and hexanucleotide repeats. Nucleic Acids Res. *46*, 942–955.

Pedroso, I.M., Duarte, L.F., Yanez, G., Burkewitz, K., and Fletcher, T.M. (2007). Sequence specificity of inter- and intramolecular G-quadruplex formation by human telomeric DNA. Biopolymers *87*, 74–84.

Pisareva, V.P., and Pisarev, A.V. (2014). eIF5 and eIF5B together stimulate 48S initiation complex formation during ribosomal scanning. Nucleic Acids Res. *42*, 12052–12069.

Porta, S., Kwong, L.K., Trojanowski, J.Q., and Lee, V.M.-Y. (2015). Drosha Inclusions Are New Components of Dipeptide-Repeat Protein Aggregates in FTLD-TDP and ALS C9orf72 Expansion Cases. J. Neuropathol. Exp. Neurol. *74*, 380–387.

Pottier, C., Ravenscroft, T.A., Sanchez-Contreras, M., and Rademakers, R. (2016). Genetics of FTLD: overview and what else we can expect from genetic studies. J. Neurochem. *138*, 32–53.

Prasad, A., Bharathi, V., Sivalingam, V., Girdhar, A., and Patel, B.K. (2019). Molecular Mechanisms of TDP-43 Misfolding and Pathology in Amyotrophic Lateral Sclerosis. Front. Mol. Neurosci. *12*.

Prudencio, M., Belzil, V.V., Batra, R., Ross, C.A., Gendron, T.F., Pregent, L.J., Murray, M.E., Overstreet, K.K., Piazza-Johnston, A.E., Desaro, P., et al. (2015). Distinct brain transcriptome profiles in C9orf72-associated and sporadic ALS. Nat. Neurosci. *18*, 1175–1182.

Prudencio, M., Gonzales, P.K., Cook, C.N., Gendron, T.F., Daughrity, L.M., Song, Y., Ebbert, M.T.W., van Blitterswijk, M., Zhang, Y.-J., Jansen-West, K., et al. (2017). Repetitive element transcripts are elevated in the brain of C9orf72 ALS/FTLD patients. Hum. Mol. Genet. *26*, 3421–3431.

Qiu, H., Hu, C., Wong, C.-M., and Hinnebusch, A.G. (2006). The Spt4p subunit of yeast DSIF stimulates association of the Paf1 complex with elongating RNA polymerase II. Mol. Cell. Biol. *26*, 3135–3148.

Qiu, H., Hu, C., Gaur, N.A., and Hinnebusch, A.G. (2012). Pol II CTD kinases Bur1 and Kin28 promote Spt5 CTR-independent recruitment of Paf1 complex. EMBO J. *31*, 3494–3505.

Raffaele, F., Claudia, M., and John, H. (2019). Genetics and molecular mechanisms of frontotemporal lobar degeneration: an update and future avenues. Neurobiol. Aging *78*, 98–110.

Reddy, K., Zamiri, B., Stanley, S.Y.R., Macgregor, R.B., and Pearson, C.E. (2013). The Disease-associated r(GGGGCC)n Repeat from the C9orf72 Gene Forms Tract Length-dependent Uni- and Multimolecular RNA G-quadruplex Structures. J. Biol. Chem. *288*, 9860–9866.

Reddy, K., Schmidt, M.H.M., Geist, J.M., Thakkar, N.P., Panigrahi, G.B., Wang, Y.-H., and Pearson, C.E. (2014). Processing of double-R-loops in (CAG)·(CTG) and C9orf72 (GGGGCC)·(GGCCCC) repeats causes instability. Nucleic Acids Res. *42*, 10473–10487.

Reinhold, W.C., Mergny, J.-L., Liu, H., Ryan, M., Pfister, T.D., Kinders, R., Parchment, R., Doroshow, J., Weinstein, J.N., and Pommier, Y. (2010). Exon array analyses across the NCI-60 reveals potential regulation of TOP1 by transcription pausing at guanosine quartets in the first intron. Cancer Res. *70*, 2191–2203.

Renton, A.E., Majounie, E., Waite, A., Simón-Sánchez, J., Rollinson, S., Gibbs, J.R., Schymick, J.C., Laaksovirta, H., van Swieten, J.C., Myllykangas, L., et al. (2011). A hexanucleotide repeat expansion in C9ORF72 is the cause of chromosome 9p21-linked ALS-FTD. Neuron *72*, 257–268.

Renton, A.E., Chiò, A., and Traynor, B.J. (2014). State of play in amyotrophic lateral sclerosis genetics. Nat. Neurosci. *17*, 17–23.

Riboldi, G., Zanetta, C., Ranieri, M., Nizzardo, M., Simone, C., Magri, F., Bresolin, N., Comi, G.P., and Corti, S. (2014). Antisense Oligonucleotide Therapy for the Treatment of C9ORF72 ALS/FTD Diseases. Molecular Neurobiology *50*, 721–732.

Richard, P., and Manley, J.L. (2017). R Loops and Links to Human Disease. J. Mol. Biol. *429*, 3168–3180.

Rodrigues, J., and Lydall, D. (2018). Paf1 and Ctr9, core components of the PAF1 complex, maintain low levels of telomeric repeat containing RNA. Nucleic Acids Res. *46*, 621–634.

Rogers, G.W., Richter, N.J., Lima, W.F., and Merrick, W.C. (2001). Modulation of the Helicase Activity of eIF4A by eIF4B, eIF4H, and eIF4F. J. Biol. Chem. *276*, 30914–30922.

Rondón, A.G., García-Rubio, M., González-Barrera, S., and Aguilera, A. (2003). Molecular evidence for a positive role of Spt4 in transcription elongation. EMBO J. *22*, 612–620.

Rondón, A.G., Gallardo, M., García-Rubio, M., and Aguilera, A. (2004). Molecular evidence indicating that the yeast PAF complex is required for transcription elongation. EMBO Rep. *5*, 47–53.

Rossi, S., Serrano, A., Gerbino, V., Giorgi, A., Francesco, L.D., Nencini, M., Bozzo, F., Schininà, M.E., Bagni, C., Cestra, G., et al. (2015). Nuclear accumulation of mRNAs underlies G4C2-repeat-induced translational repression in a cellular model of C9orf72 ALS. J Cell Sci *128*, 1787–1799.

Rozovsky, N., Butterworth, A.C., and Moore, M.J. (2008). Interactions between eIF4AI and its accessory factors eIF4B and eIF4H. RNA *14*, 2136–2148.

Russ, J., Liu, E.Y., Wu, K., Neal, D., Suh, E., Irwin, D.J., McMillan, C.T., Harms, M.B., Cairns, N.J., Wood, E.M., et al. (2015). Hypermethylation of repeat expanded C9orf72 is a clinical and molecular disease modifier. Acta Neuropathol. (Berl.) *129*, 39–52.

Saberi, S., Stauffer, J.E., Jiang, J., Garcia, S.D., Taylor, A.E., Schulte, D., Ohkubo, T., Schloffman, C.L., Maldonado, M., Baughn, M., et al. (2018). Sense-encoded poly-GR dipeptide repeat proteins correlate to neurodegeneration and uniquely co-localize with TDP-43 in dendrites of repeat-expanded C9orf72 amyotrophic lateral sclerosis. Acta Neuropathol. (Berl.) *135*, 459–474.

Sakae, N., Bieniek, K.F., Zhang, Y.-J., Ross, K., Gendron, T.F., Murray, M.E., Rademakers, R., Petrucelli, L., and Dickson, D.W. (2018). Poly-GR dipeptide repeat polymers correlate with

neurodegeneration and Clinicopathological subtypes in C9ORF72-related brain disease. Acta Neuropathol. Commun. *6*, 63.

Satoh, J., Yamamoto, Y., Kitano, S., Takitani, M., Asahina, N., and Kino, Y. (2014). Molecular Network Analysis Suggests a Logical Hypothesis for the Pathological Role of C9orf72 in Amyotrophic Lateral Sclerosis/Frontotemporal Dementia. J. Cent. Nerv. Syst. Dis. *6*, 69–78.

Sauer, M., and Paeschke, K. (2017). G-quadruplex unwinding helicases and their function *in vivo*. Biochem. Soc. Trans. *45*, 1173–1182.

Schludi, M.H., May, S., Grässer, F.A., Rentzsch, K., Kremmer, E., Küpper, C., Klopstock, T., Arzberger, T., and Edbauer, D. (2015). Distribution of dipeptide repeat proteins in cellular models and C9orf72 mutation cases suggests link to transcriptional silencing. Acta Neuropathol. (Berl.) *130*, 537–555.

Schwarzbauer, K., Bodenhofer, U., and Hochreiter, S. (2012). Genome-Wide Chromatin Remodeling Identified at GC-Rich Long Nucleosome-Free Regions. PLOS ONE *7*, e47924.

Sellier, C., Campanari, M.-L., Corbier, C.J., Gaucherot, A., Kolb-Cheynel, I., Oulad-Abdelghani, M., Ruffenach, F., Page, A., Ciura, S., Kabashi, E., et al. (2016). Loss of C9ORF72 impairs autophagy and synergizes with polyQ Ataxin-2 to induce motor neuron dysfunction and cell death. EMBO J. *35*, 1276–1297.

Seltman, R.E., and Matthews, B.R. (2012). Frontotemporal Lobar Degeneration: Epidemiology, Pathology, Diagnosis and Management. CNS Drugs *26*, 841–870.

Selvaraj, B.T., Livesey, M.R., Zhao, C., Gregory, J.M., James, O.T., Cleary, E.M., Chouhan, A.K., Gane, A.B., Perkins, E.M., Dando, O., et al. (2018). C9ORF72 repeat expansion causes vulnerability of motor neurons to Ca 2+ -permeable AMPA receptor-mediated excitotoxicity. Nat. Commun. *9*, 347.

Sen, N.D., Zhou, F., Harris, M.S., Ingolia, N.T., and Hinnebusch, A.G. (2016). eIF4B stimulates translation of long mRNAs with structured 5′ UTRs and low closed-loop potential but weak dependence on eIF4G. Proc. Natl. Acad. Sci. U. S. A. *113*, 10464–10472.

Sharma, S.D., Kraft, J.J., Miller, W.A., and Goss, D.J. (2015). Recruitment of the 40S Ribosome Subunit to the 3′-Untranslated Region (UTR) of a Viral mRNA, via the eIF4 Complex, Facilitates Cap-independent Translation. J. Biol. Chem. *290*, 11268–11281.

Shatsky, I.N., Terenin, I.M., Smirnova, V.V., and Andreev, D.E. (2018). Cap-Independent Translation: What's in a Name? Trends Biochem. Sci.

Shaw, M.P., Higgenbottom, A., McGown, A., Castelli, L.M., James, E., Hautbergue, G.M., Shaw, P.J., Ramesh, T.M. (2018) Stable transgenic C9orf72 zebrafish model key aspects of the ALS/FTD phenotype and reveal novel pathological features. Acta Neuropath Com. 6:125.

Shi, K.Y., Mori, E., Nizami, Z.F., Lin, Y., Kato, M., Xiang, S., Wu, L.C., Ding, M., Yu, Y., Gall, J.G., et al. (2017). Toxic PRn poly-dipeptides encoded by the C9orf72 repeat expansion block nuclear import and export. Proc. Natl. Acad. Sci. *114*, E1111–E1117.

Shi, Y., Lin, S., Staats, K.A., Li, Y., Chang, W.-H., Hung, S.-T., Hendricks, E., Linares, G.R., Wang, Y., Son, E.Y., et al. (2018). Haploinsufficiency leads to neurodegeneration in C9ORF72 ALS/FTD human induced motor neurons. Nature Medicine.

Shivji, M.K.K., Renaudin, X., Williams, Ç.H., and Venkitaraman, A.R. (2018). BRCA2 Regulates Transcription Elongation by RNA Polymerase II to Prevent R-Loop Accumulation. Cell Rep. *22*, 1031–1039.

Sieben, A., Van Langenhove, T., Engelborghs, S., Martin, J.-J., Boon, P., Cras, P., De Deyn, P.-P., Santens, P., Van Broeckhoven, C., and Cruts, M. (2012). The genetics and neuropathology of frontotemporal lobar degeneration. Acta Neuropathol. (Berl.) *124*, 353–372.

Simone, R., Fratta, P., Neidle, S., Parkinson, G.N., and Isaacs, A.M. (2015). G-quadruplexes: Emerging roles in neurodegenerative diseases and the non-coding transcriptome. FEBS Lett. *589*, 1653–1668.

Simone, R., Balendra, R., Moens, T.G., Preza, E., Wilson, K.M., Heslegrave, A., Woodling, N.S., Niccoli, T., Gilbert-Jaramillo, J., Abdelkarim, S., et al. (2018). G-quadruplex-binding small molecules ameliorate C9orf72 FTD/ALS pathology in vitro and in vivo. EMBO Mol. Med. *10*, 22–31.

Šket, P., Pohleven, J., Kovanda, A., Štalekar, M., Župunski, V., Zalar, M., Plavec, J., and Rogelj, B. (2015). Characterization of DNA G-quadruplex species forming from C9ORF72 G4C2-expanded repeats associated with amyotrophic lateral sclerosis and frontotemporal lobar degeneration. Neurobiol. Aging *36*, 1091–1096.

Smith, R., Pioro, E., Myers, K., Sirdofsky, M., Goslin, K., Meekins, G., Yu, H., Wymer, J., Cudkowicz, M., Macklin, E.A., et al. (2017). Enhanced Bulbar Function in Amyotrophic Lateral Sclerosis: The Nuedexta Treatment Trial. Neurotherapeutics *14*, 762–772.

Solomon, D.A., Stepto, A., Au, W.H., Adachi, Y., Diaper, D.C., Hall, R., Rekhi, A., Boudi, A., Tziortzouda, P., Lee, Y.-B., et al. (2018). A feedback loop between dipeptide-repeat protein, TDP-43 and karyopherin-α mediates C9orf72-related neurodegeneration. Brain *141*, 2908–2924.

Sonenberg, N., and Hinnebusch, A.G. (2009). Regulation of Translation Initiation in Eukaryotes: Mechanisms and Biological Targets. Cell *136*, 731–745.

Sonobe, Y., Ghadge, G., Masaki, K., Sendoel, A., Fuchs, E., and Roos, R.P. (2018). Translation of dipeptide repeat proteins from the C9ORF72 expanded repeat is associated with cellular stress. Neurobiol. Dis. *116*, 155–165.

Soto, C., and Estrada, L.D. (2008). Protein Misfolding and Neurodegeneration. Arch. Neurol. *65*, 184–189.

Soutourina, J. (2017). Transcription regulation by the Mediator complex. Nat. Rev. Mol. Cell Biol.

Spilka, R., Ernst, C., Mehta, A.K., and Haybaeck, J. (2013). Eukaryotic translation initiation factors in cancer development and progression. Cancer Lett. *340*, 9–21.

Spirin, A.S. (2009). How Does a Scanning Ribosomal Particle Move along the 5′-Untranslated Region of Eukaryotic mRNA? Brownian Ratchet Model. Biochemistry *48*, 10688–10692.

Steinacker, P., Barschke, P., and Otto, M. (2018). Biomarkers for diseases with TDP-43 pathology. Mol. Cell. Neurosci.

Su, Z., Zhang, Y., Gendron, T.F., Bauer, P.O., Chew, J., Yang, W.-Y., Fostvedt, E., Jansen-West, K., Belzil, V.V., Desaro, P., et al. (2014). Discovery of a Biomarker and Lead Small Molecules to Target r(GGGGCC)-Associated Defects in c9FTD/ALS. Neuron *83*, 1043–1050.

Sudria-Lopez, E., Koppers, M., de Wit, M., van der Meer, C., Westeneng, H.-J., Zundel, C.A.C., Youssef, S.A., Harkema, L., de Bruin, A., Veldink, J.H., et al. (2016). Full ablation of C9orf72 in mice causes immune system-related pathology and neoplastic events but no motor neuron defects. Acta Neuropathol. (Berl.) *132*, 145–147.

Sun, Y., Atas, E., Lindqvist, L., Sonenberg, N., Pelletier, J., and Meller, A. (2012). The eukaryotic initiation factor eIF4H facilitates loop-binding, repetitive RNA unwinding by the eIF4A DEAD-box helicase. Nucleic Acids Res. *40*, 6199–6207.

Sun, Z.-Y., Wang, X.-N., Cheng, S.-Q., Su, X.-X., and Ou, T.-M. (2019). Developing Novel G-Quadruplex Ligands: From Interaction with Nucleic Acids to Interfering with Nucleic Acid–Protein Interaction. Molecules *24*, 396.

Suzuki, H., Shibagaki, Y., Hattori, S., and Matsuoka, M. (2018). The proline–arginine repeat protein linked to C9-ALS/FTD causes neuronal toxicity by inhibiting the DEAD-box RNA helicase-mediated ribosome biogenesis. Cell Death Dis. *9*.

Swinnen, B., Bento-Abreu, A., Gendron, T.F., Boeynaems, S., Bogaert, E., Nuyts, R., Timmers, M., Scheveneels, W., Hersmus, N., Wang, J., et al. (2018). A zebrafish model for C9orf72 ALS reveals RNA toxicity as a pathogenic mechanism. Acta Neuropathol. (Berl.) 1–17.

Tabet, R., Schaeffer, L., Freyermuth, F., Jambeau, M., Workman, M., Lee, C.-Z., Lin, C.-C., Jiang, J., Jansen-West, K., Abou-Hamdan, H., et al. (2018). CUG initiation and frameshifting enable production of dipeptide repeat proteins from ALS/FTD C9ORF72 transcripts. Nat. Commun. *9*, 152.

Tao, Z., Wang, H., Xia, Q., Li, K., Li, K., Jiang, X., Xu, G., Wang, G., and Ying, Z. (2015). Nucleolar stress and impaired stress granule formation contribute to C9orf72 RAN translation-induced cytotoxicity. Hum. Mol. Genet. *24*, 2426–2441.

Terenin, I.M., Smirnova, V.V., Andreev, D.E., Dmitriev, S.E., and Shatsky, I.N. (2017). A researcher's guide to the galaxy of IRESs. Cell. Mol. Life Sci. *74*, 1431–1455.

Therrien, M., Rouleau, G.A., Dion, P.A., and Parker, J.A. (2013). Deletion of C9ORF72 Results in Motor Neuron Degeneration and Stress Sensitivity in C. elegans. PLoS ONE *8*.

Todd, P.K., Oh, S.Y., Krans, A., He, F., Sellier, C., Frazer, M., Renoux, A.J., Chen, K., Scaglione, K.M., Basrur, V., et al. (2013). CGG Repeat-Associated Translation Mediates Neurodegeneration in Fragile X Tremor Ataxia Syndrome. Neuron *78*, 440–455.

Toubiana, S., and Selig, S. (2018). DNA:RNA hybrids at telomeres – when it is better to be out of the (R) loop. FEBS J. *285*, 2552–2566.

Tran, H., Almeida, S., Moore, J., Gendron, T.F., Chalasani, U., Lu, Y., Du, X., Nickerson, J.A., Petrucelli, L., Weng, Z., et al. (2015). Differential Toxicity of Nuclear RNA Foci versus Dipeptide Repeat Proteins in a Drosophila Model of C9ORF72 FTD/ALS. Neuron *87*, 1207–1214.

Van Oss, S.B., Shirra, M.K., Bataille, A.R., Wier, A.D., Yen, K., Vinayachandran, V., Byeon, I.-J.L., Cucinotta, C.E., Héroux, A., Jeon, J., et al. (2016). The Histone Modification Domain of Paf1

Complex Subunit Rtf1 Directly Stimulates H2B Ubiquitylation Through an Interaction with Rad6. Mol. Cell *64*, 815–825.

Van Oss, S.B., Cucinotta, C.E., and Arndt, K.M. (2017). Emerging Insights into the Roles of the Paf1 Complex in Gene Regulation. Trends Biochem. Sci. *42*, 788–798.

Vanoosthuyse, V. (2018). Strengths and Weaknesses of the Current Strategies to Map and Characterize R-Loops. Non-Coding RNA *4*.

Vatovec, S., Kovanda, A., and Rogelj, B. (2014). Unconventional features of C9ORF72 expanded repeat in amyotrophic lateral sclerosis and frontotemporal lobar degeneration. Neurobiol. Aging *35*, 2421.e1-2421.e12.

Vatsavayai, S.C., Yoon, S.J., Gardner, R.C., Gendron, T.F., Vargas, J.N.S., Trujillo, A., Pribadi, M., Phillips, J.J., Gaus, S.E., Hixson, J.D., et al. (2016). Timing and significance of pathological features in C9orf72 expansion-associated frontotemporal dementia. Brain *139*, 3202–3216.

Vatsavayai, S.C., Nana, A.L., Yokoyama, J.S., and Seeley, W.W. (2019). C9orf72-FTD/ALS pathogenesis: evidence from human neuropathological studies. Acta Neuropathol. (Berl.) *137*, 1–26.

Vaysse, C., Philippe, C., Martineau, Y., Quelen, C., Hieblot, C., Renaud, C., Nicaise, Y., Desquesnes, A., Pannese, M., Filleron, T., et al. (2015). Key contribution of eIF4H-mediated translational control in tumor promotion. Oncotarget *6*, 39924–39940.

Veloso, A., Kirkconnell, K.S., Magnuson, B., Biewen, B., Paulsen, M.T., Wilson, T.E., and Ljungman, M. (2014). Rate of elongation by RNA polymerase II is associated with specific gene features and epigenetic modifications. Genome Res. *24*, 896.

Verma, S.P., and Das, P. (2018). G-quadruplex structure at intron 2 of TFE3 and its role in Xp11.2 translocation and splicing. Biochim Biophys Acta Gen Subj *1862*, 630–636.

Viodé, A., Fournier, C., Camuzat, A., Fenaille, F., Bank, N.B., Latouche, M., Elahi, F., Le Ber, I., Junot, C., Lamari, F., et al. (2018). New Antibody-Free Mass Spectrometry-Based Quantification Reveals That C9ORF72 Long Protein Isoform Is Reduced in the Frontal Cortex of Hexanucleotide-Repeat Expansion Carriers. Front. Neurosci. *12*.

Vos, S.M., Farnung, L., Urlaub, H., and Cramer, P. (2018). Structure of paused transcription complex Pol II–DSIF–NELF. Nature *560*, 601–606.

Wahba, L., Amon, J.D., Koshland, D., and Vuica-Ross, M. (2011). RNase H and Multiple RNA Biogenesis Factors Cooperate to Prevent RNA:DNA Hybrids from Generating Genome Instability. Mol. Cell *44*, 978–988.

Waite, A.J., Bäumer, D., East, S., Neal, J., Morris, H.R., Ansorge, O., and Blake, D.J. (2014). Reduced C9orf72 protein levels in frontal cortex of amyotrophic lateral sclerosis and frontotemporal degeneration brain with the C9ORF72 hexanucleotide repeat expansion. Neurobiol. Aging *35*, 1779.e5-1779.e13.

Walker, C., Herranz-Martin, S., Karyka, E., Liao, C., Lewis, K., Elsayed, W., Lukashchuk, V., Chiang, S.-C., Ray, S., Mulcahy, P.J., et al. (2017). C9orf72 expansion disrupts ATM-mediated chromosomal break repair. Nat. Neurosci. *20*, 1225.

Walker, S.E., Zhou, F., Mitchell, S.F., Larson, V.S., Valasek, L., Hinnebusch, A.G., and Lorsch, J.R. (2013). Yeast eIF4B binds to the head of the 40S ribosomal subunit and promotes mRNA recruitment through its N-terminal and internal repeat domains. RNA *19*, 191–207.

Wang, I.X., Grunseich, C., Fox, J., Burdick, J., Zhu, Z., Ravazian, N., Hafner, M., and Cheung, V.G. (2018a). Human proteins that interact with RNA/DNA hybrids. Genome Res. *28*, 1405–1414.

Wang, Z.-F., Ursu, A., Childs-Disney, J.L., Guertler, R., Yang, W.-Y., Bernat, V., Rzuczek, S.G., Fuerst, R., Zhang, Y.-J., Gendron, T.F., et al. (2018b). The Hairpin Form of r(G4C2)exp in c9ALS/FTD Is Repeat-Associated Non-ATG Translated and a Target for Bioactive Small Molecules. Cell Chem. Biol.

Wang, Z.-F., Ursu, A., Childs-Disney, J.L., Guertler, R., Yang, W.-Y., Bernat, V., Rzuczek, S.G., Fuerst, R., Zhang, Y.-J., Gendron, T.F., et al. (2019). The Hairpin Form of r(G4C2)exp in c9ALS/FTD Is Repeat-Associated Non-ATG Translated and a Target for Bioactive Small Molecules. Cell Chem. Biol. *26*, 179-190.e12.

Wanzek, K. (2016). The investigation of the function of repair proteins at G-quadruplex structures in Saccharomyces cerevisiae revealed that Mms1 promotes genome stability. Universität Würzburg.

Webster, C.P., Smith, E.F., Bauer, C.S., Moller, A., Hautbergue, G.M., Ferraiuolo, L., Myszczynska, M.A., Higginbottom, A., Walsh, M.J., Whitworth, A.J., et al. (2016a). The C9orf72 protein interacts with Rab1a and the ULK1 complex to regulate initiation of autophagy. EMBO J. *35*, 1656–1676.

Webster, C.P., Smith, E.F., Grierson, A.J., and De Vos, K.J. (2016b). C9orf72 plays a central role in Rab GTPase-dependent regulation of autophagy. Small GTPases 1–10.

Wen, X., Tan, W., Westergard, T., Krishnamurthy, K., Markandaiah, S.S., Shi, Y., Lin, S., Shneider, N.A., Monaghan, J., Pandey, U.B., et al. (2014). Antisense Proline-Arginine RAN Dipeptides Linked to C9ORF72-ALS/FTD Form Toxic Nuclear Aggregates that Initiate In Vitro and In Vivo Neuronal Death. Neuron 84, 1213–1225.

Westergard, T., McAvoy, K., Russell, K., Wen, X., Pang, Y., Morris, B., Pasinelli, P., Trotti, D., and Haeusler, A. (2019). Repeat-associated non-AUG translation in C9orf72-ALS/FTD is driven by neuronal excitation and stress. EMBO Mol. Med. e9423.

Wolfe, A.L., Singh, K., Zhong, Y., Drewe, P., Rajasekhar, V.K., Sanghvi, V.R., Mavrakis, K.J., Jiang, M., Roderick, J.E., Meulen, J.V. der, et al. (2014). RNA G-quadruplexes cause eIF4A-dependent oncogene translation in cancer. Nature *513*, 65.

Wu, Y., and Brosh, R.M. (2010). G-quadruplex nucleic acids and human disease. FEBS J. *277*, 3470–3488.

Xi, Z., Zinman, L., Moreno, D., Schymick, J., Liang, Y., Sato, C., Zheng, Y., Ghani, M., Dib, S., Keith, J., et al. (2013). Hypermethylation of the CpG island near the G4C2 repeat in ALS with a C9orf72 expansion. Am. J. Hum. Genet. *92*, 981–989.

Xi, Z., Rainero, I., Rubino, E., Pinessi, L., Bruni, A., Maletta, R., Nacmias, B., Sorbi, S., Galimberti, D., Surace, E., et al. (2014). Hypermethylation of the CpG-island near the C9orf72 G4C2-repeat expansion in FTLD patients. *23*, 5630–5637.

Xi, Z., Zhang, M., Bruni, A.C., Maletta, R.G., Colao, R., Fratta, P., Polke, J.M., Sweeney, M.G., Mudanohwo, E., Nacmias, B., et al. (2015). The C9orf72 repeat expansion itself is methylated in ALS and FTLD patients. Acta Neuropathol. (Berl.) *129*, 715–727.

Xiao, S., MacNair, L., McGoldrick, P., McKeever, P.M., McLean, J.R., Zhang, M., Keith, J., Zinman, L., Rogaeva, E., and Robertson, J. (2015). Isoform-specific antibodies reveal distinct subcellular localizations of C9orf72 in amyotrophic lateral sclerosis. Ann. Neurol. *78*, 568–583.

Xiao, S., MacNair, L., McLean, J., McGoldrick, P., McKeever, P., Soleimani, S., Keith, J., Zinman, L., Rogaeva, E., and Robertson, J. (2016). C9orf72 isoforms in Amyotrophic Lateral Sclerosis and Frontotemporal Lobar Degeneration. Brain Res. *1647*, 43–49.

Xie, Y., Zheng, M., Chu, X., Chen, Y., Xu, H., Wang, J., Zhou, H., and Long, J. (2018). Paf1 and Ctr9 subcomplex formation is essential for Paf1 complex assembly and functional regulation. Nat. Commun. *9*.

Xu, W., and Xu, J. (2018). C9orf72 Dipeptide Repeats Cause Selective Neurodegeneration and Cell-Autonomous Excitotoxicity in Drosophila Glutamatergic Neurons. J. Neurosci. *38*, 7741–7752.

Xu, Y., Bernecky, C., Lee, C.-T., Maier, K.C., Schwalb, B., Tegunov, D., Plitzko, J.M., Urlaub, H., and Cramer, P. (2017). Architecture of the RNA polymerase II-Paf1C-TFIIS transcription elongation complex. Nat. Commun. *8*, 15741.

Yamaguchi, Y., Shibata, H., and Handa, H. (2013). Transcription elongation factors DSIF and NELF: Promoter-proximal pausing and beyond. Biochim. Biophys. Acta BBA - Gene Regul. Mech. *1829*, 98–104.

Yeh, T.-H., Liu, H.-F., Li, Y.-W., Lu, C.-S., Shih, H.-Y., Chiu, C.-C., Lin, S.-J., Huang, Y.-C., and Cheng, Y.-C. (2018). C9orf72 is essential for neurodevelopment and motility mediated by Cyclin G1. Exp. Neurol. *304*, 114–124.

Yin, S., Lopez-Gonzalez, R., Kunz, R.C., Gangopadhyay, J., Borufka, C., Gygi, S.P., Gao, F.-B., and Reed, R. (2017). Evidence that C9ORF72 dipeptide repeat proteins associate with U2 snRNP to cause mis-splicing in ALS/FTD patients. Cell Rep. *19*, 2244–2256.

Yu, Z., Goodman, L.D., Shieh, S.-Y., Min, M., Teng, X., Zhu, Y., and Bonini, N.M. (2015). A fly model for the CCUG-repeat expansion of myotonic dystrophy type 2 reveals a novel interaction with MBNL1. Hum. Mol. Genet. *24*, 954–962.

Yuva-Aydemir, Y., Almeida, S., and Gao, F.-B. (2018). Insights into C9ORF72-Related ALS/FTD from Drosophila and iPSC Models. Trends Neurosci.

Zamft, B., Bintu, L., Ishibashi, T., and Bustamante, C. (2012). Nascent RNA structure modulates the transcriptional dynamics of RNA polymerases. Proc. Natl. Acad. Sci. U. S. A. *109*, 8948–8953.

Zamiri, B., Mirceta, M., Bomsztyk, K., Macgregor, R.B., and Pearson, C.E. (2015). Quadruplex formation by both G-rich and C-rich DNA strands of the C9orf72 (GGGGCC)8•(GGCCCC)8 repeat: effect of CpG methylation. Nucleic Acids Res. *43*, 10055–10064.

Zamiri, B., Mirceta, M., Abu-Ghazalah, R., Wold, M.S., Pearson, C.E., and Macgregor, R.B. (2018). Stress-induced acidification may contribute to formation of unusual structures in C9orf72 -repeats. Biochim. Biophys. Acta BBA - Gen. Subj. *1862*, 1482–1491.

Zhang, C., Liu, H., Zheng, K., Hao, Y., and Tan, Z. (2013). DNA G-quadruplex formation in response to remote downstream transcription activity: long-range sensing and signal transducing in DNA double helix. Nucleic Acids Res. *41*, 7144–7152.

Zhang, D., Iyer, L.M., He, F., and Aravind, L. (2012). Discovery of Novel DENN Proteins: Implications for the Evolution of Eukaryotic Intracellular Membrane Structures and Human Disease. Front. Genet. *3*.

Zhang, K., Donnelly, C.J., Haeusler, A.R., Grima, J.C., Machamer, J.B., Steinwald, P., Daley, E.L., Miller, S.J., Cunningham, K.M., Vidensky, S., et al. (2015). The C9ORF72 repeat expansion disrupts nucleocytoplasmic transport. Nature *525*, 56–61.

Zhang, K., Grima, J.C., Rothstein, J.D., and Lloyd, T.E. (2016a). Nucleocytoplasmic transport in C9orf72-mediated ALS/FTD. Nucleus *7*, 132–137.

Zhang, X., Chiang, H.-C., Wang, Y., Zhang, C., Smith, S., Zhao, X., Nair, S.J., Michalek, J., Jatoi, I., Lautner, M., et al. (2017a). Attenuation of RNA polymerase II pausing mitigates BRCA1-associated R-loop accumulation and tumorigenesis. Nat. Commun. *8*.

Zhang, Y., Roland, C., and Sagui, C. (2017b). Structure and Dynamics of DNA and RNA Double Helices Obtained from the GGGGCC and CCCCGG Hexanucleotide Repeats That Are the Hallmark of C9FTD/ALS Diseases. ACS Chem. Neurosci. *8*, 578–591.

Zhang, Y.-J., Jansen-West, K., Xu, Y.-F., Gendron, T.F., Bieniek, K.F., Lin, W.-L., Sasaguri, H., Caulfield, T., Hubbard, J., Daughrity, L., et al. (2014). Aggregation-prone c9FTD/ALS poly(GA) RAN-translated proteins cause neurotoxicity by inducing ER stress. Acta Neuropathol. (Berl.) *128*, 505.

Zhang, Y.-J., Gendron, T.F., Grima, J.C., Sasaguri, H., Jansen-West, K., Xu, Y.-F., Katzman, R.B., Gass, J., Murray, M.E., Shinohara, M., et al. (2016b). C9ORF72 poly(GA) aggregates sequester and impair HR23 and nucleocytoplasmic transport proteins. Nat. Neurosci. *19*, 668–677.

Zhang, Y.-J., Gendron, T.F., Ebbert, M.T.W., O'Raw, A.D., Yue, M., Jansen-West, K., Zhang, X., Prudencio, M., Chew, J., Cook, C.N., et al. (2018). Poly(GR) impairs protein translation and stress granule dynamics in C9orf72-associated frontotemporal dementia and amyotrophic lateral sclerosis. Nat. Med. *24*, 1136–1142.

Zhao, M., Kim, J.R., van Bruggen, R., and Park, J. (2018). RNA-Binding Proteins in Amyotrophic Lateral Sclerosis. Mol. Cells *41*, 818–829.

Zheng, K., Xiao, S., Liu, J., Zhang, J., Hao, Y., and Tan, Z. (2013). Co-transcriptional formation of DNA:RNA hybrid G-quadruplex and potential function as constitutional cis element for transcription control. Nucleic Acids Res. *41*, 5533–5541.

Zhi, X., Giroux-Leprieur, E., Wislez, M., Hu, M., Zhang, Y., Shi, H., Du, K., and Wang, L. (2015). Human RNA polymerase II associated factor 1 complex promotes tumorigenesis by activating c-MYC transcription in non-small cell lung cancer. Biochem. Biophys. Res. Commun. *465*, 685–690.

Zhou, B., Liu, C., Geng, Y., and Zhu, G. (2015). Topology of a G-quadruplex DNA formed by C9orf72 hexanucleotide repeats associated with ALS and FTD. Sci. Rep. *5*.

Zhu, B., Mandal, S.S., Pham, A.-D., Zheng, Y., Erdjument-Bromage, H., Batra, S.K., Tempst, P., and Reinberg, D. (2005). The human PAF complex coordinates transcription with events downstream of RNA synthesis. Genes Dev. *19*, 1668–1673.

Zu, T., Gibbens, B., Doty, N.S., Gomes-Pereira, M., Huguet, A., Stone, M.D., Margolis, J., Peterson, M., Markowski, T.W., Ingram, M.A.C., et al. (2011). Non-ATG-initiated translation directed by microsatellite expansions. Proc. Natl. Acad. Sci. U. S. A. *108*, 260–265.

Zu, T., Liu, Y., Bañez-Coronel, M., Reid, T., Pletnikova, O., Lewis, J., Miller, T.M., Harms, M.B., Falchook, A.E., Subramony, S.H., et al. (2013). RAN proteins and RNA foci from antisense transcripts in C9ORF72 ALS and frontotemporal dementia. Proc. Natl. Acad. Sci. U. S. A. *110*, E4968–E4977.

Zu, T., Pattamatta, A., and Ranum, L.P.W. (2018). Repeat-Associated Non-ATG Translation in Neurological Diseases. Cold Spring Harb. Perspect. Biol. *10* (12).

CHAPTER 2: TOXIC EXPANDED GGGGCC REPEAT TRANSCRIPTION IS MEDIATED BY THE PAF1 COMPLEX IN *C9ORF72*-ASSOCIATED FTD.

Nature Neuroscience, accepted March 26, 2019

Lindsey D. Goodman[1], Mercedes Prudencio[3], Nicholas J. Kramer[4], Luis F. Martinez-Ramirez[2], Ananth R. Srinivasan[2], Matthews Lan[2], Michael J. Parisi[2], Yongqing Zhu[2], Jeannie Chew[3], Casey N. Cook[3], Amit Berson[2], Aaron D. Gitler[5], Leonard Petrucelli[3], Nancy M. Bonini[1,2,*].

[1]Neuroscience Graduate Group, Perelman School of Medicine, University of Pennsylvania, Philadelphia, PA 19104, USA

[2]Department of Biology, University of Pennsylvania, Philadelphia, PA 19104, USA

[3]Department of Neuroscience, Mayo Clinic, Jacksonville, FL 32224, USA

[4]Neuroscience Graduate Program, Stanford University School of Medicine, Stanford, CA 94305, USA

[5]Department of Genetics, Stanford University School of Medicine, Stanford, CA 94305, USA

*corresponding author, email: nbonini@sas.upenn.edu

Author contributions

This work was done by LDG under the mentorship of NMB. MP contributed post-mortem patient studies and analyses under the mentorship of LP. NJK contributed yeast studies under the mentorship of ADG. NJK and ADG also provided iPS cell lysates for western immunoblots performed by LDG. LFR-M provided technical support during dPAF1C-focused studies, including qPCRs and lifespans, under the direction of LDG. AS performed ChIP experiments under the guidance of LDG. ML added technical support during fly screening and performed initial control GAL4/UAS-LacZ westerns post-screening under the direction of LDG. MJP performed technical support for fly-based studies including paraffin sectioning for vacuoles and internal eyes under the direction of LDG. YZ made G4C2 fly constructs under the direction of NMB. AB performed paraffin sectioning for fly internal eyes under the direction of LDG. JC made mouse models for G4C2 under the mentorship of LP. CNC added technical support for mammalian westerns under the mentorship of LP.

Competing interests

The authors declare that they have no conflicts of interest with the contents of this article.

Acknowledgments

We thank Andrew T. Moehlman and Helmut Krämer at UT Southwestern for ERG investigations and Tania Gendron for GP-studies in (G4C2)n animals post-screening. John T. Lis, Peter Gallant, and Michael Buszczak generously shared valuable *Drosophila* reagents targeting dPAF1C. Further thanks to Edward B. Lee, Thomas A. Jongens, Zhaolan (Joe) Zhou and members of the Bonini laboratory – notably, Jason Kennerdell, Leeanne McGurk, and Janani Saikumar – for helpful comments. Undergraduates Decklan P. Cerza and Alex Chen provided minimal technical support under the direction of L.D.G. We thank the Transgenic RNAi Project (TRiP) at Harvard Medical School (NIH/NIGMS R01-GM084947) and the Vienna *Drosophila* Research Center for developing transgenic RNAi fly stocks used in this study. We thank the NINDS Human Cell and Data Repository at Rutgers University for fibroblast cells. This work was funded by the Systems and Integrative Biology NIH/NIGMS training grant T32-GM07517 (to L.D.G.), NIH/NINDS R35-NS097263 (to A.D.G.), NIH/NINDS R35-NS097273 (to L.P.), NIH/NINDS P01-NS084974 (to L.P.), NIH/NINDS P01-NS099114 (to L.P.), Mayo Clinic Foundation (to L.P.), ALS Association (to L.P. and M.P.), Robert Packard Center for ALS Research at Johns Hopkins (to L.P.), Target ALS Foundation (to L.P.), NIH/NINDS R01-NS078283 (to N.M.B.), and NIH/NINDS R35-NS09727 (to N.M.B.).

Abstract

An expanded (G4C2)30+ repeat within *C9orf72* is the most prominent mutation in familial FTD and ALS. Through an unbiased, large-scale screen in (G4C2)49-expressing *Drosophila* we identified the CDC73/PAF1 complex (PAF1C), a transcriptional regulator of RNAPII, as a suppressor of G4C2-associated toxicity when depleted. Mechanistically, PAF1C knockdown reduces RNA and GR-dipeptide production from (G4C2)30+ transgenes. Interestingly, dPAF1C components, *dPaf1* and *dLeo1* appear selective for transcription of long, toxic repeat expansions, but not shorter, non-toxic expansions. In yeast, scPAF1C components regulate expression of both sense and anti-sense repeats. PAF1C is upregulated upon expression of (G4C2)30+ in flies and mice. hPaf1 is also upregulated in *C9*+-derived cells and its heterodimer partner, hLeo1, binds *C9*+ repeat chromatin. In *C9*+ FTD, *hPAF1* and *hLEO1* are upregulated and their expression positively correlates with expression of repeat-containing *C9orf72* transcripts. These data indicate that PAF1C activity is an important factor for transcription of the long, toxic repeat in *C9*+ FTD.

Introduction

An intronic GGGGCC hexanucleotide (G4C2) expansion of >30 repeats found within *C9orf72* is the most prominent mutation in familial frontotemporal degeneration (FTD) and amyotrophic lateral sclerosis (ALS) (DeJesus-Hernandez et al., 2011; Renton et al., 2011). These devastating neurodegenerative disorders represent a continuum of the same disease (van Blitterswijk et al., 2014a, 2014b).

While the presence of the expanded G4C2 can confer toxicity through a number of aberrant pathways, amassing evidence supports contributions by gain-of-function mechanisms (Balendra and Isaacs, 2018; Vatovec et al., 2014; Yuva-Aydemir et al., 2018). Accumulation of sense-strand G4C2- and antisense-strand G2C4-containing RNA results in RNA foci throughout the nervous system and may be toxic (Vatsavayai et al., 2019). Further, these RNAs undergo repeat-associated non-AUG (RAN) translation to produce dipeptide-repeats (DPRs) – GA, GR, GP, PA, PR – which form potentially toxic aggregates (Vatsavayai et al., 2019). Expressing (G4C2)30+ repeats, independent of changes to expression of the *C9orf72* gene product, causes toxicity in multiple model systems (Balendra and Isaacs, 2018; Vatovec et al., 2014; Yuva-Aydemir et al., 2018). In *Drosophila*, expression of (G4C2)30+ transgenes results in RNA foci formation, DPR expression, and neurodegenerative effects (Balendra and Isaacs, 2018; Yuva-Aydemir et al., 2018).

Repeat-expansions, like (G4C2)n, have been defined in a number of neurodegenerative diseases. As these repeats tend to be GC-rich, they can form secondary structures (e.g. G-quadraplexes) and R-loops which are thought to diminish RNA polymerase II (RNAPII)-driven transcription (Vatovec et al., 2014; Rhodes and Lipps, 2015; Simone et al., 2015; Hall et al., 2017; Freudenreich, 2018; Sauer and Paeschke, 2017). Specialized transcriptional machinery may be required to promote the

activity of RNAPII through such long repeat expansions (Hall et al., 2017; Sauer and Paeschke, 2017). Of note, DRB-sensitivity-inducing factor complex (DSIF) and the CDC73/PAF1 complex (PAF1C; PAF1 complex) are RNAPII regulators that may be involved since transcription of GC-rich DNA is sensitive to their loss (Rondón et al., 2003, 2004; Zhou et al., 2012).

DSIF and PAF1C are highly conserved and have non-redundant roles in activating RNAPII during elongation (Chen et al., 2009; Hartzog and Fu, 2013; Jaehning, 2010; Van Oss et al., 2017). DSIF is composed of two proteins, Spt4 and Spt5 (SPT4H/5H in humans) (Hartzog and Fu, 2013). SPT4H is implicated as a transcriptional regulator of expanded CAG and G4C2 repeats in disease (Liu et al., 2012; Cheng et al., 2015; Kramer et al., 2016). PAF1C is composed of five proteins – Paf1, Leo1, CDC73, Ctr9, and Rtf1 – and it was unknown if hPAF1C had a role in repeat expansion diseases (Jaehning, 2010; Van Oss et al., 2017). PAF1C downregulation can impact elongation rates of RNAPII, although only a subset of genes are known to require its function for expression (Porter et al., 2002; Yang et al., 2016; Fischl et al., 2017). In the nervous system, PAF1C is critical during development although it remains expressed in mature neurons (Bahrampour and Thor, 2016; Chaturvedi et al., 2016; Moniaux et al., 2009; Nguyen et al., 2010; Tan et al., 2013; Wang et al., 2008).

Here, we identified PAF1C components as modifiers of *C9orf72*-associated disease in an unbiased, large scale RNAi-based screen in *Drosophila* expressing toxic (G4C2)49. Downregulation of PAF1C components disrupted transcription of the G4C2 RNA in both *Drosophila* and *S. cerevisiae* and resulted in reduced toxicity in *Drosophila*. Importantly, components *dPaf1* and *dLeo1* were selective for transcription of long repeat transgenes, unlike the other dPAF1C subunits and *dSpt4*. Furthermore, PAF1C is upregulated in response to expression of the expanded repeat in flies, mouse models,

C9+ patient-derived cells and *C9+* FTD tissue. Notably, expression of *hPAF1* and *hLEO1* positively correlate with expression of repeat-containing *C9orf72*-transcripts in patient tissue and hLeo1 is bound to *C9orf72* chromatin in *C9+* cells. These data highlight hPAF1C as an important transcriptional regulator of expanded G4C2 within *C9orf72*.

Results

RNAPII transcriptional complexes are enriched among suppressors of (G4C2)49-toxicity. To define cellular mechanisms underlying (G4C2)30+ toxicity *in vivo*, a fly model was developed that expresses (G4C2)n repeats, utilizing the GAL4/UAS expression system **(Fig. 2-1a)**. Quantification of the number of repeats inserted into individual transgenic lines highlighted four lines: control (G4C2)8, intermediate (G4C2)29, and two expanded (G4C2)49 lines with different insertion sites **(Fig. 2-1b)**. These lines were analyzed for RNA level by northern blot to confirm similar expression **(Fig. 2-1c)**. Expression of (G4C2)8, (G4C2)29, or (G4C2)49 transgenes in the fly optic system (Gmr-GAL4) revealed that (G4C2)49 expression caused degenerative effects: disruptions to the external ommatidial organization, red pigmentation, eye size, and internal retinal tissue loss **(Fig. 2-1d)**. (G4C2)29 expression caused mild toxicity in 80% of animals: disruptions to the ommatidial organization and gaps within the internal retinal tissue.

An unbiased fly screen was developed that utilized the degenerative eye caused by (G4C2)49 expression with Gmr-GAL4 **(Fig. 2-1e; Appendix 2: Fig. S2-1a)**. Using transgenic UAS-RNAi fly lines (see methods) we defined individual genes whose downregulation altered this toxicity with enhancement or suppression. Overall, 3,932 genes were tested: ~25% of the fly genome **(Appendix 2: Sup. Data)**. 350 (8.9%) of these altered (G4C2)49-toxicity. Positive RNAi lines were then rigorously assessed to

exclude those with unspecific effects: RNAi lines that altered normal eye morphology in control animals or altered expression of a control UAS-LacZ transgene **(Appendix 2: Fig. S2-1b-c)** (Kramer et al., 2016). Overall, 119 modifiers of (G4C2)49-toxicity were identified: 55 suppressors and 64 enhancers **(Fig. 2-1f)**.

To define enriched processes, functions or components within these 119 modifiers, gene ontology (GO)-term analyses were performed (see methods). Enrichment scores (the degree to which a list of genes in a GO-term are represented within the modifier list) were plotted for GO-terms that were significantly represented within the panel of modifiers, p-value threshold of 10^-3 **(Appendix 2: Fig. S2-1d)**. Among suppressors, there was strong enrichment for genes associated with RNAPII-driven transcription **(Fig. 2-1g, green)**, including components of the dCDC73/PAF1 complex (dPAF1C; PAF1 complex) and dMediator complex (Soutourina, 2017). Additional transcription regulators included *dELL* and *dEar* of the dSuper Elongation Complex (dSEC) (Zhou et al., 2012) and *dSpt4* of the dDSIF complex. By contrast, enhancers of (G4C2)49-toxicity varied in GO-terms. Genes involved in RNA processing and splicing were identified, with components of the pre-catalytic spliceosome being the most enriched complex **(Fig. 2-1h, red)**.

Overall, dPAF1C was the most enriched complex of transcriptional regulators that suppress (G4C2)49-toxicity.

PAF1C is selective for toxicity from a G4C2-encoding RNA.

Expanded G4C2 RNA can produce dipeptide-repeat proteins GR, GA, and GP in the fly (Balendra and Isaacs, 2018; Vatovec et al., 2014; Vatsavayai et al., 2019; Yuva-Aydemir et al., 2018). Of these, (GR)30+ is strongly toxic (Mizielinska et al., 2014). As modifiers of (G4C2)49-toxicity may be acting downstream of GR-peptide production, we analyzed

the 119 RNAi lines for their ability to modulate (GR)36-toxicity **(Fig. 2-2a)**. GR models express a GR-peptide from a non-G4C2 RNA transcript, thus avoiding potential toxicity caused by a G4C2 repeat-bearing RNA (Mizielinska et al., 2014). As the PAF1 and DSIF complexes may be of particular interest in repeat-associated disease, dPAF1C and *dSpt4* RNAi were rigorously examined for modification of (GR)n-toxicity in flies and yeast **(Appendix 2: Fig. S2-2a-c**; for *scSpt4 (Kramer et al., 2016)*). Results showed no consistent or significant effects indicating that these modifiers have a minimal effect on (GR)n-associated toxicity.

In *Drosophila*, 48 of the 119 modifiers (40.3%) did not alter (GR)36-toxicity in the same manner that they altered G4C2-repeat toxicity, suggesting that they modulate expression of the RNA or RNA-derived toxicity **(Fig. 2-2b)**. GO-term analysis of these modifiers revealed that suppression by dPAF1C components was selective to the (G4C2)49 model **(Fig. 2-2c)**. In contrast, the dMediator complex and *dELL* and *dEar* of dSEC similarly suppressed both (G4C2)49- and (GR)36-toxicity in the external eye.

Overall, data suggested that dPAF1C suppression of (G4C2)49-toxicity was the result of effects upstream of toxic GR-peptide production.

dPAF1C is selective for the G4C2 expansion.

Biological connections between (G4C2)30+ expression and TAR DNA binding protein 43 (TDP43) pathology have been reported in *C9*+ FTD/ALS (Balendra and Isaacs, 2018; Vatsavayai et al., 2019). Thus, we examined the (G4C2)49 modifiers in a TDP43 model to define G4C2-unique pathways **(Fig. 2-2a)**. Expression of human TDP43 in the fly eye causes toxicity (Chung et al., 2018). Rigorous assessment of dPAF1C and *dSpt4* RNAi showed that they had no significant effect on TDP43-toxicity **(Appendix 2: Fig. S2-3a-b)**. 56 of the 119 (G4C2)49 modifiers (47.1%) were unique to (G4C2)49 **(Fig. 2-2b;**

Appendix 2: Sup. Data). GO-term analysis indicated that dPAF1C was again highly enriched, underscoring specificity of this complex to the expanded G4C2 **(Fig. 2-2d)**. By contrast, other RNAPII-regulators, such as the dMediator complex and *dELL* and *dEar* of dSEC, similarly suppressed (G4C2)49- or TDP43-toxicity in the external eye (also (Chung et al., 2018)). Furthermore, dPAF1C RNAi did not alter TDP43 protein levels **(Appendix 2: Fig. S2-3c)**.

Taken together, these data highlight dPAF1C selectivity for (G4C2)49-associated toxicity.

dPAF1C downregulation suppresses (G4C2)49-induced toxicity in fly.

We further examined if dPAF1C downregulation could impact (G4C2)49-toxicity in multiple fly tissues. First, we confirmed that the RNAi lines targeting dPAF1C components – *dPaf1 (ATMS)*, *dLeo1 (ATU)*, *dCDC73 (HYX)*, *dCtr9* and *dRtf1* –resulted in significant downregulation of the target gene, while extending reagents to include an independent set of dPAF1C RNAi lines **(Appendix 2: Fig. S2-4)**.

Consistent with effects in the external eye, co-expression of dPAF1C RNAi with (G4C2)49 rescued internal tissue loss **(Fig. 2-3a-b)**. *dPaf1*, *dLeo1*, and *dRtf1* RNAi caused ~80% recovery and *dCDC73* and *dCtr9* RNAi caused ~100% recovery of tissue depth: control =13.4±6.2μm, *dPaf1* =44.4±4.7μm, *dLeo1* =47.2±10.8μm, *dCDC73* =63±6.1μm, *dCtr9* =69.1±18.0μm, *dRtf1* =41.8±12.7μm. This indicates that dPAF1C depletion is markedly effective in mitigating (G4C2)49-toxicity in the eye. Downregulating dPAF1C components did not affect the external or internal eye on their own **(Fig. 2-3c-d)**. The second set of dPAf1C RNAi lines also suppressed (G4C2)49-toxicity, while not affecting the normal fly eye, affirming that suppression is indeed the result of targeting dPAF1C **(Appendix 2: Fig. S2-5a-b)**. To confirm the effect on G4C2-induced toxicity, an

independent (G4C2)30+ disease fly model was examined for interactions with dPAF1C. This model contains 114bp of the intronic sequence found upstream of G4C2 repeat in patients (termed “leader sequence”; LDS). Again, dPAF1C RNAi suppressed toxicity caused by LDS-(G4C2)44$^{GR\text{-}GFP}$ expression within the fly optic system **(Appendix 2: Fig. S2-5c)**.

To examine effects of downregulating dPAF1C components in the nervous system, we expressed the (G4C2)49 transgene using a conditional neuronal GAL4 driver, ElavGS. First, we assessed climbing ability of animals with adult-onset expression. At 14d, only 41% of (G4C2)49-expressing animals were able to climb 4cm up the wall of a vial within 20s **(Fig. 2-3e)**. dPAF1C RNAi significantly suppressed this effect, causing climbing abilities to be maintained at 92-96%. Suppression was again seen when using the second set of dPAF1C RNAi lines **(Appendix 2: Fig. S2-5d)**.

Next, we analyzed animals for age-dependent vacuole formation in the fly brain, an indicator of neurodegeneration. (G4C2)49 expression in the adult-fly nervous system caused large vacuoles throughout the brain at 28d. *dCDC73*, *dCtr9*, and *dRtf1* RNAi significantly reduced both vacuole size and number: mean degeneration score (3.4±0.5) was reduced to 2.10±0.6 (*dCDC73* RNAi), 2.38±0.5 (*dCtr9* RNAi), and 1.78±0.8 (*dRtf1* RNAi), with the normal brain being 1.1±0.4 **(Fig. 2-3f; Appendix 2: Fig. S2-6)**. Further, the strong suppressor *dCDC73* increased adult survival of (G4C2)49-expressing animals, with 50% survival extended by 24h and end point extended 72h **(Fig. 2-3g)**. RNAi targeting other dPAF1C components showed reduced lifespan in control flies, making it inaccurate to evaluate their activity as suppressors of (G4C2)49 lifespan **(Appendix 2: Fig. S2-7a)**. We further rigorously ruled out any possible genetic background effects of the RNAi lines within the context of (G4C2)49-expression **(Appendix 2: Fig. S2-8).**

Together, data support that dPAF1C plays an important role in (G4C2)49-induced toxicity in disease-relevant tissues in the fly.

PAF1C mediates expression of expanded G4C2 in fly and yeast.

Given that PAF1C regulates RNAPII-elongation and is important for transcription of GC-rich DNA (Jaehning, 2010; Rondón et al., 2004; Van Oss et al., 2017), we hypothesized that PAF1C may be important for successful transcription of long G4C2 repeats.

We first determined whether downregulation of dPAF1C components – *dPaf1*, *dLeo1*, *dCDC73*, *dCtr9*, and *dRtf1* – affected the amount of RNA produced from expanded (G4C2)49 transgenes in the fly nervous system, using *dSpt4* RNAi as a positive control (Kramer et al., 2016) **(Fig. 2-4a, red)**. dPAF1C RNAi caused significant reductions in (G4C2)49 RNA: *dPaf1* =41±8% reduction, *dLeo1* =54±4% reduction, *dCDC73* =57±5% reduction, *dCtr9* =62±6% reduction, *dRtf1* =62±5% reduction. These values were similar to *dSpt4* RNAi which caused a 52±5% reduction (also (Kramer et al., 2016)). This effect was consistent in a second (G4C2)49-fly model **(Appendix 2: Fig. S2-9a)**.

We evaluated the specificity of dPAF1C alterations on expanded (G4C2)49-RNA, by assessing expression from a nontoxic (G4C2)8 and an intermediate (G4C2)29 repeat. Surprisingly, *dPaf1* and *dLeo1* were selective for expanded (G4C2)49 as these RNAi did not significantly reduce expression from the shorter, nontoxic repeat transgenes **(Fig. 2-4a, black and green)**. By contrast, *dSpt4*, *dCDC73*, *dCtr9*, and *dRtf1* RNAi caused significant reductions in expression from (G4C2)8 and (G4C2)29 of >30%, similar to effects on the (G4C2)49 transgene. Statistical comparisons between each (G4C2)n transcript levels with individual RNAi **(Fig. 2-4a, top)**, confirmed that *dPaf1* and *dLeo1* RNAi show no significant difference between the expression level of (G4C2)8 and

(G4C2)29 but caused a statistically significant drop between (G4C2)<30 and (G4C2)49 RNA levels. By contrast, *dSpt4* RNAi and other dPAF1C RNAi had statistically similar decreases in RNA levels among short and expanded G4C2 repeat lengths. These findings suggest that, of the dPAF1C components, *dPaf1* and *dLeo1* appear of special importance for expression of longer repeats in the fly. We further confirmed that the reduced expression was specific to the G4C2 construct by examining expression of an alternative disease transgene, TDP43. TDP43 transcript levels were not affected by dPAF1C RNAi in the fly brain, consistent with protein data **(Fig. 2-4b; Appendix 2: Fig. S2-3c)**.

As (G4C2)30+ RNA can produce a toxic GR-dipeptide, we next asked if reduced expression of dPAF1C could alter GR production in the LDS-(G4C2)44$^{GR\text{-}GFP}$ fly model **(Fig. 2-4c)**. The GFP tag in the GR reading frame allows for fluorescence imaging and quantitation of GR-levels in the eye with Gmr-GAL4. Congruent with RNA data, dPAF1C RNAi significantly downregulated GR-GFP: *dPaf1* =40±3% reduction, *dLeo1* =42±2% reduction, *dCDC73* =56±1% reduction, *dCtr9* =50±3% reduction, *dRtf1* =51±2% reduction.

These findings were then extended to yeast to assess if scPAF1C could regulate expression of expanded G4C2 in another model system. Transgenes were expressed from a galactose-inducible promoter. *scLeo1* (*leo1Δ*) *or scCDC73* (*cdc73Δ*) deletion had mild or no effect on expression from a control eYFP transgene **(Fig. 2-4d, black)**. Deletion of other scPAF1C components had growth defects and/or significantly repressed expression of control eYFP so could not be assessed (data not shown). Interestingly, RNA levels from an expanded (G4C2)66 transgene were significantly decreased by *leo1Δ* or *cdc73Δ*: 40±14% and 38±2.5% reduction, respectively **(Fig. 2-4d, red)**. Further, as the hexanucleotide repeat in *C9*+ FTD/ALS patients can be transcribed

bidirectionally (Vatsavayai et al., 2019), we determined if scPAF1C mutants could also regulate expression from an antisense-(G2C4)66 transgene. Notably, *leo1Δ* or *cdc73Δ* had an even stronger effect on expression from this transgene with *leo1Δ* showing a significantly stronger effect than *cdc73Δ*: 77±4% and 52±11% reduction, respectively **(Fig. 2-4d, orange)**. These data confirmed that PAF1C downregulation impaired expression of expanded G4C2 repeats in an independent model system, and extended data to expanded antisense-G2C4 repeat.

Effects of PAF1C RNAi could be the result of co-regulation of PAF1C components – *Paf1*, *Leo1*, *CDC73*, *Ctr9*, and *Rtf1* – with each other and/or *Spt4*. To examine this, we expressed *dPaf1*, *dLeo1*, or *dCDC73* RNAi in adult flies using the drug-inducible ubiquitous driver, DaGS. qPCR was used to determine changes in expression from dPAF1C components not targeted by the RNAi or *dSpt4* **(Appendix 2: Fig. S2-7b)**. Data indicated that depleting these dPAF1C components does not alter expression of *dSpt4* or alternative dPAF1C components. Further, we confirmed that downregulating PAF1C in flies and in yeast did not alter general RNAPII transcription of endogenous housekeeping genes **(Appendix 2: Fig. S2-9b-c)** (Jaehning, 2010; Van Oss et al., 2017; Porter et al., 2002; Yang et al., 2016; Fischl et al., 2017).

These data support that PAF1C mediates transcription of expanded G4C2 and G2C4. Further, data in the fly argues that *dPaf1* and *dLeo1* confer repeat-length specificity to the transcriptional machinery, promoting RNAPII-driven transcription of expanded (G4C2)30+ repeats.

PAF1C is upregulated in response to expanded G4C2.

Given the important role dPAF1C is playing in (G4C2)49-expressing animals, we considered that the complex may be dysregulated in *C9+* situations. Thus, we examined

the expression of endogenous dPAF1C components – *dPaf1*, *dLeo1*, *dCDC73*, *dCtr9*, and *dRtf1* – in animals expressing (G4C2)49 in the adult fly nervous system (ElavGS, 16d). Surprisingly, all components were upregulated by qPCR **(Fig. 2-5a)**: *dPaf1* =69±10% upregulation, *dLeo1* =58±13% upregulation, *dCDC73* =71±17%upregulation, *dCtr9* =49±12% upregulation, and *dRtf1* =64±5% upregulation. This effect did not occur in response to short (G4C2)8 repeat expression. Further, dPAF1C upregulation appeared selective to G4C2 as dPAF1C components were not upregulated in TDP43 expressing animals, but rather downregulated **(Fig. 2-5b)**.

To determine if this same response to expression of the expanded G4C2 repeat occurred in mammals, protein levels of mLeo1 were measured in cortical tissue from (G4C2)2 or (G4C2)149 expressing mice **(Fig. 2-5c)**. Transgenes were expressed using an AAV2/9 vector which predominantly transduces into neurons (see methods). At 3mo post-injection, no significant differences in mLeo1 were detected between cohorts. However, at 6mo a significant upregulation of 30±8% in mLeo1 was observed in (G4C2)149 animals compared to (G4C2)2 animals.

hPaf1 is upregulated in C9+ patient-derived cells.

Our data from flies and mice indicated that PAF1C is upregulated in response to expression of an expanded G4C2 repeat in the brain. To better understand this effect in *C9+* disease, we extended our studies to patient-derived cells. Protein expression levels of four of the hPAF1C components – hPaf1, hLeo1, hCDC73, and hRtf1 – were assessed by western immunoblot in iPS cells **(Fig. 2-6a)**. The mean expression from three *C9+* patient-derived cell lines was compared to three control cell lines. Notably, hPaf1 and hRtf1 were significantly upregulated by 46±14% and 54±14%, respectively, in *C9+* derived iPS cells.

hLeo1 binds C9orf72 within the genome.

Thus far, data supported that the levels of select PAF1C components are modulated in response to expression of the repeat in flies, mice, and *C9+* patient-derived cells. Further, PAF1C is important for expression of expanded G4C2 in flies and yeast. Therefore, we considered that hPAF1C may be recruited and bound to *C9orf72* within the genome of patient-derived cells.

To assess this, chromatin immunoprecipitation (ChIP) studies were performed. Four, independent *C9+*-derived fibroblast lines **(Appendix 2: Fig. S2-10a)** were assayed, using a hLeo1 antibody **(Fig. 2-6b)**. Importantly, Leo1 forms a heterodimer with Paf1 within PAF1C when bound to RNAPII (Chu et al., 2013; Xu et al., 2017). After pull-down, the presence of the *C9orf72* gene or an *intergenic* (noncoding) sequence was assessed by qPCR and the mean enrichment was calculated from the four lines. Primers used to detect chromatin fragments from the *C9orf72* gene targeted the intronic region immediately 3' of the repeat expansion. Notably, there was a 4.9±1.8-fold enrichment of *C9orf72*-sequence over the *intergenic*-sequence and IgG controls with hLeo1 ChIP, indicating that hLeo1 was bound to the *C9orf72* gene in patient-derived *C9+* cells. Overall, data support that hLeo1 binds the *C9orf72* gene and that it is bound through the repeat.

hPAF1 and hLEO1 are upregulated in C9+ FTD and FTD/ALS.

Our data from multiple model systems indicated that PAF1C is important for expression of the expanded G4C2 and that PAF1C is upregulated in response to expression of the repeat. To better understand the role of hPAF1C in human disease, we extended our studies to FTD/ALS patient tissue.

RNA was extracted from frontal cortex tissue of *C9+* patients (n=67), *C9-* patients (n=56), or healthy controls (n=27) and the level of *hPAF1* and *hLEO1* expression were assessed by qPCR **(Fig. 2-6c; Appendix 2: Fig. S2-10b)**. In patients diagnosed with FTD (cortical disease), *hPAF1* and *hLEO1* were significantly upregulated only when the repeat expansion was present: *hPAF1* was upregulated 39% versus healthy controls and 28% versus *C9-* FTD; *hLEO1* was upregulated 23% versus healthy controls and 25% versus *C9-* FTD. Interestingly, in the frontal cortex of *C9+* ALS cases (motor neuron disease), neither *hPAF1* nor *hLEO1* showed upregulation, independent of the presence of the G4C2-repeat expansion. Patients showing symptoms of both FTD and ALS fell between FTD only and ALS only, with *C9+* FTD/ALS cases showing weaker upregulation of *hPAF1* and *hLEO1* versus healthy controls: 28% and 22%, respectively. In contrast to *hPAF1* and *hLEO1*, *hCDC73* did not show altered expression in *C9+* FTD **(Appendix 2: Fig. S2-10c)**, supporting data in *Drosophila* and patient-derived cells that Paf1 and Leo1 may play a unique role over other components.

Upregulation of *hPAF1* and *hLEO1* in *C9+* FTD is congruent with data in flies, mice, and iPS cells. Interestingly, in cortical tissue this upregulation is unique to *C9+* FTD patients compared to *C9+* ALS patients (which lack cortical diagnosis).

Expression of hPAF1 and hLEO1 positively correlate with repeat-containing C9orf72 transcripts.

As *Paf1* and *Leo1* activity were important for the expression of the expanded G4C2 repeat in flies and yeast, and hLeo1 is bound to *C9orf72* in *C9+* cells, we considered that *hPAF1* and *hLEO1* upregulation in *C9+* FTD may positively correlate with the expression of *C9orf72* transcripts containing the repeat.

To examine this, Spearman r correlations were performed between transcript levels of *hPAF1* and *hLEO1* versus *C9orf72* pre-mRNA **(Fig. 2-6d)**. Results showed strong (r>0.3 to r>0.6) and significant (p-value <0.0005) positive correlations between transcripts in *C9*+ FTD cases – for *hPAF1* vs *C9orf72*: r=0.74, 95% CI 0.5 to 0.9; for *hLEO1* vs *C9orf72*: r=0.63, 95% CI 0.3 to 0.8. No correlations were observed in *C9*- FTD cases or healthy controls supporting that this effect was in response to the presence of the repeat expansion. Further, no correlations between *hCDC73* transcripts and *C9orf72* pre-mRNA were observed, arguing that this effect was unique to *hPAF1* and *hLEO1* **(Appendix 2: Fig. S2-10d)**. No correlations were observed in *C9*+ ALS cases **(Appendix 2: Fig. S2-10e)**.

Altogether, data from multiple models and FTD cortical tissue indicate that PAF1C regulates expression of the expanded G4C2 repeats within *C9orf72* in *C9*+ situations.

Discussion

An unbiased, RNAi-based screen in *Drosophila* covering ~4000 genes revealed the CDC73/PAF1 complex (PAF1C) as a *C9orf72*-disease modifier. Downregulation of dPAF1C components – *dPaf1*, *dLeo1*, *dCDC73*, *dCtr9*, and *dRtf1* – selectively suppressed (G4C2)49-toxicity in multiple fly tissues. Mechanistically, PAF1C suppression was associated with reduced RNA and GR-dipeptide production from expanded (G4C2)n transgenes. In particular, depletion of *dPaf1* and *dLeo1*, which form a heterodimer (Chu et al., 2013; Xu et al., 2017), in the fly nervous system selectively reduced expression of long, toxic (G4C2)49 repeats versus shorter, non-toxic repeats. Moreover, *scLeo1* and *scCDC73* deletion in yeast reduced RNA production from sense-(G4C2)66 and antisense-(G2C4)66 transgenes. Additional investigations into dPAF1C in

Drosophila revealed that endogenous dPAF1C was upregulated upon expression of expanded (G4C2)30+ in neurons. This was not the result of toxicity or stress, as upregulation was selective to (G4C2)30+ versus TDP43. Interestingly, mLeo1 is also upregulated in the brain of mice expressing (G4C2)149, while hPaf1 and hRtf1 are upregulated in *C9+*-derived iPS cells. Further, we provide evidence that hPAF1C binds *C9orf72*, with ChIP for hLeo1 (of the Paf1/Leo1 heterodimer) in *C9+* cells. Using human post-mortem cortical tissue, we further found that *hPAF1* and *hLEO1* RNA levels were upregulated in *C9+* FTD patients. This upregulation positively correlated with expression of the repeat-containing *C9orf72* transcripts. Overall, these data from flies, yeast, mice, *C9+* patient-derived cells, and post-mortem patient tissue support a mechanistic link between PAF1C activity, expression of a G4C2-repeat, and *C9+* disease.

A total of 119 modifiers of (G4C2)49-toxicity were identified in our screen (**see Fig 2-1**). Remarkably, GO term analysis of the 55 suppressors showed significant enrichment for RNAPII transcriptional regulators – including dPAF1C, the dMediator complex, *dELL* and *dEar* of the dSuper Elongation Complex (dSEC), and *dSpt4* of the dDSIF complex. Not all transcription-related genes tested in the screen modify (G4C2)49 toxicity, arguing that the complexes identified are unique (see **Appendix 2: Sup. Data**). Although we focused on dPAF1C, the other RNAPII regulators may also be important in disease (Balendra and Isaacs, 2018; Vatovec et al., 2014; Vatsavayai et al., 2019; Yuva-Aydemir et al., 2018). Among the 64 enhancers of (G4C2)49-toxicity, RNA processing and splicing factors were prominent. Curiously, the majority of these enhancers similarly modulate (GR)36-toxicity (**see Fig. 2-2**). These data are consistent with reports of RNA dysregulation and splicing deficits in *C9+* FTD/ALS, while suggesting that disruptions in RNA metabolism may result from toxic GR (Balendra and Isaacs, 2018; Vatovec et al., 2014; Vatsavayai et al., 2019; Yuva-Aydemir et al., 2018).

RNAPII-driven transcription across GC-rich DNA is hypothesized to be problematic due to the propensity of the DNA/RNA to form secondary structures, such as R-loops and G-quadraplexes (Vatovec et al., 2014; Rhodes and Lipps, 2015; Simone et al., 2015; Hall et al., 2017; Freudenreich, 2018; Sauer and Paeschke, 2017). Given this, the activity of multiple elongation factors may be required for efficient transcription through expansions like (G4C2)30+ (Hall et al., 2017; Sauer and Paeschke, 2017). *Spt4* was previously implicated as a transcriptional regulator of CAG and G4C2 repeat expansions (Liu et al., 2012; Cheng et al., 2015; Kramer et al., 2016). Our data indicates that PAF1C regulates expression of G4C2 repeats in FTD/ALS (**see Fig. 2-4**). *dPaf1* and *dLeo1* of dPAF1C seem particularly important for RNAPII-transcription of expanded G4C2 as loss of these two components selectively reduced expression of a (G4C2)49 transgene in fly. While this could be the result of level of knockdown, it is compelling that Paf1 and Leo1 form a heterodimer that is important for PAF1C activation of elongating RNAPII (Yang et al., 2016; Chu et al., 2013; Xu et al., 2017; Kim et al., 2010; Yu et al., 2015a). Further, Paf1 is consistently upregulated in *C9+*-derived patient cells and tissue over other components and upregulation positively correlates to expression of repeat-containing transcripts in patient tissue (**see Fig. 2-6c-d and Appendix 2: Fig. S2-10**). Overall, these data argue that Paf1 and Leo1 are mechanistically special in *C9+* disease.

In contrast to *dPaf1/Leo1*, *dSpt4* showed similar effects on different G4C2 repeat lengths in flies (**see Fig. 2-4**). Differences in how Spt4 and Paf1/Leo1 loss impact expanded G4C2 expression may be due to their distinct roles during transcription (Chen et al., 2009; Hartzog and Fu, 2013; Jaehning, 2010; Van Oss et al., 2017). Evidence suggests that Spt4 primarily acts during the transition of RNAPII from poised to elongation or during transcription termination (Chen et al., 2009; Fischl et al., 2017;

Yang et al., 2016). In contrast, Paf1/Leo1 seems to act primarily during elongation (Chen et al., 2009; Fischl et al., 2017; Kim et al., 2010; Mayer et al., 2010; Yang et al., 2016). Notably, DSIF (composed of Spt4 and Spt5) and PAF1C may interact. In yeast, scDSIF recruits scPAF1C via the scRtf1 subunit during the transition of RNAPII from initiation to elongation (Mayekar et al., 2013). However, in higher organisms, including *Drosophila*, the dependence of PAF1C on DSIF for recruitment to elongating RNAPII is less clear. Rtf1 is less tightly associated with other PAF1C components while recent work shows that PAF1C recruitment can be DSIF-independent in mammals (Amrich et al., 2012; Cao et al., 2015; Dermody and Buratowski, 2010; Qiu et al., 2012; Xie et al., 2018). Further, Leo1 of PAF1C directly interacts with elongating RNAPII (Xu et al., 2017) and the *C9orf72* gene (**see Fig. 2-6b**). Together, these data suggest that PAF1C is playing a unique role in transcription elongation across the G4C2-repeat expansion.

FTD and ALS represent the extremes of a continuous disease spectrum. It remains unclear how one patient presents with FTD and another with ALS or combined FTD/ALS. Among many factors, unique genetic backgrounds of individuals may contribute to specific presentation (van Blitterswijk et al., 2014a, 2014b). For example, *ATXN2* and *TMEM106B* have been suggested as disease modifiers underlying the different diagnoses (van Blitterswijk et al., 2014a, 2014b). Curiously, we see selective upregulation of *hPAF1* and *hLEO1* in the frontal cortex of *C9+* FTD disease, but not *C9+* ALS (**see Fig. 2-6c**). Importantly, the frontal cortex is thought to be a primary brain region resulting in FTD-associated symptoms (Omer et al., 2017; Schönecker et al., 2018). Stage of disease progression could also contribute. Analysis of *hPAF1* and *hLEO1* expression in motor neurons from ALS patients will define if PAF1C plays a tissue-specific role. Based on current data, it is tempting to hypothesize that cortical

modulation of *Paf1* or *Leo1* in response to the repeat may be among several mechanisms contributing to the spectrum of disease phenotypes in *C9orf72*-associated disorders.

PAF1C may be an attractive therapeutic candidate for *C9*+ FTD. In yeast, *scPAF1C* has been reported to be non-essential (Jaehning, 2010; Van Oss et al., 2017). In flies, *dLeo1* is not essential to get viable adults (Gerlach et al., 2017). In mice, $mPAF1^{+/-}$ or $mLEO1^{+/-}$ heterozygosity yields no obvious abnormalities, although $mPAF1^{-/-}$ or $mLEO1^{-/-}$ null animals show pre-weaning lethality (Meehan et al., 2017). Other components of mPAF1C follow this same trend, with heterozygous mice showing no or few effects (Meehan et al., 2017). While *SUPT4H1* (human *Spt4*; non-essential in yeast) was previously proposed as a potential therapeutic target in *C9*+ FTD/ALS (Kramer et al., 2016), it may have more critical organismal functions than PAF1C in higher organisms: $SUPT4A^{+/-}$ (murine *Spt4*) heterozygous mice are viable but show a number of abnormalities and $SUPT4A^{-/-}$ null mice are embryonic lethal (Meehan et al., 2017). These investigations do not consider effects of PAF1C or Spt4 loss in a tissue- or age-specific manner, arguing that further analyses are required. Altogether, we hypothesize that specific components of PAF1C, like *Paf1* or *Leo1*, may represent a potential therapeutic target for *C9orf72*-associated disease.

This study presents the first evidence that PAF1C is an important player in *C9orf72*-associated disease, particularly in *C9*+ FTD. Further investigations into PAF1C may define the mechanisms by which it becomes upregulated—potentially in a tissue-specific manner— and its impact in other neurodegenerative situations that result from aberrant expression of repeat expansions.

Data availability statement

The authors are submitting all relevant data for publication. Any additional inquiries can be directed to the corresponding author, while any information relevant to this study will be openly shared including all raw data, unique reagents, or unique protocols.

Methods and materials

Nomenclature

For clarity “d” for *Drosophila melanogaster*, “h” for *Homo sapiens*, “m” for *Mus musculus*, or “sc” for *Saccharomyces cerevisiae* was added in front of gene/protein symbols when discussing endogenous PAF1C components in individual species.

Patient sample consents and approvals

Participants or authorized family members provided written informed consent prior to information gathering. Post-consent, autopsies were performed postmortem. Protocols were approved by the Mayo Clinic Institutional Review Board and Ethics Committee.

Clinical, genetic and pathological assessments

Patients were diagnosed with FTD and/or ALS by trained neurologists after reviewing neurological and pathological information (**Appendix 2: Fig. S2-10**). Repeat-primed polymerase chain reaction was used to determine the presence/absence of a *C9orf72* repeat expansion (DeJesus-Hernandez et al., 2011).

Mouse model and approvals

All mouse procedures were performed in agreement with the National Institutes of Health Guide for Care and Use of Experimental Animals. Approved by the Mayo Clinic Institutional Animal Care and Use Committee. The G4C2 mouse model (C57BL/6J, male mice) were previously established (Chew et al., 2019).

Drosophila work and disease models

Stocks were maintained on standard cornmeal-molasses medium. See **Appendix 2: Table S2-2** for primary fly lines used. For all experiments, multiple w^- and w^+ controls were analyzed in parallel and showed similar results. **Appendix 2: Table S2-3** details shown controls.

Fly RNAi efficacy

All control and PAF1C RNAi lines defined in **Appendix 2: Table S2-2**. RNAi efficacy was determined using Da-GAL4 (larvae) or DaGS (adult animals), previously described (Kramer et al., 2016; McGurk and Bonini, 2012). For Paf1 RNAi: larvae were collected using 20% sucrose solution. For Leo1 RNAi: wandering 3rd instar larvae were collected.

Characterization of (G4C2)n fly models

All G4C2 fly models: Transgenes inserted into pUAST vectors and randomly inserted into w^{1118} fly genomes. Original G4C2 model detailed in Fig. 2-1a and previously established (Burguete et al.; Kramer et al., 2016; Mordes et al., 2018). LDS-G4C2 model includes: 5' leader sequence (LDS; 114bp of sequence found upstream of the repeat in intron 1 of *C9orf72* in patients); 3'-GFP tag in the GR-reading frame.

Repeat-length determination: Inserted transgenes were amplified from genomic DNA using construct-specific primers that flanked the repeat (**Appendix 2: Table S2-4**) by PCR: KAPA HiFi HotStart kit (Kappa #KK2501) with GC buffer, 1M Betaine, 5% DMSO. PCR products lengths were analyzed: 1.5% agarose/TAE gel, Bioanalyzer. Repeat number was calculated from PCR product length (subtracting 5' and 3' non-G4C2 flanking sequence). Control w^{1118} animals were included and showed no signal.

RNA expression for original UAS-G4C2 model: UAS-G4C2 transgenes were expressed using HS-GAL4, 30min at 37°C. RNA was extracted 3hr post-HS and analyzed by

northern blot, probing for the SV40 terminal sequence, previously described (Yu et al., 2015b). Control w^{1118} animals were included and showed no signal.

RNAi external fly eye screen

UAS-RNAi lines developed by the Transgenic RNAi Project (TRiP) (Ni et al., 2011; Perkins et al., 2015) were purchased through Bloomington *Drosophila* Stock Center (BDSC). All available Valium 20 UAS-shRNA lines targeting unique genes were used for screening (**Appendix 2: Sup. Data**). When multiple Valium 20 fly lines were available targeting a single gene, one line was randomly selected for screening. Additional UAS-RNAi lines targeting *dPaf1* and *dLeo1* were obtained from Vienna *Drosophila* Resource Center (VDRC) (Dietzl et al., 2007).

External eye screening and imaging: UAS-RNAi males were crossed to recombinant females: UAS-(G4C2)49, Gmr-GAL4 (III) (25°C). Multiple controls were setup with every experiment to account for natural variability in (G4C2)49-toxicity, including: UAS-Luc RNAi (BDSC #31603) and w^{1118}; UAS-DSRED. The external eye phenotype for >5 1-2d progeny was observed using a standard dissection microscope. Any changes to the ommatidial organization, eye size, pigmentation, and ability to eclose from pupae were noted. Resulting phenotype was categorized into one of six groups: suppressors, mild suppressors, no effect, mild enhancers, enhancers, and lethal enhancers (**Appendix 2: Fig. S2-1a**). Animals expressing RNAi that altered (G4C2)49-toxicity were imaged on a Leica Apo16 microscope (Berson et al., 2017; Chung et al., 2018; Elden et al., 2010; Kim et al., 2014). Researchers were blinded to the RNAi targets during screening. Modifiers of (G4C2)49-toxicity were further assessed in Gmr-GAL4 > UAS-(GR)36 (Mizielinska et al., 2014) or UAS-TDP43 (Elden et al., 2010; Kim et al., 2014) animals. Modifier crosses were repeated 3+ independent times to confirm reproducibility of results.

Control experiments defining unspecific RNAi: To determine if RNAi caused toxicity in control scenarios: UAS-RNAi lines that enhanced (G4C2)49-toxicity were tested for effects in a line expressing short repeats, Gmr-GAL4 > (G4C2)6/8, and with Gmr-GAL4 only. UAS-RNAi lines were analyzed for effects on the GAL4/UAS system using β-galactosidase western immunoblots, described (Berson et al., 2017; Chung et al., 2018; Kramer et al., 2016; Mordes et al., 2018).

Gene ontology (GO) enrichment analysis

GO-term enrichment analyses were done using GOrilla software with a p-value threshold of 10^-3 (Eden et al., 2007, 2009; Subramanian et al., 2005). All genes included in the RNAi library, excluding unspecific RNAi, were set as the background. GO-terms with enrichment scores < 3.0 were excluded as these associated with umbrella categories. For final figures, redundant GO-terms were excluded using Revigo, prioritizing terms with high enrichment scores (Subramanian et al., 2005; Supek et al., 2011).

Internal eye and vacuole formation

Heads were paraffin embedded and sectioned at 8μm, described (Auluck et al., 2002; Berson et al., 2017; Chung et al., 2018; Kramer et al., 2016). Quantification of internal eye: measured depth of the retinal tissue at a consistent level of the brain (when the optic chiasm, antennal lobe and ventrolateral protocerebrum were present); retinal tissue depth was measured at the point of the optic chiasm. Animals with collapsed eyes were excluded. Quantification of vacuole formation was done using a scoring schematic (**Appendix 2: Fig. S2-6a**). The whole brain was reviewed for scoring with researchers blinded to genotype.

Drug-inducible expression using geneswitch- (GS-) GAL4 drivers

0-2d adult flies were collected and aged for 24-48h prior to transfer to 0.04mg RU486-containing food (made by pipetting 100μl of 4mg/ml RU486 in 100% ethanol onto

standard food and incubating at RT for 1-2d with slow rotation). Flies were transferred to fresh RU486-containing food every 2d.

Lifespan and negative geotaxis (climbing)

Lifespan and climbing assays were done as described with minor changes (Berson et al., 2017; Kramer et al., 2016). Assays were done at 24˚C. For the climbing assay, flies were tapped to the bottom of an empty vial and immediately video recorded. Each vial was subjected to 3 consecutive trials with a 20-30min recovery between trials. For analysis, the number of flies in a vial that crossed a 4cm line after 15 or 20s post-tapping were counted. The mean value from the 3 trials per vial was used to account for technical variability.

Western immunoblots (WB)

Fly lysates and reagents: For assays involving Gmr-GAL4 (3d animals), triplicate samples of 5-10 heads per genotype were homogenized in 1X NuPAGE LDS sample buffer using disposable pellet/pestles tissue grinders (Kimble Chase #749520-0000) and motor (Kimble Chase #749540-0000). WBs were run using a standard protocol with Invitrogen's XCell SureLock blot system, 4-12% Bis-Tris NuPAGE gels, and a iBlot dry transfer system with nitrocellulose membrane.

iPSC lysates and reagents: iPSC (**described in Appendix 2: Fig. S2-10a**) were cultured as previously described (Kramer et al., 2018) and lysates were prepared using RIPA buffer. 20µg of total protein was run using a standard WB protocol with Invitrogen's XCell SureLock blot system, 4-12% Bis-Tris NuPAGE gels and wet transfer with PVDF membrane.

Mouse lysates and reagents: Mice expressing either (G4C2)2 or (G4C2)149 were generated by intracerebroventricular administration of AAV2/9 vectors, previously described (Chew et al., 2019). Cortical tissues were harvested at 3mo and 6mo. Protein

lysates were prepped using a 1:5 weight/volume of ice-cold buffer (50mM Tris pH 7.4, 50mM NaCl, 1mM EDTA) with 2x protease and phosphatase inhibitors. 1% Triton X-100 and 2% SDS were added. Tissue homogenates were sonicated on ice and centrifuged at 4°C for 20min at 16,000xg. 30µg of total protein was run using a standard WB protocol with 10% Tris-Glycine gels and wet transfer with nitrocellulose membrane.

Fly antibodies: anti-βgalactosidase (Promega #Z3781, 1:2,000), anti-TDP43 (ProteinTech #10782-2-AP, 1:2,000), anti-αTubulin (DSHB #AA4.3, 1:2,000) (Berson et al., 2017; Chung et al., 2018; Kramer et al., 2016; Mordes et al., 2018). Antibodies targeting dCDC73 or dRtf1 were previously developed (Adelman et al., 2006).

Mammalian antibodies: anti-Paf1 (Cell Signaling #12883, 1:1,000) (Yu et al., 2015a), anti-Leo1 (ProteinTech #12281-1-AP, 1:2,000), anti-CDC73 (Cell Signaling #8126, 1:2,000) (Herr et al., 2015), anti-Rtf1 (Cell Signaling #14737, 1:2,000), anti-αTubulin-HRP (Cell Signaling #9099, 1:2,000), anti-GAPDH (IPSCs: Abcam # G8795, 1:5,000; Mice: Meridian Life Science # H86504M, 1:10,000). Antibodies validated by siRNA in fibroblast cells (data not shown): anti-Paf1, anti-Leo1, anti-Rtf1.

Secondary antibodies and imaging: Mouse or Rabbit HRP-conjugated secondary antibodies (Jackson Immunoresearch Labs #115-035-146 and 111-035-144) were used at 1:5,000 (Berson et al., 2017; Chung et al., 2018; Kramer et al., 2016; Mordes et al., 2018). Blots were analyzed using Amersham ECL Prime Detection Reagent and imaged on an Amersham Imager 600.

Real-time quantitative PCR (qPCR)

All primers are defined in **Appendix 2: Table S2-4**.

Flies: Total RNA was collected using TRIzol. For DaGS or Da-GAL4 assays, biological triplicate samples of 10 whole animals were processed per condition. For ElavGS assays, biological triplicate samples of 20-30 fly heads (16d) were processed per

condition. qPCRs were run using standard protocols. cDNA was made from 200-400ng of total RNA using random primers, High Capacity cDNA Reverse Transcription Kit (ThermoFisher #4368814). qPCR reactions were setup using SYBR Green Fast reagents, 384-welled plate, and analyzed on an Applied Biosystem's ViiA 7 Real-Time PCR System. Mean fold change was determined using the ΔΔCt method. The housekeeping gene, RP49 (RNAPI-driven), was used. Primers targeting the G4C2 fly transgenes utilized unique restriction enzyme sequences in our construct found immediately 3' of the repeat. All primers were validated using a serial dilution curve. **Appendix 2: Fig. S2-12** shows primer efficiencies between G4C2 and loading control used, RP49, to be similar.

Humans: Total RNA was extracted from frozen postmortem tissue from the frontal cortex using the RNAeasy Plus Mini Kit (QIAGEN), previously described (Prudencio et al., 2015). RNA integrity (RIN) was verified on an Agilent 2100 bioanalyzer. qPCRs were run using standard protocols. cDNA was made from 500ng of total RNA (RIN ≥7.0, mean RIN for all samples =9.3) using random primers, High Capacity cDNA Reverse Transcription Kit (ThermoFisher). qPCR was conducted using SYBR GreenER qPCR SuperMix (Invitrogen) for all samples in triplicate. qPCRs were run in an ABI Prism 7900HT Fast Real-Time PCR System (Applied Biosystems). Fold change was determined using the ΔΔCt method, comparing relative expression to healthy controls (mean=1). Housekeeping genes included RPLP0 and GAPDH. Primers targeting the *C9orf72* transcript were previously described (Niblock et al., 2016).

Yeast: Centromeric galactose-inducible plasmids that express *C9orf72* hexanucleotide repeats – sense (G4C2)66 or antisense (G2C4)66 – were transformed into yeast, described (Kramer et al., 2016). Overnight cultures were grown from transformants in 2% raffinose-containing media, then diluted into 2% galactose-containing liquid media

the next morning, and further grown at 30°C for 6 hours to allow for transgene expression. RNA was harvested from these cultures using a MasterPure Yeast RNA Extraction kit (Lucigen), including DNAseI digestions during the purification. Equal amounts of RNA were reverse transcribed using the High-Capacity cDNA Reverse Transcription Kit (Applied Biosystems) and analyzed by qPCR using SYBR green reagents.

External fly eye GR-GFP imaging

y^{1} *sc** *v*^{1};; Gmr-GAL4, UAS-LDS-(G4C2)44$^{GR\text{-}GFP}$ animals were crossed to RNAi lines or controls. Heads from 1-2d progeny were isolated and positioned for imaging on a glass slide using Vaseline. GFP imaging was immediately performed on a Leica DM6000B microscope using Z-stacks. Total GFP fluorescence in the compiled images was measured in ImageJ and normalized relative to control. Only expanded (G4C2)30+ transgenes produce GR-GFP; lines containing ≤ 22 repeats have no GFP signal by external eye fluorescence imaging or by western immunoblot.

Yeast strains and spotting assays

All yeast strains are derivatives of the haploid wildtype BY4741 strain, and all deletion strains were verified by PCR genotyping and qPCR. Centromeric galactose-inducible plasmids expressing codon-optimized *C9orf72* dipeptide repeat proteins – (PR)50 and (GR)100 (Chai and Gitler; Jovičić et al., 2015; Kramer et al., 2016) – or a control protein (CCDB) were transformed into yeast using standard methods and selected for on SD-URA agar plates. For serial dilution growth analysis, transformants were grown overnight in 2% raffinose-containing media. Overnight cultures were all normalized to OD600 = 0.8, and then each strain was diluted serially 5-fold in a 96-well plate. Yeast were spotted onto either 2% glucose or 2% galactose containing agar plates with a multi-pin 'frogger' and allowed to grow for 48h at 30°C before photographed.

Fibroblast cells and chromatin immunoprecipitation (ChIP)

Primary fibroblast cells (**described in Appendix 2: Fig. S2-10a**) were cultured in a standard 37°C / 5% CO_2 incubator using DMEM (with L-GLUT, hi glucose and sodium pyruvate) supplemented with 15% heat-inactivated FBS, 1% amino-acids, and 1% pen/strep. For ChIP, cells were collected from a confluent T-75 flask using trypsin, washed in DPBS and fixed in 1.1% formaldehyde, 10min. ChIPs were then performed as described (Lee et al., 2006) with the following details. DNA was fragmented using a bucket sonicator for 20min. Dynabeads protein A (Invitrogen # 10001D) were used at 30µl per IP. The primary antibody against hLeo1 (ProteinTech #12281-1-AP) was used at 5µg for 100µg DNA, with overnight incubation. An overnight decrosslinking was done and DNA was isolated using a standard Phenol/Chloroform/Isoamyl alcohol (PCA) protocol into 50µl. 4µl was run per reaction by qPCR using Sybr green. Ct values were normalized to input and transformed relative to Rb IgG control (Cell Signaling #2729). Intergenic sequence was as described (Kim et al., 2013). A positive control gene, p21, was used to validate Leo1 ChIPs (Kim et al., 2010). All primers are defined in **Appendix 2: Table S2-4**.

Statistical analysis, sampling, and randomization

GraphPad Prism 7.00 or 8.00 software was used to develop all graphs and for all statistical analyses. P-values ≤ 0.05 were considered significant. See **Appendix 2: Table S2-1** for details on statistics and Life Sciences Reporting Summary for additional information. No data were excluded from this study. Flies, yeast, mice, and cell lines: Data was assumed to be normal. A two-tailed unpaired student t-test, one-way ANOVA, or two-way ANOVA statistical analysis were performed when appropriate based on the experiment design. For ANOVA's Tukey's multiple comparisons tests were predominantly used. No statistical methods were used to

predetermine sample sizes and numbers were similar to previous work (Elden et al., 2010; Kim et al., 2014; Kramer et al., 2016; McGurk and Bonini, 2012; Mizielinska et al., 2014). Researchers were blinded to the genotype of all samples to maintain unbiased scoring. Humans: Data was found to not fit a normal distribution. Kruskal–Wallis, 1-way ANOVAs with Dunn's multiple comparisons test were performed to assess changes in expression of genes. Follow-up Spearman r correlations were performed. No statistical methods were used to predetermine sample sizes and numbers were similar to previous work (Kramer et al., 2016; Prudencio et al., 2015, 2017). Researchers were not blinded as data is inherently unbiased.

Chapter 2: Figures and legends

Figure 2-1

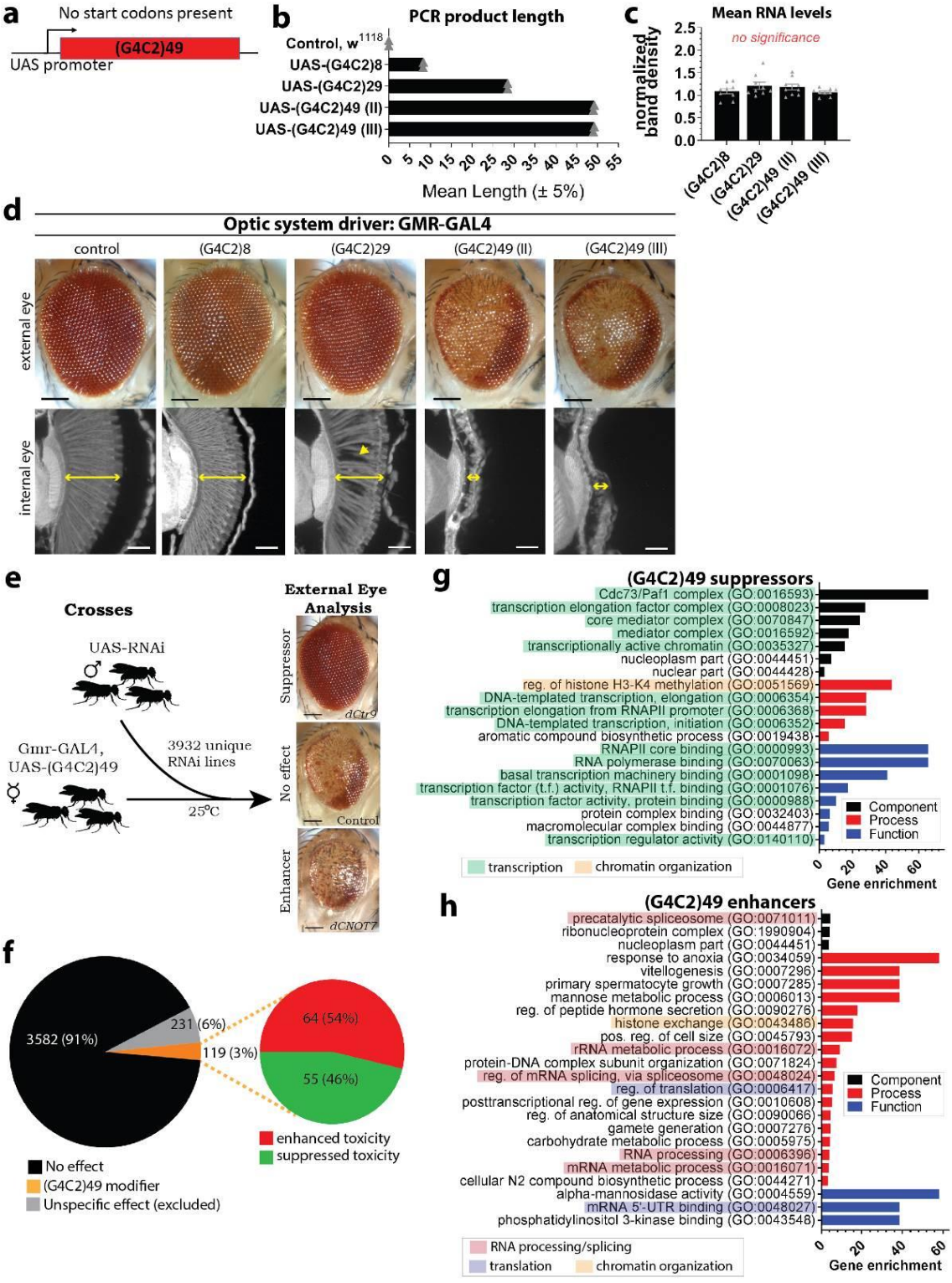
a
No start codons present
(G4C2)49
UAS promoter
b
PCR product length
Control, w1118
UAS-(G4C2)8
UAS-(G4C2)29
UAS-(G4C2)49 (II)
UAS-(G4C2)49 (III)
Mean Length (± 5%)
c
Mean RNA levels
no significance
normalized band density
(G4C2)8
(G4C2)29
(G4C2)49 (II)
(G4C2)49 (III)
d
Optic system driver: GMR-GAL4
control
(G4C2)8
(G4C2)29
(G4C2)49 (II)
(G4C2)49 (III)
external eye
internal eye
e
Crosses
UAS-RNAi
Gmr-GAL4, UAS-(G4C2)49
3932 unique RNAi lines
25°C
External Eye Analysis
Suppressor
dCtr9
No effect
Control
Enhancer
dCNOT7
f
3582 (91%)
231 (6%)
119 (3%)
64 (54%)
55 (46%)
enhanced toxicity
suppressed toxicity
No effect
(G4C2)49 modifier
Unspecific effect (excluded)
g
(G4C2)49 suppressors
Cdc73/Paf1 complex (GO:0016593)
transcription elongation factor complex (GO:0008023)
core mediator complex (GO:0070847)
mediator complex (GO:0016592)
transcriptionally active chromatin (GO:0035327)
nucleoplasm part (GO:0044451)
nuclear part (GO:0044428)
reg. of histone H3-K4 methylation (GO:0051569)
DNA-templated transcription, elongation (GO:0006354)
transcription elongation from RNAPII promoter (GO:0006368)
DNA-templated transcription, initiation (GO:0006352)
aromatic compound biosynthetic process (GO:0019438)
RNAPII core binding (GO:0000993)
RNA polymerase binding (GO:0070063)
basal transcription machinery binding (GO:0001098)
transcription factor (t.f.) activity, RNAPII t.f. binding (GO:0001076)
transcription factor activity, protein binding (GO:0000988)
protein complex binding (GO:0032403)
macromolecular complex binding (GO:0044877)
transcription regulator activity (GO:0140110)
Component
Process
Function
transcription
chromatin organization
Gene enrichment
h
(G4C2)49 enhancers
precatalytic spliceosome (GO:0071011)
ribonucleoprotein complex (GO:1990904)
nucleoplasm part (GO:0044451)
response to anoxia (GO:0034059)
vitellogenesis (GO:0007296)
primary spermatocyte growth (GO:0007285)
mannose metabolic process (GO:0006013)
reg. of peptide hormone secretion (GO:0090276)
histone exchange (GO:0043486)
pos. reg. of cell size (GO:0045793)
rRNA metabolic process (GO:0016072)
protein-DNA complex subunit organization (GO:0071824)
reg. of mRNA splicing, via spliceosome (GO:0048024)
reg. of translation (GO:0006417)
posttranscriptional reg. of gene expression (GO:0010608)
reg. of anatomical structure size (GO:0090066)
gamete generation (GO:0007276)
carbohydrate metabolic process (GO:0005975)
RNA processing (GO:0006396)
mRNA metabolic process (GO:0016071)
cellular N2 compound biosynthetic process (GO:0044271)
alpha-mannosidase activity (GO:0004559)
mRNA 5'-UTR binding (GO:0048027)
phosphatidylinositol 3-kinase binding (GO:0043548)
Component
Process
Function
RNA processing/splicing
translation
chromatin organization
Gene enrichment

Figure 1: A genetic screen reveals PAF1C as a suppressor of (G4C2)49-toxicity in the fly eye.

(a) UAS-(G4C2)n transgenes were designed expressing a pure repeat. **(b)** PCR reactions were used to quantify of the number of repeats in individual UAS-G4C2 transgenic fly lines. Shown: individual data points with mean from 2 experiments (30 flies/experiment). **(c)** RNA expression of UAS-(G4C2)n transgenes using HS-GAL4 were compared by northern blots. Statistics: ANOVA with Tukey's correction, p-value: no significance >0.05. Shown: individual data points with mean±SEM; mean value of biological triplicates (n=30 flies) from 3 independent experiments. **(d)** Expression of UAS-(G4C2)n transgenes in the fly eye compared to controls: (G4C2)8 had no effect, (G4C2)29 caused mild disruptions in 80% of animals, (G4C2)49 caused strong degeneration. Shown: data from one experiment; data reproduced in 3+ independent experiments. Arrows: internal tissue depth, lost tissue. **(e)** RNAi were co-expressed with (G4C2)49 (III) within the fly optic system. Effects of RNAi were recorded: "suppressors" reduced degeneration, "enhancers" increased degeneration. Shown: representative images. Hits were independently tested 3+ times to confirm reproducibility (>5 flies examined/cross). **(f)** 119 modifiers were identified. Control experiments excluded 231 RNAi lines with unspecific effects. **(g-h)** GO analyses revealed terms enriched in suppressors (55/3582 genes) or enhancers (64/3582 genes). Plotted: significant (p-value ≤10^-3) enrichment scores of >3.00. **(d-e)** Scale bars: external eye =100µm, internal eye =25µm. **(a-h)** Additional details for this and subsequent figures: Appendix 2: Fig. S2-1 (extended screen data), **Appendix 2: Sup. Data** (all screen results), Appendix 2: Table S2-1 (detailed sampling/reproducibility/statistics), methods.

Figure 2-2

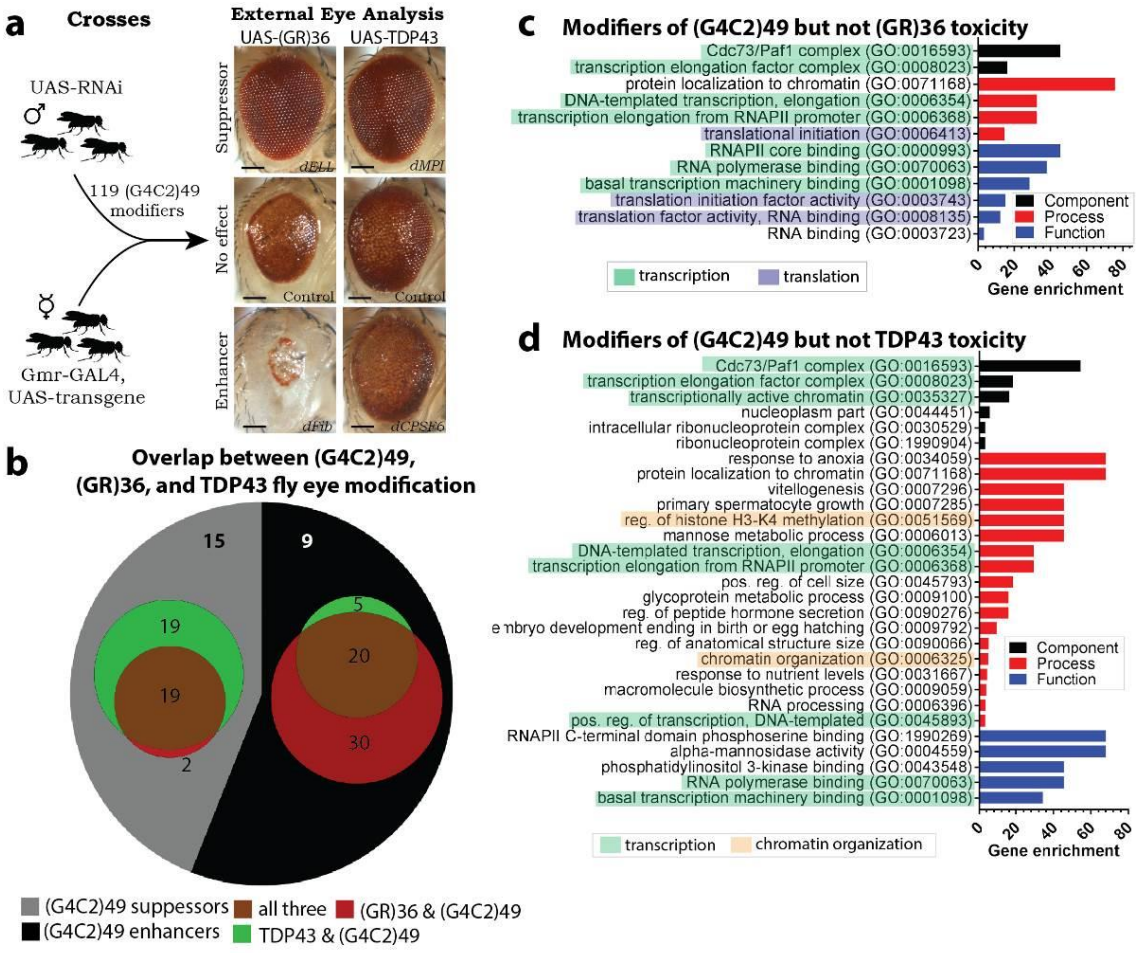
a
Crosses
UAS-RNAi
119 (G4C2)49 modifiers
Gmr-GAL4, UAS-transgene
External Eye Analysis
UAS-(GR)36
UAS-TDP43
Suppressor
No effect
Enhancer
dELL
dMPI
Control
Control
dFib
dCPSF6
b
Overlap between (G4C2)49, (GR)36, and TDP43 fly eye modification
15
9
19
5
19
20
2
30
(G4C2)49 suppressors
all three
(GR)36 & (G4C2)49
(G4C2)49 enhancers
TDP43 & (G4C2)49
c
Modifiers of (G4C2)49 but not (GR)36 toxicity
Cdc73/Paf1 complex (GO:0016593)
transcription elongation factor complex (GO:0008023)
protein localization to chromatin (GO:0071168)
DNA-templated transcription, elongation (GO:0006354)
transcription elongation from RNAPII promoter (GO:0006368)
translational initiation (GO:0006413)
RNAPII core binding (GO:0000993)
RNA polymerase binding (GO:0070063)
basal transcription machinery binding (GO:0001098)
translation initiation factor activity (GO:0003743)
translation factor activity, RNA binding (GO:0008135)
RNA binding (GO:0003723)
Component
Process
Function
transcription
translation
0
20
40
60
80
Gene enrichment
d
Modifiers of (G4C2)49 but not TDP43 toxicity
Cdc73/Paf1 complex (GO:0016593)
transcription elongation factor complex (GO:0008023)
transcriptionally active chromatin (GO:0035327)
nucleoplasm part (GO:0044451)
intracellular ribonucleoprotein complex (GO:0030529)
ribonucleoprotein complex (GO:1990904)
response to anoxia (GO:0034059)
protein localization to chromatin (GO:0071168)
vitellogenesis (GO:0007296)
primary spermatocyte growth (GO:0007285)
reg. of histone H3-K4 methylation (GO:0051569)
mannose metabolic process (GO:0006013)
DNA-templated transcription, elongation (GO:0006354)
transcription elongation from RNAPII promoter (GO:0006368)
pos. reg. of cell size (GO:0045793)
glycoprotein metabolic process (GO:0009100)
reg. of peptide hormone secretion (GO:0090276)
embryo development ending in birth or egg hatching (GO:0009792)
reg. of anatomical structure size (GO:0090066)
chromatin organization (GO:0006325)
response to nutrient levels (GO:0031667)
macromolecule biosynthetic process (GO:0009059)
RNA processing (GO:0006396)
pos. reg. of transcription, DNA-templated (GO:0045893)
RNAPII C-terminal domain phosphoserine binding (GO:1990269)
alpha-mannosidase activity (GO:0004559)
phosphatidylinositol 3-kinase binding (GO:0043548)
RNA polymerase binding (GO:0070063)
basal transcription machinery binding (GO:0001098)
Component
Process
Function
transcription
chromatin organization
0
20
40
60
80
Gene enrichment

Figure 2: PAF1C is not a modifier of (GR)36 or TDP43 toxicity in *Drosophila*.

(a) The 119 (G4C2)49 modifiers were analyzed in (GR)36 and TDP43 models to determine if they could act on GR-dipeptide toxicity or had overlapping effects on TDP43-toxicity. All were independently tested 3+ times to confirm reproducibility of results (>5 flies examined/cross). Scale bars: 100μm. **(b)** Of the 119 modifiers of (G4C2)49 toxicity, 71 (59.7%) similarly modified (GR)36, arguing they may be acting on toxic DPR. 63 (52.9%) similarly affected TDP-43 toxicity, arguing overlap between these disease models. **(c)** GO analyses revealed terms enriched in the modifiers that *did not* similarly alter (GR)36 toxicity (48/3582 genes), revealing those acting selectively on the (G4C2)49 RNA model. **(d)** GO analyses revealed terms enriched in the modifiers that *did not* similarly alter TDP43 toxicity (56/3582 genes), revealing those specific to the expanded G4C2 repeat in C9+ FTD/ALS. **(c-d)** Plotted: GO-terms with significant (p-value ≤ 10^-3) enrichment scores of >3.00.

Figure 2-3

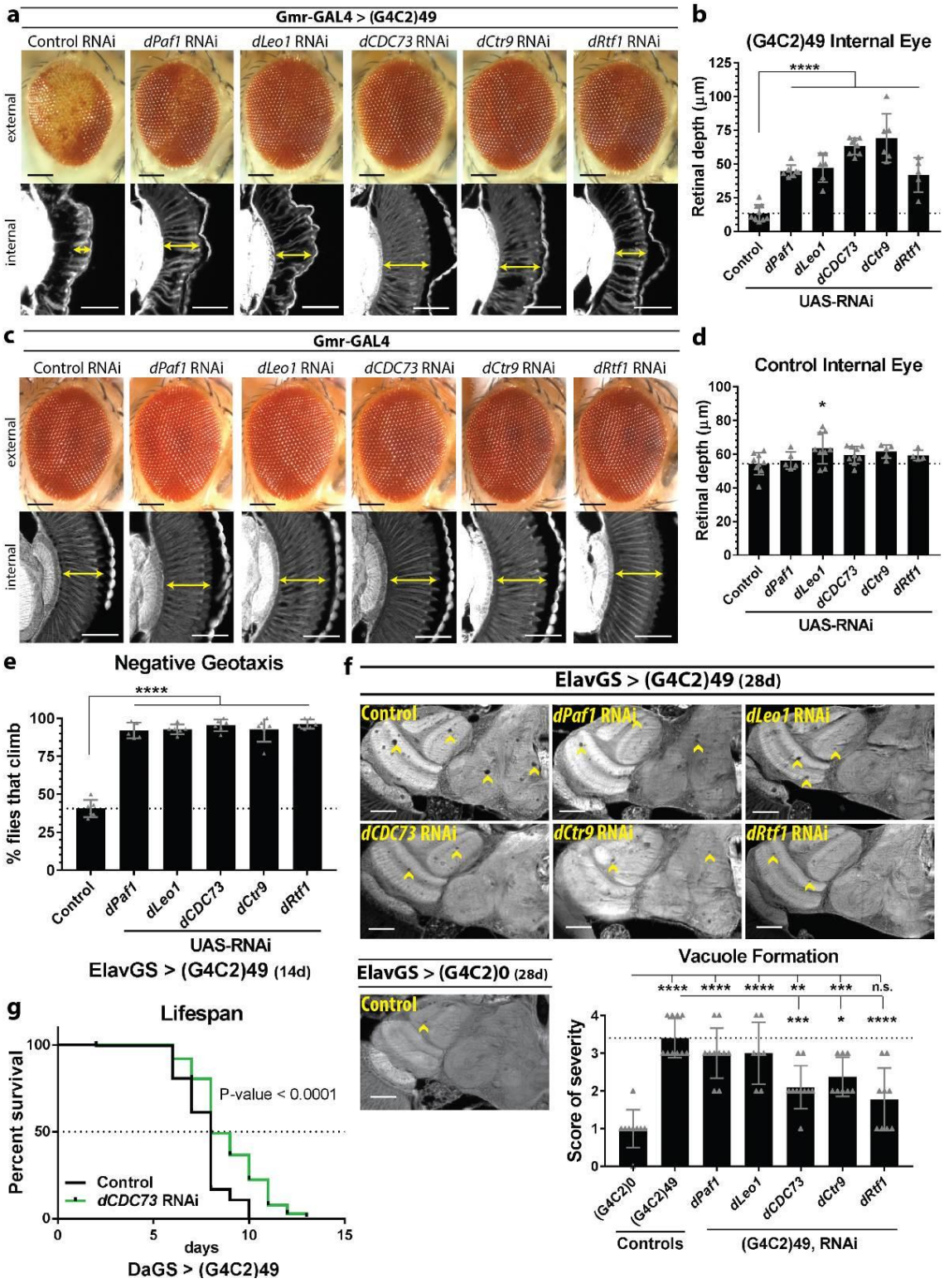
a
Gmr-GAL4 > (G4C2)49
Control RNAi
dPaf1 RNAi
dLeo1 RNAi
dCDC73 RNAi
dCtr9 RNAi
dRtf1 RNAi
external
internal
b
(G4C2)49 Internal Eye
Retinal depth (µm)
****
Control
dPaf1
dLeo1
dCDC73
dCtr9
dRtf1
UAS-RNAi
c
Gmr-GAL4
d
Control Internal Eye
*
e
Negative Geotaxis
% flies that climb
ElavGS > (G4C2)49 (14d)
f
ElavGS > (G4C2)49 (28d)
Control
dPaf1 RNAi
dLeo1 RNAi
dCDC73 RNAi
dCtr9 RNAi
dRtf1 RNAi
ElavGS > (G4C2)0 (28d)
Vacuole Formation
Score of severity
n.s.
(G4C2)0
(G4C2)49
Controls
(G4C2)49, RNAi
g
Lifespan
Percent survival
P-value < 0.0001
Control
dCDC73 RNAi
days
DaGS > (G4C2)49

Figure 3: Reduced expression of components of PAF1C suppress (G4C2)49-induced toxicity in multiple contexts in the fly.

(a-b) dPAF1C RNAi mitigates toxicity associated with (G4C2)49 expression in the eye. N flies: control=9, *dPaf1*=7, *dLeo1*=6, *dCDC73*=8, *dCtr9*=6, *dRtf1*=5. **(c-d)** dPAF1C RNAi has no effect on control fly eyes. N flies: control=9, *dPaf1*=5, *dLeo1*=9, *dCDC73*=9, *dCtr9*=5, *dRtf1*=4. **(a-d)** Internal retina depth (arrows) quantified for individual animals. Scale bars: external eye =100μm, internal eye =45μm. **(e)** Climbing deficits caused by (G4C2)49 expression in the adult nervous system (ElavGS, 14d) are rescued by dPAF1C RNAi. N flies: control=117, *dPaf1*=98, *dLeo1*=108, *dCDC73*=103, *dCtr9*=120, *dRtf1*=115. Individual data points are mean % of animals that could climb per tube; average of 19±2 animals per tube. **(f)** *dPAF1C* RNAi mitigated vacuole formation (arrowheads) in the brain with ElavGS driven expression of (G4C2)49. For quantification, a vacuole severity scoring system was developed where 0=no vacuoles and 4=medium/large, frequent (>5) vacuoles (see Sup. Fig. 6a). N flies: (G4C2)0=9, (G4C2)49: control=10, *dPaf1*=10, *dLeo1*=7, *dCDC73*=10, *dCtr9*=8, *dRtf1*=9. Scale bars: 50μm. **(g)** Knockdown of *dCDC73* in adult flies ubiquitously expressing (G4C2)49 results in lifespan extension. N flies: control=198, dCDC73=197. (b,d,f) each data point represents one animal. Statistics: (a-f) ANOVAs with Tukey's correction, (g) log-rank; p-values: ****<0.0001, ***<0.001, **<0.01, *<0.05, no significance (n.s.) >0.05. Shown on graphs: individual data points with mean±SD; data from one experiment; all experiments were repeated twice with similar results.

Figure 2-4

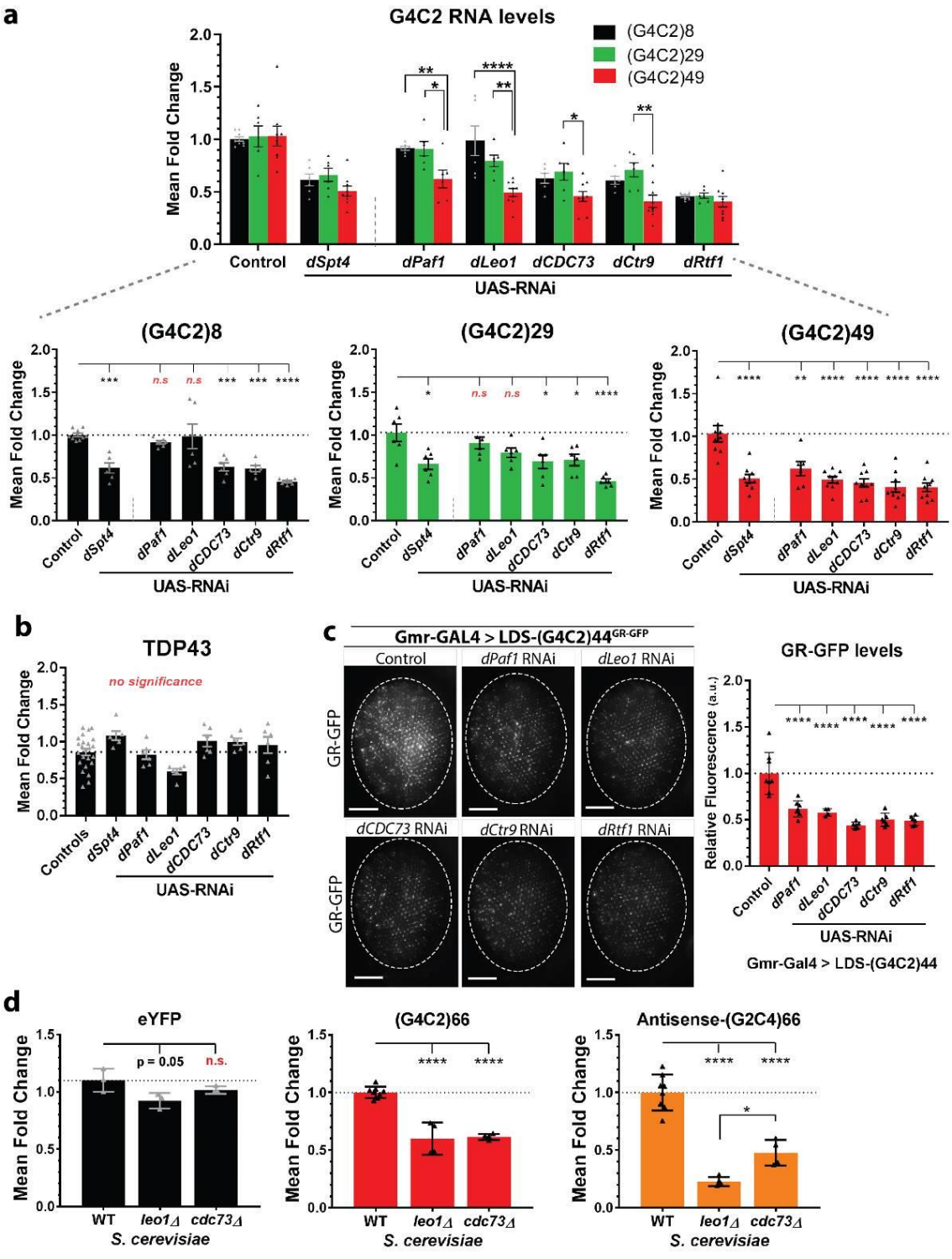
a
G4C2 RNA levels
(G4C2)8
(G4C2)29
(G4C2)49
Mean Fold Change
Control
dSpt4
dPaf1
dLeo1
dCDC73
dCtr9
dRtf1
UAS-RNAi
(G4C2)8
(G4C2)29
(G4C2)49
n.s
b
TDP43
no significance
Controls
c
Gmr-GAL4 > LDS-(G4C2)44GR-GFP
Control
dPaf1 RNAi
dLeo1 RNAi
dCDC73 RNAi
dCtr9 RNAi
dRtf1 RNAi
GR-GFP
GR-GFP levels
Relative Fluorescence (a.u.)
Gmr-Gal4 > LDS-(G4C2)44
d
eYFP
p = 0.05
n.s.
(G4C2)66
Antisense-(G2C4)66
WT
leo1Δ
cdc73Δ
S. cerevisiae

Figure 4: Downregulation of components of PAF1C selectively alter (G4C2)30+ transgene expression.

(a) (G4C2)n transgenes were co-expressed with dPAF1C RNAi lines in the adult brain using a drug inducible, neuronal driver (ElavGS, 16d). Transgene expression levels in heads measured by qPCR. *dPaf1* and *dLeo1* RNAi did not affect RNA levels of (G4C2)8 and (G4C2)29 but significantly reduced (G4C2)49 expression. *dSpt4*, *dCDC73*, *dCtr9*, *dRtf1* RNAi altered expression of all (G4C2)n transgenes. Shown: individual data points with mean±SEM; mean value of 3 biological replicates (n=25 flies/replicate) from 2-3 independent experiments. **(b)** dPAF1C RNAi did not alter TDP43 (ElavGS, 16d, heads) RNA levels by qPCR. Shown: individual data points with mean±SEM; mean value of 3 biological replicates (n=25 flies/replicate) from 2 independent experiments. **(c)** Downregulation of dPAF1C components reduces GR-GFP signal in LDS-(G4C2)44GR-GFP animals. Quantification of total GFP fluorescence relative to control animals. N flies: control=8, *dPaf1*=7, *dLeo1*=4, *dCDC73*=6, *dCtr9*=6, *dRtf1*=6. Each data point represents one eye of one animal. Shown: data from one experiment; data reproduced in two independent experiments. Scale bars: 100µm. **(d)** Effects of deleting *scCDC73* (*cdc73Δ*) or *scLeo1* (*leo1Δ*) in *S. cerevisiae* on RNA levels from transgenes assessed by qPCR. Transgenes included eYFP (control), sense-(G4C2)66 (disease) and antisense-(G2C4)66 (disease). Shown: individual data points with mean±SD; mean value of biological duplicates from 2 independent experiments. Statistics: ANOVAs with Tukey's correction, p-values: ****<0.0001, ***<0.001, **<0.01, *<0.05, no significance (n.s.) >0.05.

Figure 2-5

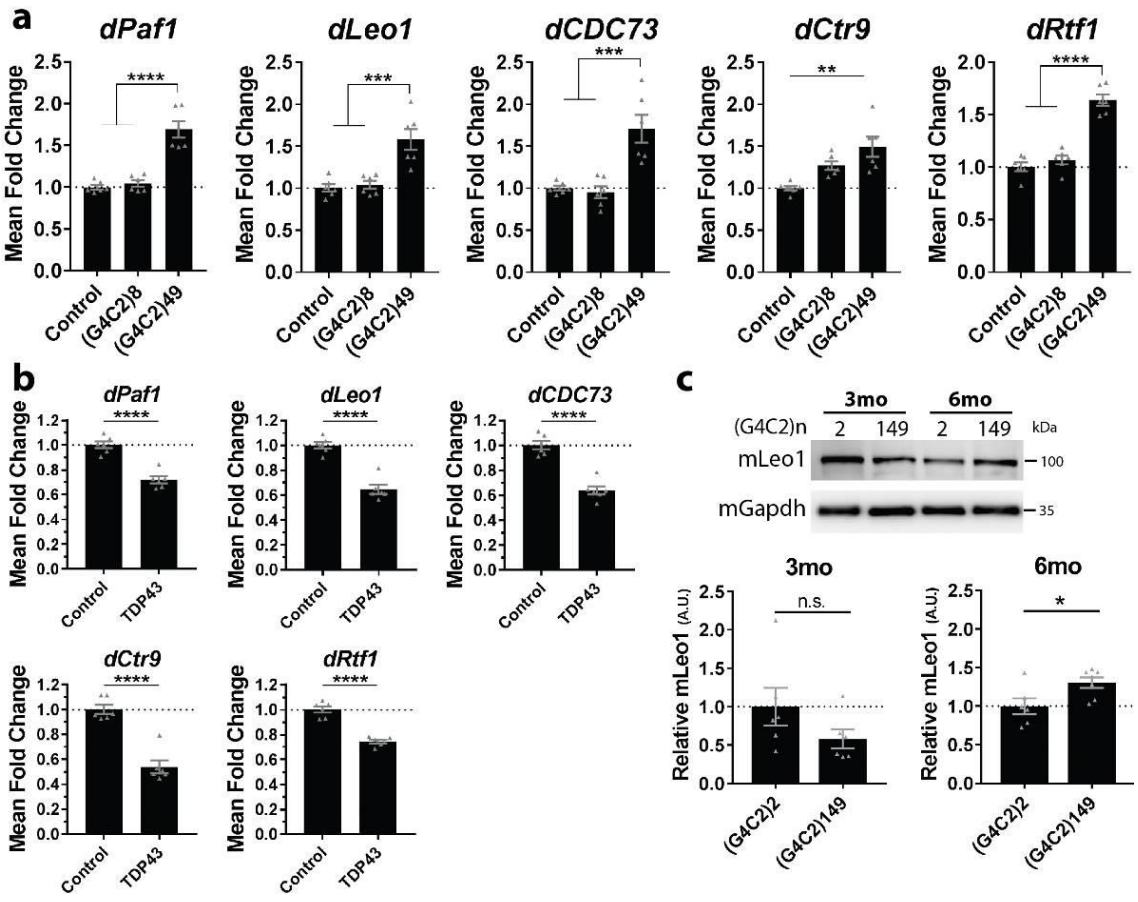
a
dPaf1
dLeo1
dCDC73
dCtr9
dRtf1
Mean Fold Change
Control
(G4C2)8
(G4C2)49
b
TDP43
c
3mo
6mo
(G4C2)n
2
149
kDa
mLeo1
100
mGapdh
35
Relative mLeo1 (A.U.)
n.s.
(G4C2)2
(G4C2)149

Figure 5: Endogenous PAF1C is upregulated in response to (G4C2)49 expression in the brain in flies and mice.

(a) Endogenous dPAF1C RNA expression is upregulated in (G4C2)49 expressing flies compared to control or (G4C2)8 expressing flies (qPCR). Transgenes expressed in the adult fly nervous system (ElavGS, 16d). Differences in expression are likely underestimated as RNA was extracted from whole head tissue, while transgenes were expressed selectively in neurons. **(b)** A non-G4C2 disease transgene, TDP43, was expressed with ElavGS (16d). Whole head analysis showed no upregulation of PAF1C components. **(a-b)** Shown: individual data points with mean±SEM; mean value of biological triplicates (n=25 flies/replicate) from 2 independent experiments. **(c)** Mouse endogenous mLeo1 protein levels measured in cortical tissue by western immunoblot using lysates from mice injected intracerebroventricularly with AAV2/9-(G4C2)2 or -(G4C2)149 at postnatal day 0. mLeo1 is upregulated by 6mo in response to expression of expanded (G4C2)149. Differences in expression are likely underestimated as protein was extracted from total cortical tissue while transgenes were expressed using AAV2/9 which predominantly transduces neurons. 3mo N animals: (G4C2)2=6, (G4C2)149=6. 6mo N animals: (G4C2)2=6, (G4C2)149=7. Shown: individual data points (each representing 1 animal) with mean±SEM. Data reproduced in two independent experiments. Statistics: (a) ANOVAs with Tukey's correction, (b-c) unpaired 2-tailed student t-test; p-values: ****<0.0001, ***<0.001, **<0.01, *<0.05, no significance (n.s.) >0.05. See Supplementary Figure 11 for uncropped western images for this and subsequent figures.

Figure 2-6

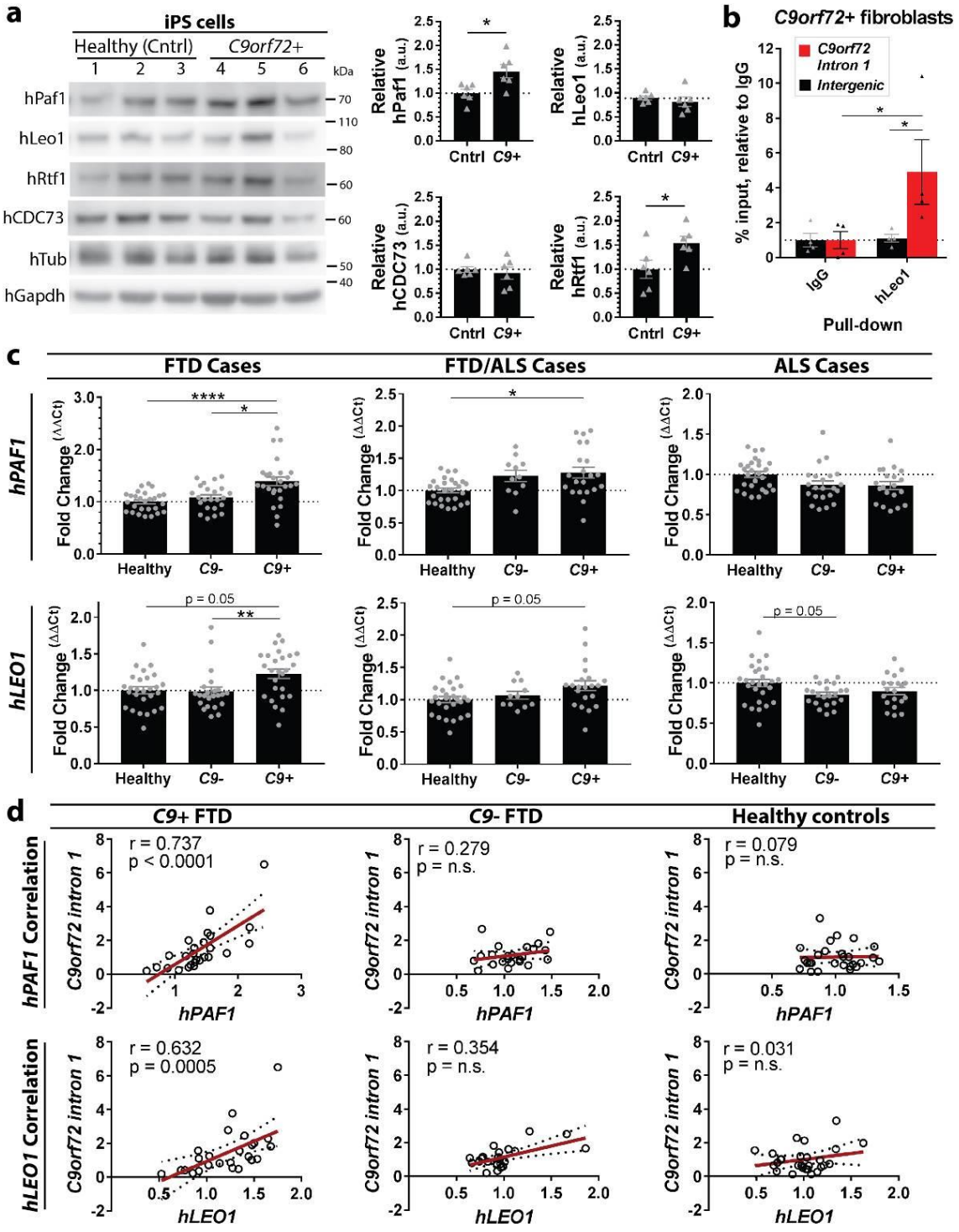
a
iPS cells
Healthy (Cntrl)
C9orf72+
1 2 3 4 5 6
kDa
hPaf1
hLeo1
hRtf1
hCDC73
hTub
hGapdh
70
110
80
60
60
50
40
Relative hPaf1 (a.u.)
Relative hLeo1 (a.u.)
Relative hCDC73 (a.u.)
Relative hRtf1 (a.u.)
Cntrl C9+
b
C9orf72+ fibroblasts
C9orf72 Intron 1
Intergenic
% input, relative to IgG
IgG
hLeo1
Pull-down
c
FTD Cases
FTD/ALS Cases
ALS Cases
hPAF1
hLEO1
Fold Change (ΔΔCt)
Healthy
C9-
C9+
p = 0.05
d
C9+ FTD
C9- FTD
Healthy controls
hPAF1 Correlation
hLEO1 Correlation
C9orf72 intron 1
r = 0.737
p < 0.0001
r = 0.279
p = n.s.
r = 0.079
p = n.s.
r = 0.632
p = 0.0005
r = 0.354
p = n.s.
r = 0.031
p = n.s.

Figure 6: Upregulated *hPAF1* and *hLEO1* positively correlate with expression of repeat-containing *C9orf72* transcripts and hLeo1 binds *C9orf72*.

(a) Western immunoblots for hPAF1C components in iPS cells. hPAF1C band densities were normalized to the mean of loading controls: hTubulin, hGAPDH. Shown: individual data points with mean±SEM; mean value of 2 biological replicates from 2 independent experiments per cell line relative to the mean signal in controls. **(b)** Chromatin immunoprecipitation studies using a hLeo1 antibody on 4 independent *C9*+-derived fibroblast lines. Data: relative to IgG controls after normalizing by input. Shown: individual data points (each representing 1 cell line) with mean±SEM; mean value of technical quadruplicates from 1 experiment. Data reproduced in 2 independent experiments per line. **(c)** qPCR analysis of *hPAF1* and *hLEO1* expression from healthy control (n=27), *C9*- (n=56), and *C9*+ patients (n=67) frontal cortex tissue. Shown: individual data points (each representing 1 individual) with mean±SEM. **(d)** Spearman r coefficients defined correlations in expression from *hPAF1* or *hLEO1* expression with *C9orf72* transcripts in individuals. r values: 0=no correlation, 1.0=100% correlated. Shown: individual data points (each representing 1 individual) with linear regression±SE. Statistics: (a) unpaired 2-tailed student t-test, (b) ANOVA with Sidak's correction, (c) Kruskal-Wallis ANOVA with Dunn's correction, (d) Spearman R correlation; p-values: ****<0.0001, ***<0.001, **<0.01, *<0.05, no significance >0.05. *C9orf72 intron 1*: intronic region immediately 3' of the G4C2 repeat in the *C9orf72* gene. See Supplementary Figure 10 for cell line and patient characteristics.

Bibliography

Adelman, K., Wei, W., Ardehali, M.B., Werner, J., Zhu, B., Reinberg, D., and Lis, J.T. (2006). Drosophila Paf1 Modulates Chromatin Structure at Actively Transcribed Genes. Mol. Cell. Biol. *26*, 250–260.

Amrich, C.G., Davis, C.P., Rogal, W.P., Shirra, M.K., Heroux, A., Gardner, R.G., Arndt, K.M., and VanDemark, A.P. (2012). Cdc73 Subunit of Paf1 Complex Contains C-terminal Ras-like Domain That Promotes Association of Paf1 Complex with Chromatin. J. Biol. Chem. *287*, 10863–10875.

Auluck, P.K., Chan, H.Y.E., Trojanowski, J.Q., Lee, V.M.-Y., and Bonini, N.M. (2002). Chaperone Suppression of α-Synuclein Toxicity in a Drosophila Model for Parkinson's Disease. Science *295*, 865–868.

Bahrampour, S., and Thor, S. (2016). Ctr9, a Key Component of the Paf1 Complex, Affects Proliferation and Terminal Differentiation in the Developing Drosophila Nervous System. G3 GenesGenomesGenetics *6*, 3229–3239.

Balendra, R., and Isaacs, A.M. (2018). C9orf72 -mediated ALS and FTD: multiple pathways to disease. Nat. Rev. Neurol. *14*, 544.

Berson, A. et al. (2017). TDP-43 Promotes Neurodegeneration by Impairing Chromatin Remodeling. Curr. Biol. *27*, 3579-3590.e6.

van Blitterswijk, M., Mullen, B., Heckman, M.G., Baker, M.C., DeJesus-Hernandez, M., Brown, P.H., Murray, M.E., Hsiung, G.-Y.R., Stewart, H., Karydas, A.M., et al. (2014a). Ataxin-2 as potential disease modifier in C9ORF72 expansion carriers. Neurobiol. Aging *35*, 2421.e13-2421.e17.

van Blitterswijk, M., Mullen, B., Nicholson, A.M., Bieniek, K.F., Heckman, M.G., Baker, M.C., DeJesus-Hernandez, M., Finch, N.A., Brown, P.H., Murray, M.E., et al. (2014b). TMEM106B protects C9ORF72 expansion carriers against frontotemporal dementia. Acta Neuropathol. (Berl.) *127*, 397–406.

Burguete, A.S., Almeida, S., Gao, F.-B., Kalb, R., Akins, M.R., and Bonini, N.M. GGGGCC microsatellite RNA is neuritically localized, induces branching defects, and perturbs transport granule function. ELife *4*.

Cao, Q.-F., Yamamoto, J., Isobe, T., Tateno, S., Murase, Y., Chen, Y., Handa, H., and Yamaguchi, Y. (2015). Characterization of the Human Transcription Elongation Factor Rtf1: Evidence for Nonoverlapping Functions of Rtf1 and the Paf1 Complex. Mol. Cell. Biol. *35*, 3459–3470.

Chai, N., and Gitler, A.D. Yeast screen for modifiers of C9orf72 poly(Glycine-Arginine) dipeptide repeat toxicity. FEMS Yeast Res.

Chaturvedi, D., Inaba, M., Scoggin, S., and Buszczak, M. (2016). Drosophila CG2469 Encodes a Homolog of Human CTR9 and Is Essential for Development. G3 GenesGenomesGenetics *6*, 3849–3857.

Chen, Y., Yamaguchi, Y., Tsugeno, Y., Yamamoto, J., Yamada, T., Nakamura, M., Hisatake, K., and Handa, H. (2009). DSIF, the Paf1 complex, and Tat-SF1 have nonredundant, cooperative roles in RNA polymerase II elongation. Genes Dev. *23*, 2765–2777.

Cheng, H.-M., Chern, Y., Chen, I.-H., Liu, C.-R., Li, S.-H., Chun, S.J., Rigo, F., Bennett, C.F., Deng, N., Feng, Y., et al. (2015). Effects on Murine Behavior and Lifespan of Selectively Decreasing Expression of Mutant Huntingtin Allele by Supt4h Knockdown. PLoS Genet. *11*.

Chew, J., Cook, C., Gendron, T.F., Jansen-West, K., del Rosso, G., Daughrity, L.M., Castanedes-Casey, M., Kurti, A., Stankowski, J.N., Disney, M.D., et al. (2019). Aberrant deposition of stress granule-resident proteins linked to C9orf72-associated TDP-43 proteinopathy. Mol. Neurodegener. *14*, 9.

Chu, X., Qin, X., Xu, H., Li, L., Wang, Z., Li, F., Xie, X., Zhou, H., Shen, Y., and Long, J. (2013). Structural insights into Paf1 complex assembly and histone binding. Nucleic Acids Res. *41*, 10619–10629.

Chung, C.-Y., Berson, A., Kennerdell, J.R., Sartoris, A., Unger, T., Porta, S., Kim, H.-J., Smith, E.R., Shilatifard, A., Van Deerlin, V., et al. (2018). Aberrant activation of non-coding RNA targets of transcriptional elongation complexes contributes to TDP-43 toxicity. Nat. Commun. *9*.

DeJesus-Hernandez, M., Mackenzie, I.R., Boeve, B.F., Boxer, A.L., Baker, M., Rutherford, N.J., Nicholson, A.M., Finch, N.A., Gilmer, H.F., Adamson, J., et al. (2011). Expanded GGGGCC hexanucleotide repeat in non-coding region of C9ORF72 causes chromosome 9p-linked frontotemporal dementia and amyotrophic lateral sclerosis. Neuron *72*, 245–256.

Dermody, J.L., and Buratowski, S. (2010). Leo1 Subunit of the Yeast Paf1 Complex Binds RNA and Contributes to Complex Recruitment. J. Biol. Chem. *285*, 33671–33679.

Dietzl, G., Chen, D., Schnorrer, F., Su, K.-C., Barinova, Y., Fellner, M., Gasser, B., Kinsey, K., Oppel, S., Scheiblauer, S., et al. (2007). A genome-wide transgenic RNAi library for conditional gene inactivation in *Drosophila*. Nature *448*, 151.

Eden, E., Lipson, D., Yogev, S., and Yakhini, Z. (2007). Discovering Motifs in Ranked Lists of DNA Sequences. PLoS Comput. Biol. *3*.

Eden, E., Navon, R., Steinfeld, I., Lipson, D., and Yakhini, Z. (2009). GOrilla: a tool for discovery and visualization of enriched GO terms in ranked gene lists. BMC Bioinformatics *10*, 48.

Elden, A.C., Kim, H.-J., Hart, M.P., Chen-Plotkin, A.S., Johnson, B.S., Fang, X., Armakola, M., Geser, F., Greene, R., Lu, M.M., et al. (2010). Ataxin-2 intermediate-length polyglutamine expansions are associated with increased risk for ALS. Nature *466*, 1069–1075.

Fischl, H., Howe, F.S., Furger, A., and Mellor, J. (2017). Paf1 Has Distinct Roles in Transcription Elongation and Differential Transcript Fate. Mol. Cell *65*, 685-698.e8.

Freudenreich, C.H. (2018). R-loops: targets for nuclease cleavage and repeat instability. Curr. Genet. 1–6.

Gerlach, J.M., Furrer, M., Gallant, M., Birkel, D., Baluapuri, A., Wolf, E., and Gallant, P. (2017). PAF1 complex component Leo1 helps recruit Drosophila Myc to promoters. Proc. Natl. Acad. Sci. *114*, E9224–E9232.

Hall, A.C., Ostrowski, L.A., Pietrobon, V., and Mekhail, K. (2017). Repetitive DNA loci and their modulation by the non-canonical nucleic acid structures R-loops and G-quadruplexes. Nucleus *8*, 162–181.

Hartzog, G.A., and Fu, J. (2013). The Spt4-Spt5 complex: a multi-faceted regulator of transcription elongation. Biochim. Biophys. Acta *1829*, 105.

Herr, P., Lundin, C., Evers, B., Ebner, D., Bauerschmidt, C., Kingham, G., Palmai-Pallag, T., Mortusewicz, O., Frings, O., Sonnhammer, E., et al. (2015). A genome-wide IR-induced RAD51 foci RNAi screen identifies CDC73 involved in chromatin remodeling for DNA repair. Cell Discov. *1*, 15034.

Jaehning, J.A. (2010). The Paf1 complex: Platform or player in RNA polymerase II transcription? Biochim. Biophys. Acta BBA - Gene Regul. Mech. *1799*, 379–388.

Jovičić, A., Mertens, J., Boeynaems, S., Bogaert, E., Chai, N., Yamada, S.B., Paul, J.W., Sun, S., Herdy, J.R., Bieri, G., et al. (2015). Modifiers of C9orf72 DPR toxicity implicate nucleocytoplasmic transport impairments in c9FTD/ALS. Nat. Neurosci. *18*, 1226–1229.

Kim, H.-J., Raphael, A.R., LaDow, E.S., McGurk, L., Weber, R., Trojanowski, J.Q., Lee, V.M.-Y., Finkbeiner, S., Gitler, A.D., and Bonini, N.M. (2014). Therapeutic modulation of eIF2α-phosphorylation rescues TDP-43 toxicity in amyotrophic lateral sclerosis disease models. Nat. Genet. *46*, 152–160.

Kim, J., Guermah, M., and Roeder, R.G. (2010). The Human PAF1 Complex Acts in Chromatin Transcription Elongation Both Independently and Cooperatively with SII/TFIIS. Cell *140*, 491–503.

Kim, N., Sun, H.-Y., Youn, M.-Y., and Yoo, J.-Y. (2013). IL-1β–specific recruitment of GCN5 histone acetyltransferase induces the release of PAF1 from chromatin for the de-repression of inflammatory response genes. Nucleic Acids Res. *41*, 4495–4506.

Kramer, N.J., Carlomagno, Y., Zhang, Y.-J., Almeida, S., Cook, C.N., Gendron, T.F., Prudencio, M., Blitterswijk, M.V., Belzil, V., Couthouis, J., et al. (2016). Spt4 selectively regulates the expression of C9orf72 sense and antisense mutant transcripts. Science *353*, 708–712.

Kramer, N.J., Haney, M.S., Morgens, D.W., Jovičić, A., Couthouis, J., Li, A., Ousey, J., Ma, R., Bieri, G., Tsui, C.K., et al. (2018). CRISPR–Cas9 screens in human cells and primary neurons identify modifiers of C9ORF72 dipeptide-repeat-protein toxicity. Nat. Genet. 1.

Lee, T.I., Johnstone, S.E., and Young, R.A. (2006). Chromatin immunoprecipitation and microarray-based analysis of protein location. Nat. Protoc. *1*, 729–748.

Liu, C.-R., Chang, C.-R., Chern, Y., Wang, T.-H., Hsieh, W.-C., Shen, W.-C., Chang, C.-Y., Chu, I.-C., Deng, N., Cohen, S.N., et al. (2012). Spt4 Is Selectively Required for Transcription of Extended Trinucleotide Repeats. Cell *148*, 690–701.

Mayekar, M.K., Gardner, R.G., and Arndt, K.M. (2013). The Recruitment of the Saccharomyces cerevisiae Paf1 Complex to Active Genes Requires a Domain of Rtf1 That Directly Interacts with the Spt4-Spt5 Complex. Mol. Cell. Biol. *33*, 3259–3273.

Mayer, A., Lidschreiber, M., Siebert, M., Leike, K., Söding, J., and Cramer, P. (2010). Uniform transitions of the general RNA polymerase II transcription complex. Nat. Struct. Mol. Biol. *17*, 1272.

McGurk, L., and Bonini, N.M. (2012). Protein interacting with C kinase (PICK1) is a suppressor of spinocerebellar ataxia 3-associated neurodegeneration in Drosophila. Hum. Mol. Genet. *21*, 76.

Meehan, T.F., Conte, N., West, D.B., Jacobsen, J.O., Mason, J., Warren, J., Chen, C.-K., Tudose, I., Relac, M., Matthews, P., et al. (2017). Disease Model Discovery from 3,328 Gene Knockouts by The International Mouse Phenotyping Consortium. Nat. Genet. *49*, 1231–1238.

Mizielinska, S., Grönke, S., Niccoli, T., Ridler, C.E., Clayton, E.L., Devoy, A., Moens, T., Norona, F.E., Woollacott, I.O.C., Pietrzyk, J., et al. (2014). C9orf72 repeat expansions cause neurodegeneration in Drosophila through arginine-rich proteins. Science *345*, 1192–1194.

Moniaux, N., Nemos, C., Deb, S., Zhu, B., Dornreiter, I., Hollingsworth, M.A., and Batra, S.K. (2009). The Human RNA Polymerase II-Associated Factor 1 (hPaf1): A New Regulator of Cell-Cycle Progression. PLoS ONE *4*.

Mordes, D.A., Prudencio, M., Goodman, L.D., Klim, J.R., Moccia, R., Limone, F., Pietilainen, O., Chowdhary, K., Dickson, D.W., Rademakers, R., et al. (2018). Dipeptide repeat proteins activate a heat shock response found in C9ORF72-ALS/FTLD patients. Acta Neuropathol. Commun. *6*.

Nguyen, C.T., Langenbacher, A., Hsieh, M., and Chen, J.-N. (2010). The Paf1 complex component Leo1 is essential for cardiac and neural crest development in zebrafish. Dev. Biol. *341*, 167–175.

Ni, J.-Q., Zhou, R., Czech, B., Liu, L.-P., Holderbaum, L., Yang-Zhou, D., Shim, H.-S., Tao, R., Handler, D., Karpowicz, P., et al. (2011). A genome-scale shRNA resource for transgenic RNAi in *Drosophila*. Nat. Methods *8*, 405.

Niblock, M., Smith, B.N., Lee, Y.-B., Sardone, V., Topp, S., Troakes, C., Al-Sarraj, S., Leblond, C.S., Dion, P.A., Rouleau, G.A., et al. (2016). Retention of hexanucleotide repeat-containing intron in C9orf72 mRNA: implications for the pathogenesis of ALS/FTD. Acta Neuropathol. Commun. *4*.

Omer, T., Finegan, E., Hutchinson, S., Doherty, M., Vajda, A., McLaughlin, R.L., Pender, N., Hardiman, O., and Bede, P. (2017). Neuroimaging patterns along the ALS-FTD spectrum: a multiparametric imaging study. Amyotroph. Lateral Scler. Front. Degener. *18*, 611–623.

Perkins, L.A., Holderbaum, L., Tao, R., Hu, Y., Sopko, R., McCall, K., Yang-Zhou, D., Flockhart, I., Binari, R., Shim, H.-S., et al. (2015). The Transgenic RNAi Project at Harvard Medical School: Resources and Validation. Genetics *201*, 843–852.

Porter, S.E., Washburn, T.M., Chang, M., and Jaehning, J.A. (2002). The Yeast Paf1-RNA Polymerase II Complex Is Required for Full Expression of a Subset of Cell Cycle-Regulated Genes. Eukaryot. Cell *1*, 830–842.

Prudencio, M., Belzil, V.V., Batra, R., Ross, C.A., Gendron, T.F., Pregent, L.J., Murray, M.E., Overstreet, K.K., Piazza-Johnston, A.E., Desaro, P., et al. (2015). Distinct brain transcriptome profiles in C9orf72-associated and sporadic ALS. Nat. Neurosci. *18*, 1175–1182.

Prudencio, M., Gonzales, P.K., Cook, C.N., Gendron, T.F., Daughrity, L.M., Song, Y., Ebbert, M.T.W., van Blitterswijk, M., Zhang, Y.-J., Jansen-West, K., et al. (2017). Repetitive element transcripts are elevated in the brain of C9orf72 ALS/FTLD patients. Hum. Mol. Genet. *26*, 3421–3431.

Qiu, H., Hu, C., Gaur, N.A., and Hinnebusch, A.G. (2012). Pol II CTD kinases Bur1 and Kin28 promote Spt5 CTR-independent recruitment of Paf1 complex. EMBO J. *31*, 3494–3505.

Renton, A.E., Majounie, E., Waite, A., Simón-Sánchez, J., Rollinson, S., Gibbs, J.R., Schymick, J.C., Laaksovirta, H., van Swieten, J.C., Myllykangas, L., et al. (2011). A hexanucleotide repeat expansion in C9ORF72 is the cause of chromosome 9p21-linked ALS-FTD. Neuron *72*, 257–268.

Rhodes, D., and Lipps, H.J. (2015). G-quadruplexes and their regulatory roles in biology. Nucleic Acids Res. *43*, 8627–8637.

Rondón, A.G., García-Rubio, M., González-Barrera, S., and Aguilera, A. (2003). Molecular evidence for a positive role of Spt4 in transcription elongation. EMBO J. *22*, 612–620.

Rondón, A.G., Gallardo, M., García-Rubio, M., and Aguilera, A. (2004). Molecular evidence indicating that the yeast PAF complex is required for transcription elongation. EMBO Rep. *5*, 47–53.

Sauer, M., and Paeschke, K. (2017). G-quadruplex unwinding helicases and their function in vivo. Biochem. Soc. Trans. *45*, 1173–1182.

Schönecker, S., Neuhofer, C., Otto, M., Ludolph, A., Kassubek, J., Landwehrmeyer, B., Anderl-Straub, S., Semler, E., Diehl-Schmid, J., Prix, C., et al. (2018). Atrophy in the Thalamus But Not Cerebellum Is Specific for C9orf72 FTD and ALS Patients – An Atlas-Based Volumetric MRI Study. Front. Aging Neurosci. *10*.

Simone, R., Fratta, P., Neidle, S., Parkinson, G.N., and Isaacs, A.M. (2015). G-quadruplexes: Emerging roles in neurodegenerative diseases and the non-coding transcriptome. FEBS Lett. *589*, 1653–1668.

Soutourina, J. (2017). Transcription regulation by the Mediator complex. Nat. Rev. Mol. Cell Biol.

Subramanian, A., Tamayo, P., Mootha, V.K., Mukherjee, S., Ebert, B.L., Gillette, M.A., Paulovich, A., Pomeroy, S.L., Golub, T.R., Lander, E.S., et al. (2005). Gene set enrichment analysis: A knowledge-based approach for interpreting genome-wide expression profiles. Proc. Natl. Acad. Sci. *102*, 15545–15550.

Supek, F., Bošnjak, M., Škunca, N., and Šmuc, T. (2011). REVIGO Summarizes and Visualizes Long Lists of Gene Ontology Terms. PLOS ONE *6*, e21800.

Tan, P.P.C., French, L., and Pavlidis, P. (2013). Neuron-Enriched Gene Expression Patterns are Regionally Anti-Correlated with Oligodendrocyte-Enriched Patterns in the Adult Mouse and Human Brain. Front. Neurosci. *7*.

Van Oss, S.B., Cucinotta, C.E., and Arndt, K.M. (2017). Emerging Insights into the Roles of the Paf1 Complex in Gene Regulation. Trends Biochem. Sci. *42*, 788–798.

Vatovec, S., Kovanda, A., and Rogelj, B. (2014). Unconventional features of C9ORF72 expanded repeat in amyotrophic lateral sclerosis and frontotemporal lobar degeneration. Neurobiol. Aging *35*, 2421.e1-2421.e12.

Vatsavayai, S.C., Nana, A.L., Yokoyama, J.S., and Seeley, W.W. (2019). C9orf72-FTD/ALS pathogenesis: evidence from human neuropathological studies. Acta Neuropathol. (Berl.) *137*, 1–26.

Wang, P., Bowl, M.R., Bender, S., Peng, J., Farber, L., Chen, J., Ali, A., Zhang, Z., Alberts, A.S., Thakker, R.V., et al. (2008). Parafibromin, a Component of the Human PAF Complex, Regulates

Growth Factors and Is Required for Embryonic Development and Survival in Adult Mice. Mol. Cell. Biol. *28*, 2930–2940.

Xie, Y., Zheng, M., Chu, X., Chen, Y., Xu, H., Wang, J., Zhou, H., and Long, J. (2018). Paf1 and Ctr9 subcomplex formation is essential for Paf1 complex assembly and functional regulation. Nat. Commun. *9*.

Xu, Y., Bernecky, C., Lee, C.-T., Maier, K.C., Schwalb, B., Tegunov, D., Plitzko, J.M., Urlaub, H., and Cramer, P. (2017). Architecture of the RNA polymerase II-Paf1C-TFIIS transcription elongation complex. Nat. Commun. *8*, 15741.

Yang, Y., Li, W., Hoque, M., Hou, L., Shen, S., Tian, B., and Dynlacht, B.D. (2016). PAF Complex Plays Novel Subunit-Specific Roles in Alternative Cleavage and Polyadenylation. PLoS Genet. *12*.

Yu, M., Yang, W., Ni, T., Tang, Z., Nakadai, T., Zhu, J., and Roeder, R.G. (2015a). RNA polymerase II–associated factor 1 regulates the release and phosphorylation of paused RNA polymerase II. Science *350*, 1383–1386.

Yu, Z., Goodman, L.D., Shieh, S.-Y., Min, M., Teng, X., Zhu, Y., and Bonini, N.M. (2015b). A fly model for the CCUG-repeat expansion of myotonic dystrophy type 2 reveals a novel interaction with MBNL1. Hum. Mol. Genet. *24*, 954–962.

Yuva-Aydemir, Y., Almeida, S., and Gao, F.-B. (2018). Insights into C9ORF72-Related ALS/FTD from Drosophila and iPSC Models. Trends Neurosci.

Zhou, Q., Li, T., and Price, D.H. (2012). RNA Polymerase II Elongation Control. Annu. Rev. Biochem. *81*, 119–143.

CHAPTER 3: *EIF4B* AND *EIF4H* MEDIATE GR PRODUCTION FROM EXPANDED G4C2 IN A *DROSOPHILA* MODEL FOR *C9ORF72*-ASSOCIATED ALS/FTD.

Acta Neuropathologica Communications, accepted March 26, 2019

Lindsey D. Goodman[1], Mercedes Prudencio[3], Ananth R. Srinivasan[2], Olivia M. Rifai[2], Virginia M-Y. Lee[4], Leonard Petrucelli[3], Nancy M. Bonini[1,2,*].

[1]Neuroscience Graduate Group, Perelman School of Medicine, University of Pennsylvania, Philadelphia, PA 19104, USA

[2]Department of Biology, University of Pennsylvania, Philadelphia, PA 19104, USA

[3]Department of Neuroscience, Mayo Clinic, Jacksonville, FL 32224, USA

[4]Center for Neurodegenerative Disease Research, Perelman School of Medicine, University of Pennsylvania, Philadelphia, PA 19104, USA

*corresponding author, email: nbonini@sas.upenn.edu

Author contributions

This work was performed by LDG under the mentorship of NMB. MP contributed post-mortem patient studies and analyses under the mentorship of LP. ARS performed western blots under the direction of LDG on fibroblast cell lysates collected by LDG. OR setup crosses and collected samples for DsRed fluorescence imaging under the direction of LDG. VYML provided a GR-antibody.

Competing interests

The authors declare that they have no conflicts of interest with the contents of this article.

Acknowledgments

We thank Shizuka B. Yamada and Aaron Gitler at Stanford University for post-screening investigations. Also, thank you to Edward B. Lee, Thomas A. Jongens, Zhaolan (Joe) Zhou and members of the Bonini laboratory for helpful comments. Further thanks to Peter Todd for discussions on unpublished translation factor data. Undergraduate and post-baccalaureate students Luis F. Martinez-Ramirez, Kimberley Newman, Benjamin Gallo, and Ken Yanagisawa provided minimal technical support under the direction of LDG. We thank the Transgenic RNAi Project (TRiP) at Harvard Medical School (NIH/NIGMS R01-GM084947) and the Vienna *Drosophila* Research Center for developing transgenic RNAi fly stocks used in this study. We thank the Center for Neurodegenerative Disease Research (CNDR) at the University of Pennsylvania for the antibody targeting GR. This work was supported by the Systems and Integrative Biology NIH/NIGMS training grant T32-GM07517 (to LDG), Amyotrophic Lateral Sclerosis Association (to MP and LP), NIH/NINDS R35-NS097273 (to LP), NIH/NINDS P01-NS084974 (to LP), NIH/NINDS P01-NS099114 (LP)], Mayo Clinic Foundation (to LP), Robert Packard Center for ALS Research at Johns Hopkins (to LP), Target ALS Foundation (to LP), NIH/NINDS R01-NS078283 (to NMB), and NIH/NINDS R35-NS09727 (to NMB).

Abstract

The discovery of an expanded (GGGGCC)n repeat (termed G4C2) within the first intron of *C9orf72* in familial ALS/FTD has led to a number of studies showing that the aberrant expression of G4C2 RNA can produce toxic dipeptides through repeat-associated non-AUG (RAN-) translation. To reveal canonical translation factors that impact this process, an unbiased loss-of-function screen was performed in a G4C2 fly model that maintained the upstream intronic sequence of the human gene and contained a GFP tag in the GR reading frame. 11 of 48 translation factors were identified that impact production of the GR-GFP protein. Further investigations into two of these, *eIF4B* and *eIF4H*, revealed that downregulation of these factors reduced toxicity caused by the expression of expanded G4C2 and reduced production of toxic GR dipeptides from G4C2 transcripts. In patient-derived cells and in post-mortem tissue from ALS/FTD patients, *EIF4H* was found to be downregulated in cases harboring the G4C2 mutation compared to patients lacking the mutation and healthy individuals. Overall, these data define eIF4B and eIF4H as disease modifiers whose activity is important for RAN-translation of the GR peptide from G4C2-transcripts.

Introduction

In Amyotrophic Lateral Sclerosis (ALS) and Frontotemporal Degeneration (FTD), the presence of a hexanucleotide expansion of >30 GGGGCC repeats (termed G4C2) within the *C9orf72* gene is the most prominent mutation in familial disease (DeJesus-Hernandez et al., 2011; Renton et al., 2011). The mechanisms underlying potential toxicity associated with G4C2 are still being defined with two leading hypotheses centering around gain-of-function mechanisms (Yuva-Aydemir et al., 2018; Balendra and Isaacs, 2018): sequestration of RNA-binding proteins by the aberrant expression of sense- and antisense- G4C2 RNA (Vatovec et al., 2014; Haeusler et al., 2016); repeat-associated non-AUG (RAN-) translation of repeat-containing transcripts produce dipeptides that are toxic to neurons (Ash et al., 2013; Mori et al., 2013; Mann et al., 2013; Gendron et al., 2013; Mackenzie et al., 2013, 2015; Niblock et al., 2016). Five dipeptides can be produced from these transcripts, depending on the reading frame: GA and GR (sense strand associated), PA and PR (antisense strand associated), and GP (produced from both sense and antisense strands).

In recent years, it has become clear that dipeptides produced from G4C2 RNA transcripts cause neurodegenerative effects (Yuva-Aydemir et al., 2018; Balendra and Isaacs, 2018). Of the 5 potential RAN-translation products, GR and PR cause particularly strong degenerative phenotypes in multiple model systems, including *Drosophila* (Freibaum et al., 2015; Mizielinska et al., 2014). Therefore, increasing understanding of the mechanisms underlying expression of these dipeptides would highlight potential therapeutic avenues centered around preventing their expression.

Many mechanistic questions remain regarding RAN-translation in G4C2-associated disease. Recent investigations have drawn a number of parallels between mechanisms underlying general translation (Browning and Bailey-Serres, 2015;

Sonenberg and Hinnebusch, 2009; Spilka et al., 2013) and RAN-translation (Kearse and Wilusz, 2017; Zu et al., 2018), finding that dipeptide production is sensitive to the inhibition/downregulation of canonical translation factors: eIF4E, eIF4G, eIF4A, eIF2α (Green et al., 2017; Tabet et al., 2018; Cheng et al., 2018). Of interest, eIF4A is a DEAD-Box helicase (Andreou and Klostermeier, 2013), and thus may be important for the unwinding of G4C2-RNA for translation. While eIF4A has relative weak helicase activity, this can be significantly stimulated by accessory proteins eIF4B and eIF4H (Rogers et al., 2001; Rozovsky et al., 2008; Nielsen et al., 2011; Sun et al., 2012; Harms et al., 2014; García-García et al., 2015; Vaysse et al., 2015; Sen et al., 2016). These latter factors contain RRM-domains and, importantly, have been reported to interact directly with the G4C2 RNA (Cooper-Knock et al., 2014; Haeusler et al., 2014; Satoh et al., 2014).

In an unbiased, directed screen for canonical translation factors, we identified 11 potential translation factors that modulate GR-production in G4C2-expressing flies. Further investigations into two of these, *eIF4B* and *eIF4H1* (fly orthologue to *eIF4H*), further defined them as modifiers of G4C2-toxicity. Their downregulation significantly reduced GR-levels in animals expressing the repeat. Further investigations into eIF4B and eIF4H in C9+ derived cells revealed that eIF4H was significantly downregulated. *EIF4H* downregulation also occurred in post-mortem tissue from C9+ ALS/FTD compared to C9- ALS/FTD and healthy individuals. This work identifies eIF4B and eIF4H as important disease modifiers that alter RAN-translation of the GR-reading frame.

Results

GFP-tagged GR dipeptides are produced in LDS-$(G4C2)_n$ flies with expanded (>30) repeats.

We previously identified a number of translation factors as modifiers of G4C2-toxicity (Goodman et al., 2019a). To investigate these and other factors in the context of RAN-translation, a new *C9orf72* fly model for ALS/FTD was designed **(Fig. 3-1A)**. This model contained the 114-base pair sequence immediately upstream of the repeat in intron 1 of *C9orf72* in ALS/FTD patient genomes (termed a "leader" sequence; LDS). The addition of this sequence puts the repeat in a more patient-relevant context while this region is likely to influence pathological mechanisms, including RAN-translation (Kearse et al., 2016; Sellier et al., 2017; Todd et al., 2013; Zu et al., 2018). G4C2 expansions can produce three sense-strand associated dipeptides: GA, GR, and GP. Importantly, of these GR is associated with extreme toxicity in multiple models, including flies (Mizielinska et al., 2014; Freibaum et al., 2015). To facilitate investigations into genes that may impact RAN-translation of GR, a GFP tag (lacking an ATG initiation codon) was added 3'-prime of the repeat in the GR-reading frame.

LDS-G4C2 transgenes were randomly inserted into the genome of w^{1118} animals. To define the number of repeats inserted into individual lines, primers that flanked the G4C2 repeat were used to PCR amplify the region (Goodman et al., 2019a). The number of repeats was then calculated from the length of the PCR products, resolved by agarose gel electrophoresis and Bioanalyzer. Two primary fly transgenic lines were defined: a control (CTRL) line containing short $(G4C2)_{\leq 12}$ repeats and an expanded (EXP) line containing $(G4C2)_{\leq 44}$ repeats **(Fig. 3-1B)**. By quantitative-real time PCR (qPCR), these two lines expressed significantly different G4C2 RNA levels **(Fig. 3-1C)**,

most likely the result of variability in insertion site within the fly genome (Levis et al., 1985).

Western immunoblots were used to determine whether a (GR)n dipeptide was produced from the LDS-G4C2 transgenes, despite the absence of an AUG in the GR-reading frame. LDS-G4C2 transgenes were expressed in the fly eye using GMR-GAL4 and protein lysates were prepared from heads. Using an antibody designed to target the GR-dipeptide (Liu et al., 2014), we found that a GR peptide was produced only from the expanded LDS-$(G4C2)_{EXP}$ fly line **(Fig. 3-1D)**. Re-probing with an anti-GFP antibody confirmed that the GR-dipeptides produced were tagged with GFP. GFP expressing control flies confirmed that the molecular weight of the GR/GFP band in LDS-$(G4C2)_{EXP}$ animals was higher than GFP alone. As LDS-$(G4C2)_{EXP}$ lines had 2.5-fold higher RNA expression than the LDS-$(G4C2)_{CTRL}$, longer exposure times were also evaluated and continued to show no GR/GFP signal in LDS-$(G4C2)_{CTRL}$ expressing animals **(Appendix 3: Fig. S3-1)**.

To define potential toxicity associated with LDS-$(G4C2)_{EXP}$, transgenes were expressed in the fly optic system using GMR-GAL4 **(Fig. 3-1E)**. LDS-$(G4C2)_{CTRL}$ animals showed external and internal eye morphologies similar to controls, supporting that the short repeat was not toxic (Freibaum et al., 2015; Goodman et al., 2019a; Kramer et al., 2016a; Mizielinska et al., 2014). In contrast, expression of LDS-$(G4C2)_{EXP}$ caused mild pigment loss externally and dramatic loss of retinal tissue internally, indicative of neurodegeneration.

To further assess GR production, fluorescence imaging of the fly eyes revealed that the LDS-$(G4C2)_{EXP}$ expressing animals produced GFP-positive puncta **(Fig. 3-1F)**. In contrast, a control fluorescence protein (DSRED) did not show puncta formation but rather had a uniform diffuse signal, indicating that the unique punctate fluorescence

pattern seen with LDS-$(G4C2)_{EXP}$ was the result of the GR. LDS-$(G4C2)_{CTRL}$ animals were also imaged and showed no GFP signal, even with 5-10x longer exposure time (data not shown).

Overall, these data indicate that expression of LDS-$(G4C2)_{EXP}$ in flies can induce toxicity and that GFP-tagged GR are produced by an expanded LDS-G4C2 transcript.

A loss of function screen for candidate RAN-translation factors.

Despite recent advances into mechanisms underlying G4C2-associated RAN-translation, a full understanding of which canonical translation factors are involved remains unclear (Green et al., 2017; Tabet et al., 2018; Cheng et al., 2018; Kearse and Wilusz, 2017; Zu et al., 2018). To define translation factors that may mediate GR-associated RAN-translation, we designed a loss-of-function (LOF) fly screen utilizing external eye imaging for toxicity, and GR-GFP fluorescence of the eyes for protein, in LDS-$(G4C2)_{EXP}$ expressing animals **(Fig. 3-2A)**. 48 RNAi (Ni et al., 2011; Perkins et al., 2015) or LOF mutant (Spradling et al., 1995, 1999; Bellen et al., 2004, 2011) fly lines were obtained that target specific translation factors, covering 86% of the 56 known translation factors in the fly (Marygold et al., 2017). 40 of 48 (83.3%) lines were RNAi and 8 of 48 (16.6%) were mutant lines.

28 of the 48 tested LOF lines altered toxicity and/or GR-GFP levels caused by LDS-$(G4C2)_{EXP}$ expression in the fly eye, assessed by comparing images with controls **(Fig. 3-2A, *step 1*)**. These 28 lines were further examined in a fly model that expresses $(GR)_{36}$ from a non-G4C2 transcript (Mizielinska et al., 2014), to determine if they acted downstream of toxic GR-production in the LDS-$(G4C2)_{EXP}$ animals **(Fig. 3-2A, *step 2*)**. 6 of the LOF lines targeting translation factors were found to similarly alter GR-induced toxicity in this model and were not further studied. The remaining 22 LOF lines were

further tested for unspecific effects using quality control experiments **(Fig. 3-2A, *step 3*)** (Chung et al., 2018; Goodman et al., 2019a; Kramer et al., 2016a; Mordes et al., 2018). Specifically, lines were examined to eliminate those that cause an effect when expressed on their own in the eye and tested to confirm no effect on the protein levels of a control (*LacZ*) transgene.

In summary, 20 of the lines did not alter toxicity or GR-GFP levels in LDS-$(G4C2)_{EXP}$ expressing animals **(Fig. 3-2B)**. 17 lines were excluded from further study because they either caused increased GR-GFP levels (1 line), altered LDS-$(G4C2)_{EXP}$ toxicity but not GR-GFP signal (4 lines), could alter GR-toxicity independent of G4C2-RNA (6 lines), or failed quality control experiments (6 lines; termed "unspecific modifiers"). Thus, from the screen of 48 factors, 11 candidate RAN-translation factors were identified **(Table 3-1, Appendix 3: Table S3-2)**.

Depletion of eIF4B or eIF4H1 mitigates toxicity in LDS-$(G4C2)_{EXP}$ animals.

Of the 11 factors that reduced GR-GFP levels, eIF4B and eIF4H1 (fly orthologue to human eIF4H) were intriguing. These two factors have independent and redundant roles in activating eIF4A (Rogers et al., 2001; Rozovsky et al., 2008; Nielsen et al., 2011; Sun et al., 2012; Harms et al., 2014; García-García et al., 2015; Vaysse et al., 2015; Sen et al., 2016) which was recently identified as a RAN-translation factor in a G4C2-model (Green et al., 2017; Tabet et al., 2018). Further, eIF4B and eIF4H had previously been reported to bind G4C2 RNA through RNA recognition motifs (RRMs) (Cooper-Knock et al., 2014; Haeusler et al., 2014; Satoh et al., 2014).

To further investigate *eIF4B* and *eIF4H1* as modifiers of LDS-$(G4C2)_{EXP}$ in flies, a second, independent set of RNAi lines targeting these genes was obtained (termed RNAi-2). All RNAi lines were confirmed to downregulate the expected targets, *eIF4B* or

eIF4H1 **(Fig. 3-3A, Appendix 3: Fig. S3-3A)**. Further, *eIF4B* RNAi did not cause reduced expression of *eIF4H1*, and vice versa, indicating that expression of these two genes is independent and that the RNAi lines are specific. Interestingly, ubiquitous downregulation of *eIF4B* or *eIF4H1* by RNAi produced viable adults with no obvious phenotype **(Fig. 3-3B)**, supporting that these genes are not essential in the fly (also (Hernández et al., 2004)).

The effects of co-expressing *eIF4B*, *eIF4H1*, or control (*Luc*) RNAi with LDS-$(G4C2)_{EXP}$ using GMR-GAL4 were analyzed in the eye. Externally, *eIF4B* or *eIF4H1* RNAi caused reduced toxicity compared to the control RNAi, seen by recovered red pigment and ommatidial organization **(Fig. 3-4A)**. Internally, retinal tissue loss caused by LDS-$(G4C2)_{EXP}$ was also mitigated by depletion of *eIF4B* or *eIF4H1*. Blinded quantification of the total surface area for retina tissue or of tissue depth (at the point of the optic chiasm) revealed that suppression was consistent and significant **(Fig. 3-4B)**. Suppression was recapitulated with a second set of RNAi lines, supporting that the effects seen are the result of downregulating these target genes **(Appendix 3: Fig. S3-4B-C)**.

To further assess if *eIF4B* and *eIF4H1* could be acting downstream of toxic GR-production, RNAi lines targeting *eIF4B*, *eIF4H1*, or control (*Luc*) were co-expressed with $(GR)_{36}$ in the fly eye using GMR-GAL4. The $(GR)_{36}$ transgene produces a GR dipeptide from a non-G4C2 repeat transcript (Mizielinska et al., 2014). In contrast to the effect in LDS-$(G4C2)_{EXP}$ animals, *eIF4B* and *eIF4H1* RNAi increased GR-toxicity in both the external and internal eye **(Fig. 3-4C-D)**. This argues that these genes do not act on the same pathway in GR animals as in LDS-$(G4C2)_{EXP}$ animals. Depletion of either *eIF4B* or *eIF4H1* on their own did not alter normal eye morphology **(Fig. 3-4E-F)**.

Depletion of eIF4B or eIF4H1 reduces GR-production in LDS-$(G4C2)_{EXP}$ animals.

As *eIF4B* and *eIF4H1* are canonical translation factors we hypothesized that they modified LDS-$(G4C2)_{EXP}$ toxicity by mediating translation from the G4C2 transcript. To further test if depletion of these factors reduced GR production, *eIF4B*, *eIF4H1*, or control (*Luc*) RNAi were co-expressed with LDS-$(G4C2)_{EXP}$ in the fly eye and fluorescence imaging was performed **(Fig. 3-5A)**. Blinded quantification of GR-GFP signal in LDS-$(G4C2)_{EXP}$ flies revealed that *eIF4B* depletion caused a 48.3±13% decrease in total GR-GFP fluorescence **(Fig. 3-5B, *grey*)**. Further, *eIF4H1* depletion caused a 65.5±3.7% decrease in GR-GFP fluorescence levels. As puncta formation was associated with fluorescently tagged GR **(see Fig 3-1.)**, additional analyses were performed to define changes in the number of bright GR-GFP puncta and the average size of these puncta (**Fig. 3-5B, *black***). *eIF4B* RNAi reduced the number of puncta from 233 per eye to 44 per eye, an 81% reduction. Additionally, the average size of the puncta per eye was reduced by 63% (7.6μm^2 to 2.8μm^2). *eIFH1* RNAi caused a 91% reduction in the number of GR-GFP puncta per eye (233 to 20) and the size of the puncta was reduced from 7.6μm^2 to 2.4 μm^2, a 68% reduction. Effects on GR-GFP levels and puncta were also seen using the second set of RNAi lines targeting *eIF4B* and *eIF4H1* **(Appendix 3: Fig. S3-3D-E)**.

While we had already determined that *eIF4B* and *eIF4H1* RNAi did not alter toxicity downstream of GR production **(see Fig. 3-4C-D)**, we considered whether their depletion could modify LDS-$(G4C2)_{EXP}$ upstream of translation, on the transcriptional level. To assess this, we used qPCR to measure transcript levels of the LDS-$(G4C2)_{EXP}$ transgene in animals co-expressing control RNAi (*Luc*), *eIF4B* or *eIF4H1* RNAi **(Fig. 3-5B, *light grey*)**. Depletion of *eIF4B* or *eIF4H1* did not alter LDS-$(G4C2)_{EXP}$ RNA levels, further supporting that they act on the translational level.

To test the specificity of *eIF4B* and *eIF4H1* to translation of a G4C2 transcript, we first confirmed specificity of the effect of *eIF4B* and *eIF4H1* RNAi, by assessing whether their depletion had an effect on eye fluorescence of a control DsRed transgene in the fly optic system (GMR-GAL4) **(Fig. 3-5C).** Blinded quantification supported that total fluorescence was unchanged, arguing that the effect in LDS-$(G4C2)_{EXP}$ animals was specific to the GR-tagged fluorescent protein **(Fig. 3-5D)**. We further used western immunoblots to analyze protein levels produced from a control (*LacZ*) transgene in animals co-expressing *eIF4B*, *eIF4H1*, or control (*Luc*) RNAi **(Fig. 3-5E)**. Transgenes were expressed using GMR-GAL4 and protein was extracted from whole heads. Consistent with fluorescence data using DsRed, no significant difference in the amount of β-galactosidase protein translated from the *LacZ* transcript was seen. The second set of RNAi lines targeting *eIF4B* and *eIF4H1* also did not alter protein expression from a control (*LacZ)* gene **(Appendix 3: Fig. S3-3F).** These data are consistent with previous reports that these factors are not essential for general translation (Altmann et al., 1993; Capossela et al., 2012; Coppolecchia et al., 1993; Hernández et al., 2004).

Overall, these data support that *eIF4B* or *eIF4H1* modify LDS-$(G4C2)_{EXP}$ toxicity by mediating toxic GR production. Importantly, translation from the G4C2 transcript is particularly sensitive to their depletion as expression from a control transcript was unaltered under similar conditions.

EIF4H is downregulated in ALS/FTD cases harboring a G4C2 expansion in C9orf72.

Data in the fly supported that *eIF4B* and *eIF4H1* were modifiers of LDS-$(G4C2)_{EXP}$ that could alter the amount of GR produced from the repeat-containing transcript. To further investigate these translation factors in disease, we considered that the expression of the

human orthologues to these factors, *eIF4B* and *eIF4H*, could be dysregulated if they played a critical role in G4C2-associated expression.

eIF4B and eIF4H protein levels were assessed by western immunoblot in primary fibroblast cell lines (**Fig. 3-6.A**; lines described in **Appendix 3: Table S3-3**). The mean expression from four independent C9+-patient derived lines was compared to the mean expression from five independent lines derived from healthy individuals. Interestingly, eIF4B total levels were unchanged while eIF4H levels were reduced by 47.5%. As eIF4B is inhibited by phosphorylation at Ser422 (Raught et al., 2004; Roux and Topisirovic, 2018), we further examined levels of phospho-eIF4B to determine whether this factor was dysregulated by protein modification. No obvious changes were observed in phospho-eIF4B levels visually or relative to total eIF4B in C9+ versus healthy cells.

Data from patient-derived cells supported that eIF4H is dysregulated in C9+ situations. To further assess this finding in patients, total RNA was extracted from post-mortem, cerebellar tissue from 112 ALS/FTD individuals or 22 healthy individuals and the expression from *EIF4B* or *EIF4H* were defined by qPCR **(Fig. 3-6B;** individuals described in **Appendix 3: Table S3-4)**. The ALS/FTD cohort were further broken down based on the presence or absence of the G4C2-repeat expansion in *C9orf72* into 46 C9-ALS/FTD and 66 C9+ ALS/FTD cases. Consistent with protein data from fibroblast lines, *eIF4B* expression was unaltered in disease. Importantly, *eIF4H* was significantly downregulated by 71.2% in C9+ ALS/FTD compared to healthy controls and 54.4% compared to C9- ALS/FTD cases.

These data indicate a significant decrease in *eIF4H* expression in response to the presence of expanded G4C2 in ALS/FTD.

Discussion

Mechanisms underlying repeat-associated non-AUG (RAN-) translation remain unclear despite evidence that this form of translation occurs in disease (Kearse and Wilusz, 2017; Zu et al., 2018). To help define potential RAN-translation factors, we developed a gain-of-function fly model for *C9orf72*-associated ALS/FTD that expressed an expanded GGGGCC hexanucleotide repeat (termed G4C2) downstream of the sequence normally found upstream of the repeat in patients (114bp of intronic DNA found 5'-prime of the repeat in intron 1 of *C9orf72* in ALS/FTD); the transgene expressed also contained a GFP tag downstream of the repeat in the GR reading frame **(see Fig. 3-1)**. Using this model, we screened 48 of 56 canonical translation factors in flies (Marygold et al., 2017) to define those that could impact expression of the GR dipeptide **(see Fig. 3-2 and Appendix 3: Table S3-2)**. 11 candidate RAN-translation factors were defined **(see Table 3-1)**. When depleted, these factors reduced GR-GFP levels, reduced G4C2-induced toxicity, and did not reduce toxicity associated with a non-G4C2 transcript generated toxic GR protein. Further investigations into two of these, *eIF4B* and *eIF4H1* (fly orthologue to *eIF4H*), revealed that their depletion reduced G4C2-induced toxicity and GR-GFP levels, but did not alter G4C2 RNA levels **(see Fig. 3-5 and Appendix 3: Fig. S3-3)**. Investigations into *EIF4B* and *EIF4H* expression in patient-derived cells and in post-mortem tissue revealed that *EIF4H* is significantly downregulated in ALS/FTD patients harboring the G4C2 expansion (C9+ ALS/FTD) **(see Fig. 3-6)**. This effect was not seen in ALS/FTD patients lacking the G4C2 mutation (C9- ALS/FTD), arguing that it is a response to the presence of the repeat. These data highlight *eIF4B* and *eIF4H* as novel factors mediating disease-associated pathways.

To our knowledge, this is the first *in vivo* investigation into canonical translation factors that impact dipeptide production in a *C9orf72*-associated disease model. The

simplest hypothesis is that these factors impact the process of RAN translation from the G4C2 repeat-containing transcript. Interestingly, our data suggest that production of the GR dipeptide requires specific factors as only 11 of 48 canonical translation factors screened altered GR-GFP levels in G4C2-expressing animals. Further, investigations into mammalian systems using DPR-specific antibodies will determine if *eIF4B* or *eIF4H* depletion disrupts expression of multiple DPR and confirm effects on GR production. Although these factors could function to alter GR-production through alternative means versus RAN-translation (i.e. stability of the protein, altered expression of more direct RAN-translation factors), it is compelling that the factors identified converge at key regulatory steps of translation and that the majority of these factors function together or with previously suggested RAN-translation factors **(see Fig. 3-7)**. We ruled out factors that similarly altered toxicity caused by the GR dipeptide, supporting that they act on pathways not associated with toxicity of the GR protein. We also ruled out mechanisms underlying G4C2 transcription and RNA stability for *eIF4B* and *eIF4H*, as G4C2 transcript levels are unaltered by their depletion **(see Fig. 3-5B)**. Although our investigations here focused on *eIF4B* and *eIF4H*, we note that we defined a number of other intriguing factors that act on either on G4C2- and/or GR-associated toxicity (**see Table 3-1**).

The fly model developed herein expresses the LDS-G4C2 transcript as an mRNA, containing a 5'-prime m^7G cap and polyadenylated (poly(A)-) tail. In disease, the G4C2-RNA could exist in multiple forms (Yuva-Aydemir et al., 2018), including: improperly spliced *C9orf72*-mRNA transcripts retaining the repeat (Niblock et al., 2016), properly spliced intronic sequence kept stable by the repeat (Vatovec et al., 2014; Haeusler et al., 2016), altered transcription initiation products (Sareen et al., 2013), or aborted *C9orf72*-transcript products (Haeusler et al., 2014). Interestingly, fly models that

express expanded G4C2 within properly spliced introns do not show dipeptide expression nor toxicity, despite the formation of RNA foci (Tran et al., 2015). Further, improperly spliced *C9orf72*-transcripts can be shuttled from the nucleus to the cytoplasm where they undergo RAN-translation (Hautbergue et al., 2017). Overall, these data support that G4C2 repeats retained in capped and polyadenylated *C9orf72*-mRNA are able to produce toxic dipeptides and are relevant to patients. Whether or not G4C2-associated RAN translation is dependent on the presence of this 5'-prime cap (and poly(A)-tail) is still debated (Cheng et al., 2018; Green et al., 2017; Tabet et al., 2018) (Cheng et al., 2018; Green et al., 2017; Tabet et al., 2018).

Our investigations draw parallels between the canonical functions of translation factors (Marygold et al., 2017) and RAN-translation **(see Model, Figure 1-3)**. However, there are multiple types of translation that may be pertinent to disease, including cap-independent mechanisms, such as IRES translation (Green et al., 2016; Kearse and Wilusz, 2017; Shatsky et al., 2018; Sonenberg and Hinnebusch, 2009). Of the 11 candidate RAN-translation factors we identified, 4 have been reported to function in cap-independent translation: eIF4B (Khan and Goss, 2012; Sharma et al., 2015), eIF4H (Vaysse et al., 2015), eIF5B (Galmozzi et al., 2012), eIF2β (Liberman et al., 2015). Interestingly, eIF4B or eIF4H significantly strengthen eIF4A-mediated unwinding of longer, more complex 5' UTRs in transcripts (Rozovsky et al., 2008; Sun et al., 2012; Vaysse et al., 2015; Sen et al., 2016). This activity is thought to mediate scanning of the 5' UTR for translation start sites (Spirin, 2009) and recruitment of ribosomal subunits (Sharma et al., 2015; Walker et al., 2013). Overall, these data suggest a model for G4C2-associated RAN-translation where eIF4B/eIF4H and eIF4A mediate dipeptide production during this scanning process (Green et al., 2016; Tabet et al., 2018). Further,

frame-shifting during scanning could result in the production of all three sense-strand associated dipeptides (GA, GR, GP) from a near-cognate alternative start codon, CUG, found upstream of the repeat in the GA-reading frame (Tabet et al., 2018).

In addition to their involvement in non-canonical translation and in stimulating eIF4A (previously reported as a RAN-translation factor (Green et al., 2017; Tabet et al., 2018), we chose to focus on eIF4B and eIF4H as they are RNA-binding proteins (RBPs) containing homologous RNA recognition motifs (RRMs) (Richter-Cook et al., 1998). Screens for RBPs that interact with G4C2-RNA identified both eIF4B and eIF4H, supporting our data that they function in translation from G4C2 transcripts (Cooper-Knock et al., 2014; Haeusler et al., 2014; Satoh et al., 2014). Both eIF4B and eIF4H can independently stimulate the helicase activity of eIF4A during translation (Rogers et al., 2001; Rozovsky et al., 2008; Nielsen et al., 2011; Sun et al., 2012; Harms et al., 2014; García-García et al., 2015; Vaysse et al., 2015; Sen et al., 2016) while key differences between them are noted. Structural data supports that eIF4H is constitutively active while eIF4B contains a regulatory carboxyl domain containing multiple phosphorylation sites (Méthot et al., 1996; Raught et al., 2004). This may explain why *EIF4H* is downregulated in C9+ ALS/FTD but not *EIF4B* **(see Fig. 3-6),** as eIF4B can be regulated by de/phosphorylation. However, no significant changes were observed for phospho-eIF4B at Ser422, an inhibitory modification (Sonenberg and Hinnebusch, 2009; Roux and Topisirovic, 2018), in four C9+ derived cell lines versus five control cell lines. Extended analyses are needed to increase the sample size and to test for eIF4B phosphorylation at other marks (Bettegazzi et al., 2017; van Gorp et al., 2009). Overall, we hypothesize that *EIF4H* is downregulated as the result of compensatory mechanisms: cells may actively downregulate *EIF4H* to reduce expression of toxic GR dipeptide. Alternatively, as eIF4H had previously been reported to bind G4C2-RNA

(Cooper-Knock et al., 2014; Haeusler et al., 2014; Satoh et al., 2014), the reduced *EIF4H* RNA levels could be the result of a more complex feedback loop: as eIF4H protein is sequestered by G4C2 RNA foci, cells may respond by downregulating *EIF4H* transcription under the assumption that there is plenty of this translation factor present. Localization studies in patient tissue are needed to determine if eIF4H is indeed sequestered into G4C2-foci. In either scenario, data supports that eIF4H plays an important role in C9+ disease while further investigations would help define its role in disease progression.

Studies in multiple model systems support that *eIF4B* and *eIF4H* loss does not inhibit global translation, including yeast (Altmann et al., 1993; Coppolecchia et al., 1993), flies (Hernández et al., 2004), and mice (Capossela et al., 2012). Interestingly, yeast and flies **(see Fig. 3-3B)** with downregulated *eIF4B* or *eIF4H* are viable (Altmann et al., 1993; Coppolecchia et al., 1993; Hernández et al., 2004) and *EIF4H*$^{+/-}$ mice do not have notable deficits (Capossela et al., 2012); although *eIF4B* and *eIF4H* have been suggested to be important for brain development (Bettegazzi et al., 2017; Capossela et al., 2012; Eom et al., 2014; Rode et al., 2018). The downstream consequences of *EIF4H* downregulation in C9+ ALS/FTD may be broader than simply altering RAN-translation: depletion of *eIF4B* and *eIF4H* in cultured cells has been shown to induce stress granule formation (Mokas et al., 2009). Interestingly, as *EIF4H* expression is reduced in C9+ ALS/FTD and C9+ derived cells, this raises a potential connection between that downregulation and mechanisms underlying TDP-43 pathology/toxicity (Coyne et al., 2017; Fernandes et al., 2018). Further, our data in GR-expressing flies argues that the depletion of these factors downstream of GR-production can feed into pathways disrupted by this toxic dipeptide **(see Fig. 3-4C-D)** (Kanekura et al., 2016; Suzuki et al., 2018; Tao et al., 2015; Zhang et al., 2018).

In conclusion, in an unbiased, targeted screen we identified *eIF4B* and *eIF4H* as canonical translation factors that, when depleted in flies, disrupted toxicity caused by the expression of expanded G4C2 RNA. Interestingly, *EIF4H* was downregulated in C9+ ALS/FTD patients, indicating a distinct role in *C9orf72*-associated disease. These factors may represent unique G4C2 modifiers that couple RAN-translation to dysregulation of RNA metabolism in disease (Coyne et al., 2017; Ito et al., 2017; Zhao et al., 2018).

Methods and materials

Patient samples and clinical, genetic and pathological assessments

Participant information is summarized in Appendix 3: Table S3-4. Protocols were approved by the Mayo Clinic Institutional Review Board and Ethics Committee. All participants (or authorized family members) were provided written informed consent before information gathering, autopsies and postmortem analyses. Trained neurologists diagnosed patients with ALS and/or FTD after reviewing neurological and pathological information. The presence or absence of an expanded G4C2 within intron 1 of *C9orf72* was done using a previously established protocol for repeat-primed polymerase chain reaction (DeJesus-Hernandez et al., 2011).

Drosophila work

Stocks were maintained on standard cornmeal-molasses medium. Fly lines used are detailed in Appendix 3: Tables S3-2 and S3-5. Fly lines obtained from Bloomington *Drosophila* Stock Center (BDSC) and Vienna *Drosophila* Resource Center (VDRC) are noted.

Characterization of LDS-(G4C2)n fly models

Transgenes were inserted into pUAST vectors and randomly inserted into w^{1118} fly genomes. The LDS-G4C2 model has a 5' leader sequence (LDS) inserted immediately

upstream of the G4C2 repeats, 114bp of sequence upstream of the repeat in intron 1 of *C9orf72* in patients, and a 3' GFP tag in the GR reading frame. Repeat-length determination: Genomic DNA was extracted from individual fly lines and the transgenes present were amplified by PCR using primers designed to flank the repeat (Appendix 3: Table S3-6). Amplification was done using a KAPA HiFi HotStart kit (Kappa #KK2501) and PCR product sizes were quantified using agarose gels and a Bioanalyzer, previously described (Goodman et al., 2019a). Control w^{1118} animals were included in experiments and showed no signal. RNA expression: Transgenes were expressed as previously described using HS-Gal4 (Goodman et al., 2019a) and RNA levels were assessed by qPCR, using primers designed to amplify the GFP tag (Appendix 3: Table S3-6). Control w^{1118} animals were included in experiments and showed no signal.

LOF external fly eye screen

Publicly available RNAi (Ni et al., 2011; Perkins et al., 2015) or mutant (Bellen et al., 2004, 2011; Spradling et al., 1995, 1999) loss-of-function (LOF) fly lines targeting canonical translation factors were obtained from the Bloomington *Drosophila* Stock Center (BDSC). Additional UAS-RNAi lines targeting *eIF4B* and *eIF4H1* were obtained from Vienna *Drosophila* Resource Center (VDRC) (Dietzl et al., 2007).

External eye imaging: LOF males were crossed to recombinant females: UAS-LDS-$(G4C2)_{EXP}$, GMR-GAL4 (III) (26°C). Multiple w^- and w^+ controls were setup with every experiment to assess any natural variability, including a UAS-Luc RNAi (BDSC # 31603) and w^{1118}; UAS-DSRED. External eyes for 1-2d progeny were imaged on a Leica APO16 microscope as described (Goodman et al., 2019a). Any changes to the ommatidia organization, eye size, pigmentation, and ability to eclose from pupae were noted. Resulting phenotype was categorized into one of six groups: suppressors, mild

suppressors, no effect, mild enhancers, enhancers, and lethal enhancers (Appendix 3: Fig. S3-2).

External eye fluorescence imaging: LOF males were crossed to recombinant females: UAS-LDS-$(G4C2)_{EXP}$, GMR-GAL4 (III) (26°C) and 1-2d progeny were imaged on a Leica DM6000B and quantified as previously described (Goodman et al., 2019a). w^- or w^+ controls were used for accurate comparisons depending on the background of the LOF lines and the final genotypes of animals. Any changes to the GR-GFP levels using LUT Z-stacked images were noted. Resulting phenotype was categorized into one of six groups: suppressors, mild suppressors, no effect, mild enhancers, enhancers, and lethal enhancers (Appendix 3: Fig. S3-2). Researchers were blinded to the LOF targets during screening. Modifiers of LDS-$(G4C2)_{EXP}$ toxicity and/or GR-GFP levels were further assessed in GMR-GAL4 > UAS-(GR)36 animals. Modifier crosses were repeated 3+ independent times to confirm reproducibility of results.

Quality control experiments defining unspecific LOF lines were performed as previously described (Goodman et al., 2019a).

Fly RNAi efficacy

All control and RNAi lines are defined in Appendix 3: Table S3-5. RNAi efficacy was determined using Da-GAL4 (adults or larvae) as previously described (Goodman et al., 2019a; McGurk and Bonini, 2012).

Fibroblast cells

Cultured using standard protocols in DMEM complete media: 15% FBS (Sigma), 1x MEM Amino Acids (ThermoSci # 11130051), 1% pen/strep, DMEM (high glucose, plus sodium pyruvate). Cells were maintained in a 5% CO_2 incubator at 37°C.

Western immunoblots (WB)

Fly tissue: Triplicate samples of 5-10 heads per genotype were homogenized using disposable pellet/pestles tissue grinders (Kimble Chase #749520-0000) and motor (Kimble Chase #749540-0000). For βgal: heads were directly homogenized into 1X NuPAGE LDS sample buffer. For GR/GFP: heads were homogenized into RIPA buffer (50mM Tris-HCL (pH 7.5), 150mM NaCl, 1% NP-40, 50mM NaF, 0.5% DOC), plus protease inhibitors (Sigma # 05892970001), 1mM PMSF, and 1mM DTT.

Fibroblast cells: cells were lysed in RIPA buffer plus protease, 1mM PMSF, and 1mM DTT, and phosphatase inhibitors (Sigma # 04906845001) for 30min at 4^{o}C. All RIPA lysates: quantified by Bradford; 20µg of protein was run per lane. All WBs: run using a standard protocol with Invitrogen's XCell SureLock blot system, 4-12% Bis-Tris NuPAGE gels and a wet transfer with PVDF membrane, except βgal which was transferred with an iBlot dry transfer system (program 2, 8min) and nitrocellulose membrane. Antibodies: anti-βgalactosidase (Promega #Z3781, 1:2,000), anti-αTubulin (DSHB #AA4.3, 1:2,000), anti-GFP^{JL8} (Takara #632380, 1:10,000), anti-GR (gift from V. M-Y. Lee #2316, 1:1,000). *H. sapiens* antibodies: anti-eIF4B (Cell Signaling #3592, 1:1,000), anti-eIF4H (Cell Signaling #3469,1:1,000), anti-phospho-eIF4B (Cell Signaling #3591,1:1,000), anti-GAPDH (Sigma #G8795, 1:5,000). Secondary antibodies: Mouse-HRP (Jackson Immunoresearch Labs #115-035-146, 1:5000), Rabbit-HRP (Jackson Immunoresearch Labs #111-035-144, 1:5000) (Berson et al., 2017). Blots were analyzed using Amersham ECL Prime Detection Reagent and imaged on an Amersham Imager 600.

Quantitative real-time PCR (qPCR)

All primers are defined in Appendix 3: Table S3-6. For both fly and human qPCRs, protocols are previously described with the following changes (Goodman et al., 2019a). Flies: For Da-GAL4 assays, triplicate samples of 5 whole animals were processed per

condition. For GMR-GAL4 assays, triplicate samples of 20 fly heads (1-2d) were processed per condition. Humans: Total RNA was extracted from frozen postmortem tissue from the cerebellum using the RNAeasy Plus Mini Kit (QIAGEN), previously described (Prudencio et al., 2015). RNA integrity (RIN) was verified on an Agilent 2100 bioanalyzer. RIN values ranged from 6.7 to 10, with most of the samples falling between 9.1 and 9.8.

Statistical analysis and data availability

GraphPad Prism 8.00 software was used to develop all graphs and for all statistical analyses. P-values < 0.05 were considered significant. All relevant data is included within the manuscript and Appendix 3. Additional inquiries can be directed to the corresponding author, including reagent requests. No statistical methods were used to predetermine sample sizes and data distributions were assumed to be normal, similar to previous work (Berson et al., 2017; Elden et al., 2010; Goodman et al., 2019a; Kim et al., 2014; Kramer et al., 2016b; McGurk and Bonini, 2012; Mizielinska et al., 2014; Prudencio et al., 2015, 2017). Fly and fibroblast data: A two-tailed unpaired student t-test or one-way ANOVA with Tukey's multiple comparisons test was performed when appropriate. Researchers were blinded to the genotype of all samples to maintain unbiased scoring. Human qPCRs: Nonparametric, one-way ANOVAs with Dunn's multiple comparisons test were performed as data distribution was not normal.

Chapter 3: Tables

Table 3-1: Candidate RAN translation factors.

Fly Gene	Human orthologue	type of LOF line	LDS-$(G4C2)_{EXP}$		$(GR)_{36}$	Alone	Control (*LacZ*) expression
			Toxicity	GR-GFP levels	Toxicity	Phenotype	
eIF4B	*EIF4B*	RNAi					
eIF4H1	*EIF4H*	RNAi					
eIF5B	*EIF5B*	RNAi					
eIF5	*EIF5*	RNAi					
eIF4E3	*EIF4E*	RNAi					
eIF4E4	*EIF4E*	RNAi					
eIF4E7	*EIF4E*	mutant					
eIF2β	*EIF2S2*	RNAi					
eIF3d1	*EIF3D*	mutant					
eIF4E5	*EIF4E*	RNAi					
eIF3i	*EIF3I*	RNAi					

Color scheme

decreased	mild decrease	no effect	mild increase	increased	not tested

Chapter 3: Figures and legends

Figure 3-1

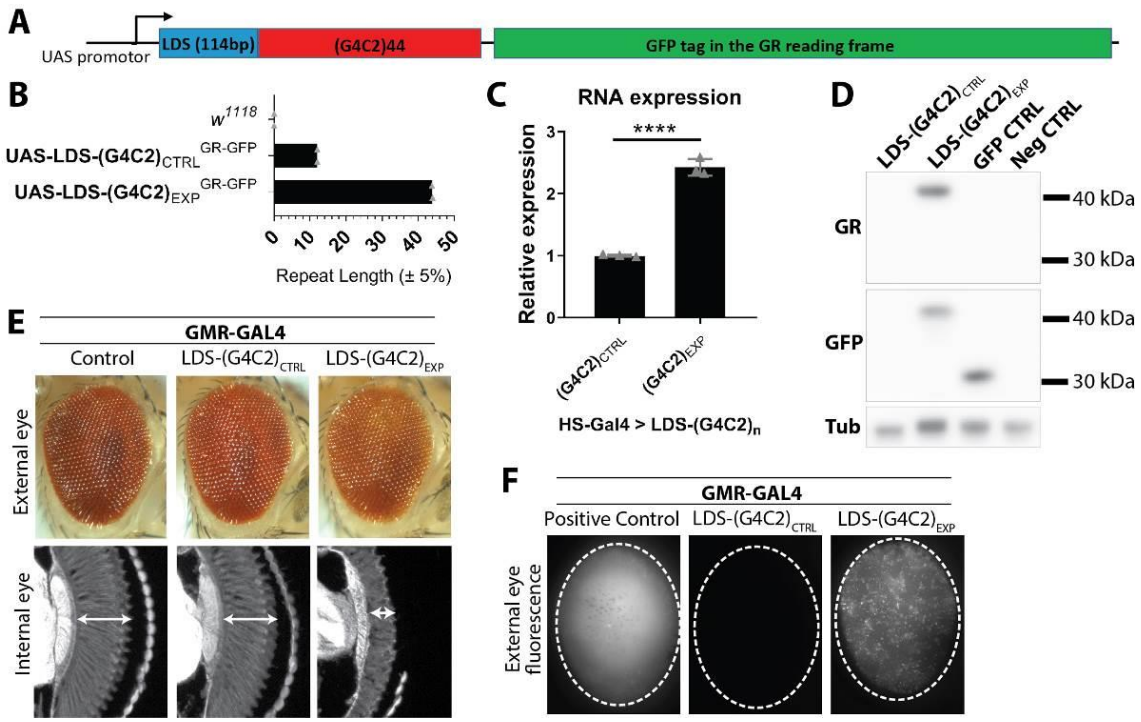

Figure 3-1: Expanded G4C2 transgenes produce GFP-tagged GR.

A. A new transgenic (G4C2)n model was developed to look at RAN-translation of the GR reading frame. A "leader" sequence (LDS) was added 5' of the repeat: 114bp of intronic sequence found upstream of the repeat in patient samples. The GR reading frame has an in-frame GFP coding sequence 3' of the repeat that lacks an ATG initiation. **B.** To define the number of repeats inserted into genomes of w^{1118} transgenic flies, PCR reactions were developed that amplified the repeat and its flanking region. The number of repeats were calculated from PCR product lengths measured on a Bioanalyzer and agarose gel. Shown: the maximum number of repeats found in the control (CTRL) or expanded (EXP) G4C2 fly lines; individual data points from 2 independent DNA preps with mean. **C.** qPCR analysis for RNA levels between control and expanded G4C2 fly lines. Shown: individual data points with mean±SD. Statistics: unpaired student t-test, p-value ****<0.0001. **D.** Western immunoblots confirmed GR is produced and successfully tagged with GFP in EXP-G4C2 flies. No GR/GFP was detected in control G4C2 flies, even with overexposure **(Appendix 3: Fig. S3-1)**. Uncropped westerns (**Appendix 3: Fig. S3-4) E.** External and internal eye analysis in animals expressing G4C2 or control (DSRED) transgenes using GMR-GAL4. Degeneration was seen only in LDS-$(G4C2)_{EXP}$ animals: external pigment loss and reduced integrity of internal retina tissue. **F.** External eye imaging for fluorescence caused by transgene expression. Positive (DSRED) control flies show uniform diffuse signal. Control G4C2 flies show no signal, even with increased exposure (data not shown). Expanded G4C2 flies show GFP puncta. Shown (E-F): representative images while all conditions were tested 2+ times. For full genotypes see **Appendix 3: Table S3-1**.

Figure 3-2

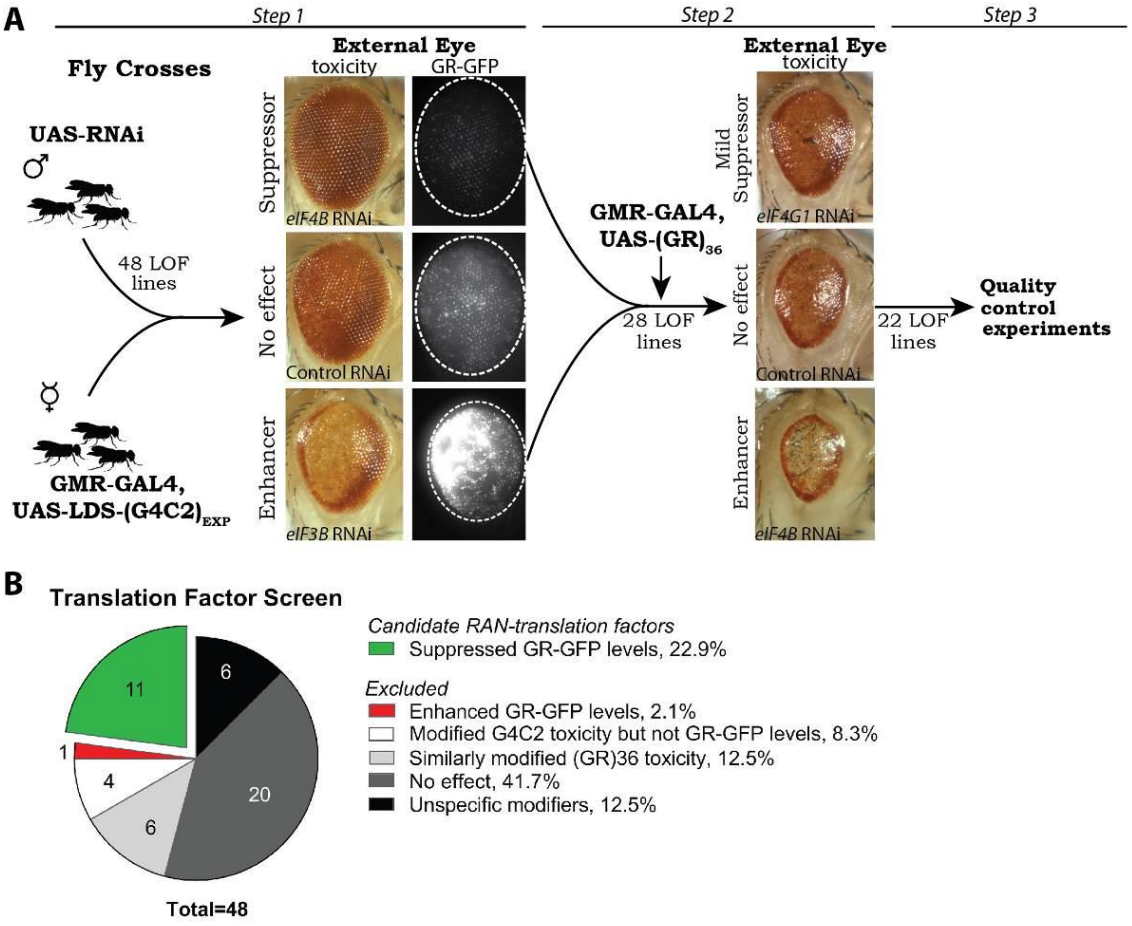
A
Step 1
Step 2
Step 3
Fly Crosses
UAS-RNAi
48 LOF lines
GMR-GAL4, UAS-LDS-(G4C2)EXP
External Eye
toxicity
GR-GFP
Suppressor
eIF4B RNAi
No effect
Control RNAi
Enhancer
eIF3B RNAi
GMR-GAL4, UAS-(GR)36
28 LOF lines
External Eye
toxicity
Mild Suppressor
eIF4G1 RNAi
No effect
Control RNAi
Enhancer
eIF4B RNAi
22 LOF lines
Quality control experiments
B
Translation Factor Screen
11
6
1
4
20
6
Total=48
Candidate RAN-translation factors
Suppressed GR-GFP levels, 22.9%
Excluded
Enhanced GR-GFP levels, 2.1%
Modified G4C2 toxicity but not GR-GFP levels, 8.3%
Similarly modified (GR)36 toxicity, 12.5%
No effect, 41.7%
Unspecific modifiers, 12.5%

Figure 3-2: A screen of translation factors reveals those important for expression of GR from $(G4C2)_{EXP}$.

A. To identify canonical translation factors that may be involved in RAN translation of G4C2 in the GR reading frame, a loss-of-function (LOF) based screen was designed utilizing previously developed RNAi (Ni et al., 2011; Perkins et al., 2015) or LOF mutant fly lines (Spradling et al., 1995, 1999; Bellen et al., 2004, 2011) targeting 48 of 56 (86%) known translation factors (Marygold et al., 2017). Individual translation factors were downregulated in animals expressing LDS-$(G4C2)_{EXP}$ and any that altered the external eye phenotype and/or GR-GFP levels were defined (Step 1). These 28 LOF lines were further tested in (GR)36 expressing animals, defining 6 that acted similarly on GR-associated toxicity (Step 2). Additional quality control experiments excluded LOF lines that altered expression from a control (LacZ) transgene by western immunoblot and/or altered a WT eye morphology when expressed alone, as described (Step 3) (Chung et al., 2018; Goodman et al., 2019a; Kramer et al., 2016a). **B.** Summary of screen results. Overall, 11 translation factors were identified as candidate RAN translation factors as their depletion reduced GR-GFP levels. Overall, excluded LOF lines either: altered toxicity of G4C2 flies but did not alter GR-GFP levels, similarly altered toxicity in a non-G4C2, GR fly model arguing that these acted downstream of GR production, had no effect on G4C2 toxicity or GR-GFP levels, or were “unspecific” modifiers identified by quality control experiments. Shown: representative images while all RNAi were tested 2+ times for effects under each condition. Details on LOF lines used and complete results with each line can be found in **Appendix 3: Table S3-2**. For full genotypes and RNAi lines see **Appendix 3: Table S3-1**.

Figure 3-3

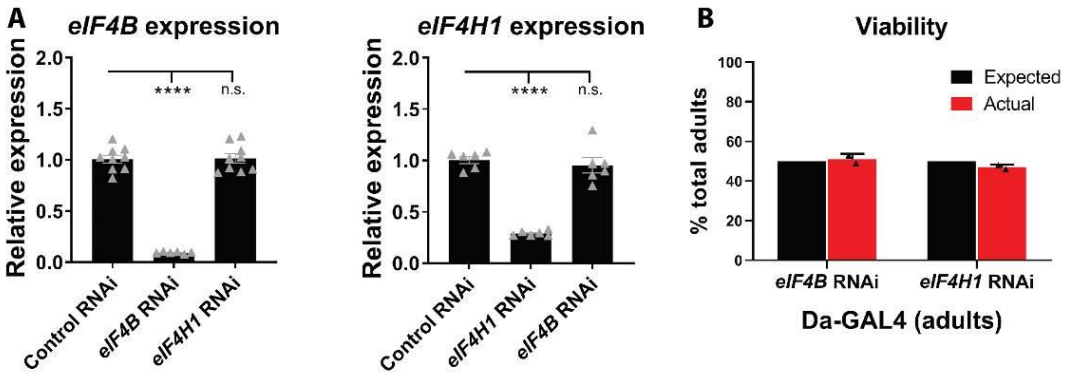

Figure 3-3: Analysis of eIF4B and eIF4H1 RNAi in control flies.

A. RNA levels produced from *eIF4B* or *eIF4H1* were assessed by qPCR in flies ubiquitously expressing RNAi (by Daughterless-GAL4). Statistics: one-way ANOVAs with Tukey's multiple comparison correction, p-values ****<0.0001, ***<0.001, **<0.01, *<0.05, no significance >0.05. Shown: individual data points from 2 independent experiments with mean±SEM. **B.** Viability studies in *Drosophila* reveal that RNAi-depletion of eIF4B or eIF4H1 do not significantly alter the number of adult flies expected to eclose. Shown: ratio of progeny from two individual crosses with RNAi compared to sibling animals with the balancer chromosome that reach adulthood (1-2d adult animals). Comparing the # progeny that eclose from a single vial compensates for differences in mating variability, fertilized eggs laid, among other variables. However, we note that the presence of the balancer chromosome could potentially cause mild sub-viability to adulthood. Crosses: *RNAi/CyO* x *Da-GAL4 (III)*; counted progeny: *RNAi/+; Da-GAL4/+* and *CyO/+; Da-GAL4/+*. RNAi lines: control (JF01355), *eIF4B* RNAi (HMS04503), *eIF4H1* RNAi (HMS04504). For full genotypes see **Appendix 3: Table S3-1**.

Figure 3-4

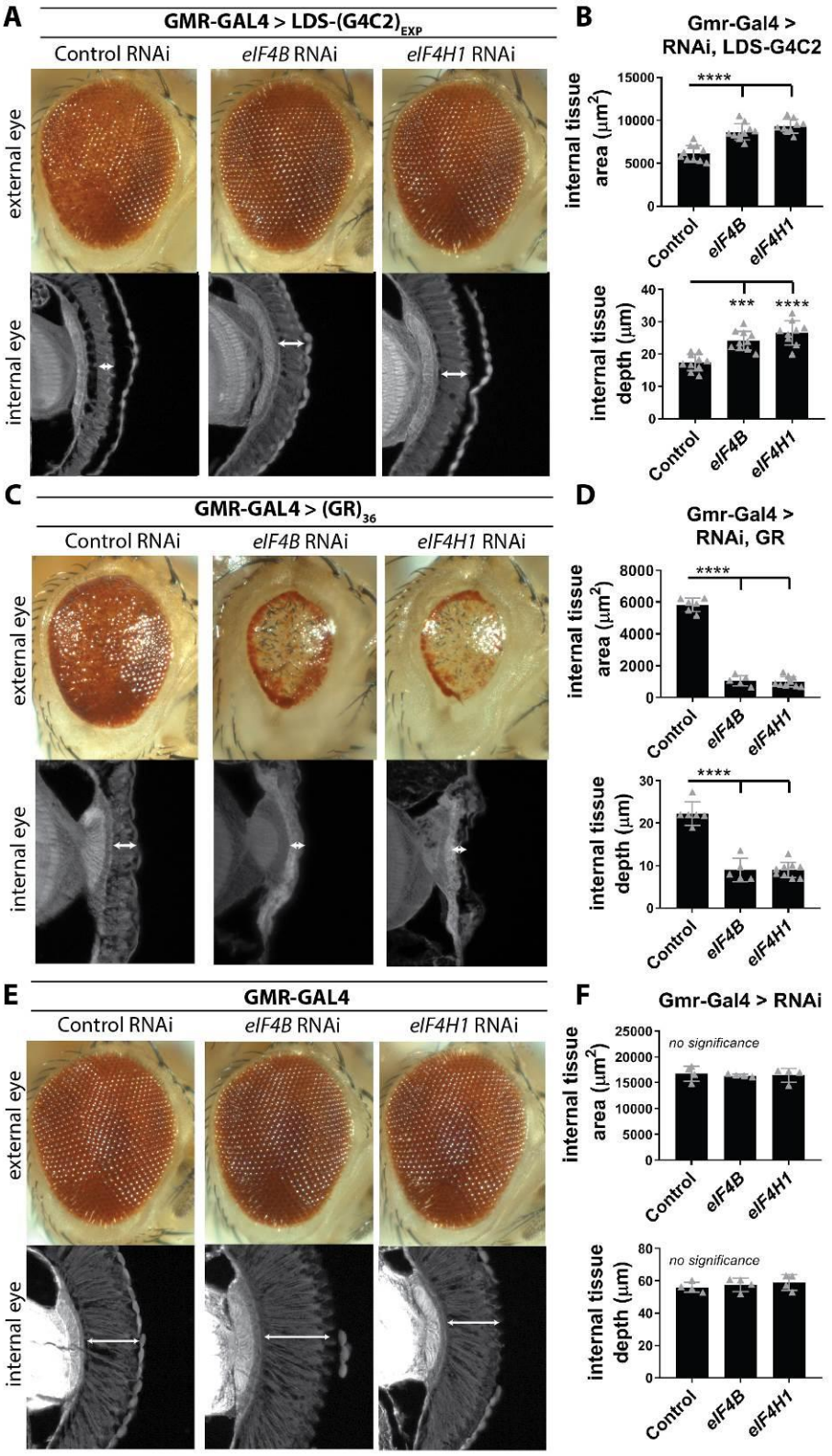
A
GMR-GAL4 > LDS-(G4C2)EXP
Control RNAi
eIF4B RNAi
eIF4H1 RNAi
external eye
internal eye
B
Gmr-Gal4 > RNAi, LDS-G4C2
internal tissue area (μm2)
****
Control
eIF4B
eIF4H1
internal tissue depth (μm)
***
****
C
GMR-GAL4 > (GR)36
D
Gmr-Gal4 > RNAi, GR
E
GMR-GAL4
F
Gmr-Gal4 > RNAi
no significance

Figure 3-4: Depletion of *eIF4B* and *eIF4H1* selectively suppresses LDS-$(G4C2)_{EXP}$ associated toxicity.

A. Using GMR-GAL4, RNAi-mediated depletion of *eIF4B* or *eIF4H1* in LDS-$(G4C2)_{EXP}$ expressing flies results in reduced toxicity in both the external and internal eye: seen externally by recovered pigment and ommatidial structure, seen internally by recovered retinal tissue integrity. **B.** Blinded quantification of internal retina tissue was done by measuring the total surface area of tissue present and by measuring the depth of the tissue at the position where the optic chiasm occurs. n=9-10 animals per genotype. **C.** *eIF4B* or *eIF4H1* RNAi was expressed in (GR)36 flies (GMR-GAL4) and effects on GR-associated toxicity were observed in the external and internal eye. **D.** Blinded quantification of internal retina tissue. n=5-9 animals per genotype. **E.** *eIF4B* or *eIF4H1* RNAi was expressed in control flies (GMR-GAL4) and effects on the normal eye were observed externally and internally. **F.** Blinded quantification of internal retina tissue. n=4 animals per genotype. For graphs, shown are individual data points representing 1 animal with mean±SD. Statistics: one-way ANOVAs with Tukey's multiple comparison correction, p-values ****<0.0001, ***<0.001, **<0.01, *<0.05, no significance >0.05. RNAi lines: control (JF01355), eIF4B (HMS04503), eIF4H1 (HMS04504). For full genotypes see **Appendix 3: Table S3-1**.

Figure 3-5

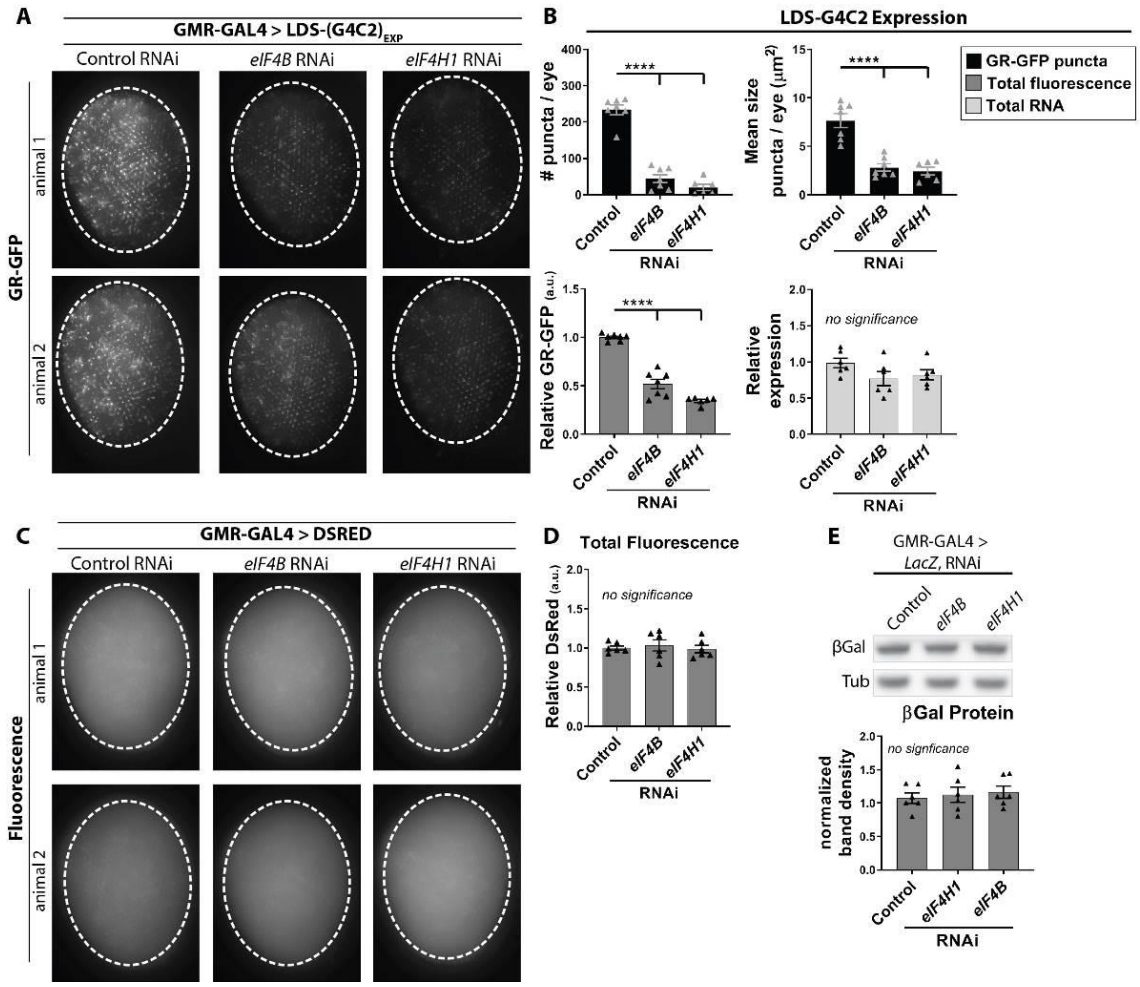
A
GMR-GAL4 > LDS-(G4C2)EXP
Control RNAi
eIF4B RNAi
eIF4H1 RNAi
GR-GFP
animal 1
animal 2
B
LDS-G4C2 Expression
GR-GFP puncta
Total fluorescence
Total RNA
puncta / eye
Mean size puncta / eye (μm2)
Relative GR-GFP (a.u.)
Relative expression
no significance
Control
eIF4B
eIF4H1
RNAi
C
GMR-GAL4 > DSRED
Fluorescence
D
Total Fluorescence
Relative DsRed (a.u.)
E
GMR-GAL4 > LacZ, RNAi
βGal
Tub
βGal Protein
normalized band density
no signficance

Figure 3-5: *eIF4B* and *eIF4H1* RNAi selectively reduce GR-GFP levels produced from LDS-$(G4C2)_{EXP}$.

A. Fluorescence imaging in LDS-$(G4C2)_{EXP}$ expressing flies shows that depletion of *eIF4B* or *eIF4H* by RNAi results in reduced GR-GFP levels (GMR-GAL4). **B.** Blinded quantification of GR-GFP signal in LDS-$(G4C2)_{EXP}$ animals relative to the signal in control RNAi animals. Analysis of GR-GFP puncta number and size are shown in *black*. Total GR-GFP signal is shown in *grey*. n=6-7 animals per genotype. Further, qPCR was used to quantify RNA levels in LDS-$(G4C2)_{EXP}$ flies co-expressing control, *eIF4B*, or *eIF4H1* RNAi, shown in *light grey*. **C.** A control fluorescent protein, DsRed, was similarly expressed in the fly eye with RNAi to control, *eIF4B*, or *eIF4H*. **D.** Blinded quantification of DsRed fluorescence shows no effect by RNAi. n=6 animals per genotype. **E.** A representative western immunoblot image for β-Galactosidase in *LacZ* flies co-expressing control, *eIF4B*, or *eIF4H1* RNAi. Uncropped westerns (**Appendix 3: Fig. S3-4).** Blinded quantification of β-Galactosidase western immunoblots normalized to the loading control, Tubulin. For graphs, shown are individual data points from 2 independent assays with mean±SEM. Statistics: one-way ANOVAs with Tukey's multiple comparison correction, p-values ****<0.0001, ***<0.001, **<0.01, *<0.05, no significance >0.05. RNAi lines: control (JF01355), *eIF4B* (HMS04503), *eIF4H1* (HMS04504). For full genotypes see **Appendix 3: Table S3-1**.

Figure 3-6

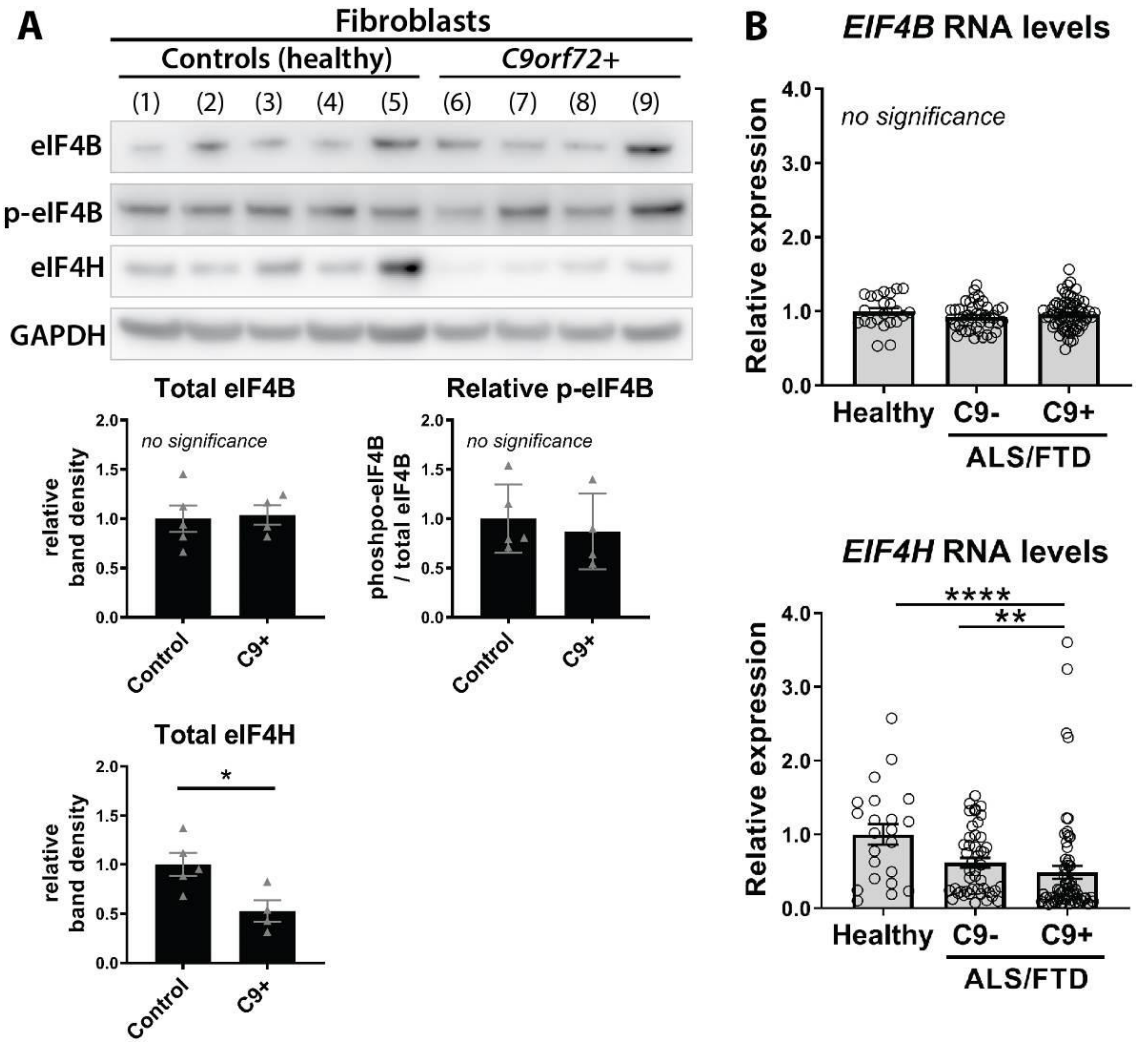
A
Fibroblasts
Controls (healthy)
C9orf72+
(1) (2) (3) (4) (5) (6) (7) (8) (9)
eIF4B
p-eIF4B
eIF4H
GAPDH
Total eIF4B
relative band density
no significance
Control
C9+
Relative p-eIF4B
phoshpo-eIF4B / total eIF4B
no significance
Control
C9+
Total eIF4H
relative band density
*
Control
C9+
B
EIF4B RNA levels
Relative expression
no significance
Healthy
C9-
C9+
ALS/FTD
EIF4H RNA levels
Relative expression
****
**
Healthy
C9-
C9+
ALS/FTD

Figure 3-6: *EIF4H* is downregulated in C9+ ALS/FTD.

A. Western immunoblots were used to define changes in eIF4B or eIF4H protein levels from 5 independent control or 4 independent C9+ derived fibroblast cell lines. Data are relative to controls. Quantification of total protein was done after normalizing to loading, using GAPDH. Phospho-eIF4B quantification was further normalized to total eIF4B. Statistics: unpaired student t-tests. Shown: each data point represents 1 cell line with mean±SEM; the mean data from 2 independent protein preparations is shown per line. **B.** RNA levels of *EIF4B* or *EIF4H* were assessed by qPCR in human cerebellar tissue from healthy individuals or ALS/FTD patients with (C9+) or without (C9-) the G4C2 expansion in *C9orf72*. n = 22 (healthy), 46 (C9- ALS/FTD), 66 (C9+ ALS/FTD). Statistics: one-way ANOVAs with Dunn's multiple comparison correction. Shown: individual data points representing 1 individual with mean±SEM. Cell line details: **Appendix 3: Table S3-3.** Patient details**: Appendix 3: Table S3-4.** p-values ****<0.0001, ***<0.001, **<0.01, *<0.05, no significance >0.05.

Bibliography

Altmann, M., Müller, P.P., Wittmer, B., Ruchti, F., Lanker, S., and Trachsel, H. (1993). A Saccharomyces cerevisiae homologue of mammalian translation initiation factor 4B contributes to RNA helicase activity. EMBO J. *12*, 3997–4003.

Andreou, A.Z., and Klostermeier, D. (2013). The DEAD-box helicase eIF4A. RNA Biol. *10*, 19–32.

Ash, P.E.A., Bieniek, K.F., Gendron, T.F., Caulfield, T., Lin, W.-L., DeJesus-Hernandez, M., van Blitterswijk, M.M., Jansen-West, K., Paul, J.W., Rademakers, R., et al. (2013). Unconventional translation of C9ORF72 GGGGCC expansion generates insoluble polypeptides specific to c9FTD/ALS. Neuron *77*, 639–646.

Balendra, R., and Isaacs, A.M. (2018). C9orf72 -mediated ALS and FTD: multiple pathways to disease. Nat. Rev. Neurol. *14*, 544.

Bellen, H.J., Levis, R.W., Liao, G., He, Y., Carlson, J.W., Tsang, G., Evans-Holm, M., Hiesinger, P.R., Schulze, K.L., Rubin, G.M., et al. (2004). The BDGP gene disruption project: single transposon insertions associated with 40% of Drosophila genes. Genetics *167*, 761–781.

Bellen, H.J., Levis, R.W., He, Y., Carlson, J.W., Evans-Holm, M., Bae, E., Kim, J., Metaxakis, A., Savakis, C., Schulze, K.L., et al. (2011). The Drosophila gene disruption project: progress using transposons with distinctive site specificities. Genetics *188*, 731–743.

Berson, A. et al. (2017). TDP-43 Promotes Neurodegeneration by Impairing Chromatin Remodeling. Curr. Biol. *27*, 3579-3590.e6.

Bettegazzi, B., Bellani, S., Roncon, P., Guarnieri, F.C., Bertero, A., Codazzi, F., Valtorta, F., Simonato, M., Grohovaz, F., and Zacchetti, D. (2017). eIF4B phosphorylation at Ser504 links synaptic activity with protein translation in physiology and pathology. Sci. Rep. *7*, 10563.

Browning, K.S., and Bailey-Serres, J. (2015). Mechanism of Cytoplasmic mRNA Translation. Arab. Book Am. Soc. Plant Biol. *13*.

Capossela, S., Muzio, L., Bertolo, A., Bianchi, V., Dati, G., Chaabane, L., Godi, C., Politi, L.S., Biffo, S., D'Adamo, P., et al. (2012). Growth Defects and Impaired Cognitive–Behavioral Abilities in Mice with Knockout for Eif4h, a Gene Located in the Mouse Homolog of the Williams-Beuren Syndrome Critical Region. Am. J. Pathol. *180*, 1121–1135.

Cheng, W., Wang, S., Mestre, A.A., Fu, C., Makarem, A., Xian, F., Hayes, L.R., Lopez-Gonzalez, R., Drenner, K., Jiang, J., et al. (2018). C9ORF72 GGGGCC repeat-associated non-AUG translation is upregulated by stress through eIF2α phosphorylation. Nat. Commun. *9*, 51.

Chung, C.-Y., Berson, A., Kennerdell, J.R., Sartoris, A., Unger, T., Porta, S., Kim, H.-J., Smith, E.R., Shilatifard, A., Van Deerlin, V., et al. (2018). Aberrant activation of non-coding RNA targets of transcriptional elongation complexes contributes to TDP-43 toxicity. Nat. Commun. *9*.

Cooper-Knock, J., Walsh, M.J., Higginbottom, A., Robin Highley, J., Dickman, M.J., Edbauer, D., Ince, P.G., Wharton, S.B., Wilson, S.A., Kirby, J., et al. (2014). Sequestration of multiple RNA recognition motif-containing proteins by C9orf72 repeat expansions. Brain *137*, 2040–2051.

Coppolecchia, R., Buser, P., Stotz, A., and Linder, P. (1993). A new yeast translation initiation factor suppresses a mutation in the eIF-4A RNA helicase. EMBO J. *12*, 4005–4011.

Coyne, A.N., Zaepfel, B.L., and Zarnescu, D.C. (2017). Failure to Deliver and Translate—New Insights into RNA Dysregulation in ALS. Front. Cell. Neurosci. *11*.

DeJesus-Hernandez, M., Mackenzie, I.R., Boeve, B.F., Boxer, A.L., Baker, M., Rutherford, N.J., Nicholson, A.M., Finch, N.A., Gilmer, H.F., Adamson, J., et al. (2011). Expanded GGGGCC hexanucleotide repeat in non-coding region of C9ORF72 causes chromosome 9p-linked frontotemporal dementia and amyotrophic lateral sclerosis. Neuron *72*, 245–256.

Dietzl, G., Chen, D., Schnorrer, F., Su, K.-C., Barinova, Y., Fellner, M., Gasser, B., Kinsey, K., Oppel, S., Scheiblauer, S., et al. (2007). A genome-wide transgenic RNAi library for conditional gene inactivation in *Drosophila*. Nature *448*, 151.

Elden, A.C., Kim, H.-J., Hart, M.P., Chen-Plotkin, A.S., Johnson, B.S., Fang, X., Armakola, M., Geser, F., Greene, R., Lu, M.M., et al. (2010). Ataxin-2 intermediate-length polyglutamine expansions are associated with increased risk for ALS. Nature *466*, 1069–1075.

Eom, T., Muslimov, I.A., Tsokas, P., Berardi, V., Zhong, J., Sacktor, T.C., and Tiedge, H. (2014). Neuronal BC RNAs cooperate with eIF4B to mediate activity-dependent translational control. J Cell Biol *207*, 237–252.

Fernandes, N., Eshleman, N., and Buchan, J.R. (2018). Stress Granules and ALS: A Case of Causation or Correlation? In RNA Metabolism in Neurodegenerative Diseases, R. Sattler, and C.J. Donnelly, eds. (Cham: Springer International Publishing), pp. 173–212.

Freibaum, B.D., Lu, Y., Lopez-Gonzalez, R., Kim, N.C., Almeida, S., Lee, K.-H., Badders, N., Valentine, M., Miller, B.L., Wong, P.C., et al. (2015). GGGGCC repeat expansion in C9ORF72 compromises nucleocytoplasmic transport. Nature *525*, 129–133.

Galmozzi, E., Aghemo, A., and Colombo, M. (2012). Eukaryotic initiation factor 5B: a new player for the anti-hepatitis C virus effect of ribavirin? Med. Hypotheses *79*, 471–473.

García-García, C., Frieda, K.L., Feoktistova, K., Fraser, C.S., and Block, S.M. (2015). Factor-dependent processivity in human eIF4A DEAD-box helicase. Science *348*, 1486–1488.

Gendron, T.F., Bieniek, K.F., Zhang, Y.-J., Jansen-West, K., Ash, P.E.A., Caulfield, T., Daughrity, L., Dunmore, J.H., Castanedes-Casey, M., Chew, J., et al. (2013). Antisense transcripts of the expanded C9ORF72 hexanucleotide repeat form nuclear RNA foci and undergo repeat-associated non-ATG translation in c9FTD/ALS. Acta Neuropathol. (Berl.) *126*, 829–844.

Goodman, L.D., Prudencio, M., Kramer, N.J., Martinez-Ramirez, L.F., Srinivasan, A.R., Lan, M., Parisi, M.J., Zhu, Y., Chew, J., Cook, C.N., et al. (2019). Expanded GGGGCC repeat transcription is mediated by the PAF1 complex in C9orf72-associated FTD. Nat. Neurosci.

van Gorp, A.G.M., van der Vos, K.E., Brenkman, A.B., Bremer, A., van den Broek, N., Zwartkruis, F., Hershey, J.W., Burgering, B.M.T., Calkhoven, C.F., and Coffer, P.J. (2009). AGC kinases regulate phosphorylation and activation of eukaryotic translation initiation factor 4B. Oncogene *28*, 95–106.

Green, K.M., Linsalata, A.E., and Todd, P.K. (2016). RAN translation—what makes it run? Brain Res. *1647*, 30–42.

Green, K.M., Glineburg, M.R., Kearse, M.G., Flores, B.N., Linsalata, A.E., Fedak, S.J., Goldstrohm, A.C., Barmada, S.J., and Todd, P.K. (2017). RAN translation at C9orf72-associated repeat expansions is selectively enhanced by the integrated stress response. Nat. Commun. *8*.

Haeusler, A.R., Donnelly, C.J., Periz, G., Simko, E.A.J., Shaw, P.G., Kim, M.-S., Maragakis, N.J., Troncoso, J.C., Pandey, A., Sattler, R., et al. (2014). C9orf72 Nucleotide Repeat Structures Initiate Molecular Cascades of Disease. Nature *507*, 195–200.

Haeusler, A.R., Donnelly, C.J., and Rothstein, J.D. (2016). The expanding biology of the C9orf72 nucleotide repeat expansion in neurodegenerative disease. Nat. Rev. Neurosci. *17*, 383–395.

Harms, U., Andreou, A.Z., Gubaev, A., and Klostermeier, D. (2014). eIF4B, eIF4G and RNA regulate eIF4A activity in translation initiation by modulating the eIF4A conformational cycle. Nucleic Acids Res. *42*, 7911–7922.

Hautbergue, G.M., Castelli, L.M., Ferraiuolo, L., Sanchez-Martinez, A., Cooper-Knock, J., Higginbottom, A., Lin, Y.-H., Bauer, C.S., Dodd, J.E., Myszczynska, M.A., et al. (2017). SRSF1-dependent nuclear export inhibition of C9ORF72 repeat transcripts prevents neurodegeneration and associated motor deficits. Nat. Commun. *8*.

Hernández, G., Vázquez-Pianzola, P., Zurbriggen, A., Altmann, M., Sierra, J.M., and Rivera-Pomar, R. (2004). Two functionally redundant isoforms of Drosophila melanogaster eukaryotic initiation factor 4B are involved in cap-dependent translation, cell survival, and proliferation. Eur. J. Biochem. *271*, 2923–2936.

Ito, D., Hatano, M., and Suzuki, N. (2017). RNA binding proteins and the pathological cascade in ALS/FTD neurodegeneration. Sci. Transl. Med. *9*, eaah5436.

Kanekura, K., Yagi, T., Cammack, A.J., Mahadevan, J., Kuroda, M., Harms, M.B., Miller, T.M., and Urano, F. (2016). Poly-dipeptides encoded by the C9ORF72 repeats block global protein translation. Hum. Mol. Genet. *25*, 1803–1813.

Kearse, M.G., and Wilusz, J.E. (2017). Non-AUG translation: a new start for protein synthesis in eukaryotes. Genes Dev. *31*, 1717–1731.

Kearse, M.G., Green, K.M., Krans, A., Rodriguez, C.M., Linsalata, A.E., Goldstrohm, A.C., and Todd, P.K. (2016). CGG Repeat-Associated Non-AUG Translation Utilizes a Cap-Dependent Scanning Mechanism of Initiation to Produce Toxic Proteins. Mol. Cell *62*, 314–322.

Khan, M.A., and Goss, D.J. (2012). Poly(A)-binding protein increases the binding affinity and kinetic rates of interaction of viral protein linked to genome with translation initiation factors eIFiso4F and eIFiso4F·4B complex. Biochemistry *51*, 1388–1395.

Kim, H.-J., Raphael, A.R., LaDow, E.S., McGurk, L., Weber, R., Trojanowski, J.Q., Lee, V.M.-Y., Finkbeiner, S., Gitler, A.D., and Bonini, N.M. (2014). Therapeutic modulation of eIF2α-phosphorylation rescues TDP-43 toxicity in amyotrophic lateral sclerosis disease models. Nat. Genet. *46*, 152–160.

Kramer, N.J., Carlomagno, Y., Zhang, Y.-J., Almeida, S., Cook, C.N., Gendron, T.F., Prudencio, M., Van Blitterswijk, M., Belzil, V., Couthouis, J., et al. (2016a). Spt4 selectively regulates the expression of C9orf72 sense and antisense mutant transcripts associated with c9FTD/ALS. Science *353*, 708–712.

Kramer, N.J., Carlomagno, Y., Zhang, Y.-J., Almeida, S., Cook, C.N., Gendron, T.F., Prudencio, M., Blitterswijk, M.V., Belzil, V., Couthouis, J., et al. (2016b). Spt4 selectively regulates the expression of C9orf72 sense and antisense mutant transcripts. Science *353*, 708–712.

Levis, R., Hazelrigg, T., and Rubin, G.M. (1985). Effects of genomic position on the expression of transduced copies of the white gene of Drosophila. Science *229*, 558–561.

Liberman, N., Gandin, V., Svitkin, Y.V., David, M., Virgili, G., Jaramillo, M., Holcik, M., Nagar, B., Kimchi, A., and Sonenberg, N. (2015). DAP5 associates with eIF2β and eIF4AI to promote Internal Ribosome Entry Site driven translation. Nucleic Acids Res. *43*, 3764–3775.

Liu, E.Y., Russ, J., Wu, K., Neal, D., Suh, E., McNally, A.G., Irwin, D.J., Van Deerlin, V.M., and Lee, E.B. (2014). C9orf72 hypermethylation protects against repeat expansion-associated pathology in ALS/FTD. Acta Neuropathol. (Berl.) *128*, 525–541.

Mackenzie, I.R., Arzberger, T., Kremmer, E., Troost, D., Lorenzl, S., Mori, K., Weng, S.-M., Haass, C., Kretzschmar, H.A., Edbauer, D., et al. (2013). Dipeptide repeat protein pathology in C9ORF72 mutation cases: clinico-pathological correlations. Acta Neuropathol. (Berl.) *126*, 859–879.

Mackenzie, I.R.A., Frick, P., Grässer, F.A., Gendron, T.F., Petrucelli, L., Cashman, N.R., Edbauer, D., Kremmer, E., Prudlo, J., Troost, D., et al. (2015). Quantitative analysis and clinico-pathological correlations of different dipeptide repeat protein pathologies in C9ORF72 mutation carriers. Acta Neuropathol. (Berl.) *130*, 845–861.

Mann, D.M., Rollinson, S., Robinson, A., Bennion Callister, J., Thompson, J.C., Snowden, J.S., Gendron, T., Petrucelli, L., Masuda-Suzukake, M., Hasegawa, M., et al. (2013). Dipeptide repeat proteins are present in the p62 positive inclusions in patients with frontotemporal lobar degeneration and motor neurone disease associated with expansions in C9ORF72. Acta Neuropathol. Commun. *1*, 68.

Marygold, S.J., Attrill, H., and Lasko, P. (2017). The translation factors of Drosophila melanogaster. Fly (Austin) *11*, 65–74.

McGurk, L., and Bonini, N.M. (2012). Protein interacting with C kinase (PICK1) is a suppressor of spinocerebellar ataxia 3-associated neurodegeneration in Drosophila. Hum. Mol. Genet. *21*, 76.

Méthot, N., Song, M.S., and Sonenberg, N. (1996). A region rich in aspartic acid, arginine, tyrosine, and glycine (DRYG) mediates eukaryotic initiation factor 4B (eIF4B) self-association and interaction with eIF3. Mol. Cell. Biol. *16*, 5328–5334.

Mizielinska, S., Grönke, S., Niccoli, T., Ridler, C.E., Clayton, E.L., Devoy, A., Moens, T., Norona, F.E., Woollacott, I.O.C., Pietrzyk, J., et al. (2014). C9orf72 repeat expansions cause neurodegeneration in Drosophila through arginine-rich proteins. Science *345*, 1192–1194.

Mokas, S., Mills, J.R., Garreau, C., Fournier, M.-J., Robert, F., Arya, P., Kaufman, R.J., Pelletier, J., and Mazroui, R. (2009). Uncoupling Stress Granule Assembly and Translation Initiation Inhibition. Mol. Biol. Cell *20*, 2673–2683.

Mordes, D.A., Prudencio, M., Goodman, L.D., Klim, J.R., Moccia, R., Limone, F., Pietilainen, O., Chowdhary, K., Dickson, D.W., Rademakers, R., et al. (2018). Dipeptide repeat proteins activate a heat shock response found in C9ORF72-ALS/FTLD patients. Acta Neuropathol. Commun. *6*.

Mori, K., Weng, S.-M., Arzberger, T., May, S., Rentzsch, K., Kremmer, E., Schmid, B., Kretzschmar, H.A., Cruts, M., Van Broeckhoven, C., et al. (2013). The C9orf72 GGGGCC repeat is translated into aggregating dipeptide-repeat proteins in FTLD/ALS. Science *339*, 1335–1338.

Ni, J.-Q., Zhou, R., Czech, B., Liu, L.-P., Holderbaum, L., Yang-Zhou, D., Shim, H.-S., Tao, R., Handler, D., Karpowicz, P., et al. (2011). A genome-scale shRNA resource for transgenic RNAi in *Drosophila*. Nat. Methods *8*, 405.

Niblock, M., Smith, B.N., Lee, Y.-B., Sardone, V., Topp, S., Troakes, C., Al-Sarraj, S., Leblond, C.S., Dion, P.A., Rouleau, G.A., et al. (2016). Retention of hexanucleotide repeat-containing intron in C9orf72 mRNA: implications for the pathogenesis of ALS/FTD. Acta Neuropathol. Commun. *4*.

Nielsen, K.H., Behrens, M.A., He, Y., Oliveira, C.L.P., Sottrup Jensen, L., Hoffmann, S.V., Pedersen, J.S., and Andersen, G.R. (2011). Synergistic activation of eIF4A by eIF4B and eIF4G. Nucleic Acids Res. *39*, 2678–2689.

Perkins, L.A., Holderbaum, L., Tao, R., Hu, Y., Sopko, R., McCall, K., Yang-Zhou, D., Flockhart, I., Binari, R., Shim, H.-S., et al. (2015). The Transgenic RNAi Project at Harvard Medical School: Resources and Validation. Genetics *201*, 843–852.

Prudencio, M., Belzil, V.V., Batra, R., Ross, C.A., Gendron, T.F., Pregent, L.J., Murray, M.E., Overstreet, K.K., Piazza-Johnston, A.E., Desaro, P., et al. (2015). Distinct brain transcriptome profiles in C9orf72-associated and sporadic ALS. Nat. Neurosci. *18*, 1175–1182.

Prudencio, M., Gonzales, P.K., Cook, C.N., Gendron, T.F., Daughrity, L.M., Song, Y., Ebbert, M.T.W., van Blitterswijk, M., Zhang, Y.-J., Jansen-West, K., et al. (2017). Repetitive element transcripts are elevated in the brain of C9orf72 ALS/FTLD patients. Hum. Mol. Genet. *26*, 3421–3431.

Raught, B., Peiretti, F., Gingras, A.-C., Livingstone, M., Shahbazian, D., Mayeur, G.L., Polakiewicz, R.D., Sonenberg, N., and Hershey, J.W. (2004). Phosphorylation of eucaryotic translation initiation factor 4B Ser422 is modulated by S6 kinases. EMBO J. *23*, 1761–1769.

Renton, A.E., Majounie, E., Waite, A., Simón-Sánchez, J., Rollinson, S., Gibbs, J.R., Schymick, J.C., Laaksovirta, H., van Swieten, J.C., Myllykangas, L., et al. (2011). A hexanucleotide repeat expansion in C9ORF72 is the cause of chromosome 9p21-linked ALS-FTD. Neuron *72*, 257–268.

Richter-Cook, N.J., Dever, T.E., Hensold, J.O., and Merrick, W.C. (1998). Purification and Characterization of a New Eukaryotic Protein Translation Factor EUKARYOTIC INITIATION FACTOR 4H. J. Biol. Chem. *273*, 7579–7587.

Rode, S., Ohm, H., Anhäuser, L., Wagner, M., Rosing, M., Deng, X., Sin, O., Leidel, S.A., Storkebaum, E., Rentmeister, A., et al. (2018). Differential Requirement for Translation Initiation Factor Pathways during Ecdysone-Dependent Neuronal Remodeling in Drosophila. Cell Rep. *24*, 2287-2299.e4.

Rogers, G.W., Richter, N.J., Lima, W.F., and Merrick, W.C. (2001). Modulation of the Helicase Activity of eIF4A by eIF4B, eIF4H, and eIF4F. J. Biol. Chem. *276*, 30914–30922.

Roux, P.P., and Topisirovic, I. (2018). Signaling Pathways Involved in the Regulation of mRNA Translation. Mol. Cell. Biol. *38*.

Rozovsky, N., Butterworth, A.C., and Moore, M.J. (2008). Interactions between eIF4AI and its accessory factors eIF4B and eIF4H. RNA *14*, 2136–2148.

Sareen, D., O'Rourke, J.G., Meera, P., Muhammad, A.K.M.G., Grant, S., Simpkinson, M., Bell, S., Carmona, S., Ornelas, L., Sahabian, A., et al. (2013). Targeting RNA foci in iPSC-derived motor neurons from ALS patients with C9ORF72 repeat expansion. Sci. Transl. Med. *5*, 208ra149.

Satoh, J., Yamamoto, Y., Kitano, S., Takitani, M., Asahina, N., and Kino, Y. (2014). Molecular Network Analysis Suggests a Logical Hypothesis for the Pathological Role of C9orf72 in Amyotrophic Lateral Sclerosis/Frontotemporal Dementia. J. Cent. Nerv. Syst. Dis. *6*, 69–78.

Sellier, C., Buijsen, R.A.M., He, F., Natla, S., Jung, L., Tropel, P., Gaucherot, A., Jacobs, H., Meziane, H., Vincent, A., et al. (2017). Translation of Expanded CGG Repeats into FMRpolyG Is Pathogenic and May Contribute to Fragile X Tremor Ataxia Syndrome. Neuron *93*, 331–347.

Sen, N.D., Zhou, F., Harris, M.S., Ingolia, N.T., and Hinnebusch, A.G. (2016). eIF4B stimulates translation of long mRNAs with structured 5′ UTRs and low closed-loop potential but weak dependence on eIF4G. Proc. Natl. Acad. Sci. U. S. A. *113*, 10464–10472.

Sharma, S.D., Kraft, J.J., Miller, W.A., and Goss, D.J. (2015). Recruitment of the 40S Ribosome Subunit to the 3′-Untranslated Region (UTR) of a Viral mRNA, via the eIF4 Complex, Facilitates Cap-independent Translation. J. Biol. Chem. *290*, 11268–11281.

Shatsky, I.N., Terenin, I.M., Smirnova, V.V., and Andreev, D.E. (2018). Cap-Independent Translation: What's in a Name? Trends Biochem. Sci.

Sonenberg, N., and Hinnebusch, A.G. (2009). Regulation of Translation Initiation in Eukaryotes: Mechanisms and Biological Targets. Cell *136*, 731–745.

Spilka, R., Ernst, C., Mehta, A.K., and Haybaeck, J. (2013). Eukaryotic translation initiation factors in cancer development and progression. Cancer Lett. *340*, 9–21.

Spirin, A.S. (2009). How Does a Scanning Ribosomal Particle Move along the 5′-Untranslated Region of Eukaryotic mRNA? Brownian Ratchet Model. Biochemistry *48*, 10688–10692.

Spradling, A.C., Stern, D.M., Kiss, I., Roote, J., Laverty, T., and Rubin, G.M. (1995). Gene disruptions using P transposable elements: an integral component of the Drosophila genome project. Proc. Natl. Acad. Sci. U. S. A. *92*, 10824–10830.

Spradling, A.C., Stern, D., Beaton, A., Rhem, E.J., Laverty, T., Mozden, N., Misra, S., and Rubin, G.M. (1999). The Berkeley Drosophila Genome Project gene disruption project: Single P-element insertions mutating 25% of vital Drosophila genes. Genetics *153*, 135–177.

Sun, Y., Atas, E., Lindqvist, L., Sonenberg, N., Pelletier, J., and Meller, A. (2012). The eukaryotic initiation factor eIF4H facilitates loop-binding, repetitive RNA unwinding by the eIF4A DEAD-box helicase. Nucleic Acids Res. *40*, 6199–6207.

Suzuki, H., Shibagaki, Y., Hattori, S., and Matsuoka, M. (2018). The proline–arginine repeat protein linked to C9-ALS/FTD causes neuronal toxicity by inhibiting the DEAD-box RNA helicase-mediated ribosome biogenesis. Cell Death Dis. *9*.

Tabet, R., Schaeffer, L., Freyermuth, F., Jambeau, M., Workman, M., Lee, C.-Z., Lin, C.-C., Jiang, J., Jansen-West, K., Abou-Hamdan, H., et al. (2018). CUG initiation and frameshifting enable production of dipeptide repeat proteins from ALS/FTD C9ORF72 transcripts. Nat. Commun. *9*, 152.

Tao, Z., Wang, H., Xia, Q., Li, K., Li, K., Jiang, X., Xu, G., Wang, G., and Ying, Z. (2015). Nucleolar stress and impaired stress granule formation contribute to C9orf72 RAN translation-induced cytotoxicity. Hum. Mol. Genet. *24*, 2426–2441.

Todd, P.K., Oh, S.Y., Krans, A., He, F., Sellier, C., Frazer, M., Renoux, A.J., Chen, K., Scaglione, K.M., Basrur, V., et al. (2013). CGG Repeat-Associated Translation Mediates Neurodegeneration in Fragile X Tremor Ataxia Syndrome. Neuron *78*, 440–455.

Tran, H., Almeida, S., Moore, J., Gendron, T.F., Chalasani, U., Lu, Y., Du, X., Nickerson, J.A., Petrucelli, L., Weng, Z., et al. (2015). Differential Toxicity of Nuclear RNA Foci versus Dipeptide Repeat Proteins in a Drosophila Model of C9ORF72 FTD/ALS. Neuron *87*, 1207–1214.

Vatovec, S., Kovanda, A., and Rogelj, B. (2014). Unconventional features of C9ORF72 expanded repeat in amyotrophic lateral sclerosis and frontotemporal lobar degeneration. Neurobiol. Aging *35*, 2421.e1-2421.e12.

Vaysse, C., Philippe, C., Martineau, Y., Quelen, C., Hieblot, C., Renaud, C., Nicaise, Y., Desquesnes, A., Pannese, M., Filleron, T., et al. (2015). Key contribution of eIF4H-mediated translational control in tumor promotion. Oncotarget *6*, 39924–39940.

Walker, S.E., Zhou, F., Mitchell, S.F., Larson, V.S., Valasek, L., Hinnebusch, A.G., and Lorsch, J.R. (2013). Yeast eIF4B binds to the head of the 40S ribosomal subunit and promotes mRNA recruitment through its N-terminal and internal repeat domains. RNA *19*, 191–207.

Yuva-Aydemir, Y., Almeida, S., and Gao, F.-B. (2018). Insights into C9ORF72-Related ALS/FTD from Drosophila and iPSC Models. Trends Neurosci.

Zhang, Y.-J., Gendron, T.F., Ebbert, M.T.W., O'Raw, A.D., Yue, M., Jansen-West, K., Zhang, X., Prudencio, M., Chew, J., Cook, C.N., et al. (2018). Poly(GR) impairs protein translation and stress granule dynamics in C9orf72-associated frontotemporal dementia and amyotrophic lateral sclerosis. Nat. Med. *24*, 1136–1142.

Zhao, M., Kim, J.R., van Bruggen, R., and Park, J. (2018). RNA-Binding Proteins in Amyotrophic Lateral Sclerosis. Mol. Cells *41*, 818–829.

Zu, T., Pattamatta, A., and Ranum, L.P.W. (2018). Repeat-Associated Non-ATG Translation in Neurological Diseases. Cold Spring Harb. Perspect. Biol. *10*, a033019.

CHAPTER 4: SIGNIFICANCE AND NEXT STEPS

An unbiased, RNAi-based screen

The discovery that an expanded hexanucleotide repeat of (G4C2)n exists within *C9orf72* and that expansions of >30 repeats are associated with ALS/FTD were made by two independent groups in 2011 (DeJesus-Hernandez et al., 2011; Renton et al., 2011). When I began this project in 2013, little was known about the impact this mutation may have on neuronal health and disease progression. Drawing parallels from previous examples of nucleotide expansions and disease (Krzyzosiak et al., 2012; Nguyen et al., 2019), multiple groups developed gain-of-function models, including ours described in **Chapter 2** (Freibaum et al., 2015; Kramer et al., 2016; Mizielinska et al., 2014; Xu et al., 2013). By using *Drosophila*, investigators could rapidly define degenerative effects associated with gain-of-function mechanisms that resulted with expression >30 G4C2 repeats *in vivo*.

While each research group uniquely used their G4C2 fly model(s) to uncover disease mechanisms only two groups, to my knowledge, took on the task of performing unbiased, forward-screens to define disease modifiers (Freibaum et al., 2015; Goodman et al., 2019a). Of these, our screen on (G4C2)49-expressing flies was unique as we analyzed individual genes whose RNAi-mediated loss may impact G4C2-associated toxicity in *Drosophila* (**see Chapter 2: Fig. 2-1e and** (Goodman et al., 2019a)). (The other report utilized chromatin deficiency fly lines that targeted multiple genes simultaneously and are predicted to result in only a 50% downregulation of encompassed genes (Freibaum et al., 2015).) We identified 119 genes whose downregulation could increase or decrease (G4C2)49-induced toxicity in the fly eye (**see Chapter 2: Fig. 2-1f and** (Goodman et al., 2019a)). Further investigations tested G4C2-associated genes in a second fly model that expressed the toxic GR-dipeptide from a non-G4C2 transcript (**see Chapter 2: Fig. 2-2a and** (Goodman et al., 2019a; Mizielinska

et al., 2014). This defined pathways selective to the G4C2-RNA (**see Chapter 2: Fig. 2-2c and** (Goodman et al., 2019a)) and genes whose loss impacted both the G4C2-RNA and its dipeptide product (**see Appendix 2: Supplementary data and** (Goodman et al., 2019a)). Last, by testing G4C2-associated genes in a fly model that overexpressed a related disease gene, TDP-43 (**see Chapter 2: Fig. 2-2a and** (Goodman et al., 2019a)), we also defined pathways selective for the *C9orf72*-mutation in C9+ ALS/FTD (**see Chapter 2: Fig. 2-2d and** (Goodman et al., 2019a)) and genes that could target both co-existing disease etiologies (**see Appendix 2: Supplementary data and** (Chew et al., 2015, 2019; DeJesus-Hernandez et al., 2011; Goodman et al., 2019a; Renton et al., 2011)). In total, our large-scale, unbiased screen highlighted genes and pathways worth further investigation to improve understanding of C9+ ALS/FTD disease mechanisms. Of these, pathways involving multiple genes identified in the screen included the following and may be worth further investigation: splicing dysfunction (Cooper-Knock et al., 2015; Prudencio et al., 2015; Yin et al., 2017), DNA damage (Farg et al., 2017; Higelin et al., 2018; Lopez-Gonzalez et al., 2016; Riemslagh et al., 2019; Walker et al., 2017), and perturbed nucleolar function (Haeusler et al., 2014; Herrmann and Parlato, 2018; Kwon et al., 2014; Mizielinska et al., 2017; Tao et al., 2015). Below I will discuss one of these, splicing dysfunction.

Splicing dysfunction

Dysregulation of RNA-metabolism is a re-occurring theme in ALS/FTD, and mutations in multiple RNA-binding proteins are linked to disease (Coyne et al., 2017; Ito et al., 2017; Zhao et al., 2018). Interestingly, 17 of 119 genes whose downregulation impacted (G4C2)49-toxicity are involved in mRNA-processing, the majority of which increased toxicity and similarly enhanced (GR)36-toxicity when depleted. In particular, GO-term

analyses revealed that reduced expression of precatalytic spliceosome components using RNAi increased (G4C2)49-toxicity (**see Chapter 2. Fig. 2-1h and** (Goodman et al., 2019a)). This included fly orthologues to *snRNP-U1-70K*, *SAP30BP*, *SF3A1*, *SF3B5*, *HSPA8*, *RACK1*, and *HNRNPUL1*. These same RNAi lines similarly enhanced (GR)36-toxicity in the fly eye, suggesting that perturbations to the spliceosome may be the result of toxic GR-dipeptide expressed from the (G4C2)49-transgene. Of these, SF3A1, HSPA8, RACK1, and HNRNPUL1 did not similarly alter toxicity in TDP-43 expressing flies.

Currently, multiple studies have reported that splicing errors occur in C9+ ALS/FTD compared to C9- ALS/FTD (Cooper-Knock et al., 2015; Prudencio et al., 2015; Yin et al., 2017). Of these, Cooper-Knock and colleagues suggested that splicing dysfunction correlated with disease progression. The majority of papers in the current literature associate changes in RNA metabolism to sequestration of RNA-binding proteins by the G4C2-RNA in C9+ disease (Conlon et al., 2016; Cooper-Knock et al., 2014; Lee et al., 2013; Mori et al., 2013; Sareen et al., 2013). However, the GR- (and PR-) dipeptide can also interact with relevant RNA binding proteins (RBPs) (Davidson et al., 2017; Kwon et al., 2014; Lee et al., 2016). As C9+ ALS/FTD is an progressive disorder and splicing dysfunction may be correlated with disease progression (Cooper-Knock et al., 2015), it is reasonable to hypothesize that initial splicing errors may be induced by G4C2-RNA while the accumulation of toxic GR-dipeptides within cells with age may further perturb this process, resulting in a rapid decline in neuron health and disease.

In support of this, a recent study presented a compelling argument that GR-dipeptides can directly interfere with splicing (Yin et al., 2017). In an *in vitro* assay, the authors found that flag-tagged GR can interact with 5 of 7 components of the precatalytic

spliceosome that we had identified as enhancers of G4C2/GR-toxicity in the fly: *snRNP-U1-70K*, *SAP30BP*, *SF3A1*, *HSPA8*, *HNRNPUL1*. Their focused studies revealed that SF3A1 was mis-localized to the cytoplasm of cells exposed to GR-dipeptides and in C9+-derived iPS neurons, suggesting a potential mechanism underlying *SF3A1* RNAi's ability to increase toxicity in our G4C2/GR animals. Notably, among the genes identified in our screen, snRNP-U1-70K is mis-localized to the cytoplasm, forms insoluble tangles, and contributes to splicing defects in Alzheimer's disease (Bai et al., 2013, 2014; Hales et al., 2014; Johnson et al., 2018). Suggesting a parallel mechanism may occur in ALS, snRNP-U1-70K mis-localization has also been associated with *FUS* mutations found in ALS (Yu et al., 2015a). In C9orf72-associated disease, Yin and colleagues have argued that GR could act specifically act on U2 snRNP over U1 snRNP (Yin et al., 2017). However, our data would suggest that U1 snRNP (of which snRNP-U1-70K is the primary component) may also be playing a role in C9+ disease. In fact, these researchers showed that blocks in splicing that resulted from exposure to GR-dipeptides occurred in the early steps of the process *in vitro.* While they argue that this is when the U2 snRNP is functioning, literature supports that both U1 and U2 snRNPs are important in early stages of splicing, with U1 acting before U2 (Wahl et al., 2009; Yan et al., 2019). Further, U1 snRNP and U2 snRNP interact while U1 recognizes the 5' splice site and U2 the 3' splice site of introns (Nik and Bowman, 2019; Plaschka et al., 2018; Shao et al., 2012; Zhan et al., 2018).

Overall, a directed study looking into the precatalytic spliceosome components identified in our screen whose loss enhances G4C2/GR toxicity may further elucidate how splicing errors occur in C9+ disease. snRNP-U1-70K may be of particular interest and it will be used as an example herein (Bai et al., 2013, 2014; Hales et al., 2014; Johnson et al., 2018). Follow-up investigations would need to confirm that altered

expression of snRNP-U1-70K can modify (G4C2)49- and (GR)36-induced toxicity specifically in the fly, using available RNAi and UAS-upregulation lines. By testing for effects of modulating snRNP-U1-70K expression on degenerative phenotypes caused by expressing (G4C2)49 or (GR)36 in the fly optic system and brain, one could determine if snRNP-U1-70K was a dose-dependent modifier of G4C2/GR toxicity *in vivo*. Follow-up RNA-sequencing studies in the fly would define genes that may be mis-spliced in disease and if snRNP-U1-70K plays a role. The fly offers the strong advantage of allowing for relatively rapid age progression studies *in vivo*. Thus, by comparing flies expressing toxic (G4C2)49, toxic (GR)36, or inert (G4C2)8 within the fly brain (ElavGS), genes that are mis-spliced in response to the toxic repeat expansion and/or its GR-dipeptide product with age would be revealed. Follow-up studies could then involve modulating snRNP-U1-70K, using RNAi and UAS lines, in G4C2/GR expressing animals. One would expect that if normal snRNP-U1-70K function was disrupted by the GR-dipeptide that increasing the expression of snRNP-U1-70K would alleviate splicing errors seen in GR-expressing animals alone. Further, downregulating snRNP-U1-70K in GR animals would likely cause an increase in splicing errors, demonstrating that the GR-dipeptide was disrupting snRNP-U1-70K's normal function. Using the fly model containing a GFP-tag in the GR reading frame (**see Chapter 3. Fig. 3-1 and** (Goodman et al., 2019a)), one could perform a number of directed mechanistic studies to define interactions between snRNP-U1-70K and the GR-dipeptide *in vivo* (e.g. immunoprecipitation studies, co-localization immunofluorescence staining). Translating findings to C9+ mouse models (Chew et al., 2015, 2019), C9+-derived cell lines and/or post-mortem tissue would explain snRNP-U1-70K's role in disease. Additional investigations could look for potential connections with splicing deficits caused by TDP-

43 mis-localization in ALS or other factors associated with splicing and neurodegeneration (e.g. SMN) (Nik and Bowman, 2019; Nussbacher et al., 2019).

The PAF1 complex

Compellingly, among the ~4000 genes screened for effects on (G4C2)-49 toxicity in *Drosophila* (**see Chapter 2: Fig. 2-1e-h and** (Goodman et al., 2019a)), RNAi-mediated depletion of 3 of the 5 core components to the PAF1 complex (PAF1C) were found to suppress (G4C2)49-toxicity – CDC73, Ctr9, and Rtf1. (The sixth, minor component of PAF1C, WDR61, was also identified as a suppressor of G4C2-toxicity in our screen; **see Appendix 2: Supplementary data and** (Goodman et al., 2019a)**.**) Ensuing investigations expanded reagents to include the 2 remaining PAF1C components – Paf1 and Leo1 – and defined PAF1C depletion for its ability to specifically suppress (G4C2)49 toxicity versus GR-induced or TDP-43-induced toxicity (**see Chapter 2: Fig. 2-2, 2-3 and** (Goodman et al., 2019a)). As PAF1C is a transcriptional regulator of RNAPII (Jaehning, 2010), mechanistic studies defined the importance of PAF1C components in G4C2‖G2C4-DNA expression, using multiple fly and yeast models (**see Chapter 2: Fig. 2-4 and** (Goodman et al., 2019a)). (RNAi to *WDR61* caused similar effects on (G4C2)49-toxicity and RNA levels in the fly; data not shown.) A key finding was that loss of *Paf1* and *Leo1*, which form a heterodimer within the PAF1C complex (Chu et al., 2013), selectively impacted expression from toxic (>30) G4C2-repeat expansions versus inert (≤ 29) G4C2-repeats in the fly (**see Chapter 2: Fig. 2-4a and** (Goodman et al., 2019a)). The effect was remarkably consistent between G4C2-fly models arguing that it was biological rather than technical (compare data in **Chapter 2: Fig. 2-4a and 2-4c and** (Goodman et al., 2019a)). In contrast, RNAi targeting *Spt4* (of the DSIF complex; (Hartzog and Fu, 2013)) or the other PAF1C components – *CDC73*, *Ctr9*, *Rtf1* (and

WDR61; data not shown) – similarly altered expression from all G4C2-transgenes independent of the repeat-length. Additionally, we showed that Leo1, of the Paf1/Leo1 heterodimer, was bound to *C9orf72*-chromatin in C9+ ALS/FTD patient cells (**see Chapter 2: Fig. 2-6b and** (Goodman et al., 2019a)). Further supporting that both Paf1 and Leo1 play a special role in disease, these components were upregulated in FTD cortical tissue only when the toxic (>30) G4C2-repeat expansion was present (**see Chapter 2: Fig. 2-6c and** (Goodman et al., 2019a)). This was not true for another PAF1C component, *CDC73* (**see Appendix 2: Fig. S2-10 and** (Goodman et al., 2019a)). Notably, the expression of *Paf1* and *Leo1* in C9+ FTD tissue positively correlated to expression of the G4C2-postive *C9orf72* gene (**see Chapter 2: Fig. 2-6d and** (Goodman et al., 2019a)).

In total, these investigations revealed the PAF1C as a transcriptional regulator of G4C2-repeats in C9+ ALS/FTD. Further investigations into Paf1 and Leo1 may reveal them to be effective therapeutic targets, while current data supports their loss in flies, yeast, and mice may be better tolerated than the previously proposed target, Spt4 (Gerlach et al., 2017; Jaehning, 2010; Kramer et al., 2016; Meehan et al., 2017; Van Oss et al., 2017). Here, I will describe key next steps that are needed to further define PAF1C's role in C9+ ALS/FTD.

PAF1C in C9+ FTD versus C9+ ALS

A surprising feature of PAF1C in C9+ disease that we found during our investigations was that components *Paf1* and *Leo1* were selectively upregulated in C9+ post-mortem cortical tissue derived from FTD patients versus ALS patients. We hypothesized that this difference was the result of the tissue assayed. Specifically, RNA was extracted from the frontal cortex of individuals, while only FTD and FTD/ALS cases have cognitive deficits

associated with neurodegeneration in the frontal and temporal cortices. In contrast, ALS patients have motor deficits associated degeneration of upper and lower motor neurons in the motor cortex, brain stem, and spinal cord. Fittingly, brain scans of FTD versus ALS patients show different atrophy patterns (Boeve et al., 2012; Omer et al., 2017; Schönecker et al., 2018). In total, further investigations into why we saw a change in *Paf1/Leo1* expression based on different patient diagnoses need to be explored.

Upregulation of PAF1C in frontal cortex tissue from FTD patients but not ALS patients could be the result of the type of tissue assayed and/or PAF1C gene variants. As mentioned, FTD affects neurons in the frontal and temporal cortices while ALS affects motor neurons. However, we analyzed *Paf1/Leo1* levels in cortical tissue from both. Further investigations are needed to determine if PAF1C components are upregulated in tissue relevant to ALS: motor neurons in the spinal cord. Thorough investigations into *PAF1* and *LEO1* using patient data may also define any unique features underlying PAF1 and LEO1 that contribute to C9+ patients developing FTD versus ALS, thus defining them as disease modifiers. For example, expression of gene variants, isoforms, or other unique genetic features may underly these genes' ability to mediate RNAPII-transcription of expanded G4C2-DNA. Examples of disease modifiers in ALS/FTD are *ATXN2 and TMEM106B. ATXN2* can carry an intermediate-length CAG-repeat associated with an increased risk for C9+ patients to develop ALS (van Blitterswijk et al., 2014a). *TMEM106B* can produce multiple mRNA variants, while homozygosity for the recessive variant rs3173615 may protect C9+ patients from developing FTD (van Blitterswijk et al., 2014b). In total, thorough clinical investigations are needed while comparing *PAF1* and *LEO1* in FTD versus ALS patients and considering factors such as tissue specificity, disease progression (discussed below), and disease severity.

An alternative hypothesis that could explain why *Paf1* and *Leo1* were upregulated in C9+ FTD cases but not C9+ ALS cases is that expression levels may change during disease progression. Interestingly, neuronal expression of (G4C2)149 compared to (G4C2)2 in mice caused no change in Leo1 levels at 3 months of transgene expression (**see Chapter 2: Fig. 2-5c and** (Goodman et al., 2019a)). However, Leo1 was significantly upregulated after 6 months of transgene expression. This argues that PAF1C upregulation occurred in a progressive manner as a response to the toxic, expanded G4C2-transgene expression. In our fly investigations, we saw that PAF1C components were upregulated in brains of (G4C2)49-expressing flies before degenerative phenotypes are expected (**see Chapter 2: Fig. 2-5a and** (Goodman et al., 2019a)). Specifically, we analyzed PAF1C expression after 16 days of transgene expression in adult fly neurons, which is before vacuole formation and animal death occurs. In total, these data argue that PAF1C expression may change over time while a more directed study is needed. A straightforward approach would be to define PAF1C expression with a time course in flies and mice. By comparing PAF1C levels to phenotypic data (e.g. lifespans, motor deficits, vacuole formation), one could define how PAF1C expression changes in response to (G4C2)30+ expression in neurons during early-, mid-, or late-stage disease progression.

While the above hypotheses focus on potential direct roles Paf1 and Leo1 may be playing in defining if C9+ patients develop FTD versus ALS, I note that these proteins may play an indirect role. Importantly, PAF1C is a transcriptional regulator that acts on multiple RNAPII-regulated genes (Jaehning, 2010). Thus, while our data show that Paf1 and Leo1 are upregulated in response to expanded (>30) G4C2-expression, its upregulation is likely to contribute to unique expression profiles in C9+ FTD patients and may affect disease relevant pathways (Cooper-Knock et al., 2015; Prudencio et al.,

2015). For example, expression of repetitive elements are increased in C9+ ALS/FTD compared to C9- ALS/FTD (Prudencio et al., 2017). PAF1C may further define differences between C9+ ALS and C9+ FTD patients in this pathway.

Overall, directed studies are needed to further define PAF1C's role in ALS/FTD while considering multiple factors such as tissue type, disease stage, and the supposition that different components of PAF1C may behave differently.

Additional mechanistic studies

In Chapter 2, we present compelling data that loss of PAF1C impacts expression from expanded G4C2-repeats using mice and yeast models. Importantly, Paf1 and Leo1 seem to be of particular importance as their depletion selectively impacted expression from toxic (>30) repeats compared to inert (≤ 29) repeats in the fly. Additional investigations are needed to further define the mechanism(s) underlying these effects in human cells and C9+ disease.

Specifically, the impact of downregulating PAF1C components on expression from an endogenous mutant *C9orf72* gene would further define its role in mediating expression of >30 G4C2-repeat expansions. Our data used overexpression G4C2-models that expressed the repeats in the absence of, or with minimal amounts of, the surrounding gene sequence in patients (**see Chapter 2: Fig. 2-4 and** (Goodman et al., 2019a)). Additional studies are needed to define if loss of PAF1C components can disrupt expression from the endogenous *C9orf72* gene harboring the G4C2-repeat expansion (>30). Utilizing C9+ versus control iPS cells and/or iPS neurons, one could downregulate expression of PAF1C components, particularly *Paf1* and *Leo1*, using RNAi or CRISPR/Cas9. Then established quantitative reverse-transcriptase PCR (qPCR) assays would define if the depletion of these genes impacted RNA expression from the

C9orf72 gene (Kramer et al., 2016; Niblock et al., 2016). Such investigations should also consider if multiple PAF1C subunits need to be depleted to see strong effects. If G4C2-expression is mediated by PAF1C in disease, one would expect that *C9orf72*-RNA transcripts would be reduced when these subunits are downregulated. This effect should only be seen in C9+ cells versus control cells if it were the result of the presence of the repeat expansion (>30).

Optimization of the above studies would also allow for follow-up chromatin immunoprecipitation (ChIP) investigations. Specifically, if PAF1C is important for regulating RNAPII during transcription of expanded G4C2-repeats (>30), one would expect that when PAF1C subunits are downregulated that RNAPII's ability to bind the *C9orf72* gene would decrease. This effect should only be seen in C9+ cells versus control cells if it is a response to the presence of the G4C2-repeat expansion (>30). Studies should also consider: whether effects are unique to components Paf1 and Leo1, whether PAF1C recruitment to mutant-*C9orf72* is independent of DSIF-activity, and whether full knockdown of PAF1C genes is needed to significantly impact G4C2-repeat expression. Last, in C9+-derived patient cells, we found that the PAF1C component, Leo1, is bound to the *C9orf72*-chromatin immediately downstream of the G4C2-repeat expansion (**see Chapter 2: Fig. 2-6b and** (Goodman et al., 2019a)**)**. The specificity or enrichment of this binding to a *C9orf72* gene harboring the repeat needs to be determined.

Follow-up investigations could also explore the mechanism underlying PAF1C-regulation of RNAPII during transcription of the G4C2-repeat expansion. For example, as discussed in Chapter 1, PAF1C may play a role in resolving G-quadruplexes and/or R-loops that may form as RNAPII moves across the G4C2-repeat expansion (Gerlach et al., 2017; Landsverk et al., 2019; Reddy et al., 2014; Shivji et al., 2018; Wahba et al.,

2011). Note that R-loop formation by the *C9orf72*-mutant gene occurs *in vivo* and the PAF1C component, Paf1, can regulate R-loop formation in human cells (Esanov et al., 2017; Shivji et al., 2018). Further, this could explain the selectivity of Paf1 and Leo1 to expanded repeats of >30 as one would expect a positive correlation between the repeat-length and formation of these inhibitory secondary structures (Shivji et al., 2018). In total, targeted studies designed to define interactions of PAF1C to G4C2-repeat DNA *in vitro*, *ex vivo*, and/or in flies would determine if PAF1C activity on G4C2-transcription involved the secondary structures these repeats can form.

PAF1C may not be acting alone to promote RNAPII-transcription across expanded G4C2-repeats as it can recruit factors meant to promote RNAPII-driven transcription (e.g. opening up the chromatin, recruiting RNA processing complexes) (Adelman et al., 2006; Jaehning, 2010). Interestingly, in our ~4000 gene screen we tested a number of relevant factors, the majority of which did not modify (G4C2)49-toxicity at all or in a manner consistent with their involvement in G4C2-transcription, including *TFIIS*, *P-TEFb*, *Chd1*, *Set1*, and components of the CCR4-NOT complex. However, this is not an extensive list and more directed studies are required to determine if PAF1C function during G4C2-transcription requires, or is impacted by, additional proteins in C9+ disease. Among potential candidates, ATXN2 may be of particular interest (van Blitterswijk et al., 2014a). Recent publications reported that this gene prevents R-loop accumulation in GC-rich ribosomal DNA and PAF1C may also regulate RNAPI-transcription, suggesting that PAF1C and ATXN2 may interact to regulated transcription of GC-rich DNA (Abraham et al., 2016; Ostrowski et al., 2018; Zhang et al., 2010, 2010). As this would be a relatively novel role of ATXN2, typically considered a cytoplasmic RNA-binding protein that mediates stress-responses (Lee et al., 2018), extensive validation of a potential role in transcription would be needed while

considering how the insertion of an intermediate polyQ within the protein mediates its role in disease.

Last, PAF1C may have effects in C9+ disease that are independent of its role as a transcriptional regulator of the G4C2-repeat expansion. As mentioned earlier, the upregulation of *Paf1* and *Leo1* may contribute to unique expression profiles of C9+ patients versus C9- patients (Cooper-Knock et al., 2015; Prudencio et al., 2015, 2017). In addition, if PAF1C is indeed able to resolve secondary structures formed by GC-rich DNA, then it may play a role in DNA damage reported to occur in C9+ disease (Konopka and Atkin, 2018). Accumulation of R-loops at GC-rich DNA/RNA during transcription can leave DNA vulnerable to breaks and induce cellular stress while the upregulation of *Paf1/Leo1* may be a protective mechanism in C9+ tissue (Crossley et al., 2019; Esanov et al., 2017; Lin and Wilson, 2011; McKay and Cabrita, 2013). Last, instability of the G4C2-repeat expansion within patient cells is a pathological feature of C9+ disease (Vatsavayai et al., 2019). R-loop formation can stimulate expansion or contraction of disease-related repeat expansions (Nakamori et al., 2011; Reddy et al., 2014; Salinas-Rios et al., 2011; Thys and Wang, 2015). A recent study implicated PAF1C in helping to remove stalled RNAPII at R-loops during replication stress, arguing that it may also regulate genomic instability in C9+ disease (Poli et al., 2016). Overall, directed investigations into how expression of expanded G4C2‖G2C4 influences these pathways and whether upregulated PAF1C is involved would further elucidate the role of PAF1C in C9+ disease.

Candidate G4C2-RAN translation factors

Herein, we developed an important, novel G4C2-fly model that includes 114bp intronic sequence found upstream of the G4C2-repeat in C9+ patients, thus putting the repeat in

a more patient-relevant context (**see Chapter 3: Fig. 3-1 and** (Goodman et al., 2019b)). Further, the inclusion of a GFP tag within the GR reading frame makes this unique model a valuable tool for studies on toxic GR-dipeptides produced from a G4C2-RNA *in vivo*. Using this model, an unbiased, targeted screen was performed to identify translation factors whose depletion caused reduced expression of the GR-GFP dipeptide from G4C2-RNA (**see Chapter 3: Fig. 3-2 and** (Goodman et al., 2019b)). To my knowledge, this represents the first *in vivo* screen for potential RAN-translation factors in disease, encompassing 48 of 56 (86%) known translation factors in *Drosophila* (Marygold et al., 2017). From this screen, 11 factors were identified that may mediate expression of toxic GR-dipeptides in G4C2-expressing models. As very little is currently known about the mechanisms underlying G4C2-RAN translation, the results from this screen will, undoubtedly, be of value to the scientific community as additional investigations are pursued (Nguyen et al., 2019). While we focused on two of these, *eIF4B* and *eIF4H* (discussed below), additional investigations into these other translation factors would further define them as RAN-translation factors. Aside from their role in RAN-translation, recent studies have also implicated the toxic GR-dipeptide in translation dysfunctions in C9+ disease (Hartmann et al., 2018; Zhang et al., 2018). Thus, as our screen also tested translation factors for their effects on toxicity caused by the GR-dipeptide, independently from a G4C2-RNA, we further highlighted potential factors involved in GR-associated disease mechanisms (**see Appendix 3: Table S3-2 and** (Goodman et al., 2019b)). Validating our data, eIF3B (also known as eIF3η) was previously shown to interact with GR-dipeptides while our screen revealed that loss of this factor could enhance GR-toxicity in the fly (Zhang et al., 2018).

Our focused investigations into eIF4B and eIF4H offers the first evidence that these two translation factors are players in G4C2-RAN translation (**see Chapter 3: Fig. 3-4, 3-5 and** (Goodman et al., 2019b)). However, additional investigations are needed to fully define their role in this mechanism. Specifically, studies utilizing antibodies specific to each of the 3 sense-strand associated dipeptides – GA, GR, GP – would show that depleted eIF4B and eIF4H could impact expression of GR dipeptides, independent of the GFP tag, and whether this was specific to the GR-reading frame in G4C2-expressing flies. Ensuing investigations should use human cells, ideally C9+-derived iPS cells and/or neurons, to determine if depletion of eIF4B alone, eIF4H alone, or co-depletion of these factors (using RNAi or CRISPR/Cas9) could impact dipeptide expression from an endogenous mutant *C9orf72*-gene. Additional variables that should be considered are: the impact of stress on translation mechanisms, whether loss of these factors causes a global reduction in translation, the impact of age, and tissue specificity. Of these, the impact of stress is of particular importance as G4C2-RAN translation may be promoted by the integrated stress response (Cheng et al., 2018; Green et al., 2017; Tabet et al., 2018). Also, a recent manuscript reported the levels of dipeptide varies between cell types and that mechanisms specific to neurons may impact G4C2-RAN translation (Westergard et al., 2019).

In Chapter 3, we also show that *eIF4H* is downregulated in C9+-derived patient cells and in C9+ ALS/FTD post-mortem cerebellar tissue (**see Chapter 3: Fig. 3-6 and** (Goodman et al., 2019b)). The simplest hypothesis is that this was a protective response by cells as reducing expression of this translation factor may help to reduce expression of toxic GR-dipeptide. However, eIF4H's downregulation could also be the response of a more complicated process since it may be sequestered by G4C2-RNA foci (Cooper-Knock et al., 2014; Haeusler et al., 2014; Satoh et al., 2014). Thus, cells may mistakenly

sense that there is plenty of eIF4H available and thus downregulate the gene's expression. However, the eIF4H that is within the cell is, in fact, unavailable to perform its normal duties as it is sequestered by G4C2-RNA. Directed investigations are needed to define which of these pathways may be occurring in C9+ disease. While it may be difficult to differentiate these mechanisms, confirmation that eIF4H is sequestered into G4C2-RNA foci, as is predicted by *in vitro* data, would add to the possibility that the more complicated hypothesis is at play. eIF4H could also be disrupted through other mechanisms independent of direct interactions with G4C2-RNA (e.g. mis-localization). Overall, this may put eIF4H in a unique position to couple RNA dysregulation in disease to RAN-translation. Aside from this, depletion of eIF4B and eIF4H had previously been reported to induce stress granule formation *ex vivo* (Mokas et al., 2009). Thus, the depletion of eIF4H may have multiple implications in C9+ disease, such as linking G4C2-disease mechanisms to the onset of TDP-43 pathology (Chew et al., 2015; McGurk et al., 2018; Zhang et al., 2018).

Other repeat diseases

Thus far, I have focused on the role of PAF1C and identified translation factors in C9+ ALS/FTD that harbor a hexanucleotide repeat expansion of >30 G4C2. However, the identified mechanisms described that mediate transcription/translation from G4C2-repeat RNA may also impact other nucleotide-repeat expansions. There are multiple examples of GC-rich repeat expansions associated with neurodegenerative disease (ND), including: CAG-repeats found in polyglutamine diseases (polyQ diseases are a heterogenous group of NDs that includes Huntington's disease (HD) and multiple spinal cerebellar ataxias (SCAs)), CTG-repeats found in myotonic dystrophy 1 (DM1), CCTG-repeats found in myotonic dystrophy 2 (DM2), and CGG-repeats found in Fragile-X-

associated tremor and ataxia syndrome (FXTAS) (Chen et al., 2018; Krzyzosiak et al., 2012; Nguyen et al., 2019; Todd Peter K. and Paulson Henry L., 2010). The location of the expanded repeat within the afflicted genes can vary amid promotors (e.g. CAG-repeat in SCA12), 5'UTR of genes (e.g. FXTAS), introns (e.g. DM2), exons (e.g. CAG-repeat multiple polyQ diseases), and 3' UTR of genes (e.g. DM1). Based on location, the repeats can cause gain-of-function toxicity, such as that described for G4C2-repeats herein, or can disrupt the normal function of the afflicted gene/gene product causing loss-of-function disease mechanisms.

Unique transcriptional machinery required to promote RNAPII-activity as it moves through GC-rich repeat expansions may be common among diseases. For example, the DSIF complex has been suggested to regulate RNAPII-transcription of multiple repetitive DNA elements, including (G4C2)8+, (CAG)99+, (CTG)105, (CAA)90 and (AAA)24+ sequences (**see Chapter 2** and (Cheng et al., 2015; Goodman et al., 2019a; Kramer et al., 2016; Liu et al., 2012)). Thus, it is reasonable to expand investigations of PAF1C to additional repeat-associated diseases. In particular, fly studies described in Chapter 2 can be extended to existing fly models that harbor CAG, CTG, or CTGG-repeat expansions (Shieh and Bonini, 2011; Yu et al., 2015b). One could define whether downregulation of PAF1C components, particularly *Paf1* and *Leo1*, using RNAi can suppress toxicity caused by the expression of these repeats in the fly. Mechanistic studies would also reveal if the RNA-transcript levels produced from the transgenes are reduced with knockdown of PAF1C components and if this knockdown disrupts RNAPII-binding to the transgene. Notably, interactions could depend on unique secondary structures formed by these repeats as they are predicted to form G-quadruplexes, R-loops, and hairpins like G4C2-DNA, which may need to be resolved during transcription (Childs-Disney et al., 2014; Cruchten et al., 2019; Freudenreich, 2018; Krzyzosiak et al.,

2012; Reddy et al., 2014). Overall, these investigations would explore if PAF1C plays a global role in multiple repeat-associated diseases while increasing our understandings of its function in C9+ ALS/FTD.

In addition to G4C2-repeats, RNA-transcripts produced by the mentioned repeat-expansions can also undergo RAN-translation. Of note, CAG repeats can produce three peptides, depending on the reading frame (Zu et al., 2011). Interestingly, peptide production was dependent on repeat-length and the RNA's ability to form hairpin structures, like ones potentially formed by G4C2 RNA (Su et al., 2014; Wang et al., 2019). Moreover, CGG-repeats can also produce peptides through mechanisms independent of an AUG-start codon (Kearse et al., 2016; Todd et al., 2013). Recently, Todd and colleagues drew parallels between CGG- and G4C2-RAN translation mechanisms, highlighting that both require eIF4E and eIF4A (Green et al., 2017; Kearse et al., 2016). Intriguingly, our studies highlight eIF4B and eIF4H for playing a role in G4C2-RAN translation (**see Chapter 3 and** (Goodman et al., 2019b)) while these two factors act on eIF4A to promote unwinding of secondary structures formed by RNA (Rogers et al., 2001; Rozovsky et al., 2008; Nielsen et al., 2011; Sun et al., 2012; Harms et al., 2014; García-García et al., 2015; Vaysse et al., 2015; Sen et al., 2016). This activity by eIF4B and eIF4H is particularly important at highly structured, repetitive RNA sequences (Sen et al., 2016; Sun et al., 2012). Thus, it is reasonable to hypothesize that these two factors may also play a role in CGG- and/or CAG-RAN translation. The connection between G4C2-, CGG-, and CAG-RAN translation may be their ability to form unique hairpin structures (Krzyzosiak et al., 2012; Wang et al., 2019). In total, while directed studies are needed to define the role of eIF4B, eIF4H, and other potential translation factors we identified in our screen as G4C2-RAN translation factors (see Chapter 3 and (Goodman et al., 2019b)), ensuing investigations that expand findings to

other repeat-RNAs that undergo RAN-translation may help to define common mechanisms underlying this unique process.

Closing statements

The devastation of neurodegenerative diseases impacts individuals and society, pushing the need for scientists and clinicians to rapidly elucidate disease mechanisms while innately uncovering potential therapeutic targets. The aberrant expression of a hexanucleotide expansion of >30 G4C2-repeats within *C9orf72* is currently the most prominent known mutation in familial ALS/FTD. Accumulating evidence suggests that this mutation confers toxicity through gain-of-function mechanisms, a finding that may prove advantageous in terms of developing an effective therapy. In fact, research is currently underway to define pharmacological reagents, such as small molecules and antisense oligonucleotides, that may be able to disrupt G4C2-associated disease mechanisms when administered to patients (Donnelly et al., 2013; Hu et al., 2016; Jiang et al., 2016; Perego et al., 2018; Simone et al., 2018; Su et al., 2014; Wang et al., 2019; Zamiri et al., 2014). While promising, there are limitations to these current approaches, such as their inability to simultaneously target both sense- and antisense- transcripts produced from the G4C2‖G2C4 DNA in patients (Jiang and Cleveland, 2016). Accordingly, inhibiting the transcription or translation of mutant-*C9orf72* in patients may be a more effective approach. Recent work has proposed using epigenetic modifiers to shut down the gene (Belzil et al., 2014; Liu et al., 2014; McMillan et al., 2015; Russ et al., 2015; Xi et al., 2013, 2014, 2015; Zeier et al., 2015). Alternatively, herein we define unique transcription and translation factors that may be important for the expression of the G4C2‖G2C4-repeat expansion in disease. Speculatively, inhibiting *Paf1* or *Leo1* of PAF1C may be an acceptable approach to downregulating bidirectional transcription of

mutant-*C9orf72*. Our data shows that these components are selective to >30 G4C2-repeats, unlike previously proposed Spt4 (**see Chapter 2 and** (Goodman et al., 2019a; Kramer et al., 2016; Naguib et al., 2019)). Further, partial inhibition of these genes may impact G4C2-transcripton while being well tolerated for cell viability. Note that PAF1C only regulates expression from a subset of genes and mice that are heterozygous null for Paf1 or Leo1 are relatively normal (Porter et al., 2002; Mueller et al., 2004; Penheiter et al., 2005; Cao et al., 2015; Yang et al., 2016; Fischl et al., 2017; Meehan et al., 2017; Ringwald et al., 2011; Skarnes et al., 2011).

Overall, the included studies help to uncover gain-of-function disease mechanisms in *C9orf72*-associated ALS/FTD while highlighting machinery important for G4C2‖G2C4 DNA/RNA expression in the context of disease. These findings have the potential to elucidate mechanisms pertinent to multiple repeat-associated diseases.

Bibliography

Abraham, K.J., Chan, J.N.Y., Salvi, J.S., Ho, B., Hall, A., Vidya, E., Guo, R., Killackey, S.A., Liu, N., Lee, J.E., et al. (2016). Intersection of calorie restriction and magnesium in the suppression of genome-destabilizing RNA–DNA hybrids. Nucleic Acids Research *44*, 8870.

Adelman, K., Wei, W., Ardehali, M.B., Werner, J., Zhu, B., Reinberg, D., and Lis, J.T. (2006). Drosophila Paf1 Modulates Chromatin Structure at Actively Transcribed Genes. Mol Cell Biol *26*, 250–260.

Ash, P.E.A., Bieniek, K.F., Gendron, T.F., Caulfield, T., Lin, W.-L., DeJesus-Hernandez, M., van Blitterswijk, M.M., Jansen-West, K., Paul, J.W., Rademakers, R., et al. (2013). Unconventional translation of C9ORF72 GGGGCC expansion generates insoluble polypeptides specific to c9FTD/ALS. Neuron *77*, 639–646.

Bai, B., Hales, C.M., Chen, P.-C., Gozal, Y., Dammer, E.B., Fritz, J.J., Wang, X., Xia, Q., Duong, D.M., Street, C., et al. (2013). U1 small nuclear ribonucleoprotein complex and RNA splicing alterations in Alzheimer's disease. Proc Natl Acad Sci U S A *110*, 16562–16567.

Bai, B., Chen, P.-C., Hales, C.M., Wu, Z., Pagala, V., High, A.A., Levey, A.I., Lah, J.J., and Peng, J. (2014). Integrated Approaches for Analyzing U1-70K Cleavage in Alzheimer's Disease. J Proteome Res *13*, 4526–4534.

Baral, A., Kumar, P., Pathak, R., and Chowdhury, S. (2013). Emerging trends in G-quadruplex biology – role in epigenetic and evolutionary events. Mol. BioSyst. *9*, 1568–1575.

Bauer, P.O. (2016). Methylation of C9orf72 expansion reduces RNA foci formation and dipeptide-repeat proteins expression in cells. Neuroscience Letters *612*, 204–209.

Belzil, V.V., Bauer, P.O., Gendron, T.F., Murray, M.E., Dickson, D., and Petrucelli, L. (2014). Characterization of DNA hypermethylation in the cerebellum of c9FTD/ALS patients. Brain Res. *1584*, 15–21.

van Blitterswijk, M., DeJesus-Hernandez, M., Niemantsverdriet, E., Murray, M.E., Heckman, M.G., Diehl, N.N., Brown, P.H., Baker, M.C., Finch, N.A., Bauer, P.O., et al. (2013). Associations of repeat sizes with clinical and pathological characteristics in C9ORF72 expansion carriers (Xpansize-72): a cross-sectional cohort study. Lancet Neurol *12*.

van Blitterswijk, M., Mullen, B., Heckman, M.G., Baker, M.C., DeJesus-Hernandez, M., Brown, P.H., Murray, M.E., Hsiung, G.-Y.R., Stewart, H., Karydas, A.M., et al. (2014a). Ataxin-2 as potential disease modifier in C9ORF72 expansion carriers. Neurobiol Aging *35*, 2421.e13-2421.e17.

van Blitterswijk, M., Mullen, B., Nicholson, A.M., Bieniek, K.F., Heckman, M.G., Baker, M.C., DeJesus-Hernandez, M., Finch, N.A., Brown, P.H., Murray, M.E., et al. (2014b). TMEM106B protects C9ORF72 expansion carriers against frontotemporal dementia. Acta Neuropathol *127*, 397–406.

Boeve, B.F., Boylan, K.B., Graff-Radford, N.R., DeJesus-Hernandez, M., Knopman, D.S., Pedraza, O., Vemuri, P., Jones, D., Lowe, V., Murray, M.E., et al. (2012). Characterization of frontotemporal dementia and/or amyotrophic lateral sclerosis associated with the GGGGCC repeat expansion in C9ORF72. Brain *135*, 765–783.

Brázda, V., Hároníková, L., Liao, J.C.C., and Fojta, M. (2014). DNA and RNA Quadruplex-Binding Proteins. International Journal of Molecular Sciences *15*, 17493.

Buchman, V.L., Cooper-Knock, J., Connor-Robson, N., Higginbottom, A., Kirby, J., Razinskaya, O.D., Ninkina, N., and Shaw, P.J. (2013). Simultaneous and independent detection of C9ORF72 alleles with low and high number of GGGGCC repeats using an optimised protocol of Southern blot hybridisation. Molecular Neurodegeneration *8*, 12.

Cao, Q.-F., Yamamoto, J., Isobe, T., Tateno, S., Murase, Y., Chen, Y., Handa, H., and Yamaguchi, Y. (2015). Characterization of the Human Transcription Elongation Factor Rtf1: Evidence for Nonoverlapping Functions of Rtf1 and the Paf1 Complex. Mol Cell Biol *35*, 3459–3470.

Chen, Z., Sequeiros, J., Tang, B., and Jiang, H. (2018). Genetic modifiers of age-at-onset in polyglutamine diseases. Ageing Research Reviews *48*, 99–108.

Cheng, H.-M., Chern, Y., Chen, I.-H., Liu, C.-R., Li, S.-H., Chun, S.J., Rigo, F., Bennett, C.F., Deng, N., Feng, Y., et al. (2015). Effects on Murine Behavior and Lifespan of Selectively Decreasing Expression of Mutant Huntingtin Allele by Supt4h Knockdown. PLoS Genet *11*.

Cheng, W., Wang, S., Mestre, A.A., Fu, C., Makarem, A., Xian, F., Hayes, L.R., Lopez-Gonzalez, R., Drenner, K., Jiang, J., et al. (2018). C9ORF72 GGGGCC repeat-associated non-AUG translation is upregulated by stress through eIF2α phosphorylation. Nature Communications *9*, 51.

Chew, J., Gendron, T.F., Prudencio, M., Sasaguri, H., Zhang, Y.-J., Castanedes-Casey, M., Lee, C.W., Jansen-West, K., Kurti, A., Murray, M.E., et al. (2015). C9ORF72 repeat expansions in mice cause TDP-43 pathology, neuronal loss, and behavioral deficits. Science *348*, 1151–1154.

Chew, J., Cook, C., Gendron, T.F., Jansen-West, K., del Rosso, G., Daughrity, L.M., Castanedes-Casey, M., Kurti, A., Stankowski, J.N., Disney, M.D., et al. (2019). Aberrant deposition of stress granule-resident proteins linked to C9orf72-associated TDP-43 proteinopathy. Molecular Neurodegeneration *14*, 9.

Childs-Disney, J.L., Yildirim, I., Park, H., Lohman, J.R., Guan, L., Tran, T., Sarkar, P., Schatz, G.C., and Disney, M.D. (2014). Structure of the Myotonic Dystrophy Type 2 RNA and Designed Small Molecules That Reduce Toxicity. ACS Chemical Biology *9*, 538.

Chu, X., Qin, X., Xu, H., Li, L., Wang, Z., Li, F., Xie, X., Zhou, H., Shen, Y., and Long, J. (2013). Structural insights into Paf1 complex assembly and histone binding. Nucleic Acids Res *41*, 10619–10629.

Conlon, E.G., Lu, L., Sharma, A., Yamazaki, T., Tang, T., Shneider, N.A., and Manley, J.L. (2016). The C9ORF72 GGGGCC expansion forms RNA G-quadruplex inclusions and sequesters hnRNP H to disrupt splicing in ALS brains. ELife Sciences *5*, e17820.

Cooper-Knock, J., Walsh, M.J., Higginbottom, A., Robin Highley, J., Dickman, M.J., Edbauer, D., Ince, P.G., Wharton, S.B., Wilson, S.A., Kirby, J., et al. (2014). Sequestration of multiple RNA recognition motif-containing proteins by C9orf72 repeat expansions. Brain *137*, 2040–2051.

Cooper-Knock, J., Bury, J.J., Heath, P.R., Wyles, M., Higginbottom, A., Gelsthorpe, C., Highley, J.R., Hautbergue, G., Rattray, M., Kirby, J., et al. (2015). C9ORF72 GGGGCC Expanded

Repeats Produce Splicing Dysregulation which Correlates with Disease Severity in Amyotrophic Lateral Sclerosis. PLoS One *10*.

Coyne, A.N., Zaepfel, B.L., and Zarnescu, D.C. (2017). Failure to Deliver and Translate—New Insights into RNA Dysregulation in ALS. Front. Cell. Neurosci. *11*.

Crossley, M.P., Bocek, M., and Cimprich, K.A. (2019). R-Loops as Cellular Regulators and Genomic Threats. Molecular Cell *73*, 398–411.

Cruchten, R.T.P. van, Wieringa, B., and Wansink, D.G. (2019). Expanded CUG repeats in DMPK transcripts adopt diverse hairpin conformations without influencing the structure of the flanking sequences. RNA *25*, 481–495.

Davidson, Y.S., Flood, L., Robinson, A.C., Nihei, Y., Mori, K., Rollinson, S., Richardson, A., Benson, B.C., Jones, M., Snowden, J.S., et al. (2017). Heterogeneous ribonuclear protein A3 (hnRNP A3) is present in dipeptide repeat protein containing inclusions in Frontotemporal Lobar Degeneration and Motor Neurone disease associated with expansions in C9orf72 gene. Acta Neuropathologica Communications *5*, 31.

DeJesus-Hernandez, M., Mackenzie, I.R., Boeve, B.F., Boxer, A.L., Baker, M., Rutherford, N.J., Nicholson, A.M., Finch, N.A., Gilmer, H.F., Adamson, J., et al. (2011). Expanded GGGGCC hexanucleotide repeat in non-coding region of C9ORF72 causes chromosome 9p-linked frontotemporal dementia and amyotrophic lateral sclerosis. Neuron *72*, 245–256.

Deshpande, S.M., Sadhale, P.P., and Vijayraghavan, U. (2014). Involvement of S. cerevisiae Rpb4 in subset of pathways related to transcription elongation. Gene *545*, 126–131.

Dobson-Stone, C., Hallupp, M., Loy, C.T., Thompson, E.M., Haan, E., Sue, C.M., Panegyres, P.K., Razquin, C., Seijo-Martínez, M., Rene, R., et al. (2013). C9ORF72 Repeat Expansion in Australian and Spanish Frontotemporal Dementia Patients. PLOS ONE *8*, e56899.

Donnelly, C.J., Zhang, P.-W., Pham, J.T., Heusler, A.R., Mistry, N.A., Vidensky, S., Daley, E.L., Poth, E.M., Hoover, B., Fines, D.M., et al. (2013). RNA Toxicity from the ALS/FTD C9ORF72 Expansion Is Mitigated by Antisense Intervention. Neuron *80*, 415–428.

Duarte, A.R., Cadoni, E., Ressurreição, A.S., Moreira, R., and Paulo, A. (2018). Design of Modular G-quadruplex Ligands. ChemMedChem *13*, 869–893.

Esanov, R., Cabrera, G.T., Andrade, N.S., Gendron, T.F., Brown, R.H., Benatar, M., Wahlestedt, C., Mueller, C., and Zeier, Z. (2017). A C9ORF72 BAC mouse model recapitulates key epigenetic perturbations of ALS/FTD. Molecular Neurodegeneration *12*, 46.

Farg, M.A., Konopka, A., Soo, K.Y., Ito, D., and Atkin, J.D. (2017). The DNA damage response (DDR) is induced by the C9orf72 repeat expansion in amyotrophic lateral sclerosis. Hum Mol Genet *26*, 2882–2896.

Faudale, M., Cogoi, S., and Xodo, L.E. (2011). Photoactivated cationic alkyl-substituted porphyrin binding to g4-RNA in the 5′-UTR of KRAS oncogene represses translation. Chem. Commun. *48*, 874–876.

Fischl, H., Howe, F.S., Furger, A., and Mellor, J. (2017). Paf1 Has Distinct Roles in Transcription Elongation and Differential Transcript Fate. Mol Cell *65*, 685-698.e8.

Fratta, P., Mizielinska, S., Nicoll, A.J., Zloh, M., Fisher, E.M.C., Parkinson, G., and Isaacs, A.M. (2012). C9orf72 hexanucleotide repeat associated with amyotrophic lateral sclerosis and frontotemporal dementia forms RNA G-quadruplexes. Sci Rep *2*.

Freibaum, B.D., Lu, Y., Lopez-Gonzalez, R., Kim, N.C., Almeida, S., Lee, K.-H., Badders, N., Valentine, M., Miller, B.L., Wong, P.C., et al. (2015). GGGGCC repeat expansion in C9ORF72 compromises nucleocytoplasmic transport. Nature *525*, 129–133.

Freudenreich, C.H. (2018). R-loops: targets for nuclease cleavage and repeat instability. Curr Genet 1–6.

García, A., Collin, A., and Calvo, O. (2012). Sub1 associates with Spt5 and influences RNA polymerase II transcription elongation rate. MBoC *23*, 4297–4312.

García-García, C., Frieda, K.L., Feoktistova, K., Fraser, C.S., and Block, S.M. (2015). Factor-dependent processivity in human eIF4A DEAD-box helicase. Science *348*, 1486–1488.

Gerlach, J.M., Furrer, M., Gallant, M., Birkel, D., Baluapuri, A., Wolf, E., and Gallant, P. (2017). PAF1 complex component Leo1 helps recruit Drosophila Myc to promoters. PNAS *114*, E9224–E9232.

Goodman, L.D., Prudencio, M., Kramer, N.J., Martinez-Ramirez, L.F., Srinivasan, A.R., Lan, M., Parisi, M.J., Zhu, Y., Chew, J., Cook, C.N., et al. (2019a). Expanded GGGGCC repeat transcription is mediated by the PAF1 complex in C9orf72-associated FTD. Nat Neurosci.

Goodman, L.D., Prudencio, M., Srinivasan, A.R., Rifai, O.M., Lee, V.M.-Y., Petrucelli, L., and Bonini, N.M. (2019b). eIF4B and eIF4H mediate GR production from expanded G4C2 in a Drosophila model for C9orf72-associated ALS. Acta Neuropathol Commun.

Green, K.M., Glineburg, M.R., Kearse, M.G., Flores, B.N., Linsalata, A.E., Fedak, S.J., Goldstrohm, A.C., Barmada, S.J., and Todd, P.K. (2017). RAN translation at C9orf72-associated repeat expansions is selectively enhanced by the integrated stress response. Nat Commun *8*.

Haeusler, A.R., Donnelly, C.J., Periz, G., Simko, E.A.J., Shaw, P.G., Kim, M.-S., Maragakis, N.J., Troncoso, J.C., Pandey, A., Sattler, R., et al. (2014). C9orf72 Nucleotide Repeat Structures Initiate Molecular Cascades of Disease. Nature *507*, 195–200.

Hales, C.M., Dammer, E.B., Diner, I., Yi, H., Seyfried, N.T., Gearing, M., Glass, J.D., Montine, T.J., Levey, A.I., and Lah, J.J. (2014). Aggregates of Small Nuclear Ribonucleic Acids (snRNAs) in Alzheimer's Disease. Brain Pathology *24*, 344–351.

Hall, A.C., Ostrowski, L.A., Pietrobon, V., and Mekhail, K. (2017). Repetitive DNA loci and their modulation by the non-canonical nucleic acid structures R-loops and G-quadruplexes. Nucleus *8*, 162–181.

Harms, U., Andreou, A.Z., Gubaev, A., and Klostermeier, D. (2014). eIF4B, eIF4G and RNA regulate eIF4A activity in translation initiation by modulating the eIF4A conformational cycle. Nucleic Acids Res *42*, 7911–7922.

Hartmann, H., Hornburg, D., Czuppa, M., Bader, J., Michaelsen, M., Farny, D., Arzberger, T., Mann, M., Meissner, F., and Edbauer, D. (2018). Proteomics and C9orf72 neuropathology identify ribosomes as poly-GR/PR interactors driving toxicity. Life Science Alliance *1*, e201800070.

Hartzog, G.A., and Fu, J. (2013). The Spt4-Spt5 complex: a multi-faceted regulator of transcription elongation. Biochimica et Biophysica Acta *1829*, 105.

Herrmann, D., and Parlato, R. (2018). C9orf72-associated neurodegeneration in ALS-FTD: breaking new ground in ribosomal RNA and nucleolar dysfunction. Cell Tissue Res 1–10.

Higelin, J., Catanese, A., Semelink-Sedlacek, L.L., Oeztuerk, S., Lutz, A.-K., Bausinger, J., Barbi, G., Speit, G., Andersen, P.M., Ludolph, A.C., et al. (2018). NEK1 loss-of-function mutation induces DNA damage accumulation in ALS patient-derived motoneurons. Stem Cell Research *30*, 150–162.

Hu, J., Rigo, F., Prakash, T.P., and Corey, D.R. (2016). Recognition of c9orf72 Mutant RNA by Single-Stranded Silencing RNAs. Nucleic Acid Therapeutics *27*, 87–94.

Hübers, A., Marroquin, N., Schmoll, B., Vielhaber, S., Just, M., Mayer, B., Högel, J., Dorst, J., Mertens, T., Just, W., et al. (2014). Polymerase chain reaction and Southern blot-based analysis of the C9orf72 hexanucleotide repeat in different motor neuron diseases. Neurobiol. Aging *35*, 1214.e1-6.

Ishiguro, A., Kimura, N., Watanabe, Y., Watanabe, S., and Ishihama, A. (2016). TDP-43 binds and transports G-quadruplex-containing m RNAs into neurites for local translation. Genes to Cells *21*, 466–481.

Ito, D., Hatano, M., and Suzuki, N. (2017). RNA binding proteins and the pathological cascade in ALS/FTD neurodegeneration. Science Translational Medicine *9*, eaah5436.

Jaehning, J.A. (2010). The Paf1 Complex: Platform or Player in RNA Polymerase II Transcription? Biochimica et Biophysica Acta *1799*, 379.

Jiang, J., and Cleveland, D.W. (2016). Bidirectional Transcriptional Inhibition as Therapy for ALS/FTD Caused by Repeat Expansion in C9orf72. Neuron *92*, 1160–1163.

Jiang, J., Zhu, Q., Gendron, T.F., Saberi, S., McAlonis-Downes, M., Seelman, A., Stauffer, J.E., Jafar-nejad, P., Drenner, K., Schulte, D., et al. (2016). Gain of toxicity from ALS/FTD-linked repeat expansions in C9ORF72 is alleviated by antisense oligonucleotides targeting GGGGCC-containing RNAs. Neuron *90*, 535–550.

Johnson, E.C.B., Dammer, E.B., Duong, D.M., Yin, L., Thambisetty, M., Troncoso, J.C., Lah, J.J., Levey, A.I., and Seyfried, N.T. (2018). Deep proteomic network analysis of Alzheimer's disease brain reveals alterations in RNA binding proteins and RNA splicing associated with disease. Molecular Neurodegeneration *13*, 52.

Jung, J., and Bonini, N. (2007). CREB-Binding Protein Modulates Repeat Instability in a Drosophila Model for PolyQ Disease. Science *315*, 1857–1859.

Jung, J., Jaarsveld, M.T.M. van, Shieh, S.-Y., Xu, K., and Bonini, N.M. (2011). Defining Genetic Factors That Modulate Intergenerational CAG Repeat Instability in Drosophila melanogaster. Genetics *187*, 61–71.

Kearse, M.G., Green, K.M., Krans, A., Rodriguez, C.M., Linsalata, A.E., Goldstrohm, A.C., and Todd, P.K. (2016). CGG Repeat-Associated Non-AUG Translation Utilizes a Cap-Dependent Scanning Mechanism of Initiation to Produce Toxic Proteins. Molecular Cell *62*, 314–322.

Kejnovsky, E., Tokan, V., and Lexa, M. (2015). Transposable elements and G-quadruplexes. Chromosome Res *23*, 615–623.

Konopka, A., and Atkin, J.D. (2018). The Emerging Role of DNA Damage in the Pathogenesis of the C9orf72 Repeat Expansion in Amyotrophic Lateral Sclerosis. International Journal of Molecular Sciences *19*, 3137.

Kramer, N.J., Carlomagno, Y., Zhang, Y.-J., Almeida, S., Cook, C.N., Gendron, T.F., Prudencio, M., Van Blitterswijk, M., Belzil, V., Couthouis, J., et al. (2016). Spt4 selectively regulates the expression of C9orf72 sense and antisense mutant transcripts associated with c9FTD/ALS. Science *353*, 708–712.

Krzyzosiak, W.J., Sobczak, K., Wojciechowska, M., Fiszer, A., Mykowska, A., and Kozlowski, P. (2012). Triplet repeat RNA structure and its role as pathogenic agent and therapeutic target. Nucleic Acids Res *40*, 11–26.

Kumar, V., kashav, T., Islam, A., Ahmad, F., and Hassan, M.I. (2016). Structural insight into C9orf72 hexanucleotide repeat expansions: Towards new therapeutic targets in FTD-ALS. Neurochemistry International *100*, 11–20.

Kwon, I., Xiang, S., Kato, M., Wu, L., Theodoropoulos, P., Wang, T., Kim, J., Yun, J., Xie, Y., and McKnight, S.L. (2014). Poly-dipeptides encoded by the C9orf72 repeats bind nucleoli, impede RNA biogenesis, and kill cells. Science *345*, 1139–1145.

Landsverk, H.B., Sandquist, L.E., Sridhara, S.C., Rødland, G.E., Sabino, J.C., de Almeida, S.F., Grallert, B., Trinkle-Mulcahy, L., and Syljuåsen, R.G. (2019). Regulation of ATR activity via the RNA polymerase II associated factors CDC73 and PNUTS-PP1. Nucleic Acids Res *47*, 1797–1813.

Lee, J., Kim, M., Itoh, T.Q., and Lim, C. (2018). Ataxin-2: A versatile posttranscriptional regulator and its implication in neural function. Wiley Interdisciplinary Reviews: RNA *9*, e1488.

Lee, K.-H., Zhang, P., Kim, H.J., Mitrea, D.M., Sarkar, M., Freibaum, B.D., Cika, J., Coughlin, M., Messing, J., Molliex, A., et al. (2016). C9orf72 Dipeptide Repeats Impair the Assembly, Dynamics, and Function of Membrane-Less Organelles. Cell *167*, 774-788.e17.

Lee, Y.-B., Chen, H.-J., Peres, J.N., Gomez-Deza, J., Attig, J., Štalekar, M., Troakes, C., Nishimura, A.L., Scotter, E.L., Vance, C., et al. (2013). Hexanucleotide Repeats in ALS/FTD Form Length-Dependent RNA Foci, Sequester RNA Binding Proteins, and Are Neurotoxic. Cell Reports *5*, 1178–1186.

Lin, Y., and Wilson, J.H. (2011). Transcription-induced DNA toxicity at trinucleotide repeats. Cell Cycle *10*, 611–618.

Liu, C.-R., Chang, C.-R., Chern, Y., Wang, T.-H., Hsieh, W.-C., Shen, W.-C., Chang, C.-Y., Chu, I.-C., Deng, N., Cohen, S.N., et al. (2012). Spt4 Is Selectively Required for Transcription of Extended Trinucleotide Repeats. Cell *148*, 690–701.

Liu, E.Y., Russ, J., Wu, K., Neal, D., Suh, E., McNally, A.G., Irwin, D.J., Van Deerlin, V.M., and Lee, E.B. (2014). C9orf72 hypermethylation protects against repeat expansion-associated pathology in ALS/FTD. Acta Neuropathol *128*, 525–541.

Lopez-Gonzalez, R., Lu, Y., Gendron, T.F., Karydas, A., Tran, H., Yang, D., Petrucelli, L., Miller, B.L., Almeida, S., and Gao, F.-B. (2016). Poly(GR) in C9ORF72-Related ALS/FTD Compromises Mitochondrial Function and Increases Oxidative Stress and DNA Damage in iPSC-Derived Motor Neurons. Neuron *92*, 383–391.

Marygold, S.J., Attrill, H., and Lasko, P. (2017). The translation factors of Drosophila melanogaster. Fly *11*, 65–74.

McGurk, L., Gomes, E., Guo, L., Mojsilovic-Petrovic, J., Tran, V., Kalb, R.G., Shorter, J., and Bonini, N.M. (2018). Poly(ADP-Ribose) Prevents Pathological Phase Separation of TDP-43 by Promoting Liquid Demixing and Stress Granule Localization. Molecular Cell *71*, 703-717.e9.

McKay, B.C., and Cabrita, M.A. (2013). Arresting transcription and sentencing the cell: The consequences of blocked transcription. Mechanisms of Ageing and Development *134*, 243–252.

McMillan, C.T., Russ, J., Wood, E.M., Irwin, D.J., Grossman, M., McCluskey, L., Elman, L., Van Deerlin, V., and Lee, E.B. (2015). C9orf72 promoter hypermethylation is neuroprotective: Neuroimaging and neuropathologic evidence. Neurology *84*, 1622–1630.

Meehan, T.F., Conte, N., West, D.B., Jacobsen, J.O., Mason, J., Warren, J., Chen, C.-K., Tudose, I., Relac, M., Matthews, P., et al. (2017). Disease Model Discovery from 3,328 Gene Knockouts by The International Mouse Phenotyping Consortium. Nat Genet *49*, 1231–1238.

Mizielinska, S., Grönke, S., Niccoli, T., Ridler, C.E., Clayton, E.L., Devoy, A., Moens, T., Norona, F.E., Woollacott, I.O.C., Pietrzyk, J., et al. (2014). C9orf72 repeat expansions cause neurodegeneration in Drosophila through arginine-rich proteins. Science *345*, 1192–1194.

Mizielinska, S., Ridler, C.E., Balendra, R., Thoeng, A., Woodling, N.S., Grässer, F.A., Plagnol, V., Lashley, T., Partridge, L., and Isaacs, A.M. (2017). Bidirectional nucleolar dysfunction in C9orf72 frontotemporal lobar degeneration. Acta Neuropathologica Communications *5*, 29.

Mokas, S., Mills, J.R., Garreau, C., Fournier, M.-J., Robert, F., Arya, P., Kaufman, R.J., Pelletier, J., and Mazroui, R. (2009). Uncoupling Stress Granule Assembly and Translation Initiation Inhibition. Mol Biol Cell *20*, 2673–2683.

Mori, K., Lammich, S., Mackenzie, I.R.A., Forné, I., Zilow, S., Kretzschmar, H., Edbauer, D., Janssens, J., Kleinberger, G., Cruts, M., et al. (2013). hnRNP A3 binds to GGGGCC repeats and is a constituent of p62-positive/TDP43-negative inclusions in the hippocampus of patients with <Emphasis Type="Italic">C9orf72</Emphasis> mutations. Acta Neuropathol *125*, 413–423.

Mueller, C.L., Porter, S.E., Hoffman, M.G., and Jaehning, J.A. (2004). The Paf1 Complex Has Functions Independent of Actively Transcribing RNA Polymerase II. Molecular Cell *14*, 447–456.

Mukherjee, A.K., Sharma, S., and Chowdhury, S. (2019). Non-duplex G-Quadruplex Structures Emerge as Mediators of Epigenetic Modifications. Trends in Genetics *35*, 129–144.

Naguib, A., Sandmann, T., Yi, F., Watts, R.J., Lewcock, J.W., and Dowdle, W.E. (2019). SUPT4H1 Depletion Leads to a Global Reduction in RNA. Cell Reports *26*, 45-53.e4.

Nakamori, M., Pearson, C.E., and Thornton, C.A. (2011). Bidirectional transcription stimulates expansion and contraction of expanded (CTG)•(CAG) repeats. Hum Mol Genet *20*, 580–588.

Nguyen, L., Cleary, J.D., and Ranum, L.P.W. (2019). Repeat-Associated Non-ATG Translation: Molecular Mechanisms and Contribution to Neurological Disease. Annual Review of Neuroscience *42*.

Niblock, M., Smith, B.N., Lee, Y.-B., Sardone, V., Topp, S., Troakes, C., Al-Sarraj, S., Leblond, C.S., Dion, P.A., Rouleau, G.A., et al. (2016). Retention of hexanucleotide repeat-containing intron in C9orf72 mRNA: implications for the pathogenesis of ALS/FTD. Acta Neuropathol Commun *4*.

Nielsen, K.H., Behrens, M.A., He, Y., Oliveira, C.L.P., Sottrup Jensen, L., Hoffmann, S.V., Pedersen, J.S., and Andersen, G.R. (2011). Synergistic activation of eIF4A by eIF4B and eIF4G. Nucleic Acids Research *39*, 2678–2689.

Nik, S., and Bowman, T.V. (2019). Splicing and neurodegeneration: Insights and mechanisms. Wiley Interdisciplinary Reviews: RNA *0*, e1532.

Nussbacher, J.K., Tabet, R., Yeo, G.W., and Lagier-Tourenne, C. (2019). Disruption of RNA Metabolism in Neurological Diseases and Emerging Therapeutic Interventions. Neuron *102*, 294–320.

Omer, T., Finegan, E., Hutchinson, S., Doherty, M., Vajda, A., McLaughlin, R.L., Pender, N., Hardiman, O., and Bede, P. (2017). Neuroimaging patterns along the ALS-FTD spectrum: a multiparametric imaging study. Amyotrophic Lateral Sclerosis and Frontotemporal Degeneration *18*, 611–623.

Ostrowski, L.A., Hall, A.C., Szafranski, K.J., Oshidari, R., Abraham, K.J., Chan, J.N.Y., Krustev, C., Zhang, K., Wang, A., Liu, Y., et al. (2018). Conserved Pbp1/Ataxin-2 regulates retrotransposon activity and connects polyglutamine expansion-driven protein aggregation to lifespan-controlling rDNA repeats. Communications Biology *1*.

Penheiter, K.L., Washburn, T.M., Porter, S.E., Hoffman, M.G., and Jaehning, J.A. (2005). A Posttranscriptional Role for the Yeast Paf1-RNA Polymerase II Complex Is Revealed by Identification of Primary Targets. Molecular Cell *20*, 213–223.

Perego, M.G.L., Taiana, M., Bresolin, N., Comi, G.P., and Corti, S. (2018). R-Loops in Motor Neuron Diseases. Mol Neurobiol 1–11.

Plaschka, C., Lin, P.-C., Charenton, C., and Nagai, K. (2018). Prespliceosome structure provides insights into spliceosome assembly and regulation. Nature *559*, 419.

Poli, J., Gerhold, C.-B., Tosi, A., Hustedt, N., Seeber, A., Sack, R., Herzog, F., Pasero, P., Shimada, K., Hopfner, K.-P., et al. (2016). Mec1, INO80, and the PAF1 complex cooperate to limit transcription replication conflicts through RNAPII removal during replication stress. Genes Dev. *30*, 337–354.

Porter, S.E., Washburn, T.M., Chang, M., and Jaehning, J.A. (2002). The Yeast Paf1-RNA Polymerase II Complex Is Required for Full Expression of a Subset of Cell Cycle-Regulated Genes. Eukaryot Cell *1*, 830–842.

Prudencio, M., Belzil, V.V., Batra, R., Ross, C.A., Gendron, T.F., Pregent, L.J., Murray, M.E., Overstreet, K.K., Piazza-Johnston, A.E., Desaro, P., et al. (2015). Distinct brain transcriptome profiles in C9orf72-associated and sporadic ALS. Nat Neurosci *18*, 1175–1182.

Prudencio, M., Gonzales, P.K., Cook, C.N., Gendron, T.F., Daughrity, L.M., Song, Y., Ebbert, M.T.W., van Blitterswijk, M., Zhang, Y.-J., Jansen-West, K., et al. (2017). Repetitive element transcripts are elevated in the brain of C9orf72 ALS/FTLD patients. Hum Mol Genet *26*, 3421–3431.

Raiber, E.-A., Kranaster, R., Lam, E., Nikan, M., and Balasubramanian, S. (2012). A non-canonical DNA structure is a binding motif for the transcription factor SP1 in vitro. Nucleic Acids Research *40*, 1499.

Reddy, K., Schmidt, M.H.M., Geist, J.M., Thakkar, N.P., Panigrahi, G.B., Wang, Y.-H., and Pearson, C.E. (2014). Processing of double-R-loops in (CAG)·(CTG) and C9orf72 (GGGGCC)·(GGCCCC) repeats causes instability. Nucleic Acids Res *42*, 10473–10487.

Reese, J.C. (2013). The control of elongation by the yeast Ccr4-Not complex. Biochim Biophys Acta *1829*, 127–133.

Renton, A.E., Majounie, E., Waite, A., Simón-Sánchez, J., Rollinson, S., Gibbs, J.R., Schymick, J.C., Laaksovirta, H., van Swieten, J.C., Myllykangas, L., et al. (2011). A hexanucleotide repeat expansion in C9ORF72 is the cause of chromosome 9p21-linked ALS-FTD. Neuron *72*, 257–268.

Riemslagh, F.W., Lans, H., Seelaar, H., Severijnen, L.-A.W.F.M., Melhem, S., Vermeulen, W., Aronica, E., Pasterkamp, R.J., Swieten, J.C. van, and Willemsen, R. (2019). HR23B pathology preferentially co-localizes with p62, pTDP-43 and poly-GA in C9ORF72-linked frontotemporal dementia and amyotrophic lateral sclerosis. Acta Neuropathologica Communications *7*.

Ringwald, M., Iyer, V., Mason, J.C., Stone, K.R., Tadepally, H.D., Kadin, J.A., Bult, C.J., Eppig, J.T., Oakley, D.J., Briois, S., et al. (2011). The IKMC web portal: a central point of entry to data and resources from the International Knockout Mouse Consortium. Nucleic Acids Res *39*, D849–D855.

Rogers, G.W., Richter, N.J., Lima, W.F., and Merrick, W.C. (2001). Modulation of the Helicase Activity of eIF4A by eIF4B, eIF4H, and eIF4F. J. Biol. Chem. *276*, 30914–30922.

Rozovsky, N., Butterworth, A.C., and Moore, M.J. (2008). Interactions between eIF4AI and its accessory factors eIF4B and eIF4H. RNA *14*, 2136–2148.

Russ, J., Liu, E.Y., Wu, K., Neal, D., Suh, E., Irwin, D.J., McMillan, C.T., Harms, M.B., Cairns, N.J., Wood, E.M., et al. (2015). Hypermethylation of repeat expanded C9orf72 is a clinical and molecular disease modifier. Acta Neuropathol *129*, 39–52.

Salinas-Rios, V., Belotserkovskii, B.P., and Hanawalt, P.C. (2011). DNA slip-outs cause RNA polymerase II arrest in vitro: potential implications for genetic instability. Nucleic Acids Res *39*, 7444–7454.

Sareen, D., O'Rourke, J.G., Meera, P., Muhammad, A.K.M.G., Grant, S., Simpkinson, M., Bell, S., Carmona, S., Ornelas, L., Sahabian, A., et al. (2013). Targeting RNA foci in iPSC-derived motor neurons from ALS patients with C9ORF72 repeat expansion. Sci Transl Med *5*, 208ra149.

Satoh, J., Yamamoto, Y., Kitano, S., Takitani, M., Asahina, N., and Kino, Y. (2014). Molecular Network Analysis Suggests a Logical Hypothesis for the Pathological Role of C9orf72 in Amyotrophic Lateral Sclerosis/Frontotemporal Dementia. J Cent Nerv Syst Dis *6*, 69–78.

Sauer, M., and Paeschke, K. (2017). G-quadruplex unwinding helicases and their function *in vivo*. Biochemical Society Transactions *45*, 1173–1182.

Schönecker, S., Neuhofer, C., Otto, M., Ludolph, A., Kassubek, J., Landwehrmeyer, B., Anderl-Straub, S., Semler, E., Diehl-Schmid, J., Prix, C., et al. (2018). Atrophy in the Thalamus But Not Cerebellum Is Specific for C9orf72 FTD and ALS Patients – An Atlas-Based Volumetric MRI Study. Front Aging Neurosci *10*.

Selth, L.A., Sigurdsson, S., and Svejstrup, J.Q. (2010). Transcript Elongation by RNA Polymerase II. Annu. Rev. Biochem. *79*, 271–293.

Sen, N.D., Zhou, F., Harris, M.S., Ingolia, N.T., and Hinnebusch, A.G. (2016). eIF4B stimulates translation of long mRNAs with structured 5′ UTRs and low closed-loop potential but weak dependence on eIF4G. Proc Natl Acad Sci U S A *113*, 10464–10472.

Shao, W., Kim, H.-S., Cao, Y., Xu, Y.-Z., and Query, C.C. (2012). A U1-U2 snRNP Interaction Network during Intron Definition. Molecular and Cellular Biology *32*, 470–478.

Shieh, S.-Y., and Bonini, N.M. (2011). Genes and pathways affected by CAG-repeat RNA-based toxicity in Drosophila. Human Molecular Genetics *20*, 4810.

Shivji, M.K.K., Renaudin, X., Williams, Ç.H., and Venkitaraman, A.R. (2018). BRCA2 Regulates Transcription Elongation by RNA Polymerase II to Prevent R-Loop Accumulation. Cell Reports *22*, 1031–1039.

Sikorski, T.W., Ficarro, S.B., Holik, J., Kim, T., Rando, O.J., Marto, J.A., and Buratowski, S. (2011). Sub1 and RPA associate with RNA Polymerase II at different stages of transcription. Mol Cell *44*, 397–409.

Simone, R., Balendra, R., Moens, T.G., Preza, E., Wilson, K.M., Heslegrave, A., Woodling, N.S., Niccoli, T., Gilbert-Jaramillo, J., Abdelkarim, S., et al. (2018). G-quadruplex-binding small molecules ameliorate C9orf72 FTD/ALS pathology in vitro and in vivo. EMBO Mol Med *10*, 22–31.

Skarnes, W.C., Rosen, B., West, A.P., Koutsourakis, M., Bushell, W., Iyer, V., Mujica, A.O., Thomas, M., Harrow, J., Cox, T., et al. (2011). A conditional knockout resource for the genome–wide study of mouse gene function. Nature *474*, 337–342.

Su, Z., Zhang, Y., Gendron, T.F., Bauer, P.O., Chew, J., Yang, W.-Y., Fostvedt, E., Jansen-West, K., Belzil, V.V., Desaro, P., et al. (2014). Discovery of a Biomarker and Lead Small Molecules to Target r(GGGGCC)-Associated Defects in c9FTD/ALS. Neuron *83*, 1043–1050.

Sun, J., Rothschild, G., Pefanis, E., and Basu, U. (2013). Transcriptional stalling in B-lymphocytes. Transcription *4*, 127–135.

Sun, Y., Atas, E., Lindqvist, L., Sonenberg, N., Pelletier, J., and Meller, A. (2012). The eukaryotic initiation factor eIF4H facilitates loop-binding, repetitive RNA unwinding by the eIF4A DEAD-box helicase. Nucleic Acids Res *40*, 6199–6207.

Szlachta, K., Thys, R.G., Atkin, N.D., Pierce, L.C.T., Bekiranov, S., and Wang, Y.-H. (2018). Alternative DNA secondary structure formation affects RNA polymerase II promoter-proximal pausing in human. Genome Biology *19*, 89.

Tabet, R., Schaeffer, L., Freyermuth, F., Jambeau, M., Workman, M., Lee, C.-Z., Lin, C.-C., Jiang, J., Jansen-West, K., Abou-Hamdan, H., et al. (2018). CUG initiation and frameshifting enable production of dipeptide repeat proteins from ALS/FTD C9ORF72 transcripts. Nature Communications *9*, 152.

Tao, Z., Wang, H., Xia, Q., Li, K., Li, K., Jiang, X., Xu, G., Wang, G., and Ying, Z. (2015). Nucleolar stress and impaired stress granule formation contribute to C9orf72 RAN translation-induced cytotoxicity. Hum Mol Genet *24*, 2426–2441.

Thys, R.G., and Wang, Y.-H. (2015). DNA Replication Dynamics of the GGGGCC Repeat of the C9orf72 Gene. J. Biol. Chem. *290*, 28953–28962.

Todd, P.K., Oh, S.Y., Krans, A., He, F., Sellier, C., Frazer, M., Renoux, A.J., Chen, K., Scaglione, K.M., Basrur, V., et al. (2013). CGG Repeat-Associated Translation Mediates Neurodegeneration in Fragile X Tremor Ataxia Syndrome. Neuron *78*, 440–455.

Todd Peter K., and Paulson Henry L. (2010). RNA-mediated neurodegeneration in repeat expansion disorders. Annals of Neurology *67*, 291–300.

Van Oss, S.B., Cucinotta, C.E., and Arndt, K.M. (2017). Emerging Insights into the Roles of the Paf1 Complex in Gene Regulation. Trends in Biochemical Sciences *42*, 788–798.

Vatsavayai, S.C., Nana, A.L., Yokoyama, J.S., and Seeley, W.W. (2019). C9orf72-FTD/ALS pathogenesis: evidence from human neuropathological studies. Acta Neuropathol *137*, 1–26.

Vaysse, C., Philippe, C., Martineau, Y., Quelen, C., Hieblot, C., Renaud, C., Nicaise, Y., Desquesnes, A., Pannese, M., Filleron, T., et al. (2015). Key contribution of eIF4H-mediated translational control in tumor promotion. Oncotarget *6*, 39924–39940.

Verma-Gaur, J., Rao, S.N., Taya, T., and Sadhale, P. (2008). Genomewide Recruitment Analysis of Rpb4, a Subunit of Polymerase II in Saccharomyces cerevisiae, Reveals Its Involvement in Transcription Elongation. Eukaryotic Cell *7*, 1009–1018.

Wahba, L., Amon, J.D., Koshland, D., and Vuica-Ross, M. (2011). RNase H and Multiple RNA Biogenesis Factors Cooperate to Prevent RNA:DNA Hybrids from Generating Genome Instability. Molecular Cell *44*, 978–988.

Wahl, M.C., Will, C.L., and Lührmann, R. (2009). The Spliceosome: Design Principles of a Dynamic RNP Machine. Cell *136*, 701–718.

Walker, C., Herranz-Martin, S., Karyka, E., Liao, C., Lewis, K., Elsayed, W., Lukashchuk, V., Chiang, S.-C., Ray, S., Mulcahy, P.J., et al. (2017). C9orf72 expansion disrupts ATM-mediated chromosomal break repair. Nature Neuroscience *20*, 1225.

Wang, Z.-F., Ursu, A., Childs-Disney, J.L., Guertler, R., Yang, W.-Y., Bernat, V., Rzuczek, S.G., Fuerst, R., Zhang, Y.-J., Gendron, T.F., et al. (2019). The Hairpin Form of r(G4C2)exp in c9ALS/FTD Is Repeat-Associated Non-ATG Translated and a Target for Bioactive Small Molecules. Cell Chemical Biology *26*, 179-190.e12.

Westergard, T., McAvoy, K., Russell, K., Wen, X., Pang, Y., Morris, B., Pasinelli, P., Trotti, D., and Haeusler, A. (2019). Repeat-associated non-AUG translation in C9orf72-ALS/FTD is driven by neuronal excitation and stress. EMBO Molecular Medicine e9423.

Xi, Z., Zinman, L., Moreno, D., Schymick, J., Liang, Y., Sato, C., Zheng, Y., Ghani, M., Dib, S., Keith, J., et al. (2013). Hypermethylation of the CpG island near the G4C2 repeat in ALS with a C9orf72 expansion. Am. J. Hum. Genet. *92*, 981–989.

Xi, Z., Rainero, I., Rubino, E., Pinessi, L., Bruni, A., Maletta, R., Nacmias, B., Sorbi, S., Galimberti, D., Surace, E., et al. (2014). Hypermethylation of the CpG-island near the C9orf72 G4C2-repeat expansion in FTLD patients. *23*, 5630–5637.

Xi, Z., Zhang, M., Bruni, A.C., Maletta, R.G., Colao, R., Fratta, P., Polke, J.M., Sweeney, M.G., Mudanohwo, E., Nacmias, B., et al. (2015). The C9orf72 repeat expansion itself is methylated in ALS and FTLD patients. Acta Neuropathol. *129*, 715–727.

Xu, Z., Poidevin, M., Li, X., Li, Y., Shu, L., Nelson, D.L., Li, H., Hales, C.M., Gearing, M., Wingo, T.S., et al. (2013). Expanded GGGGCC repeat RNA associated with amyotrophic lateral sclerosis and frontotemporal dementia causes neurodegeneration. Proc Natl Acad Sci U S A *110*, 7778–7783.

Yan, C., Wan, R., and Shi, Y. (2019). Molecular Mechanisms of pre-mRNA Splicing through Structural Biology of the Spliceosome. Cold Spring Harb Perspect Biol *11*, a032409.

Yang, Y., Li, W., Hoque, M., Hou, L., Shen, S., Tian, B., and Dynlacht, B.D. (2016). PAF Complex Plays Novel Subunit-Specific Roles in Alternative Cleavage and Polyadenylation. PLoS Genet *12*.

Yin, S., Lopez-Gonzalez, R., Kunz, R.C., Gangopadhyay, J., Borufka, C., Gygi, S.P., Gao, F.-B., and Reed, R. (2017). Evidence that C9ORF72 dipeptide repeat proteins associate with U2 snRNP to cause mis-splicing in ALS/FTD patients. Cell Rep *19*, 2244–2256.

Yu, Y., Chi, B., Xia, W., Gangopadhyay, J., Yamazaki, T., Winkelbauer-Hurt, M.E., Yin, S., Eliasse, Y., Adams, E., Shaw, C.E., et al. (2015a). U1 snRNP is mislocalized in ALS patient fibroblasts bearing NLS mutations in FUS and is required for motor neuron outgrowth in zebrafish. Nucleic Acids Res 43, 3208–3218.

Yu, Z., Goodman, L.D., Shieh, S.-Y., Min, M., Teng, X., Zhu, Y., and Bonini, N.M. (2015b). A fly model for the CCUG-repeat expansion of myotonic dystrophy type 2 reveals a novel interaction with MBNL1. Hum. Mol. Genet. *24*, 954–962.

Zamiri, B., Reddy, K., Macgregor, R.B., and Pearson, C.E. (2014). TMPyP4 Porphyrin Distorts RNA G-quadruplex Structures of the Disease-associated r(GGGGCC)n Repeat of the C9orf72 Gene and Blocks Interaction of RNA-binding Proteins. J. Biol. Chem. *289*, 4653–4659.

Zamiri, B., Mirceta, M., Abu-Ghazalah, R., Wold, M.S., Pearson, C.E., and Macgregor, R.B. (2018). Stress-induced acidification may contribute to formation of unusual structures in C9orf72 -repeats. Biochimica et Biophysica Acta (BBA) - General Subjects *1862*, 1482–1491.

Zeier, Z., Esanov, R., Belle, K.C., Volmar, C.-H., Johnstone, A.L., Halley, P., DeRosa, B.A., Khoury, N., van Blitterswijk, M., Rademakers, R., et al. (2015). Bromodomain inhibitors regulate the C9ORF72 locus in ALS. Experimental Neurology *271*, 241–250.

Zhan, X., Yan, C., Zhang, X., Lei, J., and Shi, Y. (2018). Structures of the human pre-catalytic spliceosome and its precursor spliceosome. Cell Research *28*, 1129.

Zhang, Y., Smith, A.D., Renfrow, M.B., and Schneider, D.A. (2010). The RNA Polymerase-associated Factor 1 Complex (Paf1C) Directly Increases the Elongation Rate of RNA Polymerase I and Is Required for Efficient Regulation of rRNA Synthesis. J. Biol. Chem. *285*, 14152–14159.

Zhang, Y.-J., Gendron, T.F., Ebbert, M.T.W., O'Raw, A.D., Yue, M., Jansen-West, K., Zhang, X., Prudencio, M., Chew, J., Cook, C.N., et al. (2018). Poly(GR) impairs protein translation and stress granule dynamics in C9orf72-associated frontotemporal dementia and amyotrophic lateral sclerosis. Nat. Med. *24*, 1136–1142.

Zhao, M., Kim, J.R., van Bruggen, R., and Park, J. (2018). RNA-Binding Proteins in Amyotrophic Lateral Sclerosis. Mol Cells *41*, 818–829.

Zu, T., Gibbens, B., Doty, N.S., Gomes-Pereira, M., Huguet, A., Stone, M.D., Margolis, J., Peterson, M., Markowski, T.W., Ingram, M.A.C., et al. (2011). Non-ATG-initiated translation directed by microsatellite expansions. Proc. Natl. Acad. Sci. U.S.A. *108*, 260–265.

APPENDIX 1: ABREVIATIONS

80S ribosome (subunits: 40S and 60S ribosomes)

ALS (amyotrophic lateral sclerosis)

ASO (antisense oligonucleotides)

C9- ALS/FTD (ALS/FTD cases lacking the G4C2 expansion in C9orf72)

C9+ ALS/FTD (ALS/FTD cases harboring the G4C2 expansion in C9orf72)

CAG (expanded (CAG)30+ mutation found in multiple neurological disorders)

CDC73 (component of PAF1C)

Ctr9 (component of PAF1C)

DPR (dipeptide repeats; includes GA, GR, GP, PA, PR)

DSIF (DRB-sensitivity-inducing transcription factor complex; subunits: Spt4 and Spt5)

eIF (eukaryotic initiation factor)

eIF4F complex (subunits: eIF4E, eIF4G, eIF4A)

FTD (frontotemporal degeneration)

G4C2 (expanded (GGGGCC)30+ mutation found within C9orf72)

G4C2||G2C4 (sense-G4C2 and antisense-G2C4; bidirectional gene products from the G4C2 mutation within C9orrf72)

GA (glycine-alanine dipeptide; RAN-translation product from sense-G4C2 RNA)

GC-rich (DNA or RNA enriched for guanine and cytosine bases)

GFP (green fluorescent protein)

GP (glycine-proline dipeptide; RAN-translation product from sense-G4C2 and antisense-G2C4 RNA)

GR (glycine-arginine dipeptide; RAN-translation product from sense-G4C2 RNA; highly toxic)

IRES-translation (internal ribosome entry-site translation)

ISR (integrated stress response)

Leo1 (component of PAF1C)

LDS (“leader sequence”; truncated 5’ UTR derived from the 114bp sequence found upstream of G4C2 in intron 1 of *C9orf72* in C9+ ALS/FTD patients)

NELF (Negative Elongation Factor)

P-TEFb (positive elongation factor-b; also called CDK9)

PA (proline-alanine dipeptide; RAN-translation product from antisense-G2C4 RNA)

Paf1 (component of PAF1C)

PAF1C (Polymerase II Associating Factor 1 transcription elongation complex; subunits: Paf1, Leo1, CDC73, Ctr9, Rtf1)

PIC (preinitiation complex; subunits: 40s ribosome, eIF1, eIF1A, eIF5, eIF3 complex)

poly(A) tail (3’ mRNA modification of a polyadenylated tail)

PR (proline-arginine dipeptide; RAN-translation product from antisense-G2C4 RNA; highly toxic)

qPCR (quantitative reverse transcribed polymerase chain reaction; also **qRT-PCR**)

RAN-translation (Repeat Associated Non-AUG translation; also **RANT**)

RBP (RNA binding protein)

RNAPII (RNA polymerase II)

RRM (RNA recognition motif)

Rtf1 (component of PAF1C)

Spt4 (component of DSIF)

Spt5 (component of DSIF)

TDP-43 (Tar DNA-binding protein -43)

UTR (untranslated-region)

WB (western immunoblot)

WT (wild-type)

APPENDIX 2: CHAPTER 2 SUPPLEMENTARY TABLES, FIGURES, AND DATA

Chapter 2: Supplementary tables

Table S2-1: detailed sampling/ reproducibility/ statistics

Fig. 1b: (no statistics)						
Sample size (n)	30 per sample					
Independent Expt. Runs	2 runs					
Data point	Total repeat length calculated from PCR-product size minus non-G4C2 surrounding sequence and divided by 6 for 6 nucleotides per repeat					
Fig. 1c: 1-way ANOVA						
ANOVA table	SS	DF	MS	F (DFn, DFd)	P value	
Treatment (between columns)	0.1391	3	0.04637	F (3, 46) = 0.9539	P=0.4225	
Residual (within columns)	2.236	46	0.04861			
Total	2.375	49				
Sample size (n)	30 per sample					
Independent Expt. Runs	3-5 runs w/ biological triplicates					
Data point	normalized band density per well					
Tukey's multiple comparisons test	Mean Diff.	95.00% CI of diff.	Significant?	Summary	Adjusted P Value	
(G4C2)8 vs. (G4C2)29	-0.1222	-0.3525 to 0.1080	No	ns	0.4856	
(G4C2)8 vs. (G4C2)49 (II)	-0.09463	-0.3249 to 0.1356	No	ns	0.6839	
(G4C2)8 vs. (G4C2)49 (III)	0.01956	-0.2107 to 0.2498	No	ns	0.9956	
(G4C2)29 vs. (G4C2)49 (II)	0.02758	-0.2027 to 0.2578	No	ns	0.9880	
(G4C2)29 vs. (G4C2)49 (III)	0.1418	-0.08847 to 0.3720	No	ns	0.3566	

(G4C2)49 (II) vs. (G4C2)49 (III)	0.1142	-0.1160 to 0.3444	No	ns	0.5428	
GO-term analyses (Fig. 1g-h, Fig. 2c-d, and Sup Fig. 1d)						
p-value cut-off	> 0.001					
Enrichment score cut-off	< 3.00					
Fig. 3b: 1-way ANOVA						
ANOVA table	SS	DF	MS	F (DFn, DFd)	P value	
Treatment (between columns)	15173	5	3035	F (5, 35) = 30.19	P<0.0001	
Residual (within columns)	3518	35	100.5			
Total	18691	40				
Sample sizes (n)	Control (9); Paf1 RNAi (7); Leo1 RNAi (6), CDC73 RNAi (8); Ctr9 RNAi (6); Rtf1 RNAi (5)					
Independent Expt. Runs	2 with >4 animals per genotype					
Data point	retina depth from 1 eye per animal					
Tukey's multiple comparisons test	Mean Diff.	95.00% CI of diff.	Significant?	Summary	Adjusted P Value	
Control vs. Paf1	-31.02	-46.25 to -15.8	Yes	****	<0.0001	
Control vs. Leo1	-33.82	-49.75 to -17.9	Yes	****	<0.0001	
Control vs. CDC73	-49.71	-64.39 to -35.03	Yes	****	<0.0001	
Control vs. Ctr9	-55.68	-71.61 to -39.76	Yes	****	<0.0001	
Control vs. Rtf1	-28.4	-45.25 to -11.55	Yes	***	0.0002	
Paf1 vs. Leo1	-2.799	-19.61 to 14.01	No	ns	0.9958	
Paf1 vs. CDC73	-18.68	-34.32 to -3.048	Yes	*	0.0115	

Paf1 vs. Ctr9	-24.66	-41.47 to -7.851	Yes	**	0.0012	
Paf1 vs. Rtf1	2.621	-15.07 to 20.31	No	ns	0.9976	
Leo1 vs. CDC73	-15.89	-32.2 to 0.431	No	ns	0.0601	
Leo1 vs. Ctr9	-21.86	-39.3 to -4.418	Yes	**	0.0072	
Leo1 vs. Rtf1	5.42	-12.87 to 23.71	No	ns	0.9457	
CDC73 vs. Ctr9	-5.975	-22.29 to 10.34	No	ns	0.8766	
CDC73 vs. Rtf1	21.3	4.081 to 38.53	Yes	**	0.0082	
Ctr9 vs. Rtf1	27.28	8.986 to 45.57	Yes	***	0.001	
Fig. 3d: 1-way ANOVA						
ANOVA table	SS	DF	MS	F (DFn, DFd)	P value	
Treatment (between columns)	449.3	5	89.87	F (5, 35) = 2.209	P=0.0754	
Residual (within columns)	1424	35	40.68			
Total	1873	40				
Sample sizes (n)	Control (9); Paf1 RNAi (5); Leo1 RNAi (9), CDC73 RNAi (9); Ctr9 RNAi (5); Rtf1 RNAi (4)					
Independent Expt. Runs	2 with >4 animals per genotype					
Data point	retina depth from 1 eye per animal					
Tukey's multiple comparisons test	Mean Diff.	95.00% CI of diff.	Significant?	Summary	Adjusted P Value	
Control vs. Paf1	-1.877	-12.6 to 8.843	No	ns	0.9947	
Control vs. Leo1	-9.136	-18.2 to -0.0763	Yes	*	0.0471	

Control vs. CDC73	-5.15	-14.21 to 3.91	No	ns	0.5328	
Control vs. Ctr9	-7.211	-17.93 to 3.509	No	ns	0.3483	
Control vs. Rtf1	-4.944	-16.49 to 6.606	No	ns	0.7884	
Paf1 vs. Leo1	-7.26	-17.98 to 3.46	No	ns	0.3411	
Paf1 vs. CDC73	-3.273	-13.99 to 7.447	No	ns	0.9387	
Paf1 vs. Ctr9	-5.334	-17.49 to 6.822	No	ns	0.7709	
Paf1 vs. Rtf1	-3.067	-15.96 to 9.826	No	ns	0.9786	
Leo1 vs. CDC73	3.986	-5.074 to 13.05	No	ns	0.769	
Leo1 vs. Ctr9	1.926	-8.794 to 12.65	No	ns	0.994	
Leo1 vs. Rtf1	4.193	-7.357 to 15.74	No	ns	0.8805	
CDC73 vs. Ctr9	-2.061	-12.78 to 8.659	No	ns	0.9918	
CDC73 vs. Rtf1	0.2064	-11.34 to 11.76	No	ns	>0.9999	
Ctr9 vs. Rtf1	2.267	-10.63 to 15.16	No	ns	0.9946	

Fig. 3e: 1-way ANOVA

ANOVA table	SS	DF	MS	F (DFn, DFd)	P value	
Treatment (between columns)	14205	5	2841	F (5, 29) = 107.9	P<0.0001	
Residual (within columns)	763.8	29	26.34			
Total	14969	34				
Sample sizes (n)	Control (117); Paf1 RNAi (98); Leo1 RNAi (108), CDC73 RNAi (103); Ctr9 RNAi (120); Rtf1 RNAi (115)					

Independent Expt. Runs	2 with >90 animals per genotype					
Data point	mean % animals that climb per tube; 19+/-2.1 animals per tube for each genotype					
Tukey's multiple comparisons test	Mean Diff.	95.00% CI of diff.	Significant?	Summary	Adjusted P Value	
Control vs. *dRtf1*	-55.67	-64.7 to -46.63	Yes	****	<0.0001	
Control vs. *dCDC73*	-54.83	-63.87 to -45.8	Yes	****	<0.0001	
Control vs. *dLeo1*	-52.17	-61.2 to -43.13	Yes	****	<0.0001	
Control vs. *dPaf1*	-51.33	-60.81 to -41.86	Yes	****	<0.0001	
Control vs. *dCtr9*	-52.17	-61.2 to -43.13	Yes	****	<0.0001	
dRtf1 vs. *dCDC73*	0.8333	-8.199 to 9.866	No	ns	0.9997	
dRtf1 vs. *dLeo1*	3.5	-5.533 to 12.53	No	ns	0.8421	
dRtf1 vs. *dPaf1*	4.333	-5.14 to 13.81	No	ns	0.7299	
dRtf1 vs. *dCtr9*	3.5	-5.533 to 12.53	No	ns	0.8421	
dCDC73 vs. *dLeo1*	2.667	-6.366 to 11.7	No	ns	0.9434	
dCDC73 vs. *dPaf1*	3.5	-5.974 to 12.97	No	ns	0.8665	
dCDC73 vs. *dCtr9*	2.667	-6.366 to 11.7	No	ns	0.9434	
dLeo1 vs. *dPaf1*	0.8333	-8.64 to 10.31	No	ns	0.9998	
dLeo1 vs. *dCtr9*	0	-9.033 to 9.033	No	ns	>0.9999	
dPaf1 vs. *dCtr9*	-0.8333	-10.31 to 8.64	No	ns	0.9998	

Fig. 3f: 1-way ANOVA						
ANOVA table	SS	DF	MS	F (DFn, DFd)	P value	
Treatment (between columns)	38.13	6	6.354	F (6, 56) = 15.66	P<0.0001	
Residual (within columns)	22.73	56	0.4059			
Total	60.86	62				
Sample sizes (n)	(G4C2)0 (9); (G4C2)49 (10); Paf1 RNAi (10); Leo1 RNAi (7), CDC73 RNAi (10); Ctr9 RNAi (8); Rtf1 RNAi (9)					
Independent Expt. Runs	2 with >5 animals per genotype					
Data point	vacuole score for 1 animal					
Tukey's multiple comparisons test	Mean Diff.	95.00% CI of diff.	Significant?	Summary	Adjusted P Value	
(G4C2)49 vs. *dPaf1*	0.4	-0.4713 to 1.271	No	ns	0.7974	
(G4C2)49 vs. *dLeo1*	0.4	-0.5601 to 1.36	No	ns	0.8608	
(G4C2)49 vs. *dCDC73*	1.3	0.4287 to 2.171	Yes	***	0.0005	
(G4C2)49 vs. *dCtr9*	1.025	0.1009 to 1.949	Yes	*	0.0205	
(G4C2)49 vs. *dRtf1*	1.622	0.7271 to 2.517	Yes	****	<0.0001	
(G4C2)49 vs. (G4C2)0	2.4	1.505 to 3.295	Yes	****	<0.0001	
dPaf1 vs. *dLeo1*	0	-0.9601 to 0.9601	No	ns	>0.9999	
dPaf1 vs. *dCDC73*	0.9	0.02871 to 1.771	Yes	*	0.0386	
dPaf1 vs. *dCtr9*	0.625	-0.2991 to 1.549	No	ns	0.3854	
dPaf1 vs. *dRtf1*	1.222	0.3271 to 2.117	Yes	**	0.0019	

dPaf1 vs. (G4C2)0	2	1.105 to 2.895	Yes	****	<0.0001	
dLeo1 vs. *dCDC73*	0.9	-0.06012 to 1.86	No	ns	0.08	
dLeo1 vs. *dCtr9*	0.625	-0.3833 to 1.633	No	ns	0.4918	
dLeo1 vs. *dRtf1*	1.222	0.2404 to 2.204	Yes	**	0.0061	
dLeo1 vs. (G4C2)0	2	1.018 to 2.982	Yes	****	<0.0001	
dCDC73 vs. *dCtr9*	-0.275	-1.199 to 0.6491	No	ns	0.9695	
dCDC73 vs. *dRtf1*	0.3222	-0.5729 to 1.217	No	ns	0.9253	
dCDC73 vs. (G4C2)0	1.1	0.2048 to 1.995	Yes	**	0.0071	
dCtr9 vs. *dRtf1*	0.5972	-0.3495 to 1.544	No	ns	0.4703	
dCtr9 vs. (G4C2)0	1.375	0.4283 to 2.322	Yes	***	0.0008	
dRtf1 vs. (G4C2)0	0.7778	-0.1406 to 1.696	No	ns	0.1489	

Fig. 3g: Log-rank (Mantel-Cox) test and Gehan-Breslow-Wilcoxon test

Sample Sizes (n)		Control (198); CDC73 RNAi (197)				
Independent Expt Runs		2 repeats with >150 animals per genotype				
Test	Chi square	df	P value	Significant?	Summary	95% CI of ratio
Log-rank (Mantel-Cox)	62.43	1	<0.0001	Yes	****	0.8185 to 1.222/ 0.8185 to 1.222
Gehan-Breslow-Wilcoxon	49.24	1	<0.0001	Yes	****	

Fig. 4a, top: 2-way ANOVA

ANOVA table, Top	SS	DF	MS	F (DFn, DFd)	P value	

Interaction	0.7888	12	0.06573	F (12, 126) = 2.309	P=0.0107	
Row Factor	4.781	6	0.7969	F (6, 126) = 28	P<0.0001	
Column Factor	1.222	2	0.6109	F (2, 126) = 21.46	P<0.0001	
Residual	3.586	126	0.02846			
Sample size (n)	25					
Independent Expt. Runs	2 for (G4C2)8 and (G4C2)29; 3 for (G4C2)49; all runs included biological triplicates					
Data point	mean fold change for 1 replicate relative to mean of controls					
Tukey's multiple comparisons test	Mean Diff.	95.00% CI of diff.	Significant?	Summary	Adjusted P Value	
Control						
(G4C2)8 vs. (G4C2)29	-0.02547	-0.2364 to 0.1854	No	ns	0.9558	
(G4C2)8 vs. (G4C2)49	-0.02856	-0.2172 to 0.1601	No	ns	0.9314	
(G4C2)29 vs. (G4C2)49	-0.003088	-0.214 to 0.2078	No	ns	0.9993	
dSpt4						
(G4C2)8 vs. (G4C2)29	-0.0468	-0.2778 to 0.1842	No	ns	0.8807	
(G4C2)8 vs. (G4C2)49	0.1073	-0.1036 to 0.3182	No	ns	0.4512	
(G4C2)29 vs. (G4C2)49	0.1541	-0.05676 to 0.365	No	ns	0.1968	
dPaf1						
(G4C2)8 vs. (G4C2)29	0.006048	-0.225 to 0.2371	No	ns	0.9979	
(G4C2)8 vs. (G4C2)49	0.2943	0.06331 to 0.5254	Yes	**	0.0085	

(G4C2)29 vs. (G4C2)49	0.2883	0.05727 to 0.5193	Yes	*	0.0102	
dLeo1						
(G4C2)8 vs. (G4C2)29	0.1915	-0.03957 to 0.4225	No	ns	0.1251	
(G4C2)8 vs. (G4C2)49	0.4914	0.2805 to 0.7023	Yes	****	<0.0001	
(G4C2)29 vs. (G4C2)49	0.3	0.08907 to 0.5109	Yes	**	0.0028	
dCDC73						
(G4C2)8 vs. (G4C2)29	-0.06161	-0.2926 to 0.1694	No	ns	0.8025	
(G4C2)8 vs. (G4C2)49	0.1718	-0.03906 to 0.3827	No	ns	0.1338	
(G4C2)29 vs. (G4C2)49	0.2334	0.02256 to 0.4443	Yes	*	0.0261	
dCtr9						
(G4C2)8 vs. (G4C2)29	-0.1007	-0.3317 to 0.1303	No	ns	0.5568	
(G4C2)8 vs. (G4C2)49	0.1994	-0.01145 to 0.4103	No	ns	0.068	
(G4C2)29 vs. (G4C2)49	0.3002	0.08928 to 0.5111	Yes	**	0.0028	
dRtf1						
(G4C2)8 vs. (G4C2)29	-0.008195	-0.2392 to 0.2228	No	ns	0.9961	
(G4C2)8 vs. (G4C2)49	0.05067	-0.1602 to 0.2616	No	ns	0.8364	
(G4C2)29 vs. (G4C2)49	0.05886	-0.152 to 0.2698	No	ns	0.7859	
Fig. 4a, bottom, (G4C2)8: 1-way ANOVA						
ANOVA table	SS	DF	MS	F (DFn, DFd)	P value	
Treatment (between	1.898	6	0.3163	F (6, 38)	P<0.0001	

columns)				= 13.99		
Residual (within columns)	0.8592	38	0.02261			
Total	2.757	44				
Independent Expt. Runs	(same data as 4a, top)					
Data point	(same data as 4a, top)					
Tukey's multiple comparisons test	Mean Diff.	95.00% CI of diff.	Significant?	Summary	Adjusted P Value	
Control vs. *dSpt4*	0.3869	0.1403 to 0.6335	Yes	***	0.0004	
Control vs. *dPaf1*	0.08589	-0.1607 to 0.3325	No	ns	0.9291	
Control vs. *dLeo1*	0.0158	-0.2308 to 0.2624	No	ns	>0.9999	
Control vs. *dCDC73*	0.3731	0.1265 to 0.6196	Yes	***	0.0006	
Control vs. *dCtr9*	0.3926	0.146 to 0.6391	Yes	***	0.0003	
Control vs. *dRtf1*	0.5456	0.299 to 0.7921	Yes	****	<0.0001	
dSpt4 vs. *dPaf1*	-0.301	-0.5711 to -0.03088	Yes	*	0.0206	
dSpt4 vs. *dLeo1*	-0.3711	-0.6412 to -0.101	Yes	**	0.0022	
dSpt4 vs. *dCDC73*	-0.01383	-0.284 to 0.2563	No	ns	>0.9999	
dSpt4 vs. *dCtr9*	0.005667	-0.2645 to 0.2758	No	ns	>0.9999	
dSpt4 vs. *dRtf1*	0.1587	-0.1115 to 0.4288	No	ns	0.5385	
dPaf1 vs. *dLeo1*	-0.07009	-0.3402 to 0.2	No	ns	0.9828	
dPaf1 vs. *dCDC73*	0.2872	0.01705 to 0.5573	Yes	*	0.0309	

dPaf1 vs. *dCtr9*	0.3067	0.03655 to 0.5768	Yes	*	0.0173	
dPaf1 vs. *dRtf1*	0.4597	0.1895 to 0.7298	Yes	***	0.0001	
dLeo1 vs. *dCDC73*	0.3573	0.08713 to 0.6274	Yes	**	0.0035	
dLeo1 vs. *dCtr9*	0.3768	0.1066 to 0.6469	Yes	**	0.0018	
dLeo1 vs. *dRtf1*	0.5298	0.2596 to 0.7999	Yes	****	<0.0001	
dCDC73 vs. *dCtr9*	0.0195	-0.2506 to 0.2896	No	ns	>0.9999	
dCDC73 vs. *dRtf1*	0.1725	-0.09762 to 0.4426	No	ns	0.4391	
dCtr9 vs. *dRtf1*	0.153	-0.1171 to 0.4231	No	ns	0.5803	

Fig. 4a, bottom, (G4C2)29: 1-way ANOVA

ANOVA table	SS	DF	MS	F (DFn, DFd)	P value	Independent Expt. Runs
Treatment (between columns)	1.193	6	0.1989	F (6, 35) = 6.968	P<0.0001	2-3 w/ triplicates
Residual (within columns)	0.9991	35	0.02855			
Total	2.193	41				
Independent Expt. Runs	(same data as 4a, top)					
Data point	(same data as 4a, top)					

Tukey's multiple comparisons test	Mean Diff.	95.00% CI of diff.	Significant?	Summary	Adjusted P Value	
Control vs. *dSpt4*	0.3656	0.06063 to 0.6705	Yes	*	0.0104	
Control vs. *dPaf1*	0.1174	-0.1875 to 0.4223	No	ns	0.8881	

Control vs. *dLeo1*	0.2327	-0.0722 to 0.5377	No	ns	0.2347	
Control vs. *dCDC73*	0.3369	0.03198 to 0.6418	Yes	*	0.0224	
Control vs. *dCtr9*	0.3173	0.01237 to 0.6222	Yes	*	0.0369	
Control vs. *dRtf1*	0.5628	0.2579 to 0.8678	Yes	****	<0.0001	
dSpt4 vs. *dPaf1*	-0.2482	-0.5531 to 0.05677	No	ns	0.1751	
dSpt4 vs. *dLeo1*	-0.1328	-0.4378 to 0.1721	No	ns	0.8177	
dSpt4 vs. *dCDC73*	-0.02865	-0.3336 to 0.2763	No	ns	>0.9999	
dSpt4 vs. *dCtr9*	-0.04826	-0.3532 to 0.2567	No	ns	0.9988	
dSpt4 vs. *dRtf1*	0.1973	-0.1077 to 0.5022	No	ns	0.4195	
dPaf1 vs. *dLeo1*	0.1153	-0.1896 to 0.4202	No	ns	0.8961	
dPaf1 vs. *dCDC73*	0.2195	-0.08542 to 0.5244	No	ns	0.2962	
dPaf1 vs. *dCtr9*	0.1999	-0.105 to 0.5048	No	ns	0.4038	
dPaf1 vs. *dRtf1*	0.4454	0.1405 to 0.7504	Yes	**	0.0011	
dLeo1 vs. *dCDC73*	0.1042	-0.2007 to 0.4091	No	ns	0.9333	
dLeo1 vs. *dCtr9*	0.08457	-0.2204 to 0.3895	No	ns	0.9752	
dLeo1 vs. *dRtf1*	0.3301	0.02517 to 0.635	Yes	*	0.0267	
dCDC73 vs. *dCtr9*	-0.01961	-0.3245 to 0.2853	No	ns	>0.9999	
dCDC73 vs. *dRtf1*	0.2259	-0.07901 to 0.5308	No	ns	0.2652	

dCtr9 vs. *dRtf1*	0.2455	-0.0594 to 0.5505	No	ns	0.1843	
Fig. 4a, bottom, (G4C2)49: 1-way ANOVA						
ANOVA table	SS	DF	MS	F (DFn, DFd)	P value	
Treatment (between columns)	2.59	6	0.4317	F (6, 53) = 13.24	P<0.0001	
Residual (within columns)	1.728	53	0.03261			
Total	4.318	59				
Independent Expt. Runs	(same data as 4a, top)					
Data point	(same data as 4a, top)					
Tukey's multiple comparisons test	Mean Diff.	95.00% CI of diff.	Significant?	Summary	Adjusted P Value	
Control vs. *dSpt4*	0.5228	0.2619 to 0.7836	Yes	****	<0.0001	
Control vs. *dPaf1*	0.4088	0.1171 to 0.7004	Yes	**	0.0014	
Control vs. *dLeo1*	0.5358	0.2749 to 0.7966	Yes	****	<0.0001	
Control vs. *dCDC73*	0.5734	0.3126 to 0.8343	Yes	****	<0.0001	
Control vs. *dCtr9*	0.6206	0.3597 to 0.8814	Yes	****	<0.0001	
Control vs. *dRtf1*	0.6248	0.3639 to 0.8856	Yes	****	<0.0001	
dSpt4 vs. *dPaf1*	-0.114	-0.4056 to 0.1776	No	ns	0.8919	
dSpt4 vs. *dLeo1*	0.013	-0.2478 to 0.2738	No	ns	>0.9999	
dSpt4 vs. *dCDC73*	0.05067	-0.2102 to 0.3115	No	ns	0.9967	
dSpt4 vs. *dCtr9*	0.09778	-0.1631 to 0.3586	No	ns	0.9097	

dSpt4 vs. *dRtf1*	0.102	-0.1588 to 0.3628	No	ns	0.8917	
dPaf1 vs. *dLeo1*	0.127	-0.1646 to 0.4186	No	ns	0.8326	
dPaf1 vs. *dCDC73*	0.1647	-0.127 to 0.4563	No	ns	0.5994	
dPaf1 vs. *dCtr9*	0.2118	-0.07985 to 0.5034	No	ns	0.2999	
dPaf1 vs. *dRtf1*	0.216	-0.07563 to 0.5076	No	ns	0.2778	
dLeo1 vs. *dCDC73*	0.03767	-0.2232 to 0.2985	No	ns	0.9994	
dLeo1 vs. *dCtr9*	0.08478	-0.1761 to 0.3456	No	ns	0.9527	
dLeo1 vs. *dRtf1*	0.089	-0.1718 to 0.3498	No	ns	0.9407	
dCDC73 vs. *dCtr9*	0.04711	-0.2137 to 0.308	No	ns	0.9978	
dCDC73 vs. *dRtf1*	0.05133	-0.2095 to 0.3122	No	ns	0.9965	
dCtr9 vs. *dRtf1*	0.004222	-0.2566 to 0.2651	No	ns	>0.9999	

Fig. 4b: 1-way ANOVA

ANOVA table	SS	DF	MS	F (DFn, DFd)	P value	
Treatment (between columns)	0.9645	6	0.1608	F (6, 53) = 4.235	P=0.0015	
Residual (within columns)	2.012	53	0.03796			
Total	2.976	59				
Sample Size (n)	25					
Independent Expt. Runs	2 runs w/ biological triplicates					
Data point	mean fold change for 1 replicate relative to mean of controls					
Tukey's multiple	Mean	95.00% CI	Significant?	Summar	Adjusted P	

comparisons test	Diff.	of diff.		y	Value	
Controls vs. dSpt4	-0.2208	-0.4933 to 0.05168	No	ns	0.1863	
Controls vs. dPaf1	0.03427	-0.2382 to 0.3068	No	ns	0.9997	
Controls vs. dLeo1	0.2632	-0.009266 to 0.5358	No	ns	0.0647	
Controls vs. dCDC73	-0.1495	-0.422 to 0.123	No	ns	0.6312	
Controls vs. dCtr9	-0.1402	-0.4127 to 0.1323	No	ns	0.6973	
Controls vs. dRtf1	-0.09473	-0.3672 to 0.1778	No	ns	0.9354	
dSpt4 vs. dPaf1	0.2551	-0.0896 to 0.5998	No	ns	0.2787	
dSpt4 vs. dLeo1	0.4841	0.1394 to 0.8288	Yes	**	0.0013	
dSpt4 vs. dCDC73	0.07132	-0.2734 to 0.416	No	ns	0.9953	
dSpt4 vs. dCtr9	0.0806	-0.2641 to 0.4253	No	ns	0.991	
dSpt4 vs. dRtf1	0.1261	-0.2186 to 0.4708	No	ns	0.9188	
dPaf1 vs. dLeo1	0.229	-0.1157 to 0.5737	No	ns	0.4054	
dPaf1 vs. dCDC73	-0.1838	-0.5285 to 0.1609	No	ns	0.6615	
dPaf1 vs. dCtr9	-0.1745	-0.5192 to 0.1702	No	ns	0.7129	
dPaf1 vs. dRtf1	-0.129	-0.4737 to 0.2157	No	ns	0.9103	
dLeo1 vs. dCDC73	-0.4128	-0.7575	Yes	**	0.0096	

		to -0.06805				
dLeo1 vs. dCtr9	-0.4035	-0.7482 to -0.05877	Yes	*	0.0121	
dLeo1 vs. dRtf1	-0.358	-0.7027 to -0.01327	Yes	*	0.037	
dCDC73 vs. dCtr9	0.009283	-0.3354 to 0.354	No	ns	>0.9999	
dCDC73 vs. dRtf1	0.05478	-0.2899 to 0.3995	No	ns	0.9989	
dCtr9 vs. dRtf1	0.0455	-0.2992 to 0.3902	No	ns	0.9996	

Fig. 4c: 1-way ANOVA

ANOVA table	SS	DF	MS	F (DFn, DFd)	P value	
Treatment (between columns)	1.546	5	0.3092	F (5, 31) = 21.2	P<0.0001	
Residual (within columns)	0.4523	31	0.01459			
Total	1.998	36				
Sample sizes (n)	Control (8); Paf1 RNAi (7); Leo1 RNAi (4), CDC73 RNAi (6); Ctr9 RNAi (6); Rtf1 RNAi (6)					
Independent Expt. Runs	2 w/ >4 animals per genotype					
Data point	total fluorescence per animal relative to mean of controls					

Tukey's multiple comparisons test	Mean Diff.	95.00% CI of diff.	Significant?	Summary	Adjusted P Value	
Control vs. dPaf1	0.3824	0.1927 to 0.5722	Yes	****	<0.0001	
Control vs. dLeo1	0.4228	0.1983 to 0.6473	Yes	****	<0.0001	
Control vs. dCDC73	0.5605	0.3625 to 0.7585	Yes	****	<0.0001	

Control vs. dCtr9	0.4994	0.3015 to 0.6974	Yes	****	<0.0001	
Control vs. dRtf1	0.5118	0.3138 to 0.7098	Yes	****	<0.0001	
dPaf1 vs. dLeo1	0.04043	-0.1894 to 0.2702	No	ns	0.9943	
dPaf1 vs. dCDC73	0.1781	-0.02586 to 0.3821	No	ns	0.1151	
dPaf1 vs. dCtr9	0.117	-0.08694 to 0.321	No	ns	0.5163	
dPaf1 vs. dRtf1	0.1294	-0.07456 to 0.3334	No	ns	0.4064	
dLeo1 vs. dCDC73	0.1377	-0.09897 to 0.3743	No	ns	0.5013	
dLeo1 vs. dCtr9	0.07659	-0.16 to 0.3132	No	ns	0.9201	
dLeo1 vs. dRtf1	0.08897	-0.1477 to 0.3256	No	ns	0.8603	
dCDC73 vs. dCtr9	-0.06108	-0.2727 to 0.1506	No	ns	0.9495	
dCDC73 vs. dRtf1	-0.0487	-0.2604 to 0.163	No	ns	0.9808	
dCtr9 vs. dRtf1	0.01238	-0.1993 to 0.224	No	ns	>0.9999	

Fig. 4d, eYFP: 1-way ANOVA						
ANOVA table	SS	DF	MS	F (DFn, DFd)	P value	
Treatment (between columns)	0.04774	2	0.02387	F (2, 6) = 4.589	P=0.0618	
Residual (within columns)	0.03121	6	0.005202			
Total	0.07895	8				
Independent Expt. Runs	1 with biological triplicates					

Data point	mean fold change for 1 replicate relative to mean of controls					
Tukey's multiple comparisons test	Mean Diff.	95.00% CI of diff.	Significant?	Summary	Adjusted P Value	
WT vs. leo1Δ	0.1783	-0.002355 to 0.359	No	ns	0.0525	
WT vs. cdc73Δ	0.085	-0.09569 to 0.2657	No	ns	0.3794	
leo1Δ vs. cdc73Δ	-0.09333	-0.274 to 0.08735	No	ns	0.3217	
Fig. 4d, sense (G4C2)66: 1-way ANOVA						
ANOVA table	SS	DF	MS	F (DFn, DFd)	P value	
Treatment (between columns)	0.6141	2	0.307	F (2, 13) = 51.44	P<0.0001	
Residual (within columns)	0.0776	13	0.005969			
Total	0.6917	15				
Independent Expt. Runs	2 with biological duplicates					
Data point	mean fold change for 1 replicate relative to mean of controls					
Tukey's multiple comparisons test	Mean Diff.	95.00% CI of diff.	Significant?	Summary	Adjusted P Value	
WT vs. leo1Δ	0.3993	0.2743 to 0.5242	Yes	****	<0.0001	
WT vs. cdc73Δ	0.3841	0.2592 to 0.509	Yes	****	<0.0001	
leo1Δ vs. cdc73Δ	-0.01517	-0.1594 to 0.1291	No	ns	0.9585	
Fig. 4d, antisense (G2C4)66: 1-way ANOVA						
ANOVA table	SS	DF	MS	F (DFn, DFd)	P value	
Treatment (between	1.802	2	0.9012	F (2, 13)	P<0.0001	

columns)				= 55.8		
Residual (within columns)	0.21	13	0.01615			
Total	2.012	15				
Independent Expt. Runs	2 with biological duplicates					
Data point	mean fold change for 1 replicate relative to mean of controls					
Tukey's multiple comparisons test	Mean Diff.	95.00% CI of diff.	Significant?	Summary	Adjusted P Value	
WT vs. leo1Δ	0.7723	0.5668 to 0.9778	Yes	****	<0.0001	
WT vs. cdc73Δ	0.5232	0.3177 to 0.7287	Yes	****	<0.0001	
leo1Δ vs. cdc73Δ	-0.2491	-0.4864 to -0.01182	Yes	*	0.0394	
Fig. 5a, dPaf1: 1-way ANOVA						
ANOVA table	SS	DF	MS	F (DFn, DFd)	P value	
Treatment (between columns)	1.803	2	0.9015	F (2, 15) = 38.41	P<0.0001	
Residual (within columns)	0.3521	15	0.02347			
Total	2.155	17				
Sample size (n)	25					
Independent Expt. Runs	2 w/ biological triplicates					
Data point	mean fold change for 1 replicate relative to mean of controls					
Tukey's multiple comparisons test	Mean Diff.	95.00% CI of diff.	Significant?	Summary	Adjusted P Value	
Control vs. (G4C2)8	-0.04403	-0.2738 to 0.1857	No	ns	0.8734	
Control vs.	-0.6923	-0.922 to	Yes	****	<0.0001	

(G4C2)49		-0.4626				
(G4C2)8 vs. (G4C2)49	-0.6483	-0.878 to -0.4185	Yes	****	<0.0001	
Fig. 5a, dLeo1: 1-way ANOVA						
ANOVA table	SS	DF	MS	F (DFn, DFd)	P value	
Treatment (between columns)	1.257	2	0.6285	F (2, 15) = 15.74	P<0.0001	
Residual (within columns)	0.5989	15	0.03993			
Total	1.856	17				
Sample size (n)	25					
Independent Expt. Runs	2 w/ biological triplicates					
Data point	mean fold change for 1 replicate relative to mean of controls					
Tukey's multiple comparisons test	Mean Diff.	95.00% CI of diff.	Significant?	Summary	Adjusted P Value	
Control vs. (G4C2)8	-0.03623	-0.3359 to 0.2634	No	ns	0.9473	
Control vs. (G4C2)49	-0.5778	-0.8775 to -0.2782	Yes	***	0.0004	
(G4C2)8 vs. (G4C2)49	-0.5416	-0.8412 to -0.2419	Yes	***	0.0008	
Fig. 5a, dCDC73: 1-way ANOVA						
ANOVA table	SS	DF	MS	F (DFn, DFd)	P value	
Treatment (between columns)	2.143	2	1.071	F (2, 15) = 16.13	P=0.0002	
Residual (within columns)	0.9963	15	0.06642			
Total	3.139	17				

Sample size (n)	25					
Independent Expt. Runs	2 w/ biological triplicates					
Data point	mean fold change for 1 replicate relative to mean of controls					
Tukey's multiple comparisons test	Mean Diff.	95.00% CI of diff.	Significant?	Summary	Adjusted P Value	
Control vs. (G4C2)8	0.04675	-0.3397 to 0.4332	No	ns	0.9472	
Control vs. (G4C2)49	-0.7074	-1.094 to -0.3209	Yes	***	0.0007	
(G4C2)8 vs. (G4C2)49	-0.7542	-1.141 to -0.3677	Yes	***	0.0004	
Fig. 5a, dCtr9: 1-way ANOVA						
ANOVA table	SS	DF	MS	F (DFn, DFd)	P value	
Treatment (between columns)	0.7279	2	0.364	F (2, 15) = 10.35	P=0.0015	
Residual (within columns)	0.5273	15	0.03515			
Total	1.255	17				
Sample size (n)	25					
Independent Expt. Runs	2 w/ biological triplicates					
Data point	mean fold change for 1 replicate relative to mean of controls					
Tukey's multiple comparisons test	Mean Diff.	95.00% CI of diff.	Significant?	Summary	Adjusted P Value	
Control vs. (G4C2)8	-0.2668	-0.548 to 0.01439	No	ns	0.0641	
Control vs. (G4C2)49	-0.492	-0.7732 to -0.2108	Yes	**	0.0011	
(G4C2)8 vs. (G4C2)49	-0.2252	-0.5064 to 0.05596	No	ns	0.1277	

Fig. 5a, dRtf1: 1-way ANOVA						
ANOVA table	SS	DF	MS	F (DFn, DFd)	P value	
Treatment (between columns)	1.465	2	0.7324	F (2, 15) = 56.77	P<0.0001	
Residual (within columns)	0.1935	15	0.0129			
Total	1.658	17				
Sample size (n)	25					
Independent Expt. Runs	2 w/ biological triplicates					
Data point	mean fold change for 1 replicate relative to mean of controls					
Tukey's multiple comparisons test	Mean Diff.	95.00% CI of diff.	Significant?	Summary	Adjusted P Value	
Control vs. (G4C2)8	-0.06468	-0.235 to 0.1056	No	ns	0.5963	
Control vs. (G4C2)49	-0.6349	-0.8052 to -0.4646	Yes	****	<0.0001	
(G4C2)8 vs. (G4C2)49	-0.5702	-0.7405 to -0.3999	Yes	****	<0.0001	

Fig. 5b: unpaired, two-tailed student t-tests						
Sample size (n)	25					
Independent Expt. Runs	2 w/ biological triplicates					
Data point	mean fold change for 1 replicate relative to mean of controls					
	P value	Significant?	Summary	F, DFn, Dfd	F test P value	F test significant?
Control vs. Paf1 RNAi	<0.0001	Yes	****	1.043, 5, 5	0.9647	No
Control vs. Leo1 RNAi	<0.0001	Yes	****	1.925, 5, 5	0.4897	No

Control vs. CDC73 shRNA	<0.0001	Yes	****	1.035, 5, 5	0.9708	No
Control vs. Ctr9 shRNA	<0.0001	Yes	****	2.088, 5, 5	0.4382	No
Control vs. Rtf1 shRNA	<0.0001	Yes	****	2.827, 5, 5	0.2786	No

Fig. 5c: unpaired, two-tailed student t-tests						
Independent Expt. Runs	2 w/ > 3 animals per run					
Sample sizes (n)	3mo: (G4C2)2 (6), (G4C2)149 (6); 6mo: (G4C2)2 (6), (G4C2)149 (7)					
Data point	relative band density normalized to mGAPDH					
	P value	Significant?	Summary	F, DFn, Dfd	F test P value	F test significant?
(G4C2)2 vs. (G4C2)149 (3mo)	0.1585	No	ns	3.931, 5, 5	0.1593	No
(G4C2)2 vs. (G4C2)149 (6mo)	0.0292	Yes	*	1.94, 5, 6	0.4432	No

Fig. 6a: unpaired, two-tailed student t-tests						
Independent Expt. Runs	2 w/ technical triplicates					
Data point	relative band density normalized to mean of hTub and hGAPDH					
	P value	Significant?	Summary	F, DFn, Dfd	F test P value	F test significant?
hPaf1: Cntrl vs. C9+	0.0178	Yes	*	2.996, 5, 5	0.2537	No
hLeo1: Cntrl vs. C9+	0.4751	No	ns	5.62, 5, 5	0.0812	No
hCDC73: Cntrl vs. C9+	0.5874	No	ns	4.455, 5, 5	0.1267	No
hRtf1: Cntrl vs. C9+	0.0419	Yes	*	1.808, 5, 5	0.5316	No

Fig. 6b: 2-way ANOVA						
ANOVA table, Top	SS	DF	MS	F (DFn,	P value	

				DFd)		
Interaction	14.42	1	14.42	F (1, 12) = 3.704	P=0.0783	
Row Factor	16.24	1	16.24	F (1, 12) = 4.169	P=0.0638	
Column Factor	14.42	1	14.42	F (1, 12) = 3.704	P=0.0783	
Residual	46.73	12	3.894			
Independent Expt. Runs	2 per line w/ technical quadruplicates					
Data point	relative signal normalized to % input relative to IgG; mean for individual lines					
Sidak's multiple comparisons test	Mean Diff.	95.00% CI of diff.	Significant?	Summary	Adjusted P Value	
hLeo1 - IgG						
C9orf72 Intron 1	3.914	0.351 to 7.476	Yes	*	0.0316	
Intergenic	0.1158	-3.447 to 3.678	No	ns	0.9958	
C9orf72 Intron 1 - Intergenic						
hLeo1	3.798	0.2353 to 7.36	Yes	*	0.0368	
IgG	0	-3.563 to 3.563	No	ns	>0.9999	
Fig. 6c, Paf1, FTD cases: 1-way Kruskal-Wallis ANOVA (see Supplementary Fig. 10a for sample sizes and patient details)						
P value	Exact or approx?	Summary	medians vary signif. (P < 0.05)?	Number of groups	Kruskal-Wallis statistic	
<0.0001	Approximate	****	Yes	3	18.57	
Independent Expt. Runs	2 for individual patients w/ technical duplicates					
Data point	mean fold change for 1 patient relative to mean of healthy controls					
Dunn's multiple	Mean	Significant	Summary	Adjusted		

comparisons test	rank diff.	?		P Value		
Healthy vs. C9-	-7.029	No	ns	0.7859		
Healthy vs. C9+	-25.45	Yes	****	<0.0001		
C9- vs. C9+	-18.42	Yes	*	0.0107		
Fig. 6c, Paf1, FTD/ALS cases: 1-way Kruskal-Wallis ANOVA (see Supplementary Fig. 10a for sample sizes and patient details)						
P value	Exact or approx?	Summary	medians vary signif. (P < 0.05)?	Number of groups	Kruskal-Wallis statistic	
0.0074	Approximate	**	Yes	3	9.823	
Independent Expt. Runs	2 for individual patients w/ technical duplicates					
Data point	mean fold change for 1 patient relative to mean of healthy controls					
Dunn's multiple comparisons test	Mean rank diff.	Significant?	Summary	Adjusted P Value		
Healthy vs. C9-	-13.99	No	ns	0.0682		
Healthy vs. C9+	-14.11	Yes	*	0.0143		
C9- vs. C9+	-0.1126	No	ns	>0.9999		
Fig. 6c, Paf1, ALS cases: 1-way Kruskal-Wallis ANOVA (see Supplementary Fig. 10a for sample sizes and patient details)						
P value	Exact or approx?	Summary	medians vary signif. (P < 0.05)?	Number of groups	Kruskal-Wallis statistic	
0.0285	Approximate	*	Yes	3	7.119	
Independent Expt. Runs	2 for individual patients w/ technical duplicates					
Data point	mean fold change for 1 patient relative to mean of healthy controls					
Dunn's multiple comparisons test	Mean rank	Significant?	Summary	Adjusted P Value		

	diff.					
Healthy vs. C9-	13.26	No	ns	0.064		
Healthy vs. C9+	13.14	No	ns	0.0794		
C9- vs. C9+	-0.1273	No	ns	>0.9999		

Fig. 6c, Leo1, FTD cases: 1-way Kruskal-Wallis ANOVA (see Supplementary Fig. 10a for sample sizes and patient details)						
P value	Exact or approx?	Summary	medians vary signif. (P < 0.05)?	Number of groups	Kruskal-Wallis statistic	
0.0077	Approximate	**	Yes	3	9.74	
Independent Expt. Runs	2 for individual patients w/ technical duplicates					
Data point	mean fold change for 1 patient relative to mean of healthy controls					
Dunn's multiple comparisons test	Mean rank diff.	Significant?	Summary	Adjusted P Value		
Healthy vs. C9-	4.317	No	ns	>0.9999		
Healthy vs. C9+	-14.27	No	ns	0.0561		
C9- vs. C9+	-18.58	Yes	**	0.0099		

Fig. 6c, Leo1, FTD/ALS cases: 1-way Kruskal-Wallis ANOVA (see Supplementary Fig. 10a for sample sizes and patient details)						
P value	Exact or approx?	Summary	medians vary signif. (P < 0.05)?	Number of groups	Kruskal-Wallis statistic	
0.0588	Approximate	ns	No	3	5.668	
Independent Expt. Runs	1-2 for individual patients w/ replicates					
Data point	mean fold change for 1 patient relative to mean of healthy controls					
Dunn's multiple comparisons test	Mean rank diff.	Significant?	Summary	Adjusted P Value		

Healthy vs. C9-	-4.529	No	ns	>0.9999		
Healthy vs. C9+	-11.88	No	ns	0.0522		
C9- vs. C9+	-7.355	No	ns	0.7498		

Fig. 6c, Leo1, ALS cases: 1-way Kruskal-Wallis ANOVA (see Supplementary Fig. 10a for sample sizes and patient details)

P value	Exact or approx?	Summary	medians vary signif. (P < 0.05)?	Number of groups	Kruskal-Wallis statistic	
0.0534	Approximate	ns	No	3	5.859	

Independent Expt. Runs	2 for individual patients w/ technical duplicates					
Data point	mean fold change for 1 patient relative to mean of healthy controls					
Dunn's multiple comparisons test	Mean rank diff.	Significant?	Summary	Adjusted P Value		
Healthy vs. C9-	13.5	No	ns	0.0574		
Healthy vs. C9+	9.3	No	ns	0.3484		
C9- vs. C9+	-4.2	No	ns	>0.9999		

Fig. 6d: Spearman r correlations (see Supplementary Fig. 10a for sample sizes and patient details)

Independent Expt. Runs	For C9orf72-intron 1: 2 for individual patients w/ technical duplicates; For Paf1, Leo1: same data as Fig. 6c.					
Data point	mean fold change for 1 patient relative to mean of healthy controls					
	Spearman r	P value (two-tailed)	Summary	Exact or Approx?	Significant? (α = 0.05)	95% CI
C9+ FTD only: C9orf72 Intron 1 vs PAF1	0.7374	<0.0001	****	Approx.	Yes	0.4808 to 0.8777
C9- FTD only: C9orf72 Intron 1 vs PAF1	0.2787	0.1979	ns	Approx.	No	-0.1635 to 0.627

						6
Healthy Cntrls: C9orf72 Intron 1 vs PAF1	0.07937	0.6939	ns	Approx.	No	-0.3206 to 0.4554
C9+ FTD only: C9orf72 Intron 1 vs LEO1	0.6321	0.0005	***	Approx.	Yes	0.3133 to 0.8229
C9- FTD only: C9orf72 Intron 1 vs LEO1	0.3538	0.0977	ns	Approx.	No	-0.08131 to 0.6756
Healthy Cntrls: C9orf72 Intron 1 vs LEO1	0.03114	0.8775	ns	Approx.	No	-0.3634 to 0.4162

Sup. Fig 2b: 1-way ANOVA						
RNAi lines						
ANOVA table	SS	DF	MS	F (DFn, DFd)	P value	
Treatment (between columns)	1118	6	186.3	F (6, 53) = 5.729	P=0.0001	
Residual (within columns)	1724	53	32.52			
Total	2842	59				
Sample sizes (n)	w+ control RNAi (9), Paf1 RNAi (10), Leo1 RNAi (9), CDC73 RNAi (4), Ctr9 RNAi (8), Rtf1 RNAi (6), Spt4 RNAi (14)					
Independent Expt. Runs	>3					
Data point	retina depth from 1 eye per animal					
Dunnett's multiple comparisons test	Mean Diff.	95.00% CI of diff.	Significant?	Summary	Adjusted P Value	
w+ Control vs. dCDC73	9.77	0.6823 to 18.86	Yes	*	0.0305	

w+ Control vs. dRtf1	5.473	-2.498 to 13.44	No	ns	0.2854	
w+ Control vs. dCtr9	-3.253	-10.6 to 4.096	No	ns	0.705	
w+ Control vs. dLeo1	2.247	-4.883 to 9.376	No	ns	0.9073	
w+ Control vs. dPaf1	5.883	-1.066 to 12.83	No	ns	0.1259	
w+ Control vs. dSpt4	-3.536	-9.998 to 2.925	No	ns	0.5073	
RNAi-2 lines						
ANOVA table	SS	DF	MS	F (DFn, DFd)	P value	
Treatment (between columns)	251.2	5	50.24	F (5, 18) = 2.616	P=0.0602	
Residual (within columns)	345.7	18	19.2			
Total	596.9	23				
Sample sizes (n)	w- control (4), Paf1 RNAi-2 (4), Leo1 RNAi-2 (4), CDC73 RNAi-2 (4), Ctr9 RNAi-2 (4), Rtf1 RNAi-2 (4)					
Independent Expt. Runs	>2					
Data point	retina depth from 1 eye per animal					
Tukey's multiple comparisons test	Mean Diff.	95.00% CI of diff.	Significant?	Summary	Adjusted P Value	
w- Control vs. dPaf1	9.036	-0.8125 to 18.88	No	ns	0.0831	
w- Control vs. dLeo1	3.161	-6.687 to 13.01	No	ns	0.9051	
w- Control vs. dCDC73	0.5823	-9.266 to 10.43	No	ns	>0.9999	
w- Control vs. dCtr9	6.508	-3.341 to 16.36	No	ns	0.3302	
w- Control vs.	5.715	-4.134 to	No	ns	0.4645	

dRtf1		15.56				
dPaf1 vs. dLeo1	-5.875	-15.72 to 3.974	No	ns	0.4356	
dPaf1 vs. dCDC73	-8.453	-18.3 to 1.395	No	ns	0.1177	
dPaf1 vs. dCtr9	-2.528	-12.38 to 7.32	No	ns	0.9608	
dPaf1 vs. dRtf1	-3.321	-13.17 to 6.527	No	ns	0.8862	
dLeo1 vs. dCDC73	-2.579	-12.43 to 7.269	No	ns	0.9574	
dLeo1 vs. dCtr9	3.347	-6.502 to 13.19	No	ns	0.883	
dLeo1 vs. dRtf1	2.554	-7.295 to 12.4	No	ns	0.9591	
dCDC73 vs. dCtr9	5.925	-3.923 to 15.77	No	ns	0.4266	
dCDC73 vs. dRtf1	5.132	-4.716 to 14.98	No	ns	0.575	
dCtr9 vs. dRtf1	-0.793	-10.64 to 9.055	No	ns	0.9998	

Sup. Fig 3b: 1-way ANOVA

RNAi lines

ANOVA table	SS	DF	MS	F (DFn, DFd)	P value	
Treatment (between columns)	3259	6	543.1	F (6, 41) = 11.29	P<0.0001	
Residual (within columns)	1973	41	48.12			
Total	5231	47				
Sample sizes (n)	w+ control RNAi (13), Paf1 RNAi (9), Leo1 RNAi (4), CDC73 RNAi (5), Ctr9 RNAi (4), Rtf1 RNAi (4), Spt4 RNAi (9)					
Independent Expt. Runs	>3					

Data point	retina depth from 1 eye per animal					
Tukey's multiple comparisons test	Mean Diff.	95.00% CI of diff.	Significant?	Summary	Adjusted P Value	
w+ Control vs. dPaf1	-0.3164	-9.639 to 9.006	No	ns	>0.9999	
w+ Control vs. dLeo1	-7.64	-19.93 to 4.652	No	ns	0.4754	
w+ Control vs. dCDC73	-26.81	-38.12 to -15.5	Yes	****	<0.0001	
w+ Control vs. dCtr9	-2.375	-14.67 to 9.917	No	ns	0.9965	
w+ Control vs. dRtf1	3.072	-9.22 to 15.36	No	ns	0.9862	
w+ Control vs. dSpt4	-1.241	-10.56 to 8.081	No	ns	0.9996	
dPaf1 vs. dLeo1	-7.324	-20.24 to 5.595	No	ns	0.5833	
dPaf1 vs. dCDC73	-26.5	-38.49 to -14.5	Yes	****	<0.0001	
dPaf1 vs. dCtr9	-2.059	-14.98 to 10.86	No	ns	0.9988	
dPaf1 vs. dRtf1	3.388	-9.531 to 16.31	No	ns	0.9823	
dPaf1 vs. dSpt4	-0.9246	-11.06 to 9.21	No	ns	>0.9999	
dLeo1 vs. dCDC73	-19.17	-33.59 to -4.75	Yes	**	0.0031	
dLeo1 vs. dCtr9	5.265	-9.936 to 20.47	No	ns	0.9323	
dLeo1 vs. dRtf1	10.71	-4.49 to 25.91	No	ns	0.3261	
dLeo1 vs. dSpt4	6.399	-6.52 to 19.32	No	ns	0.7225	
dCDC73 vs. dCtr9	24.44	10.01 to	Yes	****	<0.0001	

		38.86				
dCDC73 vs. dRtf1	29.88	15.46 to 44.3	Yes	****	<0.0001	
dCDC73 vs. dSpt4	25.57	13.58 to 37.56	Yes	****	<0.0001	
dCtr9 vs. dRtf1	5.447	-9.755 to 20.65	No	ns	0.9213	
dCtr9 vs. dSpt4	1.134	-11.78 to 14.05	No	ns	>0.9999	
dRtf1 vs. dSpt4	-4.313	-17.23 to 8.606	No	ns	0.9428	
RNAi-2 lines						
ANOVA table	SS	DF	MS	F (DFn, DFd)	P value	
Treatment (between columns)	234.6	5	46.91	F (5, 28) = 2.695	P=0.0414	
Residual (within columns)	487.4	28	17.41			
Total	722	33				
Sample sizes (n)	w- control (6), Paf1 RNAi-2 (4), Leo1 RNAi-2 (6), CDC73 RNAi-2 (6), Ctr9 RNAi-2 (6), Rtf1 RNAi-2 (6)					
Independent Expt. Runs	>2					
Data point	retina depth from 1 eye per animal					
Tukey's multiple comparisons test	Mean Diff.	95.00% CI of diff.	Significant?	Summary	Adjusted P Value	
w- Control vs. dPaf1	-1.265	-9.495 to 6.965	No	ns	0.9968	
w- Control vs. dLeo1	1.952	-5.409 to 9.313	No	ns	0.9632	
w- Control vs. dCDC73	2.304	-5.057 to 9.665	No	ns	0.9276	
w- Control vs. dCtr9	1.869	-5.492 to 9.23	No	ns	0.9694	

w- Control vs. dRtf1	-5.042	-12.4 to 2.319	No	ns	0.3194	
dPaf1 vs. dLeo1	3.217	-5.013 to 11.45	No	ns	0.8357	
dPaf1 vs. dCDC73	3.57	-4.66 to 11.8	No	ns	0.7688	
dPaf1 vs. dCtr9	3.134	-5.096 to 11.36	No	ns	0.8499	
dPaf1 vs. dRtf1	-3.777	-12.01 to 4.453	No	ns	0.7252	
dLeo1 vs. dCDC73	0.3523	-7.009 to 7.713	No	ns	>0.9999	
dLeo1 vs. dCtr9	-0.08333	-7.444 to 7.278	No	ns	>0.9999	
dLeo1 vs. dRtf1	-6.994	-14.36 to 0.3668	No	ns	0.0698	
dCDC73 vs. dCtr9	-0.4357	-7.797 to 6.925	No	ns	>0.9999	
dCDC73 vs. dRtf1	-7.347	-14.71 to 0.01449	No	ns	0.0507	
dCtr9 vs. dRtf1	-6.911	-14.27 to 0.4502	No	ns	0.0752	

Sup. Fig 3c: 1-way ANOVA						
RNAi lines						
ANOVA table	SS	DF	MS	F (DFn, DFd)	P value	
Treatment (between columns)	1.398	5	0.2796	F (5, 12) = 1.647	P=0.2217	
Residual (within columns)	2.038	12	0.1698			
Total	3.436	17				
Sample size (n)	10					
Independent Expt.	2 w/ biological triplicates					

Runs						
Data point	normalized band density per lane					
Tukey's multiple comparisons test	Mean Diff.	95.00% CI of diff.	Significant?	Summary	Adjusted P Value	
w+ Control vs. dPaf1	-0.0001803	-1.13 to 1.13	No	ns	>0.9999	
w+ Control vs. dLeo1	0.06474	-1.065 to 1.195	No	ns	>0.9999	
w+ Control vs. dCDC73	0.5331	-0.5971 to 1.663	No	ns	0.6224	
w+ Control vs. dCtr9	0.6254	-0.5048 to 1.756	No	ns	0.4682	
w+ Control vs. dRtf1	0.5654	-0.5647 to 1.696	No	ns	0.5672	
dPaf1 vs. dLeo1	0.06492	-1.065 to 1.195	No	ns	>0.9999	
dPaf1 vs. dCDC73	0.5333	-0.5969 to 1.663	No	ns	0.6221	
dPaf1 vs. dCtr9	0.6255	-0.5046 to 1.756	No	ns	0.4679	
dPaf1 vs. dRtf1	0.5656	-0.5645 to 1.696	No	ns	0.5669	
dLeo1 vs. dCDC73	0.4683	-0.6618 to 1.598	No	ns	0.7311	
dLeo1 vs. dCtr9	0.5606	-0.5695 to 1.691	No	ns	0.5754	
dLeo1 vs. dRtf1	0.5007	-0.6294 to 1.631	No	ns	0.6775	
dCDC73 vs. dCtr9	0.09229	-1.038 to 1.222	No	ns	0.9997	
dCDC73 vs. dRtf1	0.03237	-1.098 to 1.163	No	ns	>0.9999	
dCtr9 vs. dRtf1	-0.0599	-1.19 to	No	ns	>0.9999	

	2	1.07				
RNAi-2 lines						
ANOVA table	SS	DF	MS	F (DFn, DFd)	P value	
Treatment (between columns)	1.241	5	0.2483	F (5, 12) = 0.9149	P=0.5035	
Residual (within columns)	3.256	12	0.2714			
Total	4.498	17				
Sample size (n)	10					
Independent Expt. Runs	2 w/ biological triplicates					
Data point	normalized band density per lane					
Tukey's multiple comparisons test	Mean Diff.	95.00% CI of diff.	Significant?	Summary	Adjusted P Value	
w- Control vs. dPaf1	0.1544	-1.274 to 1.583	No	ns	0.9989	
w- Control vs. dLeo1	0.2261	-1.203 to 1.655	No	ns	0.9937	
w- Control vs. dCDC73	-0.2988	-1.727 to 1.13	No	ns	0.9781	
w- Control vs. dCtr9	-0.2684	-1.697 to 1.16	No	ns	0.9863	
w- Control vs. dRtf1	-0.5079	-1.936 to 0.9208	No	ns	0.8316	
dPaf1 vs. dLeo1	0.07162	-1.357 to 1.5	No	ns	>0.9999	
dPaf1 vs. dCDC73	-0.4532	-1.882 to 0.9754	No	ns	0.8858	
dPaf1 vs. dCtr9	-0.4228	-1.851 to 1.006	No	ns	0.9112	
dPaf1 vs. dRtf1	-0.6623	-2.091 to 0.7663	No	ns	0.6381	

dLeo1 vs. dCDC73	-0.5249	-1.953 to 0.9038	No	ns	0.8128	
dLeo1 vs. dCtr9	-0.4944	-1.923 to 0.9342	No	ns	0.8459	
dLeo1 vs. dRtf1	-0.7339	-2.163 to 0.6947	No	ns	0.5417	
dCDC73 vs. dCtr9	0.03042	-1.398 to 1.459	No	ns	>0.9999	
dCDC73 vs. dRtf1	-0.2091	-1.638 to 1.22	No	ns	0.9956	
dCtr9 vs. dRtf1	-0.2395	-1.668 to 1.189	No	ns	0.9917	
Sup. Fig 4a, Paf1: 1-way ANOVA						
ANOVA table	SS	DF	MS	F (DFn, DFd)	P value	
Treatment (between columns)	3.236	2	1.618	F (2, 21) = 175.6	P<0.0001	
Residual (within columns)	0.1935	21	0.009215			
Total	3.43	23				
Independent Expt. Runs	2 w/ biological triplicates					
Data point	mean fold change for 1 replicate relative to mean of controls					
Tukey's multiple comparisons test	Mean Diff.	95.00% CI of diff.	Significant?	Summary	Adjusted P Value	
w- Control vs. w-RNAi	0.8853	0.7644 to 1.006	Yes	****	<0.0001	
w- Control vs. w-RNAi-2	0.445	0.324 to 0.566	Yes	****	<0.0001	
w- RNAi vs. w-RNAi-2	-0.4403	-0.58 to -0.3006	Yes	****	<0.0001	
Sup. Fig 4a, Leo1: 1-way ANOVA						
ANOVA table	SS	DF	MS	F (DFn, DFd)	P value	

Treatment (between columns)	3.867	2	1.933	F (2, 18) = 115.1	P<0.0001	
Residual (within columns)	0.3023	18	0.0168			
Total	4.169	20				
Independent Expt. Runs	2 w/ triplicates					
Data point	mean fold change for 1 replicate relative to mean of controls					
Tukey's multiple comparisons test	Mean Diff.	95.00% CI of diff.	Significant?	Summary	Adjusted P Value	
w- Control vs. w- RNAi	0.9047	0.7303 to 1.079	Yes	****	<0.0001	
w- Control vs. w- RNAi-2	0.8253	0.651 to 0.9997	Yes	****	<0.0001	
w- RNAi vs. w- RNAi-2	-0.07933	-0.2703 to 0.1116	No	ns	0.5499	
Sup. Fig 4a, CDC73: unpaired, two-tailed student t-test						
Independent Expt. Runs	2 w/ triplicates					
Data point	mean fold change for 1 replicate relative to mean of controls					
	P value	Significant?	Summary	F, DFn, Dfd	F test P value	F test significant?
w+ Control vs. w+ RNAi	<0.0001	Yes	****	15.18, 2, 2	0.1236	No
w- Control vs. w- RNAi	<0.0001	Yes	****	2.525, 5, 5	0.3324	No
Sup. Fig 4a, Ctr9: unpaired, two-tailed student t-test						
Independent Expt. Runs	2 w/ triplicates					
Data point	mean fold change for 1 replicate relative to mean of controls					
	P value	Significant?	Summary	F, DFn, Dfd	F test P value	F test significant?

w+ Control vs. w+ RNAi	0.0002	Yes	***	27.15, 2, 2	0.0711	No
w- Control vs. w- RNAi	0.0459	Yes	*	34.8, 8, 5	0.0011	Yes
Sup. Fig 4a, Rtf1: unpaired, two-tailed student t-test						
Independent Expt. Runs	2 w/ triplicates					
Data point	mean fold change for 1 replicate relative to mean of controls					
	P value	Significant?	Summary	F, DFn, Dfd	F test P value	F test significant?
w+ Control vs. w+ RNAi	0.0005	Yes	***	5.439, 2, 2	0.3106	No
w- Control vs. w- RNAi	0.023	Yes	*	2.27, 2, 2	0.6116	No
Sup. Fig 4b: unpaired, two-tailed student t-test						
Independent Expt. Runs	2 w/ triplicates					
Data point	normalized band density per lane relative to mean of controls					
	P value	Significant?	Summary	F, DFn, Dfd	F test P value	F test significant?
w+ Control vs. w+ RNAi	0.0285	Yes	*	4.041, 2, 2	0.3967	No
w- Control vs. w- RNAi	0.0281	Yes	*	2.861, 5, 5	0.2734	No
Sup. Fig 4c: unpaired, two-tailed student t-test						
Independent Expt. Runs	2 w/ triplicates					
Data point	normalized band density per lane relative to mean of controls					
	P value	Significant?	Summary	F, DFn, Dfd	F test P value	F test significant?
w+ Control vs. w+ RNAi	0.0026	Yes	**	2.027, 2, 2	0.6608	No

w- Control vs. w-RNAi	0.0026	Yes	**	2.235, 5, 5	0.398	No
Sup. Fig 5a: 1-way ANOVA						
ANOVA table	SS	DF	MS	F (DFn, DFd)	P value	
Treatment (between columns)	10728	5	2146	F (5, 32) = 32.34	P<0.0001	
Residual (within columns)	2123	32	66.35			
Total	12851	37				
Sample sizes (n)	w- Control (12); Paf1 RNAi-2 (5); Leo1 RNAi-2 (6), CDC73 RNAi-2 (6); Ctr9 RNAi-2 (6); Rtf1 RNAi-2 (3)					
Independent Expt. Runs	2 with > 4 animals per genotype					
Data point	retina depth from 1 eye per animal					
Tukey's multiple comparisons test	Mean Diff.	95.00% CI of diff.	Significant?	Summary	Adjusted P Value	
w- Control vs. dPaf1	-18.42	-31.55 to -5.284	Yes	**	0.0022	
w- Control vs. dLeo1	-42.18	-54.52 to -29.84	Yes	****	<0.0001	
w- Control vs. dCDC73	-39.4	-51.73 to -27.06	Yes	****	<0.0001	
w- Control vs. dCtr9	-26.82	-39.16 to -14.48	Yes	****	<0.0001	
w- Control vs. dRtf1	-34.38	-50.31 to -18.46	Yes	****	<0.0001	
dPaf1 vs. dLeo1	-23.76	-38.7 to -8.818	Yes	***	0.0004	
dPaf1 vs. dCDC73	-20.98	-35.92 to -6.036	Yes	**	0.0022	
dPaf1 vs. dCtr9	-8.404	-23.35 to 6.538	No	ns	0.5394	
dPaf1 vs. dRtf1	-15.96	-33.98 to 2.056	No	ns	0.1067	

dLeo1 vs. dCDC73	2.782	-11.46 to 17.03	No	ns	0.9909	
dLeo1 vs. dCtr9	15.36	1.109 to 29.6	Yes	*	0.0286	
dLeo1 vs. dRtf1	7.795	-9.653 to 25.24	No	ns	0.7535	
dCDC73 vs. dCtr9	12.57	-1.672 to 26.82	No	ns	0.1089	
dCDC73 vs. dRtf1	5.013	-12.43 to 22.46	No	ns	0.9509	
dCtr9 vs. dRtf1	-7.561	-25.01 to 9.887	No	ns	0.776	
Sup. Fig 5b: 1-way ANOVA						
ANOVA table	SS	DF	MS	F (DFn, DFd)	P value	
Treatment (between columns)	203.3	5	40.65	F (5, 17) = 1.997	P=0.1307	
Residual (within columns)	346.1	17	20.36			
Total	549.3	22				
Sample sizes (n)	w- Control (4); Paf1 RNAi-2 (3); Leo1 RNAi-2 (4), CDC73 RNAi-2 (4); Ctr9 RNAi-2 (3); Rtf1 RNAi-2 (5)					
Independent Expt. Runs	2 with > 4 animals per genotype					
Data point	retina depth from 1 eye per animal					
Tukey's multiple comparisons test	Mean Diff.	95.00% CI of diff.	Significant?	Summary	Adjusted P Value	
w- Control vs. dPaf1	-0.3168	-11.34 to 10.71	No	ns	>0.9999	
w- Control vs. dLeo1	-2.17	-12.37 to 8.035	No	ns	0.9818	
w- Control vs. dCDC73	-1.276	-11.48 to 8.929	No	ns	0.9984	
w- Control vs. dCtr9	1.859	-9.164 to 12.88	No	ns	0.9936	

w- Control vs. dRtf1	-7.137	-16.82 to 2.544	No	ns	0.2252	
dPaf1 vs. dLeo1	-1.853	-12.88 to 9.169	No	ns	0.9937	
dPaf1 vs. dCDC73	-0.9592	-11.98 to 10.06	No	ns	0.9997	
dPaf1 vs. dCtr9	2.176	-9.608 to 13.96	No	ns	0.9903	
dPaf1 vs. dRtf1	-6.82	-17.36 to 3.719	No	ns	0.3469	
dLeo1 vs. dCDC73	0.894	-9.311 to 11.1	No	ns	0.9997	
dLeo1 vs. dCtr9	4.029	-6.994 to 15.05	No	ns	0.8451	
dLeo1 vs. dRtf1	-4.967	-14.65 to 4.714	No	ns	0.5848	
dCDC73 vs. dCtr9	3.135	-7.888 to 14.16	No	ns	0.9387	
dCDC73 vs. dRtf1	-5.861	-15.54 to 3.82	No	ns	0.4151	
dCtr9 vs. dRtf1	-8.996	-19.54 to 1.544	No	ns	0.1199	

Sup. Fig 5c: 1-way ANOVA						
ANOVA table	SS	DF	MS	F (DFn, DFd)	P value	
Treatment (between columns)	2096	5	419.2	F (5, 27) = 32.81	P<0.0001	
Residual (within columns)	345	27	12.78			
Total	2441	32				
Sample sizes (n)	w- Control (6); Paf1 RNAi-2 (5); Leo1 RNAi-2 (5), CDC73 RNAi-2 (5); Ctr9 RNAi-2 (6); Rtf1 RNAi-2 (6)					
Independent Expt. Runs	2 with > 4 animals per genotype					
Data point	retina depth from 1 eye per animal					

Tukey's multiple comparisons test	Mean Diff.	95.00% CI of diff.	Significant?	Summary	Adjusted P Value	
Control vs. dPaf1	-19.16	-25.79 to -12.53	Yes	****	<0.0001	
Control vs. dLeo1	-12.03	-18.66 to -5.394	Yes	****	<0.0001	
Control vs. dCDC73	-24.63	-31.26 to -18	Yes	****	<0.0001	
Control vs. dCtr9	-19.74	-26.07 to -13.42	Yes	****	<0.0001	
Control vs. dRtf1	-12.78	-19.11 to -6.461	Yes	****	<0.0001	
dPaf1 vs. dLeo1	7.137	0.2107 to 14.06	Yes	*	0.0406	
dPaf1 vs. dCDC73	-5.467	-12.39 to 1.46	No	ns	0.1856	
dPaf1 vs. dCtr9	-0.5815	-7.213 to 6.05	No	ns	0.9998	
dPaf1 vs. dRtf1	6.378	-0.2533 to 13.01	No	ns	0.0646	
dLeo1 vs. dCDC73	-12.6	-19.53 to -5.678	Yes	****	<0.0001	
dLeo1 vs. dCtr9	-7.719	-14.35 to -1.087	Yes	*	0.0156	
dLeo1 vs. dRtf1	-0.7589	-7.391 to 5.873	No	ns	0.9992	
dCDC73 vs. dCtr9	4.885	-1.747 to 11.52	No	ns	0.2461	
dCDC73 vs. dRtf1	11.85	5.213 to 18.48	Yes	***	0.0001	
dCtr9 vs. dRtf1	6.96	0.6368 to 13.28	Yes	*	0.0247	
Sup. Fig 5d: 1-way ANOVA						
ANOVA table	SS	DF	MS	F (DFn, DFd)	P value	
Treatment (between	2290	5	457.9	F (5, 19)	P<0.0001	

columns)				= 10.68		
Residual (within columns)	815	19	42.89			
Total	3105	24				
Sample sizes (n)	Control (51); Paf1 RNAi-2 (85); Leo1 RNAi-2 (73), CDC73 RNAi-2 (67); Ctr9 RNAi-2 (87); Rtf1 RNAi-2 (31)					
Independent Expt. Runs	2 with > 30 animals per genotype					
Data point	mean % animals that climb per tube; 10-20 animals per tube for each genotype					
Tukey's multiple comparisons test	Mean Diff.	95.00% CI of diff.	Significant?	Summary	Adjusted P Value	
w- Control vs. dPaf1	-28.5	-43.13 to -13.87	Yes	****	<0.0001	
w- Control vs. dLeo1	-23.5	-39.3 to -7.695	Yes	**	0.0019	
w- Control vs. dCDC73	-30.5	-46.3 to -14.7	Yes	****	<0.0001	
w- Control vs. dCtr9	-29.8	-44.91 to -14.69	Yes	****	<0.0001	
w- Control vs. dRtf1	-30.67	-47.56 to -13.77	Yes	***	0.0002	
dPaf1 vs. dLeo1	5	-8.358 to 18.36	No	ns	0.8395	
dPaf1 vs. dCDC73	-2	-15.36 to 11.36	No	ns	0.9966	
dPaf1 vs. dCtr9	-1.3	-13.83 to 11.23	No	ns	0.9994	
dPaf1 vs. dRtf1	-2.167	-16.8 to 12.47	No	ns	0.9968	
dLeo1 vs. dCDC73	-7	-21.63 to 7.633	No	ns	0.6615	
dLeo1 vs. dCtr9	-6.3	-20.18 to 7.582	No	ns	0.7071	
dLeo1 vs. dRtf1	-7.167	-22.97 to 8.638	No	ns	0.7078	

dCDC73 vs. dCtr9	0.7	-13.18 to 14.58	No	ns	>0.9999	
dCDC73 vs. dRtf1	-0.1667	-15.97 to 15.64	No	ns	>0.9999	
dCtr9 vs. dRtf1	-0.8667	-15.98 to 14.25	No	ns	>0.9999	
Sup. Fig 7b, Paf1: 1-way ANOVA						
ANOVA table	SS	DF	MS	F (DFn, DFd)	P value	
Treatment (between columns)	0.2299	2	0.115	F (2, 18) = 1.864	P=0.1837	
Residual (within columns)	1.11	18	0.06167			
Total	1.34	20				
Sample size (n)	10					
Independent Expt. Runs	2 w/ biological triplicates					
Data point	mean fold change for 1 replicate relative to mean of controls					
Tukey's multiple comparisons test	Mean Diff.	95.00% CI of diff.	Significant?	Summary	Adjusted P Value	
Controls vs. dLeo1	0.09034	-0.2437 to 0.4244	No	ns	0.7721	
Controls vs. dCDC73	0.2525	-0.08157 to 0.5865	No	ns	0.1594	
dLeo1 vs. dCDC73	0.1621	-0.2038 to 0.528	No	ns	0.5082	
Sup. Fig 7b, Leo1: 1-way ANOVA						
ANOVA table	SS	DF	MS	F (DFn, DFd)	P value	
Treatment (between columns)	0.5062	2	0.2531	F (2, 15) = 9.4	P=0.0023	
Residual (within columns)	0.4039	15	0.02693			
Total	0.9101	17				

Sample size (n)	10					
Independent Expt. Runs	2 w/ biological triplicates					
Data point	mean fold change for 1 replicate relative to mean of controls					
Tukey's multiple comparisons test	Mean Diff.	95.00% CI of diff.	Significant?	Summary	Adjusted P Value	
Control vs. dPaf1	-0.2364	-0.4825 to 0.009665	No	ns	0.0606	
Control vs. dCDC73	0.1727	-0.07338 to 0.4188	No	ns	0.1959	
dPaf1 vs. dCDC73	0.4091	0.163 to 0.6552	Yes	**	0.0017	

Sup. Fig 7b, Cdc73: 1-way ANOVA

ANOVA table	SS	DF	MS	F (DFn, DFd)	P value	
Treatment (between columns)	0.3349	2	0.1675	F (2, 15) = 1.59	P=0.2365	
Residual (within columns)	1.58	15	0.1053			
Total	1.915	17				
Sample size (n)	10					
Independent Expt. Runs	2 w/ biological triplicates					
Data point	mean fold change for 1 replicate relative to mean of controls					
Tukey's multiple comparisons test	Mean Diff.	95.00% CI of diff.	Significant?	Summary	Adjusted P Value	
Control vs. dPaf1	-0.1228	-0.6095 to 0.3639	No	ns	0.7921	
Control vs. dLeo1	0.2077	-0.279 to 0.6944	No	ns	0.5237	
dPaf1 vs. dLeo1	0.3305	-0.1562 to 0.8172	No	ns	0.2151	

Sup. Fig 7b, Ctr9: 1-way ANOVA

ANOVA table	SS	DF	MS	F (DFn, DFd)	P value	
Treatment (between columns)	0.671	3	0.2237	F (3, 20) = 6.055	P=0.0042	
Residual (within columns)	0.7388	20	0.03694			
Total	1.41	23				
Sample size (n)	10					
Independent Expt. Runs	2 w/ biological triplicates					
Data point	mean fold change for 1 replicate relative to mean of controls					
Tukey's multiple comparisons test	Mean Diff.	95.00% CI of diff.	Significant?	Summary	Adjusted P Value	
Control vs. dPaf1	-0.05303	-0.3636 to 0.2576	No	ns	0.9631	
Control vs. dLeo1	0.1977	-0.1129 to 0.5083	No	ns	0.3107	
Control vs. dCDC73	0.3685	0.05788 to 0.6791	Yes	*	0.0165	
dPaf1 vs. dLeo1	0.2508	-0.05983 to 0.5613	No	ns	0.1415	
dPaf1 vs. dCDC73	0.4215	0.1109 to 0.7321	Yes	**	0.0057	
dLeo1 vs. dCDC73	0.1708	-0.1398 to 0.4813	No	ns	0.4343	
Sup. Fig 7b, Rtf1: 1-way ANOVA						
ANOVA table	SS	DF	MS	F (DFn, DFd)	P value	
Treatment (between columns)	0.9819	3	0.3273	F (3, 20) = 4.88	P=0.0105	
Residual (within columns)	1.341	20	0.06706			
Total	2.323	23				

Sample size (n)	10					
Independent Expt. Runs	2 w/ biological triplicates					
Data point	mean fold change for 1 replicate relative to mean of controls					
Tukey's multiple comparisons test	Mean Diff.	95.00% CI of diff.	Significant?	Summary	Adjusted P Value	
Controls vs. dPaf1	-0.2141	-0.6326 to 0.2044	No	ns	0.495	
Controls vs. dLeo1	0.04407	-0.3744 to 0.4625	No	ns	0.9908	
Controls vs. dCDC73	0.3524	-0.06609 to 0.7709	No	ns	0.1185	
dPaf1 vs. dLeo1	0.2582	-0.1603 to 0.6766	No	ns	0.3366	
dPaf1 vs. dCDC73	0.5665	0.148 to 0.985	Yes	**	0.0058	
dLeo1 vs. dCDC73	0.3083	-0.1102 to 0.7268	No	ns	0.1995	
Sup. Fig 7b, Spt4: 1-way ANOVA						
ANOVA table	SS	DF	MS	F (DFn, DFd)	P value	
Treatment (between columns)	0.5222	3	0.1741	F (3, 23) = 2.823	P=0.0612	
Residual (within columns)	1.418	23	0.06165			
Total	1.94	26				
Sample size (n)	10					
Independent Expt. Runs	2 w/ biological triplicates					
Data point	mean fold change for 1 replicate relative to mean of controls					
Tukey's multiple comparisons test	Mean Diff.	95.00% CI of diff.	Significant?	Summary	Adjusted P Value	
Control vs. dPaf1	-0.1918	-0.5539 to 0.1703	No	ns	0.4735	

Control vs. dLeo1	-0.04617	-0.4083 to 0.316	No	ns	0.9846	
Control vs. dCDC73	0.2195	-0.1426 to 0.5817	No	ns	0.3578	
dPaf1 vs. dLeo1	0.1456	-0.2511 to 0.5423	No	ns	0.7419	
dPaf1 vs. dCDC73	0.4113	0.01462 to 0.808	Yes	*	0.0402	
dLeo1 vs. dCDC73	0.2657	-0.131 to 0.6624	No	ns	0.2752	

Sup Fig 7a, Control vs. Paf1 RNAi: Log-rank (Mantel-Cox) test and Gehan-Breslow-Wilcoxon test

Sample Sizes (n)	Control (301); Paf1 RNAi (200)
Independent Expt Runs	2 with > 150 animals per genotype

Test	Chi square	df	P value	Significant?	Summary	95% CI of ratio
Log-rank (Mantel-Cox)	133	1	<0.0001	Yes	****	1.119 to 1.653/ 0.605 to 0.8936
Gehan-Breslow-Wilcoxon	72.23	1	<0.0001	Yes	****	

Sup Fig 7a, Control vs. Leo1 RNAi: Log-rank (Mantel-Cox) test and Gehan-Breslow-Wilcoxon test

Sample Sizes (n)	Control (301); Leo1 RNAi (275)
Independent Expt Runs	2 with > 150 animals per genotype

Test	Chi square	df	P value	Significant?	Summary	95% CI of ratio
Log-rank (Mantel-Cox)	86.2	1	<0.0001	Yes	****	1.081 to 1.582/ 0.6322 to 0.9249
Gehan-Breslow-Wilcoxon	59.88	1	<0.0001	Yes	****	

Sup Fig 7a, Control vs. CDC73 RNAi: Log-rank (Mantel-Cox) test and Gehan-Breslow-Wilcoxon

test						
Sample Sizes (n)		Control (301); CDC73 RNAi (200)				
Independent Expt Runs		2 with > 150 animals per genotype				
Test	Chi square	df	P value	Significant?	Summary	95% CI of ratio
Log-rank (Mantel-Cox)	2.125	1	0.1449	No	ns	0.7966 to 1.185/ 0.8442 to 1.255
Gehan-Breslow-Wilcoxon	2.474	1	0.1158	No	ns	
Sup Fig 7a, Control vs. Ctr9 RNAi: Log-rank (Mantel-Cox) test and Gehan-Breslow-Wilcoxon test						
Sample Sizes (n)		Control (301); Ctr9 RNAi (210)				
Independent Expt Runs		2 with > 150 animals per genotype				
Test	Chi square	df	P value	Significant?	Summary	95% CI of ratio
Log-rank (Mantel-Cox)	207.8	1	<0.0001	Yes	****	1.272 to 1.878/ 0.5324 to 0.7864
Gehan-Breslow-Wilcoxon	163.8	1	<0.0001	Yes	****	
Sup Fig 7a, Control vs. Rtf1 RNAi: Log-rank (Mantel-Cox) test and Gehan-Breslow-Wilcoxon test						
Sample Sizes (n)		Control (301); Rtf1 RNAi (200)				
Independent Expt Runs		2 with > 150 animals per genotype				
Test	Chi square	df	P value	Significant?	Summary	95% CI of ratio
Log-rank (Mantel-Cox)	48.15	1	<0.0001	Yes	****	0.9055 to 1.328/ 0.7528 to 1.104
Gehan-Breslow-Wilcoxon	19.29	1	<0.0001	Yes	****	
Sup. Fig 8a: unpaired, two-tailed student t-test						

Sample sizes (n)	w+ Control (9); w- Control (12)					
Independent Expt. Runs	>3 with >4 animals per genotype					
Data point	retina depth from 1 eye per animal					
	P value	Significant?	Summary	F, DFn, Dfd	F test P value	F test significant?
w+ control vs. w- control	0.8479	No	ns	1.465, 8, 11	0.5451	No

Sup Fig 8b: Log-rank (Mantel-Cox) test and Gehan-Breslow-Wilcoxon test						
Sample Sizes (n)	w- Control (188); w+ control (106)					
Independent Expt Runs	2 with >100 animals per genotype					
Test	Chi square	df	P value	Significant?	Summary	95% CI of ratio
Log-rank (Mantel-Cox)	0.5859	1	0.444	No	ns	0.8822 to 1.435/ 0.697 to 1.134
Gehan-Breslow-Wilcoxon	0.04529	1	0.8315	No	ns	

Sup. Fig 8c: unpaired, two-tailed student t-test						
Sample sizes (n)	w+ Control (72); w- Control (51)					
Independent Expt. Runs	2 with >50 animals per genotype					
Data point	mean % animals that climb per tube; 10-20 animals per tube for each genotype					
	P value	Significant?	Summary	F, DFn, Dfd	F test P value	F test significant?
w+ control vs. w- control	0.3479	No	ns	4.687, 6, 5	0.1111	No

Sup. Fig 8d: 1-way ANOVA						
ANOVA table	SS	DF	MS	F (DFn, DFd)	P value	
Treatment (between	0.6252	3	0.2084	F (3, 20)	P=0.1584	

columns)				= 1.923		
Residual (within columns)	2.167	20	0.1084			
Total	2.792	23				
Sample size (n)	25					
Independent Expt. Runs	2 w/ biological triplicates					
Data point	mean fold change for 1 replicate relative to mean of controls					
Tukey's multiple comparisons test	Mean Diff.	95.00% CI of diff.	Significant?	Summary	Adjusted P Value	
w- Control 1 vs. w- Control 2	-0.3957	-0.9276 to 0.1363	No	ns	0.193	
w- Control 1 vs. w+ Control 1	-0.06283	-0.5948 to 0.4691	No	ns	0.9872	
w- Control 1 vs. w+ Control 2	-0.01733	-0.5493 to 0.5146	No	ns	0.9997	
w- Control 2 vs. w+ Control 1	0.3328	-0.1991 to 0.8648	No	ns	0.3249	
w- Control 2 vs. w+ Control 2	0.3783	-0.1536 to 0.9103	No	ns	0.2245	
w+ Control 1 vs. w+ Control 2	0.0455	-0.4864 to 0.5774	No	ns	0.995	
Sup. Fig 8e: unpaired, two-tailed student t-test						
Sample sizes (n)	w+ Control (8); w- Control (8)					
Independent Expt. Runs	2 with >4 animals per genotype					
Data point	total fluorescence per animal relative to mean of w- control					
	P value	Significant?	Summary	F, DFn, Dfd	F test P value	F test significant?
w+ control vs. w- control	0.0688	No	ns	8.09, 7, 7	0.0132	Yes

Sup. Fig 9a: 1-way ANOVA						
ANOVA table	SS	DF	MS	F (DFn, DFd)	P value	
Treatment (between columns)	2.065	5	0.4131	F (5, 30) = 11.67	P<0.0001	
Residual (within columns)	1.062	30	0.03539			
Total	3.127	35				
Sample size (n)	25					
Independent Expt. Runs	2 w/ biological triplicates for all except Rtf1 which was run once					
Data point	mean fold change for 1 replicate relative to mean of controls					
Tukey's multiple comparisons test	Mean Diff.	95.00% CI of diff.	Significant?	Summary	Adjusted P Value	
Control vs. dPaf1	0.4965	0.1949 to 0.7981	Yes	***	0.0003	
Control vs. dLeo1	0.3727	0.07111 to 0.6742	Yes	**	0.0087	
Control vs. dCDC73	0.4903	0.1888 to 0.7919	Yes	***	0.0004	
Control vs. dCtr9	0.4308	0.1293 to 0.7324	Yes	**	0.0019	
Control vs. dRtf1	0.8277	0.4462 to 1.209	Yes	****	<0.0001	
dPaf1 vs. dLeo1	-0.1238	-0.4542 to 0.2065	No	ns	0.8606	
dPaf1 vs. dCDC73	-0.006167	-0.3365 to 0.3242	No	ns	>0.9999	
dPaf1 vs. dCtr9	-0.06567	-0.396 to 0.2647	No	ns	0.9899	
dPaf1 vs. dRtf1	0.3312	-0.07342 to 0.7358	No	ns	0.1593	

dLeo1 vs. dCDC73	0.1177	-0.2127 to 0.448	No	ns	0.8841	
dLeo1 vs. dCtr9	0.05817	-0.2722 to 0.3885	No	ns	0.9942	
dLeo1 vs. dRtf1	0.455	0.05041 to 0.8596	Yes	*	0.0204	
dCDC73 vs. dCtr9	-0.0595	-0.3898 to 0.2708	No	ns	0.9936	
dCDC73 vs. dRtf1	0.3373	-0.06725 to 0.7419	No	ns	0.1457	
dCtr9 vs. dRtf1	0.3968	-0.007752 to 0.8014	No	ns	0.057	
Sup. Fig 9b, Tub: 1-way ANOVA						
ANOVA table	SS	DF	MS	F (DFn, DFd)	P value	
Treatment (between columns)	0.278	6	0.04633	F (6, 14) = 0.8653	P=0.5433	
Residual (within columns)	0.7496	14	0.05354			
Total	1.028	20				
Sample size (n)	10					
Independent Expt. Runs	2 w/ biological triplicates					
Data point	mean fold change for 1 replicate relative to mean of controls					
Tukey's multiple comparisons test	Mean Diff.	95.00% CI of diff.	Significant?	Summary	Adjusted P Value	
Control vs. dSpt4	0.0787	-0.5664 to 0.7238	No	ns	0.9994	
Control vs. dCDC73	0.2742	-0.3709 to 0.9194	No	ns	0.7668	
Control vs. dRtf1	-0.0189	-0.664 to 0.6262	No	ns	>0.9999	
Control vs. dCtr9	-0.0877	-0.7329	No	ns	0.999	

	3	to 0.5574				
Control vs. dPaf1	-0.0849	-0.73 to 0.5602	No	ns	0.9991	
Control vs. dLeo1	0.04713	-0.598 to 0.6923	No	ns	>0.9999	
dSpt4 vs. dCDC73	0.1955	-0.4496 to 0.8407	No	ns	0.9369	
dSpt4 vs. dRtf1	-0.0976	-0.7427 to 0.5475	No	ns	0.9981	
dSpt4 vs. dCtr9	-0.1664	-0.8116 to 0.4787	No	ns	0.9698	
dSpt4 vs. dPaf1	-0.1636	-0.8087 to 0.4815	No	ns	0.9722	
dSpt4 vs. dLeo1	-0.03157	-0.6767 to 0.6136	No	ns	>0.9999	
dCDC73 vs. dRtf1	-0.2931	-0.9383 to 0.352	No	ns	0.7122	
dCDC73 vs. dCtr9	-0.362	-1.007 to 0.2832	No	ns	0.5018	
dCDC73 vs. dPaf1	-0.3591	-1.004 to 0.286	No	ns	0.5103	
dCDC73 vs. dLeo1	-0.2271	-0.8722 to 0.418	No	ns	0.8822	
dRtf1 vs. dCtr9	-0.06883	-0.714 to 0.5763	No	ns	0.9997	
dRtf1 vs. dPaf1	-0.066	-0.7111 to 0.5791	No	ns	0.9998	
dRtf1 vs. dLeo1	0.06603	-0.5791 to 0.7112	No	ns	0.9998	
dCtr9 vs. dPaf1	0.002833	-0.6423 to 0.648	No	ns	>0.9999	
dCtr9 vs. dLeo1	0.1349	-0.5103	No	ns	0.9894	

		to 0.78				
dPaf1 vs. dLeo1	0.132	-0.5131 to 0.7772	No	ns	0.9905	
Sup. Fig 9b, Actin: 1-way ANOVA						
ANOVA table	SS	DF	MS	F (DFn, DFd)	P value	
Treatment (between columns)	0.1481	6	0.02469	F (6, 17) = 0.484	P=0.8112	
Residual (within columns)	0.8672	17	0.05101			
Total	1.015	23				
Sample size (n)	10					
Independent Expt. Runs	2 w/ biological triplicates					
Data point	mean fold change for 1 replicate relative to mean of controls					
Tukey's multiple comparisons test	Mean Diff.	95.00% CI of diff.	Significant?	Summary	Adjusted P Value	
Control vs. dSpt4	0.1449	-0.3864 to 0.6762	No	ns	0.9663	
Control vs. dCDC73	0.04818	-0.4831 to 0.5795	No	ns	>0.9999	
Control vs. dRtf1	0.1723	-0.359 to 0.7035	No	ns	0.9261	
Control vs. dCtr9	0.1424	-0.3889 to 0.6737	No	ns	0.969	
Control vs. dPaf1	0.06598	-0.4653 to 0.5973	No	ns	0.9995	
Control vs. dLeo1	0.2285	-0.3028 to 0.7598	No	ns	0.7787	
dSpt4 vs. dCDC73	-0.0967	-0.7102 to 0.5168	No	ns	0.9981	
dSpt4 vs. dRtf1	0.02737	-0.5861 to 0.6408	No	ns	>0.9999	

dSpt4 vs. dCtr9	-0.0025	-0.616 to 0.611	No	ns	>0.9999	
dSpt4 vs. dPaf1	-0.0789	-0.6924 to 0.5346	No	ns	0.9994	
dSpt4 vs. dLeo1	0.0836	-0.5299 to 0.6971	No	ns	0.9991	
dCDC73 vs. dRtf1	0.1241	-0.4894 to 0.7375	No	ns	0.9925	
dCDC73 vs. dCtr9	0.0942	-0.5193 to 0.7077	No	ns	0.9983	
dCDC73 vs. dPaf1	0.0178	-0.5957 to 0.6313	No	ns	>0.9999	
dCDC73 vs. dLeo1	0.1803	-0.4332 to 0.7938	No	ns	0.9523	
dRtf1 vs. dCtr9	-0.02987	-0.6433 to 0.5836	No	ns	>0.9999	
dRtf1 vs. dPaf1	-0.1063	-0.7197 to 0.5072	No	ns	0.9967	
dRtf1 vs. dLeo1	0.05623	-0.5572 to 0.6697	No	ns	>0.9999	
dCtr9 vs. dPaf1	-0.0764	-0.6899 to 0.5371	No	ns	0.9995	
dCtr9 vs. dLeo1	0.0861	-0.5274 to 0.6996	No	ns	0.999	
dPaf1 vs. dLeo1	0.1625	-0.451 to 0.776	No	ns	0.9707	

Sup. Fig 9c, TDH3: 1-way ANOVA

ANOVA table	SS	DF	MS	F (DFn, DFd)	P value	
Treatment (between columns)	0.002645	2	0.001323	F (2, 9) = 0.2174	P=0.8087	
Residual (within columns)	0.05475	9	0.006083			

Total	0.05739	11				
Independent Expt. Runs	1 w/ biological triplicates					
Data point	mean fold change for 1 replicate relative to mean of controls					
Tukey's multiple comparisons test	Mean Diff.	95.00% CI of diff.	Significant?	Summary	Adjusted P Value	
WT vs. leo1Δ	0.003941	-0.15 to 0.1579	No	ns	0.9972	
WT vs. cdc73Δ	-0.02934	-0.1833 to 0.1246	No	ns	0.8579	
leo1Δ vs. cdc73Δ	-0.03328	-0.1873 to 0.1207	No	ns	0.8218	
Sup. Fig 9c, FBA1: 1-way ANOVA						
ANOVA table	SS	DF	MS	F (DFn, DFd)	P value	
Treatment (between columns)	0.1229	2	0.06147	F (2, 9) = 2.248	P=0.1615	
Residual (within columns)	0.2461	9	0.02734			
Total	0.369	11				
Independent Expt. Runs	2 w/ biological triplicates					
Data point	mean fold change for 1 replicate relative to mean of controls					
Tukey's multiple comparisons test	Mean Diff.	95.00% CI of diff.	Significant?	Summary	Adjusted P Value	
WT vs. leo1Δ	-0.06865	-0.3951 to 0.2578	No	ns	0.8303	
WT vs. cdc73Δ	-0.2406	-0.5671 to 0.0858	No	ns	0.154	
leo1Δ vs. cdc73Δ	-0.172	-0.4984 to 0.1544	No	ns	0.3485	
Sup. Fig 10c: 1-way Kruskal-Wallis ANOVA (see Supplementary Fig. 10a for sample sizes and						

patient details)						
P value	Exact or approx?	Summary	medians vary signif. (P < 0.05)?	Number of groups	Kruskal-Wallis statistic	
0.0167	Approximate	ns	Yes	3	8.186	
Independent Expt. Runs	1-2 for individual patients w/ technical replicates					
Data point	mean fold change for 1 patient relative to mean of healthy controls					
Dunn's multiple comparisons test	Mean rank diff.	Significant?	Summary	Adjusted P Value		
Healthy vs. C9-	-17.78	Yes	*	0.0152		
Healthy vs. C9+	-11	No	ns	0.2017		
C9- vs. C9+	6.783	No	ns	0.8547		

Sup. Fig. 10d-e: Spearman r correlations (see Supplementary Fig. 10a for sample sizes and patient details)						
Independent Expt. Runs	1-2 for individual patients w/ technical replicates					
Data point	mean fold change for 1 patient relative to mean of healthy controls					
	Spearman r	P value (two-tailed)	Summary	Exact or Approx?	Significant? (α = 0.05)	95% CI
C9+ FTD only: C9orf72 Intron 1 vs CDC73	0.1338	0.5527	ns	Approx.	No	-0.317 to 0.5353
C9- FTD only: C9orf72 Intron 1 vs CDC73	0.09289	0.6734	ns	Approx.	No	-0.3435 to 0.4963
C9+ ALS only: C9orf72 Intron 1 vs Paf1	-0.2857	0.9048	ns	Approx.	No	-0.4761 to 0.4308

C9+ ALS only: C9orf72 Intron 1 vs Leo1	0.3293	0.1562	ns	Approx.	No	-0.1463 to 0.6813
C9- ALS only: C9orf72 Intron 1 vs Paf1	0.6183	0.0022	Yes	Approx.	**	0.2536 to 0.8291
C9- ALS only: C9orf72 Intron 1 vs Leo1	0.4952	0.0191	Yes	Approx.	*	0.07982 to 0.764

Sup. Fig. 12: linear regression						
Independent Expt. Runs	2					
	Slope	95% CI of slope	F (DFn, DFd)	Significant?	P-value	
G4C2 primers	-3.622 ± 0.1514	-5.546 to -1.699	572.4 (1, 1)	Yes	0.0266	
RP49 primers	-3.487 ± 0.1511	-5.407 to -1.568	532.8 (1, 1)	Yes	0.0276	

Table S2-2: Fly lines

Name	Collection	ID #	Full genotype	References
Gmr-GAL4	n/a	n/a	w*;; Gmr-GAL4^{YH3}	[1]
ElavGS	BDSC	43642	y[1] w[*];; P{w[+mC]=elav-Switch.O}GSG301	[2]
DaGS	n/a	n/a	w*; Da-GAL4[Geneswitch];	[2]
Da-GAL4	n/a	n/a	w*;; Da-GAL4	[3]
HS-GAL4	BDSC	2077	w[*]; P{w[+mC]=GAL4-Hsp70.PB}2;	[4]
Control	n/a	n/a	w[1118]; UAS-DSRED;	[5]
(G4C2)8	n/a	n/a	w[1118];; UAS-(G4C2)8	this paper
(G4C2)29	n/a	n/a	w[1118]; UAS-(G4C2)29;	[6]
(G4C2)49 (II)	n/a	n/a	w[1118]; UAS-(G4C2)49;	this paper
(G4C2)49	n/a	n/a	w[1118];; UAS-(G4C2)49	[6]
LDS-(G4C2)44^{GR-GFP}	n/a	n/a	w[1118];; UAS-LDS-(G4C2)$_{4,42,44}$[GR-GFP]	this paper
TDP43^{52S}	n/a	n/a	w[1118];; UAS-TDP43	[7]
TDP43^{37M}	n/a	n/a	w[1118]; UAS-TDP43;	[7]
w- Control	BDSC	5905	w[1118];;	
Control RNAi/w+ control 1	BDSC	31603	y[1] v[1];; P{y[+t7.7] v[+t1.8]=TRiP.JF01355}attP2	previously used in[8,9]
w+ control 2	BDSC	35788	y[1] v[1]; P{y[+t7.7] v[+t1.8]=UAS-LUC.VALIUM10}attP2	
(GR)36	BDSC	58692	w[1118]; P{{y[+t7.7] w[+mC]=UAS-poly-GR.PO-36}attP40;	[10]
Paf1 RNAi	VDRC	20876	w[1118]; P{GD9782}v20876;	previously used in[11]
Paf1 RNAi-2	VDRC	108826	w[1118]; P{KK100080}VIE-260B;	
Leo1 RNAi	VDRC	17490	w[1118];; P{GD8296}v17490	previously used in[11]

Leo1 RNAi-2	VDRC	106074	w[1118]; P{KK104959}VIE-260B;	
CDC73 RNAi	BDSC	53278	y[1] v[1]; P{y[+t7.7] v[+t1.8]=TRiP.HMC03494}attP40;	
CDC73 RNAi-2	VDRC	28318	w[1118];; P{GD12640}v28318	
Ctr9 RNAi	BDSC	33736	y[1] sc[*] v[1];; P{y[+t7.7] v[+t1.8]=TRiP.HMS00619}attP2	
Ctr9 RNAi-2	VDRC	108874	w[1118]; P{KK101412}VIE-260B;	
Rtf1 RNAi	BDSC	34850	y[1] sc[*] v[1];; P{y[+t7.7] v[+t1.8]=TRiP.HMS00168}attP2	
Rtf1 RNAi-2	VDRC	110392	w[1118]; P{KK101209}VIE-260B;	
Spt4 RNAi	BDSC	32896	y[1] sc[*] v[1]; P{y[+t7.7] v[+t1.8]=TRiP.HMS00685}attP2	previously used in[6]

References

1. Kim, H.-J. *et al.* Therapeutic modulation of eIF2α-phosphorylation rescues TDP-43 toxicity in amyotrophic lateral sclerosis disease models. *Nat Genet* **46**, 152–160 (2014).
2. Tricoire, H. *et al.* The steroid hormone receptor EcR finely modulates Drosophila lifespan during adulthood in a sex-specific manner. *Mechanisms of Ageing and Development* **130**, 547–552 (2009).
3. Wodarz, A., Hinz, U., Engelbert, M. & Knust, E. Expression of crumbs confers apical character on plasma membrane domains of ectodermal epithelia of drosophila. *Cell* **82**, 67–76 (1995).
4. Harrison, D. A., Binari, R., Nahreini, T. S., Gilman, M. & Perrimon, N. Activation of a Drosophila Janus kinase (JAK) causes hematopoietic neoplasia and developmental defects. *EMBO J* **14**, 2857–2865 (1995).
5. Yu, Z. *et al.* A fly model for the CCUG-repeat expansion of myotonic dystrophy type 2 reveals a novel interaction with MBNL1. *Hum. Mol. Genet.* **24**, 954–962 (2015).
6. Kramer, N. J. *et al.* Spt4 selectively regulates the expression of C9orf72 sense and antisense mutant transcripts. *Science* **353**, 708–712 (2016).
7. Elden, A. C. *et al.* Ataxin-2 intermediate-length polyglutamine expansions are associated with increased risk for ALS. *Nature* **466**, 1069–1075 (2010).
8. Berson, A. *et al.* TDP-43 Promotes Neurodegeneration by Impairing Chromatin Remodeling. *Current Biology* **27**, 3579-3590.e6 (2017).
9. Chung, C.-Y. *et al.* Aberrant activation of non-coding RNA targets of transcriptional elongation complexes contributes to TDP-43 toxicity. *Nat Commun* **9**, (2018).
10. Mizielinska, S. *et al.* C9orf72 repeat expansions cause neurodegeneration in Drosophila through arginine-rich proteins. *Science* **345**, 1192–1194 (2014).
11. Gerlach, J. M. *et al.* PAF1 complex component Leo1 helps recruit Drosophila Myc to promoters. *PNAS* **114**, E9224–E9232 (2017).

Table S2-3: Full Genotypes

Fig. 1c	Genotype (driver: HS-GAL4, BL2077)	Includes	Temp
Control	*w^{1118}/w*; HS-GAL4/+;*	n/a	25°C
UAS-G4C2 (II)	*w^{1118}/w*; HS-GAL4/UAS-(G4C2)n;*	(G4C2)29 and (G4C2)49 (II)	25°C
UAS-G4C2 (III)	*w^{1118}/w*; HS-GAL4/+; UAS-(G4C2)n/+*	(G4C2)8 and (G4C2)49 (III)	25°C
Fig. 1d	**Genotype (driver: Gmr-GAL4^{YH3})**	**Includes**	**Temp**
Control	*w^{1118}/Y;; Gmr-GAL4/+*	n/a	25°C
UAS-G4C2 (II)	*w^{1118}/Y; UAS-(G4C2)n/+; Gmr-GAL4/+*	(G4C2)29 and (G4C2)49 (II)	25°C
UAS-G4C2 (III)	*w^{1118}/Y;; UAS-(G4C2)n/Gmr-GAL4*	(G4C2)8 and (G4C2)49 (III)	25°C
Fig. 1e	**Genotype (driver: Gmr-GAL4^{YH3})**	**Shown RNAi lines**	**Temp**
Control	*w^{1118}/Y;; Gmr-GAL4, UAS-(G4C2)n/UAS-RNAi*	Luc (BL31603)	25°C
UAS-RNAi (II)	*w^{1118}/Y; UAS-RNAi/+; Gmr-GAL4, UAS-(G4C2)n/+*	CNOT7 (BL52947)	25°C
UAS-RNAi (III)	*w^{1118}/Y;; Gmr-GAL4, UAS-(G4C2)n/UAS-RNAi*	Ctr9 (BL33736)	25°C
Fig. 2a	**Genotype (driver: Gmr-GAL4^{YH3})**	**Shown RNAi lines**	**Temp**
(GR)36			
Control	*w^{1118}/$y^{1}v^{1}$;UAS-(GR)36/+; Gmr-GAL4/UAS-RNAi*	Luc (BL31603)	25°C
UAS-RNAi (II)	*w^{1118}/$y^{1}v^{1}$;UAS-(GR)36/UAS-RNAi; Gmr-GAL4/+*	Fib (BL42553)	25°C
UAS-RNAi (III)	*w^{1118}/$y^{1}v^{1}$;UAS-(GR)36/+; Gmr-GAL4/UAS-RNAi*	ELL (BL33399)	25°C
TDP43			
Control	*w^{1118}/$y^{1}v^{1}$;UAS-TDP43^{37M}/+; Gmr-GAL4/UAS-RNAi*	Luc (BL31603)	25°C
UAS-RNAi (III)	*w^{1118}/$y^{1}v^{1}$;UAS-TDP43^{37M}/+; Gmr-GAL4/UAS-RNAi*	MPI (BL34379), CPSF6 (BL34804)	25°C

Figure 3a-b	Genotype (driver: Gmr-GAL4^{YH3})	Line	Temp
Control	*w^{1118}/Y;; Gmr-GAL4, UAS-(G4C2)49/UAS-RNAi*	Luc RNAi (BL31603)	24℃
UAS-RNAi (II)	*w^{1118}/Y; UAS-RNAi/+; Gmr-GAL4, UAS-(G4C2)49/+*	Paf1 RNAi (v20876), CDC73 RNAi (BL53278)	24℃
UAS-RNAi (III)	*w^{1118}/Y;; Gmr-GAL4, UAS-(G4C2)49/UAS-RNAi*	Leo1 RNAi (v17490), Ctr9 RNAi (BL33736), Rtf1 RNAi (BL34850)	24℃
Figure 3c-d	Genotype (driver: Gmr-GAL4^{YH3})	Line	Temp
Control	*w^{1118}/Y;; Gmr-GAL4/UAS-RNAi*	Luc RNAi (BL31603)	24℃
UAS-RNAi (II)	*w^{1118}/Y; UAS-RNAi/+; Gmr-GAL4/+*	Paf1 RNAi (v20876), CDC73 RNAi (BL53278)	24℃
UAS-RNAi (III)	*w^{1118}/Y;; Gmr-GAL4/UAS-RNAi*	Leo1 RNAi (v17490), Ctr9 RNAi (BL33736), Rtf1 RNAi (BL34850)	24℃
Figure 3e	Genotype (driver: Elav-GS)	Line	Temp
Control	*w^{1118}; UAS-DSRED/+; Elav-GS, UAS-(G4C2)49/+*	UAS-DSRED	24℃
dPaf1 RNAi	*w^{1118}; UAS-RNAi/+; Elav-GS, UAS-(G4C2)49/+*	v20876	24℃
dLeo1 RNAi	*w^{1118};; Elav-GS, UAS-(G4C2)49/UAS-RNAi*	v17490	24℃
dCDC73 RNAi	*w^{1118}/y^1v^1; UAS-RNAi/+; Elav-GS, UAS-(G4C2)49/+*	BL53278	24℃
UAS-TRiP (III)	*$w^{1118}/y^1sc^*v^1$;; Elav-GS, UAS-(G4C2)49/UAS-RNAi*	Ctr9 RNAi (BL33736), Rtf1 RNAi (BL34850)	24℃
Figure 3f and Supplemental Fig 6	Genotype (driver: Elav-GS)	Line	Temp
(G4C2)0 Control	*w^{1118}; UAS-DSRED/+; Elav-GS/+*	UAS-DSRED	24℃
(G4C2)49 Control	*w^{1118}; UAS-DSRED/+; Elav-GS, UAS-(G4C2)49/+*	UAS-DSRED	24℃
dPaf1 RNAi	*w^{1118}; UAS-RNAi/+; Elav-GS, UAS-(G4C2)49/+*	v20876	24℃
dLeo1 RNAi	*w^{1118};; Elav-GS, UAS-(G4C2)49/UAS-RNAi*	v17490	24℃

dCDC73 RNAi	*w^{1118}/y^1v^1; UAS-RNAi/+; Elav-GS, UAS-(G4C2)49/+*	BL53278	24℃
UAS-TRiP (III)	*$w^{1118}/y^1sc^*v^1$;; Elav-GS, UAS-(G4C2)49/UAS-RNAi*	Ctr9 RNAi (BL33736), Rtf1 RNAi (BL34850)	24℃
Figure 3g	Genotype (driver: Da-GS)	Line	Temp
Control	*w^{1118}/Y; Da-GS, UAS-(G4C2)49/UAS-DSRED;*	UAS-DSRED	24℃
dCDC73 RNAi	*w^{1118}/Y; Da-GS, UAS-(G4C2)49/UAS-RNAi;*	BL53278	24℃
Figure 4a	Genotype (driver: Elav-GS)	Line	Temp
(G4C2)8 and (G4C2)49			
Control	*w^{1118}; UAS-DSRED/+; Elav-GS, UAS-(G4C2)n/+*	UAS-DSRED	24℃
dPaf1 RNAi	*w^{1118}; UAS-RNAi/+; Elav-GS, UAS-(G4C2)n/+*	v20876	24℃
dLeo1 RNAi	*w^{1118};; Elav-GS, UAS-(G4C2)n/UAS-RNAi*	v17490	24℃
dCDC73 RNAi	*w^{1118}/y^1v^1; UAS-RNAi/+; Elav-GS, UAS-(G4C2)n/+*	BL53278	24℃
UAS-TRiP (III)	*$w^{1118}/y^1sc^*v^1$;; Elav-GS, UAS-(G4C2)n/UAS-RNAi*	Ctr9 RNAi (BL33736), Rtf1 RNAi (BL34850)	24℃
(G4C2)29			
Control	*w^{1118}; UAS-DSRED/UAS-(G4C2)29; Elav-GS/+*	UAS-DSRED	24℃
dPaf1 RNAi	*w^{1118}; UAS-RNAi/UAS-(G4C2)29; Elav-GS/+*	v20876	24℃
dLeo1 RNAi	*w^{1118}; UAS-(G4C2)29/+; Elav-GS/UAS-RNAi*	v17490	24℃
dCDC73 RNAi	*w^{1118}/y^1v^1; UAS-RNAi/UAS-(G4C2)29; Elav-GS/+*	BL53278	24℃
UAS-TRiP (III)	*$w^{1118}/y^1sc^*v^1$; UAS-(G4C2)29/+; Elav-GS/UAS-RNAi*	Ctr9 RNAi (BL33736), Rtf1 RNAi (BL34850)	24℃
Figure 4b	Genotype (driver: Elav-GS)	Line	Temp
Control 1*	*w^{1118};; Elav-GS, UAS-$TDP43^{52S}$/+*	(n/a)	24℃

Control 2*	*w^{1118}; UAS-DSRED/+; Elav-GS, UAS-TDP43^{52S}/+*	UAS-DSRED	24°C
dPaf1 RNAi	*w^{1118}; UAS-RNAi/+; Elav-GS, UAS-TDP43^{52S}/+*	v20876	24°C
dCDC73 RNAi	*w^{1118}/$y^{1}v^{1}$; UAS-RNAi/+; Elav-GS, UAS-TDP43^{52S}/+*	BL53278	24°C
dLeo1 RNAi	*w^{1118};; Elav-GS, UAS-TDP43^{52S}/UAS-RNAi*	v17490	24°C
UAS-TRiP RNAi (III)	*w^{1118}/$y^{1}sc^{*}v^{1}$;; Elav-GS, UAS-TDP43^{52S}/UAS-RNAi*	Ctr9 RNAi (BL33736), Rtf1 RNAi (BL34850)	24°C
* all controls merged to compensate for technical variability; results further validated (Sup Fig 3c)			
Figure 4c	Genotype (driver: Gmr-GAL4^{YH3})	Line	Temp
Control	*$y^{1}sc^{*}v^{1}$/Y;; Gmr-GAL4, UAS-(G4C2)$_{4,42,44}^{GR-GFP}$/+*	(n/a)	26°C
UAS-RNAi (II)	*$y^{1}sc^{*}v^{1}$/Y; UAS-RNAi/+; Gmr-GAL4, UAS-(G4C2)$_{4,42,44}^{GR-GFP}$/+*	Paf1 RNAi (v20876), CDC73 RNAi (BL53278)	26°C
UAS-RNAi (III)	*$y^{1}sc^{*}v^{1}$/Y;; Gmr-GAL4, UAS-(G4C2)$_{4,42,44}^{GR-GFP}$/UAS-RNAi*	Leo1 RNAi (v17490), Ctr9 RNAi (BL33736), Rtf1 RNAi (BL34850)	26°C
Figure 4d	Genotype	Strain	
WT	*MATa his3Δ1 leu2Δ0 met15Δ0 ura3Δ0*	BY4741	
leo1Δ	*MATa his3Δ1 leu2Δ0 met15Δ0 ura3Δ0 leo1Δ::KanMX*	BY4741	
cdc73Δ	*MATa his3Δ1 leu2Δ0 met15Δ0 ura3Δ0 cdc73Δ::KanMX*	BY4741	
Figure 5a	Genotype (driver: Elav-GS)	Line	Temp
Control	*w^{1118};; Elav-GS/+*	(n/a)	24°C
(G4C2)8 and (G4C2)49	*w^{1118};; Elav-GS/UAS-(G4C2)n*	(n/a)	24°C
Figure 5b	Genotype (driver: Elav-GS)	Line	Temp
Control	*w^{1118};; Elav-GS/+*	(n/a)	24°C
TDP43	*w^{1118}; UAS-TDP43^{37m}/+; Elav-GS/+*	(n/a)	24°C
Supplemental	Genotype (driver: Gmr-GAL4^{YH3})	Shown RNAi lines	Temp

Figure 1a			
UAS-RNAi (II)	*w^{1118}/Y; UAS-RNAi/+; Gmr-GAL4, UAS-(G4C2)n/+*	Trs33 (BL51393), NXF1 (BL42013), His2Av (BL44056)	25°C
UAS-RNAi (III)	*w^{1118}/Y;; Gmr-GAL4, UAS-(G4C2)n/UAS-RNAi*	Med17 (BL34664), Med6 (BL33743), Hel25E (BL33666), SMC2 (BL32369), RagC-D (BL32342), CG3829 (BL55245), Cdk12 (BL34838), Brd8 (BL42658), Hrg (BL33378), Atg3 (BL34359), Dom (BL38385), Not3 (BL33002)	25°C
Supplemental Figure 1b	**Genotype (driver: Gmr-GAL4^{YH3})**	**Shown RNAi lines**	**Temp**
(G4C2)8 and (G4C2)49			
Control	*w^{1118}/Y;; Gmr-GAL4, UAS-(G4C2)n/UAS-RNAi*	Luc RNAi (BL31603)	25°C
UAS-RNAi (II)	*w^{1118}/Y; UAS-RNAi/+; Gmr-GAL4, UAS-(G4C2)n/+*	Fib (BL42553)	25°C
UAS-RNAi (III)	*w^{1118}/Y;; Gmr-GAL4, UAS-(G4C2)n/UAS-RNAi*	Ct (BL33967)	25°C
Control			
Control	*w^{1118}/Y;; Gmr-GAL4/UAS-RNAi*	Luc RNAi (BL31603)	25°C
UAS-RNAi (II)	*w^{1118}/Y; UAS-RNAi/+; Gmr-GAL4/+*	Fib (BL42553)	25°C
UAS-RNAi (III)	*w^{1118}/Y;; Gmr-GAL4/UAS-RNAi*	Ct (BL33967)	25°C
Supplemental Figure 1c	**Genotype (driver: Gmr-GAL4, BL1104)**	**Shown RNAi lines**	**Temp**
Control	*w^{1118}/Y; Gmr-GAL4, UAS-LacZ/+; UAS-RNAi/+*	Luc RNAi (BL31603)	25°C
UAS-RNAi (II)	*w^{1118}/Y; UAS-RNAi/Gmr-GAL4, UAS-LacZ;*	(n/a)	25°C
UAS-RNAi (III)	*w^{1118}/Y; Gmr-GAL4, UAS-LacZ/+; UAS-RNAi/+*	AFF1-4 (BL34592), MRTO4 (BL33730)	25°C
Supplemental Figure 2a-b	**Genotype (driver: Gmr-GAL4^{YH3})**	**Line**	**Temp**
w^{-} control	*w^{1118}; UAS-DSRED/UAS-*	UAS-DSRED	24°C

	(GR)36; Gmr-GAL4/+		
w^+ control	*w^{1118}/y^1v^1;UAS-(GR)36/+; Gmr-GAL4/UAS-RNAi*	Luc RNAi (BL31603)	24℃
UAS-GD/KK RNAi (II)	*w^{1118}; UAS-RNAi/UAS-(GR)36; Gmr-GAL4/+*	Paf1 RNAi (v20876), Paf1 RNAi-2 (v108826), Leo1 RNAi-2 (v106074), Ctr9 RNAi-2 (v108874), Rtf1 RNAi-2 (v110932)	24℃
UAS-RNAi (III)	*w^{1118}; UAS-(GR)36/+; Gmr-GAL4/UAS-RNAi*	Leo1 RNAi (v17490), Cdc73 RNAi-2 (v28318)	24℃
UAS-TRiP RNAi (II)	*w^{1118}/y^1v^1; UAS-RNAi/UAS-(GR)36; Gmr-GAL4/+*	Cdc73 RNAi (BL53278)	24℃
UAS-TRiP RNAi (III)	*$w^{1118}/y^1sc^*v^1$;UAS-(GR)36/+; Gmr-GAL4/UAS-RNAi*	Ctr9 RNAi (BL33736), Rtf1 RNAi (BL34850), Spt4 RNAi (BL32896)	24℃
Supplemental Figure 3	Genotype (driver: Gmr-GAL4^{YH3})	Line	Temp
w^- control	*w^{1118}; UAS-$TDP43^{37M}$/+; Gmr-GAL4/+*	(n/a)	26℃
w^+ control	*w^{1118}/y^1v^1;UAS-$TDP43^{37M}$/+; Gmr-GAL4/UAS-RNAi*	Luc RNAi (BL31603)	26℃
UAS-GD/KK RNAi (II)	*w^{1118}; UAS-RNAi/UAS-$TDP43^{37M}$; Gmr-GAL4/+*	Paf1 RNAi (v20876), Paf1 RNAi-2 (v108826), Leo1 RNAi-2 (v106074), Ctr9 RNAi-2 (v108874), Rtf1 RNAi-2 (v110932)	26℃
UAS-GD RNAi (III)	*w^{1118}; UAS-$TDP43^{37M}$/+; Gmr-GAL4/UAS-RNAi*	Leo1 RNAi (v17490), Cdc73 RNAi-2 (v28318)	26℃
UAS-TRiP RNAi (II)	*w^{1118}/y^1v^1; UAS-RNAi/UAS-$TDP43^{37M}$; Gmr-GAL4/+*	Cdc73 RNAi (BL53278)	26℃
UAS-TRiP RNAi (III)	*$w^{1118}/y^1sc^*v^1$;UAS-$TDP43^{37M}$/+; Gmr-GAL4/UAS-RNAi*	Ctr9 RNAi (BL33736), Rtf1 RNAi (BL34850), Spt4 RNAi (BL32896)	26℃
Supplemental Figure 4a	Genotype	Line	Temp
Da-GAL4			
w- control	*w^{1118};; Da-GAL4/+*	(n/a)	26℃
w- RNAi (II)	*w^{1118}; UAS-RNAi/+; Da-GAL4/+*	Paf1 RNAi (v20876), Paf1 RNAi-2 (v108826), Ctr9 RNAi-2 (v108874), Leo1 RNAi-2 (v106074)	26℃
w- RNAi (III)	*w^{1118};; Da-GAL4/UAS-RNAi*	Leo1 RNAi (v17490)	26℃

Da-GS			
w- control	*w^{1118}; Da-GS/+;*	(n/a)	26°C
w- RNAi (II)	*w^{1118}; UAS-RNAi/Da-GS;*	Rtf1 RNAi-2 (v110932)	26°C
w- RNAi (III)	*w^{1118}; Da-GS/+; UAS-RNAi/+*	Cdc73 RNAi-2 (v28318)	26°C
w^{+} control	*w^{1118}/y^{1}v^{1}; Da-GS/+; UAS-RNAi/+*	Luc RNAi (BL31603)	26°C
w+ RNAi (II)	*w^{1118}/y^{1}v^{1}; UAS-RNAi/Da-GS;*	Cdc73 RNAi (BL53278)	26°C
w+ RNAi (III)	*w^{1118}/y^{1}sc*v^{1}; Da-GS/+; UAS-RNAi/+*	Ctr9 RNAi (BL33736), Rtf1 RNAi (BL34850), Spt4 RNAi (BL32896)	26°C
Supplemental Figure 4b	Genotype (driver: Da-GS)	Line	Temp
w- control	*w^{1118}/Y; Da-GS/+;*	(n/a)	26°C
w^{+} control	*w^{1118}/Y; Da-GS/+; UAS-RNAi/+*	Luc RNAi (BL31603)	26°C
w- RNAi	*w^{1118}/Y; Da-GS/+; UAS-RNAi/+*	v28318	26°C
w+ RNAi	*w^{1118}/Y; UAS-RNAi/Da-GS;*	BL53278	26°C
Supplemental Figure 4c	Genotype (driver: Da-GS)	Line	Temp
w- control	*w^{1118}/Y; Da-GS/+;*	(n/a)	26°C
w^{+} control	*w^{1118}/Y; Da-GS/+; UAS-RNAi/+*	Luc RNAi (BL31603)	26°C
w- RNAi	*w^{1118}/Y; UAS-RNAi/Da-GS;*	v110392	26°C
w+ RNAi	*w^{1118}/Y; Da-GS/+; UAS-RNAi/+*	BL34850	26°C
Supplemental Figure 5a	Genotype (driver: Gmr-GAL4^{YH3})	Line	Temp
w- control	*w^{1118}/Y;; Gmr-GAL4, UAS-(G4C2)49/+*	(n/a)	25°C
UAS-GD/KK RNAi (II)	*w^{1118}/Y; UAS-RNAi/+; Gmr-GAL4, UAS-(G4C2)49/+*	Paf1 RNAi-2 (v108826), Leo1 RNAi-2 (v106074), Ctr9 RNAi-2 (v108874), Rtf1 RNAi-2 (v110932)	25°C
UAS-GD RNAi (III)	*w^{1118}/Y;; Gmr-GAL4, UAS-(G4C2)49/UAS-RNAi*	Cdc73 RNAi-2 (v28318)	25°C
Supplemental Figure 5b	Genotype (driver: Gmr-GAL4^{YH3})	Line	Temp

w- control	*w^{1118}/Y;; Gmr-GAL4/+*	(n/a)	25°C
UAS-GD/KK RNAi (II)	*w^{1118}/Y; UAS-RNAi/+; Gmr-GAL4/+*	Paf1 RNAi-2 (v108826), Leo1 RNAi-2 (v106074), Ctr9 RNAi-2 (v108874), Rtf1 RNAi-2 (v110932)	25°C
UAS-GD RNAi (III)	*w^{1118}/Y;; Gmr-GAL4/UAS-RNAi*	Cdc73 RNAi-2 (v28318)	25°C
Supplemental Figure 5c	Genotype (driver: Gmr-GAL4^{YH3})	Line	Temp
Control	*w^{1118}/Y;; Gmr-GAL4, UAS-(G4C2)$_{4,42,44}^{GR-GFP}$/UAS-RNAi*	Luc RNAi (BL31603)	26°C
UAS-RNAi (II)	*w^{1118}/Y; UAS-RNAi/+; Gmr-GAL4, UAS-(G4C2)$_{4,42,44}^{GR-GFP}$/+*	Paf1 RNAi (v20876), CDC73 RNAi (BL53278)	26°C
UAS-RNAi (III)	*w^{1118}/Y;; Gmr-GAL4, UAS-(G4C2)$_{4,42,44}^{GR-GFP}$/UAS-RNAi*	Leo1 RNAi (v17490), Ctr9 RNAi (BL33736), Rtf1 RNAi (BL34850)	26°C
Supplemental Figure 5d	Genotype (driver: Elav-GS)	Line	Temp
Control	*w^{1118}/Y; UAS-DSRED/+; Elav-GS, UAS-(G4C2)49/+*	UAS-DSRED	24°C
RNAi (II)	*w^{1118}/Y; UAS-RNAi/+; Elav-GS, UAS-(G4C2)49/+*	Paf1 RNAi-2 (v108826), Leo1 RNAi-2 (v106074), Ctr9 RNAi-2 (v108874), Rtf1 RNAi-2 (v110932)	24°C
RNAi (III)	*w^{1118}/Y;; Elav-GS, UAS-(G4C2)49/UAS-RNAi*	Cdc73 RNAi-2 (v28318)	24°C
Supplemental Figure 7a	Genotype (driver: Da-GS)	Line	Temp
Control	*w^{1118}; UAS-DSRED/Da-GS;*	UAS-DSRED	25°C
dPaf1 RNAi	*w^{1118}; UAS-RNAi/Da-GS;*	v20876	25°C
dCDC73 RNAi	*w^{1118}/y^{1}v^{1}; UAS-RNAi/Da-GS;*	BL53278	25°C
dLeo1 RNAi	*w^{1118}; Da-GS/+; UAS-RNAi/+*	v17490	25°C
Supplemental Figure 7b	Genotype (driver: Elav-GS)	Line	Temp
Control	*w^{1118}/Y;; Elav-GS/+*	(n/a)	24°C
UAS-RNAi (II)	*w^{1118}/Y; UAS-RNAi/+; Elav-GS/+*	Paf1 RNAi (v20876), CDC73 RNAi (BL53278)	24°C
UAS-RNAi	*w^{1118}/Y;; Elav-GS/UAS-RNAi*	Leo1 RNAi (v17490), Ctr9 RNAi	24°C

(III)		(BL33736), Rtf1 RNAi (BL34850)	
Supplemental Figure 8a	Genotype (driver: Gmr-GAL4^{YH3})	Line	Temp
w- control	*w^{1118}/Y;; Gmr-GAL4, UAS-(G4C2)49/+*	(n/a)	25°C
w^{+} control	*w^{1118}/Y;; Gmr-GAL4, UAS-(G4C2)49/UAS-RNAi*	Luc RNAi (BL31603)	25°C
Supplemental Figure 8b	Genotype (driver: Da-GS)	Line	Temp
w- control	*w^{1118}/Y; Da-GS, UAS-(G4C2)49/UAS-DSRED;*	UAS-DSRED	24°C
w^{+} control	*w^{1118}/Y; Da-GS, UAS-(G4C2)49/+; UAS-RNAi/+*	Luc RNAi (BL31603)	24°C
Supplemental Figure 8c	Genotype (driver: Elav-GS)	Line	Temp
w- control	*w^{1118}/Y; UAS-DSRED/+; Elav-GS, UAS-(G4C2)49/+*	UAS-DSRED	24°C
w^{+} control	*w^{1118}/Y;; Elav-GS, UAS-(G4C2)49/UAS-Luc*	Luc (BL35788)	24°C
Supplemental Figure 8d	Genotype (driver: Elav-GS)	Line	Temp
w- control 1	*w^{1118};; Elav-GS, UAS-(G4C2)49/+*	(n/a)	24°C
w- control 2	*w^{1118}; UAS-DSRED/+; Elav-GS, UAS-(G4C2)49/+*	UAS-DSRED	24°C
w^{+} control 1	*w^{1118}/$y^{1}v^{1}$;; Elav-GS, UAS-(G4C2)49/UAS-RNAi*	Luc RNAi (BL31603)	24°C
w^{+} control 2	*w^{1118}/$y^{1}v^{1}$;; Elav-GS, UAS-(G4C2)49/UAS-Luc*	Luc (BL35788)	24°C
Supplemental Figure 8e	Genotype (driver: Gmr-GAL4^{YH3})	Line	Temp
w- control	*$y^{1}sc^{*}v^{1}$/Y;; Gmr-GAL4, UAS-$(G4C2)_{4,42,44}^{GR\text{-}GFP}$/+*	(n/a)	26°C
w^{+} control	*$y^{1}sc^{*}v^{1}$/Y;; Gmr-GAL4, UAS-$(G4C2)_{4,42,44}^{GR\text{-}GFP}$/UAS-RNAi*	Luc RNAi (BL31603)	26°C
Supplemental	Genotype (driver: ElavGS)	Line	Temp

Figure 9a			
Control	*w^{1118}; UAS-DSRED/UAS-(G4C2)49; Elav-GS/+*	UAS-DSRED	24℃
dPaf1 RNAi	*w^{1118}; UAS-RNAi/UAS-(G4C2)49; Elav-GS/+*	v20876	24℃
dCDC73 RNAi	*w^{1118}/y^1v^1; UAS-RNAi/UAS-(G4C2)49; Elav-GS/+*	BL53278	24℃
dLeo1 RNAi	*w^{1118}; UAS-(G4C2)49/+; Elav-GS/UAS-RNAi*	v17490	24℃
UAS-TRiP RNAi (III)	*$w^{1118}/y^1sc^*v^1$; UAS-(G4C2)49/+; Elav-GS/UAS-RNAi*	Ctr9 RNAi (BL33736), Rtf1 RNAi (BL34850)	24℃
Supplemental Figure 9b	Genotype (driver: Da-GS)	Line	Temp
Control	*w^{1118}; UAS-DSRED/Da-GS;*	UAS-DSRED	25℃
dPaf1 RNAi	*w^{1118}; UAS-RNAi/Da-GS;*	v20876	25℃
dCDC73 RNAi	*w^{1118}/y^1v^1; UAS-RNAi/Da-GS;*	BL53278	25℃
dLeo1 RNAi	*w^{1118}; Da-GS/+; UAS-RNAi/+*	v17490	25℃
UAS-TRiP RNAi (III)	*$w^{1118}/y^1sc^*v^1$; Da-GS/+; UAS-RNAi/+*	Ctr9 RNAi (BL33736), Rtf1 RNAi (BL34850)	25℃

Table S2-4: Primers

Target	Species	Assay	Forward Primer (5' to 3')	Reverse Primer (5' to 3')
UAS-G4C2	n/a	PCR	GAATTCGAGCTCAGATCTCCCG	TCTAGAGGATCCGGTACCGAGTCTCGAG
UAS-LDS-	n/a	PCR	CTCGCTGAGGGTGAACAAGA	ACTTGTGGCCGTTTACGTCG
Actin5C	Dmel.	qPCR	CGAAGAAGTTGCTGCTCTGGTTGT	GGACGTCCCACAATCGATGGGAAG
dCDC73	Dmel.	qPCR	AGCGTGAAGACCAACTATCTCA	CGCACGTAGACCGAGTGTT
dCtr9	Dmel.	qPCR	ATTGCGCACGTTTATGTCGA	GACGGGCCTTAAGTAGCACT
dLeo1	Dmel.	qPCR	ACGGCTGATCGACACTGATA	TGGCTCTCGACTTTATCCCG
dPaf1	Dmel.	qPCR	CCAAAGCTTCCAAGGGCTAC	CGATAGCGCTGCATACGATG
dRP49	Dmel.	qPCR	TGTCCTTCCAGCTTCAAGATGACCATC	CTTGGGCTTGCGCCATTTGTG
dRtf1	Dmel.	qPCR	CGGACGCAATCCCTGATCG	CCGTTTGGGGCTTCTTTCG
βTub56D	Dmel.	qPCR	CATCCAAGCTGGTCAGTG	GCCATGCTCATCGGAGAT
UAS-G4C2	n/a	qPCR	AGACTCGGTACCGGATCCTC	GCTCCCATTCATCAGTTCCA
UAS-TDP43	n/a	qPCR	TGTCTTCATCCCCAAGCCAT	TGTGCTTAGGTTCGGCATTG
hRPLP0	Hsap	qPCR	TCTACAACCCTGAAGTGCTTGAT	CAATCTGCAGACAGACACTGG
hGAPDH	Hsap	qPCR	GTTCGACAGTCAGCCGCATC	GGAATTTGCCATGGGTGGA
C9orf72 3'-repeat	Hsap.	qPCR & ChIP	CCTGATAGGAGATAACAGGATTCCAC	CGACATCACTGCATTCCAACTGTC
hPAF1	Hsap.	qPCR	CCACTGAGTTCAACCGTTATGG	TCCTCGGTAAACTGCTGCTTC
hLEO1	Hsap	qPCR	CAAGTGGTCAGATGGAAGCA	TGGGGCTTTGTACACATCAA
hCDC73	Hsap.	qPCR	GGGGCACTGCAATTAGTGTT	CTGCACAAAAACGGCTACAA
Intergenic	Hsap.	ChIP	CCAACTGGGTGCTGCCTAGA	AGGGTGCCCATCACAGATGG
scACT1	Sce.	qPCR	ATTCTGAGGTTGCTGCTTTGG	TGTCTTGGTCTACCGACGATAG
scTDH3	Sce.	qPCR	TTGCCATGGGGTTCTTCCAA	CACCAGCGTCAATGTGCTTT
scFBA1	Sce.	qPCR	AACCTCTAACGGTGGTGCTG	ATCTGATGTAGTGGGCAGCG
eYFP	Sce.	qPCR	GAGCTGAAGGGCATCGACTT	TTCTTCTGCTTGTCGGCCAT
C9 repeat	Sce.	qPCR	AGCTTAGTACTCGCTGAGGGTG	GACTCCTGAGTTCCAGAGCTTG
scLEO1	Sce.	qPCR	AGGGAGGATCAACTGGACGA	ATGTACCGTCTGACCACTGC
scCDC73	Sce.	qPCR	ATCTGAAAGCACCCGGTCAG	CCACCACAACTGGATCGGAA

Chapter 2: Supplementary figures and legends

Figure S2-1

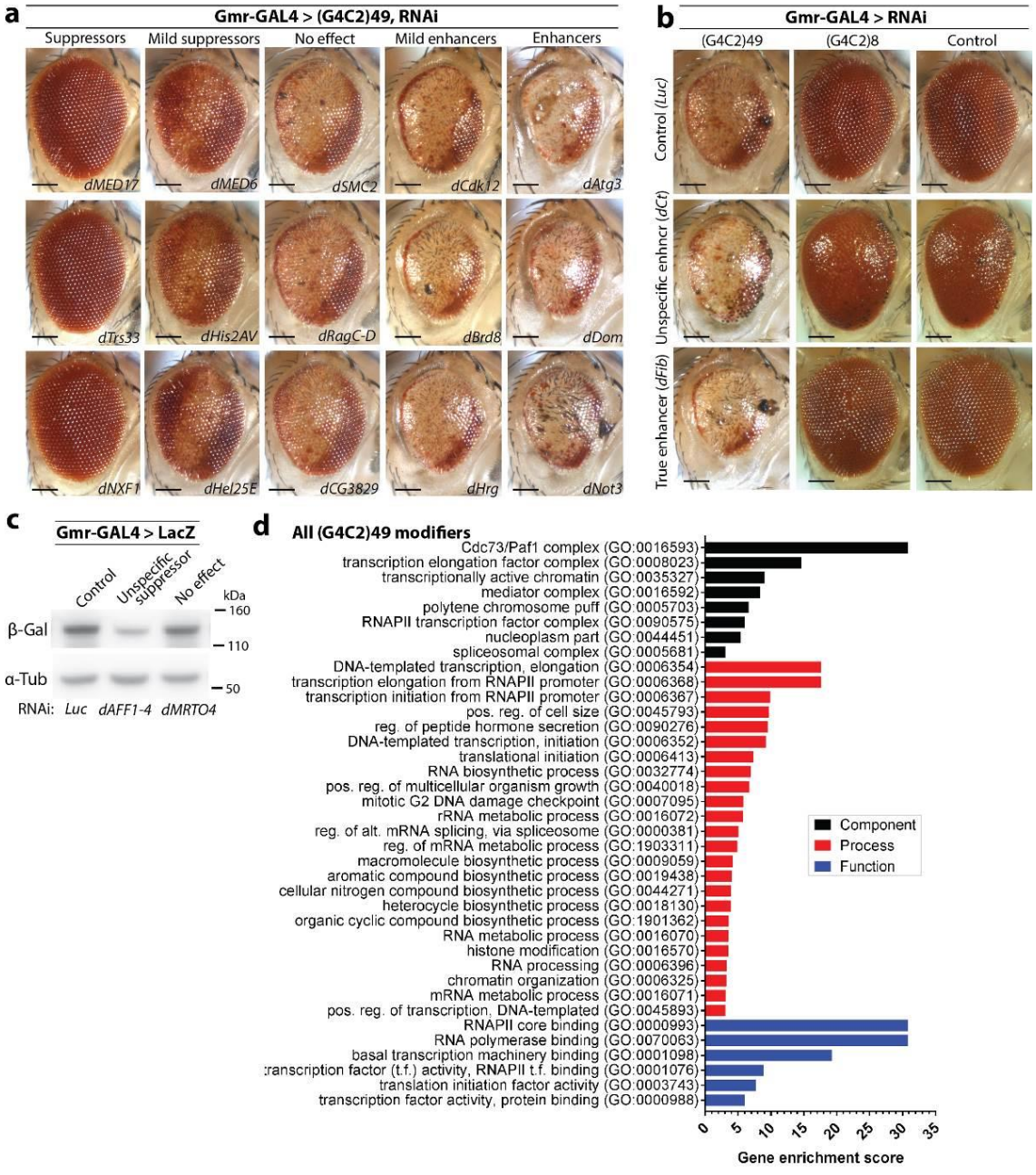

Supplementary Figure S2-1: Screen extended data.

(a) Representative images for the categories identified during the RNAi-based screen in Gmr-GAL4 > (G4C2)49 expressing animals: “suppressors” (strong recovery of ommatidial organization, eye color, and eye size), “mild suppressors” (recovery of ommatidial organization, eye color, and eye size while degenerative effects were still present), “no effect” (indistinguishable from controls), “mild enhancers” (increased disruptions in ommatidial organization and pigment loss), “enhancers” (strongly increased disruptions in ommatidial organization, pigment loss, and eye size), and “lethal enhancers” (lethality in the late pupal stage ; rare (n<2) escapers’ eyes looked like “enhancers”). All hits were independently tested 2+ times to confirm reproducibility (n>5 flies/cross). **(b)** Mild enhancers, enhancers, and lethal enhancers were expressed alone or in control (G4C2)8 expressing animals to define those that were toxic in control scenarios. Shown are representative images for an “unspecific enhancer” (RNAi line that caused toxicity in controls) and a “true enhancer” (RNAi line that had no effect in controls while enhancing (G4C2)49-toxicity). Unspecific enhancers were excluded. **(a-b)** Scale bars: 100μm **(c)** To identify RNAi lines that altered (G4C2)49-toxicity indirectly by effecting the GAL4/UAS expression system, RNAi lines were co-expressed with a control LacZ transgene. β-Galactosidase protein levels were quantified by western immunoblot. RNAi lines that significantly increased or decreased LacZ expression in a manner consistent with its effect on (G4C2)49-toxicity were reclassified as either “LacZ-suppressors” or “LacZ-enhancers” and excluded. Shown is a representative western immunoblot. All lines with potential effects were independently tested twice with biological duplicates to confirm reproducibility. **(d)** Gene ontology analyses revealed GO terms enriched in the panel of modifiers identified in the screen that alter (G4C2)49-toxicity (119/3582 genes). To compensate for any biases introduced in the RNAi library,

the genes screened were used as the background. RNAi lines that failed control scenarios (b-c) were excluded. Plotted: significant (p-value ≤ 10^-3) enrichment scores of >3.00. Additional details for this and subsequent figures: Supplemental Data (all screen data and significant GO-terms), Supplemental Table S2-1 (detailed sampling, reproducibility and statistics), methods (sampling methods).

Figure S2-2

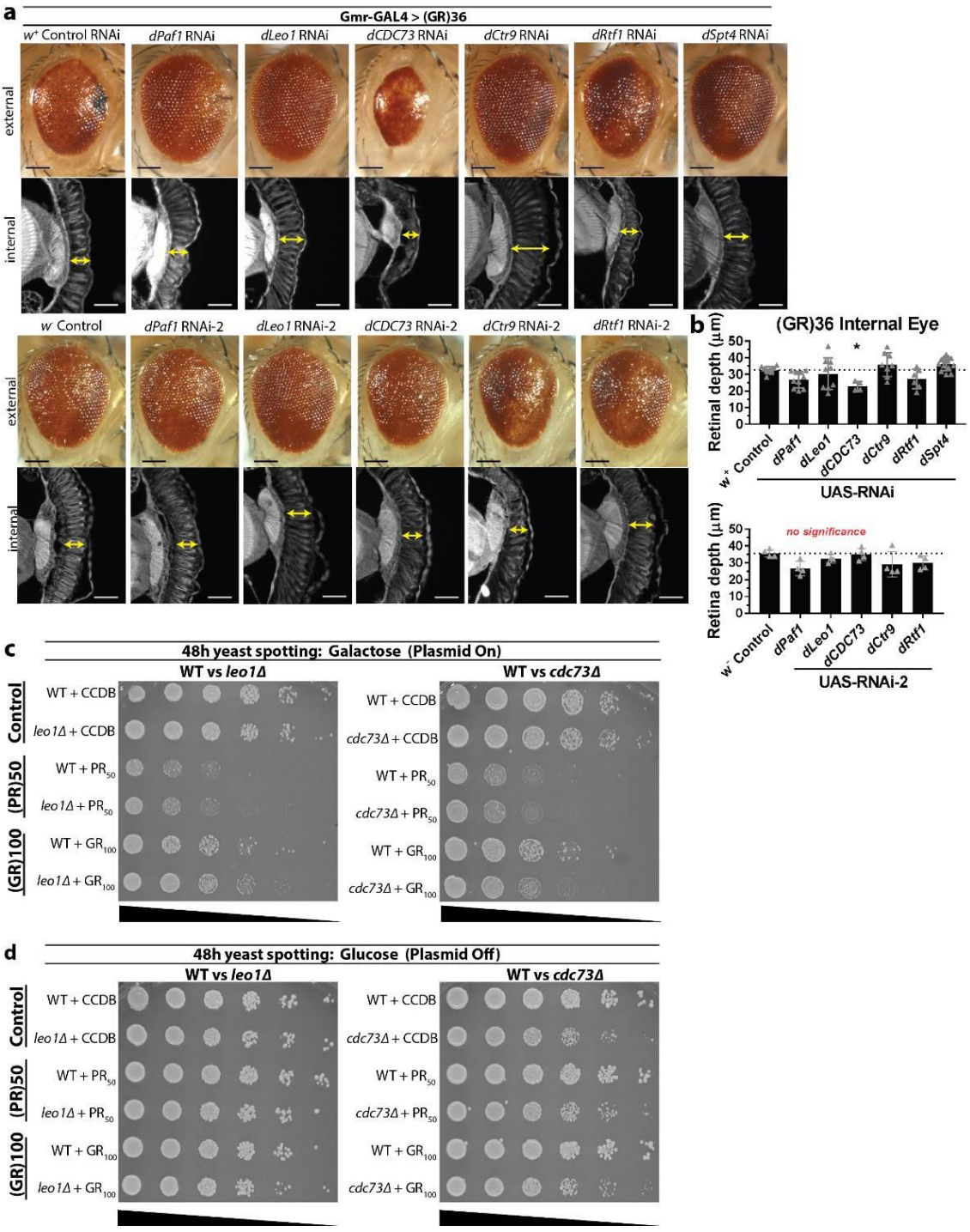
a
Gmr-GAL4 > (GR)36
w+ Control RNAi
dPaf1 RNAi
dLeo1 RNAi
dCDC73 RNAi
dCtr9 RNAi
dRtf1 RNAi
dSpt4 RNAi
external
internal
w- Control
dPaf1 RNAi-2
dLeo1 RNAi-2
dCDC73 RNAi-2
dCtr9 RNAi-2
dRtf1 RNAi-2
b
(GR)36 Internal Eye
Retinal depth (µm)
UAS-RNAi
no significance
Retina depth (µm)
UAS-RNAi-2
c
48h yeast spotting: Galactose (Plasmid On)
WT vs leo1Δ
WT vs cdc73Δ
Control
(PR)50
(GR)100
WT + CCDB
leo1Δ + CCDB
cdc73Δ + CCDB
WT + PR50
leo1Δ + PR50
cdc73Δ + PR50
WT + GR100
leo1Δ + GR100
cdc73Δ + GR100
d
48h yeast spotting: Glucose (Plasmid Off)

Supplementary Figure S2-2: Downregulation of PAF1C and dSpt4 does not suppress toxicity caused by expression of (GR)30+ or (PR)50.

(a-b) dPAF1C components and *dSpt4* were examined for modification of (GR)36-toxicity in the fly optic system (Gmr-GAL4). Internally, there was no significant recovery in retinal tissue loss with multiple RNAi lines targeting *dPaf1*, *dLeo1*, *dCtr9*, and *dRtf1*. *dCDC73* RNAi enhanced toxicity both externally and internally while this effect was not reproducible with *dCDC73* RNAi-2. Internal retina depth (arrows) was quantified for individual animals. N flies for RNAi: control=9, *dPaf1*=10, *dLeo1*=9, *dCDC73*=4, *dCtr9*=8, *dRtf1*=6, *dSpt4*=14. N flies for RNAi-2 = 4 for all genotypes. Shown: individual data points (each representing 1 animal) with mean±SD. Statistics: ANOVAs with Dunnett's correction (RNAi), ANOVA with Tukey's correction (RNAi-2), p-values: *=0.03, no significance (n.s.) >0.05. Scale bars: external eye = 100μm, internal eye = 35μm. **(c-d)** To further assess the specificity of PAF1C to (G4C2)30+ RNA models, yeast spotting assays were used. Control (CCDB), (PR)50 or (GR)100 were expressed in yeast using galactose-inducible transgenes (see methods). Expression of (PR)50 and (GR)100 reduced colony formation in WT cells. This effect was unaltered in *leo1Δ* yeast. Interestingly, *cdc73Δ* caused further reduced growth in (GR)100 expressing yeast but had no effect on yeast expressing (PR)50. This is consistent with *dCDC73* RNAi data in (GR)36-expressing flies where loss of this component, in one RNAi line, increased GR-associated toxicity. Note that any mild effects observed with individual PAF1C components and *dSpt4* can be explained by the fact that a GR-producing mRNA transcript, despite being G4C2-independent, will still be GC-rich based on the standard codon table. PAF1C and *Spt4* are important for transcription of GC-rich DNA (Rondón, A. G. et al, 2004; Rondón, A. G. et al, 2003). Shown: data from one experiment; all experiments were independently repeated with similar results.

Figure S2-3

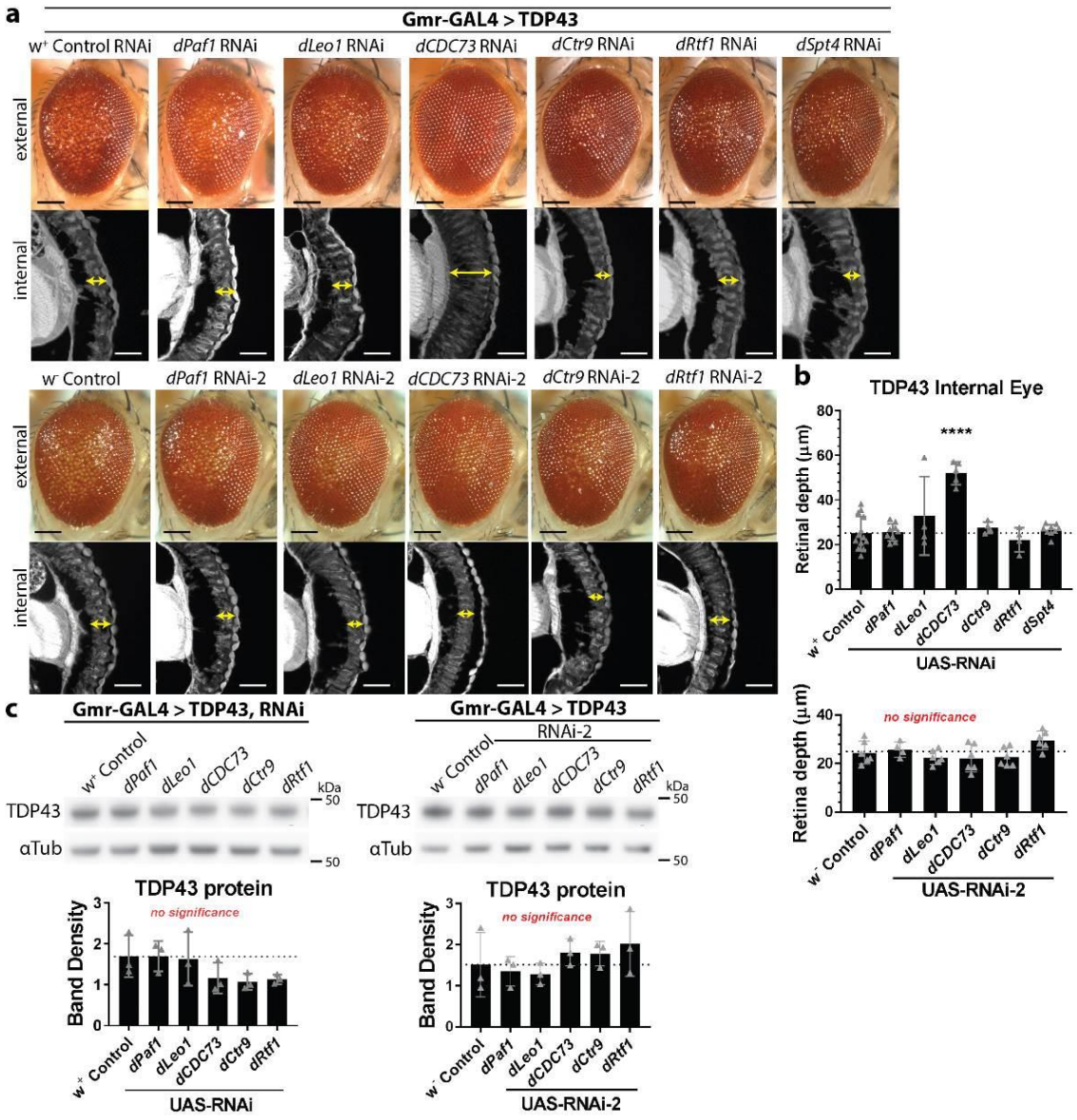
a
Gmr-GAL4 > TDP43
w+ Control RNAi
dPaf1 RNAi
dLeo1 RNAi
dCDC73 RNAi
dCtr9 RNAi
dRtf1 RNAi
dSpt4 RNAi
external
internal
w- Control
dPaf1 RNAi-2
dLeo1 RNAi-2
dCDC73 RNAi-2
dCtr9 RNAi-2
dRtf1 RNAi-2
b
TDP43 Internal Eye
Retinal depth (µm)
****
w+ Control
dPaf1
dLeo1
dCDC73
dCtr9
dRtf1
dSpt4
UAS-RNAi
no significance
w- Control
UAS-RNAi-2
c
Gmr-GAL4 > TDP43, RNAi
Gmr-GAL4 > TDP43
RNAi-2
TDP43
αTub
kDa
50
TDP43 protein
Band Density
no significance
UAS-RNAi
UAS-RNAi-2

Supplementary Figure S2-3: Downregulation of dPAF1C and dSpt4 does not suppress toxicity caused by expression of TDP43 in the fly eye.

(a-b) dPAF1C and *Spt4* RNAi were tested as modifiers of TDP43-toxicity in the fly optic system (Gmr-GAL4). Only *dCDC73* RNAi caused significant suppression of the external and internal eye in these animals. This effect was not reproduced with a second, independent RNAi lines targeting *dCDC73*. Internal retina depth (arrows) was quantified for individual animals. N flies for RNAi: control=13, *dPaf1*=9, *dLeo1*=4, *dCDC73*=5, *dCtr9*=4, *dRtf1*=4, *dSpt4*=9. N flies for RNAi-2: control=6, *dPaf1*=4, *dLeo1*=6, *dCDC73*=6, *dCtr9*=6, *dRtf1*=6. Shown: individual data points (each representing 1 animal) with mean±SD. Scale bars: external eye = 100µm, internal eye = 35µm. **(c)** Expression from the TDP43 transgene was analyzed by western immunoblot when dPAF1C was downregulated revealing no change in TDP43 protein levels. Shown: individual data points with mean±SD; mean value of biological triplicates (n=10 flies/replicate). Statistics: ANOVAs with Tukey's correction, p-values: ****< 0.0001, no significance (n.s.) >0.05. Shown: data from one experiment while all experiments were independently repeated with similar results. See Supplemental Figure S2-11 for uncropped western images for this and subsequent figures.

Figure S2-4

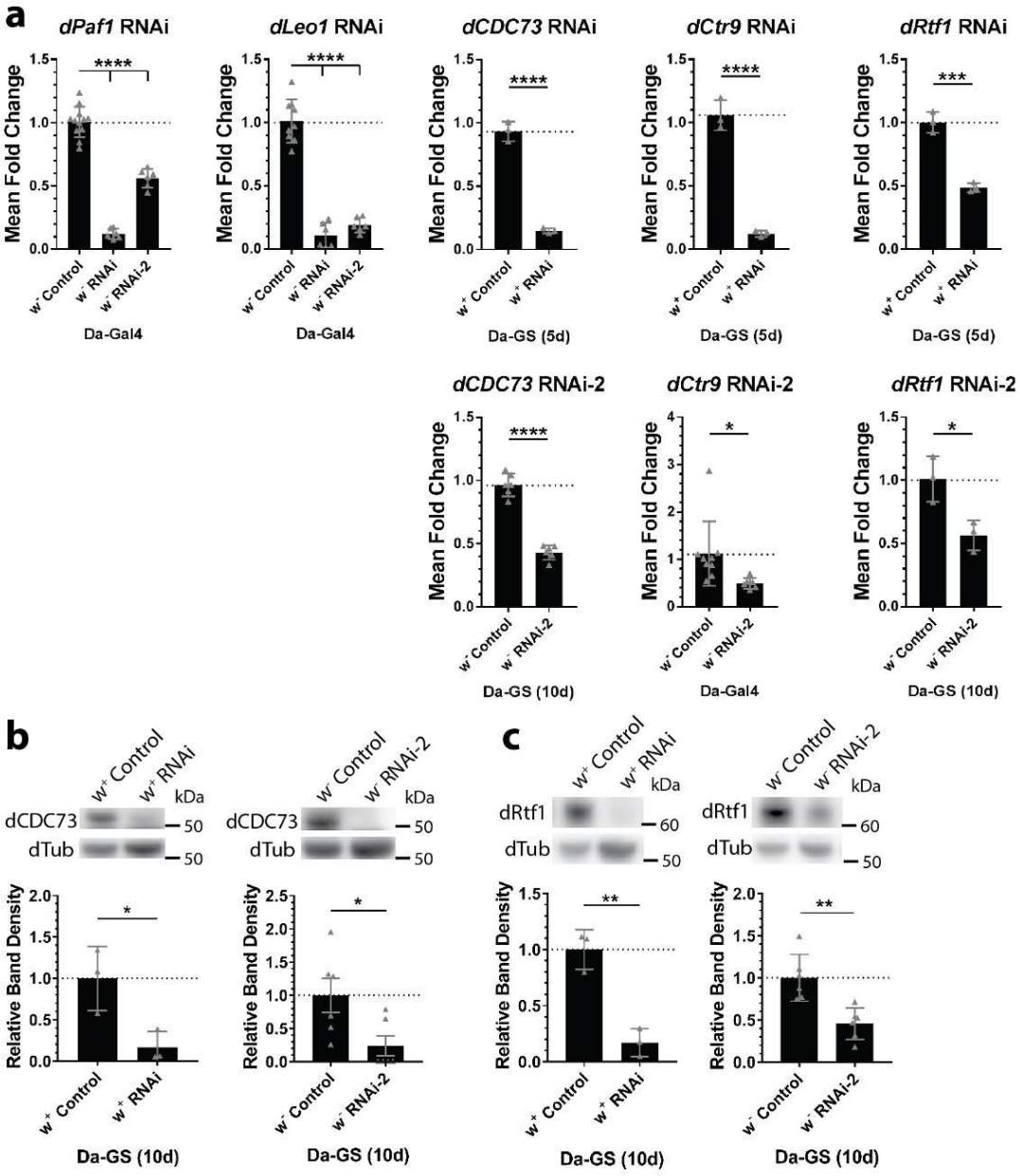
a
dPaf1 RNAi
dLeo1 RNAi
dCDC73 RNAi
dCtr9 RNAi
dRtf1 RNAi
dCDC73 RNAi-2
dCtr9 RNAi-2
dRtf1 RNAi-2
Mean Fold Change
w+ Control
w+ RNAi
w- RNAi-2
Da-Gal4
Da-GS (5d)
Da-GS (10d)
b
c
dCDC73
dTub
dRtf1
kDa
Relative Band Density

Supplementary Figure S2-4: Characterization of dPAF1C RNAi fly lines.

(a) RNA levels of dPAF1C components were assessed by qPCR to define RNAi efficacy in flies. UAS-RNAi fly lines were ubiquitously expressed and compared to background-matched controls. For samples analyzed with Da-GAL4, expression was measured in larvae. For samples analyzed with Da-GS, expression was measured in adult animals (n=10) after 5d or 10d of drug-induced expression. Shown: individual data points with mean±SD; mean value of 3-6 biological replicates. **(b-c)** RNAi lines targeting *dCDC73* or *dRtf1* were analyzed for level of protein knockdown by western immunoblot. Shown: individual data points with mean±SD; mean value of 3 biological replicates (n=10 flies/replicate). Statistics: ANOVAs with Tukey's correction (*dPaf1* and *dLeo1* RNAi only), unpaired 2-tailed student t-test; p-values: ****<0.0001, ***<0.001, **<0.01, *<0.05. Shown: data from one experiment while all experiments were independently repeated with similar results.

Figure S2-5

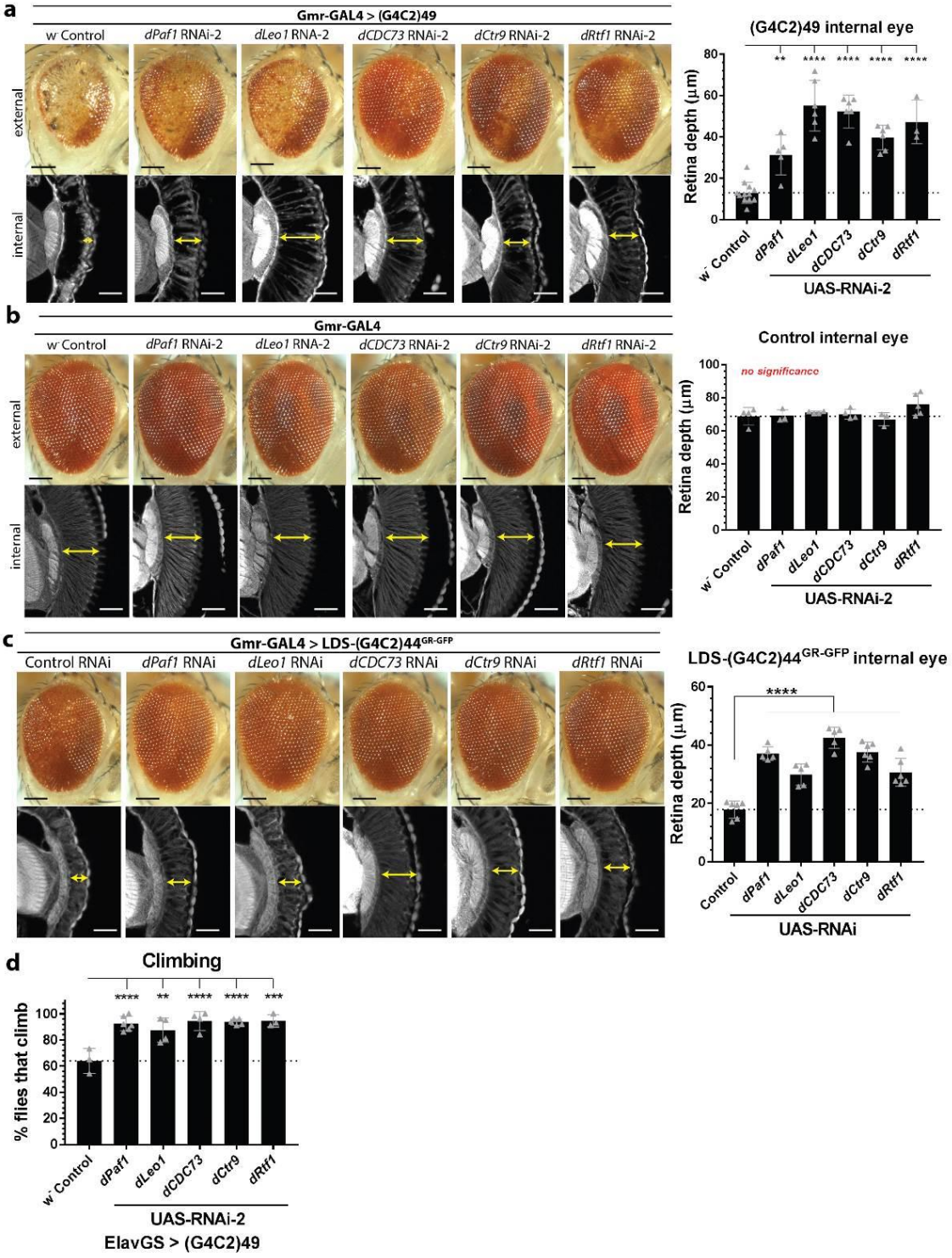
a
Gmr-GAL4 > (G4C2)49
w- Control
dPaf1 RNAi-2
dLeo1 RNA-2
dCDC73 RNAi-2
dCtr9 RNAi-2
dRtf1 RNAi-2
external
internal
(G4C2)49 internal eye
Retina depth (µm)
w- Control
dPaf1
dLeo1
dCDC73
dCtr9
dRtf1
UAS-RNAi-2
b
Gmr-GAL4
Control internal eye
no significance
c
Gmr-GAL4 > LDS-(G4C2)44GR-GFP
Control RNAi
LDS-(G4C2)44GR-GFP internal eye
Control
UAS-RNAi
d
Climbing
% flies that climb
ElavGS > (G4C2)49

Supplementary Figure S2-5: Extended data showing dPAF1C RNAi lines suppress (G4C2)30+ toxicity in the fly.

(a) Downregulation of each of the components of dPAF1C with a second set of RNAi lines mitigates toxicity associated with (G4C2)49 expression in the fly eye, seen externally by reduced pigment loss and reduced disruption in ommatidial organization and internally by increased integrity of the retinal tissue. All RNAi-2 lines are in a *w*- genetic background. Internal retina depth (arrows) was quantified for individual animals. N flies: control=12, *dPaf1*=5, *dLeo1*=6, *dCDC73*=6, *dCtr9*=6, *dRtf1*=3. **(b)** Downregulation of components of dPAF1C with a second set of RNAi lines has no effect on control fly eyes. Internal retina depth (arrows) was quantified for individual animals. N flies: control=4, *dPaf1*=3, *dLeo1*=4, *dCDC73*=4, *dCtr9*=3, *dRtf1*=5. **(c)** dPAF1C RNAi were tested in a second, independent fly model expressing expanded (G4C2)30+ in the fly eye. This model contains a sequence 5' of the repeat (leader sequence, LDS; 114bp of intronic sequence found upstream of the repeat in *C9orf72*) and a 3' GFP tag in the GR reading frame. Toxicity in this model is also suppressed by dPAF1C RNAi co-expression, seen externally by reduced pigment loss and reduced disruption in ommatidial organization and internally by increased integrity of the retinal tissue. Internal retina depth (arrows) was quantified for individual animals. N flies: control=6, *dPaf1*=5, *dLeo1*=5, *dCDC73*=5, *dCtr9*=6, *dRtf1*=6. (a-c) each data point represents one animal. Scale bars: external eye = 100μm, internal eye = 35μm. **(d)** At 20d, climbing deficits caused by (G4C2)49 expression in the adult male nervous system are rescued when dPAF1C RNAi-2 lines are co-expressed. N flies: control=51, dPaf1=85, dLeo1=73, dCDC73=67, dCtr9=87, dRtf1=31. Individual data points are the mean % of animals that could climb per tube. Average of 16±3.6 animals per tube. Statistics: ANOVAs with Tukey's correction, p-values: ****<0.0001, ***<0.001, **<0.01, *<0.05. Shown: individual

data points with mean±SD; data from one experiment; all experiments were independently repeated twice with similar results.

Figure S2-6

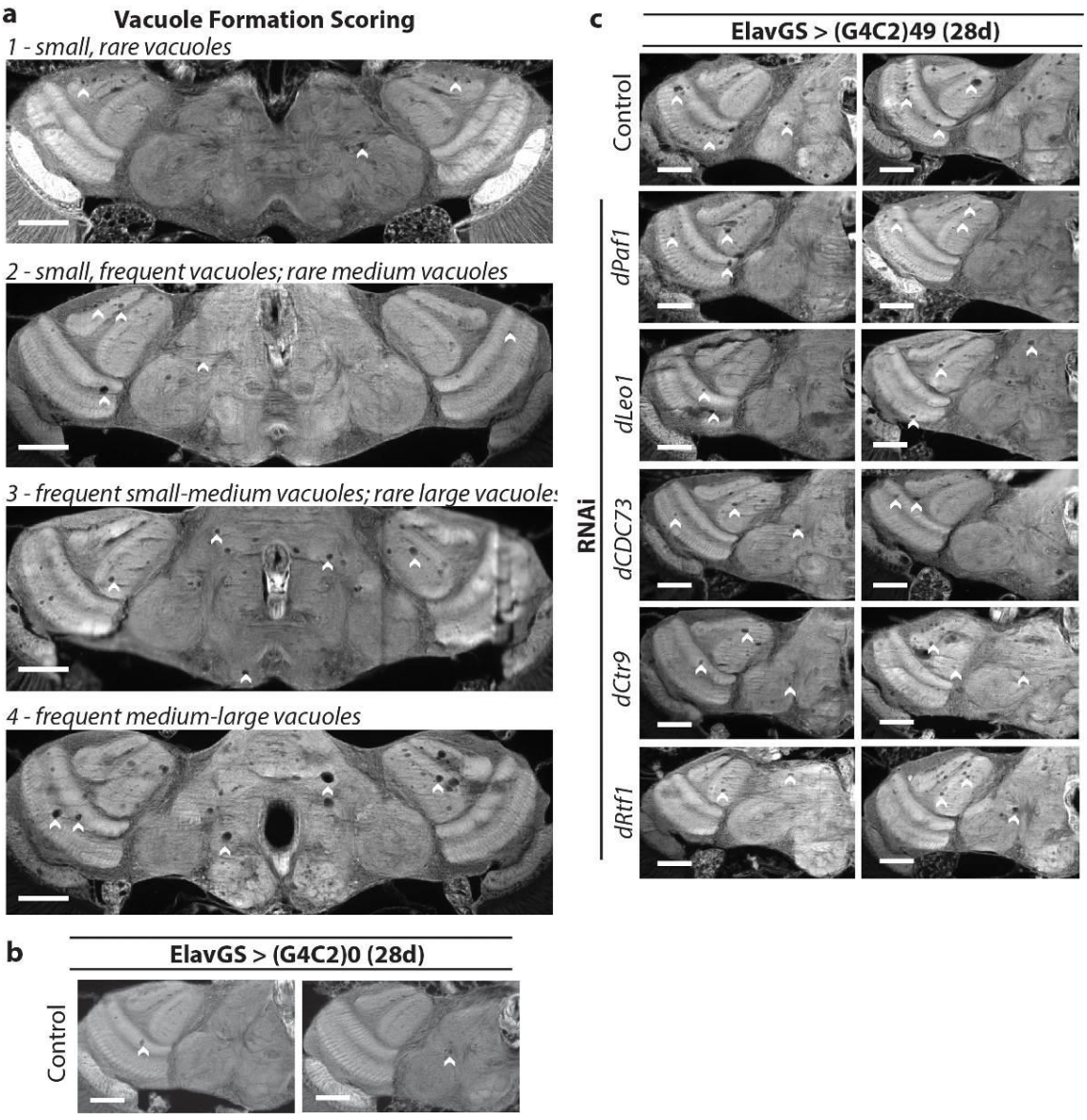
a
Vacuole Formation Scoring
1 - small, rare vacuoles
2 - small, frequent vacuoles; rare medium vacuoles
3 - frequent small-medium vacuoles; rare large vacuoles
4 - frequent medium-large vacuoles
b
ElavGS > (G4C2)0 (28d)
Control
c
ElavGS > (G4C2)49 (28d)
Control
RNAi
dPaf1
dLeo1
dCDC73
dCtr9
dRtf1

Supplementary Figure S2-6: Vacuole formation scoring schematic and additional examples of genotypes reported.

(a) Scoring of vacuole formation (arrowheads) in the adult fly brain. A scale was developed from 0-4 where 0 = no vacuoles and 4 = frequent medium-large vacuoles. “rare” means ≤5 vacuoles and “frequent” means >5 vacuoles. Sections through the entire brain of each animal were assessed in scoring. (G4C2)49 expression in 8d animals typically receives a score of 1. (G4C2)49 expression in 28d animals typically receives a score of 3-4. Expression is driven by the drug-inducible neuronal driver, ElavGS. **(b)** Additional representative images of non-G4C2, age matched controls at 28d. **(c)** Additional representative images of vacuoles observed in (G4C2)49 brains at 28d (see Fig 3f). dPAF1C components are targeted by RNAi and result in suppression of vacuole formation in (G4C2)49 expressing animals. Shown: data from one experiment; experiment was repeated twice with similar results. Scale bars: 50μm

Figure S2-7

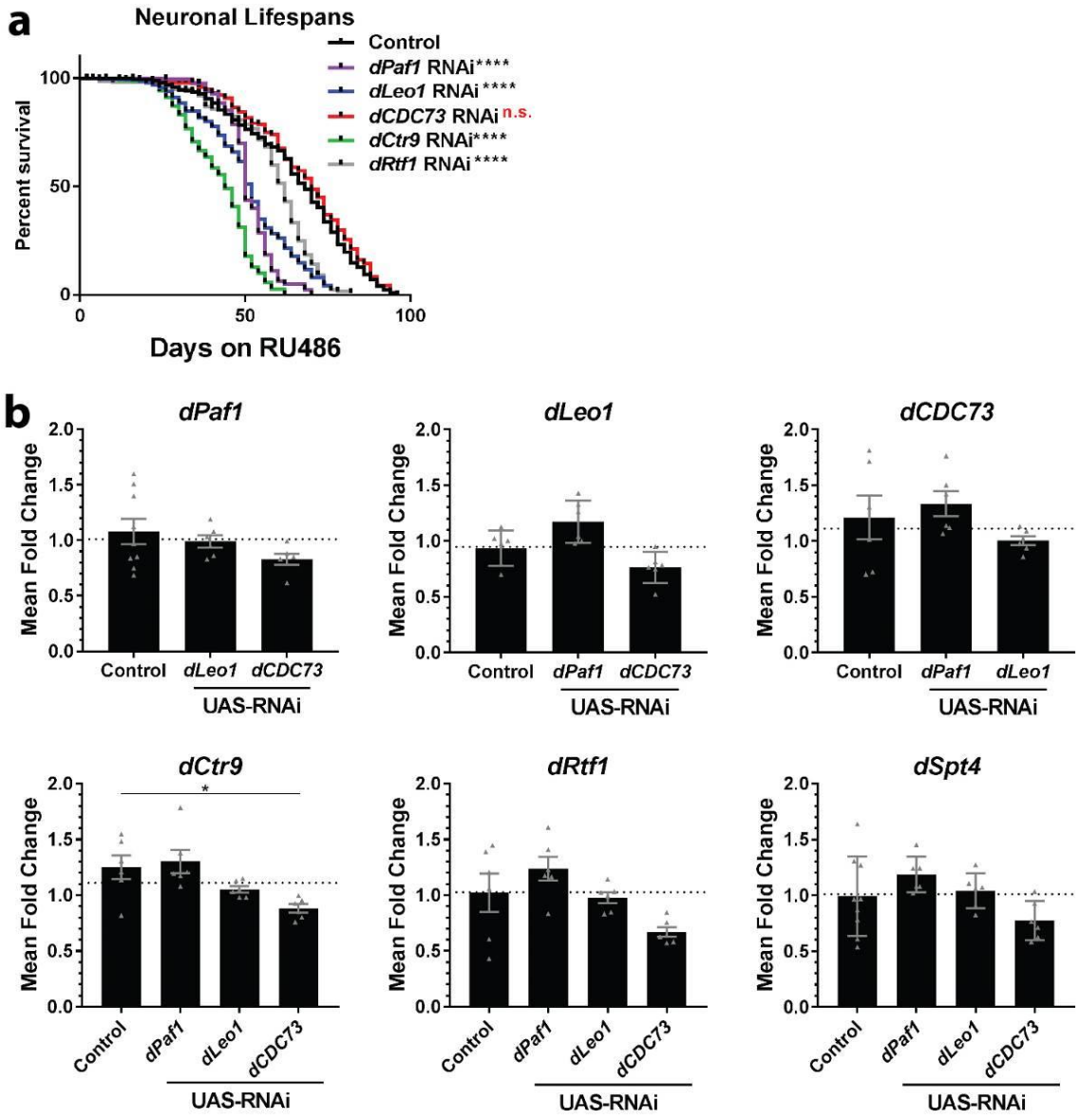
a
Neuronal Lifespans
Control
dPaf1 RNAi****
dLeo1 RNAi****
dCDC73 RNAi n.s.
dCtr9 RNAi****
dRtf1 RNAi****
Percent survival
Days on RU486
b
dPaf1
dLeo1
dCDC73
dCtr9
dRtf1
dSpt4
Mean Fold Change
Control
UAS-RNAi

Supplementary Figure S2-7: Characterization of the dPAF1C in the fly.

(a) RNAi for dPAF1C components were expressed in the adult fly nervous system using the drug-inducible neuronal driver, ElavGS. Survival of animals with age was evaluated. All RNAi but *dCDC73* RNAi results in reduced lifespan compared to control animals. N flies: control=301, *dPaf1*=200, *dLeo1*=275, *dCDC73*=200, *dCtr9*=210, *dRtf1*=200. **(b)** Co-regulation of dPAF1C components and dSpt4 were determined by looking for reduced expression of components when *dPaf1*, *dLeo1*, or *dCDC73* were downregulated by RNAi ubiquitously in adult animals (DaGS, 6d). No significance was detected except for *dCtr9* showing downregulation with *dCDC73* RNAi. Shown: individual data points with mean±SD; mean value of biological triplicates (n=10 flies/replicate). Statistics: (a) log-rank tests, (b) ANOVA with Tukey's correction; p-values: ****<0.0001, ***<0.001, **<0.01, *<0.05, no significance (n.s.) >0.05. Shown: data from one experiment; all experiments were independently repeated with similar results.

Figure S2-8

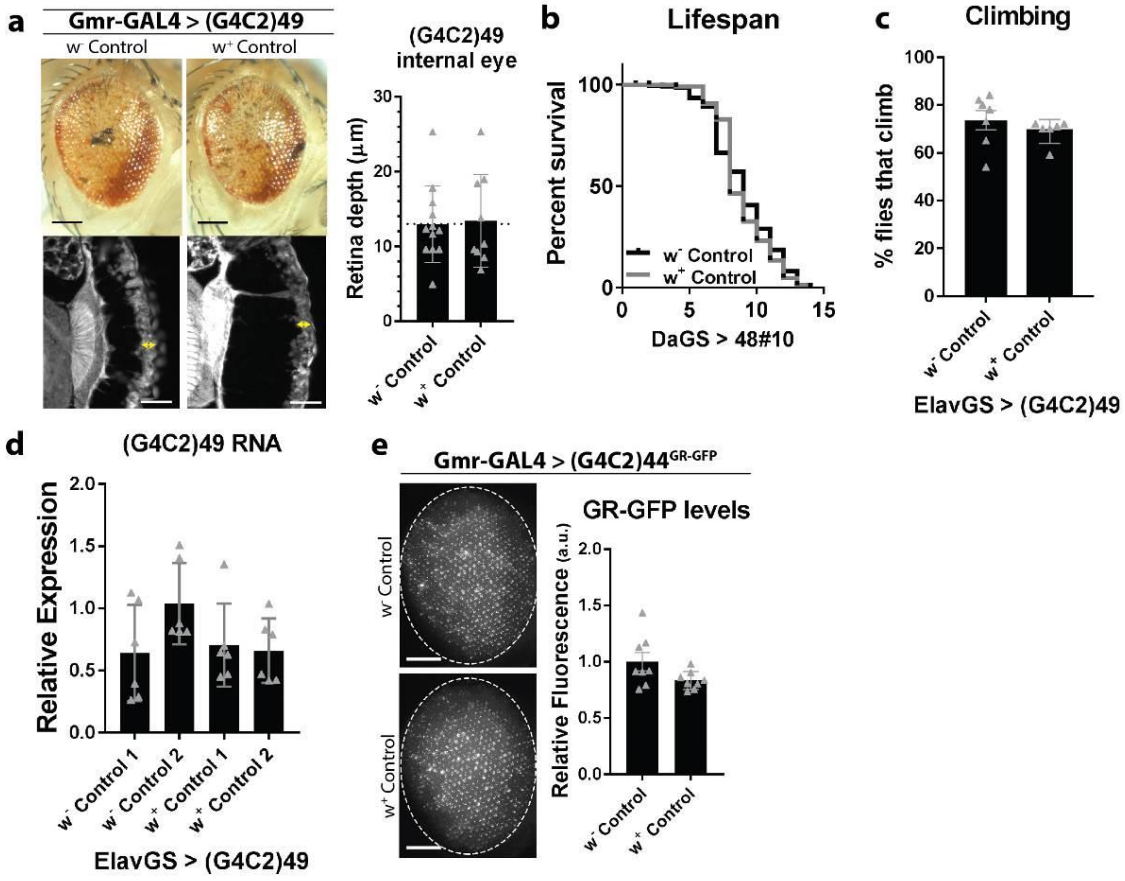
a
Gmr-GAL4 > (G4C2)49
w⁻ Control
w⁺ Control
(G4C2)49 internal eye
Retina depth (µm)
w⁻ Control
w⁺ Control
b
Lifespan
Percent survival
w⁻ Control
w⁺ Control
DaGS > 48#10
c
Climbing
% flies that climb
w⁻ Control
w⁺ Control
ElavGS > (G4C2)49
d
(G4C2)49 RNA
Relative Expression
w⁻ Control 1
w⁻ Control 2
w⁺ Control 1
w⁺ Control 2
ElavGS > (G4C2)49
e
Gmr-GAL4 > (G4C2)44GR-GFP
w⁻ Control
w⁺ Control
GR-GFP levels
Relative Fluorescence (a.u.)
w⁻ Control
w⁺ Control

Supplementary Figure S2-1: Comparisons of w^- vs w^+ genetic background controls in (G4C2)30+ expressing flies shows no significant differences.

To address potential concerns of different RNAi genetic backgrounds of the lines used in this study, multiple controls with different genetic backgrounds were examined. Here we show representative data. **(a)** Toxicity associated with (G4C2)49 expression looks similar both externally and internally in the fly eye when the transgene is expressed in the optic system (Gmr-GAL4) in w^- vs w^+ genetic backgrounds. Internal retina depth (arrows) was quantified for individual animals. N flies: w^-=12, w^+=9. Shown: individual data points (each representing 1 animal) with mean±SD. Scale bars: external eye = 100µm, internal eye = 35µm. **(b)** Ubiquitous expression of (G4C2)49 in adult flies results in similar lifespans in w^- vs w^+ genetic backgrounds. N flies: w^-=188, w^+=106. **(c)** Climbing deficits develop with age in animals expressing (G4C2)49 in the adult fly nervous system, ElavGS. The % flies that can climb is comparable in w^- and w^+ controls (20d, males). N flies: w^-=51, w^+=72. Shown: Individual data points are mean % of animals that could climb per tube; individual data points with mean±SD. **(d)** qPCR analysis of (G4C2)49 RNA levels in the adult fly nervous system is statistically similar in multiple genetic backgrounds. Shown: individual data points with mean±SD; mean value of biological triplicates (n=25 flies/replicate) from 2 independent experiments. **(e)** External eye imaging of GR-GFP in Gmr-GAL4 > LDS-(G4C2)44$^{GR\text{-}GFP}$ animals results in similar GFP fluorescence independent of genetic background. N flies: w^-=8, w^+=8. Shown: individual data points (each representing 1 animal) with mean±SD. Scale bars: 100µm. Statistics: (a,c,e) unpaired 2-tailed student t-tests, (b) log-rank test, (d) ANOVA with Tukey's correction; p-value: no significance >0.05. See Supplemental Figure 12 for optimization of fly G4C2 qPCR reactions for this and subsequent figures.

Figure S2-9

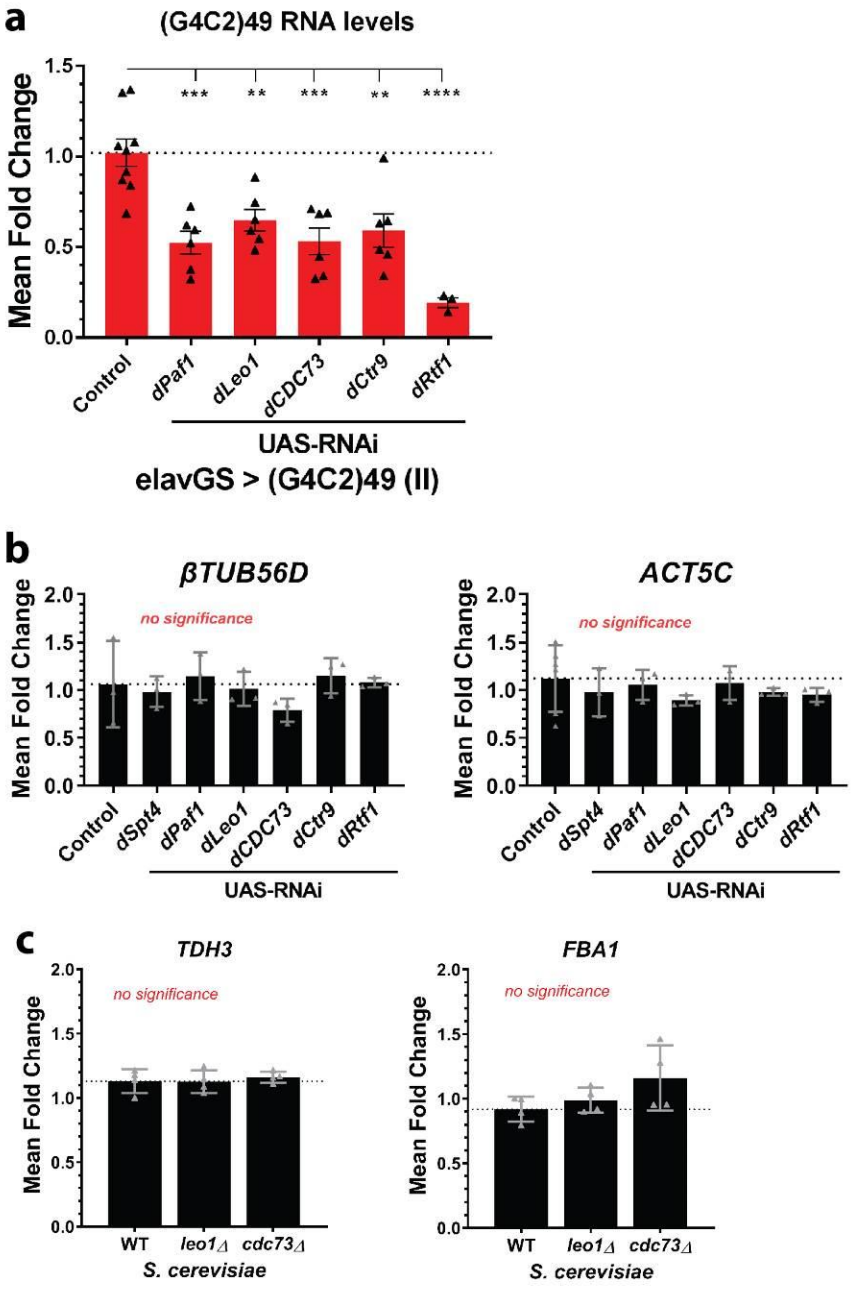
a
(G4C2)49 RNA levels
Mean Fold Change
1.5
1.0
0.5
0.0
***
**
***
**
****
Control
dPaf1
dLeo1
dCDC73
dCtr9
dRtf1
UAS-RNAi
elavGS > (G4C2)49 (II)
b
βTUB56D
no significance
Mean Fold Change
2.0
1.5
1.0
0.5
0.0
Control
dSpt4
dPaf1
dLeo1
dCDC73
dCtr9
dRtf1
UAS-RNAi
ACT5C
no significance
Mean Fold Change
2.0
1.5
1.0
0.5
0.0
Control
dSpt4
dPaf1
dLeo1
dCDC73
dCtr9
dRtf1
UAS-RNAi
c
TDH3
no significance
Mean Fold Change
2.0
1.5
1.0
0.5
0.0
WT
leo1Δ
cdc73Δ
S. cerevisiae
FBA1
no significance
Mean Fold Change
2.0
1.5
1.0
0.5
0.0
WT
leo1Δ
cdc73Δ
S. cerevisiae

Supplementary Figure S2-9: Extended qPCR fly and yeast data.

(a) A second, independent (G4C2)49 transgene was co-expressed with dPAF1C RNAi lines in the adult brain using a drug inducible, neuronal driver (ElavGS, 16d). Downregulation of all dPAF1C components caused significantly less RNA to be produced from the (G4C2)49 transgene by qPCR, consistent with data in Fig. 4a. Shown: individual data points with mean±SEM; mean value of biological triplicates (n=25 flies/replicate) from 2 independent experiments. **(b)** RNA levels for endogenous dRNAPII driven genes *βTUB56D* (β-Tubulin) and *ACT5C* (β-Actin) are unchanged upon knockdown of dPAF1C by qPCR. The ubiquitous, drug-inducible driver, DaGS, was used to drive RNAi expression in whole animals (6d). Shown: individual data points with mean±SD; mean value of biological triplicates (n=10 flies/replicate); data from 1 experiment while data reproduced in a second, independent experiment. **(c)** leo1Δ or cdc73Δ yeast strains do not alter RNA levels produced from endogenous scRNAPII genes, *TDH3* and *FBA1*. RNA levels were measured by qPCR. Shown: individual data points with mean±SD; mean value of biological triplicates from 1 experiment. Statistics: ANOVAs with Tukey's correction, p-values: ****<0.0001, ***<0.001, **<0.01, *<0.05, no significance >0.05.

Figure S2-10

a

		Fig	NINDS/Coriell Code	Rutgers ID	Target ALS ID	Mutation	Diagnosis	Age at onset	Age at sampling	Gender	Source
iPSC, Line 1	#011	6a		FA0000011	TALSCTRL15.12	n/a	Healthy	n/a	49	F	Gitler Lab
iPSC, Line 2	#2242	6a				n/a	Healthy	n/a			Gitler Lab
iPSC, Line 3	#8783	6a				n/a	Healthy	n/a			Gitler Lab
iPSC, Line 4	#002	6a		150000002	TALS9-9.3	*C9orf72*	ALS	60	64	F	Gitler Lab
iPSC, Line 5	#33	6a				*C9orf72*	(spinal)	61			Gitler Lab
iPSC, Line 6	#92	6a				*C9orf72*	(bulbar)	48			Gitler Lab
Fibroblast #1		6b	ND42504			*C9orf72*	FTD	At Risk	53	F	Rutgers
Fibroblast #2		6b	ND42506			*C9orf72*	FTD	At Risk	46	F	Rutgers
Fibroblast #3		6b	ND42496			*C9orf72*	FTD	At Risk	57	M	Rutgers
Fibroblast #4		6b	ND40069			*C9orf72: Intermediate*	Parkinsonism	71	75	F	Rutgers

b

	C9orf72-positive			
	All	FTLD	ALS/FTLD	ALS
Number of cases	67	26	21	20
Gender (male)	36 (53.73%)	18 (69.23%)	11 (52.38%)	7 (35.00%)
Age at onset	61 (41,54,67,79)	66 (44,56,70,79)	58 (50,53,65,74)	57 (41,49,62,76)
Age at death	64 (43,59,72,90)	72 (52,66,80,90)	62 (51,60,68,80)	60 (43,52,66,77)
Disease duration	3.7 (1.0,2.2,6.7,14.5)	6.9 (2.4,5.7,8.5,14.5)	4.8 (1.1,2.7,7.4,10.4)	1.9 (1.0,1.4,3.0,6.3)

	C9orf72-negative				Healthy controls
	All	FTLD	ALS/FTLD	ALS	
Number of cases	56	23	11	22	27
Gender (male)	25 (44.64%)	10 (43.48%)	4 (36.36%)	12 (54.55%)	15 (55.56%)
Age at onset	66 (45,57,73,86)	73 (57,66,80,86)	69 (46,56,70,78)	59 (45,49,67,76)	-
Age at death	73 (47,66,83,100)	83 (66,78,88,100)	73 (49,65,78,85)	66 (47,59,71,79)	81 (57,65,88,99)
Disease duration	4.3 (0.6,2.9,8.4,21.9)	8.5 (3.9,8.2,10.1,20.5)	2.9 (0.6,1.8,7.4,21.9)	3.5 (0.9,2.3,4.7,21.5)	-

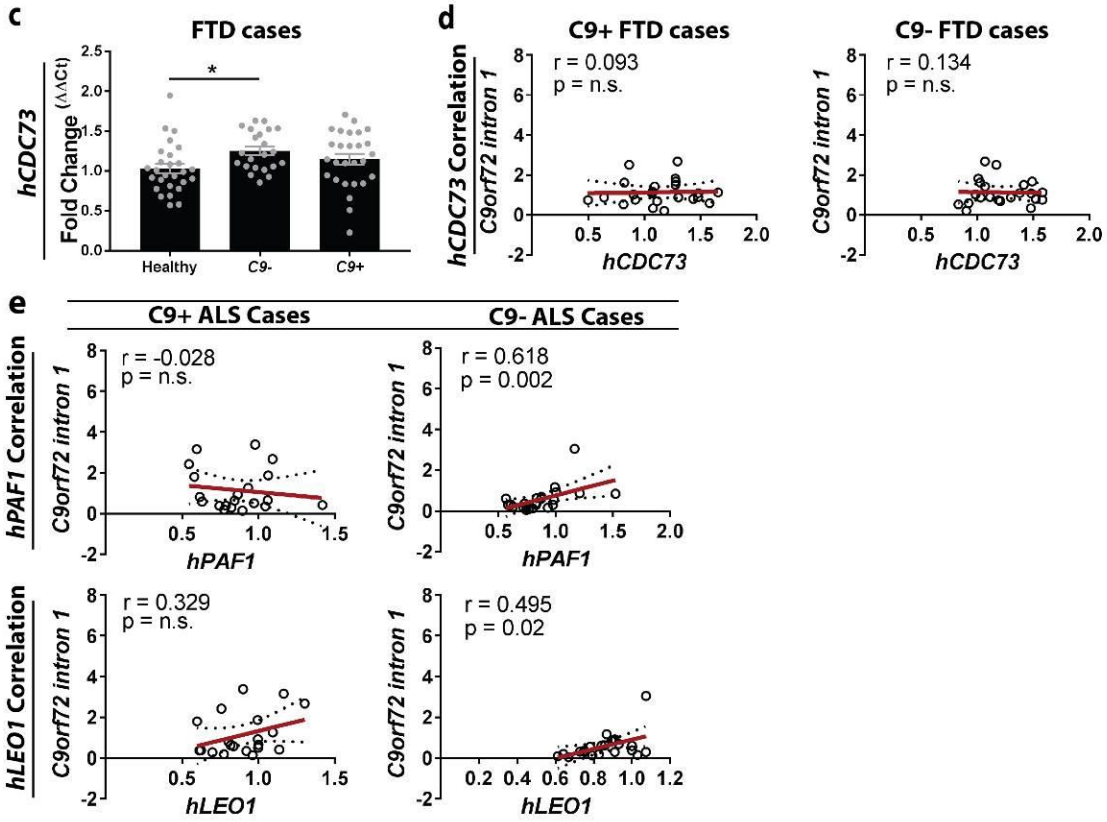

Supplementary Figure S2-10: Extended patient data.

(a) Summary of iPS and fibroblast cell lines used in Fig 6a-b, respectively. **(b)** Summary of patient cohort used in this study. Total number, cases that were male (%) and average age at onset/death/duration: median (minimum, 25th percentile, 75th percentile, and maximum). **(c)** In frontal cortex tissue from FTD cases qPCR analysis of endogenous expression of *hCDC73* revealed no significant change in expression in *C9+* versus *C9-* cases. *C9-* cases did show a significant upregulation of *hCDC73* compared to healthy controls. Shown: individual data points (each representing 1 individual) with mean±SEM. **(d)** Spearman correlation coefficients for *C9+* or *C9-* FTD cases show no correlation in *hCDC73* expression and *C9orf72* expression in the frontal cortex of patients. **(e)** Spearman correlation coefficients for *C9+* or *C9-* ALS cases showed no correlation in expression of *hPAF1* and *hLEO1* and expression of *C9orf72* in the frontal cortex of *C9+* patients. In *C9-* ALS patients, there were weak correlations that were markedly lower than those in *C9+* FTD patients (see Fig. 6d). *C9orf72 intron 1*: the intronic gene region immediately 3' of the G4C2 repeat in the *C9orf72* pre-mRNA transcript. (d,e) Shown: individual data points (each representing 1 individual) with linear regression±SE. Statistics: (c) ANOVA with Tukey's correction, (d,e) Spearman R correlations; p-values: ****<0.0001, ***<0.001, **<0.01, *<0.05, no significance (n.s.) >0.05.

Figure S2-11

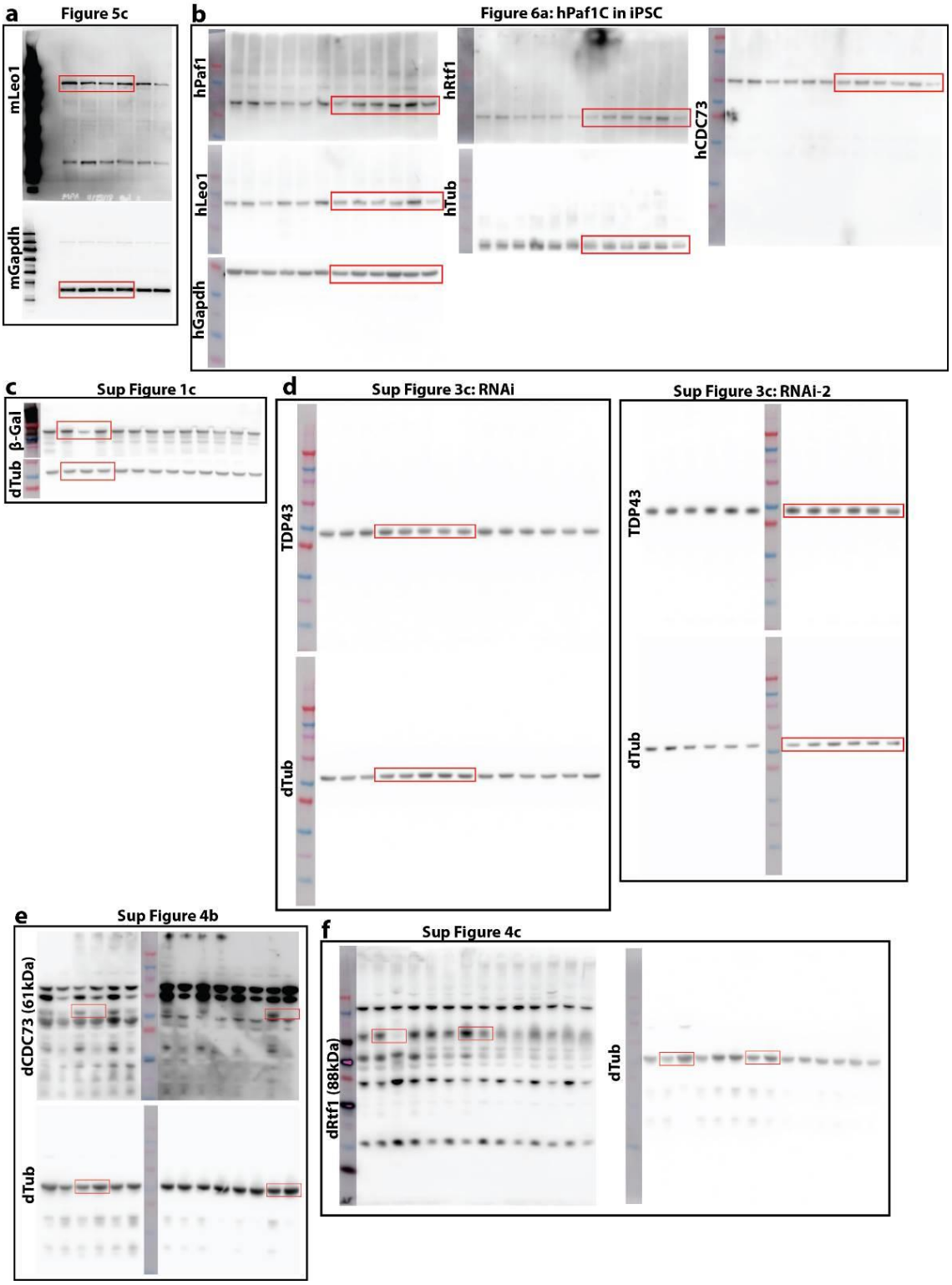
a
Figure 5c
mLeo1
mGapdh
b
Figure 6a: hPaf1C in iPSC
hPaf1
hRtf1
hCDC73
hLeo1
hTub
hGapdh
c
Sup Figure 1c
β-Gal
dTub
d
Sup Figure 3c: RNAi
TDP43
dTub
Sup Figure 3c: RNAi-2
TDP43
dTub
e
Sup Figure 4b
dCDC73 (61kDa)
dTub
f
Sup Figure 4c
dRtf1 (88kDa)
dTub

Supplementary Figure S2-11: Full, uncropped western immunoblot images with protein standards.

Uncropped western immunoblot images for all relevant figures. **(a)** protein ladder shown is SuperSignal Enhanced Molecular Weight Protein Ladder (Fisher Sci #84786). **(b-f)** protein ladder shown is Novex Sharp Pre-stained Protein Standard (Invitrogen #LC5800).

Figure S2-12

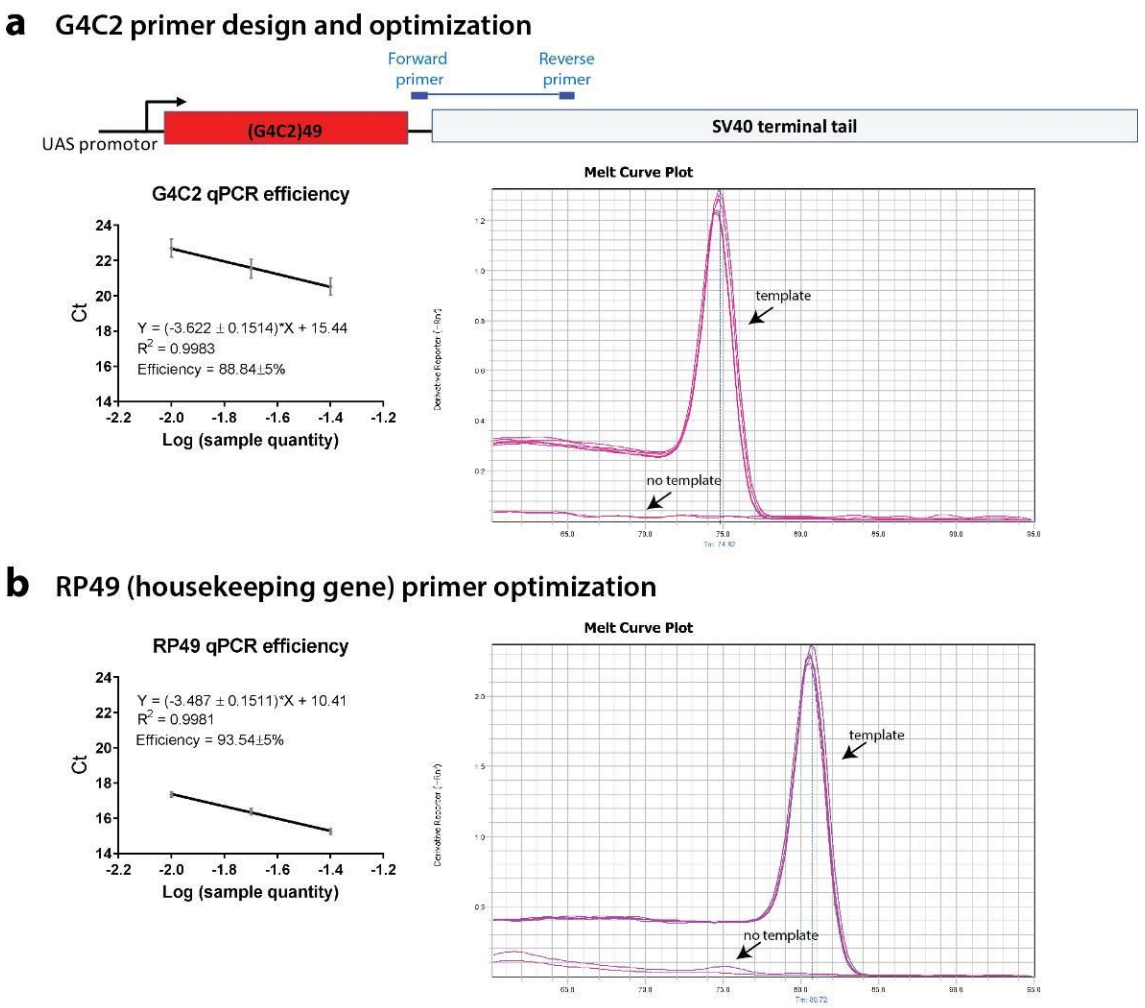
a G4C2 primer design and optimization
Forward primer
Reverse primer
UAS promotor
(G4C2)49
SV40 terminal tail
G4C2 qPCR efficiency
Ct
Y = (-3.622 ± 0.1514)*X + 15.44
R2 = 0.9983
Efficiency = 88.84±5%
Log (sample quantity)
Melt Curve Plot
template
no template
b RP49 (housekeeping gene) primer optimization
RP49 qPCR efficiency
Y = (-3.487 ± 0.1511)*X + 10.41
R2 = 0.9981
Efficiency = 93.54±5%
Log (sample quantity)
Melt Curve Plot
template
no template

Supplementary Figure S2-12. G4C2 and RP49 primer optimization for qPCR.

During optimization of primers for qPCR reactions used in this study, primer efficiencies and melt curves were closely examined to ensure validity of all reactions. **(a)** For measuring (G4C2)n mRNA levels in flies, qPCR primers were designed that utilized unique restriction enzyme sequences located 3' of the repeat. **(b)** RP49, a common housekeeping gene, shows a similar primer efficiency to the G4C2 primers, both ~90%, and was used as the main reference gene. Primer efficiencies were calculated using serial dilutions of cDNA made from control samples expressing (G4C2)49 in the fly nervous system (using ElavGS). Shown: mean value of biological triplicates from 2 independent experiments and the resulting trendline is shown±SD. Representative melt curves from one of the biological triplicates is shown. Further, qPCR products were run on an agarose gel to confirm that there was one product and that it was the expected size (data not shown).

Chapter 2: Supplementary data

KEY
NE = no effect
MS = mild suppression
S = suppression
ME = mild enhancer
E = enhancer
E-L = lethal enhancer
A = additive enhancer
LacZ-E = enhancer of Gal4/UAS system
LacZ-S = suppressor of Gal4/UAS system

shRNA target			shRNA fly line		Final call as a potential modifier of (G4C2)49	Effects on the external eye phenotype					Affect on UAS-LacZ protein
CG #	FBgn	Gene Symbol	stock #	RNAi		UAS-(G4C2)49	UAS-(G4C2)6-8	UAS-TDP43	UAS-(GR)36	alone (gmr-gal4)	
CG1433	FBgn0019637	atu/Leo1	v17490	GD8296	S	S		NE	S	NE	NE
CG2503	FBgn0010750	atms/Paf1	v20876	GD9782	S	MS		NE	NE	NE	NE
CG11990	FBgn0037657	hyx/Cdc73	BL53278	HMC03494	S	S		S	E	NE	NE
CG2469	FBgn0035205	CG2469/Ctr9	BL33736	HMS00619	S	S		NE	S	NE	NE
CG10955	FBgn0034722	Rtf1	BL34850	HMS00168	MS	MS		NE	NE	NE	NE
CG3909	FBgn0027524	Wdr61/Ski8	BL57377	HMC04664	MS	MS		NE	E	NE	NE
CG12372	FBgn0028683	spt4	BL32896	HMS00685	MS	MS		NE	NE	NE	NE
CG7626	FBgn0040273	Spt5	BL34837	HMS00153	LacZ-S	S		S	MS	ME	MS
CG12225	FBgn0028982	Spt6	BL32373	HMS00364	LacZ-S	S	ME	S	S	E	S
CG11397	FBgn0015391	glu	BL32350	HMS00341		NE					
CG7578	FBgn0028538	sec71	BL32366	HMS00357		NE					
CG5001	FBgn0031322	CG5001	BL32392	HMS00386		NE					
CG10691	FBgn0002031	l(2)37Cc	BL32404	HMS00399		NE					
CG10528	FBgn0004811	fs(2)ltoPP43	BL32452	HMS00451		NE					
CG5229	FBgn0028387	chm	BL32484	HMS00487	A	E	E			E	
CG7420	FBgn0031344	CG7420	BL32510	HMS00514	E-L	E-L	NE	NE	ME		(ME POSSIBLE)
CG17566	FBgn0010097	gammaTub37C	BL32513	HMS00517		NE					
CG9078	FBgn0001941	ifc	BL32514	HMS00518		NE					
CG4184	FBgn0027592	MED15	BL32517	HMS00522	(MS POSSIBLE)	NE		S	MS	ME	

CG4389	FBgn0028479	Mtpalpha	BL32873	HMS00660		NE					
CG3131	FBgn0031464	Duox	BL32903	HMS00692		NE					
CG3399	FBgn0000256	capu	BL32922	HMS00712		NE					
CG14472	FBgn0011230	poe	BL32945	HMS00739		NE					
CG10043	FBgn0015803	rtGEF	BL32947	HMS00741		NE					
CG17941	FBgn0000497	ds	BL32964	HMS00759		NE					
CG2720	FBgn0024352	Hop	BL32979	HMS00779		NE					
CG4889	FBgn0004009	wg	BL32994	HMS00794		NE					
CG4965	FBgn0002673	twe	BL33044	HMS00642		NE					
CG13692	FBgn0031254	CG13692	BL33341	HMS00207		NE					
CG4785	FBgn0031314	CG4785	BL33358	HMS00230		NE					
CG3423	FBgn0020616	SA	BL33395	HMS00272		NE					
CG8749	FBgn0016978	snRNP-U1-70K	BL33396	HMS00274	E	E	NE	E	NE		(not viable)
CG18497	FBgn0016977	spen	BL33398	HMS00276	A	ME	ME			E	
CG8409	FBgn0003607	Su(var)205	BL33400	HMS00278		NE					
CG4894	FBgn0001991	Ca-alpha1D	BL33413	HMS00294		NE					
CG1768	FBgn0011202	dia	BL33424	HMS00308		NE					
CG9885	FBgn0000490	dpp	BL33618	HMS00011		NE					
CG7254	FBgn0004507	GlyP	BL33634	HMS00032		NE					
CG5671	FBgn0026379	Pten	BL33643	HMS00044	A	ME	ME			ME	
CG2807	FBgn0031266	CG2807	BL33650	HMS00055	A	E-L	E-L			E	
CG3605	FBgn0031493	CG3605	BL33651	HMS00056	A	E	E			E	
CG3938	FBgn0010382	CycE	BL33654	HMS00060		NE					
CG18174	FBgn0028694	Rpn11	BL33662	HMS00071	A	E-L	E			E	
CG7269	FBgn0014189	Hel25E	BL33666	HMS00076	MS	MS		S	S		NE
CG4916	FBgn0004419	me31B	BL33675	HMS00539	LacZ-E	ME	NE	ME	NE		E
CG3736	FBgn0002989	okr	BL33707	HMS00585		NE					
CG3542	FBgn0031492	CG3542	BL33711	HMS00589		NE					
CG10377	FBgn0004838	Hrb27C	BL33716	HMS00597	E-L	E-L	NE	E	E-L		NE
CG33955	FBgn0031414	eys	BL33766	JF02708		NE					
CG14028	FBgn0015031	cype	BL33878	HMS00815		NE					
CG5366	FBgn0027568	Cand1	BL33920	HMS00864		NE					
CG10387	FBgn0015553	tos	BL33937	HMS00887		NE					
CG5203	FBgn0027052	CHIP	BL33938	HMS00889		NE					
CG5092	FBgn0021796	mTor	BL33951	HMS00904		NE					

CG9961	FBgn0031451	CG9961	BL33959	HMS00916		NE					
CG6716	FBgn0003145	prd	BL33965	HMS00922		NE					
CG9075	FBgn0001942	eIF-4a	BL33970	HMS00927	A	E-L	E-L			E-L	
CG15438	FBgn0025684	MFS18	BL33998	HMS00961		NE					
CG13387	FBgn0020497	emb	BL34021	HMS00991		NE					
CG9244	FBgn0010100	Acon	BL34028	HMS00998		NE					
CG15218	FBgn0025674	CycK	BL34032	HMS01003		NE					
CG10726	FBgn0014127	barr	BL34068	HMS00049		NE					
CG2903	FBgn0031450	Hrs	BL34086	HMS00840		NE					
CG18405	FBgn0011259	Sema-1a	BL34320	HMS01307		NE					
CG3851	FBgn0002985	odd	BL34328	HMS01315		NE					
CG9553	FBgn0000308	chic	BL34523	HMS00550		NE					
CG7885	FBgn0026373	RpII33	BL34567	HMS01040	A	E	E	E	ME	E	
CG18780	FBgn0013531	MED20	BL34577	HMS01051		NE		MS	NE		
CG5481	FBgn0002543	lea	BL34589	HMS01063		NE					
CG10034	FBgn0000964	tj	BL34595	HMS01069		NE					
CG3858	FBgn0019809	gcm2	BL34597	HMS01071		NE					
CG4897	FBgn0005593	RpL7	BL34600	HMS01074	A	E-L	E			E-L	
CG16738	FBgn0003430	slp1	BL34633	HMS01107		NE					
CG2939	FBgn0004567	slp2	BL34634	HMS01108		NE					
CG3710	FBgn0010422	TfIIS	BL34642	HMS01117		NE					
CG10334	FBgn0005672	spi	BL34645	HMS01120	A	E	E			E	
CG10719	FBgn0010300	brat	BL34646	HMS01121	E	E	NE	NE	NE		NE
CG3242	FBgn0004892	sob	BL34648	HMS01123		NE					
CG4212	FBgn0015791	Rab14	BL34654	HMS01130		NE					
CG3469	FBgn0015000	betaggt-I	BL34687	HMS01165		NE					
CG7111	FBgn0020618	Rack1	BL34694	HMS01173	E	E	NE	NE	ME		(ME POSSIBLE)
CG4579	FBgn0021761	Nup154	BL34710	HMS01189		NE					
CG5848	FBgn0000250	cact	BL34775	HMS00084		NE					
CG13389	FBgn0010265	RpS13	BL34820	HMS00135	A	E	E			E	
CG7793	FBgn0001965	Sos	BL34833	HMS00149		NE					
CG11490	FBgn0031233	CG11490	BL34859	HMS00177		NE					
CG13243	FBgn0028903	CG13243	BL34861	HMS00179		NE					
CG6122	FBgn0004872	piwi	BL34866	HMS00185	A	E	ME			E	

CG18028	FBgn0002566	lt	BL34871	HMS00190		NE					
CG11372	FBgn0031213	galectin	BL34880	HMS01225		NE					
CG9242	FBgn0000239	bur	BL34889	HMS01234		NE					
CG18627	FBgn0028970	betaggt-II	BL34902	HMS01247		NE					
CG3956	FBgn0003448	sna	BL34906	HMS01252		NE					
CG3166	FBgn0000097	aop	BL34909	HMS01256	A	E-L	E			E	
CG7082	FBgn0031401	papi	BL34932	HMS01282		NE					
CG10699	FBgn0002023	Lim3	BL34962	HMS00596		NE					
CG4114	FBgn0004583	ex	BL34968	HMS00874		NE					
CG3352	FBgn0001075	ft	BL34970	HMS00932		NE					
CG3752	FBgn0012036	Aldh	BL34989	HMS01399		NE					
CG17259	FBgn0031497	CG17259	BL34992	HMS01402		NE					
CG12789	FBgn0025697	santa-maria	BL34995	HMS01405	(ME POSSIBLE)	NE	NE		ME		
CG4824	FBgn0000182	BicC	BL34997	HMS01407		NE					
CG6521	FBgn0027363	Stam	BL35016	HMS01429		NE					
CG4952	FBgn0005677	dac	BL35022	HMS01435		NE					
CG1374	FBgn0003866	tsh	BL35030	HMS01443		NE					
CG18507	FBgn0028527	CG18507	BL35033	HMS01447		NE					
CG3779	FBgn0002973	numb	BL35045	HMS01459		NE					
CG4428	FBgn0031298	Atg4	BL35740	HMS01482		NE					
CG6601	FBgn0015797	Rab6	BL35744	HMS01486		NE					
CG3523	FBgn0027571	CG3523	BL35775	HMS01524		NE					
CG12630	FBgn0028979	tio	BL35812	HMS01527		NE					
CG10360	FBgn0003231	ref(2)P	BL36111	HMS00551		NE					
CG6699	FBgn0025724	beta'Cop	BL36113	HMS01038		NE	NE	NE	NE	NE	NE
CG5363	FBgn0004106	cdc2	BL36117	HMS01531	A	E	ME	MS	E	ME	
CG5686	FBgn0024248	chico	BL36665	HMS01553	E-L	E-L	NE	NE	ME		NE
CG1071	FBgn0024371	E2f2	BL36674	HMS01562		NE					
CG9127	FBgn0000052	ade2	BL36686	HMS01574		NE					
CG17265	FBgn0031488	CG17265	BL36687	HMS01575		NE					
CG33090	FBgn0028916	CG33090	BL36688	HMS01576		NE					
CG3214	FBgn0031436	CG3214	BL36695	HMS01584		NE					
CG6382	FBgn0020443	Elf	BL36703	HMS01592		NE					
CG5304	FBgn0010497	dmGlut	BL36724	HMS01615		NE					

CG8827	FBgn0012037	Ance	BL36749	HMS03009	A	E-L	E-L			E-L	
CG9261	FBgn0015777	nrv2	BL37495	HMS01637		NE					
CG5722	FBgn0024320	Npc1a	BL37504	HMS01646		NE					
CG3018	FBgn0010602	lwr	BL37506	HMS01648		NE					
CG10692	FBgn0028707	Mt2	BL38224	HMS01667		NE					
CG7291	FBgn0031381	Npc2a	BL38237	HMS01681		NE		S	E		
CG12676	FBgn0000547	ed	BL38243	HMS01687		NE					
CG2855	FBgn0031458	aph-1	BL38249	HMS01693		NE					
CG3326	FBgn0031519	CG3326	BL38266	HMS01711		NE					
CG9258	FBgn0015776	nrv1	BL38275	HMS01725		NE					
CG3903	FBgn0001987	Gli	BL38284	HMS01737		NE					
CG2774	FBgn0031534	Snx1	BL38301	HMS01763		NE					
CG15358	FBgn0031373	CG15358	BL38313	HMS01777		NE					
CG10637	FBgn0015772	Nak	BL38326	HMS01793		NE					
CG7109	FBgn0004177	mts	BL38337	HMS01804	E-L	E-L	ME	MS	E-L	ME	NE
CG9115	FBgn0025742	mtm	BL38339	HMS01806		NE					
CG4993	FBgn0024734	PRL-1	BL38358	HMS01826		NE					
CG5102	FBgn0000413	da	BL38382	HMS01851		NE					
CG18095	FBgn0028872	CG18095	BL38521	HMS01705		NE					
CG8667	FBgn0023091	dimm	BL38530	HMS01742		NE					
CG3365	FBgn0020304	drongo	BL38960	HMS01874		NE					
CG4764	FBgn0031310	CG4764	BL38963	HMS01877		NE					
CG31762	FBgn0000114	aret	BL38983	HMS01899		NE					
CG2671	FBgn0002121	l(2)gl	BL38989	HMS01905		NE					
CG2699	FBgn0020622	Pi3K21B	BL38991	HMS01907		NE					
CG3766	FBgn0011232	scat	BL38994	HMS01910		NE					
CG17348	FBgn0015380	drl	BL39002	HMS01918		NE					
CG10385	FBgn0005617	msl-1	BL39012	HMS01930		NE					
CG6137	FBgn0000146	aub	BL39026	HMS01945		NE					
CG16928	FBgn0020270	mre11	BL39028	HMS01947		NE					
CG3994	FBgn0028516	ZnT35C	BL39049	HMS01969		NE					
CG7115	FBgn0027515	CG7115	BL39065	HMS01985	A	ME	ME			E	
CG2914	FBgn0005660	Ets21C	BL39069	HMS01989		NE					
CG4280	FBgn0015924	crq	BL40831	HMS01997		NE					
CG3159	FBgn0026438	Eaat2	BL40832	HMS01998		NE					

CG2718	FBgn0001142	Gs1	BL40836	HMS02002		NE					
CG14029	FBgn0016076	vri	BL40862	HMS02029		NE					
CG3234	FBgn0014396	tim	BL40864	HMS02031		NE					
CG2843	FBgn0031452	Cwc25	BL40887	HMS02135		NE					
CG17332	FBgn0027779	VhaSFD	BL40896	HMS02144		NE					
CG9884	FBgn0011818	oaf	BL40926	HMS02174		NE					
CG9887	FBgn0031424	VGlut	BL40927	HMS02175		NE					
CG4274	FBgn0001086	fzy	BL40933	HMS02181		NE					
CG14026	FBgn0003716	tkv	BL40937	HMS02185		NE					
CG10443	FBgn0000464	Lar	BL40938	HMS02186		NE					
CG14938	FBgn0020309	crol	BL41669	HMS02202		NE					
CG7595	FBgn0000317	ck	BL41690	HMS02254		NE					
CG12317	FBgn0028425	Jhl-21	BL41706	HMS02271	A	E-L	E			E	
CG9019	FBgn0015381	dsf	BL41707	HMS02272	MS	MS		NE	E		NE
CG11835	FBgn0031264	CG11835	BL41725	HMS02291		NE					
CG11324	FBgn0025777	homer	BL41908	HMS02301		NE					
CG11592	FBgn0025686	CG11592	BL41956	HMS02353		NE					
CG4220	FBgn0004858	elB	BL41960	HMS02357		NE					
CG5655	FBgn0011305	Rsf1	BL41971	HMS02368		NE					
CG7100	FBgn0015609	CadN	BL41982	HMS02380		NE					
CG11723	FBgn0031391	CG11723	BL42514	HMJ02079		NE					
CG11617	FBgn0031232	CG11617	BL42525	HMJ02091		NE					
CG13388	FBgn0027932	Akap200	BL42539	HMJ02109		NE					
CG10016	FBgn0024244	drm	BL42548	HMJ02120		NE					
CG18660	FBgn0028704	Nckx30C	BL42581	HMS01955		NE					
CG5556	FBgn0031332	CG5556	BL42594	HMS02426		NE					
CG10655	FBgn0002021	l(2)37Bb	BL42608	HMS02443		NE					
CG3758	FBgn0001981	esg	BL42846	HMS02538		NE					
CG12403	FBgn0020368	Vha68-1	BL42888	HMS02581		NE					
CG12245	FBgn0014179	gcm	BL42889	HMS02582		NE					
CG5353	FBgn0027081	Aats-thr	BL42902	HMS02595		NE					
CG9092	FBgn0001089	Gal	BL42922	HMS02615		NE					
CG6605	FBgn0000183	BicD	BL42929	HMS02622		NE					
CG9564	FBgn0015316	Try29F	BL42949	HMS02642		NE					
CG3747	FBgn0026439	Eaat1	BL43287	HMS02659		NE					

CG2975	FBgn0031468	CG2975	BL43290	HMS02662		NE					
CG10604	FBgn0000529	bsh	BL43994	HMS02708		NE					
CG5371	FBgn0011703	RnrL	BL44022	HMS02737		NE					
CG8867	FBgn0020906	Jon25Bi	BL44025	HMS02740		NE					
CG2762	FBgn0003963	ush	BL44041	HMS02757		NE					
CG3647	FBgn0001978	stc	BL44051	HMS02768		NE					
CG3763	FBgn0000640	Fbp2	BL44052	HMS02769		NE			E		
CG6176	FBgn0026431	Grip75	BL44072	HMS02789		NE					
CG17240	FBgn0011832	Ser12	BL44086	HMS02803		NE					
CG31795	FBgn0031294	IA-2	BL44099	HMS02819		NE					
CG9643	FBgn0031485	CG9643	BL44110	HMS02831		NE					
CG18641	FBgn0031426	CG18641	BL44492	HMC02414		NE					
CG10739	FBgn0010309	pigeon	BL44507	HMC02897		NE					
CG4341	FBgn0028481	CG4341	BL44509	HMC02899		NE					
CG4145	FBgn0000299	Cg25C	BL44520	HMC02910		NE					
CG4180	FBgn0001977	l(2)35Bg	BL44644	HMC02348		NE					
CG4892	FBgn0028884	CG4892	BL44648	HMC02356		NE					
CG31783	FBgn0002939	ninaD	BL44652	HMC02392		NE					
CG3022	FBgn0031275	GABA-B-R3	BL50622	HMC02989		NE					
CG4491	FBgn0005771	noc	BL50659	HMC03060		NE					
CG31670	FBgn0031375	erm	BL50661	HMC03062		NE					
CG12287	FBgn0004394	pdm2	BL50665	HMC03066		NE					
CG16890	FBgn0028932	CG16890	BL50671	HMC03072		NE					
CG6713	FBgn0011676	Nos	BL50675	HMC03076		NE					
CG18783	FBgn0028420	Kr-h1	BL50685	HMC03086		NE					
CG11607	FBgn0001170	H2.0	BL50690	HMC03091		NE					
CG14396	FBgn0011829	Ret	BL50700	HMC03102		NE					
CG7400	FBgn0021953	Fatp	BL50709	HMC03111		NE					
CG2851	FBgn0010323	Gsc	BL50894	HMC02397		NE					
CG16858	FBgn0016075	vkg	BL50895	HMC02400		NE					
CG16987	FBgn0031461	daw	BL50911	HMJ03135		NE					
CG15387	FBgn0031403	CG15387	BL50952	HMJ21053		NE					
CG17158	FBgn0011570	cpb	BL50954	HMJ21056		NE					
CG5813	FBgn0000307	chif	BL51016	HMJ21138		NE					
CG11907	FBgn0031250	Ent1	BL51055	HMJ21190		NE					

CG16873	FBgn0028936	nimB5	BL51162	HMC02406		NE					
CG3047	FBgn0003372	Sgs1	BL51421	HMC02393		NE					
CG11331	FBgn0028990	Spn27A	BL51445	HMC03159		NE					
CG10800	FBgn0017551	Rca1	BL51450	HMC03180		NE					
CG5869	FBgn0028894	CG5869	BL51452	HMC03184		NE					
CG10697	FBgn0000422	Ddc	BL51462	HMC03200		NE					
CG10203	FBgn0028554	x16	BL51468	HMC03209		NE					
CG9042	FBgn0001128	Gpdh	BL51474	HMC03218		NE					
CG4162	FBgn0002524	lace	BL51475	HMC03219		NE					
CG17320	FBgn0015808	ScpX	BL51479	HMC03224		NE					
CG3210	FBgn0026479	Drp1	BL51483	HMC03230		NE					
CG15269	FBgn0028878	CG15269	BL51506	HMC03273		NE					
CG4426	FBgn0015905	ast	BL51700	HMC03173		NE					
CG11325	FBgn0025595	GRHR	BL51710	HMC03228		NE					
CG4163	FBgn0001992	Cyp303a1	BL51716	HMC03249		NE					
CG11020	FBgn0016920	nompC	BL51722	HMC03261		NE					
CG5526	FBgn0013810	Dhc36C	BL51726	HMC03270	(ME POSSIBLE)	NE	NE				
CG10619	FBgn0003896	tup	BL51763	HMC03317		NE					
CG4488	FBgn0011737	wee	BL51776	HMC03331		NE					
CG5876	FBgn0028375	heix	BL51780	HMC03335		NE					
CG3057	FBgn0019830	colt	BL51798	HMC03354		NE					
CG13397	FBgn0014417	CG13397	BL51808	HMC03368		NE					
CG11567	FBgn0015623	Cpr	BL51809	HMC03369		NE					
CG3664	FBgn0014010	Rab5	BL51847	HMC03420		NE					
CG17678	FBgn0000384	cta	BL51848	HMC03421		NE					
CG7144	FBgn0025687	LKR	BL51850	HMC03424		NE					
CG9886	FBgn0031428	CG9886	BL51857	HMC03431	A	ME	ME		E	ME	
CG15444	FBgn0011603	ine	BL51919	HMS03378	A	E	E			E	
CG4271	FBgn0031409	CG4271	BL52873	HMC03611		NE					
CG11911	FBgn0031249	CG11911	BL52894	HMC03633		NE					
CG10084	FBgn0002044	swm	BL52935	HMC03677	MS	MS		S	ME		NE
CG4276	FBgn0029095	aru	BL52976	HMJ21663		NE					
CG6206	FBgn0027611	CG6206	BL53294	HMC03510	E	E-L	NE	S	E	ME	NE
CG3639	FBgn0031282	Pex12	BL53308	HMC03536		NE					

CG5680	FBgn0000229	bsk	BL53310	HMC03539		NE					
CG5920	FBgn0004867	RpS2	BL53319	HMC03548	A	E-L	E			E	
CG13690	FBgn0031252	CG13690	BL53326	HMC03555		NE					
CG16784	FBgn0003141	pr	BL53346	HMC03575	MS	MS	ME	E	E-L	ME	NE
CG11561	FBgn0003444	smo	BL53348	HMC03577		NE					
CG8674	FBgn0021856	l(2)k14505	BL53352	HMC03581		NE					
CG17012	FBgn0031406	Send1	BL53369	HMC03598		NE					
CG18557	FBgn0031470	CG18557	BL53373	HMC03602		NE					
CG3117	FBgn0031471	CG3117	BL53673	HMC03606		NE					
CG5216	FBgn0024291	Sir2	BL53697	HMJ21708	(ME POSSIBLE)	NE	NE				
CG15362	FBgn0031378	CG15362	BL53919	HMJ21254	MS	MS		S	E		NE
CG11376	FBgn0031216	Zir	BL53946	HMJ21308	A	ME	ME			ME	
CG3625	FBgn0031245	CG3625	BL53962	HMJ21344		NE					
CG7364	FBgn0028541	TM9SF4	BL54019	HMJ21445		NE					
CG4164	FBgn0031256	CG4164	BL54797	HMJ21390		NE					
CG4846	FBgn0013433	beat-Ia	BL54820	HMJ21539		NE					
CG3557	FBgn0031423	CG3557	BL54829	HMJ21548		NE					
CG15427	FBgn0010473	tutl	BL54850	HMJ21587		NE					
CG11912	FBgn0031248	CG11912	BL55141	HMC03737		NE					
CG11455	FBgn0031228	CG11455	BL55180	HMC03861		NE					
CG6582	FBgn0027885	Aac11	BL55187	HMC03881		NE					
CG3436	FBgn0031229	CG3436	BL55207	HMC03922		NE					
CG4602	FBgn0024285	Srp54	BL55254	HMC03941		NE					
CG10206	FBgn0026196	nop5	BL55262	HMC03949		NE					
CG17652	FBgn0031361	CG17652	BL55287	HMC03974		NE					
CG3433	FBgn0021944	Coprox	BL55318	HMC04005		NE					
CG7061	FBgn0027505	rab3-GAP	BL55328	HMC04015		NE					
CG5125	FBgn0002938	ninaC	BL55335	HMC04022		NE					
CG3151	FBgn0010263	Rbp9	BL55360	HMC04047		NE					
CG10449	FBgn0002022	Catsup	BL55396	HMC04084		NE					
CG7210	FBgn0001301	kel	BL55612	HMC03751		NE					
CG4793	FBgn0028514	CG4793	BL55621	HMC03765		NE					
CR32879	FBgn0003931	snRNA:U4:38AB	BL55689	HMC03903		NE					
CG4629	FBgn0031299	CG4629	BL55889	HMC04163		NE					

CG4501	FBgn0027348	bgm	BL55918	HMC04204	A	ME	ME	S	NE	ME	
CG17610	FBgn0001137	grk	BL55926	HMC04213		NE					
CG9280	FBgn0001114	Glt	BL55929	HMC04217		NE					
CG5430	FBgn0011294	a5	BL55932	HMC04220		NE					
CG4475	FBgn0020415	Idgf2	BL55935	HMC04223		NE					
CG33119	FBgn0027929	nimB1	BL55937	HMC04225		NE					
CG7644	FBgn0028645	beat-Ib	BL55938	HMC04226		NE					
CG16995	FBgn0031412	CG16995	BL55942	HMC04230		NE					
CG33115	FBgn0028542	nimB4	BL55963	HMC04257		NE					
CG4099	FBgn0014033	Sr-CI	BL56012	HMC04308		NE					
CG5619	FBgn0003751	trk	BL56040	HMC04348		NE					
CG4267	FBgn0264979	CG4267	BL32332	HMS00323		NE					
CG5337	FBgn0032249	CG5337	BL32333	HMS00324		NE					
CG7627	FBgn0032026	CG7627	BL32337	HMS00328	A	ME	ME			ME	
CG9548	FBgn0031822	CG9548	BL32344	HMS00335		NE					
CG6181	FBgn0032340	Ge-1	BL32349	HMS00340		NE					
CG11628	FBgn0086779	step	BL32374	HMS00365	A	E	E			E	
CG9252	FBgn0086251	del	BL32375	HMS00366		NE					
CG42768	FBgn0261836	Msp-300	BL32377	HMS00368		NE					
CG43860	FBgn0264442	ab	BL32378	HMS00369		NE					
CG7840	FBgn0032014	CG7840	BL32379	HMS00370		NE					
CG14945	FBgn0032402	CG14945	BL32384	HMS00376		NE					
CG17331	FBgn0032596	CG17331	BL32390	HMS00384		NE					
CG4738	FBgn0262647	Nup160	BL32391	HMS00385		NE					
CG31753	FBgn0045852	ham	BL32470	HMS00470		NE					
CG16975	FBgn0032475	Sfmbt	BL32473	HMS00473		NE					
CG17494	FBgn0040011	CG17494	BL32509	HMS00513		NE					
CG7787	FBgn0032020	CG7787	BL32843	HMS00625		NE					
CG18096	FBgn0041183	Tep1	BL32856	HMS00641		NE					
CG4260	FBgn0264855	alpha-Adaptin	BL32866	HMS00653		NE					
CG13109	FBgn0041092	tai	BL32885	HMS00673		NE					
CG5181	FBgn0031909	CG5181	BL32888	HMS00676	(ME POSSIBLE)	NE	NE	ME	NE	NE	
CG17293	FBgn0032030	Wdr82	BL32926	HMS00718		NE					
CG33979	FBgn0261458	capt	BL33010	HMS00810		NE					

CG31873	FBgn0260750	Mulk	BL33046	HMS00699		NE					
CG17107	FBgn0032281	CG17107	BL33057	HMS00717		NE					
CG5022	FBgn0032225	CG5022	BL33359	HMS00231		NE					
CG9226	FBgn0031782	WDR79	BL33363	HMS00235		NE					
CG42522	FBgn0261437	CSN8	BL33370	HMS00243		NE					
CG12787	FBgn0041150	hoe1	BL33377	HMS00251		NE					
CG10305	FBgn0261597	RpS26	BL33393	HMS00270	A	E	E			E	
CG12393	FBgn0031768	CG12393	BL33428	HMS00312		NE					
CG8676	FBgn0261239	Hr39	BL33624	HMS00018		NE					
CG3127	FBgn0250906	Pgk	BL33632	HMS00030	ME	ME	NE	ME	NE		NE
CG31666	FBgn0086758	chinmo	BL33638	HMS00036		NE					
CG18591	FBgn0261790	SmE	BL33664	HMS00074		NE					
CG9188	FBgn0031878	sip2	BL33691	HMS00559		NE					
CG3753	FBgn0031655	Marcal1	BL33709	HMS00587		NE					
CG6464	FBgn0261648	salm	BL33714	HMS00594		NE					
CG31884	FBgn0040070	Trx-2	BL33721	HMS00603		NE					
CG14034	FBgn0250847	CG14034	BL33732	HMS00615		NE					
CG5034	FBgn0032223	GATAd	BL33747	HMS01086		NE					
CG33129	FBgn0053129	CG33129	BL33751	HMS01091		NE					
CG42840	FBgn0262029	d	BL33754	HMS01096		NE					
CG10679	FBgn0032725	Nedd8	BL33881	HMS00818		NE					
CG18398	FBgn0032728	Tango6	BL33883	HMS00820		NE					
CG5899	FBgn0032157	Etl1	BL33891	HMS00829		NE					
CG9493	FBgn0031799	Pez	BL33918	HMS00861		NE					
CG12299	FBgn0032295	CG12299	BL33957	HMS00912		NE					
CG7438	FBgn0086347	Myo31DF	BL33971	HMS00928		NE					
CG7830	FBgn0032015	CG7830	BL33979	HMS00939		NE					
CG14939	FBgn0032378	CycY	BL34009	HMS00974		NE					
CG15414	FBgn0031542	CG15414	BL34010	HMS00975		NE					
CG7851	FBgn0032013	Scgalpha	BL34027	HMS00997		NE					
CG9270	FBgn0032908	CG9270	BL34029	HMS00999		NE					
CG5640	FBgn0260749	Utx	BL34076	HMS00575		NE					
CG7870	FBgn0261020	wol	BL34365	HMS01354		NE					
CG6116	FBgn0032499	Uvrag	BL34368	HMS01357		NE					
CG33123	FBgn0053123	CG33123	BL34483	HMS01335		NE					

CG7392	FBgn0044323	Cka	BL34522	HMS00081		NE					
CG10302	FBgn0032679	bsf	BL34550	HMS01022		NE					
CG15628	FBgn0031632	CG15628	BL34555	HMS01027		NE					
CG42641	FBgn0261396	Rpn3	BL34561	HMS01033		NE					
CG9282	FBgn0032518	RpL24	BL34569	HMS01043		NE					
CG3762	FBgn0263598	Vha68-2	BL34582	HMS01056		NE					
CG9273	FBgn0032906	RPA2	BL34587	HMS01061		NE					
CG8817	FBgn0041111	lilli	BL34592	HMS01066	LacZ-S	S		S	S		S
CG13998	FBgn0040949	CG13998	BL34599	HMS01073		NE					
CG34341	FBgn0085370	Pde11	BL34611	HMS01286		NE					
CG3733	FBgn0250786	Chd1	BL34665	HMS01142	E-L	E-L	NE	ME	E-L		NE
CG40006	FBgn0058006	CG40006	BL34691	HMS01170		NE					
CG2615	FBgn0086657	ik2	BL34709	HMS01188		NE					
CG8678	FBgn0032935	Atg18b	BL34715	HMS01194		NE					
CG7138	FBgn0031951	r2d2	BL34784	HMS00093	ME	ME	NE	NE	NE		(ME POSSIBLE)
CG9267	FBgn0032524	CG9267	BL34800	HMS00109		NE					
CG6866	FBgn0032515	loqs	BL34851	HMS00169		NE					
CG10333	FBgn0032690	CG10333	BL34857	HMS00175		NE					
CG31855	FBgn0051855	CG31855	BL34903	HMS01248		NE					
CG8475	FBgn0031995	CG8475	BL34904	HMS01249		NE					
CG15415	FBgn0031549	Spindly	BL34933	HMS01283		NE					
CG6724	FBgn0032298	CG6724	BL34934	HMS01284		NE					
CG6667	FBgn0260632	dl	BL34938	HMS00028		NE					
CG31792	FBgn0051792	CG31792	BL34942	HMS00219		NE					
CG43081	FBgn0262526	vas	BL34950	HMS00373		NE					
CG14023	FBgn0031698	Ncoa6	BL34964	HMS00664	A	ME	ME	MS	NE	E	
CG4063	FBgn0263933	ebi	BL34981	HMS01390		NE					
CG31632	FBgn0051632	sens-2	BL34984	HMS01394		NE					
CG1512	FBgn0032956	Cul-2	BL34988	HMS01398		NE					
CG42685	FBgn0261571	CG42685	BL35005	HMS01415		NE					
CG6453	FBgn0032643	CG6453	BL35008	HMS01418		NE					
CG10722	FBgn0032848	nesd	BL35009	HMS01419		NE					
CG15154	FBgn0041184	Socs36E	BL35036	HMS01450		NE					
CG31676	FBgn0051676	CG31676	BL35727	HMS01469		NE					

CG17927	FBgn0264695	Mhc	BL35729	HMS01471		NE					
CG9539	FBgn0086357	Sec61alpha	BL35730	HMS01472	A	E-L	E-L			E-L	
CG4644	FBgn0261938	mtRNApol	BL35732	HMS01474		NE					
CG17906	FBgn0032086	CG17906	BL35767	HMS01516		NE					
CG6055	FBgn0031918	CG6055	BL35778	HMS01528		NE					
CG7380	FBgn0031977	baf	BL36108	HMS00195		NE					
CG42366	FBgn0259712	CG42366	BL36112	HMS00987	A	ME	ME			E	
CG4494	FBgn0264922	smt3	BL36125	HMS01540	A	E	ME			E	
CG8846	FBgn0261560	Thor/4E-BP	BL36667	HMS01555		NE					
CG14016	FBgn0031715	tomb	BL36669	HMS01557		NE					
CG33196	FBgn0053196	dp	BL36673	HMS01561		NE					
CG9573	FBgn0032089	Rcd-1r	BL36683	HMS01571		NE					
CG42616	FBgn0261268	Cul-3	BL36684	HMS01572	A	ME	ME		NE	ME	
CG17161	FBgn0261278	grp/Chk1	BL36685	HMS01573	S	S		S	MS		NE
CG18662	FBgn0040963	CG18662	BL36710	HMS01600		NE					
CG8902	FBgn0031886	Nuf2	BL36725	HMS01616		NE					
CG12314	FBgn0261266	zuc	BL36742	HMS03002		NE					
CG13969	FBgn0045064	bwa	BL36765	HMS03026		NE					
CG31886	FBgn0032079	CG31886	BL36769	HMS03030		NE					
CG12292	FBgn0032451	spict	BL37505	HMS01647		NE					
CG8222	FBgn0032006	Pvr	BL37520	HMS01662		NE					
CG31708	FBgn0051708	CG31708	BL38227	HMS01671		NE					
CG31694	FBgn0051694	CG31694	BL38228	HMS01672		NE					
CG14010	FBgn0031725	CG14010	BL38229	HMS01673		NE					
CG11320	FBgn0031837	CG11320	BL38231	HMS01675		NE					
CG31930	FBgn0045498	Gr22d	BL38248	HMS01692		NE					
CG3305	FBgn0032949	Lamp1	BL38254	HMS01698		NE					
CG3338	FBgn0031598	CG3338	BL38267	HMS01712		NE					
CG7371	FBgn0031710	CG7371	BL38268	HMS01713		NE					
CG4427	FBgn0043364	cbt	BL38276	HMS01726		NE					
CG8282	FBgn0032005	Snx6	BL38278	HMS01729		NE					
CG10538	FBgn0032821	CdGAPr	BL38279	HMS01730		NE					
CG17840	FBgn0031611	CG17840	BL38291	HMS01749		NE					
CG9298	FBgn0260861	Trs23	BL38303	HMS01765		NE					
CG31860	FBgn0051860	CG31860	BL38312	HMS01776		NE					

CG6214	FBgn0032456	MRP	BL38316	HMS01780		NE					
CG31793	FBgn0051793	CG31793	BL38319	HMS01783		NE					
CG8679	FBgn0032934	CG8679	BL38348	HMS01816		NE					
CG9138	FBgn0031879	uif	BL38354	HMS01822	A	E	ME			E	
CG10413	FBgn0032689	CG10413	BL38364	HMS01833		NE					
CG42368	FBgn0259714	CG42368	BL38936	HMS01718		NE					
CG7102	FBgn0031961	CG7102	BL38939	HMS01789		NE					
CG10188	FBgn0032796	CG10188	BL38942	HMS01856		NE					
CG9426	FBgn0032485	CG9426	BL38946	HMS01860		NE					
Pvf3	FBgn0085407	Pvf3	BL38962	HMS01876		NE					
holn1	FBgn0032250	holn1	BL38968	HMS01882		NE					
CG7806	FBgn0032018	CG7806	BL38997	HMS01913		NE					
Tsp29Fb	FBgn0032075	Tsp29Fb	BL39042	HMS01962		NE					
Tsp33B	FBgn0032376	Tsp33B	BL39043	HMS01963		NE					
CG5446	FBgn0032429	CG5446	BL40824	HMS00624		NE					
Tsp29Fa	FBgn0032074	Tsp29Fa	BL40829	HMS01995		NE					
CYLD	FBgn0032210	CYLD	BL40840	HMS02006		NE					
CadN2	FBgn0262018	CadN2	BL40889	HMS02137		NE					
CG5261	FBgn0031912	CG5261	BL40922	HMS02170		NE					
CG34345	FBgn0085374	CG34345	BL40941	HMS02189		NE					
Klp31E	FBgn0032243	Klp31E	BL40943	HMS02191		NE					
Tsp26A	FBgn0031760	Tsp26A	BL40946	HMS02194		NE					
CG6750	FBgn0032292	CG6750	BL41678	HMS02242		NE					
CG4747	FBgn0043456	CG4747	BL41698	HMS02263		NE					
CG13384	FBgn0032036	CG13384	BL41703	HMS02268		NE					
Myo28B1	FBgn0040299	Myo28B1	BL41717	HMS02282		NE					
CG10376	FBgn0032702	CG10376	BL41907	HMS02300		NE					
CG4495	FBgn0031893	CG4495	BL41909	HMS02302		NE					
CG3513	FBgn0031559	CG3513	BL41918	HMS02315		NE					
CG13996	FBgn0031763	CG13996	BL41921	HMS02318		NE					
Dpy-30L1	FBgn0032293	Dpy-30L1	BL41946	HMS02343		NE					
Spf45	FBgn0086683	Spf45	BL41954	HMS02351		NE					
Dh31	FBgn0032048	Dh31	BL41957	HMS02354		NE					
CG8671	FBgn0032938	CG8671	BL41965	HMS02362		NE					
CG18563	FBgn0032639	CG18563	BL41974	HMS02372		NE					

CG12404	FBgn0032465	CG12404	BL41989	HMS02388		NE					
CG10621	FBgn0032726	CG10621	BL42011	HMS02412		NE					
CG31716	FBgn0051716	Cnot4	BL42513	HMJ02078		NE					
CG31720	FBgn0051720	mthl15	BL42515	HMJ02080		NE					
CG14001	FBgn0043362	bchs	BL42517	HMJ02083		NE					
CG5545	FBgn0032651	Oli	BL42560	HMJ02216		NE					
CG9257	FBgn0032916	CG9257	BL42582	HMS02123		NE					
CG15630	FBgn0031627	CG15630	BL42589	HMS02421		NE					
CG16974	FBgn0032479	CG16974	BL42590	HMS02422		NE					
CG9029	FBgn0031746	CG9029	BL42593	HMS02425		NE					
CG31794	FBgn0041789	Pax	BL42614	HMS02449		NE					
CG7123	FBgn0261800	LanB1	BL42616	HMS02451		NE					
CG31774	FBgn0051774	fred	BL42621	HMS02456		NE					
CG42820	FBgn0262002	CG42820	BL42623	HMS02458		NE					
CG10806	FBgn0031865	Nha1	BL42648	HMS02484		NE					
CG7094	FBgn0032650	CG7094	BL42653	HMS02489		NE					
CG10178	FBgn0032684	CG10178	BL42657	HMS02493		NE					
CG10702	FBgn0032752	CG10702	BL42663	HMS02499		NE					
CG33643	FBgn0053643	CG33643	BL42823	HMS02505		NE					
CG3604	FBgn0031562	CG3604	BL42829	HMS02513		NE					
CG4584	FBgn0250837	dUTPase	BL42835	HMS02527		NE					
CG31730	FBgn0051730	CG31730	BL42848	HMS02540		NE					
CG18125	FBgn0264253	Send2	BL42850	HMS02542		NE					
CG15443	FBgn0031609	CG15443	BL42864	HMS02557		NE					
CG4482	FBgn0086711	mol	BL42867	HMS02560		NE					
CG5972	FBgn0031781	Arpc4	BL42875	HMS02568		NE					
CG10651	FBgn0032853	CG10651	BL42885	HMS02578		NE					
CG10470	FBgn0032746	CG10470	BL42896	HMS02589		NE					
CG31776	FBgn0051776	CG31776	BL42897	HMS02590		NE					
CG31901	FBgn0051901	Mur29B	BL42918	HMS02611		NE					
CG6766	FBgn0032398	CG6766	BL42924	HMS02617		NE					
CG17104	FBgn0040496	CG17104	BL42925	HMS02618		NE					
CG33120	FBgn0053120	CG33120	BL42934	HMS02627		NE					
CG9994	FBgn0032782	Rab9	BL42942	HMS02635		NE					
CG5075	FBgn0032464	Vha68-3	BL42954	HMS02647		NE					

CG17291	FBgn0260439	Pp2A-29B	BL43283	HMS01921		NE					
CG42403	FBgn0259822	Ca-beta	BL43292	HMS02664		NE					
CG5776	FBgn0032450	CG5776	BL43299	HMS02672		NE					
CG4988	FBgn0032372	CG4988	BL43303	HMS02676		NE					
CG17108	FBgn0032285	CG17108	BL43313	HMS02697		NE					
CG9107	FBgn0031764	CG9107	BL43547	HMS02555	S	S		S	E		NE
CG15627	FBgn0031634	Ir25a	BL43985	HMC02682		NE					
CG10623	FBgn0032727	CG10623	BL43986	HMC02683		NE					
CG13965	FBgn0032834	CG13965	BL44015	HMS02729		NE					
CG6153	FBgn0032445	CG6153	BL44017	HMS02732		NE					
CG31849	FBgn0051849	CG31849	BL44020	HMS02735		NE					
CG15479	FBgn0032493	CG15479	BL44024	HMS02739		NE					
CG42296	FBgn0259192	CG42296	BL44028	HMS02744		NE					
CG2976	FBgn0031633	CG2976	BL44032	HMS02748		NE					
CG12264	FBgn0032393	CG12264	BL44037	HMS02753		NE					
CG16771	FBgn0032779	CG16771	BL44042	HMS02758		NE					
CG33510	FBgn0053510	CG33510	BL44069	HMS02786		NE					
CG34380	FBgn0085409	CG34380	BL44089	HMS02806		NE					
CG10348	FBgn0032707	CG10348	BL44091	HMS02808		NE					
CG11326	FBgn0031850	Tsp	BL44116	HMS02838		NE					
CG10431	FBgn0032730	CG10431	BL44470	HMC02345		NE					
CG5322	FBgn0032253	Lysosomal α-mannosidase I	BL44473	HMC02357	E	E	NE	S	NE		NE
CG43227	FBgn0262872	milt	BL44477	HMC02365		NE					
CG8869	FBgn0031654	Jon25Bii	BL44504	HMC02890		NE					
CG31741	FBgn0051741	CG31741	BL44518	HMC02908		NE					
CG31690	FBgn0051690	CG31690	BL44525	HMC02919		NE					
CG5423	FBgn0041097	robo3	BL44539	HMC02934		NE					
CG3696	FBgn0086902	kis	BL44542	HMC02937		NE					
CG5352	FBgn0262601	SmB	BL44544	HMC02939	A	ME	ME			ME	
CG4140	FBgn0261881	l(2)35Be	BL44545	HMC02941		NE					
CG7221	FBgn0031972	Wwox	BL44546	HMC02942		NE					
CG13948	FBgn0041250	Gr21a	BL44554	HMS02850		NE					
CG9547	FBgn0031824	CG9547	BL44556	HMS02852		NE					
CG7299	FBgn0032282	CG7299	BL44557	HMS02853		NE					
CG11630	FBgn0032964	CG11630	BL44566	HMS02862		NE					

CG2637	FBgn0262743	Fs(2)Ket	BL44576	HMS02872	A	E-L	ME	E	ME	ME	
CG33801	FBgn0053801	His1:CG33801	BL44582	HMS02879		NE					
CG7309	FBgn0032314	CG7309	BL44653	HMC02417	S	S		S	MS		NE
CG7228	FBgn0031969	pes	BL50612	HMC02979		NE					
CG7227	FBgn0031970	CG7227	BL50613	HMC02980		NE					
CG43065	FBgn0262475	bru-2	BL50627	HMC02994		NE					
CG18619	FBgn0032202	Reptor-BP	BL50658	HMC03059	ME	ME	NE	ME	ME		NE
CG7219	FBgn0031973	Spn28D	BL50670	HMC03071		NE					
CG6634	FBgn0261963	mid	BL50681	HMC03082		NE					
CG16869	FBgn0032535	Ance-2	BL50691	HMC03092		NE					
CG5325	FBgn0032407	Pex19	BL50702	HMC03104		NE					
CG10166	FBgn0032799	CG10166	BL50713	HMS02947		NE					
CG1428	FBgn0032967	CG1428	BL50715	HMS02949		NE					
CG14036	FBgn0031677	CG14036	BL50717	HMS02951		NE					
CG8663	FBgn0032946	nrv3	BL50725	HMS02961		NE					
CG5427	FBgn0032433	Oatp33Ea	BL50736	HMS02972		NE					
CG6860	FBgn0032633	Lrch	BL50901	HMJ03119		NE					
CG9246	FBgn0032925	CG9246	BL50907	HMJ03129		NE					
CG34136	FBgn0083972	CG34136	BL50936	HMJ21031		NE					
CG3539	FBgn0264978	Slh	BL50940	HMJ21035		NE					
CG15138	FBgn0032629	beat-IIIc	BL50941	HMJ21036		NE					
CG17098	FBgn0032276	CG17098	BL50950	HMJ21051	A	ME	ME	MS	E	E	
CG10268	FBgn0032811	CG10268	BL50955	HMJ21057	A	E	E			E	
CG5439	FBgn0032476	CG5439	BL50957	HMJ21059		NE					
CG33194	FBgn0053194	CheA29a	BL50978	HMJ21084		NE					
CG6717	FBgn0083141	Spn28B	BL50996	HMJ21109		NE					
CG42238	FBgn0250867	CG42238	BL51023	HMJ21149		NE					
CG9568	FBgn0032087	CG9568	BL51025	HMJ21151	(MS POSSIBLE)	NE		S	E		
CG13784	FBgn0031897	CG13784	BL51027	HMJ21154		NE					
CG42474	FBgn0259964	Sfp33A3	BL51052	HMJ21186		NE					
CG4496	FBgn0031894	CG4496	BL51428	HMC03034	ME	ME	NE	ME	NE		NE
CG14351	FBgn0261509	haf	BL51438	HMC03152		NE					
CG9256	FBgn0040297	Nhe2	BL51491	HMC03243		NE					
CG6504	FBgn0041195	Pkd2	BL51502	HMC03263		NE					

CG31660	FBgn0051660	pog	BL51705	HMC03192		NE					
CG14014	FBgn0031718	CG14014	BL51737	HMS03168		NE					
CG4636	FBgn0041781	SCAR	BL51803	HMC03361		NE					
CG15274	FBgn0260446	GABA-B-R1	BL51817	HMC03388		NE					
CG31729	FBgn0051729	CG31729	BL51819	HMC03390		NE					
CG31760	FBgn0051760	CG31760	BL51838	HMC03410		NE					
CG33298	FBgn0032120	CG33298	BL51841	HMC03414		NE			NE		
CG14043	FBgn0031659	CG14043	BL51858	HMC03432		NE					
CG8891	FBgn0031663	CG8891	BL51859	HMC03433		NE					
CG8680	FBgn0031684	CG8680	BL51860	HMC03434		NE					
CG10399	FBgn0031877	CG10399	BL51861	HMC03435		NE					
CG13778	FBgn0031885	Mnn1	BL51862	HMC03436		NE					
CG4908	FBgn0032195	CG4908	BL51863	HMC03437		NE					
CG5037	FBgn0032222	CG5037	BL51864	HMC03438		NE					
CG5091	FBgn0032234	gny	BL51865	HMC03439		NE					
CG6415	FBgn0032287	CG6415	BL51867	HMC03441		NE					
CG17036	FBgn0032449	CG17036	BL51868	HMC03442		NE					
CG5287	FBgn0032477	CG5287	BL51869	HMC03443		NE					
CG10639	FBgn0032729	CG10639	BL51870	HMC03444		NE					
CG31692	FBgn0032820	fbp	BL51871	HMC03445		NE					
CG9342	FBgn0032904	Mtp	BL51872	HMC03446		NE					
CG3262	FBgn0032986	CG3262	BL51873	HMC03447		NE					
CG8349	FBgn0032003	CG8349	BL51914	HMS03372		NE					
CG8353	FBgn0032002	CG8353	BL51915	HMS03373		NE					
CG8360	FBgn0032001	CG8360	BL51916	HMS03374		NE					
CG14535	FBgn0031955	CG14535	BL51936	HMC03285		NE					
CG15828	FBgn0032136	CG15828	BL51937	HMC03294		NE					
CG31605	FBgn0261822	Bsg	BL52110	HMC03195		NE					
CG5390	FBgn0032213	CG5390	BL52875	HMC03613		NE					
CG4128	FBgn0032151	nAcRalpha-30D	BL52885	HMC03623		NE					
CG17597	FBgn0032715	cad	BL52886	HMC03624		NE					
CG3355	FBgn0031619	CG3355	BL52897	HMC03636		NE					
CG31739	FBgn0051739	CG31739	BL52909	HMC03649		NE					
CG15434	FBgn0040705	CG15434	BL52913	HMC03653		NE					
CG6287	FBgn0032350	CG6287	BL52928	HMC03669		NE					

CG13277	FBgn0261068	LSm7	BL52932	HMC03674		NE					
CG9140	FBgn0031771	CG9140	BL52939	HMJ21591		NE					
CG34174	FBgn0085203	CG34174	BL52943	HMJ21610		NE					
CG11050	FBgn0031836	CG11050	BL52970	HMJ21655		NE					
CG12795	FBgn0031535	CG12795	BL52988	HMJ21680		NE					
CG17134	FBgn0032304	CG17134	BL53023	HMJ21746		NE					
CG3651	FBgn0032974	CG3651	BL53028	HMJ21753		NE					
CG15167	FBgn0032709	CG15167	BL53031	HMJ21757		NE					
CG17118	FBgn0032291	CG17118	BL53304	HMC03531		NE					
CG5996	FBgn0032593	trpgamma	BL53313	HMC03542		NE					
CG31803	FBgn0051803	CG31803	BL53338	HMC03567		NE					
CG31954	FBgn0051954	CG31954	BL53674	HMC03607		NE					
CG10473	FBgn0263198	Acn	BL53676	HMC03673		NE					
CG7456	FBgn0032258	CG7456	BL53679	HMJ21592		NE					
CG11199	FBgn0046704	Liprin-alpha	BL53868	HMC03183		NE					
CG10833	FBgn0031689	Cyp28d1	BL53892	HMJ21210		NE					
CG31802	FBgn0051802	CG31802	BL53893	HMJ21211		NE					
CG8890	FBgn0031661	Gmd	BL53912	HMJ21245	A	E-L	E			E	
CG10338	FBgn0032700	CG10338	BL53913	HMJ21246		NE					
CG9305	FBgn0032512	CG9305	BL53915	HMJ21248		NE					
CG10414	FBgn0032691	Atac2	BL53918	HMJ21253		NE					
CG31641	FBgn0051641	stai	BL53925	HMJ21270		NE					
CG13270	FBgn0040262	Ugt36Ba	BL53931	HMJ21279		NE					
CG16825	FBgn0032503	CG16825	BL53973	HMJ21358		NE					
CG4904	FBgn0250843	Pros35	BL53974	HMJ21359	A	ME	ME	MS	E	ME	
CG14011	FBgn0031722	CG14011	BL53993	HMJ21397	MS	MS		NE	E		NE
CG6392	FBgn0040232	cmet	BL54004	HMJ21427	A	ME	E			E	
CG5727	FBgn0032193	CG5727	BL54021	HMJ21447		NE					
CG14031	FBgn0031695	Cyp4ac3	BL54023	HMJ21449		NE					
CG43720	FBgn0263873	sick	BL54037	HMJ21480		NE					
CG10174	FBgn0032680	Ntf-2r	BL54462	HMS03723		NE					
CG16997	FBgn0263235	Phae2	BL54805	HMJ21499		NE					
CG42533	FBgn0260486	CG42533	BL54817	HMJ21536		NE					
CG15145	FBgn0032649	CG15145	BL54837	HMJ21556		NE					
CG5381	FBgn0032218	CG5381	BL54847	HMJ21584		NE					

CG31950	FBgn0051950	CG31950	BL55161	HMC03836		NE					
CG3058	FBgn0031601	Dim1	BL55171	HMC03851		NE					
CG13999	FBgn0031753	CG13999	BL55177	HMC03858		NE					
CG8885	FBgn0262467	Scox	BL55179	HMC03860		NE					
CG9232	FBgn0263200	Galt	BL55191	HMC03885		NE					
CG6488	FBgn0032361	CG6488	BL55192	HMC03886		NE					
CG17242	FBgn0250841	CG17242	BL55198	HMC03896	A	ME	ME			E	
CG6686	FBgn0032388	CG6686	BL55202	HMC03913	A	ME	ME		E	ME	
CG5648	FBgn0032492	Prosalpha6T	BL55243	HMC02418		NE					
CG5343	FBgn0032248	CG5343	BL55258	HMC03945		NE					
CG10466	FBgn0032822	CG10466	BL55263	HMC03950		NE					
CG12512	FBgn0031703	CG12512	BL55269	HMC03956		NE					
CG31619	FBgn0051619	CG31619	BL55296	HMC03983		NE					
CG17988	FBgn0032536	Ance-3	BL55298	HMC03985		NE					
CG34395	FBgn0085424	nub	BL55305	HMC03992		NE					
CG4132	FBgn0040079	pkaap	BL55333	HMC04020		NE					
CG17239	FBgn0042186	CG17239	BL55336	HMC04023		NE					
CG8871	FBgn0031653	Jon25Biii	BL55344	HMC04031		NE					
CG14934	FBgn0032381	Mal-B1	BL55346	HMC04033		NE					
CR32881	FBgn0043022	snRNA:U5:38ABa	BL55361	HMC04048		NE					
CG3225	FBgn0031631	CG3225	BL55365	HMC04053		NE					
CG18787	FBgn0042125	CG18787	BL55375	HMC04063		NE					
CG17571	FBgn0259998	CG17571	BL55408	HMC04096		NE					
CG17234	FBgn0042187	CG17234	BL55611	HMC03750		NE					
CG9377	FBgn0032507	CG9377	BL55623	HMC03767		NE					
CG31852	FBgn0051852	Tap42	BL55625	HMC03769		NE					
CG31728	FBgn0051728	CG31728	BL55628	HMC03773		NE					
CG4779	FBgn0040211	hgo	BL55629	HMC03775		NE					
CG17657	FBgn0086698	frtz	BL55649	HMC03798		NE					
CG31812	FBgn0051812	CG31812	BL55659	HMC03813		NE					
CR32989	FBgn0041717	snRNA:U6atac:29B	BL55666	HMC03821		NE					
CG3294	FBgn0031628	CG3294	BL55691	HMC03905		NE					
CG11266	FBgn0031883	Caper	BL55742	HMC03924	(MS POSSIBLE)	NE			E		
CG6639	FBgn0032638	CG6639	BL55853	HMC03740		NE					

CG9333	FBgn0032891	Oseg5	BL55856	HMC03888		NE					
CG43756	FBgn0264087	Slob	BL55879	HMC04152		NE					
CG9222	FBgn0031784	CG9222	BL55890	HMC04165		NE					
CG4839	FBgn0032187	CG4839	BL55891	HMC04168		NE					
CG33531	FBgn0053531	Ddr	BL55906	HMC04190		NE					
CG15284	FBgn0264810	pburs	BL55924	HMC04211		NE					
CG44007	FBgn0264815	Pde1c	BL55925	HMC04212		NE					
CG6431	FBgn0032289	CG6431	BL55943	HMC04231		NE					
CG17905	FBgn0032598	ChLD3	BL55944	HMC04232		NE					
CG14405	FBgn0032888	CheB38c	BL55945	HMC04233	A	ME	ME	MS		ME	
CG33117	FBgn0053117	Victoria	BL55953	HMC04242		NE					
CG13990	FBgn0040950	Muc26B	BL55986	HMC04282		NE					
CG17814	FBgn0040959	Peritrophin-15a	BL55987	HMC04283		NE					
CG31681	FBgn0051681	CG31681	BL55994	HMC04290		NE					
CG31704	FBgn0051704	CG31704	BL55995	HMC04291		NE					
CG31973	FBgn0051973	Cda5	BL55996	HMC04292		NE					
CG34102	FBgn0083938	BG642163	BL56001	HMC04297		NE					
CG34447	FBgn0085476	CG34447	BL56002	HMC04298		NE					
CG34448	FBgn0085477	CG34448	BL56003	HMC04299	A	E	E			E	
CG31893	FBgn0040958	Peritrophin-15b	BL56019	HMC04315		NE					
CG7068	FBgn0041181	Tep3	BL56020	HMC04316		NE					
CG7532	FBgn0261534	l(2)34Fc	BL56023	HMC04319		NE			E		
CG16820	FBgn0032495	CG16820	BL56027	HMC04323		NE					
CG10730	FBgn0032843	CG10730	BL56028	HMC04324		NE					
CG31751	FBgn0086909	CG31751	BL56030	HMC04338		NE					
CG12288	FBgn0032620	CG12288	BL56037	HMC04345		NE					
CG16712	FBgn0031561	CG16712	BL56047	HMS04250		NE					
CG5726	FBgn0034313	CG5726	BL32335	HMS00326		NE					
CG8707	FBgn0033272	RagC-D	BL32342	HMS00333		NE					
CG3845	FBgn0010488	NAT1	BL32357	HMS00348	S	S		NE	ME		NE
CG2173	FBgn0021995	Rs1	BL32363	HMS00354		NE					
CG8815	FBgn0022764	Sin3A	BL32368	HMS00359		NE					
CG10212	FBgn0027783	SMC2	BL32369	HMS00360		NE					
CG6805	FBgn0034179	CG6805	BL32380	HMS00371		NE					
CG8416	FBgn0014020	Rho1	BL32383	HMS00375	A	E	E			E	

CG32885	FBgn0016053	pgc	BL32386	HMS00378		NE					
CG34207	FBgn0085236	CG34207	BL32387	HMS00379		NE					
CG5820	FBgn0013272	Gp150	BL32400	HMS00395		NE					
CG3879	FBgn0004512	Mdr49	BL32405	HMS00400		NE					
CG17704	FBgn0026401	Nipped-B	BL32406	HMS00401	ME	ME	NE	NE	NE		NE
CG2917	FBgn0023181	Orc4	BL32409	HMS00404		NE					
CG11084	FBgn0003090	pk	BL32413	HMS00408		NE					
CG8804	FBgn0016078	wun	BL32429	HMS00424		NE					
CG10082	FBgn0034644	CG10082	BL32431	HMS00427		NE					
CG34399	FBgn0085428	Nox	BL32433	HMS00429		NE					
CG2044	FBgn0002535	Lcp4	BL32455	HMS00454		NE					
CG1825	FBgn0010342	Map60	BL32458	HMS00457		NE					
CG6061	FBgn0033846	mip120	BL32461	HMS00461		NE					
CG7200	FBgn0032671	CG7200	BL32485	HMS00488		NE					
CG8411	FBgn0005695	gcl	BL32492	HMS00495		NE					
CG30356	FBgn0050356	CG30356	BL32493	HMS00496		NE					
CG8905	FBgn0010213	Sod2	BL32496	HMS00499		NE					
CG12405	FBgn0033520	Prx2540-1	BL32497	HMS00500		NE					
CG15119	FBgn0034430	mip40	BL32834	HMS00524		NE					
CG34407	FBgn0085436	Not1	BL32836	HMS00526	A	E	ME	ME		E	
CG12110	FBgn0033075	Pld	BL32839	HMS00529		NE					
CG7843	FBgn0033062	Ars2	BL32844	HMS00626		NE					
CG8625	FBgn0011604	Iswi	BL32845	HMS00628		NE					
CG10155	FBgn0020767	Spred	BL32852	HMS00637		NE					
CG8975	FBgn0011704	RnrS	BL32864	HMS00651		NE					
CG6050	FBgn0024556	EfTuM	BL32868	HMS00655		NE					
CG5170	FBgn0027835	Dp1	BL32872	HMS00659		NE					
CG8266	FBgn0033339	sec31	BL32878	HMS00666		NE					
CG8309	FBgn0033902	Tango7/eIF3m	BL32879	HMS00667	A	ME	ME			ME	
CG4878	FBgn0034237	eIF3-S9	BL32880	HMS00668	E	E	NE	E-L	E-L		NE
CG5174	FBgn0034345	CG5174	BL32881	HMS00669		NE					
CG9862	FBgn0034646	Rae1	BL32882	HMS00670		NE					
CG10578	FBgn0263106	DnaJ-1	BL32899	HMS00688		NE					
CG3722	FBgn0003391	shg	BL32904	HMS00693	A	E	E			E	
CG12252	FBgn0035026	Fcp1	BL32925	HMS00716		NE					

CG8529	FBgn0033739	Dyb	BL32935	HMS00728		NE					
CG11482	FBgn0011659	Mlh1	BL32940	HMS00734		NE					
CG8274	FBgn0013756	Mtor	BL32941	HMS00735		NE					
CG8068	FBgn0003612	Su(var)2-10	BL32956	HMS00750	A	ME	ME			ME	
CG13350	FBgn0033890	Ctf4	BL32968	HMS00764		NE					
CG13745	FBgn0033354	FANCI	BL32972	HMS00769	ME	ME	NE	NE	E-L		NE
CG1242	FBgn0001233	Hsp83	BL32996	HMS00796		NE					
CG8426	FBgn0033029	l(2)NC136/Not3	BL33002	HMS00802	LacZ-E	E	NE	ME	E-L		E
CG4466	FBgn0001226	Hsp27	BL33007	HMS00807		NE					
CG3825	FBgn0034948	Gadd34/PPP1R15	BL33011	HMS00811		NE					
CG9193	FBgn0005655	mus209	BL33043	HMS00634		NE					
CG5859	FBgn0025830	IntS8	BL33048	HMS00721	E	E	NE	NE	ME	NE	NE
CG12340	FBgn0027499	wde	BL33339	HMS00205		NE					
CG13096	FBgn0032050	CG13096	BL33340	HMS00206		NE					
CG44153	FBgn0265002	CG44153	BL33350	HMS00218		NE					
CG3253	FBgn0041706	CG3253	BL33351	HMS00220		NE					
CG9005	FBgn0033638	CG9005	BL33362	HMS00234		NE					
CG6556	FBgn0021818	cnk	BL33366	HMS00238		NE					
CG8710	FBgn0033265	coil	BL33368	HMS00240		NE					
CG4654	FBgn0011763	Dp	BL33372	HMS00245		NE					
CG9854	FBgn0015949	hrg	BL33378	HMS00252	ME	ME	NE	E	ME		(MS POSSIBLE)
CG5373	FBgn0015277	Pi3K59F	BL33384	HMS00261		NE					
CG12367	FBgn0033686	Hen1	BL33385	HMS00262		NE					
CG8991	FBgn0033654	Sobp	BL33397	HMS00275		NE					
CG3905	FBgn0008654	Su(z)2	BL33403	HMS00281		NE					
CG30388	FBgn0034590	Magi	BL33411	HMS00291		NE					
CG10249	FBgn0027596	CG10249	BL33432	HMS00319		NE					
CG1389	FBgn0003733	tor	BL33627	HMS00021		NE					
CG6493	FBgn0034246	Dcr-2	BL33656	HMS00062		NE					
CG8730	FBgn0026722	drosha	BL33657	HMS00064		NE					
CG1519	FBgn0023175	Prosalpha7	BL33660	HMS00068	A	E	E			E	
CG2038	FBgn0028836	CSN7	BL33663	HMS00073		NE					
CG4254	FBgn0011726	tsr	BL33670	HMS00534		NE					
CG1406	FBgn0033210	U2A	BL33671	HMS00535		NE					

CG15117	FBgn0034417	CG15117	BL33693	HMS00562		NE					
CG9015	FBgn0000577	en	BL33715	HMS00595		NE					
CG1381	FBgn0033485	RpLP0-like	BL33730	HMS00613	E	E	NE	NE	ME		NE
CG17385	FBgn0033934	CG17385	BL33734	HMS00617		NE					
CG18446	FBgn0033458	CG18446	BL33735	HMS00618		NE					
CG6370	FBgn0034277	CG6370	BL33752	HMS01092		NE					
CG8166	FBgn0034013	unc-5	BL33756	HMS01099		NE					
CG4921	FBgn0016701	Rab4	BL33757	HMS01100		NE					
CG6518	FBgn0004784	inaC	BL33768	JF02958		NE					
CG8397	FBgn0034066	CG8397	BL33877	HMS00814		NE					
CG16720	FBgn0004168	5-HT1A	BL33885	HMS00823		NE					
CG10241	FBgn0015714	Cyp6a17	BL33887	HMS00825		NE					
CG3820	FBgn0010660	Nup214	BL33897	HMS00837		NE					
CG8243	FBgn0033349	CG8243	BL33927	HMS00876		NE					
CG17064	FBgn0033845	mars	BL33929	HMS00878		NE					
CG1341	FBgn0028687	Rpt1	BL33930	HMS00879	A	E	E			E	
CG8983	FBgn0033663	ERp60	BL33935	HMS00885		NE					
CG16932	FBgn0035060	Eps-15	BL33942	HMS00893		NE					
CG5109	FBgn0003044	Pcl	BL33946	HMS00897		NE					
CG8280	FBgn0000556	Ef1alpha48D	BL33960	HMS00917		NE					
CG12190	FBgn0034763	RYBP	BL33974	HMS00931		NE					
CG30345	FBgn0050345	CG30345	BL33994	HMS00957		NE					
CG12128	FBgn0033473	CG12128	BL33997	HMS00960		NE					
CG15095	FBgn0010651	l(2)08717	BL33999	HMS00962		NE					
CG33519	FBgn0053519	Unc-89	BL34000	HMS00963		NE					
CG10207	FBgn0016684	NaPi-T	BL34003	HMS00966		NE					
CG12324	FBgn0033555	RpS15Ab	BL34008	HMS00973		NE					
CG5465	FBgn0034707	MED16	BL34012	HMS00978		NE					
CG4038	FBgn0011824	CG4038	BL34013	HMS00979	(ME POSSIBLE)	NE					
CG30067	FBgn0050067	Obp50a	BL34023	HMS00993		NE					
CG4005	FBgn0034970	yki	BL34067	HMS00041	A	ME	ME	NE	NE	ME	
CG10683	FBgn0004400	rhi	BL34071	HMS00069		NE					
CG8728	FBgn0033235	CG8728	BL34074	HMS00561		NE					
CG4049	FBgn0034976	CG4049	BL34077	HMS00584		NE					

CG33348	FBgn0053348	CheB42a	BL34078	HMS00590		NE					
CG2065	FBgn0033204	CG2065	BL34098	HMS00984		NE					
CG10917	FBgn0000658	fj	BL34323	HMS01310		NE					
CG2328	FBgn0000606	eve	BL34325	HMS01312		NE					
CG9485	FBgn0034618	CG9485	BL34333	HMS01321		NE					
CG4001	FBgn0003071	Pfk	BL34336	HMS01324		NE					
CG4062	FBgn0027079	Aats-val	BL34338	HMS01326		NE					
CG10253	FBgn0033983	CG10253	BL34350	HMS01339		NE					
CG8075	FBgn0015838	Vang	BL34354	HMS01343		NE					
CG5489	FBgn0034366	Atg7	BL34369	HMS01358		NE					
CG8261	FBgn0004921	Ggamma1	BL34372	HMS01361		NE					
CG6562	FBgn0034691	synj	BL34378	HMS01368		NE					
CG30456	FBgn0050456	CG30456	BL34380	HMS01370		NE					
CG13192	FBgn0033653	CG13192	BL34390	HMS01384		NE					
CG8298	FBgn0033673	CG8298	BL34524	HMS00813		NE					
CG4581	FBgn0025352	Thiolase	BL34546	HMS01017		NE					
CG13551	FBgn0040660	CG13551	BL34554	HMS01026		NE					
CG2158	FBgn0033264	Nup50	BL34580	HMS01054		NE					
CG6459	FBgn0034259	P32	BL34585	HMS01059		NE					
CG2163	FBgn0005648	Pabp2	BL34602	HMS00553		NE					
CG8472	FBgn0000253	Cam	BL34609	HMS01318		NE					
CG40293	FBgn0046692	Stlk	BL34620	HMS01295		NE					
CG8877	FBgn0033688	Prp8	BL34622	HMS01297		NE					
CG15835	FBgn0033233	Kdm4A	BL34629	HMS01304		NE					
CG3340	FBgn0001325	Kr	BL34632	HMS01106		NE					
CG9635	FBgn0023172	RhoGEF2	BL34643	HMS01118		NE					
CG16778	FBgn0003715	CG16778	BL34651	HMS01126		NE					
CG8819	FBgn0033749	achi	BL34652	HMS01127		NE					
CG2204	FBgn0001122	G-oalpha47A	BL34653	HMS01129		NE					
CG7576	FBgn0005586	Rab3	BL34655	HMS01131		NE					
CG8367	FBgn0000289	cg	BL34668	HMS01145		NE					
CG15104	FBgn0034410	Topors	BL34671	HMS01149	MS	MS		NE	NE		NE
CG14767	FBgn0040777	CG14767	BL34679	HMS01157		NE					
CG7734	FBgn0003396	shn	BL34689	HMS01167		NE					
CG8980	FBgn0026402	NiPp1	BL34696	HMS01175		NE					

CG6622	FBgn0003091	Pkc53E	BL34716	HMS01195		NE					
CG18324	FBgn0033905	CG18324	BL34720	HMS01199		NE					
CG8791	FBgn0033234	CG8791	BL34728	HMS01207		NE					
CG8920	FBgn0027529	CG8920	BL34738	HMS01218		NE					
CG5575	FBgn0011236	ken	BL34739	HMS01219	E	E	NE	ME	ME		NE
CG8293	FBgn0015247	Iap2	BL34776	HMS00085		NE					
CG10938	FBgn0016697	Prosalpha5	BL34786	HMS00095	A	E	E			E	
CG3644	FBgn0000181	bic	BL34790	HMS00099		NE					
CG3090	FBgn0005612	Sox14	BL34794	HMS00103		NE					
CG12323	FBgn0029134	Prosbeta5	BL34810	HMS00119	A	E-L	E			E	
CG9291	FBgn0023211	Elongin-C	BL34818	HMS00128		NE					
CG9646	FBgn0034184	CG9646	BL34819	HMS00134		NE					
CG8639	FBgn0033313	Cirl	BL34821	HMS00136		NE					
CG8392	FBgn0010590	Prosbeta1	BL34824	HMS00139	A	E	E			E-L	
CG8912	FBgn0014870	Psi	BL34825	HMS00140		NE					
CG2910	FBgn0027548	nito	BL34848	HMS00166		NE					
CG33554	FBgn0053554	Nipped-A	BL34849	HMS00167		NE					
CG11419	FBgn0034231	Apc10	BL34858	HMS00176		NE					
CG11680	FBgn0002774	mle/nap	BL34864	HMS00182	(MS POSSIBLE)	NE	NE	MS			
CG10915	FBgn0034308	CG10915	BL34879	HMS00199		NE					
CG11198	FBgn0033246	ACC	BL34885	HMS01230		NE					
CG15667	FBgn0026369	Sara	BL34894	HMS01239		NE					
CG18250	FBgn0034072	Dg	BL34895	HMS01240		NE					
CG4816	FBgn0022987	qkr54B	BL34896	HMS01241		NE					
CG5562	FBgn0024234	gbb	BL34898	HMS01243		NE					
CG3615	FBgn0034110	Atg9	BL34901	HMS01246		NE					
CG10080	FBgn0034641	mahj	BL34912	HMS01260		NE	NE	NE	NE		
CG8996	FBgn0010516	wal	BL34915	HMS01263		NE					
CG3269	FBgn0014009	Rab2	BL34922	HMS01271		NE					
CG13867	FBgn0034503	MED8	BL34926	HMS01275	MS	MS		S	MS		NE
CG9834	FBgn0034433	endoB	BL34935	HMS01285		NE					
CG4696	FBgn0002789	Mp20	BL34963	HMS00630		NE					
CG8858	FBgn0033698	CG8858	BL34975	HMS01128	E	E	NE	NE	NE		NE
CG13345	FBgn0086356	tum	BL35007	HMS01417		NE					

CG11086	FBgn0033153	Gadd45	BL35023	HMS01436		NE					
CG11121	FBgn0003460	so	BL35028	HMS01441	E-L	E-L	NE	E	E-L		NE
CG13183	FBgn0033667	CG13183	BL35031	HMS01444		NE					
CG13188	FBgn0033668	CG13188	BL35032	HMS01445		NE					
CG8523	FBgn0010241	Mdr50	BL35034	HMS01448		NE					
CG8440	FBgn0015754	Lis-1	BL35043	HMS01457		NE					
CG11895	FBgn0024836	stan	BL35050	HMS01464		NE					
CG30173	FBgn0061198	HSPC300	BL35051	HMS01465		NE					
CG8821	FBgn0033748	vis	BL35738	HMS01480		NE					
CG8238	FBgn0040491	Buffy	BL35742	HMS01484		NE					
CG30176	FBgn0034918	wibg	BL35746	HMS01488		NE					
CG9397	FBgn0086655	jing	BL35750	HMS01493	A	E	ME			E	
CG8988	FBgn0033656	S2P	BL35760	HMS01508		NE					
CG4832	FBgn0013765	cnn	BL35761	HMS01509		NE					
CG8648	FBgn0025832	Fen1	BL35764	HMS01512		NE					
CG13442	FBgn0034546	CG13442	BL35769	HMS01518		NE					
CG7765	FBgn0001308	Khc	BL35770	HMS01519		NE					
CG9083	FBgn0035077	CG9083	BL35791	HMS01505	E-L	E-L	ME	E	ME	ME	NE
CG2078	FBgn0033402	Myd88	BL36107	HMS00183		NE					
CG30443	FBgn0050443	Opbp	BL36120	HMS01535		NE					
CG18408	FBgn0033504	CAP	BL36663	HMS01551		NE					
CG16935	FBgn0033883	CG16935	BL36671	HMS01559		NE					
CG10105	FBgn0033935	Sin1	BL36677	HMS01565		NE					
CG30379	FBgn0050379	CG30379	BL36679	HMS01567		NE					
CG8200	FBgn0024754	Flo-1	BL36700	HMS01589		NE					
CG1772	FBgn0010316	dap	BL36720	HMS01610		NE					
CG3318	FBgn0019643	Dat	BL36726	HMS01617		NE					
CG3624	FBgn0034724	babos	BL36728	HMS01619		NE					
CG8183	FBgn0019968	Khc-73	BL36733	HMS01624		NE					
CG13441	FBgn0041240	Gr57a	BL36738	HMS01629		NE					
CG30324	FBgn0050324	CG30324	BL36751	HMS03011		NE					
CG33988	FBgn0053988	CG33988	BL36754	HMS03014		NE					
CG9415	FBgn0021872	Xbp1	BL36755	HMS03015		NE					
CG3376	FBgn0034997	CG3376	BL36760	HMS03021		NE					
CG5345	FBgn0000566	Eip55E	BL36766	HMS03027		NE					

CG8430	FBgn0001124	Got1	BL36768	HMS03029		NE					
CG10079	FBgn0003731	Egfr	BL36773	JF02384	A	E	E			E	
CG17759	FBgn0004435	Galpha49B	BL36775	JF02390		NE					
CG10924	FBgn0034356	CG10924	BL36915	HMS00200		NE					
CG6542	FBgn0027506	EDTP	BL36917	HMS01577		NE					
CG4589	FBgn0019886	Letm1	BL37502	HMS01644	A	ME	ME			E	
CG3691	FBgn0035047	Pof	BL37508	HMS01650		NE					
CG15707	FBgn0034098	krimp	BL37511	HMS01653		NE					
CG15671	FBgn0000395	cv-2	BL37514	HMS01656		NE					
CG5473	FBgn0034371	SP2637	BL37522	HMS01664		NE					
CG18468	FBgn0034217	Lhr	BL38240	HMS01684		NE					
CG33558	FBgn0053558	mim	BL38246	HMS01690		NE					
CG1429	FBgn0011656	Mef2	BL38247	HMS01691		NE					
CG12864	FBgn0026427	Su(var)2-HP2	BL38255	HMS01699		NE					
CG5330	FBgn0015268	Nap1	BL38257	HMS01701		NE					
CG15792	FBgn0005634	zip	BL38259	HMS01703	A	E	E			E	
CG3886	FBgn0005624	Psc	BL38261	HMS01706		NE					
CG10933	FBgn0034264	CG10933	BL38263	HMS01708		NE					
CG2093	FBgn0033194	Vps13	BL38270	HMS01715		NE		S	E-L		
CG10808	FBgn0033876	synaptogyrin	BL38274	HMS01724		NE					
CG15087	FBgn0034380	CG15087	BL38280	HMS01731		NE					
CG1298	FBgn0033032	kune	BL38295	HMS01755		NE					
CG1599	FBgn0033452	CG1599	BL38300	HMS01762		NE					
CG8055	FBgn0086656	shrb	BL38305	HMS01767		NE					
CG5370	FBgn0010501	Dcp-1	BL38315	HMS01779		NE					
CG10505	FBgn0034612	CG10505	BL38317	HMS01781		NE					
CG33465	FBgn0053465	CG33465	BL38323	HMS01787		NE					
CG3530	FBgn0028497	CG3530	BL38340	HMS01807		NE					
CG11312	FBgn0011674	insc	BL38351	HMS01819		NE					
CG8722	FBgn0033247	Nup44A	BL38357	HMS01825		NE					
CG3419	FBgn0035002	CG3419	BL38360	HMS01828		NE					
CG13570	FBgn0015544	spag	BL38371	HMS01840		NE					
CG9696	FBgn0020306	dom	BL38385	HMS01854	E	E	NE	E	ME		NE
CG3121	FBgn0034957	CG3121	BL38524	HMS01721		NE					
CG9236	FBgn0034558	CG9236	BL38532	HMS01745		NE					

CG12369	FBgn0010238	Lac	BL38536	HMS01756	ME	ME	NE	NE	E		NE
CG15097	FBgn0034396	CG15097	BL38538	HMS01790		NE					
CG5576	FBgn0013983	imd	BL38933	HMS00253		NE					
CG5625	FBgn0034708	Vps35	BL38944	HMS01858		NE					
CG17800	FBgn0033159	Dscam	BL38945	HMS01859		NE					
CG12273	FBgn0016762	angel	BL38947	HMS01861		NE					
CG8024	FBgn0002567	ltd	BL38956	HMS01870		NE					
CG8095	FBgn0003328	scb	BL38959	HMS01873		NE					
CG11217	FBgn0015614	CanB2	BL38971	HMS01886		NE					
CG8964	FBgn0033674	CG8964	BL38973	HMS01889		NE					
CG6410	FBgn0034265	Snx16	BL38992	HMS01908		NE					
CG30390	FBgn0050390	Sgf29	BL39000	HMS01916		NE					
CG5581	FBgn0003022	Ote	BL39009	HMS01926		NE					
CG10327	FBgn0025790	TBPH	BL39014	HMS01932		NE			E		
CG8604	FBgn0027356	Amph	BL39015	HMS01933		NE					
CG13521	FBgn0005631	robo	BL39027	HMS01946		NE					
CG16801	FBgn0034012	Hr51	BL39032	HMS01951		NE					
CG15112	FBgn0000578	ena	BL39034	HMS01953		NE					
CG18817	FBgn0029508	Tsp42Ea	BL39044	HMS01964		NE					
CG11303	FBgn0020372	TM4SF	BL39048	HMS01968		NE					
CG10417	FBgn0033021	CG10417	BL39051	HMS01971		NE					
CG13197	FBgn0062449	CG13197	BL39052	HMS01972		NE					
CG34191	FBgn0085220	CG34191	BL39054	HMS01974		NE					
CG12210	FBgn0003660	Syb	BL39067	HMS01987	(ME POSSIBLE)	NE	NE	MS	E		NE
CG30092	FBgn0028371	jbug	BL39070	HMS01990		NE					
CG8581	FBgn0011592	fra	BL40826	HMS01147		NE					
CG15081	FBgn0010551	l(2)03709	BL40835	HMS02001		NE					
CG9446	FBgn0033109	coro	BL40841	HMS02007	MS	MS		S	E		NE
CG12391	FBgn0033581	CG12391	BL40847	HMS02014		NE					
CG9954	FBgn0034534	maf-S	BL40853	HMS02020		NE					
CG3060	FBgn0002791	mr	BL40856	HMS02023		NE					
CG12821	FBgn0040780	CG12821	BL40859	HMS02026		NE					
CG33138	FBgn0053138	CG33138	BL40860	HMS02027		NE					
CG8224	FBgn0011300	babo	BL40866	HMS02033		NE					

CG13594	FBgn0035041	CG13594	BL40891	HMS02139		NE					
CG4071	FBgn0034744	Vps20	BL40894	HMS02142	A	ME	ME			ME	
CG14468	FBgn0033042	Tsp42A	BL40900	HMS02148		NE	NE	MS	E		
CG4943	FBgn0029006	lack	BL40905	HMS02153	(MS POSSIBLE)	NE		NE	E		
CG30483	FBgn0040752	Prosap	BL40909	HMS02157		NE					
CG13329	FBgn0040477	cid	BL40912	HMS02160		NE					
CG3510	FBgn0000405	CycB	BL40915	HMS02163		NE					
CG30011	FBgn0050011	gem	BL40934	HMS02182		NE					
CG11770	FBgn0002552	lin	BL40939	HMS02187		NE					
CG34379	FBgn0085408	Shroom	BL40942	HMS02190		NE					
CG2727	FBgn0010435	emp	BL40947	HMS02195		NE					
CG8376	FBgn0000099	ap	BL41673	HMS02207		NE					
CG17835	FBgn0001269	inv	BL41675	HMS02209		NE					
CG9422	FBgn0033092	CG9422	BL41679	HMS02243	MS	MS		NE	NE		NE
CG10540	FBgn0034577	cpa	BL41685	HMS02249		NE					
CG1399	FBgn0033212	CG1399	BL41686	HMS02250		NE					
CG2105	FBgn0033192	Corin	BL41721	HMS02287		NE					
CG9453	FBgn0028985	Spn4	BL41722	HMS02288		NE					
CG6530	FBgn0028956	mthl3	BL41887	HMS02309		NE					
CG4812	FBgn0019928	Ser8	BL41920	HMS02317		NE					
CG7229	FBgn0034423	CG7229	BL41922	HMS02319		NE					
CG8589	FBgn0033921	tej	BL41929	HMS02326		NE					
CG5179	FBgn0019949	Cdk9/p-TEFb	BL41932	HMS02329		NE					
CG6692	FBgn0013770	Cp1	BL41939	HMS02336		NE					
CG33133	FBgn0001133	grau	BL41940	HMS02337		NE					
CG34361	FBgn0085390	Dgk	BL41944	HMS02341		NE					
CG8190	FBgn0034029	eIF2B-gamma	BL41948	HMS02345		NE					
CG8856	FBgn0020377	Sr-CII	BL41949	HMS02346		NE					
CG34054	FBgn0054054	CG34054	BL41951	HMS02348		NE					
CG4302	FBgn0027073	CG4302	BL41967	HMS02364		NE					
CG12172	FBgn0024294	Spn43Aa	BL41972	HMS02370		NE					
CG30161	FBgn0050161	CG30161	BL41977	HMS02375		NE					
CG11107	FBgn0033160	CG11107	BL41992	HMS02393		NE					
CG3572	FBgn0022960	vimar	BL41996	HMS02397		NE					

CG9441	FBgn0003162	Pu	BL41998	HMS02399		NE					
CG2040	FBgn0010114	hig	BL42000	HMS02401		NE					
CG8453	FBgn0025454	Cyp6g1	BL42006	HMS02407		NE					
CG8834	FBgn0033733	CG8834	BL42010	HMS02411		NE					
CG1845	FBgn0033155	Br140	BL42502	HMJ02067		NE					
CG10344	FBgn0034729	CG10344	BL42505	HMJ02070		NE					
CG8090	FBgn0033995	CG8090	BL42507	HMJ02072		NE					
CG13493	FBgn0034667	comr	BL42522	HMJ02088		NE					
CG3260	FBgn0021875	Zfrp8	BL42528	HMJ02095		NE					
CG9418	FBgn0026582	CG9418	BL42542	HMJ02112		NE					
CG9304	FBgn0034674	CG9304	BL42544	HMJ02115		NE					
CG1891	FBgn0003317	sax	BL42546	HMJ02118		NE					
CG9888	FBgn0003062	Fib	BL42553	HMJ02126	E-L	E-L	NE	NE	E		NE
CG18247	FBgn0015295	shark	BL42555	HMJ02128		NE					
CG9480	FBgn0034603	Glycogenin	BL42565	HMJ02222		NE					
CG2049	FBgn0020621	Pkn	BL42567	HMJ02226		NE					
CG15605	FBgn0034196	CG15605	BL42586	HMS02418		NE					
CG9896	FBgn0034808	CG9896	BL42587	HMS02419		NE					
CG11423	FBgn0034251	CG11423	BL42591	HMS02423		NE					
CG7865	FBgn0033050	Pngl	BL42592	HMS02424		NE					
CG18108	FBgn0034329	IM1	BL42599	HMS02431		NE					
CG4905	FBgn0034135	Syn2	BL42601	HMS02433		NE					
CG3821	FBgn0002069	Aats-asp	BL42606	HMS02439		NE					
CG3894	FBgn0035059	CG3894	BL42618	HMS02453		NE					
CG5825	FBgn0014857	His3.3A	BL42620	HMS02455		NE					
CG4294	FBgn0034742	CG4294	BL42624	HMS02459		NE					
CG18471	FBgn0024232	gprs	BL42630	HMS02465		NE					
CG8427	FBgn0023167	SmD3	BL42633	HMS02469		NE					
CG4847	FBgn0034229	CG4847	BL42655	HMS02491		NE					
CG1362	FBgn0013435	cdc2rk	BL42661	HMS02497		NE					
CG15105	FBgn0034412	abba	BL42826	HMS02508		NE					
CG2160	FBgn0033266	Socs44A	BL42830	HMS02515		NE					
CG3502	FBgn0046253	CG3502	BL42839	HMS02531		NE					
CG3608	FBgn0035039	CG3608	BL42841	HMS02533		NE					
CG3814	FBgn0025692	CG3814	BL42852	HMS02544		NE					

CG6033	FBgn0004638	drk	BL42855	HMS02547		NE					
CG30259	FBgn0050259	CG30259	BL42856	HMS02548		NE					
CG3209	FBgn0034971	CG3209	BL42863	HMS02556		NE					
CG30035	FBgn0050035	Tret1-1	BL42880	HMS02573		NE					
CG8315	FBgn0034058	Pex11	BL42883	HMS02576		NE					
CG3495	FBgn0034794	Gmer	BL42884	HMS02577		NE					
CG13189	FBgn0033665	CG13189	BL42894	HMS02587		NE					
CG8399	FBgn0034067	CG8399	BL42910	HMS02603		NE					
CG5033	FBgn0028744	CG5033	BL42930	HMS02623		NE					
CG8929	FBgn0034504	CG8929	BL42936	HMS02629		NE					
CG3633	FBgn0034727	mRpS29	BL42938	HMS02631		NE					
CG15609	FBgn0034180	Ehbp1	BL42939	HMS02632		NE					
CG11388	FBgn0034959	CG11388	BL42940	HMS02633		NE					
CG11290	FBgn0034975	enok	BL42941	HMS02634		NE					
CG3803	FBgn0034938	CG3803	BL42948	HMS02641		NE					
CG1882	FBgn0033226	CG1882	BL42957	HMS02650		NE					
CG15084	FBgn0034402	CG15084	BL42958	HMS02651		NE					
CG12858	FBgn0033958	CG12858	BL43284	HMS02655	A	E	ME			E	
CG18255	FBgn0013988	Strn-Mlck	BL43291	HMS02663		NE					
CG30010	FBgn0050010	CG30010	BL43293	HMS02665		NE					
CG10265	FBgn0033990	CG10265	BL43294	HMS02667		NE					
CG8946	FBgn0010591	Sply	BL43304	HMS02684		NE					
CG30371	FBgn0050371	CG30371	BL43307	HMS02691		NE					
CG10913	FBgn0028983	Spn6	BL43309	HMS02693		NE					
CG12133	FBgn0033469	CG12133	BL43312	HMS02696		NE					
CG9456	FBgn0028988	Spn1	BL43991	HMS02704		NE					
CG13424	FBgn0034520	lms	BL43995	HMS02709		NE					
CG1809	FBgn0033423	CG1809	BL44016	HMS02731		NE		NE	E		
CG8400	FBgn0034068	casp	BL44027	HMS02742		NE					
CG13739	FBgn0033403	CG13739	BL44030	HMS02746		NE					
CG1865	FBgn0024293	Spn43Ab	BL44043	HMS02759		NE					
CG6155	FBgn0014877	Roe1	BL44060	HMS02777		NE					
CG10023	FBgn0020440	Fak56D	BL44075	HMS02792		NE					
CG30361	FBgn0050361	mtt	BL44076	HMS02793	A	ME	ME			E	
CG30496	FBgn0050496	CG30496	BL44078	HMS02795		NE					

CG12699	FBgn0046294	CG12699	BL44111	HMS02833		NE					
CG9428	FBgn0033096	ZIP1	BL44120	HMS02842		NE					
CG30277	FBgn0050277	Oatp58Da	BL44122	HMS02844		NE					
CG1916	FBgn0004360	Wnt2	BL44271	HMS02826		NE					
CG4356	FBgn0000037	mAcR-60C	BL44469	HMC02343		NE					
CG1708	FBgn0000352	cos	BL44472	HMC02347		NE					
CG8325	FBgn0021847	l(2)k14710	BL44482	HMC02372		NE					
CG8579	FBgn0001285	Jon44E	BL44486	HMC02391		NE					
CG10306	FBgn0034654	CG10306	BL44493	HMC02415	MS	MS		NE	NE		NE
CG5190	FBgn0034351	CG5190	BL44494	HMC02423		NE					
CG9090	FBgn0034497	CG9090	BL44495	HMC02425		NE					
CG34123	FBgn0083959	trpm	BL44503	HMC02889		NE					
CG7881	FBgn0033048	CG7881	BL44505	HMC02891		NE					
CG18609	FBgn0034382	CG18609	BL44510	HMC02900		NE					
CG12490	FBgn0034782	CG12490	BL44511	HMC02901		NE					
CG17818	FBgn0027872	rdgBbeta	BL44523	HMC02916		NE					
CG4871	FBgn0035050	ST6Gal	BL44528	HMC02922		NE					
CG30495	FBgn0050495	CG30495	BL44531	HMC02925		NE					
CG2070	FBgn0033203	CG2070	BL44532	HMC02926		NE					
CG8520	FBgn0033734	CG8520	BL44533	HMC02927		NE					
CG16827	FBgn0034005	alphaPS4	BL44534	HMC02928		NE					
CG3388	FBgn0001148	gsb	BL44548	HMC02944		NE					
CG3649	FBgn0034785	CG3649	BL44549	HMC02946		NE					
CG18107	FBgn0034330	CG18107	BL44562	HMS02858		NE					
CG11184	FBgn0034923	Upf3	BL44565	HMS02861		NE		NE	E		
CG8746	FBgn0033330	CG8746	BL44567	HMS02863		NE					
CG7861	FBgn0033055	tbce	BL44569	HMS02865		NE					
CG33087	FBgn0053087	LRP1	BL44579	HMS02875		NE					
CG5409	FBgn0011743	Arp53D	BL44580	HMS02876		NE					
CG3380	FBgn0034716	Oatp58Dc	BL44583	HMS02880		NE					
CG5036	FBgn0028743	CG5036	BL44632	HMC02405		NE					
CG5709	FBgn0025186	ari-2	BL44646	HMC02353		NE					
CG1821	FBgn0025286	RpL31	BL44647	HMC02354		NE					
CG12909	FBgn0033507	CG12909	BL44654	HMC02419		NE					
CG2736	FBgn0035090	CG2736	BL44655	HMC02427	S	S		MS	NE		NE

CG30194	FBgn0050194	CG44252	BL44658	HMC02440	A	ME	ME	MS	NE	ME	
CG9023	FBgn0015872	Drip	BL44661	HMC02945		NE					
CG8711	FBgn0033260	Cul-4	BL50614	HMC02981		NE					
CG30463	FBgn0050463	CG30463	BL50617	HMC02984		NE					
CG8380	FBgn0034136	DAT	BL50619	HMC02986		NE					
CG12051	FBgn0000043	Act42A	BL50625	HMC02992		NE					
CG10130	FBgn0010638	Sec61beta	BL50626	HMC02993	A	E-L	E			E	
CG6953	FBgn0026721	fat-spondin	BL50629	HMC02996		NE					
CG30491	FBgn0050491	CG30491	BL50630	HMC02997		NE					
CG5436	FBgn0001230	Hsp68	BL50637	HMC03036		NE					
CG9825	FBgn0034783	CG9825	BL50639	HMC03039		NE					
CG9876	FBgn0034821	CG9876	BL50655	HMC03056		NE					
CG15101	FBgn0010053	Jheh1	BL50676	HMC03077		NE					
CG7230	FBgn0003254	rib	BL50682	HMC03083		NE					
CG9858	FBgn0000326	clt	BL50683	HMC03084		NE					
CG7777	FBgn0033635	CG7777	BL50695	HMC03097		NE					
CG4663	FBgn0033812	Pex13	BL50697	HMC03099		NE					
CG10142	FBgn0035076	Ance-5	BL50703	HMC03105		NE					
CG2835	FBgn0001123	G-salpha60A	BL50704	HMC03106		NE					
CG1765	FBgn0000546	EcR	BL50712	HMC03114	A	E-L	E			E	
CG5770	FBgn0034291	CG5770	BL50719	HMS02953		NE					
CG3183	FBgn0033081	geminin	BL50720	HMS02954		NE					
CG13221	FBgn0041174	Vhl	BL50727	HMS02963		NE					
CG30265	FBgn0050265	CG30265	BL50731	HMS02967		NE					
CG8950	FBgn0034186	CG8950	BL50897	HMC02421		NE					
CG17821	FBgn0034383	CG17821	BL50898	HMC02424		NE					
CG18011	FBgn0033491	CG18011	BL50900	HMJ03118		NE					
CG9001	FBgn0034175	ste24b	BL50913	HMJ21002		NE					
CG10062	FBgn0034439	CG10062	BL50970	HMJ21076		NE					
CG12567	FBgn0039958	CG12567	BL50973	HMJ21079		NE					
CG1663	FBgn0033449	CG1663	BL50974	HMJ21080		NE					
CG8457	FBgn0033697	Cyp6t3	BL50976	HMJ21082		NE					
CG13561	FBgn0034906	CG13561	BL50995	HMJ21108		NE					
CG8735	FBgn0033309	CG8735	BL50998	HMJ21111		NE					
CG2121	FBgn0033289	CG2121	BL51014	HMJ21133		NE					

CG1850	FBgn0033154	CG1850	BL51046	HMJ21179		NE					
CG30085	FBgn0050085	Rif1	BL51051	HMJ21185		NE					
CG13579	FBgn0035010	CG13579	BL51053	HMJ21188		NE					
CG2956	FBgn0003900	twi	BL51164	HMJ03122		NE					
CG30106	FBgn0050106	CCHa1r	BL51168	HMJ21029		NE					
CR42452	FBgn0083123	Uhg5	BL51176	HMJ21153		NE					
CG6646	FBgn0033885	DJ-1alpha	BL51177	HMJ21180		NE					
CG8704	FBgn0010109	dpn	BL51440	HMC03154		NE					
CG3668	FBgn0004896	fd59A	BL51441	HMC03155		NE					
CG33183	FBgn0000448	Hr46	BL51442	HMC03156		NE					
CG10474	FBgn0034427	CG10474	BL51444	HMC03158		NE					
CG9033	FBgn0033629	Tsp47F	BL51458	HMC03194		NE					
CG10117	FBgn0020245	ttv	BL51480	HMC03225		NE					
CG8766	FBgn0026619	Taz	BL51484	HMC03231		NE					
CG30272	FBgn0050272	CG30272	BL51493	HMC03245		NE					
CG12251	FBgn0033807	AQP	BL51504	HMC03266		NE					
CG11295	FBgn0013548	l(2)dtl	BL51510	HMC03280		NE					
CG4817	FBgn0010278	Ssrp	BL51519	HMS03169		NE					
CG2064	FBgn0033205	CG2064	BL51693	HMC03137		NE					
CG2827	FBgn0023477	Tal	BL51709	HMC03227		NE					
CG30060	FBgn0050060	CG30060	BL51712	HMC03235		NE					
CG10497	FBgn0010415	Sdc	BL51723	HMC03265		NE	NE	NE	E		
CG9826	FBgn0034784	CG9826	BL51728	HMC03274		NE					
CG8403	FBgn0034070	SP2353	BL51732	HMC03287		NE					
CG3499	FBgn0034792	CG3499	BL51752	HMC03303	MS	MS		NE	NE		NE
CG11099	FBgn0034485	CG11099	BL51766	HMC03321		NE					
CG9450	FBgn0003891	tud	BL51771	HMC03326		NE					
CG3298	FBgn0028426	JhI-1	BL51781	HMC03336		NE					
CG30438	FBgn0050438	CG30438	BL51790	HMC03346		NE					
CG8251	FBgn0003074	Pgi/gpi	BL51804	HMC03362		NE					
CG9364	FBgn0003748	Treh	BL51810	HMC03381		NE					
CG4533	FBgn0011296	l(2)efl	BL51816	HMC03387		NE					
CG11140	FBgn0010548	Aldh-III	BL51820	HMC03391		NE					
CG30054	FBgn0050054	CG30054	BL51823	HMC03395		NE					
CG18444	FBgn0003863	alphaTry	BL51824	HMC03396		NE					

CG11182	FBgn0025334	PHDP	BL51832	HMC03404		NE					
CG15860	FBgn0060296	pain	BL51835	HMC03407		NE					
CG3204	FBgn0025806	Rap2l	BL51840	HMC03412		NE					
CG9183	FBgn0003114	plu	BL51844	HMC03417		NE					
CG11949	FBgn0010434	cora	BL51845	HMC03418		NE					
CG8432	FBgn0026378	Rep	BL51851	HMC03425		NE					
CG8235	FBgn0033351	CG8235	BL51874	HMC03448		NE					
CG2292	FBgn0033479	CG2292	BL51875	HMC03449		NE					
CG12895	FBgn0033523	CG12895	BL51876	HMC03450		NE					
CG8594	FBgn0033755	ClC-b	BL51877	HMC03451		NE					
CG18278	FBgn0033836	CG18278	BL51878	HMC03452		NE					
CG8067	FBgn0033891	CG8067	BL51879	HMC03453		NE					
CG9000	FBgn0034176	ste24a	BL51880	HMC03454		NE					
CG6550	FBgn0034214	CG6550	BL51881	HMC03455		NE					
CG6401	FBgn0034270	CG6401	BL51882	HMC03456		NE					
CG6385	FBgn0034276	CG6385	BL51883	HMC03457		NE					
CG15111	FBgn0034419	CG15111	BL51885	HMC03459		NE					
CG7735	FBgn0034446	CG7735	BL51886	HMC03460		NE					
CG11237	FBgn0034452	Oseg6	BL51887	HMC03461		NE					
CG9313	FBgn0034566	CG9313	BL51888	HMC03462		NE					
CG15651	FBgn0034567	CG15651	BL51889	HMC03463		NE					
CG10315	FBgn0034858	eIF2B-delta	BL51891	HMC03465	A	E	ME	ME	E-L	E	
CG5411	FBgn0034886	Pde8	BL51892	HMC03466		NE					
CG11173	FBgn0034913	usnp	BL51893	HMC03467		NE					
CG5569	FBgn0034919	CG5569	BL51894	HMC03468		NE					
CG16912	FBgn0035064	CG16912	BL51895	HMC03469		NE					
CG32904	FBgn0028991	seq	BL51923	HMC03316	A	ME	ME			ME	
CG3613	FBgn0022986	qkr58E-1	BL51934	HMC03215		NE					
CG3504	FBgn0001263	inaD	BL52313	HMC03170	A	E	E			E	
CG30090	FBgn0050090	CG30090	BL52878	HMC03616		NE					
CG5009	FBgn0027572	CG5009	BL52882	HMC03620		NE					
CG3270	FBgn0033093	CG3270	BL52887	HMC03625		NE					
CG14749	FBgn0033316	CG14749	BL52888	HMC03626		NE					
CG12129	FBgn0033475	CG12129	BL52889	HMC03627		NE					
CG13320	FBgn0033785	Sans	BL52890	HMC03628		NE					

CG11192	FBgn0034507	CG11192	BL52893	HMC03631		NE					
CG4386	FBgn0034661	CG4386	BL52898	HMC03637		NE					
CG33460	FBgn0053460	CG33460	BL52900	HMC03639		NE					
CG11665	FBgn0033028	CG11665	BL52902	HMC03642		NE					
CG33198	FBgn0053198	pen-2	BL52908	HMC03648		NE					
CG30359	FBgn0050359	Mal-A5	BL52910	HMC03650		NE					
CG3267	FBgn0042083	CG3267	BL52912	HMC03652		NE					
CG8311	FBgn0034141	CG8311	BL52926	HMC03667		NE					
CG6251	FBgn0034118	Nup62	BL52927	HMC03668		NE					
CG10215	FBgn0028434	Ercc1	BL52929	HMC03670		NE					
CG2072	FBgn0026326	Mad1	BL52930	HMC03671		NE					
CG30457	FBgn0050457	CG30457	BL52964	HMJ21647		NE					
CG2921	FBgn0034689	CG2921	BL52965	HMJ21649		NE					
CG13427	FBgn0034514	CG13427	BL52967	HMJ21652		NE					
CG9235	FBgn0034560	CG9235	BL52971	HMJ21656		NE					
CG13423	FBgn0034513	CG13423	BL52972	HMJ21657		NE					
CG13434	FBgn0034523	Nnf1a	BL52973	HMJ21658		NE					
CG13220	FBgn0033608	CG13220	BL52984	HMJ21671		NE					
CG9993	FBgn0034553	CG9993	BL52985	HMJ21675		NE					
CG8824	FBgn0045063	fdl	BL52987	HMJ21679		NE					
CG30128	FBgn0046879	Obp56c	BL53001	HMJ21717		NE					
CG11209	FBgn0034489	ppk6	BL53010	HMJ21728		NE					
CR32886	FBgn0045800	Uhg1	BL53014	HMJ21736		NE					
CG8694	FBgn0002569	Mal-A2	BL53017	HMJ21740		NE					
CG6967	FBgn0034187	CG6967	BL53030	HMJ21756		NE					
CG17952	FBgn0034657	LBR	BL53269	HMC02426		NE					
CG4554	FBgn0034734	CG4554	BL53270	HMC03176		NE					
CG8800	FBgn0033408	CG8800	BL53295	HMC03511		NE					
CG8566	FBgn0034155	unc-104	BL53296	HMC03512		NE					
CG3661	FBgn0010078	RpL23	BL53300	HMC03527	A	E-L	E			E	
CG13232	FBgn0033578	BBS4	BL53305	HMC03532		NE					
CG4354	FBgn0005638	slbo	BL53309	HMC03538		NE					
CG9856	FBgn0016641	PTP-ER	BL53311	HMC03540		NE					
CG11430	FBgn0041585	olf186-F	BL53333	HMC03562		NE					
CG30022	FBgn0050022	CG30022	BL53334	HMC03563		NE					

CG30493	FBgn0050493	CG30493	BL53336	HMC03565		NE					
CG5912	FBgn0000119	arr	BL53342	HMC03571		NE					
CG11546	FBgn0010504	kermit	BL53349	HMC03578		NE					
CG4084	FBgn0011297	l(2)not	BL53350	HMC03579		NE					
CG12385	FBgn0011555	thetaTry	BL53362	HMC03591		NE					
CG13527	FBgn0034776	CG13527	BL53364	HMC03593		NE					
CG14760	FBgn0033277	CG14760	BL53366	HMC03595		NE					
CG1773	FBgn0033439	CG1773	BL53371	HMC03600		NE					
CG18681	FBgn0010425	epsilonTry	BL53374	HMC03603		NE					
CG18735	FBgn0042098	CG18735	BL53375	HMC03604		NE					
CG9640	FBgn0034182	CG9640	BL53681	HMJ21594		NE					
CG30280	FBgn0050280	CG30280	BL53693	HMJ21678		NE					
CG15920	FBgn0034157	resilin	BL53702	HMJ21733		NE					
CG1548	FBgn0029093	cathD	BL53882	HMJ21197		NE					
CG12763	FBgn0004240	Dpt	BL53923	HMJ21267		NE					
CG7137	FBgn0034422	CG7137	BL53924	HMJ21269		NE					
CG15862	FBgn0022382	Pka	BL53930	HMJ21276	A	ME	E			E	
CG13585	FBgn0035020	CG13585	BL53933	HMJ21281		NE					
CG5721	FBgn0034315	CG5721	BL53949	HMJ21313		NE					
CG18537	FBgn0034323	CG18537	BL53960	HMJ21342		NE					
CG10240	FBgn0013773	Cyp6a22	BL53963	HMJ21345		NE					
CG11061	FBgn0034697	GM130	BL53966	HMJ21349		NE					
CG13589	FBgn0035011	CG13589	BL53978	HMJ21367		NE					
CG6262	FBgn0034121	CG6262	BL53987	HMJ21391		NE					
CG12464	FBgn0033861	CG12464	BL53988	HMJ21392		NE					
CG3570	FBgn0035035	CG3570	BL54010	HMJ21433		NE					
CG3074	FBgn0034709	Swim	BL54015	HMJ21440		NE					
CG4329	FBgn0034745	CG4329	BL54035	HMJ21478		NE					
CG14478	FBgn0028953	CG14478	BL54040	HMJ21483		NE					
CG11788	FBgn0034495	CG11788	BL54043	HMJ21486		NE					
CG10927	FBgn0034360	CG10927	BL54050	HMS03521		NE					
CG6477	FBgn0034249	RhoGAP54D	BL54051	HMS03522		NE					
CG34033	FBgn0054033	CG34033	BL54055	HMS03716		NE					
CG7863	FBgn0033051	dream	BL54059	HMJ21268		NE					
CG14757	FBgn0033274	CG14757	BL54465	HMC03733		NE					

CG18369	FBgn0033860	S-Lap5	BL54796	HMJ21193		NE					
CG9344	FBgn0034564	CG9344	BL54798	HMJ21492		NE					
CG30338	FBgn0050338	CG30338	BL54809	HMJ21503		NE					
CG7759	FBgn0033633	CG7759	BL54811	HMJ21530		NE					
CG3017	FBgn0020764	Alas	BL54815	HMJ21534		NE					
CG10543	FBgn0034570	CG10543	BL54816	HMJ21535		NE					
CG30042	FBgn0050042	Cpr49Ab	BL54825	HMJ21544		NE					
CG14750	FBgn0022027	Vps25	BL54831	HMJ21550		NE					
CG3162	FBgn0034834	LS2	BL54832	HMJ21551		NE					
CG4688	FBgn0033817	GstE14	BL54836	HMJ21555		NE					
CG9460	FBgn0033115	Spn42De	BL54840	HMJ21559		NE					
CG30187	FBgn0050187	CG30187	BL54841	HMJ21560		NE					
CG33139	FBgn0053139	Ranbp11	BL55142	HMC03738		NE					
CG12388	FBgn0043471	kappaTry	BL55148	HMC03772		NE					
CG2063	FBgn0033400	CG2063/SAP30BP	BL55173	HMC03853	E	E	NE	E	E		NE
CG30414	FBgn0050414	CG30414	BL55176	HMC03857		NE					
CG3850	FBgn0033782	sug	BL55182	HMC03866		NE					
CG4007	FBgn0020391	Nrk	BL55184	HMC03875		NE					
CG8690	FBgn0033297	Mal-A8	BL55193	HMC03889		NE					
CG7637	FBgn0033548	CG7637	BL55194	HMC03890		NE					
CG4827	FBgn0034225	veil	BL55195	HMC03891		NE					
CG2852	FBgn0034753	CG2852	BL55196	HMC03892		NE					
CG6209	FBgn0033862	CG6209	BL55203	HMC03916		NE					
CG2980	FBgn0034939	thoc5	BL55206	HMC03921		NE					
CG30122	FBgn0050122	CG30122	BL55209	HMC03927	E	E	NE	NE	E		(MEPOSSIBLE)
CG6536	FBgn0034219	mthl4	BL55244	HMC02422		NE					
CG3829	FBgn0035091	CG3829	BL55245	HMC02428		NE					
CG12759	FBgn0010220	Dbp45A	BL55253	HMC03940		NE					
CG9401	FBgn0002736	mago	BL55260	HMC03947		NE					
CG12919	FBgn0033483	egr	BL55276	HMC03963		NE					
CG5821	FBgn0022985	qkr58E-2	BL55279	HMC03966		NE					
CG13168	FBgn0033705	CG13168	BL55288	HMC03975		NE					
CG18455	FBgn0025360	Optix	BL55306	HMC03993	S	S		MS	NE		NE
CG8643	FBgn0033310	rgr	BL55307	HMC03994		NE					

CG10052	FBgn0020617	Rx	BL55308	HMC03995		NE					
CG8256	FBgn0022160	Gpo-1	BL55319	HMC04006		NE					
CG3140	FBgn0022708	Adk2	BL55320	HMC04007		NE					
CG8230	FBgn0027607	CG8230	BL55329	HMC04016		NE					
CG7461	FBgn0034432	CG7461	BL55347	HMC04034		NE					
CG8213	FBgn0033359	CG8213	BL55350	HMC04037		NE					
CG8738	FBgn0033321	CG8738	BL55351	HMC04038		NE					
CG4266	FBgn0034598	CG4266	BL55354	HMC04041		NE					
CG5002	FBgn0034275	CG5002	BL55359	HMC04046		NE					
CG8781	FBgn0033378	tsu	BL55367	HMC04055	MS	MS		MS	E		NE
CG18067	FBgn0034512	CG18067	BL55383	HMC04071		NE					
CG2668	FBgn0004181	Peb	BL55390	HMC04078		NE					
CG3832	FBgn0019948	Phm	BL55392	HMC04080		NE					
CG12387	FBgn0011556	zetaTry	BL55407	HMC04095	A	ME	ME			E	
CG4927	FBgn0034139	CG4927	BL55409	HMC04097		NE					
CG8172	FBgn0033362	CG8172	BL55608	HMC03746		NE					
CG8169	FBgn0011660	Pms2	BL55614	HMC03753		NE					
CG9294	FBgn0034666	CG9294	BL55618	HMC03761		NE					
CG4527	FBgn0035001	slik	BL55626	HMC03770		NE					
CG18375	FBgn0034606	ASPP	BL55639	HMC03787	E	E	NE	MS	E		NE
CG8079	FBgn0034002	CG8079	BL55654	HMC03804		NE					
CG6315	FBgn0000662	fl(2)d	BL55674	HMC03833		NE					
CG3594	FBgn0035063	Eap	BL55678	HMC03845		NE					
CG30104	FBgn0050104	NT5E-2	BL55684	HMC03869		NE					
CG4016	FBgn0086532	Spt-I	BL55685	HMC03870		NE					
CG2411	FBgn0003892	ptc	BL55686	HMC03872		NE					
CG3496	FBgn0003977	vir	BL55694	HMC03908		NE					
CG11066	FBgn0033033	scaf	BL55695	HMC03909		NE					
CG12343	FBgn0033556	CG12343	BL55697	HMC03911		NE					
CG10110	FBgn0024698	Cpsf160	BL55698	HMC03912		NE					
CG18426	FBgn0021895	ytr	BL55704	HMC03929		NE					
CG12386	FBgn0011554	etaTry	BL55731	HMC03744		NE					
CG6701	FBgn0033889	CG6701	BL55854	HMC03849		NE					
CG8967	FBgn0004839	otk	BL55869	HMC04139		NE					
CG3915	FBgn0033791	Drl-2	BL55893	HMC04172		NE					

CG4945	FBgn0034137	CG4945	BL55894	HMC04173		NE					
CG3216	FBgn0034568	CG3216	BL55895	HMC04174		NE					
CG33467	FBgn0053467	CG33467	BL55905	HMC04189		NE					
CG9874	FBgn0003687	Tbp	BL55911	HMC04197		NE					
CG8205	FBgn0023441	fus	BL55921	HMC04208		NE					
CG3584	FBgn0022984	qkr58E-3	BL55922	HMC04209		NE					
CG11390	FBgn0011695	PebIII	BL55933	HMC04221		NE					
CG7754	FBgn0015001	iotaTry	BL55934	HMC04222		NE					
CG8642	FBgn0033312	CG8642	BL55946	HMC04234	A	E-L	E-L			E-L	
CG10143	FBgn0033952	Adgf-E	BL55947	HMC04236		NE					
CG9849	FBgn0034803	CG9849	BL55948	HMC04237		NE					
CG5756	FBgn0034301	CG5756	BL55964	HMC04259		NE					
CG30293	FBgn0050293	Cht12	BL55989	HMC04285		NE					
CG30486	FBgn0050486	CG30486	BL55990	HMC04286		NE					
CG9070	FBgn0086519	Cpr47Eg	BL56004	HMC04300		NE					
CG15100	FBgn0034401	CG15100	BL56007	HMC04303		NE					
CG4802	FBgn0034215	CG4802	BL56010	HMC04306		NE					
CG3666	FBgn0034094	Tsf3	BL56015	HMC04311		NE					
CG1656	FBgn0040093	lectin-46Ca	BL56016	HMC04312		NE					
CG15231	FBgn0040653	IM4	BL56018	HMC04314		NE					
CG30467	FBgn0050467	CG30467	BL56021	HMC04317		NE					
CG30040	FBgn0086677	jeb	BL56022	HMC04318		NE					
CG3394	FBgn0034999	CG3394	BL56032	HMC04340		NE					
CG5589	FBgn0036754	CG5589	BL32334	HMS00325		NE					
CG6914	FBgn0037172	CG6914	BL32336	HMS00327		NE					
CG7692	FBgn0036714	CG7692	BL32338	HMS00329		NE					
CG8765	FBgn0036900	CG8765	BL32343	HMS00334		NE					
CG8479	FBgn0261276	opa1-like	BL32358	HMS00349		NE					
CG10077	FBgn0035720	CG10077	BL32388	HMS00380		NE					
CG10107	FBgn0035713	velo	BL32389	HMS00383		NE					
CG5144	FBgn0035957	CG5144	BL32393	HMS00387		NE					
CG32172	FBgn0026197	noe	BL32407	HMS00402		NE					
CG8201	FBgn0260934	par-1	BL32410	HMS00405	A	E	E			E	
CG10228	FBgn0264962	lnr-a/Pcf11	BL32411	HMS00406	A	E-L	E-L			E-L	
CG9750	FBgn0040075	rept	BL32415	HMS00410		NE					

CG32149	FBgn0036518	RhoGAP71E	BL32417	HMS00412		NE					
CG14112	FBgn0036349	SNCF	BL32420	HMS00415		NE					
CG9181	FBgn0003138	Ptp61F	BL32426	HMS00421		NE					
CG12262	FBgn0035811	CG12262	BL32436	HMS00434		NE					
CG6418	FBgn0036104	CG6418	BL32441	HMS00439		NE					
CG32138	FBgn0052138	CG32138	BL32447	HMS00445		NE					
CG11100	FBgn0037207	Mes2	BL32460	HMS00460		NE					
CG2103	FBgn0035375	pgant6	BL32463	HMS00463		NE					
CG4879	FBgn0027375	RecQ5	BL32466	HMS00466		NE					
CG8167	FBgn0036046	Ilp2	BL32475	HMS00476		NE					
CG32062	FBgn0052062	A2bp1	BL32476	HMS00478		NE					
CG8567	FBgn0013799	Deaf1	BL32512	HMS00516		NE					
CG11440	FBgn0037163	laza	BL32515	HMS00519		NE					
CG32156	FBgn0005536	Mbs	BL32516	HMS00521		NE					
CG5994	FBgn0017430	Nelf-E	BL32835	HMS00525		NE					
CG8241	FBgn0086895	pea	BL32838	HMS00528	A	E	ME			ME	
CG6586	FBgn0028980	tan	BL32855	HMS00640		NE					
CG14173	FBgn0044051	Ilp1	BL32861	HMS00648		NE					
CG5519	FBgn0261119	Prp19	BL32865	HMS00652	A	ME	ME	ME		ME	
CG4978	FBgn0020633	Mcm7	BL32867	HMS00654		NE					
CG2331	FBgn0261014	TER94	BL32869	HMS00656		NE					
CG3689	FBgn0035987	CG3689	BL32883	HMS00671		NE					
CG11793	FBgn0003462	Sod	BL32909	HMS00698		NE					
CG9311	FBgn0036448	mop	BL32916	HMS00706		NE					
CG13887	FBgn0035165	CG13887	BL32917	HMS00707		NE					
CG11593	FBgn0035488	CG11593	BL32924	HMS00715		NE					
CG18178	FBgn0036035	CG18178	BL32927	HMS00719		NE					
CG7324	FBgn0037074	CG7324	BL32929	HMS00722		NE					
CG8108	FBgn0027567	CG8108	BL32930	HMS00723		NE					
CG6143	FBgn0004401	Pep	BL32944	HMS00738		NE					
CG17962	FBgn0004052	Z600	BL32953	HMS00747		NE					
CG10672	FBgn0035588	CG10672	BL32958	HMS00753		NE					
CG10163	FBgn0035697	CG10163	BL32959	HMS00754		NE					
CG6964	FBgn0010825	Gug	BL32961	HMS00756	A	ME	ME			E	
CG12755	FBgn0002440	l(3)mbn	BL32962	HMS00757		NE					

CG8091	FBgn0026404	Nc	BL32963	HMS00758		NE					
CG32109	FBgn0052109	CG32109	BL32970	HMS00767		NE					
CG6292	FBgn0025455	CycT	BL32976	HMS00776	A	E	E			E	
CG14563	FBgn0037139	CG14563	BL33045	HMS00643		NE					
CG13720	FBgn0035555	CG13720	BL33342	HMS00208		NE					
CG17746	FBgn0035425	CG17746	BL33347	HMS00214		NE					
CG3919	FBgn0036423	CG3919	BL33355	HMS00226		NE					
CG18332	FBgn0027055	CSN3	BL33369	HMS00242		NE					
CG10269	FBgn0022935	D19A	BL33371	HMS00244		NE					
CG4432	FBgn0035976	PGRP-LC	BL33383	HMS00259		NE					
CG8865	FBgn0026376	Rgl	BL33389	HMS00266		NE					
CG3395	FBgn0010408	RpS9	BL33394	HMS00271		NE					
CG32217	FBgn0014037	ELL	BL33399	HMS00277	S	S		S	S		NE
CG8013	FBgn0020887	Su(z)12	BL33402	HMS00280		NE					
CG11624	FBgn0003943	Ubi-p63E	BL33405	HMS00284	A	E-L	E-L			E-L	
CG6539	FBgn0011802	Gem3	BL33408	HMS00287		NE					
CG7143	FBgn0037141	DNApol-eta	BL33410	HMS00290		NE					
CG9594	FBgn0023395	Chd3	BL33420	HMS00302		NE					
CG8057	FBgn0260972	alc	BL33429	HMS00316		NE					
CG42257	FBgn0259142	Snp	BL33434	HMS00321		NE					
CG11228	FBgn0261456	hpo	BL33614	HMS00006		NE					
CG32443	FBgn0003042	Pc	BL33622	HMS00016		NE					
CG4059	FBgn0001078	ftz-f1	BL33625	HMS00019	A	ME	ME			ME	
CG7935	FBgn0026252	msk	BL33626	HMS00020		NE					
CG10160	FBgn0001258	ImpL3	BL33640	HMS00039		NE					
CG6272	FBgn0036126	CG6272	BL33652	HMS00057		NE					
CG32346	FBgn0000541	E(bx)	BL33658	HMS00065		NE					
CG6502	FBgn0000629	E(z)	BL33659	HMS00066		NE			MS		
CG10630	FBgn0035608	blanks	BL33667	HMS00078		NE					
CG14167	FBgn0044050	Ilp3	BL33681	HMS00546		NE					
CG33273	FBgn0044048	Ilp5	BL33683	HMS00548		NE					
CG9191	FBgn0004378	Klp61F	BL33685	HMS00552	A	ME	ME			ME	
CG11661	FBgn0010352	Nc73EF	BL33686	HMS00554		NE					
CG4609	FBgn0014163	fax	BL33687	HMS00555		NE					
CG7421	FBgn0037137	Nopp140	BL33694	HMS00564	E-L	E-L	NE	E	E-L		NE

CG10133	FBgn0036366	CG10133	BL33701	HMS00578		NE					
CG13902	FBgn0035166	CG13902	BL33702	HMS00579		NE					
CG8887	FBgn0005386	ash1	BL33705	HMS00582		NE					
CG5546	FBgn0036761	MED19	BL33710	HMS00588	S	S		S	MS		NE
CG15022	FBgn0035547	CG15022	BL33713	HMS00593		NE					
CG13900	FBgn0035162	CG13900	BL33731	HMS00614		NE					
Hsc70Cb	FBgn0026418	Hsc70Cb	BL33742	HMS01080		NE					
MED24	FBgn0035851	MED24	BL33755	HMS01097		NE					
Vha44	FBgn0262511	Vha44	BL33884	HMS00821		NE					
Eaf6	FBgn0035624	Eaf6	BL33904	HMS00846		NE					
Ark	FBgn0263864	Ark	BL33924	HMS00870		NE					
Chmp1	FBgn0036805	Chmp1	BL33928	HMS00877		NE					
kst	FBgn0004167	kst	BL33933	HMS00882		NE					
PHGPx	FBgn0035438	PHGPx	BL33939	HMS00890		NE					
Ack	FBgn0028484	Ack	BL33941	HMS00892		NE					
GXIVsPLA2	FBgn0036545	GXIVsPLA2	BL33961	HMS00918		NE					
Pcaf	FBgn0020388	Pcaf	BL33981	HMS00941		NE					
nxf2	FBgn0036640	nxf2	BL33985	HMS00945		NE					
SrpRbeta	FBgn0011509	SrpRbeta	BL34011	HMS00977		NE					
CG12012	FBgn0035444	CG12012	BL34015	HMS00982		NE					
Cat	FBgn0000261	Cat	BL34020	HMS00990		NE					
CG14966	FBgn0035415	CG14966	BL34022	HMS00992		NE					
CG6497	FBgn0036704	CG6497	BL34026	HMS00996		NE					
MED10	FBgn0036581	MED10	BL34031	HMS01001		NE					
CG7497	FBgn0036742	CG7497	BL34035	HMS01008		NE					
whd	FBgn0261862	whd	BL34066	HMS00040		NE					
Eip63E	FBgn0005640	Eip63E	BL34075	HMS00569		NE					
CG5830	FBgn0036556	CG5830	BL34079	HMS01077		NE					
Grasp65	FBgn0036919	Grasp65	BL34082	HMS01093		NE					
MED11	FBgn0036811	MED11	BL34083	HMS01094		NE					
dlp	FBgn0041604	dlp	BL34089	HMS00875		NE					
eIF-4E	FBgn0015218	eIF-4E	BL34096	HMS00969		NE					
CG9425	FBgn0036451	CG9425	BL34099	HMS01002		NE					
fz	FBgn0001085	fz	BL34321	HMS01308		NE					
h	FBgn0001168	h	BL34326	HMS01313		NE					

CG9148	FBgn0025682	scf	BL34331	HMS01319		NE					
CG5660	FBgn0035942	CG5660	BL34339	HMS01327	A	E	E			E	
CG6512	FBgn0036702	CG6512	BL34343	HMS01331		NE					
CG5165	FBgn0003076	Pgm	BL34345	HMS01333		NE					
CG7762	FBgn0028695	Rpn1	BL34348	HMS01337	A	E-L	E			E	
CG17514	FBgn0039959	CG17514	BL34355	HMS01344		NE					
CG6877	FBgn0036813	Aut1/Atg3	BL34359	HMS01348	E	E	NE	S	ME		NE
CG10419	FBgn0036850	Gem2	BL34366	HMS01355		NE					
CG43722	FBgn0263934	esn	BL34371	HMS01360		NE					
CG5186	FBgn0261477	slim	BL34376	HMS01366		NE					
CG40452	FBgn0011288	Snap25	BL34377	HMS01367		NE					
CG11534	FBgn0046296	CG11534	BL34384	HMS01374		NE					
CG10576	FBgn0035630	CG10576	BL34388	HMS01382		NE					
CG10741	FBgn0036373	CG10741	BL34394	HMS00981		NE					
CG4877	FBgn0036624	RAF2	BL34395	HMS01012		NE					
CG5942	FBgn0000212	brm	BL34520	HMS00050		NE					
CG8937	FBgn0001216	Hsc70-1	BL34527	HMS00888		NE					
CG9451	FBgn0036876	CG9451	BL34545	HMS01016	A	E	E			E	
CG10483	FBgn0035649	CG10483	BL34551	HMS01023		NE					
CG10850	FBgn0041147	ida	BL34552	HMS01024		NE					
CG12084	FBgn0043458	CG12084	BL34553	HMS01025		NE					
CG4098	FBgn0036648	CG4098	BL34559	HMS01031		NE					
CG4157	FBgn0028693	Rpn12	BL34560	HMS01032	A	E	ME	MS	E-L	ME	
CG7619	FBgn0015283	Pros54	BL34566	HMS01039		NE					
CG8268	FBgn0035827	Srp9	BL34568	HMS01041		NE					
CG12031	FBgn0035145	MED14	BL34575	HMS01049	S	S		S	MS		NE
CG10289	FBgn0035688	CG10289	BL34579	HMS01053		NE					
CG4769	FBgn0035600	CG4769	BL34583	HMS01057		NE					
CG5594	FBgn0261794	kcc	BL34584	HMS01058		NE					
CG8491	FBgn0001324	kto/MED12	BL34588	HMS01062		NE					
CG10960	FBgn0036316	CG10960	BL34598	HMS01072		NE					
CG8339	FBgn0020251	sfl	BL34601	HMS00543		NE					
CG11009	FBgn0036318	Wbp2	BL34603	HMS00563		NE					
CG7062	FBgn0015793	Rab19	BL34607	HMS00592		NE					
CG9614	FBgn0003089	pip	BL34613	HMS01288		NE					

CG11621	FBgn0015278	Pi3K68D	BL34621	HMS01296		NE					
CG12076	FBgn0027616	YT521-B	BL34627	HMS01302		NE					
CG5069	FBgn0014143	croc	BL34647	HMS01122		NE					
CG11526	FBgn0035437	CG11526	BL34657	HMS01134		NE					
CG7162	FBgn0037109	MED1	BL34662	HMS01139		NE					
CG32435	FBgn0021760	chb	BL34669	HMS01146		NE					
CG5893	FBgn0000411	D	BL34672	HMS01150		NE					
CG10861	FBgn0036255	Atg12	BL34675	HMS01153		NE					
CG32076	FBgn0052076	Alg10	BL34681	HMS01159		NE					
CG7504	FBgn0035842	CG7504	BL34683	HMS01161		NE					
CG30149	FBgn0250850	rig	BL34684	HMS01162		NE					
CG6896	FBgn0036801	MYPT-75D	BL34688	HMS01166		NE					
CG7283	FBgn0036213	RpL10Ab	BL34695	HMS01174	A	E-L	E			E	
CG8609	FBgn0035754	MED4	BL34697	HMS01176		NE					
CG4717	FBgn0001320	kni	BL34705	HMS01184	A	E	ME			E	
CG7986	FBgn0035850	Atg18	BL34714	HMS01193		NE					
CG18647	FBgn0045759	bin	BL34718	HMS01197		NE					
CG1241	FBgn0044452	Atg2	BL34719	HMS01198		NE					
CG6662	FBgn0035907	GstO1	BL34727	HMS01206		NE					
CG7405	FBgn0022936	CycH	BL34732	HMS01212		NE					
CG6975	FBgn0005198	gig	BL34737	HMS01217		NE					
CG12085	FBgn0028577	pUf68	BL34785	HMS00094	(ME POSSIBLE)	NE	NE				
CG11513	FBgn0041164	armi	BL34789	HMS00098		NE					
CG11254	FBgn0016034	mael	BL34793	HMS00102		NE					
CG4097	FBgn0002284	Pros26	BL34801	HMS00110	A	E	E			E	
CG15010	FBgn0041171	ago	BL34802	HMS00111		NE					
CG12196	FBgn0086908	egg	BL34803	HMS00112		NE					
CG7185	FBgn0035872	CPSF6	BL34804	HMS00113	E	E	NE	E	E		NE
CG6169	FBgn0036534	Dcp2	BL34806	HMS00115		NE					
CG7597	FBgn0037093	Cdk12	BL34838	HMS00155	ME	ME	NE	ME	ME		MS
CG7471	FBgn0015805	Rpd3	BL34846	HMS00164		NE					
CG5528	FBgn0036978	Toll-9	BL34853	HMS00171	A	ME	ME			E	
CG12559	FBgn0003256	rl	BL34855	HMS00173		NE					
CG7008	FBgn0035121	Tudor-SN	BL34865	HMS00184		NE					

CG10863	FBgn0027552	CG10863	BL34878	HMS00198		NE					
CG5103	FBgn0036784	CG5103	BL34882	HMS01227		NE					
CG2248	FBgn0010333	Rac1	BL34910	HMS01258		NE					
CG6199	FBgn0036147	Plod	BL34911	HMS01259		NE					
CG7961	FBgn0025725	alphaCop	BL34923	HMS01272	A	E-L	E-L			E-L	
CG1210	FBgn0020386	Pdk1	BL34936	HMS01250		NE					
CG6311	FBgn0036735	Edc3	BL34953	HMS00392		NE					
CG4086	FBgn0004465	Su(P)	BL34955	HMS00430		NE					
CG1171	FBgn0004552	Akh	BL34960	HMS00477		NE					
CG8993	FBgn0035334	CG8993	BL34973	HMS01042		NE					
CG7112	FBgn0035879	CG7112	BL34976	HMS01132		NE					
CG10103	FBgn0035715	CG10103	BL34979	HMS01388		NE					
CG7659	FBgn0015550	tap	BL34985	HMS01395		NE					
CG8487	FBgn0264560	garz	BL34987	HMS01397	A	E-L	E-L			E-L	
CG12019	FBgn0011573	Cdc37	BL34991	HMS01401		NE					
CG11268	FBgn0036336	ste14	BL34996	HMS01406		NE					
CG32029	FBgn0052029	Cpr66D	BL35011	HMS01421		NE					
CG34229	FBgn0259832	CG34229	BL35019	HMS01432		NE					
CG10181	FBgn0004513	Mdr65	BL35035	HMS01449		NE					
CG12342	FBgn0086898	dgo	BL35040	HMS01454		NE					
CG1956	FBgn0004636	R	BL35047	HMS01461		NE					
CG17698	FBgn0040056	CG17698	BL35733	HMS01475		NE					
CG5582	FBgn0036756	cln3	BL35734	HMS01476		NE					
CG7003	FBgn0036486	Msh6	BL35737	HMS01479		NE					
CG33486	FBgn0041607	asparagine-synthetase	BL35739	HMS01481		NE					
CG6776	FBgn0035904	GstO3	BL35762	HMS01510		NE					
CG3371	FBgn0035153	ebd1	BL35765	HMS01513		NE					
CG40127	FBgn0262116	CG40127	BL35779	HMS01529		NE					
CG8127	FBgn0000568	Eip75B	BL35780	HMS01530	A	E-L	E-L			E-L	
CG42595	FBgn0262124	uex	BL36116	HMS01492		NE					
CG13474	FBgn0036439	CG13474	BL36124	HMS01539		NE					
CG5119	FBgn0261619	pAbp	BL36127	HMS01542		NE					
CG6718	FBgn0036053	iPLA2-VIA	BL36129	HMS01544		NE					
CG6114	FBgn0036544	sff	BL36656	HMS01280		NE					
CG33130	FBgn0263197	Patronin	BL36659	HMS01547		NE					

CG11451	FBgn0037025	Spc105R	BL36660	HMS01548		NE					
CG4761	FBgn0001323	knrl	BL36664	HMS01552		NE					
CG4999	FBgn0035936	Tsp66E	BL36696	HMS01585		NE					
CG12306	FBgn0003124	polo	BL36702	HMS01591		NE					
CG13503	FBgn0243516	Vrp1	BL36704	HMS01593		NE					
CG1921	FBgn0014388	sty	BL36709	HMS01599	A	E	E	E	NE	E	
CG17183	FBgn0035149	MED30	BL36711	HMS01601		NE					
CG17046	FBgn0001316	klar	BL36721	HMS01612		NE					
CG2075	FBgn0004372	aly	BL36723	HMS01614		NE					
CG11308	FBgn0002842	sa	BL36730	HMS01621		NE					
CG2086	FBgn0027594	drpr	BL36732	HMS01623		NE					
CG9006	FBgn0086712	Egm	BL36739	HMS01630		NE					
CG12034	FBgn0035421	CG12034	BL36759	HMS03020		NE					
CG32052	FBgn0044328	CG32052	BL36763	HMS03024		NE					
CG5962	FBgn0000121	Arr2	BL36772	JF02290		NE					
CG5751	FBgn0035934	TrpA1	BL36780	JF02461		NE					
CG7478	FBgn0000045	Act79B	BL36857	HMS00303		NE					
CG9160	FBgn0011361	mtacp1	BL37492	HMS01634		NE					
CG7314	FBgn0036199	Bmcp	BL37498	HMS01640		NE					
CG42678	FBgn0261564	CG42678	BL37500	HMS01642		NE					
CG7540	FBgn0037092	M6	BL37503	HMS01645	MS	MS		MS	E		NE
CG10523	FBgn0041100	park	BL37509	HMS01651		NE					
CG5665	FBgn0036977	CG5665	BL37517	HMS01659		NE					
CG9186	FBgn0035206	CG9186	BL37518	HMS01660		NE					
CG10308	FBgn0010317	CycJ	BL37521	HMS01663		NE					
CG32433	FBgn0045474	Gr77a	BL38236	HMS01680		NE					
CG42572	FBgn0260959	MCPH1	BL38244	HMS01688		NE					
CG42783	FBgn0261854	aPKC	BL38245	HMS01689		NE					
CG5654	FBgn0022959	yps	BL38250	HMS01694		NE					
CG10624	FBgn0010894	sinu	BL38258	HMS01702		NE					
CG15014	FBgn0035532	CG15014	BL38273	HMS01722		NE					
CG10083	FBgn0036372	CG10083	BL38282	HMS01735		NE					
CG43443	FBgn0263391	hts	BL38283	HMS01736		NE					
CG4893	FBgn0036616	CG4893	BL38287	HMS01740		NE					
CG9712	FBgn0036666	TSG101	BL38306	HMS01768		NE					

CG7565	FBgn0035833	CG7565	BL38307	HMS01770		NE					
CG5026	FBgn0035945	CG5026	BL38309	HMS01773		NE					
CG32113	FBgn0052113	CG32113	BL38320	HMS01784		NE					
CG8194	FBgn0010406	RNaseX25	BL38322	HMS01786		NE					
CG3705	FBgn0023129	aay	BL38338	HMS01805		NE					
CG10738	FBgn0036368	CG10738	BL38346	HMS01814		NE					
CG7804	FBgn0036496	CG7804	BL38355	HMS01823	(MS POSSIBLE)	NE			E		
CG12006	FBgn0035464	CG12006	BL38359	HMS01827		NE					
CG10975	FBgn0014007	Ptp69D	BL38370	HMS01839		NE					
CG18803	FBgn0019947	Psn	BL38374	HMS01843		NE					
CG4618	FBgn0035589	CHMP2B	BL38375	HMS01844		NE					
CG13676	FBgn0035844	CG13676	BL38376	HMS01845		NE					
CG10971	FBgn0036309	Hip1	BL38377	HMS01846		NE					
CG13293	FBgn0035677	CG13293	BL38380	HMS01849		NE					
CG7446	FBgn0001134	Grd	BL38384	HMS01853		NE					
CG8029	FBgn0262515	VhaAC45	BL38522	HMS01717		NE					
CG11278	FBgn0036341	Syx13	BL38525	HMS01723		NE					
CG18156	FBgn0035725	Mis12	BL38535	HMS01753		NE					
CG6224	FBgn0040230	dbo	BL38940	HMS01791		NE					
CG8104	FBgn0036059	nudE	BL38954	HMS01868	A	ME	ME			ME	
CG7067	FBgn0024945	NitFhit	BL38961	HMS01875		NE					
CG32300	FBgn0015360	oxt	BL38985	HMS01901		NE					
CG6851	FBgn0027786	Mtch	BL38986	HMS01902		NE					
CG17947	FBgn0010215	alpha-Cat	BL38987	HMS01903		NE					
CG42856	FBgn0262103	Sik3	BL39005	HMS01922		NE					
CG12327	FBgn0036492	Best3	BL39040	HMS01960		NE					
CG32136	FBgn0043550	Tsp68C	BL39045	HMS01965		NE					
CG5492	FBgn0036769	Tsp74F	BL39046	HMS01966		NE					
CG6117	FBgn0000489	Pka-C3	BL39050	HMS01970		NE					
CG32434	FBgn0026179	siz	BL39060	HMS01980		NE					
CG8739	FBgn0086784	stmA	BL39062	HMS01982		NE					
CG6827	FBgn0013997	Nrx-IV	BL39071	HMS01991		NE					
CG8798	FBgn0036892	Lon	BL40162	HMS01940		NE					
CG9949	FBgn0003410	sina	BL40842	HMS02008		NE					

CG8442	FBgn0004619	Glu-RI	BL40844	HMS02010		NE					
CG42332	FBgn0259234	Camta	BL40849	HMS02016		NE					
CG8591	FBgn0035769	CTCF	BL40850	HMS02017		NE					
CG9648	FBgn0017578	Max	BL40851	HMS02018		NE					
CG3654	FBgn0036004	Jarid2	BL40855	HMS02022		NE					
CG17888	FBgn0016694	Pdp1	BL40863	HMS02030		NE					
CG8786	FBgn0036897	CG8786	BL40882	HMS02130		NE					
CG10060	FBgn0001104	G-ialpha65A	BL40890	HMS02138		NE					
CG7259	FBgn0036491	Best4	BL40897	HMS02145		NE					
CG7823	FBgn0036921	RhoGDI	BL40902	HMS02150		NE					
CG8005	FBgn0035854	CG8005	BL40921	HMS02169		NE					
CG3161	FBgn0262736	Vha16-1	BL40923	HMS02171		NE					
CG44154	FBgn0265003	koi	BL40924	HMS02172		NE					
CG8390	FBgn0259978	vlc	BL40925	HMS02173		NE					
CG12091	FBgn0035228	CG12091	BL40936	HMS02184		NE					
CG10642	FBgn0004380	Klp64D	BL40945	HMS02193		NE					
CG10743	FBgn0036376	Liprin-beta	BL41672	HMS02206		NE					
CG5714	FBgn0000543	ecd	BL41676	HMS02211		NE					
CG6456	FBgn0036713	Mip	BL41680	HMS02244		NE					
CG7018	FBgn0005658	Ets65A	BL41682	HMS02246		NE					
CG5837	FBgn0011771	Hem	BL41688	HMS02252		NE					
CG9155	FBgn0010246	Myo61F	BL41689	HMS02253		NE					
CG33232	FBgn0035347	CG33232	BL41696	HMS02261		NE					
CG32031	FBgn0000116	Argk	BL41697	HMS02262		NE					
CG1004	FBgn0004635	rho	BL41699	HMS02264		NE					
CG10426	FBgn0036273	CG10426	BL41701	HMS02266		NE					
CG7176	FBgn0001248	Idh	BL41708	HMS02273		NE					
CG8732	FBgn0263120	Acsl	BL41885	HMS02307	A	E-L	E-L			E	
CG10776	FBgn0024179	wit	BL41906	HMS02298		NE					
CG9390	FBgn0012034	AcCoAS	BL41917	HMS02314		NE					
CG10625	FBgn0035612	CG10625	BL41923	HMS02320		NE					
CG43340	FBgn0263077	CG43340	BL41926	HMS02323	A	E	E			E	
CG43741	FBgn0263998	PR2	BL41931	HMS02328		NE					
CG7729	FBgn0036688	Fit2	BL41941	HMS02338		NE					
CG7272	FBgn0036501	CG7272	BL41950	HMS02347		NE					

CG12009	FBgn0035430	CG12009	BL41968	HMS02365		NE					
CG12169	FBgn0035143	Ppm1	BL41987	HMS02386		NE					
CG6811	FBgn0036257	RhoGAP68F	BL41990	HMS02390		NE					
CG6642	FBgn0011293	a10	BL41993	HMS02394		NE					
CG11486	FBgn0035397	CG11486	BL42492	HMJ02056		NE					
CG5059	FBgn0037007	CG5059	BL42494	HMJ02058		NE					
CG4933	FBgn0036615	CG4933	BL42496	HMJ02060		NE					
CG9238	FBgn0036428	CG9238	BL42498	HMJ02062		NE					
CG6049	FBgn0037081	barc	BL42504	HMJ02069		NE					
CG16973	FBgn0010909	msn	BL42518	HMJ02084		NE					
CG7177	FBgn0037098	Wnk	BL42521	HMJ02087		NE					
CG5408	FBgn0028978	trbl	BL42523	HMJ02089		NE					
CG8606	FBgn0035761	RhoGEF4	BL42550	HMJ02122		NE					
CG9619	FBgn0036862	Gbs-76A	BL42551	HMJ02124		NE					
CG6064	FBgn0036746	Crtc	BL42561	HMJ02217		NE					
CG7450	FBgn0004396	CrebA	BL42562	HMJ02218		NE					
CG8727	FBgn0023094	cyc	BL42563	HMJ02219		NE					
CG7391	FBgn0023076	Clk	BL42566	HMJ02224		NE					
CG7892	FBgn0011817	nmo	BL42570	HMJ02229		NE					
CG6297	FBgn0020412	JIL-1	BL42571	HMJ02230		NE					
CG10539	FBgn0015806	S6k	BL42572	HMJ02231		NE					
CG1258	FBgn0011692	pav	BL42573	HMJ02232		NE					
CG17528	FBgn0261387	CG17528	BL42575	HMJ02234		NE					
CG18769	FBgn0042185	CG18769	BL42580	HMS01927		NE					
CG9205	FBgn0035181	CG9205	BL42588	HMS02420		NE					
CG5433	FBgn0010235	Klc	BL42597	HMS02429		NE					
CG7020	FBgn0024806	DIP2	BL42598	HMS02430		NE					
CG9018	FBgn0035318	CG9018	BL42603	HMS02436		NE					
CG4190	FBgn0001229	Hsp67Bc	BL42607	HMS02440		NE					
CG4183	FBgn0001225	Hsp26	BL42610	HMS02445		NE					
CG42311	FBgn0259211	grh	BL42611	HMS02446		NE					
CG43202	FBgn0262838	CG43202	BL42617	HMS02452		NE					
CG8368	FBgn0035707	CG8368	BL42635	HMS02471		NE					
CG8620	FBgn0040837	CG8620	BL42638	HMS02474		NE					
CG7989	FBgn0262560	wcd	BL42642	HMS02478	A	E	ME	E		E	

CG9695	FBgn0000414	Dab	BL42646	HMS02482		NE					
CG4821	FBgn0023479	Tequila	BL42650	HMS02486		NE					
CG10173	FBgn0035696	Best2	BL42654	HMS02490		NE					
CG3922	FBgn0005533	RpS17	BL42656	HMS02492	A	E	E			E	
CG11352	FBgn0027339	jim	BL42662	HMS02498		NE					
CG5585	FBgn0036973	Rbbp5	BL42819	HMJ02113		NE					
CG7133	FBgn0037150	CG7133	BL42820	HMS02502		NE					
CG7460	FBgn0036749	CG7460	BL42827	HMS02509		NE					
CG11238	FBgn0010830	l(3)04053	BL42859	HMS02551		NE					
CG32315	FBgn0024510	dlt	BL42866	HMS02559		NE					
CG13298	FBgn0035692	CG13298	BL42873	HMS02566	A	E	ME	MS	E	E	
CG14168	FBgn0036044	CG14168	BL42874	HMS02567	A	E	ME	ME	E	ME	
CG7266	FBgn0000565	Eip71CD	BL42877	HMS02570		NE					
CG13737	FBgn0036382	CG13737	BL42886	HMS02579		NE					
CG13716	FBgn0035563	CG13716	BL42895	HMS02588		NE					
CG13917	FBgn0035237	CG13917	BL42903	HMS02596	A	E	ME	S	E	ME	
CG4216	FBgn0003683	term	BL42921	HMS02614		NE					
CG16998	FBgn0035795	CG16998	BL42923	HMS02616		NE					
CG14137	FBgn0036178	CG14137	BL42937	HMS02630		NE					
CG10688	FBgn0036300	CG10688	BL42956	HMS02649		NE					
CG6736	FBgn0044049	Ilp4	BL43288	HMS02660		NE					
CG11658	FBgn0036196	CG11658	BL43298	HMS02671		NE					
CG10585	FBgn0037044	CG10585	BL43301	HMS02674		NE					
CG32236	FBgn0046793	CG32236	BL43305	HMS02685		NE					
CG32134	FBgn0005592	btl	BL43544	HMS02656		NE					
CG10472	FBgn0035670	CG10472	BL43548	HMS02654		NE					
CG18214	FBgn0024277	trio	BL43549	HMS02690		NE					
CG10605	FBgn0015919	caup	BL44002	HMS02716		NE					
CG7139	FBgn0027532	CG7139	BL44007	HMS02721		NE					
CG4195	FBgn0002283	l(3)73Ah	BL44011	HMS02725		NE					
CG4463	FBgn0001224	Hsp23	BL44029	HMS02745		NE					
CG40263	FBgn0058263	MFS17	BL44033	HMS02749		NE					
CG33991	FBgn0013718	nuf	BL44035	HMS02751		NE					
CG44128	FBgn0264959	Src42A	BL44039	HMS02755		NE					
CG1262	FBgn0020509	Acp62F	BL44047	HMS02763		NE					

CG10574	FBgn0028429	l-2	BL44050	HMS02767		NE					
CG5187	FBgn0035956	Doc2	BL44087	HMS02804		NE					
CG6451	FBgn0041161	blue	BL44094	HMS02814		NE					
CG1072	FBgn0013751	Awh	BL44097	HMS02817		NE					
CG16724	FBgn0003741	tra	BL44109	HMS02830		NE					
CG33528	FBgn0260964	Vmat	BL44471	HMC02346		NE					
CG10616	FBgn0036286	CG10616	BL44474	HMC02359		NE					
CG5701	FBgn0036980	RhoBTB	BL44478	HMC02368		NE					
CG12030	FBgn0035147	Gale	BL44496	HMC02429		NE					
CG16992	FBgn0035789	mthl6	BL44497	HMC02432		NE					
CG7476	FBgn0035847	mthl7	BL44498	HMC02433		NE					
CG18331	FBgn0036181	Muc68Ca	BL44499	HMC02435		NE					
CG4994	FBgn0026409	Mpcp	BL44508	HMC02898		NE					
CG10361	FBgn0036208	CG10361	BL44512	HMC02902		NE					
CG14353	FBgn0036771	CG14353	BL44513	HMC02903		NE					
CG6905	FBgn0035136	CG6905	BL44524	HMC02918	A	ME	ME			E	
CG32082	FBgn0052082	CG32082	BL44526	HMC02920		NE					
CG12079	FBgn0035404	CG12079	BL44535	HMC02929		NE					
CG14991	FBgn0035498	Fit1	BL44536	HMC02930		NE					
CG6498	FBgn0036511	CG6498	BL44547	HMC02943		NE					
CG10681	FBgn0036291	CG10681	BL44558	HMS02854		NE					
CG6289	FBgn0036970	Spn77Bc	BL44563	HMS02859		NE					
CG3725	FBgn0263006	Ca-P60A	BL44581	HMS02878		NE					
CG5486	FBgn0016756	Ubp64E	BL44645	HMC02352		NE					
CG10475	FBgn0035667	Jon65Ai	BL44656	HMC02430		NE					
CG6449	FBgn0036101	NijA	BL50632	HMC02999		NE					
CG8474	FBgn0025874	Meics	BL50636	HMC03035		NE					
CG10590	FBgn0035622	CG10590	BL50638	HMC03038		NE					
CG7002	FBgn0029167	Hml	BL50640	HMC03040		NE					
CG6592	FBgn0035669	CG6592	BL50645	HMC03045		NE					
CG11801	FBgn0036128	Elo68beta	BL50646	HMC03046		NE					
CG7414	FBgn0037135	CG7414	BL50649	HMC03050		NE					
CG6391	FBgn0036111	Aps	BL50651	HMC03052		NE					
CG10704	FBgn0036285	toe	BL50660	HMC03061		NE					
CG7499	FBgn0028699	Rh50	BL50666	HMC03067		NE					

CG7140	FBgn0037147	CG7140	BL50677	HMC03078		NE					
CG17334	FBgn0035626	lin-28	BL50679	HMC03080		NE					
CG7404	FBgn0035849	ERR	BL50686	HMC03087		NE					
CG7960	FBgn0013755	Bro	BL50689	HMC03090		NE					
CG32055	FBgn0052055	CG32055	BL50692	HMC03093		NE					
CG6859	FBgn0036484	Pex3	BL50694	HMC03096		NE					
CG6749	FBgn0036040	CG6749	BL50696	HMC03098	A	ME	ME			ME	
CG5485	FBgn0036770	Prestin	BL50706	HMC03108		NE					
CG32105	FBgn0052105	CG32105	BL50711	HMC03113		NE					
CG5690	FBgn0035295	Cnb	BL50714	HMS02948		NE					
CG10591	FBgn0035621	CG10591	BL50722	HMS02956		NE					
CG44167	FBgn0265052	St3	BL50728	HMS02964		NE					
CG7398	FBgn0024921	Trn	BL50732	HMS02968		NE					
CG4347	FBgn0035978	UGP	BL50902	HMJ03120		NE					
CG7260	FBgn0011723	byn	BL50906	HMJ03127		NE					
CG10392	FBgn0261403	sxc	BL50909	HMJ03131		NE					
CG9279	FBgn0036882	CG9279	BL50914	HMJ21003		NE					
CG10622	FBgn0029118	Sucb	BL50939	HMJ21034		NE					
CG5290	FBgn0036772	CG5290	BL50949	HMJ21050		NE					
CG10124	FBgn0035709	eIF4E-4	BL50951	HMJ21052		NE					
CG5642	FBgn0036258	eIF3l	BL50959	HMJ21061		NE					
CG14177	FBgn0036013	CG14177	BL50984	HMJ21094		NE					
CG5444	FBgn0010280	Taf4	BL50985	HMJ21095	A	E	E			E	
CG6527	FBgn0036085	CG6527	BL50994	HMJ21107		NE					
CG14962	FBgn0035407	CG14962	BL51002	HMJ21116		NE					
CG12918	FBgn0263260	sel	BL51015	HMJ21136		NE					
CG10596	FBgn0015766	Msr-110	BL51034	HMJ21161		NE					
CG9670	FBgn0028380	fal	BL51048	HMJ21182		NE					
CG14572	FBgn0037128	CG14572	BL51050	HMJ21184		NE					
CG11637	FBgn0036822	CG11637	BL51156	HMC02367		NE					
CG4457	FBgn0015298	Srp19	BL51160	HMC02399	A	E	E			E	
CG6298	FBgn0023197	Jon74E	BL51161	HMC02401		NE					
CG11115	FBgn0037202	Ssl1	BL51165	HMJ03124		NE					
CG10270	FBgn0022699	D19B	BL51166	HMJ03125		NE					
CG2264	FBgn0262169	magu	BL51169	HMJ21055		NE					

CG14838	FBgn0035799	CG14838	BL51175	HMJ21140		NE					
CG7580	FBgn0036728	CG7580	BL51357	HMC03242		NE					
CG8276	FBgn0263144	bin3	BL51427	HMC02940		NE					
CG7542	FBgn0036738	CG7542	BL51429	HMC03048		NE					
CG7422	FBgn0035815	Snmp2	BL51432	HMC03144		NE					
CG7409	FBgn0035817	CG7409	BL51433	HMC03145		NE					
CG9007	FBgn0036398	CG9007	BL51447	HMC03177		NE					
CG18179	FBgn0036023	CG18179	BL51451	HMC03181		NE					
CG16838	FBgn0036574	CG16838	BL51453	HMC03187		NE					
CG7510	FBgn0036741	CG7510	BL51463	HMC03201		NE					
CG11529	FBgn0036264	CG11529	BL51469	HMC03210		NE					
CG43795	FBgn0264339	CG43795	BL51472	HMC03214		NE					
CG8782	FBgn0022774	Oat	BL51481	HMC03226		NE					
CG10078	FBgn0041194	Prat2	BL51492	HMC03244		NE					
CG10594	FBgn0003486	spo	BL51496	HMC03251		NE					
CG6760	FBgn0013563	Pex1	BL51497	HMC03252		NE					
CG6765	FBgn0035903	CG6765	BL51500	HMC03258		NE					
CG17181	FBgn0035144	CG17181	BL51517	HMS03165		NE					
CG6483	FBgn0035665	Jon65Aiii	BL51692	HMC02917		NE					
CG17084	FBgn0035131	mthl9	BL51695	HMC03141		NE					
CG7955	FBgn0035244	ABCB7	BL51696	HMC03142		NE					
CG10477	FBgn0035661	CG10477	BL51697	HMC03143		NE					
CG8329	FBgn0036022	CG8329	BL51698	HMC03146		NE					
CG17027	FBgn0036553	CG17027	BL51701	HMC03174		NE					
CG5272	FBgn0001120	gnu	BL51703	HMC03185		NE					
CG6869	FBgn0036485	FucTA	BL51715	HMC03247		NE					
CG17484	FBgn0260799	p120ctn	BL51729	HMC03276		NE					
CG9701	FBgn0036659	CG9701	BL51733	HMC03293		NE					
CG17061	FBgn0035132	mthl10	BL51753	HMC03304		NE					
CG7118	FBgn0035886	Jon66Ci	BL51754	HMC03305		NE					
CG5262	FBgn0036988	CG5262	BL51755	HMC03306		NE					
CG8585	FBgn0263397	Ih	BL51765	HMC03319		NE					
CG5747	FBgn0035935	mfr	BL51769	HMC03324		NE					
CG7758	FBgn0027945	ppl	BL51778	HMC03333		NE					
CG9943	FBgn0029117	Surf1	BL51783	HMC03338		NE					

CG5258	FBgn0029148	NHP2	BL51784	HMC03339		NE					
CG14994	FBgn0004516	Gad1	BL51794	HMC03350		NE					
CG14993	FBgn0016013	Faa	BL51796	HMC03352		NE					
CG17146	FBgn0022709	Adk1	BL51799	HMC03355		NE					
CG6097	FBgn0003292	rt	BL51805	HMC03363		NE					
CG8615	FBgn0035753	RpL18	BL51812	HMC03383	A	E	E				
CG7977	FBgn0026372	RpL23A	BL51818	HMC03389		NE					
CG9384	FBgn0036446	CG9384	BL51821	HMC03393		NE					
CG7864	FBgn0035233	Pex10	BL51826	HMC03398		NE					
CG8177	FBgn0036043	CG8177	BL51827	HMC03399		NE					
CG17142	FBgn0035113	pyx	BL51836	HMC03408		NE					
CG4319	FBgn0011706	rpr	BL51846	HMC03419		NE					
CG18374	FBgn0025592	Gyk	BL51849	HMC03423		NE					
CG7049	FBgn0035102	CG7049	BL51896	HMC03470		NE					
CG13927	FBgn0035245	GC	BL51897	HMC03471		NE					
CG2069	FBgn0035264	Oseg4	BL51898	HMC03472		NE					
CG1140	FBgn0035298	CG1140	BL51899	HMC03473		NE					
CG2107	FBgn0035383	CG2107	BL51900	HMC03474		NE					
CG12014	FBgn0035445	CG12014	BL51901	HMC03475		NE					
CG10849	FBgn0035471	Sc2	BL51902	HMC03476		NE					
CG4623	FBgn0035587	CG4623	BL51903	HMC03477		NE					
CG7161	FBgn0035891	Oseg1	BL51904	HMC03478		NE					
CG12272	FBgn0036571	CG12272	BL51906	HMC03481		NE					
CG9706	FBgn0036662	CG9706	BL51908	HMC03483		NE					
CG6841	FBgn0036828	CG6841	BL51909	HMC03484		NE					
CG7470	FBgn0037146	CG7470	BL51911	HMC03487		NE					
CG6951	FBgn0036959	CG6951	BL51913	HMS03371		NE					
CG15811	FBgn0004574	Rop	BL51925	HMC03422	A	E-L	E-L			E-L	
CG7757	FBgn0036915	CG7757	BL51940	HMC03485	A	E	ME	ME		ME	
CG10586	FBgn0037036	Sems	BL52892	HMC03630		NE					
CG10537	FBgn0004244	Rdl	BL52903	HMC03643		NE					
CG6020	FBgn0037001	CG6020	BL52922	HMC03662		NE					
CG11796	FBgn0036992	CG11796	BL52923	HMC03663		NE					
CG4300	FBgn0036272	CG4300	BL52924	HMC03665		NE					
CG8583	FBgn0035771	sec63	BL52925	HMC03666		NE					

CG7971	FBgn0035253	CG7971	BL52936	HMC03678	A	E-L	E			E-L	
CG5684	FBgn0036239	Pop2/CNOT7	BL52947	HMJ21614	E	E	NE	NE	E		NE
CG13891	FBgn0035139	CG13891	BL52950	HMJ21619		NE					
CG5602	FBgn0262619	DNA-ligI	BL52951	HMJ21620		NE					
CG42600	FBgn0261016	clos	BL52966	HMJ21651		NE					
CG32088	FBgn0052088	CG32088	BL52969	HMJ21654		NE					
CG32102	FBgn0052102	CG32102	BL52975	HMJ21661		NE					
CG10588	FBgn0037037	CG10588	BL52977	HMJ21664		NE					
CG9710	FBgn0021768	nudC	BL52980	HMJ21667		NE					
CG3743	FBgn0040305	MTF-1	BL52986	HMJ21677		NE					
CG9129	FBgn0035196	CG9129	BL52995	HMJ21707		NE					
CG43729	FBgn0263980	CG43729	BL52999	HMJ21714		NE					
CG4167	FBgn0001227	Hsp67Ba	BL53007	HMJ21725		NE					
CG3529	FBgn0035995	CG3529	BL53008	HMJ21726		NE					
CG13924	FBgn0035286	CG13924	BL53013	HMJ21735		NE					
CG8001	FBgn0035268	CG8001	BL53021	HMJ21744		NE					
CG7327	FBgn0014849	Eig71Ei	BL53022	HMJ21745		NE					
CG6215	FBgn0015025	CkIIalpha-i1	BL53025	HMJ21750		NE					
CG6850	FBgn0014075	Ugt	BL53027	HMJ21752		NE					
CG4153	FBgn0004926	eIF-2beta	BL53268	HMC02396		NE					
CG4365	FBgn0037024	CG4365	BL53290	HMC03506	A	E	E			E	
CG6671	FBgn0262739	AGO1	BL53293	HMC03509	A	E	E			E	
CG7506	FBgn0035805	CG7506	BL53297	HMC03513	A	ME	ME			E	
CG4461	FBgn0035982	CG4461	BL53298	HMC03517		NE					
CG14077	FBgn0036830	CG14077	BL53303	HMC03530		NE					
CG32072	FBgn0052072	Elo68alpha	BL53307	HMC03535		NE					
CG5842	FBgn0036414	nan	BL53312	HMC03541		NE					
CG10359	FBgn0035452	CG10359	BL53316	HMC03545		NE					
CG17028	FBgn0036552	CG17028	BL53320	HMC03549		NE					
CG15015	FBgn0035533	Cip4	BL53321	HMC03550		NE					
CG8019	FBgn0001179	hay	BL53345	HMC03574		NE					
CG10522	FBgn0002466	sti	BL53357	HMC03586		NE					
CG2092	FBgn0261385	scra	BL53358	HMC03587		NE					
CG10587	FBgn0037039	CG10587	BL53359	HMC03588	A	ME	ME			ME	
CG11037	FBgn0037038	CG11037	BL53360	HMC03589		NE					

CG14990	FBgn0035496	CG14990	BL53367	HMC03596		NE					
CG30283	FBgn0260477	CG30283	BL53376	HMC03605		NE					
CG7328	FBgn0036942	CG7328	BL53675	HMC03664		NE					
CG13285	FBgn0035611	CG13285	BL53680	HMJ21593		NE					
Smyd4	FBgn0036282	Smyd4	BL53682	HMJ21595		NE					
tow	FBgn0035719	tow	BL53704	HMJ21747		NE					
Cpr72Ea	FBgn0036617	Cpr72Ea	BL53878	HMJ21191		NE					
CG11426	FBgn0037166	CG11426	BL53879	HMJ21194		NE					
hppy	FBgn0263395	hppy	BL53884	HMJ21199		NE					
pdm3	FBgn0261588	pdm3	BL53887	HMJ21205		NE					
CG7202	FBgn0037086	CG7202	BL53895	HMJ21214		NE					
CG32444	FBgn0043783	CG32444	BL53929	HMJ21275		NE					
Cyt-b5	FBgn0264294	Cyt-b5	BL53950	HMJ21314		NE					
CG32026	FBgn0052026	CG32026	BL53953	HMJ21319		NE					
tral	FBgn0041775	tral	BL53961	HMJ21343	A	E	E-L			E-L	
Nplp2	FBgn0040813	Nplp2	BL53967	HMJ21350		NE					
Eig71Ea	FBgn0004588	Eig71Ea	BL53984	HMJ21384		NE					
Sox21a	FBgn0036411	Sox21a	BL53991	HMJ21395		NE					
Xpd	FBgn0261850	Xpd	BL53992	HMJ21396	ME	ME	NE	NE	E		NE
Tie	FBgn0014073	Tie	BL54005	HMJ21428		NE					
5-HT1B	FBgn0263116	5-HT1B	BL54006	HMJ21429	A	E	E			E	
CG2021	FBgn0035271	CG2021	BL54007	HMJ21430		NE					
loopin-1	FBgn0259795	loopin-1	BL54012	HMJ21436		NE					
Ndfip	FBgn0052177	Ndfip	BL54018	HMJ21444		NE					
Gr61a	FBgn0035167	Gr61a	BL54030	HMJ21473		NE					
CG14147	FBgn0036112	CG14147	BL54046	HMJ21489		NE					
CG8549	FBgn0035714	CG8549	BL54466	HMC03734		NE					
mas	FBgn0011653	mas	BL54475	HMC03732	MS	MS		S	S		(ME POSSIBLE)
CG13810	FBgn0035313	CG13810	BL54802	HMJ21496		NE					
CG42663	FBgn0261545	CG42663	BL54808	HMJ21502		NE					
robl62A	FBgn0028567	robl62A	BL54813	HMJ21532		NE					
Nca	FBgn0013303	Nca	BL54814	HMJ21533		NE					
CG32036	FBgn0052036	CG32036	BL54818	HMJ21537		NE					
CG8833	FBgn0036386	CG8833	BL54824	HMJ21543		NE					

CG6757	FBgn0040475	SH3PX1	BL54833	HMJ21552		NE					
CG6933	FBgn0036952	CG6933	BL54842	HMJ21579		NE					
CG7385	FBgn0036937	Ir76b	BL54846	HMJ21583		NE					
CG1919	FBgn0035281	Cpr62Bc	BL54849	HMJ21586		NE					
CG3396	FBgn0040296	Ocho	BL54851	HMJ21588	A	E	E			E	
CG1828	FBgn0002183	dre4	BL54855	HMS02240		NE					
CG7433	FBgn0036927	CG7433	BL54993	HMC03730		NE					
CG3088	FBgn0036015	CG3088	BL55145	HMC03755		NE					
CG8610	FBgn0012058	Cdc27	BL55155	HMC03814	A	ME	E			E	
CG16725	FBgn0036641	Smn	BL55158	HMC03832		NE					
CR32162	FBgn0041721	snRNA:U12:73B	BL55164	HMC03841		NE					
CG10907	FBgn0036207	CG10907	BL55204	HMC03919		NE					
CG11274	FBgn0036340	SRm160	BL55205	HMC03920		NE					
CG6322	FBgn0036733	U4-U6-60K	BL55210	HMC03931		NE					
CG9383	FBgn0029094	asf1	BL55250	HMC03937		NE					
CG7564	FBgn0036734	CG7564	BL55252	HMC03939		NE					
CG18586	FBgn0035642	CG18586	BL55270	HMC03957		NE					
CG44252	FBgn0265187	CG44252	BL55271	HMC03958		NE					
CG10948	FBgn0036317	CG10948	BL55280	HMC03967		NE					
CG6817	FBgn0024236	foi	BL55281	HMC03968		NE					
CG10469	FBgn0035678	CG10469	BL55291	HMC03978		NE					
CG6457	FBgn0040060	yip7	BL55293	HMC03980	ME	ME	NE	ME	NE		NE
CG1130	FBgn0004880	scrt	BL55309	HMC03996		NE					
CG32120	FBgn0002573	sens	BL55310	HMC03997		NE					
CG10564	FBgn0024150	Ac78C	BL55312	HMC03999		NE					
CG4561	FBgn0027080	Aats-tyr	BL55326	HMC04013		NE					
CG6778	FBgn0027088	Aats-gly	BL55327	HMC04014		NE					
CG6580	FBgn0035666	Jon65Aii	BL55343	HMC04030	A	ME	E			E	
CG6865	FBgn0036817	CG6865	BL55349	HMC04036		NE					
CG4911	FBgn0035959	CG4911	BL55353	HMC04040		NE					
CG6876	FBgn0036487	Prp31	BL55364	HMC04052		NE					
CG33228	FBgn0261373	CG33228	BL55372	HMC04060		NE					
CG10006	FBgn0036461	CG10006	BL55376	HMC04064		NE					
CG13076	FBgn0044028	Notum	BL55379	HMC04067		NE					
CG1934	FBgn0001254	ImpE2	BL55380	HMC04068		NE					

CG8783	FBgn0036397	CG8783	BL55384	HMC04072		NE					
CG10717	FBgn0001256	ImpL1	BL55387	HMC04075		NE					
CG3322	FBgn0002528	LanB2	BL55388	HMC04076		NE					
CG6821	FBgn0002564	Lsp1gamma	BL55389	HMC04077		NE					
CG10810	FBgn0010381	Drs	BL55391	HMC04079		NE					
CG18321	FBgn0029002	miple2	BL55393	HMC04081		NE					
CG13906	FBgn0028999	nerfin-1	BL55395	HMC04083		NE					
CG1887	FBgn0035290	CG1887	BL55401	HMC04089		NE					
CG9116	FBgn0004429	LysP	BL55606	HMC03743		NE					
CG7028	FBgn0027587	CG7028	BL55640	HMC03788		NE					
CG6664	FBgn0036685	CG6664	BL55643	HMC03792		NE					
CG10754	FBgn0036314	CG10754	BL55650	HMC03799		NE					
CG42382	FBgn0259728	CG42382	BL55652	HMC03801		NE					
CG10582	FBgn0028402	Sin	BL55656	HMC03807		NE					
CG6822	FBgn0035909	ergic53	BL55657	HMC03809		NE					
CG7942	FBgn0035838	ldbr	BL55661	HMC03816		NE					
CG8596	FBgn0035767	CG8596	BL55664	HMC03819		NE					
CG11489	FBgn0025702	srpk79D	BL55667	HMC03822		NE					
CG1291	FBgn0035401	CG1291	BL55671	HMC03827		NE					
CR32908	FBgn0003938	snRNA:U5:63BC	BL55676	HMC03840		NE					
CG18180	FBgn0036024	CG18180	BL55680	HMC03862		NE					
CG4083	FBgn0017572	Mo25	BL55681	HMC03865		NE					
CG5649	FBgn0024887	kin17	BL55692	HMC03906	A	E	ME			E	
CG5971	FBgn0035918	Cdc6	BL55734	HMC03802	A	ME	ME			ME	
CG10663	FBgn0036287	CG10663	BL55737	HMC03876		NE					
CG2146	FBgn0261397	didum	BL55740	HMC03900		NE					
CG9054	FBgn0015075	Ddx1	BL55744	HMC03930		NE					
CG10418	FBgn0036277	CG10418	BL55746	HMC03933		NE					
CG15009	FBgn0001257	ImpL2	BL55855	HMC03863		NE					
CG4279	FBgn0261067	LSm1	BL55912	HMC04198		NE					
CG32176	FBgn0052176	CG32176	BL55923	HMC04210		NE					
CG6917	FBgn0000592	Est-6	BL55927	HMC04215		NE					
CG17148	FBgn0000594	Est-P	BL55928	HMC04216		NE					
CG7599	FBgn0004593	Eig71Ef	BL55930	HMC04218	MS	MS		S	E		E
CG13312	FBgn0035931	CG13312	BL55949	HMC04238		NE					

CG6628	FBgn0036072	CG6628	BL55950	HMC04239		NE					
CG17826	FBgn0036227	CG17826	BL55951	HMC04240		NE					
CG10116	FBgn0036367	CG10116	BL55952	HMC04241		NE					
CG40733	FBgn0085512	RYamide	BL55957	HMC04246		NE					
CG17575	FBgn0250842	CG17575	BL55958	HMC04247		NE					
CG8614	FBgn0024542	Neos	BL55960	HMC04254		NE					
CG13806	FBgn0035325	CG13806	BL55965	HMC04260		NE					
CG14957	FBgn0035412	CG14957	BL55966	HMC04261		NE					
CG14959	FBgn0035427	ckd	BL55967	HMC04262		NE					
CG8072	FBgn0036070	CG8072	BL55968	HMC04263		NE					
CG5897	FBgn0036220	CG5897	BL55969	HMC04264		NE					
CG5883	FBgn0036225	CG5883	BL55970	HMC04265		NE					
CG10154	FBgn0036361	CG10154	BL55971	HMC04266	A	E	E			E	
CG6996	FBgn0036950	CG6996	BL55972	HMC04267		NE					
CG17145	FBgn0036953	CG17145	BL55974	HMC04269		NE					
CG5008	FBgn0040321	GNBP3	BL55984	HMC04280		NE					
CG32024	FBgn0052024	CG32024	BL55997	HMC04293		NE					
CG32068	FBgn0052068	CG32068	BL56008	HMC04304	A	ME	ME			ME	
CG9128	FBgn0035195	Sac1	BL56013	HMC04309		NE					
CG10592	FBgn0035619	CG10592	BL56014	HMC04310		NE					
CG1274	FBgn0040308	Jafrac2	BL56043	HMC04351		NE					
CG32178	FBgn0043025	Msi	BL56044	HMC04352		NE					
CG7250	FBgn0036494	Toll-6	BL56048	HMS04251		NE					
CG8021	FBgn0037602	CG8021	BL32339	HMS00330		NE					
CG6226	FBgn0013269	FK506-bp1	BL32348	HMS00339		NE					
CG9983	FBgn0001215	Hrb98DE	BL32351	HMS00342	E	E	NE	E	ME		NE
CG9484	FBgn0002431	hyd	BL32352	HMS00343	ME	ME	NE	E	E		NE
CG12249	FBgn0021776	mira	BL32356	HMS00347		NE					
CG1064	FBgn0011715	Snr1	BL32372	HMS00363		NE					
CG6791	FBgn0037918	CG6791	BL32395	HMS00389		NE					
CG9775	FBgn0037261	CG9775	BL32396	HMS00390		NE					
CG42799	FBgn0261934	dikar	BL32397	HMS00391		NE					
CG33556	FBgn0053556	form3	BL32398	HMS00393	A	E	E			E	
CG7788	FBgn0019972	Ice	BL32403	HMS00398	A	E	E			E	
CG5650	FBgn0004103	Pp1-87B	BL32414	HMS00409	A	E-L	E			E	

CG17603	FBgn0010355	Taf1	BL32421	HMS00416	ME	ME	NE	E	ME		NE
CG3143	FBgn0038197	foxo	BL32427	HMS00422		NE					
CG7483	FBgn0037573	eIF4AIII	BL32444	HMS00442	(MS POSSIBLE)	NE					
CG6923	FBgn0037944	CG6923	BL32448	HMS00447		NE					
CG5248	FBgn0020278	loco	BL32456	HMS00455		NE					
CG4720	FBgn0014006	Pk92B	BL32464	HMS00464		NE					
CG6773	FBgn0024509	sec13	BL32468	HMS00468		NE					
CG12073	FBgn0004573	5-HT7	BL32471	HMS00471		NE					
CG5422	FBgn0005649	Rox8	BL32472	HMS00472		NE					
CG7771	FBgn0004666	sim	BL32488	HMS00491		NE					
CG4637	FBgn0004644	hh	BL32489	HMS00492		NE					
CG31137	FBgn0011725	twin	BL32490	HMS00493		NE					
CG7015	FBgn0263352	Unr	BL32491	HMS00494		NE					
CG8308	FBgn0087040	alphaTub67C	BL32502	HMS00506		NE					
CG1193	FBgn0037375	kat-60L1	BL32506	HMS00510		NE					
CG11984	FBgn0037655	CG11984	BL32507	HMS00511		NE					
CG9366	FBgn0014380	RhoL	BL32841	HMS00532		NE					
CG3354	FBgn0086915	Mst77F	BL32849	HMS00633		NE					
CG5374	FBgn0003676	T-cp1	BL32854	HMS00639		NE					
CG3637	FBgn0025865	Cortactin	BL32871	HMS00658		NE					
CG8036	FBgn0037607	CG8036	BL32884	HMS00672		NE					
CG7583	FBgn0020496	CtBP	BL32889	HMS00677		NE					
CG4565	FBgn0037841	CG4565	BL32893	HMS00682		NE					
CG4261	FBgn0022787	Hel89B	BL32895	HMS00684		NE					
CG3508	FBgn0038251	CG3508	BL32898	HMS00687		NE					
CG4800	FBgn0037874	Tctp	BL32911	HMS00701	A	E-L	E-L			E-L	
CG2899	FBgn0015402	ksr	BL32937	HMS00730		NE					
CG1483	FBgn0002645	Map205	BL32939	HMS00733		NE					
CG12819	FBgn0037810	sle	BL32969	HMS00766		NE					
CG32251	FBgn0052251	CG32251	BL32974	HMS00772		NE					
CG8165	FBgn0037703	JHDM2	BL32975	HMS00775		NE					
CG5637	FBgn0002962	nos	BL32985	HMS00785		NE					
CG32491	FBgn0002781	mod(mdg4)	BL32995	HMS00795		NE					
CG6343	FBgn0019957	ND42	BL32998	HMS00798		NE					

CG6831	FBgn0260442	rhea	BL32999	HMS00799		NE					
CG5252	FBgn0037894	Ranbp9	BL33004	HMS00804		NE					
CG12812	FBgn0037781	Fancl	BL33050	HMS00771		NE					
CG12201	FBgn0037970	CG12201	BL33338	HMS00204		NE					
CG14377	FBgn0038148	CG14377	BL33344	HMS00210		NE					
CG9386	FBgn0037708	CG9386	BL33364	HMS00236		NE					
CG42665	FBgn0261547	Exn	BL33373	HMS00246		NE					
CG9351	FBgn0024555	flfl	BL33374	HMS00247		NE					
CG8874	FBgn0000723	Fps85D	BL33375	HMS00249		NE					
CG9434	FBgn0037724	Fst	BL33376	HMS00250		NE					
CG33956	FBgn0001297	kay	BL33379	HMS00254		NE					
CG9412	FBgn0015778	rin	BL33392	HMS00269		NE					
CG42734	FBgn0261788	Ank2	BL33414	HMS00295		NE					
CG6993	FBgn0003513	ss	BL33415	HMS00296		NE					
CG2198	FBgn0000071	Ama	BL33416	HMS00297	A	ME	ME			E	
CG31132	FBgn0011785	BRWD3	BL33421	HMS00304		NE					
CG12284	FBgn0260635	th	BL33597	HMS00752		NE					
CG42865	FBgn0262139	trh	BL33612	HMS00002		NE					
CG4006	FBgn0010379	Akt1	BL33615	HMS00007	E-L	E-L	ME	MS	E-L	ME	NE
CG10422	FBgn0000158	bam	BL33631	HMS00029		NE					
CG4257	FBgn0016917	Stat92E	BL33637	HMS00035		NE					
CG32206	FBgn0052206	CG32206	BL33645	HMS00046		NE					
CG5670	FBgn0002921	Atpalpha	BL33646	HMS00047	E-L	E-L	NE	NE	E-L		NE
CG9745	FBgn0000412	D1	BL33655	HMS00061	A	E	E			E	
CG11992	FBgn0014018	Rel	BL33661	HMS00070		NE					
CG1462	FBgn0016123	Aph-4	BL33673	HMS00537		NE					
CG7917	FBgn0016685	Nlp	BL33688	HMS00556		NE					
CG6148	FBgn0016693	Past1	BL33689	HMS00557		NE					
CG3978	FBgn0003117	pnr	BL33697	HMS00570		NE					
CG11033	FBgn0037659	Kdm2	BL33699	HMS00574		NE					
CG8651	FBgn0003862	trx	BL33703	HMS00580		NE					
CG17149	FBgn0260397	Su(var)3-3	BL33726	HMS00608		NE					
CG6030	FBgn0016120	ATPsyn-d	BL33740	HMS01078		NE					
CG9473	FBgn0024330	MED6	BL33743	HMS01081	MS	MS		S	MS		NE
CG7281	FBgn0004597	CycC	BL33753	HMS01095		NE					

CG5201	FBgn0020493	Dad	BL33759	HMS01102		NE					
CG10002	FBgn0000659	fkh	BL33760	HMS01103		NE					
CG2047	FBgn0001077	ftz	BL33761	HMS01104		NE					
CG1034	FBgn0000166	bcd	BL33886	HMS00824		NE					
CG17594	FBgn0028993	scro	BL33890	HMS00828		NE					
CG7951	FBgn0015542	sima	BL33894	HMS00832		NE					
CG3412	FBgn0023423	slmb	BL33898	HMS00838		NE					
CG8573	FBgn0003567	su(Hw)	BL33906	HMS00848		NE					
CG9809	FBgn0037248	Spargel	BL33914	HMS00857		NE					
CG9809	FBgn0037248	Spargel	BL33915	HMS00858		NE					
CG4974	FBgn0263930	dally	BL33952	HMS00905		NE					
CG9769	FBgn0037270	eIF3f1	BL33980	HMS00940		NE					
CG1112	FBgn0015575	alpha-Est7	BL33992	HMS00955		NE					
CG17273	FBgn0027493	CG17273	BL33993	HMS00956		NE					
CG9656	FBgn0001138	grn	BL34014	HMS00980		NE					
CG42669	FBgn0261551	CG42669	BL34016	HMS00985		NE					
CG10230	FBgn0028691	Rpn9	BL34034	HMS01007		NE					
CG8580	FBgn0082598	akirin	BL34036	HMS01010		NE					
CG33484	FBgn0052311	zormin	BL34039	HMS01014		NE					
CG12072	FBgn0011739	wts	BL34064	HMS00026		NE					
CG8522	FBgn0261283	HLH106	BL34073	HMS00080		NE					
CG6625	FBgn0250791	Snap	BL34088	HMS00872		NE					
CG2017	FBgn0037391	CG2017	BL34097	HMS00976		NE					
CG3619	FBgn0000463	Dl	BL34322	HMS01309	A	E-L	E-L			E-L	
CG1378	FBgn0003720	tll	BL34329	HMS01316		NE					
CG12360	FBgn0038111	CG12360	BL34341	HMS01329		NE					
CG9805	FBgn0037249	eIF3-S10	BL34353	HMS01342	(MS POSSIBLE)	NE	ME	MS	ME	E	
CG5232	FBgn0038045	Sas	BL34357	HMS01346		NE					
CG9374	FBgn0038167	lkb1	BL34362	HMS01351		NE					
CG32226	FBgn0052226	Pex23	BL34370	HMS01359		NE					
CG8287	FBgn0262518	Rab8	BL34373	HMS01363		NE					
CG8417	FBgn0037744	MPI	BL34379	HMS01369	E	E	NE	S	NE		NE
CG18525	FBgn0028984	Spn5	BL34381	HMS01371		NE					
CG1218	FBgn0037377	CG1218	BL34389	HMS01383		NE					

CG18549	FBgn0038053	CG18549	BL34391	HMS01385		NE					
CG6284	FBgn0037802	Sirt6	BL34530	HMS01009		NE					
CG1100	FBgn0028690	Rpn5	BL34532	HMS00971		NE					
CG42575	FBgn0260795	CG42575	BL34549	HMS01021		NE					
CG1982	FBgn0024289	Sodh-1	BL34556	HMS01028		NE					
CG3027	FBgn0037513	pyd3	BL34557	HMS01029		NE					
CG9773	FBgn0037609	CG9773	BL34570	HMS01044		NE					
CG4608	FBgn0014135	bnl	BL34572	HMS01046		NE					
CG1057	FBgn0037262	MED31	BL34574	HMS01048		NE					
CG1245	FBgn0037359	MED27	BL34576	HMS01050		NE					
CG2943	FBgn0037530	CG2943	BL34581	HMS01055		NE					
CG11968	FBgn0037647	RagA	BL34590	HMS01064		NE					
CG11999	FBgn0037312	CG11999	BL34604	HMS00565		NE					
CG9375	FBgn0003205	Ras85D	BL34619	HMS01294		NE					
CG1101	FBgn0010774	Ref1	BL34626	HMS01301		NE					
CG1046	FBgn0004053	zen	BL34635	HMS01109		NE					
CG17117	FBgn0001235	hth	BL34637	HMS01112		NE					
CG1048	FBgn0004054	zen2	BL34649	HMS01124		NE					
CG4674	FBgn0037856	CG4674	BL34660	HMS01137		NE					
CG5208	FBgn0028470	Patr-1	BL34667	HMS01144		NE					
CG3320	FBgn0016700	Rab1	BL34670	HMS01148		NE					
CG33976	FBgn0038063	Octbeta2R	BL34673	HMS01151		NE					
CG1009	FBgn0261243	Psa	BL34674	HMS01152		NE					
CG42584	FBgn0260874	Ir76a	BL34678	HMS01156		NE					
CG8412	FBgn0037743	CG8412	BL34680	HMS01158		NE					
CG17023	FBgn0024804	Dbp80	BL34682	HMS01160		NE					
CG2023	FBgn0037383	CG2023	BL34693	HMS01172		NE					
CG6134	FBgn0003495	spz	BL34699	HMS01178		NE					
CG6127	FBgn0004197	Ser	BL34700	HMS01179		NE					
CG2102	FBgn0004878	cas	BL34701	HMS01180		NE					
CG5460	FBgn0001169	H	BL34703	HMS01182	A	ME	ME			ME	
CG9786	FBgn0001180	hb	BL34704	HMS01183		NE					
CG1133	FBgn0003002	opa	BL34706	HMS01185		NE					
CG9475	FBgn0037742	Rpt3R	BL34713	HMS01192		NE					
CG17397	FBgn0040020	MED21	BL34731	HMS01211	S	S		S	MS		NE

CG42279	FBgn0259174	Nedd4	BL34741	HMS01221		NE					
CG5475	FBgn0015765	Mpk2	BL34744	HMS01224		NE					
CG2128	FBgn0025825	Hdac3	BL34778	HMS00087		NE					
CG5378	FBgn0028688	Rpn7	BL34787	HMS00096	A	E-L	E			E	
CG5289	FBgn0015282	Pros26.4	BL34795	HMS00104	A	E-L	E			E	
CG4913	FBgn0026441	ear	BL34798	HMS00107	MS	MS		MS	MS		NE
CG7439	FBgn0087035	AGO2	BL34799	HMS00108		NE					
CG8273	FBgn0037716	CG8273	BL34805	HMS00114		NE					
CG9772	FBgn0037236	Skp2	BL34807	HMS00116		NE					
CG3158	FBgn0003483	spn-E	BL34808	HMS00117		NE					
CG10279	FBgn0003261	Rm62	BL34829	HMS00144		NE					
CG1395	FBgn0003525	stg	BL34831	HMS00146	A	E	E			E	
CG10753	FBgn0261933	SmD1	BL34834	HMS00150		NE					
CG2925	FBgn0014366	noi	BL34845	HMS00163		NE					
CG17358	FBgn0011290	Taf12	BL34852	HMS00170		NE					
CG43772	FBgn0264272	mwh	BL34862	HMS00180		NE					
CG8120	FBgn0037675	HP1e	BL34863	HMS00181		NE					
CG1084	FBgn0037240	Cont	BL34867	HMS00186	E-L	E-L	NE	MS	MS		NE
CG11981	FBgn0026380	Prosbeta3	BL34868	HMS00187	A	E-L	ME	S	E-L	E	
CG1451	FBgn0015589	Apc	BL34869	HMS00188		NE					
CG7437	FBgn0262737	mub	BL34870	HMS00189		NE					
CG31196	FBgn0020238	14-3-3epsilon	BL34884	HMS01229		NE					
CG2244	FBgn0027951	MTA1-like	BL34905	HMS01251		NE					
CG33101	FBgn0013998	Nsf2	BL34914	HMS01262		NE					
CG18740	FBgn0002783	mor	BL34919	HMS01267		NE					
CG33214	FBgn0264561	Glg1	BL34921	HMS01270		NE					
CG7508	FBgn0010433	ato	BL34929	HMS01278		NE					
CG8351	FBgn0037632	Tcp-1eta	BL34931	HMS01281		NE					
CG6598	FBgn0011768	Fdh	BL34937	HMS01268		NE					
CG2926	FBgn0037344	CG2926	BL34941	HMS00216		NE					
CG42674	FBgn0261556	CG42674	BL34943	HMS00228		NE					
CG6203	FBgn0028734	Fmr1	BL34944	HMS00248		NE					
CG18271	FBgn0037263	slx1	BL34949	HMS00313		NE					
CG11888	FBgn0028692	Rpn2	BL34961	HMS00533		NE					
CG8977	FBgn0015019	Cctgamma	BL34969	HMS00884		NE					

CG2684	FBgn0002542	lds	BL34980	HMS01389		NE					
CG10388	FBgn0003944	Ubx	BL34993	HMS01403		NE					
CG9347	FBgn0002937	ninaB	BL34994	HMS01404	A	ME	ME			E	
CG6017	FBgn0259824	Hip14	BL35012	HMS01422		NE					
CG14887	FBgn0004087	Dhfr	BL35015	HMS01428		NE					
CG7937	FBgn0004863	C15	BL35018	HMS01431		NE					
CG7223	FBgn0010389	htl	BL35024	HMS01437		NE					
CG1135	FBgn0263832	Rcd5	BL35026	HMS01439		NE					
CG17077	FBgn0003118	pnt	BL35038	HMS01452	A	E	E			E	
CG10061	FBgn0011020	Sas-4	BL35049	HMS01463		NE					
CG5954	FBgn0002441	l(3)mbt	BL35052	HMS01466		NE					
CG1945	FBgn0005632	faf	BL35728	HMS01470		NE					
CG8279	FBgn0038237	Pde6	BL35743	HMS01485		NE					
CG12021	FBgn0067864	Patj	BL35747	HMS01489		NE					
CG6338	FBgn0004510	Ets97D	BL35749	HMS01491		NE					
CG15887	FBgn0038132	CG15887	BL35751	HMS01494		NE					
CG3937	FBgn0014141	cher	BL35755	HMS01501		NE					
CG8384	FBgn0001139	gro	BL35759	HMS01506		NE					
CG7538	FBgn0014861	Mcm2	BL35771	HMS01520		NE					
CG5844	FBgn0038049	CG5844	BL35776	HMS01525		NE					
CG9925	FBgn0038191	CG9925	BL35811	HMS01514		NE					
CG3992	FBgn0003507	srp	BL35813	HMS01208		NE					
CG4115	FBgn0038017	CG4115	BL35814	HMS01446	A	E-L	E			E	
CG9764	FBgn0004049	yrt	BL36118	HMS01532		NE					
CG6376	FBgn0011766	E2f	BL36126	HMS01541		NE					
CG10498	FBgn0004107	cdc2c	BL36128	HMS01543		NE					
CG7643	FBgn0000063	ald	BL36658	HMS01546		NE					
CG9734	FBgn0027657	glob1	BL36668	HMS01556		NE					
CG14675	FBgn0037385	glob3	BL36670	HMS01558		NE					
CG6008	FBgn0027785	NP15.6	BL36672	HMS01560		NE					
CG3265	FBgn0027066	Eb1	BL36680	HMS01568		NE					
CG6235	FBgn0004889	tws	BL36689	HMS01578		NE					
CG2184	FBgn0002773	Mlc2	BL36694	HMS01583	S	S		MS	NE		NE
CG7507	FBgn0261797	Dhc64C	BL36698	HMS01587		NE					
CG32464	FBgn0013576	mtd/OXR1	BL36718	HMS01608		NE					

CG32484	FBgn0052484	Sk2	BL36741	HMS03001		NE					
CG1856	FBgn0003870	ttk	BL36748	HMS03008		NE					
CG14669	FBgn0037326	CG14669	BL36750	HMS03010		NE					
CG32364	FBgn0052364	CG32364	BL36752	HMS03012	A	E	ME			E	
CG11997	FBgn0037662	CG11997	BL36753	HMS03013		NE					
CG1347	FBgn0037363	CG1347	BL36918	HMS01611		NE					
CG5518	FBgn0015541	sda	BL37494	HMS01636		NE					
CG12001	FBgn0037265	CG12001	BL37499	HMS01641		NE					
CG5206	FBgn0023097	bon	BL37515	HMS01657		NE					
CG10851	FBgn0004587	B52	BL37519	HMS01661		NE					
CG11739	FBgn0037239	CG11739	BL38230	HMS01674		NE					
CG6213	FBgn0026753	Vha13	BL38233	HMS01677		NE					
CG3153	FBgn0038198	Npc2b	BL38238	HMS01682		NE					
CG8208	FBgn0027950	MBD-like	BL38239	HMS01683		NE					
CG9755	FBgn0003165	pum	BL38241	HMS01685		NE					
CG10120	FBgn0002719	Men	BL38256	HMS01700		NE					
CG9779	FBgn0037231	vps24	BL38281	HMS01733		NE					
CG10711	FBgn0086785	Vps36	BL38286	HMS01739		NE					
CG9379	FBgn0000244	by	BL38288	HMS01743		NE					
CG3911	FBgn0260859	Bet3	BL38302	HMS01764		NE					
CG9424	FBgn0037719	bocksbeutel	BL38349	HMS01817		NE					
CG3571	FBgn0037978	KLHL18	BL38352	HMS01820		NE					
CG5730	FBgn0000083	AnnIX	BL38523	HMS01719		NE					
CG3279	FBgn0260862	Vti1	BL38526	HMS01727		NE					
CG4848	FBgn0037998	CG4848	BL38943	HMS01857		NE					
CG6238	FBgn0029157	ssh	BL38948	HMS01862	A	E	E			E	
CG5643	FBgn0027492	wdb	BL38950	HMS01864		NE					
CG42247	FBgn0259099	DCX-EMAP	BL38964	HMS01878		NE					
CG31012	FBgn0027598	cindr	BL38976	HMS01892		NE					
CG1715	FBgn0010808	l(3)03670	BL38984	HMS01900		NE					
CG5000	FBgn0027948	msps	BL38990	HMS01906		NE					
CG1088	FBgn0015324	Vha26	BL38996	HMS01912		NE					
CG9601	FBgn0037578	CG9601	BL39003	HMS01919		NE					
CG11516	FBgn0004369	Ptp99A	BL39006	HMS01923	MS	MS		S	NE		NE
CG1228	FBgn0261985	Ptpmeg	BL39007	HMS01924		NE					

CG5720	FBgn0028471	Nab2	BL39008	HMS01925		NE					
CG10047	FBgn0028400	Syt4	BL39016	HMS01934		NE					
CG14718	FBgn0037939	CG14718	BL39018	HMS01936		NE					
CG7904	FBgn0003169	put	BL39025	HMS01944		NE					
CG8478	FBgn0037746	CG8478	BL39033	HMS01952		NE					
CG5658	FBgn0004387	Klp98A	BL39037	HMS01957		NE					
CG2097	FBgn0037371	Sym	BL39041	HMS01961		NE					
CG1058	FBgn0022981	rpk	BL39053	HMS01973	MS	MS	ME	S	E	ME	NE
CG14998	FBgn0264693	ens	BL40825	HMS00933		NE					
CG2185	FBgn0037358	elm	BL40843	HMS02009		NE					
CG5505	FBgn0260936	scny	BL40865	HMS02032		NE					
CG12170	FBgn0037356	CG12170	BL40867	HMS02034		NE					
CG17369	FBgn0005671	Vha55	BL40884	HMS02132		NE					
CG6378	FBgn0026562	BM-40-SPARC	BL40885	HMS02133		NE					
CG7749	FBgn0261574	kug	BL40888	HMS02136		NE					
CG5608	FBgn0038058	CG5608	BL40892	HMS02140		NE					
CG6120	FBgn0027865	Tsp96F	BL40901	HMS02149		NE					
CG2330	FBgn0037447	Neurochondrin	BL40903	HMS02151		NE					
CG43946	FBgn0264574	Glut1	BL40904	HMS02152		NE					
CG6593	FBgn0003134	Pp1alpha-96A	BL40906	HMS02154		NE					
CG43743	FBgn0264000	Glu-RIB	BL40908	HMS02156		NE					
CG7581	FBgn0025457	Bub3	BL40910	HMS02158		NE					
CG7807	FBgn0261953	AP-2	BL40911	HMS02159		NE					
CG8136	FBgn0037616	CG8136	BL40918	HMS02166		NE					
CG11286	FBgn0037516	CG11286	BL40919	HMS02167		NE					
CG40351	FBgn0040022	Set1	BL40931	HMS02179		NE					
CG2902	FBgn0010399	Nmdar1	BL41667	HMS02200		NE					
CG5507	FBgn0004359	T48	BL41684	HMS02248		NE					
CG4843	FBgn0004117	Tm2	BL41695	HMS02260		NE					
CG44099	FBgn0264908	pHCl	BL41700	HMS02265		NE					
CG1106	FBgn0010225	Gel	BL41704	HMS02269		NE					
CG10295	FBgn0014001	Pak	BL41714	HMS02279		NE					
CG7996	FBgn0003450	snk	BL41723	HMS02289		NE					
CG8342	FBgn0002578	m1	BL41886	HMS02308		NE					
CG3068	FBgn0000147	aur	BL41889	HMS02205		NE					

CG11958	FBgn0015622	Cnx99A	BL41911	HMS02304		NE					
CG32183	FBgn0052183	Ccn	BL41913	HMS02310		NE					
CG10772	FBgn0004509	Fur1	BL41914	HMS02311		NE					
CG3373	FBgn0015737	Hmu	BL41915	HMS02312		NE					
CG14084	FBgn0260857	Bet1	BL41927	HMS02324		NE					
CG5974	FBgn0010441	pll	BL41935	HMS02332		NE					
CG9797	FBgn0037621	CG9797	BL41937	HMS02334		NE					
CG6359	FBgn0038065	Snx3	BL41947	HMS02344		NE					
CG5814	FBgn0015625	CycB3	BL41979	HMS02377		NE					
CG6932	FBgn0028837	CSN6	BL41991	HMS02392		NE					
CG43128	FBgn0262593	Shab	BL41999	HMS02400		NE					
CG7756	FBgn0001217	Hsc70-2	BL42014	HMS02415		NE					
CG2051	FBgn0037376	CG2051	BL42488	HMJ02050		NE					
CG9727	FBgn0037445	CG9727	BL42495	HMJ02059		NE					
CG2087	FBgn0037327	PERK/PEK	BL42499	HMJ02063		NE					
CG42458	FBgn0259935	CG42458	BL42506	HMJ02071		NE					
CG43976	FBgn0264707	RhoGEF3	BL42526	HMJ02092		NE					
CG1098	FBgn0027497	Madm	BL42529	HMJ02096		NE					
CG5264	FBgn0014949	btn	BL42530	HMJ02097		NE					
CG11762	FBgn0037618	CG11762	BL42531	HMJ02098		NE					
CG2210	FBgn0000150	awd	BL42532	HMJ02099		NE					
CG6384	FBgn0000283	Cp190	BL42536	HMJ02105		NE					
CG32296	FBgn0052296	Mrtf	BL42537	HMJ02106	MS	MS		MS	E		NE
CG17228	FBgn0004595	pros	BL42538	HMJ02107	A	ME	E	S		E-L	
CG32130	FBgn0086708	stv	BL42564	HMJ02221		NE					
CG6027	FBgn0004876	cdi	BL42568	HMJ02227		NE					
CG7693	FBgn0023083	fray	BL42569	HMJ02228		NE					
CG43173	FBgn0262792	CG43173	BL42584	HMS02369		NE					
CG43896	FBgn0264488	CG43896	BL42585	HMS02417		NE					
CG12357	FBgn0022943	Cbp20	BL42596	HMS02428		NE					
CG12147	FBgn0037325	CG12147	BL42612	HMS02447		NE					
CG17367	FBgn0028717	Lnk	BL42613	HMS02448		NE					
CG6014	FBgn0261258	rgn	BL42619	HMS02454		NE					
CG6489	FBgn0013279	Hsp70Bc	BL42626	HMS02461		NE					
CG2530	FBgn0010313	corto	BL42629	HMS02464		NE					

CG2013	FBgn0004436	UbcD6	BL42631	HMS02466	A	E-L	E			E	
CG6188	FBgn0038074	CG6188	BL42637	HMS02473		NE					
CG4316	FBgn0003319	Sb	BL42647	HMS02483		NE					
CG18290	FBgn0000046	Act87E	BL42652	HMS02488		NE					
CG9738	FBgn0024326	Mkk4	BL42832	HMS02524		NE					
CG12242	FBgn0010041	GstD5	BL42842	HMS02534		NE					
CG14355	FBgn0038208	CG14355	BL42857	HMS02549		NE					
CG8793	FBgn0260655	l(3)76BDm	BL42870	HMS02563		NE					
CG1897	FBgn0000492	Dr	BL42891	HMS02584		NE					
CG9476	FBgn0003886	alphaTub85E	BL42905	HMS02598		NE					
CG1239	FBgn0037368	CG1239	BL42912	HMS02605		NE					
CG11672	FBgn0037563	CG11672	BL42913	HMS02606		NE					
CG9345	FBgn0038173	Adgf-C	BL42915	HMS02608	E-L	E-L	ME	ME	E	NE	NE
CG4067	FBgn0020385	pug	BL42950	HMS02643		NE					
CG8489	FBgn0038225	soti	BL42955	HMS02648		NE					
CG31449	FBgn0013277	Hsp70Ba	BL43289	HMS02661		NE					
CG2867	FBgn0004901	Prat	BL43296	HMS02669		NE					
CG1169	FBgn0037428	Osi18	BL43302	HMS02675		NE					
CG6467	FBgn0250815	Jon65Aiv	BL43306	HMS02689		NE					
CG33217	FBgn0053217	CG33217	BL43315	HMS02699		NE					
CG14676	FBgn0037388	CG14676	BL43316	HMS02700		NE					
CG43744	FBgn0264001	bru-3	BL43318	HMS02702		NE					
CG32423	FBgn0052423	shep	BL43545	HMS02666		NE					
CG3916	FBgn0038003	CG3916	BL43992	HMS02705		NE					
CG6438	FBgn0023179	amon	BL44001	HMS02715		NE					
CG11671	FBgn0037562	CG11671	BL44003	HMS02717		NE					
CG6939	FBgn0025802	Sbf	BL44004	HMS02718		NE					
CG1115	FBgn0037299	CG1115	BL44010	HMS02724		NE					
CG32190	FBgn0052190	NUCB1	BL44019	HMS02734		NE					
CG10967	FBgn0260945	Atg1	BL44034	HMS02750		NE					
CG32451	FBgn0052451	SPoCk	BL44040	HMS02756		NE					
CG11966	FBgn0037645	CG11966	BL44046	HMS02762	A	ME	ME			E	
CG5499	FBgn0001197	His2Av	BL44056	HMS02773	MS	MS		NE	E		NE
CG31293	FBgn0003227	rec	BL44057	HMS02774		NE					
CG8362	FBgn0028997	nmdyn-D7	BL44058	HMS02775		NE					

CG14841	FBgn0038218	CG14841	BL44059	HMS02776		NE					
CG11422	FBgn0010403	Obp83b	BL44065	HMS02782		NE					
CG1469	FBgn0015221	Fer2LCH	BL44067	HMS02784		NE					
CG1954	FBgn0003093	Pkc98E	BL44074	HMS02791		NE					
CG1910	FBgn0022349	CG1910	BL44082	HMS02799		NE					
CG16749	FBgn0037678	CG16749	BL44096	HMS02816		NE					
CG3971	FBgn0260960	Baldspot	BL44101	HMS02821		NE					
CG3066	FBgn0037515	Sp7	BL44108	HMS02829		NE					
CG3397	FBgn0037975	CG3397	BL44115	HMS02837		NE					
CG4029	FBgn0015396	jumu	BL44117	HMS02839		NE					
CG40160	FBgn0058160	CG40160	BL44268	HMS02730		NE					
CG31039	FBgn0003358	Jon99Ci	BL44269	HMS02766		NE					
CG6567	FBgn0037842	CG6567	BL44479	HMC02369		NE					
CG10032	FBgn0037493	CG10032	BL44501	HMC02437	MS	MS		NE	NE		NE
CG10059	FBgn0037481	MAGE	BL44514	HMC02904	A	ME	ME			E	
CG12817	FBgn0037798	CG12817	BL44529	HMC02923		NE					
CG40300	FBgn0250816	AGO3	BL44543	HMC02938		NE					
CG9995	FBgn0027655	htt	BL44550	HMS02845		NE					
CG15589	FBgn0037409	Osi24	BL44564	HMS02860		NE					
CG14683	FBgn0037822	CG14683	BL44571	HMS02867		NE					
CG1119	FBgn0004913	Gnf1	BL44572	HMS02868		NE					
CG32372	FBgn0052372	ltl	BL44577	HMS02873		NE					
CG40178	FBgn0058178	CG40178	BL44578	HMS02874		NE					
CG5553	FBgn0259676	DNApol-alpha60	BL44584	HMS02881		NE					
CG6672	FBgn0037875	CG6672	BL44586	HMS02884		NE					
CG2019	FBgn0029088	disp	BL44633	HMS02877		NE					
CG9920	FBgn0038200	CG9920	BL44657	HMC02438		NE					
CG2747	FBgn0037541	CG2747	BL44662	HMS02848		NE					
CG10250	FBgn0002922	nau	BL50607	HMC02974		NE					
CG6706	FBgn0027575	GABA-B-R2	BL50608	HMC02975		NE					
CG1263	FBgn0261602	RpL8	BL50610	HMC02977	A	E	E			E	
CG33265	FBgn0053265	Muc68E	BL50618	HMC02985		NE					
CG31062	FBgn0016061	side	BL50642	HMC03042		NE					
CG9459	FBgn0037764	CG9459	BL50647	HMC03047		NE					
CG5214	FBgn0037891	CG5214	BL50650	HMC03051		NE					

CG10037	FBgn0086680	vvl	BL50657	HMC03058	A	ME	ME			ME	
CG1030	FBgn0003339	Scr	BL50662	HMC03063		NE					
CG7895	FBgn0004110	tin	BL50663	HMC03064		NE					
CG33323	FBgn0037475	Fer1	BL50672	HMC03073		NE					
CG2988	FBgn0000576	ems	BL50673	HMC03074		NE					
CG14548	FBgn0002733	HLHmbeta	BL50674	HMC03075		NE					
CG32354	FBgn0052354	CG32354	BL50693	HMC03095		NE					
CG12951	FBgn0037677	CG12951	BL50698	HMC03100		NE					
CG31034	FBgn0003356	Jon99Cii	BL50705	HMC03107		NE					
CG2781	FBgn0037534	CG2781	BL50710	HMC03112		NE					
CG5931	FBgn0263599	l(3)72Ab	BL50716	HMS02950	A	ME	ME			E	
CG43894	FBgn0264486	CG43894	BL50718	HMS02952		NE					
CG31240	FBgn0011701	repo	BL50735	HMS02971		NE					
CG2189	FBgn0000439	Dfd	BL50792	HMC03094		NE					
CG1957	FBgn0027873	Cpsf100	BL50893	HMC02355		NE					
CG34356	FBgn0085385	CG34356	BL50912	HMJ03136		NE					
CG33290	FBgn0053290	CG33290	BL50916	HMJ21005		NE					
CG33267	FBgn0053267	CG33267	BL50929	HMJ21023		NE					
CG43163	FBgn0262719	CG43163	BL50958	HMJ21060		NE					
CG12173	FBgn0037305	CG12173	BL50977	HMJ21083		NE					
CG11598	FBgn0038067	CG11598	BL51000	HMJ21113		NE					
Ir62a	FBgn0053971	Ir62a	BL51026	HMJ21152		NE					
CG33286	FBgn0053286	CG33286	BL51029	HMJ21156		NE					
CG14655	FBgn0037275	CG14655	BL51031	HMJ21158		NE					
CG3772	FBgn0025680	cry	BL51033	HMJ21160		NE					
CG7129	FBgn0010877	l(3)05822	BL51159	HMC02398		NE					
CG5807	FBgn0027539	CG5807	BL51163	HMJ03117		NE					
CG11648	FBgn0000015	Abd-B	BL51167	HMJ03133		NE					
CG3379	FBgn0013981	His4r	BL51172	HMJ21134		NE					
CG18234	FBgn0265268	CG18234	BL51173	HMJ21135		NE					
CG10005	FBgn0037972	CG10005	BL51174	HMJ21137		NE					
CG4706	FBgn0037862	CG4706	BL51359	HMC03203		NE					
CG42610	FBgn0261259	Fhos	BL51391	HMJ21037		NE					
CG14394	FBgn0038079	CG14394	BL51420	HMC02385		NE					
CG18741	FBgn0015129	DopR2	BL51423	HMC02893		NE					

CG6225	FBgn0038072	CG6225	BL51435	HMC03149		NE					
CG32203	FBgn0052203	Spn75F	BL51437	HMC03151		NE					
CG9749	FBgn0020510	Abi	BL51455	HMC03190		NE					
CG31045	FBgn0026059	Mhcl	BL51456	HMC03191		NE					
CG32425	FBgn0052425	CG32425	BL51457	HMC03193		NE					
CG7665	FBgn0016650	Lgr1	BL51465	HMC03205		NE					
CG6096	FBgn0002631	HLHm5	BL51466	HMC03206		NE					
CG5320	FBgn0001098	Gdh	BL51473	HMC03217		NE					
CG11899	FBgn0014427	CG11899	BL51476	HMC03221		NE					
CG13598	FBgn0016754	sba	BL51488	HMC03239		NE					
CG6868	FBgn0003719	tld	BL51507	HMC03275		NE					
CG42330	FBgn0263219	Dscam4	BL51508	HMC03277		NE					
CG5557	FBgn0010768	sqz	BL51509	HMC03279		NE					
CG3723	FBgn0013812	Dhc93AB	BL51511	HMC03281		NE					
CG12162	FBgn0037329	CG12162	BL51514	HMC03291		NE					
CG18402	FBgn0013984	InR/IR	BL51518	HMS03166	E	E	NE	NE	E		NE
CG7910	FBgn0037547	CG7910	BL51702	HMC03182		NE					
CG5663	FBgn0000455	Dip-C	BL51708	HMC03216		NE					
CG4412	FBgn0016119	ATPsyn-Cf6	BL51714	HMC03238		NE					
CG6703	FBgn0013759	CASK	BL51721	HMC03260		NE					
CG9492	FBgn0037726	CG9492	BL51725	HMC03269		NE					
CG4312	FBgn0002869	MtnB	BL51731	HMC03286		NE					
CG7939	FBgn0002626	RpL32	BL51746	HMC02350	A	E-L	E			E	
CG10345	FBgn0027562	CG10345	BL51751	HMC03302		NE					
CG16779	FBgn0037698	CG16779	BL51756	HMC03308		NE					
CG9458	FBgn0037765	CG9458	BL51757	HMC03309		NE					
CG8333	FBgn0002735	HLHmgamma	BL51762	HMC03315		NE					
CG32281	FBgn0052281	CG32281	BL51764	HMC03318		NE					
CG7524	FBgn0262733	Src64B	BL51772	HMC03327		NE					
CG8103	FBgn0262519	Mi-2	BL51774	HMC03329	A	ME	ME			ME	
CG5796	FBgn0020018	Ppox	BL51777	HMC03332		NE					
CG1063	FBgn0010051	Itp-r83A	BL51795	HMC03351		NE					
CG3944	FBgn0017567	ND23	BL51797	HMC03353		NE					
CG9741	FBgn0000447	Dhod	BL51801	HMC03359		NE					
CG1520	FBgn0024273	WASp	BL51802	HMC03360	A	ME	ME			E	

CG6303	FBgn0037808	Bruce	BL51814	HMC03385		NE					
CG42256	FBgn0263218	Dscam2	BL51839	HMC03411		NE					
CG5018	FBgn0263605	l(3)72Dn	BL51907	HMC03482		NE					
CG1092	FBgn0037228	CG1092	BL51912	HMS03370		NE					
CG7948	FBgn0003479	spn-A	BL51926	HMC03364		NE					
CG17645	FBgn0011270	Pglym87	BL51939	HMC03367		NE					
CG32374	FBgn0052374	CG32374	BL52870	HMC03608		NE					
CG42341	FBgn0259243	Pka-R1	BL52906	HMC03646		NE					
CG5276	FBgn0037900	CG5276	BL52918	HMC03658		NE					
CG6584	FBgn0037847	SelR	BL52919	HMC03659		NE					
CG11722	FBgn0037777	CG11722	BL52920	HMC03660		NE					
CG1041	FBgn0037440	CG1041	BL52921	HMC03661		NE					
CG6147	FBgn0026317	Tsc1	BL52931	HMC03672		NE					
CG10328	FBgn0015520	nonA-l	BL52934	HMC03676		NE					
CG12749	FBgn0004237	Hrb87F	BL52937	HMC03679		NE					
CG5836	FBgn0025571	SF1	BL52938	HMC03680		NE					
CG14715	FBgn0037930	CG14715	BL52940	HMJ21596		NE					
CG43079	FBgn0262509	nrm	BL52945	HMJ21612		NE					
CG32488	FBgn0052488	CG32488	BL52949	HMJ21618		NE					
CG42543	FBgn0260660	mp	BL52981	HMJ21668		NE					
CG2911	FBgn0037350	CG2911	BL52998	HMJ21713		NE					
CG14513	FBgn0005596	yemalpha	BL53000	HMJ21716		NE					
CG42576	FBgn0261526	NT1	BL53003	HMJ21720		NE					
CG14694	FBgn0037845	CG14694	BL53012	HMJ21734		NE					
CG14708	FBgn0037910	CG14708	BL53020	HMJ21743		NE					
CG34420	FBgn0085449	CG34420	BL53032	HMJ21758		NE					
CG12582	FBgn0037215	CG12582	BL53272	HMC03488		NE					
CG17387	FBgn0037276	CG17387	BL53273	HMC03489		NE					
CG1236	FBgn0037370	CG1236	BL53274	HMC03490	A	ME	ME			ME	
CG10092	FBgn0037526	CG10092	BL53275	HMC03491		NE					
CG9613	FBgn0037574	Coq2	BL53276	HMC03492		NE					
CG9836	FBgn0037637	CG9836	BL53277	HMC03493		NE					
CG9361	FBgn0037690	Task7	BL53279	HMC03495		NE					
CG9362	FBgn0037696	GstZ1	BL53280	HMC03496		NE					
CG6666	FBgn0037873	SdhC	BL53281	HMC03497		NE					

CG8534	FBgn0037761	CG8534	BL53299	HMC03518		NE					
CG18005	FBgn0037660	beag	BL53306	HMC03533		NE					
CG8318	FBgn0015269	Nf1	BL53322	HMC03551		NE					
CG1315	FBgn0026565	CG1315	BL53323	HMC03552		NE					
CG5161	FBgn0263604	l(3)72Dh	BL53328	HMC03557		NE					
CG4649	FBgn0022359	Sodh-2	BL53353	HMC03582		NE					
CG1411	FBgn0023023	CRMP	BL53354	HMC03583		NE					
CG7535	FBgn0024963	GluClalpha	BL53356	HMC03585		NE					
CG14642	FBgn0037222	CG14642	BL53365	HMC03594	(ME POSSIBLE)	NE					
CG17404	FBgn0038001	CG17404	BL53370	HMC03599		NE					
CG17944	FBgn0037500	CG17944	BL53690	HMJ21673		NE					
CG8023	FBgn0265089	eIF4E-3	BL53880	HMJ21195		NE					
CG10370	FBgn0028684	Tbp-1	BL53886	HMJ21204	A	E	E			E	
CG31037	FBgn0000247	ca	BL53888	HMJ21206	A	ME	ME			E	
CG14723	FBgn0037950	HisCl1	BL53932	HMJ21280		NE					
CG16905	FBgn0037762	eloF	BL53947	HMJ21310		NE					
CG32159	FBgn0261799	dsx-c73A	BL53964	HMJ21346		NE					
CG7558	FBgn0262716	Arp3	BL53972	HMJ21357		NE					
CG12420	FBgn0037797	CG12420	BL53976	HMJ21365		NE					
CG11281	FBgn0086916	snky	BL53986	HMJ21388		NE					
CG42333	FBgn0261090	Sytbeta	BL53996	HMJ21400		NE					
CG9636	FBgn0037556	CG9636	BL54009	HMJ21432		NE					
CG32238	FBgn0052238	CG32238	BL54016	HMJ21441		NE					
CG5245	FBgn0038047	CG5245	BL54036	HMJ21479		NE					
CG10038	FBgn0038013	CG10038	BL54039	HMJ21482		NE					
CG9285	FBgn0000454	Dip-B	BL54045	HMJ21488		NE					
CG33703	FBgn0053703	CG33703	BL54054	HMS03715		NE					
CG3925	FBgn0037780	CG3925	BL54467	HMC03735		NE					
CG32382	FBgn0052382	sphinx2	BL54468	HMS03736		NE					
CG4264	FBgn0001219	Hsc70-4	BL54810	HMJ21529	ME	ME	NE	S	E-L		NE
CG1331	FBgn0004778	Ccp84Af	BL54821	HMJ21540		NE					
CG15596	FBgn0037418	Osi11	BL54839	HMJ21558		NE					
CG32220	FBgn0052220	Csas	BL54843	HMJ21580		NE					
CG7642	FBgn0003308	ry	BL54845	HMJ21582		NE					

CG13318	FBgn0037627	CG13318	BL55143	HMC03739		NE					
CG2098	FBgn0024891	ferrochelatase	BL55146	HMC03757		NE					
CG5099	FBgn0011666	msi	BL55152	HMC03808		NE					
CG8464	FBgn0038233	HtrA2	BL55165	HMC03843		NE					
CG11963	FBgn0037643	skap	BL55168	HMC03847		NE					
CG7878	FBgn0037549	CG7878	BL55170	HMC03850		NE					
CG3593	FBgn0003257	r-l	BL55183	HMC03871		NE					
CG9631	FBgn0027563	CG9631	BL55185	HMC03879		NE					
CG9649	FBgn0038211	CG9649	BL55200	HMC03899		NE					
CG5808	FBgn0027617	CG5808	BL55208	HMC03925		NE					
CG9652	FBgn0011582	DopR	BL55239	HMC02344		NE					
CG9684	FBgn0037583	CG9684	BL55259	HMC03946		NE					
CG9495	FBgn0003334	Scm	BL55278	HMC03965		NE					
CG6913	FBgn0037937	Fer3	BL55300	HMC03987		NE					
CG7672	FBgn0004618	gl	BL55301	HMC03988	LacZ-S	MS		S	MS		S
CG8346	FBgn0002609	HLHm3	BL55302	HMC03989		NE					
CG6054	FBgn0005355	Su(fu)	BL55315	HMC04002		NE					
CG3671	FBgn0011672	Mvl	BL55316	HMC04003		NE					
CG6386	FBgn0027889	ball	BL55330	HMC04017		NE					
CG33160	FBgn0053160	CG33160	BL55341	HMC04028		NE					
CG3505	FBgn0038250	CG3505	BL55342	HMC04029		NE					
CG2108	FBgn0037364	Rab23	BL55352	HMC04039		NE					
CG32438	FBgn0052438	Smc5	BL55371	HMC04059		NE					
CG31509	FBgn0028396	TotA	BL55378	HMC04066		NE					
CG1361	FBgn0000094	Anp	BL55385	HMC04073		NE					
CG3325	FBgn0003480	spn-B	BL55403	HMC04091		NE					
CG10693	FBgn0003429	slo	BL55405	HMC04093		NE					
CG32383	FBgn0052383	sphinx1	BL55601	HMC03898		NE					
CG33052	FBgn0053052	CG33052	BL55610	HMC03748	A	E	ME			E	
CG9363	FBgn0037697	CG9363	BL55634	HMC03781		NE					
CG5215	FBgn0263603	Zn72D	BL55635	HMC03782		NE					
CG33522	FBgn0261872	scaf6	BL55644	HMC03793		NE					
CG11094	FBgn0000504	dsx	BL55646	HMC03795		NE					
CG31000	FBgn0011224	heph	BL55655	HMC03805		NE					
CG6354	FBgn0004903	Rb97D	BL55662	HMC03817		NE					

CG9776	FBgn0027866	CG9776	BL55673	HMC03831		NE					
CG1438	FBgn0015032	Cyp4c3	BL55687	HMC03873		NE					
CG33057	FBgn0053057	CG33057	BL55699	HMC03914		NE					
CG17187	FBgn0037882	CG17187	BL55702	HMC03923		NE					
CG7887	FBgn0004622	Takr99D	BL55732	HMC03749		NE					
CG11668	FBgn0038113	CG11668	BL55733	HMC03756		NE					
CG11670	FBgn0038114	CG11670	BL55738	HMC03877		NE					
CG33159	FBgn0053159	CG33159	BL55739	HMC03893	A	ME	ME			E	
CG8383	FBgn0037737	Pnn	BL55743	HMC03928		NE					
CG32277	FBgn0052277	CG32277	BL55857	HMC03895		NE					
CG31043	FBgn0026239	gukh	BL55858	HMC03681		NE					
CG12066	FBgn0000274	Pka-C2	BL55859	HMC04129		NE					
CG10244	FBgn0022800	Cad96Ca	BL55877	HMC04150		NE					
CG6011	FBgn0027784	Prp18	BL55915	HMC04201		NE					
CG33263	FBgn0053263	CG33263	BL55954	HMC04243		NE					
CG33276	FBgn0053276	CG33276	BL55955	HMC04244		NE					
CG14643	FBgn0037225	TwdlG	BL55975	HMC04271		NE					
CG5207	FBgn0037889	scpr-A	BL55976	HMC04272		NE					
CG32304	FBgn0052304	obst-I	BL55998	HMC04294		NE					
CG32313	FBgn0052313	CG32313	BL55999	HMC04295		NE					
CG31322	FBgn0027083	Aats-met	BL56005	HMC04301		NE					
CG8956	FBgn0015011	Ahcy89E	BL56009	HMC04305		NE					
CG8327	FBgn0037723	SpdS	BL56011	HMC04307		NE					
CG5192	FBgn0019940	Rh6	BL56029	HMC04325		NE					
CG6474	FBgn0000617	e(y)1	BL32345	HMS00336		NE					
CG3923	FBgn0001337	Exp6	BL32347	HMS00338		NE					
CG7073	FBgn0038947	sar1	BL32364	HMS00355	A	E-L	E-L			E-L	
CG1250	FBgn0262125	sec23	BL32365	HMS00356		NE					
CG6987	FBgn0040284	SF2	BL32367	HMS00358	MS	MS		S	S		NE
CG7660	FBgn0261987	Pxt	BL32382	HMS00374		NE					
CG5745	FBgn0038855	CG5745	BL32394	HMS00388		NE					
CG33546	FBgn0250732	gfzf	BL32399	HMS00394		NE					
CG4147	FBgn0001218	Hsc70-3	BL32402	HMS00397	A	E	E			E	
CG7050	FBgn0038975	Nrx-1	BL32408	HMS00403		NE					
CG4574	FBgn0004611	Plc21C	BL32438	HMS00436		NE					

CG4235 8	FBgn02 59704	CG42358	BL32440	HMS0 0438		NE					
CG1710	FBgn00 39904	Hcf	BL32453	HMS0 0452	E	E	NE	NE	ME		NE
CG5121	FBgn00 39337	MED28	BL32459	HMS0 0458		NE					
CG4448	FBgn00 39067	wda	BL32469	HMS0 0469		NE					
CG3111 9	FBgn00 51119	HdacX	BL32480	HMS0 0483		NE					
CG5085	FBgn00 38788	Sirt2	BL32482	HMS0 0485		NE					
CG1130 5	FBgn00 39631	Sirt7	BL32483	HMS0 0486		NE					
CG1464	FBgn00 05558	ey	BL32486	HMS0 0489		NE					
CG3115 6	FBgn00 51156	CG31156	BL32495	HMS0 0498		NE					
CG1137 5	FBgn00 39227	polybromo	BL32840	HMS0 0531		NE					
CG4562	FBgn00 38740	CG4562	BL32842	HMS0 0623		NE					
CG1569 7	FBgn00 38834	RpS30	BL32851	HMS0 0636	A	E	E			E	
CG4548	FBgn00 39338	XNP	BL32894	HMS0 0683		NE					
CG5874	FBgn00 38872	Nelf-A	BL32897	HMS0 0686		NE					
CG1976	FBgn00 39883	RhoGAP100F	BL32946	HMS0 0740		NE					
CG6898	FBgn00 38412	Zip3	BL32954	HMS0 0748		NE					
CG1861 6	FBgn02 60444	CG18616	BL32957	HMS0 0751		NE					
CG3319 3	FBgn00 53193	sav	BL32965	HMS0 0760		NE					
CG2152	FBgn00 86768	Pcmt	BL32971	HMS0 0768		NE					
CG5834	FBgn00 51354	Hsp70Bbb	BL33000	HMS0 0800		NE					
CG1185 6	FBgn00 39302	Nup358	BL33003	HMS0 0803		NE					
CG7940	FBgn00 38576	Arp5	BL33009	HMS0 0809		NE					
CG1081 1	FBgn00 23213	eIF4G	BL33049	HMS0 0762	ME	ME	NE	ME	MS	NE	NE
CG1450 7	FBgn00 39655	CG14507	BL33345	HMS0 0211		NE					
CG3309 5	FBgn00 53095	CG33095	BL33352	HMS0 0223		NE					
CG5646	FBgn00 39525	CG5646	BL33360	HMS0 0232		NE					
CG4231 2	FBgn02 59212	cno	BL33367	HMS0 0239	A	E	E			E	
CG1639	FBgn00 01491	l(1)10Bb	BL33380	HMS0 0255		NE					
CG4314 0	FBgn02 62614	pyd	BL33386	HMS0 0263		NE					
CG1106 4	FBgn00 87002	Rfabg	BL33388	HMS0 0265		NE					
CG4755	FBgn00 38747	RhoGAP92B	BL33391	HMS0 0268		NE					
CG3348 5	FBgn00 38282	dpr9	BL33409	HMS0 0288		NE					
CG4231 6	FBgn02 59216	RhoGAP102A	BL33425	HMS0 0309		NE					
CG4267 0	FBgn02 61552	ps	BL33426	HMS0 0310		NE					
CG3954	FBgn00 00382	csw	BL33619	HMS0 0012	A	ME	ME			E	

CG3218	FBgn0000810	fs(1)K10	BL33630	HMS00027		NE					
CG6946	FBgn0259139	glo	BL33668	HMS00079		NE					
CG34354	FBgn0085383	CG34354	BL33674	HMS00538		NE					
CG11186	FBgn0019650	toy	BL33679	HMS00544		NE					
CG5383	FBgn0038948	PSR	BL33700	HMS00576		NE					
CG31212	FBgn0086613	Ino80	BL33708	HMS00586		NE					
CG12241	FBgn0038304	CG12241	BL33729	HMS00612		NE					
CG5451	FBgn0038666	Smu1	BL33739	HMS01075		NE					
CG1458	FBgn0062442	CG1458	BL33749	HMS01088		NE					
CG1487	FBgn0040206	krz	BL33880	HMS00817		NE					
CG7922	FBgn0038889	CG7922	BL33889	HMS00827		NE					
CG31022	FBgn0039776	PH4alphaEFB	BL33896	HMS00835		NE					
CG16705	FBgn0039102	SPE	BL33926	HMS00873	A	E	E			E	
CG12163	FBgn0260462	CG12163	BL33955	HMS00910		NE					
CG11848	FBgn0039282	Bili	BL33956	HMS00911		NE					
CG6990	FBgn0039019	HP1c	BL33962	HMS00919		NE					
CG1081	FBgn0041191	Rheb	BL33966	HMS00923		NE					
CG10420	FBgn0039296	CG10420	BL33968	HMS00925		NE					
CG31224	FBgn0051224	CG31224	BL33969	HMS00926		NE					
CG1800	FBgn0039861	pasha	BL33972	HMS00929		NE					
CG31426	FBgn0041588	ligatin/eIF2D	BL33995	HMS00958		NE					
CG11522	FBgn0039857	RpL6	BL34004	HMS00967	A	E-L	E-L			E	
CG12230	FBgn0000257	car	BL34007	HMS00972		NE					
CG4976	FBgn0039559	Mes-4	BL34033	HMS01004		NE					
CG4963	FBgn0039561	mfrn	BL34038	HMS01013		NE					
CG4236	FBgn0263979	Caf1	BL34069	HMS00051		NE					
CG3665	FBgn0000635	Fas2	BL34084	HMS01098		NE					
CG9746	FBgn0260935	ird1	BL34092	HMS00908		NE					
CG1973	FBgn0260990	yata	BL34100	HMS01005		NE					
CG4572	FBgn0038738	CG4572	BL34337	HMS01325		NE					
CG2241	FBgn0039788	Rpt6R	BL34342	HMS01330		NE					
CG5520	FBgn0039562	Gp93	BL34346	HMS01334		NE					
CG3590	FBgn0038467	CG3590	BL34347	HMS01336		NE					
CG6057	FBgn0040283	SMC1	BL34351	HMS01340		NE					
CG5706	FBgn0039175	CG5706	BL34356	HMS01345		NE					

CG31033	FBgn0039705	CG31033	BL34358	HMS01347		NE					
CG10007	FBgn0260744	Tango9	BL34364	HMS01353		NE					
CG31048	FBgn0264324	spg	BL34367	HMS01356		NE					
CG6560	FBgn0038916	dnd	BL34383	HMS01373		NE					
CG7719	FBgn0260399	gwl	BL34525	HMS00834		NE					
CG5527	FBgn0039564	CG5527	BL34531	HMS01076		NE					
CG3509	FBgn0038252	CG3509	BL34548	HMS01020		NE					
CG4510	FBgn0038746	Surf6	BL34563	HMS01035		NE					
CG6015	FBgn0038927	CG6015	BL34565	HMS01037	A	E	E			E	
CG33106	FBgn0043884	mask	BL34571	HMS01045		NE					
CG42788	FBgn0261859	CG42788	BL34594	HMS01068		NE					
CG9617	FBgn0260939	Sgt1	BL34605	HMS00566		NE					
CG43320	FBgn0263025	CG43320	BL34606	HMS00577		NE					
CG1862	FBgn0040324	Ephrin	BL34614	HMS01289		NE					
CG7952	FBgn0001150	gt	BL34631	HMS01105		NE					
CG10278	FBgn0038391	GATAe	BL34641	HMS01116		NE					
CG1901	FBgn0039914	mav	BL34650	HMS01125		NE					
CG31390	FBgn0051390	MED7	BL34663	HMS01140	S	S		S	S		NE
CG7957	FBgn0038578	MED17	BL34664	HMS01141	S	S		S	MS		NE
CG6921	FBgn0260942	bond	BL34676	HMS01154		NE					
CG44015	FBgn0264785	Hph	BL34717	HMS01196		NE					
CG31251	FBgn0051251	CG31251	BL34721	HMS01200		NE					
CG7700	FBgn0044871	Gos28	BL34724	HMS01203		NE					
CG17299	FBgn0264357	SNF4Agamma	BL34726	HMS01205		NE					
CG9768	FBgn0261434	hkb	BL34736	HMS01216		NE					
CG1345	FBgn0039580	Gfat2	BL34740	HMS01220		NE					
CG9012	FBgn0000319	Chc	BL34742	HMS01222		NE					
CG42668	FBgn0261550	CG42668	BL34743	HMS01223		NE					
CG6892	FBgn0039225	Ets96B	BL34783	HMS00092		NE					
CG11985	FBgn0040534	CG11985	BL34788	HMS00097	E	E	NE	ME	ME		NE
CG5441	FBgn0263118	tx	BL34792	HMS00101		NE					
CG31992	FBgn0051992	gw	BL34796	HMS00105	A	E	E			E	
CG12000	FBgn0250746	Prosbeta7	BL34812	HMS00122	A	E-L	E			E	
CG12297	FBgn0038928	BG4	BL34813	HMS00123		NE					
CG5454	FBgn0261792	snRNP-U1-C	BL34822	HMS00137		NE					

CG16941	FBgn0038464	CG16941	BL34840	HMS00157	E	E	NE	NE	ME		NE
CG11920	FBgn0039274	CG11920	BL34860	HMS00178		NE					
CG4376	FBgn0000667	Actn	BL34874	HMS00193		NE					
CG41099	FBgn0039955	CG41099	BL34883	HMS01228		NE					
CG18347	FBgn0260743	CG18347	BL34890	HMS01235		NE					
CG8933	FBgn0000611	exd	BL34897	HMS01242		NE					
CG12334	FBgn0038539	Atg8b	BL34900	HMS01245		NE					
CG1618	FBgn0000346	comt/NSF	BL34913	HMS01261		NE					
CG14508	FBgn0039651	CG14508	BL34916	HMS01264		NE					
CG1894	FBgn0039585	CG1894	BL34925	HMS01274		NE					
CG13852	FBgn0038965	mats	BL34959	HMS00475		NE					
CG42233	FBgn0250755	CG42233	BL34986	HMS01396		NE					
CG11579	FBgn0000117	arm	BL35004	HMS01414	A	E	E			E	
CG32474	FBgn0039411	dys	BL35010	HMS01420		NE					
CG42250	FBgn0261279	lqfR	BL35013	HMS01423		NE					
CG6688	FBgn0039038	CG6688	BL35021	HMS01434		NE					
CG1922	FBgn0028996	onecut	BL35025	HMS01438		NE					
CG3421	FBgn0038853	RhoGAP93B	BL35027	HMS01440		NE					
CG31009	FBgn0039709	Cad99C	BL35037	HMS01451		NE					
CG2919	FBgn0261004	asl	BL35039	HMS01453		NE					
CG10545	FBgn0001105	Gbeta13F	BL35041	HMS01455		NE					
CG1666	FBgn0001565	Hlc	BL35308	HMS01424		NE					
CG42542	FBgn0260659	CG42542	BL35736	HMS01478		NE					
CG5429	FBgn0264325	Atg6	BL35741	HMS01483		NE					
CG5466	FBgn0038815	CG5466	BL35758	HMS01504		NE					
CG14892	FBgn0038447	CG14892	BL35766	HMS01515		NE					
CG9743	FBgn0039756	CG9743	BL36675	HMS01563		NE					
CG7929	FBgn0041102	ocn	BL36681	HMS01569	A	E	ME			E	
CG10423	FBgn0039300	RpS27	BL36692	HMS01581		NE					
CG15180	FBgn0250846	glob2	BL36693	HMS01582		NE					
CG5083	FBgn0038390	Rbf2	BL36697	HMS01586		NE					
CG14866	FBgn0038315	CG14866	BL36706	HMS01596		NE					
CG32018	FBgn0011642	Zyx	BL36716	HMS01606		NE					
CG6963	FBgn0250823	gish	BL36719	HMS01609		NE					
CG31060	FBgn0046886	Gr98c	BL36735	HMS01626		NE					

CG6668	FBgn0039213	atl	BL36736	HMS01627		NE					
CG4583	FBgn0261984	Ire1	BL36743	HMS03003		NE					
CG31140	FBgn0051140	CG31140	BL36746	HMS03006		NE					
CG17100	FBgn0259938	cwo	BL36756	HMS03016		NE					
CG15533	FBgn0039768	CG15533	BL36761	HMS03022		NE					
CG15534	FBgn0039769	CG15534	BL36762	HMS03023		NE					
CG1471	FBgn0039774	CDase	BL36764	HMS03025		NE					
CG6755	FBgn0039066	EloA	BL37017	HMS01255	LacZ-S	S		S	S		MS
CG5887	FBgn0086687	desat1	BL37512	HMS01654		NE					
CG8228	FBgn0261049	Vps45	BL38252	HMS01696		NE					
CG34127	FBgn0083963	CG34127	BL38264	HMS01709		NE					
CG34139	FBgn0083975	CG34139	BL38265	HMS01710		NE					
CG8454	FBgn0261241	Vps16A	BL38271	HMS01716	A	ME	E			E	
CG9579	FBgn0000084	AnnX	BL38272	HMS01720		NE					
CG7467	FBgn0261885	osa	BL38285	HMS01738		NE					
CG6637	FBgn0260940	lsn	BL38289	HMS01747		NE					
CG4931	FBgn0038320	Sra-1	BL38294	HMS01754		NE					
CG7670	FBgn0038608	WRNexo	BL38297	HMS01758		NE					
CG11897	FBgn0039644	CG11897	BL38318	HMS01782		NE					
CG2096	FBgn0000711	flw	BL38336	HMS01803		NE					
CG13636	FBgn0039232	CG13636	BL38362	HMS01831		NE					
CG6383	FBgn0259685	crb	BL38373	HMS01842		NE					
CG1349	FBgn0039802	dj-1beta	BL38378	HMS01847		NE					
CG31148	FBgn0051148	CG31148	BL38379	HMS01848		NE					
CG6733	FBgn0039052	CG6733	BL38520	HMS01668		NE					
CG18112	FBgn0039702	Vps16B	BL38527	HMS01732		NE					
CG3525	FBgn0000536	eas	BL38528	HMS01734		NE					
CG6525	FBgn0082831	pps	BL38529	HMS01741		NE					
CG5802	FBgn0250820	CG5802	BL38938	HMS01771		NE					
CG14903	FBgn0038446	CG14903	BL38949	HMS01863		NE					
CG31522	FBgn0051522	CG31522	BL38952	HMS01866		NE					
CG9623	FBgn0001250	if	BL38958	HMS01872		NE					
CG1500	FBgn0001083	fw	BL38975	HMS01891		NE					
CG31414	FBgn0051414	CG31414	BL38977	HMS01893		NE					
CG5798	FBgn0038862	Ubpy	BL38982	HMS01898	A	ME	ME	S	E	E	

CG1359	FBgn0260860	Bet5	BL38993	HMS01909		NE					
CG14542	FBgn0039402	vps2	BL38995	HMS01911		NE					
CG1907	FBgn0039674	CG1907	BL38998	HMS01914		NE					
CG43226	FBgn0262871	lute	BL39011	HMS01929		NE					
CG7727	FBgn0000108	Appl	BL39013	HMS01931		NE					
CG5483	FBgn0038816	Lrrk	BL39019	HMS01937		NE					
CG6738	FBgn0039053	CG6738	BL39020	HMS01938		NE					
CG2520	FBgn0086372	lap	BL39021	HMS01939		NE					
CG1725	FBgn0001624	dlg1	BL39035	HMS01954		NE					
CG17785	FBgn0039188	Golgin84	BL39039	HMS01959		NE					
CG6323	FBgn0039465	Tsp97E	BL39047	HMS01967		NE					
CG1070	FBgn0261238	Alh	BL39057	HMS01977		NE					
CG7156	FBgn0038588	CG7156	BL39063	HMS01983		NE					
CG1511	FBgn0025936	Eph	BL39066	HMS01986		NE					
CG5055	FBgn0000163	baz	BL39072	HMS01992		NE					
CG43398	FBgn0263289	scrib	BL39073	HMS01993		NE					
CG17119	FBgn0039045	CG17119	BL40823	HMS00213		NE					
CG4849	FBgn0039566	CG4849	BL40828	HMS01994		NE					
CG34403	FBgn0085432	pan	BL40848	HMS02015		NE					
CG43286	FBgn0262975	cnc	BL40854	HMS02021		NE					
CG11877	FBgn0039636	CG11877	BL40858	HMS02025		NE					
CG7331	FBgn0261108	Atg13	BL40861	HMS02028		NE					
CG1906	FBgn0086361	alph	BL40873	HMS02040		NE					
CG2118	FBgn0039877	CG2118	BL40874	HMS02041		NE					
CG31057	FBgn0051057	tau	BL40875	HMS02042		NE					
CG41087	FBgn0069947	CG41087	BL40876	HMS02043		NE					
CG4413	FBgn0038767	trem	BL40881	HMS02049		NE					
CG31146	FBgn0051146	Nlg1	BL40883	HMS02131		NE					
CG17461	FBgn0039925	Kif3C	BL40886	HMS02134		NE					
CG14250	FBgn0039448	TwdlQ	BL40893	HMS02141		NE					
CG5864	FBgn0039132	AP-1sigma	BL40895	HMS02143		NE					
CG44012	FBgn0264754	btsz	BL40898	HMS02146		NE					
CG10371	FBgn0039111	Plip	BL40913	HMS02161		NE					
CG3678	FBgn0038461	CG3678	BL40920	HMS02168		NE					
CG3962	FBgn0038475	Keap1	BL40932	HMS02180	A	E-L	E-L			E	

CG10225	FBgn0039110	RanBP3	BL40948	HMS02196		NE					
CG1743	FBgn0001145	Gs2	BL40949	HMS02197		NE					
CG11144	FBgn0019985	mGluRA	BL41668	HMS02201		NE					
CG2246	FBgn0039790	CG2246	BL41694	HMS02259		NE					
CG42317	FBgn0262081	Csk	BL41712	HMS02277		NE					
CG13418	FBgn0038903	RpI12	BL41715	HMS02280		NE					
CG5148	FBgn0038478	cal1	BL41716	HMS02281		NE					
CG1539	FBgn0082582	tmod	BL41718	HMS02283		NE					
CG33336	FBgn0039044	p53	BL41720	HMS02286		NE					
CG5407	FBgn0038504	Sur-8	BL41883	HMS02299		NE					
CG6189	FBgn0001341	l(1)1Bi	BL41916	HMS02313		NE					
CG4815	FBgn0039568	CG4815	BL41919	HMS02316		NE					
CG13597	FBgn0039124	CG13597	BL41924	HMS02321		NE					
CG31343	FBgn0051343	CG31343	BL41925	HMS02322		NE					
CG17998	FBgn0261988	Gprk2	BL41933	HMS02330		NE					
CG31221	FBgn0051221	CG31221	BL41953	HMS02350		NE					
CG7794	FBgn0038565	CG7794	BL41970	HMS02367		NE					
CG17380	FBgn0039077	CG17380	BL41973	HMS02371	E-L	E-L	NE	MS	E-L		NE
CG4203	FBgn0038300	CG4203	BL41976	HMS02374		NE					
CG40378	FBgn0058378	CG40378	BL41980	HMS02378		NE					
CG4370	FBgn0039081	Irk2	BL41981	HMS02379		NE					
CG2041	FBgn0039907	lgs	BL41983	HMS02381		NE					
CG2316	FBgn0039890	CG2316	BL41984	HMS02382		NE					
CG7769	FBgn0260962	pic	BL41997	HMS02398		NE					
CG32490	FBgn0041605	cpx	BL42017	HMS02442	A	E	ME			ME	
CG11062	FBgn0024913	Actbeta	BL42493	HMJ02057		NE					
CG12254	FBgn0038760	MED25	BL42501	HMJ02066		NE					
CG11504	FBgn0039733	CG11504	BL42509	HMJ02074		NE					
CG12290	FBgn0039419	CG12290	BL42520	HMJ02086		NE					
CG15191	FBgn0000618	e(y)2	BL42524	HMJ02090		NE					
CG4656	FBgn0039055	Rassf	BL42534	HMJ02102		NE					
CG11420	FBgn0000826	png	BL42535	HMJ02104		NE					
CG10951	FBgn0045980	niki	BL42543	HMJ02114		NE					
CG42803	FBgn0264495	gpp	BL42556	HMJ02129	A	ME	ME			ME	
CG3350	FBgn0039509	bigmax	BL42559	HMJ02215		NE					

CG13850	FBgn0038961	CG13850	BL42574	HMJ02233		NE					
CG42551	FBgn0261618	larp	BL42578	HMJ02239		NE					
CG4907	FBgn0039010	CG4907	BL42602	HMS02435		NE					
CG7292	FBgn0038269	Rrp6	BL42604	HMS02437		NE					
CG7146	FBgn0038593	CG7146	BL42605	HMS02438		NE					
CG3837	FBgn0038279	CG3837	BL42609	HMS02444		NE					
CG31127	FBgn0046685	Wsck	BL42628	HMS02463		NE					
CG31195	FBgn0051195	CG31195	BL42632	HMS02468	E-L	E-L	NE	MS	E		NE
CG10407	FBgn0038395	CG10407	BL42636	HMS02472		NE					
CG44159	FBgn0265042	Irk1/ir	BL42644	HMS02480		NE					
CG4027	FBgn0000042	Act5C	BL42651	HMS02487	A	E	E			E	
CG14514	FBgn0039654	Brd8	BL42658	HMS02494	ME	ME	NE	NE	E-L		NE
CG31445	FBgn0051445	CG31445	BL42660	HMS02496		NE					
CG14895	FBgn0044826	Pak3	BL42664	HMS02500		NE					
CG9373	FBgn0260010	rump	BL42665	HMS02501		NE					
CG17477	FBgn0038479	CG17477	BL42821	HMS02503		NE					
CG5934	FBgn0039505	CG5934	BL42822	HMS02504		NE					
CG13977	FBgn0039519	Cyp6a18	BL42824	HMS02506		NE					
CG4854	FBgn0038766	CG4854	BL42833	HMS02525		NE					
CG4390	FBgn0038771	CG4390	BL42836	HMS02528		NE					
CG7715	FBgn0038646	CG7715	BL42837	HMS02529		NE					
CG31407	FBgn0051407	CG31407	BL42840	HMS02532	A	E	E			E	
CG10675	FBgn0039328	CHKov2	BL42843	HMS02535		NE					
CG15582	FBgn0046878	Obp83cd	BL42844	HMS02536		NE					
CG11873	FBgn0039633	CG11873	BL42847	HMS02539		NE					
CG6353	FBgn0038893	CG6353	BL42851	HMS02543		NE					
CG33329	FBgn0053329	Sp212	BL42858	HMS02550		NE					
CG4677	FBgn0039039	lmd	BL42871	HMS02564		NE					
CG12213	FBgn0260742	CG12213	BL42872	HMS02565		NE					
CG42827	FBgn0262009	CG42827	BL42878	HMS02571		NE					
CG6588	FBgn0262742	Fas1	BL42887	HMS02580		NE					
CG12449	FBgn0027341	Gfat1	BL42892	HMS02585		NE					
CG10192	FBgn0260634	eIF4G2	BL42893	HMS02586		NE					
CG13838	FBgn0039041	CG13838	BL42898	HMS02591		NE					
CG4792	FBgn0039016	Dcr-1	BL42901	HMS02594		NE					

CG7832	FBgn0086686	l(3)L1231	BL42907	HMS02600		NE					
CG6265	FBgn0039478	Nep5	BL42909	HMS02602		NE					
CG31016	FBgn0051016	CG31016	BL42911	HMS02604		NE					
CG3773	FBgn0038692	CG3773	BL42917	HMS02610	A	ME	ME	MS		ME	
CG6420	FBgn0039451	CG6420	BL42920	HMS02613		NE					
CG17743	FBgn0002521	pho	BL42926	HMS02619		NE					
CG11837	FBgn0039627	CG11837	BL42932	HMS02625		NE					
CG7993	FBgn0038585	CG7993	BL42935	HMS02628		NE					
CG15224	FBgn0000259	CkIIbeta	BL42943	HMS02636		NE					
CG14516	FBgn0039640	CG14516	BL42947	HMS02640		NE					
CG3796	FBgn0000022	ac	BL42953	HMS02646		NE					
CG3180	FBgn0262955	RpII140	BL43282	HMC02681		NE					
CG11836	FBgn0039272	CG11836	BL43308	HMS02692		NE					
CG1544	FBgn0039827	CG1544	BL43310	HMS02694		NE					
CG8147	FBgn0043791	CG8147	BL43314	HMS02698		NE					
CG33100	FBgn0053100	eIF4EHP	BL43990	HMS02703		NE					
CG42828	FBgn0262010	CG42828	BL43996	HMS02710		NE					
CG11956	FBgn0263236	SP1029	BL43997	HMS02711		NE					
CG32000	FBgn0052000	CG32000	BL44005	HMS02719		NE					
CG5127	FBgn0039335	Vps33B	BL44006	HMS02720		NE					
CG13978	FBgn0039518	CG13978	BL44008	HMS02722		NE					
CG5166	FBgn0041188	Atx2	BL44012	HMS02726	A	ME	ME	E		ME	
CG31065	FBgn0051065	CG31065	BL44013	HMS02727		NE					
CG1836	FBgn0026777	Rad23	BL44031	HMS02747		NE					
CG11152	FBgn0039937	fd102C	BL44045	HMS02761		NE					
CG31216	FBgn0051216	Naam	BL44053	HMS02770		NE					
CG5432	FBgn0039425	CG5432	BL44062	HMS02779	E	E	NE	MS	E		NE
CG1983	FBgn0039751	CG1983	BL44064	HMS02781		NE					
CG7265	FBgn0038272	CG7265	BL44066	HMS02783		NE					
CG10823	FBgn0038880	SIFR	BL44068	HMS02785		NE					
CG31118	FBgn0051118	RabX4	BL44070	HMS02787		NE					
CG31446	FBgn0051446	CG31446	BL44071	HMS02788		NE					
CG6535	FBgn0045035	tefu	BL44073	HMS02790		NE					
CG4367	FBgn0038783	CG4367	BL44077	HMS02794		NE					
CG5510	FBgn0039160	CG5510	BL44080	HMS02797	MS	MS	ME	S	E	ME	NE

CG13857	FBgn0038958	CG13857	BL44083	HMS02800		NE					
CG11093	FBgn0039932	CG11093	BL44085	HMS02802		NE					
CG33203	FBgn0053203	CG33203	BL44088	HMS02805		NE					
CG11843	FBgn0039630	CG11843	BL44092	HMS02809		NE					
CG3578	FBgn0000179	bi	BL44095	HMS02815		NE					
CG31141	FBgn0051141	CG31141	BL44107	HMS02828		NE					
CG7829	FBgn0039703	CG7829	BL44112	HMS02834		NE					
CG11880	FBgn0039637	CG11880	BL44113	HMS02835	A	ME	ME			ME	
CG14883	FBgn0038432	CG14883	BL44114	HMS02836		NE					
CG17780	FBgn0039197	CG17780	BL44119	HMS02841		NE					
CG5791	FBgn0040582	CG5791	BL44121	HMS02843		NE					
CG6439	FBgn0038922	CG6439	BL44475	HMC02361		NE					
modSP	FBgn0051217	modSP	BL44476	HMC02363		NE					
CG17271	FBgn0038829	CG17271	BL44480	HMC02370		NE					
ctrip	FBgn0260794	ctrip	BL44481	HMC02371		NE					
CG1172	FBgn0264712	CG1172	BL44500	HMC02436		NE					
CG5278	FBgn0038986	CG5278	BL44515	HMC02905		NE					
mthl12	FBgn0045442	mthl12	BL44516	HMC02906		NE					
CG33110	FBgn0053110	CG33110	BL44519	HMC02909		NE					
CG13830	FBgn0039054	CG13830	BL44530	HMC02924		NE					
CG13604	FBgn0039137	CG13604	BL44537	HMC02932		NE					
CG1909	FBgn0039911	CG1909	BL44538	HMC02933		NE					
Rim	FBgn0053547	Rim	BL44541	HMC02936		NE					
cdm	FBgn0261532	cdm	BL44551	HMS02846		NE					
ase	FBgn0000137	ase	BL44552	HMS02847		NE					
CG3281	FBgn0260741	CG3281	BL44555	HMS02851		NE					
CG33099	FBgn0053099	CG33099	BL44559	HMS02855		NE					
Pros25	FBgn0086134	Pros25	BL44560	HMS02856		NE					
Mitf	FBgn0263112	Mitf	BL44561	HMS02857		NE					
CG7695	FBgn0038631	CG7695	BL44568	HMS02864		NE					
CG32850	FBgn0052850	CG32850	BL44570	HMS02866		NE					
CG34290	FBgn0085319	CG34290	BL44573	HMS02869		NE					
CG15556	FBgn0039821	CG15556	BL44574	HMS02870		NE					
CG6432	FBgn0039184	CG6432	BL44575	HMS02871		NE					
CG5326	FBgn0038983	CG5326	BL44659	HMC02892		NE					

CG1937	FBgn0039875	sip3	BL50609	HMC02976		NE					
CG4210	FBgn0038302	CG4210	BL50615	HMC02982		NE					
CG1969	FBgn0039690	CG1969	BL50616	HMC02983		NE					
CG7816	FBgn0039714	CG7816	BL50635	HMC03033		NE					
CG1449	FBgn0004607	zfh2	BL50643	HMC03043		NE					
CG2229	FBgn0039777	Jon99Fii	BL50648	HMC03049		NE					
CG10367	FBgn0263782	Hmgcr	BL50652	HMC03053	A	E-L	E-L			E-L	
CG31075	FBgn0051075	CG31075	BL50654	HMC03055		NE					
CG5737	FBgn0038851	dmrt93B	BL50656	HMC03057		NE					
CG31481	FBgn0051481	pb	BL50664	HMC03065		NE					
CG18208	FBgn0038653	CG18208	BL50678	HMC03079		NE					
CG15504	FBgn0039683	dmrt99B	BL50687	HMC03088		NE					
CG6919	FBgn0038980	oa2	BL50701	HMC03103		NE					
CG1401	FBgn0039632	Cul-5	BL50707	HMC03109		NE					
CG15525	FBgn0039732	CG15525	BL50708	HMC03110		NE					
CG42235	FBgn0250757	CG42235	BL50724	HMS02960		NE					
CG31094	FBgn0066101	LpR1	BL50737	HMS02973		NE					
CG42320	FBgn0259220	Doa	BL50903	HMJ03121		NE					
CG12054	FBgn0039831	CG12054	BL50910	HMJ03134		NE					
CG14313	FBgn0038579	CG14313	BL50915	HMJ21004		NE					
CG10157	FBgn0039099	CG10157	BL50938	HMJ21033		NE					
CG6904	FBgn0038293	CG6904	BL50956	HMJ21058		NE					
CG5952	FBgn0038402	Fer2	BL50971	HMJ21077		NE					
CG4003	FBgn0040078	pont	BL50972	HMJ21078		NE					
CG10559	FBgn0039323	CG10559	BL50975	HMJ21081		NE					
CG3631	FBgn0038268	CG3631	BL50997	HMJ21110		NE					
CG33698	FBgn0261291	CheA86a	BL51001	HMJ21115		NE					
CG7911	FBgn0039735	CG7911	BL51021	HMJ21147		NE					
CG13634	FBgn0039224	CG13634	BL51024	HMJ21150		NE					
CG7789	FBgn0039698	CG7789	BL51028	HMJ21155		NE					
CG6277	FBgn0039475	CG6277	BL51030	HMJ21157		NE					
CR34649	FBgn0085056	tre-1	BL51032	HMJ21159		NE					
CG17836	FBgn0261113	Xrp1	BL51054	HMJ21189	E-L	E-L	NE	E	E		NE
CG11886	FBgn0041186	Slbp	BL51171	HMJ21114		NE					
CG6196	FBgn0038323	Trs33	BL51393	HMJ21139	S	S		S	MS		NE

CG2126	FBgn0039876	CG2126	BL51424	HMC02894		NE					
CG12753	FBgn0038427	ema	BL51426	HMC02913		NE					
CG10694	FBgn0039147	CG10694	BL51434	HMC03147		NE					
CG6271	FBgn0039476	CG6271	BL51436	HMC03150	MS	MS		S	S		NE
CG34376	FBgn0085405	CG34376	BL51439	HMC03153		NE					
CG3839	FBgn0002561	l(1)sc	BL51443	HMC03157		NE					
CG15803	FBgn0038606	CG15803	BL51449	HMC03179		NE					
CG7834	FBgn0039697	CG7834	BL51464	HMC03204	A	ME	ME			E	
CG5237	FBgn0038693	unc79	BL51471	HMC03213		NE					
CG6657	FBgn0015562	veg	BL51478	HMC03223		NE					
CG31064	FBgn0051064	CG31064	BL51494	HMC03246		NE					
CG31523	FBgn0051523	CG31523	BL51495	HMC03248		NE					
CG6283	FBgn0039474	CG6283	BL51498	HMC03253		NE					
CG33967	FBgn0262127	kibra	BL51499	HMC03256		NE					
CG11849	FBgn0039286	dan	BL51501	HMC03259		NE					
CG31284	FBgn0260005	wtrw	BL51503	HMC03264		NE					
CG43224	FBgn0262869	mun	BL51505	HMC03267		NE					
CG6930	FBgn0265276	l(3)neo38	BL51515	HMC03292		NE					
CG7242	FBgn0087021	Spc25	BL51516	HMS03161		NE					
CG2003	FBgn0039886	CG2003	BL51699	HMC03148		NE					
CG6660	FBgn0039030	CG6660	BL51707	HMC03202		NE					
CG41624	FBgn0086917	spok	BL51718	HMC03254		NE					
CG1783	FBgn0024728	Slip1	BL51724	HMC03268		NE					
CG11951	FBgn0039656	CG11951	BL51735	HMS03163	(MS POSSIBLE)	NE		NE			
CG7262	FBgn0038274	CG7262	BL51758	HMC03310	A	ME	ME	E		ME	
CG6995	FBgn0039229	Saf-B	BL51759	HMC03311		NE					
CG6295	FBgn0039471	CG6295	BL51760	HMC03312		NE					
CG11318	FBgn0039818	CG11318	BL51792	HMC03348		NE					
CG1065	FBgn0004888	Scsalpha	BL51807	HMC03366		NE					
CG4360	FBgn0038787	CG4360	BL51813	HMC03384		NE					
CG3731	FBgn0038271	CG3731	BL51822	HMC03394		NE					
CG5911	FBgn0038874	ETHR	BL51828	HMC03400		NE					
CG2171	FBgn0086355	Tpi	BL51829	HMC03401		NE					
CG12265	FBgn0264291	Det	BL51837	HMC03409		NE					

CG34383	FBgn0085412	CG34383	BL51917	HMS03376		NE					
CG11839	FBgn0039271	CG11839	BL51924	HMS03375		NE					
Mtl	FBgn0039532	Mtl	BL51932	HMC03186		NE					
CG4053	FBgn0038482	CG4053	BL52872	HMC03610		NE					
CG5255	FBgn0038485	CG5255	BL52874	HMC03612		NE					
CG5909	FBgn0039495	CG5909	BL52876	HMC03614		NE					
CG10232	FBgn0039108	CG10232	BL52891	HMC03629		NE					
CG17475	FBgn0038481	CG17475	BL52895	HMC03634		NE					
CG7142	FBgn0038595	CG7142	BL52899	HMC03638		NE					
mfas	FBgn0260745	mfas	BL52905	HMC03645		NE					
Dhap-at	FBgn0040212	Dhap-at	BL52914	HMC03654		NE					
CG15523	FBgn0039727	CG15523	BL52915	HMC03655		NE					
CG14870	FBgn0038342	CG14870	BL52916	HMC03656		NE					
CG5044	FBgn0038326	CG5044	BL52917	HMC03657		NE					
grass	FBgn0039494	grass	BL52946	HMJ21613		NE					
CG34307	FBgn0085336	CG34307	BL52953	HMJ21622		NE					
CG43427	FBgn0263346	CG43427	BL52982	HMJ21669		NE					
CG4538	FBgn0038745	CG4538	BL52989	HMJ21681		NE					
CG5514	FBgn0039560	CG5514	BL52994	HMJ21706		NE					
CG42327	FBgn0259227	CG42327	BL52997	HMJ21710		NE					
CG7582	FBgn0039681	CG7582	BL53002	HMJ21718		NE					
Npl4	FBgn0039348	Npl4	BL53004	HMJ21721		NE					
CG14894	FBgn0038428	CG14894	BL53005	HMJ21722		NE					
CG31259	FBgn0051259	CG31259	BL53009	HMJ21727		NE					
CG33630	FBgn0053630	CG33630	BL53015	HMJ21738		NE					
DNApol-epsilon	FBgn0264326	DNApol-epsilon	BL53016	HMJ21739		NE					
Muc91C	FBgn0038642	Muc91C	BL53018	HMJ21741		NE					
puc	FBgn0243512	puc	BL53019	HMJ21742	(MS POSSIBLE)	NE				ME	
CG31178	FBgn0064912	CG31178	BL53024	HMJ21748		NE					
CG17565	FBgn0038424	CG17565	BL53029	HMJ21755		NE					
CG5073	FBgn0038331	CG5073	BL53283	HMC03499		NE					
Hmt-1	FBgn0038376	Hmt-1	BL53284	HMC03500		NE					
CG5220	FBgn0038471	CG5220	BL53285	HMC03501		NE					
CG18012	FBgn0038552	CG18012	BL53286	HMC03502		NE					

CG4703	FBgn0038742	Arc42	BL53287	HMC03503		NE					
CG4159	FBgn0038811	CG4159	BL53288	HMC03504		NE					
CG15923	FBgn0038814	CG15923	BL53289	HMC03505		NE					
CG5097	FBgn0038790	MtnC	BL53292	HMC03508		NE					
CG7622	FBgn0002579	RpL36	BL53302	HMC03529	A	E	E			E	
CG42601	FBgn0261053	Cad86C	BL53314	HMC03543		NE					
CG5634	FBgn0039528	dsd	BL53318	HMC03547		NE					
CG17269	FBgn0038827	Fancd2	BL53329	HMC03558		NE					
CG4917	FBgn0039003	wfs1	BL53330	HMC03559		NE					
CG5977	FBgn0039141	spas	BL53331	HMC03560		NE					
CG31116	FBgn0051116	ClC-a	BL53337	HMC03566		NE					
CG6349	FBgn0259113	DNApol-alpha180	BL53341	HMC03570		NE					
CG32498	FBgn0000479	dnc	BL53344	HMC03573		NE					
CG11987	FBgn0264075	tgo	BL53351	HMC03580		NE					
CG1890	FBgn0039869	CG1890	BL53677	HMJ21731		NE					
CG31050	FBgn0051050	CG31050	BL53691	HMJ21674		NE					
CG14260	FBgn0039504	CG14260	BL53698	HMJ21719	A	ME	ME			E	
CG13646	FBgn0039255	CG13646	BL53701	HMJ21732		NE					
CG31164	FBgn0051164	Ir94a	BL53703	HMJ21737		NE					
CG16901	FBgn0263396	sqd	BL53891	HMJ21209		NE					
CG31438	FBgn0051438	CheB93b	BL53911	HMJ21244		NE					
CG31418	FBgn0051418	CG31418	BL53914	HMJ21247		NE					
CG32944	FBgn0052944	CG32944	BL53916	HMJ21251		NE					
CG14326	FBgn0038528	CG14326	BL53952	HMJ21318		NE					
CG7362	FBgn0038258	CG7362	BL53954	HMJ21320		NE					
CG5913	FBgn0039385	CG5913	BL53965	HMJ21347		NE					
CG5692	FBgn0040080	raps	BL53968	HMJ21351		NE					
CG31262	FBgn0051262	CG31262	BL53970	HMJ21355		NE					
CG17382	FBgn0039080	Ir94h	BL53975	HMJ21363		NE					
CG5377	FBgn0038974	CG5377	BL53977	HMJ21366		NE					
CG4803	FBgn0039015	Takl2	BL53985	HMJ21386		NE					
CG6066	FBgn0039488	CG6066	BL53997	HMJ21401		NE					
CG31244	FBgn0051244	CG31244	BL54011	HMJ21435		NE					
CG32473	FBgn0052473	CG32473	BL54013	HMJ21437		NE					
CG2219	FBgn0039889	CG2219	BL54014	HMJ21438		NE					

CG31453	FBgn0051453	pch2	BL54022	HMJ21448	MS	MS		S	E		NE
CG13664	FBgn0039294	Cad96Cb	BL54029	HMJ21472		NE					
CG17109	FBgn0039051	CG17109	BL54033	HMJ21476		NE					
CG14549	FBgn0039403	Sld5	BL54047	HMJ21490		NE					
CG5292	FBgn0038491	CG5292	BL54052	HMS03523		NE					
CG3093	FBgn0000482	dor	BL54460	HMS03720		NE					
CG31092	FBgn0051092	LpR2	BL54461	HMS03722		NE					
CG14332	FBgn0038509	CG14332	BL54800	HMJ21494		NE					
CG5677	FBgn0039172	Spase22-23	BL54801	HMJ21495		NE					
CG6447	FBgn0039437	TwdlL	BL54804	HMJ21498		NE					
CG31258	FBgn0086697	Cenp-C	BL54806	HMJ21500	A	ME	ME			ME	
CG14298	FBgn0038654	CG14298	BL54807	HMJ21501		NE					
CG8495	FBgn0261599	RpS29	BL54822	HMJ21541	A	ME	ME			E	
CG17121	FBgn0039043	CG17121	BL54830	HMJ21549		NE					
CG6073	FBgn0039417	CG6073	BL54844	HMJ21581		NE					
CG43343	FBgn0263048	CG43343	BL54848	HMJ21585		NE					
CG11820	FBgn0039270	PQBP1	BL54852	HMJ21589		NE					
CG31040	FBgn0051040	Cog7	BL55147	HMC03758		NE					
CG9733	FBgn0039759	CG9733	BL55149	HMC03774		NE					
CG6422	FBgn0039261	CG6422 (dYTHDF1)	BL55151	HMC03791	A	ME	ME			E	
CG10877	FBgn0038804	CG10877	BL55160	HMC03835		NE					
CG2177	FBgn0039902	Zip102B	BL55162	HMC03837	MS	MS		S	ME		NE
CG1249	FBgn0261789	SmD2	BL55163	HMC03839		NE					
CG6178	FBgn0039156	CG6178	BL55166	HMC03844		NE					
CG4334	FBgn0038312	CG4334	BL55167	HMC03846		NE					
CG31368	FBgn0051368	CG31368	BL55172	HMC03852		NE					
CG11313	FBgn0039798	CG11313	BL55197	HMC03894		NE					
CG14648	FBgn0263594	lost	BL55201	HMC03901		NE					
CG1109	FBgn0046222	CG1109	BL55249	HMC03936		NE					
CG6300	FBgn0038730	CG6300	BL55264	HMC03951		NE					
CG11391	FBgn0038732	CG11391	BL55266	HMC03953		NE					
CG11453	FBgn0038734	CG11453	BL55267	HMC03954		NE					
CG11659	FBgn0038731	CG11659	BL55268	HMC03955		NE					
CG7946	FBgn0039743	CG7946	BL55274	HMC03961		NE					
CG1587	FBgn0024811	Crk	BL55277	HMC03964		NE					

CG6006	FBgn0063649	CG6006	BL55282	HMC03969	E	E	NE	S	E		NE
CG1647	FBgn0039602	CG1647	BL55292	HMC03979		NE					
CG34073	FBgn0013672	mt:ATPase6	BL55297	HMC03984		NE					
CG31199	FBgn0051199	CG31199	BL55339	HMC04026		NE					
CG31200	FBgn0051200	CG31200	BL55340	HMC04027	A	E	E			E	
CG18754	FBgn0042106	CG18754	BL55348	HMC04035		NE					
CG12250	FBgn0261287	ymp	BL55356	HMC04043		NE					
CG42724	FBgn0261641	CG42724	BL55357	HMC04044		NE					
CG1420	FBgn0039626	Slu7	BL55366	HMC04054		NE					
CG7907	FBgn0038887	CG7907	BL55370	HMC04058		NE					
CG4934	FBgn0000221	brn	BL55386	HMC04074		NE					
CG5555	FBgn0038686	CG5555	BL55402	HMC04090		NE					
CG5246	FBgn0038484	CG5246	BL55410	HMC04098		NE					
CG3339	FBgn0039510	CG3339	BL55605	HMC03741		NE					
CG5938	FBgn0046247	CG5938	BL55613	HMC03752		NE					
CG12558	FBgn0039599	CG12558	BL55615	HMC03754		NE					
CG11842	FBgn0039629	CG11842	BL55617	HMC03760		NE					
CG11876	FBgn0039635	CG11876	BL55619	HMC03762		NE					
CG7883	FBgn0039726	eIF2B-alpha	BL55624	HMC03768		NE					
CG31326	FBgn0051326	CG31326	BL55630	HMC03777		NE					
CG17856	FBgn0039576	CG17856	BL55631	HMC03778		NE					
CG34157	FBgn0260003	Dys	BL55641	HMC03789		NE					
CG10210	FBgn0039117	tst	BL55647	HMC03796		NE					
CG7903	FBgn0039730	CG7903	BL55651	HMC03800	A	ME	ME			ME	
CG1964	FBgn0039688	Kul	BL55653	HMC03803		NE					
CG7598	FBgn0039689	CG7598	BL55660	HMC03815		NE					
CG10293	FBgn0264491	how	BL55665	HMC03820		NE					
CG5338	FBgn0039129	RpS19b	BL55670	HMC03825		NE					
CG4685	FBgn0039349	Ssadh	BL55683	HMC03868		NE					
CG17136	FBgn0260944	Rbp1	BL55688	HMC03902		NE					
CG7698	FBgn0261065	Cpsf73	BL55696	HMC03910		NE					
CG40478	FBgn0027101	Dyrk3	BL55882	HMC04155		NE					
CG7125	FBgn0038603	PKD	BL55898	HMC04179		NE					
CG10177	FBgn0039083	CG10177	BL55900	HMC04182		NE					
CG12069	FBgn0039796	CG12069	BL55901	HMC04183		NE					

CG11533	FBgn0039908	Asator	BL55902	HMC04184		NE					
CG31421	FBgn0046689	Takl1	BL55903	HMC04186		NE					
CG31096	FBgn0039354	Lgr3	BL55910	HMC04196		NE					
CG5728	FBgn0039182	CG5728	BL55916	HMC04202		NE					
CG34034	FBgn0054034	CG34034	BL55956	HMC04245		NE					
CG34129	FBgn0083965	CG34129	BL55959	HMC04253		NE					
CG4546	FBgn0038373	CG4546	BL55977	HMC04273		NE					
CG14880	FBgn0038422	CG14880	BL55978	HMC04274		NE					
CG7629	FBgn0038530	AttD	BL55979	HMC04275	A	E	E			E	
CG13837	FBgn0039042	CG13837	BL55980	HMC04276		NE					
CG6173	FBgn0039155	Kal1	BL55981	HMC04277		NE					
CG11853	FBgn0039298	to	BL55982	HMC04278		NE					
CG6403	FBgn0039453	CG6403	BL55983	HMC04279		NE					
CG3348	FBgn0040609	CG3348	BL55985	HMC04281		NE					
CG18550	FBgn0041710	yellow-f	BL55988	HMC04284		NE					
CG31077	FBgn0051077	CG31077	BL55991	HMC04287		NE					
CG31286	FBgn0051286	CG31286	BL55992	HMC04288		NE					
CG31296	FBgn0051296	CG31296	BL55993	HMC04289		NE					
CG14882	FBgn0038429	CG14882	BL56006	HMC04302		NE					
CG13643	FBgn0040601	CG13643	BL56017	HMC04313		NE					
CG4743	FBgn0039357	CG4743	BL56025	HMC04321		NE					
CG6126	FBgn0038407	CG6126	BL56038	HMC04346	MS	MS		NE	E		NE
CG2559	FBgn0002562	Lsp1alpha	BL56039	HMC04347		NE					
CG4090	FBgn0038492	Mur89F	BL56041	HMC04349		NE					
CG17192	FBgn0039472	CG17192	BL56042	HMC04350		NE					
CG42813	FBgn0261995	CG42813	BL56045	HMS04248		NE					
CG6194	FBgn0038325	CG6194	BL56046	HMS04249		NE					
CG8433	FBgn0029175	Ext2	BL52883	HMC03621		NE					
CG33502	FBgn0053502	CG33502	BL52907	HMC03647		NE					
CG4030	FBgn0034585	CG4030	BL52996	HMJ21709		NE					
CG7300	FBgn0032286	CG7300	BL53927	HMJ21272		NE					
CG13323	FBgn0033788	CG13323	BL53969	HMJ21352		NE					
CG9249	FBgn0032922	CG9249	BL54042	HMJ21485		NE					
CG1317	FBgn0035333	CG1317	BL54802	HMJ21301		NE					
CG43073	FBgn0262483	Rbp	BL54828	HMJ21547		NE					

CG14145	FBgn0036118	blos2	BL54835	HMJ21554		NE					
CG5953	FBgn0032587	CG5953	BL57287	HMJ21225		NE					
CG5336	FBgn0032409	Ced-12	BL58153	HMJ22104		NE					
CG3312	FBgn0014024	Rnp4F	BL58168	HMJ22145		NE					
CG14030	FBgn0031696	Bub1	BL58185	HMJ22162		NE					
CG14724	FBgn0019624	CoVa	BL58282	HMJ22367		NE					
CG30411	FBgn0050411	CG30411	BL58318	HMJ22443		NE					
CG8628	FBgn0250836	CG8628	BL58343	HMJ22474		NE					
CG8034	FBgn0031011	CG8034	BL32340	HMS00331		NE					
CG43658	FBgn0263706	CG43658	BL32341	HMS00332		NE					
CG12238	FBgn0087008	e(y)3	BL32346	HMS00337		NE					
CG12794	FBgn0028583	lcs	BL32353	HMS00344		NE					
CG1412	FBgn0031118	RhoGAP19D	BL32361	HMS00352		NE					
CG16982	FBgn0025638	Roc1a	BL32362	HMS00353		NE					
CG3051	FBgn0023169	SNF1A	BL32371	HMS00362		NE					
CG8805	FBgn0041087	wun2	BL32381	HMS00372		NE					
CG4200	FBgn0003416	sl	BL32385	HMS00377		NE					
CG7041	FBgn0030082	HP1b	BL32401	HMS00396		NE					
CG42276	FBgn0259171	Pde9	BL32412	HMS00407		NE					
CG10944	FBgn0261592	RpS6	BL32418	HMS00413	E	E	NE	S	MS		NE
CG3595	FBgn0003514	sqh	BL32439	HMS00437		NE					
CG12124	FBgn0260789	mxc	BL32446	HMS00444		NE					
CG7065	FBgn0030091	CG7065	BL32449	HMS00448		NE					
CG7098	FBgn0030891	dik	BL32451	HMS00450		NE					
CG3480	FBgn0023509	mip130	BL32462	HMS00462		NE					
CG9156	FBgn0003132	Pp1-13C	BL32465	HMS00465		NE					
CG4336	FBgn0003302	rux	BL32467	HMS00467		NE					
CG11427	FBgn0003210	rb	BL32477	HMS00479		NE					
CG12109	FBgn0030054	Caf1-180	BL32478	HMS00480		NE					
CG14446	FBgn0262730	CG14446	BL32487	HMS00490		NE					
CG1633	FBgn0040309	Jafrac1	BL32498	HMS00501		NE					
CG4303	FBgn0025463	Bap60	BL32503	HMS00507		NE					
CG1636	FBgn0030030	CG1636	BL32508	HMS00512		NE					
CG7556	FBgn0030990	CG7556	BL32511	HMS00515		NE					
CG4453	FBgn0061200	Nup153	BL32837	HMS00527		NE					

CG9057	FBgn0030608	Lsd-2	BL32846	HMS00629		NE					
CG1810	FBgn0030556	mRNA-cap	BL32847	HMS00631	LacZ-S	MS	ME	MS	MS	E	MS
CG2998	FBgn0030136	RpS28b	BL32850	HMS00635		NE					
CG33542	FBgn0053542	upd3	BL32859	HMS00646		NE					
CG13317	FBgn0044046	Ilp7	BL32862	HMS00649		NE					
CG16983	FBgn0025637	skpA	BL32870	HMS00657		NE					
CG3455	FBgn0028685	Rpt4	BL32874	HMS00661	A	ME	ME			E	
CG3226	FBgn0029882	CG3226	BL32875	HMS00662		NE					
CG5599	FBgn0030612	CG5599	BL32876	HMS00663		NE					
CG13363	FBgn0025639	Hmt4-20	BL32892	HMS00681		NE					
CG8915	FBgn0030833	CG8915	BL32908	HMS00697		NE					
CG13374	FBgn0011822	pcl	BL32943	HMS00737		NE					
CG2272	FBgn0030018	slpr	BL32948	HMS00742		NE					
CG7107	FBgn0004169	up	BL32949	HMS00743		NE					
CG17437	FBgn0040066	wds	BL32952	HMS00746		NE					
CG4313	FBgn0025632	CG4313	BL32960	HMS00755		NE					
CG1594	FBgn0004864	hop	BL32966	HMS00761		NE					
CG12141	FBgn0027084	Aats-lys	BL32967	HMS00763		NE					
CG4078	FBgn0029798	CG4078	BL32973	HMS00770		NE					
CG8128	FBgn0030668	CG8128	BL33012	HMS00812		NE					
CG11585	FBgn0030543	CG11585	BL33337	HMS00203		NE					
CG14816	FBgn0023517	Pgam5	BL33346	HMS00212		NE					
CG18262	FBgn0030012	CG18262	BL33348	HMS00215		NE					
CG34145	FBgn0083981	RunxA	BL33353	HMS00224		NE					
CG8289	FBgn0030854	CG8289	BL33361	HMS00233		NE					
CG10998	FBgn0031142	r-cup	BL33387	HMS00264		NE					
CG40494	FBgn0025836	RhoGAP1A	BL33390	HMS00267		NE					
CG18492	FBgn0026323	Tak1	BL33404	HMS00282		NE					
CG5227	FBgn0021764	sdk	BL33412	HMS00292		NE					
CG3711	FBgn0040344	CG3711	BL33422	HMS00306		NE					
CG6903	FBgn0029737	CG6903	BL33423	HMS00307		NE					
CG3917	FBgn0026430	Grip84	BL33548	HMS00627		NE					
CG12737	FBgn0025864	Crag	BL33594	HMS00241		NE					
CG3936	FBgn0004647	N	BL33611	HMS00001	A	E-L	E-L			E-L	
CG2759	FBgn0003996	w	BL33613	HMS00004	A	E-L	E-L			E-L	

CG15793	FBgn0010269	Dsor1	BL33639	HMS00037		NE					
CG1560	FBgn0004657	mys	BL33642	HMS00043		NE					
CG7035	FBgn0022942	Cbp80	BL33648	HMS00052		NE					
CG2577	FBgn0030384	CG2577	BL33649	HMS00054		NE					
CG9096	FBgn0010315	CycD	BL33653	HMS00059		NE					
CG42666	FBgn0261548	CG42666	BL33665	HMS00075		NE					
CG18412	FBgn0004861	ph-p	BL33669	HMS00082		NE					
CG5993	FBgn0004956	os	BL33680	HMS00545		NE					
CG14049	FBgn0044047	Ilp6	BL33684	HMS00549		NE					
CG2221	FBgn0028331	l(1)G0289	BL33690	HMS00558		NE					
CG3025	FBgn0014340	mof	BL33698	HMS00573		NE					
CG3171	FBgn0046687	Tre1	BL33718	HMS00599		NE					
CG1637	FBgn0030245	CG1637	BL33733	HMS00616		NE					
CG34104	FBgn0083940	CG34104	BL33738	HMS00622		NE					
CG6223	FBgn0008635	betaCop	BL33741	HMS01079	A	E-L	E-L			E-L	
CG2186	FBgn0030243	CG2186	BL33750	HMS01090		NE					
CG2655	FBgn0011276	HLH3B	BL33758	HMS01101		NE					
CG4399	FBgn0261954	east	BL33879	HMS00816		NE					
CG40440	FBgn0046697	Ppr-Y	BL33882	HMS00819		NE					
CG11092	FBgn0027537	CG11092	BL33908	HMS00850		NE					
CG2286	FBgn0017566	ND75	BL33910	HMS00853		NE					
CG14224	FBgn0031057	Ubqn	BL33917	HMS00860		NE					
CG9907	FBgn0264255	para	BL33923	HMS00868		NE					
CG11941	FBgn0026175	skpC	BL33925	HMS00871		NE					
CG10961	FBgn0026318	Traf6	BL33931	HMS00880		NE					
CG10701	FBgn0011661	Moe	BL33936	HMS00886		NE					
CG42611	FBgn0261260	mgl	BL33940	HMS00891		NE					
CG12212	FBgn0003053	peb	BL33943	HMS00894		NE					
CG5988	FBgn0030904	upd2	BL33949	HMS00901		NE					
CG10992	FBgn0030521	CtsB1	BL33953	HMS00906		NE					
CG1453	FBgn0030268	Klp10A	BL33963	HMS00920		NE					
CG11387	FBgn0004198	ct	BL33967	HMS00924	A	E	E			E	
CG8649	FBgn0024238	Fim	BL33977	HMS00937		NE					
CG6222	FBgn0003575	su(s)	BL33982	HMS00942		NE					
CG34412	FBgn0086899	tlk	BL33983	HMS00943	A	E	E			E	

CG3187	FBgn0029783	Sirt4	BL33984	HMS00944		NE					
CG2033	FBgn0010198	RpS15Aa	BL34005	HMS00968	A	E-L	E			E	
CG2947	FBgn0029676	HIP-R	BL34018	HMS00988		NE					
CG9609	FBgn0030787	CG9609	BL34030	HMS01000		NE					
CG12743	FBgn0003023	otu	BL34065	HMS00038		NE					
CG7486	FBgn0020381	Dredd	BL34070	HMS00063		NE					
CG6170	FBgn0026428	HDAC6	BL34072	HMS00077		NE					
CG18259	FBgn0030956	CG18259	BL34081	HMS01089		NE					
CG4013	FBgn0263865	Smr	BL34087	HMS00842	A	E	E			E	
CG9774	FBgn0026181	rok	BL34324	HMS01311		NE					
CG12154	FBgn0004102	oc	BL34327	HMS01314		NE					
CG14476	FBgn0027588	CG14476	BL34334	HMS01322		NE					
CG32672	FBgn0052672	Atg8a	BL34340	HMS01328		NE					
CG12703	FBgn0031069	Pmp70	BL34349	HMS01338		NE					
CG4332	FBgn0030456	CG4332	BL34352	HMS01341		NE					
CG7053	FBgn0030960	CG7053	BL34360	HMS01349	A	ME	ME			E	
CG3004	FBgn0264691	Lst8	BL34361	HMS01350	MS	MS	ME	S	S	ME	NE
CG1749	FBgn0030305	CG1749	BL34363	HMS01352		NE					
CG32670	FBgn0052670	Rab9Fb	BL34374	HMS01364		NE					
CG2849	FBgn0015286	Rala	BL34375	HMS01365	A	ME	E	E	E-L	E	
CG9355	FBgn0004511	dy	BL34382	HMS01372		NE					
CG43770	FBgn0264270	Sxl	BL34393	HMS00609		NE					
CG15784	FBgn0029766	CG15784	BL34529	HMS00983		NE					
CG9581	FBgn0031093	CG9581	BL34547	HMS01018		NE					
CG3239	FBgn0029769	CG3239	BL34558	HMS01030		NE					
CG4330	FBgn0030452	MFS10	BL34562	HMS01034		NE					
CG3034	FBgn0040339	MED22	BL34573	HMS01047		NE					
CG42699	FBgn0261610	CG42699	BL34591	HMS01065		NE					
CG4528	FBgn0003449	snf	BL34593	HMS01067	(ME POSSIBLE)	NE	NE	NE	NE	NE	
CG3585	FBgn0023458	Rbcn-3A	BL34612	HMS01287		NE					
CG9022	FBgn0014868	Ost48	BL34628	HMS01303		NE					
CG12065	FBgn0030052	CG12065	BL34636	HMS01111		NE					
CG6407	FBgn0010194	Wnt5	BL34644	HMS01119		NE					
CG13366	FBgn0025633	CG13366	BL34656	HMS01133		NE					

CG15735	FBgn0030364	CG15735	BL34666	HMS01143		NE					
CG4206	FBgn0024332	Mcm3	BL34686	HMS01164		NE					
CG3291	FBgn0020261	pcm	BL34690	HMS01169		NE					
CG10521	FBgn0015774	NetB	BL34698	HMS01177		NE					
CG1849	FBgn0003300	run	BL34707	HMS01186		NE					
CG1490	FBgn0030366	Usp7	BL34708	HMS01187		NE					
CG7033	FBgn0030086	CG7033	BL34711	HMS01190		NE					
CG1489	FBgn0020369	Pros45	BL34712	HMS01191		NE					
CG3573	FBgn0023508	Ocrl	BL34722	HMS01201		NE					
CG9784	FBgn0030761	CG9784	BL34723	HMS01202		NE					
CG12101	FBgn0015245	Hsp60	BL34729	HMS01209		NE					
CG3129	FBgn0015794	Rab18	BL34734	HMS01214		NE					
CG1770	FBgn0041210	HDAC4	BL34774	HMS00083		NE					
CG8264	FBgn0004856	Bx42	BL34777	HMS00086	A	E-L	E			E	
CG2995	FBgn0040372	G9a	BL34817	HMS00127		NE					
CG7434	FBgn0015288	RpL22	BL34828	HMS00143	A	E	E			E	
CG3606	FBgn0011571	caz	BL34839	HMS00156		NE					
CG9177	FBgn0030719	eIF5	BL34841	HMS00159	S	S		MS	NE		NE
CG1430	FBgn0010292	bys	BL34876	HMS00196	E	E	NE	NE	NE		(ME possible)
CG9212	FBgn0030724	Nipsnap	BL34887	HMS01232		NE					
CG7359	FBgn0260855	Sec22	BL34893	HMS01238		NE					
CG1643	FBgn0029943	Atg5	BL34899	HMS01244		NE					
CG16916	FBgn0028686	Rpt3	BL34917	HMS01265		NE					
CG12690	FBgn0029504	CHES-1-like	BL34928	HMS01277		NE					
CG8989	FBgn0004828	His3.3B	BL34940	HMS00148		NE					
CG32775	FBgn0066114	GlcAT-I	BL34946	HMS00289		NE					
CG17841	FBgn0028480	CG17841	BL34948	HMS00305		NE					
CG12135	FBgn0040235	c12.1	BL34952	HMS00382	A	ME	ME			ME	
CG14228	FBgn0086384	Mer	BL34958	HMS00459		NE					
CG1691	FBgn0262735	Imp	BL34977	HMS01168		NE					
CG12202	FBgn0031020	Nat1	BL34990	HMS01400		NE					
CG42594	FBgn0260971	CG42594	BL35006	HMS01416		NE					
CG2934	FBgn0028665	VhaAC39-1	BL35029	HMS01442	A	ME	E			E	
CG12047	FBgn0002873	mud	BL35044	HMS01458		NE					
CG3346	FBgn0025739	pon	BL35046	HMS01460		NE					

CG9045	FBgn0002914	Myb	BL35053	HMS01467		NE					
CG9038	FBgn0026076	UBL3	BL35745	HMS01487		NE					
CG15459	FBgn0031108	CG15459	BL35757	HMS01503		NE					
CG14791	FBgn0025382	Rab27	BL35774	HMS01523		NE					
CG1343	FBgn0020378	Sp1	BL35777	HMS01526		NE					
CG33253	FBgn0030992	CG33253	BL36106	HMS00158		NE					
CG11398	FBgn0040366	CG11398	BL36109	HMS00201		NE					
CG32703	FBgn0052703	Erk7	BL36110	HMS00222		NE					
CG42273	FBgn0259168	mnb	BL36657	HMS01545	A	E	ME			E	
CG16944	FBgn0003360	sesB	BL36661	HMS01549		NE					
CG6352	FBgn0026058	OdsH	BL36666	HMS01554		NE					
CG15319	FBgn0261617	nej	BL36682	HMS01570	A	E	ME			E	
CG8002	FBgn0031006	rictor	BL36699	HMS01588		NE					
CG1803	FBgn0030362	regucalcin	BL36708	HMS01598		NE					
CG15929	FBgn0029800	lin-52	BL36712	HMS01602		NE					
CG6269	FBgn0024184	unc-4	BL36713	HMS01603		NE					
CG8184	FBgn0030674	CG8184	BL36714	HMS01604		NE					
CG1681	FBgn0030484	GstT4	BL36717	HMS01607		NE					
CG4380	FBgn0003964	usp	BL36729	HMS01620		NE					
CG3972	FBgn0010019	Cyp4g1	BL36737	HMS01628		NE					
CG3861	FBgn0261955	kdn	BL36740	HMS01631		NE					
CG7413	FBgn0015799	Rbf	BL36744	HMS03004		NE					
CG1747	FBgn0030300	Sk1	BL36747	HMS03007		NE					
CG1583	FBgn0030013	GIIIspla2	BL36757	HMS03017		NE					
CG42628	FBgn0261379	rad	BL36758	HMS03018		NE					
CG1753	FBgn0031148	Cbs	BL36767	HMS03028		NE					
CG13762	FBgn0040333	brv3	BL36774	JF02389		NE					
CG18085	FBgn0003366	sev	BL36778	JF02393		NE					
CG15365	FBgn0030077	CG15365	BL36856	HMS00293		NE					
CG3848	FBgn0023518	trr	BL36916	HMS01019		NE					
CG18102	FBgn0003392	shi	BL36921	HMS00154		NE					
CG1634	FBgn0264975	Nrg	BL37496	HMS01638		NE					
CG9904	FBgn0040336	Seipin	BL37501	HMS01643		NE					
CG32758	FBgn0052758	CG32758	BL38225	HMS01669		NE					
CG6873	FBgn0030951	CG6873	BL38226	HMS01670		NE					

CG4898	FBgn0003721	Tm1	BL38232	HMS01676		NE					
CG10260	FBgn0261922	PI4KIIIalpha	BL38242	HMS01686		NE					
CG7925	FBgn0003714	tko	BL38251	HMS01695		NE					
CG9938	FBgn0030500	Ndc80	BL38260	HMS01704		NE					
CG4523	FBgn0029891	Pink1	BL38262	HMS01707		NE					
CG9195	FBgn0040285	Scamp	BL38277	HMS01728		NE					
CG1685	FBgn0015527	pen	BL38290	HMS01748		NE					
CG2621	FBgn0003371	sgg	BL38293	HMS01751	A	E	E			E	
CG12092	FBgn0261675	Npc1b	BL38296	HMS01757		NE					
CG33950	FBgn0261451	trol	BL38298	HMS01759		NE					
CG9214	FBgn0028397	Tob	BL38299	HMS01760		NE					
CG17828	FBgn0016038	mod(r)	BL38304	HMS01766		NE					
CG42343	FBgn0259245	CG42343	BL38310	HMS01774		NE					
CG9968	FBgn0030749	Anxb11	BL38311	HMS01775		NE					
CG1826	FBgn0030228	CG1826	BL38324	HMS01788		NE					
CG6606	FBgn0027335	Rip11	BL38325	HMS01792		NE					
CG3632	FBgn0030735	CG3632	BL38341	HMS01808		NE					
CG14211	FBgn0031044	MKP-4	BL38342	HMS01809		NE					
CG14216	FBgn0031054	Ssu72	BL38344	HMS01811		NE					
CG17598	FBgn0031194	CG17598	BL38345	HMS01812		NE					
CG13758	FBgn0260753	Pdfr	BL38347	HMS01815		NE					
CG11727	FBgn0262740	CG11727	BL38350	HMS01818		NE					
CG1718	FBgn0031170	CG1718	BL38353	HMS01821		NE					
CG34120	FBgn0083956	CG34120	BL38356	HMS01824	E-L	E-L	ME	E	E-L	ME	NE
CG1673	FBgn0030482	CG1673	BL38363	HMS01832		NE					
CG6899	FBgn0004368	Ptp4E	BL38369	HMS01838		NE					
CG32505	FBgn0023177	Pp4-19C	BL38372	HMS01841		NE					
CG32814	FBgn0052814	CG32814	BL38383	HMS01852		NE					
CG9198	FBgn0004391	shtd	BL38531	HMS01744	A	E	E			E	
CG5870	FBgn0250788	beta-Spec	BL38533	HMS01746		NE					
CG1554	FBgn0003277	RpII215	BL38537	HMS01761		NE					
CG17754	FBgn0030114	CG17754	BL38539	HMS01830		NE					
CG9984	FBgn0010416	TH1	BL38934	HMS00283		NE					
CG32697	FBgn0028341	l(1)G0232	BL38935	HMS00731		NE					
CG14804	FBgn0014411	Vps26	BL38937	HMS01769		NE					

CG32626	FBgn0052626	CG32626	BL38953	HMS01867		NE					
CG42249	FBgn0259101	CG42249	BL38955	HMS01869		NE					
CG32791	FBgn0052791	CG32791	BL38965	HMS01879		NE					
CanA-14F	FBgn0030758	CanA-14F	BL38966	HMS01880		NE					
Ubi-p5E	FBgn0086558	Ubi-p5E	BL38967	HMS01881		NE					
Pdp	FBgn0029958	Pdp	BL38972	HMS01888		NE					
CG1812	FBgn0031119	CG1812	BL38974	HMS01890		NE					
Syt12	FBgn0261085	Syt12	BL38978	HMS01894		NE					
sdt	FBgn0261873	sdt	BL38988	HMS01904		NE					
Ptp10D	FBgn0004370	Ptp10D	BL39001	HMS01917		NE					
par-6	FBgn0026192	par-6	BL39010	HMS01928		NE					
aux	FBgn0037218	aux	BL39017	HMS01935		NE					
Ca-alpha1T	FBgn0264386	Ca-alpha1T	BL39029	HMS01948		NE					
CG3842	FBgn0029866	CG3842	BL39030	HMS01949		NE					
CG8916	FBgn0030707	CG8916	BL39031	HMS01950		NE					
snz	FBgn0029976	snz	BL39036	HMS01956		NE					
CG33181	FBgn0053181	CG33181	BL39056	HMS01976		NE					
DAAM	FBgn0025641	DAAM	BL39058	HMS01978		NE					
vav	FBgn0040068	vav	BL39059	HMS01979		NE					
CG10920	FBgn0029963	CG10920	BL39068	HMS01988		NE					
Pp2C1	FBgn0022768	Pp2C1	BL40827	HMS01887		NE					
kek5	FBgn0031016	kek5	BL40830	HMS01996		NE					
Flo-2	FBgn0264078	Flo-2	BL40833	HMS01999		NE					
futsch	FBgn0259108	futsch	BL40834	HMS02000		NE					
CG7192	FBgn0030894	CG7192	BL40838	HMS02004		NE					
CG9650	FBgn0029939	CG9650	BL40852	HMS02019		NE					
CG2124	FBgn0030217	CG2124	BL40868	HMS02035		NE					
Pp2B-14D	FBgn0011826	Pp2B-14D	BL40872	HMS02039		NE					
per	FBgn0003068	per	BL40878	HMS02045		NE					
Tsp2A	FBgn0024361	Tsp2A	BL40899	HMS02147		NE					
Nmdar2	FBgn0053513	Nmdar2	BL40928	HMS02176		NE					
Grip	FBgn0029830	Grip	BL40930	HMS02178		NE					
CG14411	FBgn0030582	CG14411	BL40935	HMS02183		NE					
Klp3A	FBgn0011606	Klp3A	BL40944	HMS02192		NE					
Smox	FBgn0025800	Smox	BL41670	HMS02203		NE					

CG4690	FBgn0029837	Tsp5D	BL41681	HMS02245		NE					
CG32577	FBgn0042650	disco-r	BL41683	HMS02247		NE					
CG42864	FBgn0262111	f	BL41687	HMS02251		NE					
CG43657	FBgn0263705	Myo10A	BL41691	HMS02255	A	E	NE	NE	NE	E	NE
CG2252	FBgn0004656	fs(1)h	BL41693	HMS02257	A	E	E			E	
CG4532	FBgn0029903	pod1	BL41705	HMS02270		NE					
CG2028	FBgn0015024	CkIalpha	BL41711	HMS02276	A	ME	ME			E	
CG18582	FBgn0025743	mbt	BL41713	HMS02278		NE					
CG7113	FBgn0021765	scu	BL41884	HMS02305		NE					
CG14426	FBgn0004143	nullo	BL41905	HMS02297		NE					
CG4320	FBgn0029840	raptor	BL41912	HMS02306		NE					
CG4521	FBgn0030766	mthl1	BL41930	HMS02327		NE					
CG4252	FBgn0004367	mei-41	BL41934	HMS02331		NE					
CG14217	FBgn0031030	Tao	BL41936	HMS02333		NE					
CG11063	FBgn0030530	jub	BL41938	HMS02335		NE					
CG32743	FBgn0263968	nonC	BL41945	HMS02342		NE					
CG8394	FBgn0033911	VGAT	BL41958	HMS02355		NE					
CG3299	FBgn0004397	Vinc	BL41959	HMS02356		NE					
CG11265	FBgn0030049	Trf4-1	BL41966	HMS02363		NE					
CG2111	FBgn0030223	CG2111	BL41969	HMS02366		NE					
CG32694	FBgn0052694	CG32694	BL41975	HMS02373		NE					
CG9806	FBgn0030222	CG9806	BL41994	HMS02395		NE					
CG14424	FBgn0025644	CG14424	BL41995	HMS02396		NE					
CG6927	FBgn0029733	CG6927	BL42001	HMS02402		NE					
CG15730	FBgn0030395	CG15730	BL42002	HMS02403		NE					
CG12115	FBgn0030097	CG12115	BL42003	HMS02404		NE					
CG7206	FBgn0030892	CG7206	BL42004	HMS02405	A	E	ME			ME	
CG15916	FBgn0030704	CG15916	BL42008	HMS02409		NE					
CG15350	FBgn0014465	Cp7Fb	BL42009	HMS02410		NE					
CG4653	FBgn0030776	CG4653	BL42012	HMS02413		NE					
CG1664	FBgn0003321	sbr/NXF1	BL42013	HMS02414	S	S		S	MS		NE
CG2890	FBgn0030208	PPP4R2r	BL42015	HMS02416		NE					
CG12701	FBgn0259789	vfl	BL42016	HMS02441		NE					
CG8142	FBgn0030871	CG8142	BL42489	HMJ02051		NE					
CG1657	FBgn0030286	CG1657	BL42490	HMJ02054		NE					

CG8924	FBgn0030710	CG8924	BL42491	HMJ02055		NE					
CG15744	FBgn0030466	CG15744	BL42497	HMJ02061		NE					
CG1830	FBgn0011754	PhKgamma	BL42500	HMJ02065		NE					
CG1716	FBgn0030486	Set2	BL42511	HMJ02076		NE					
CG2116	FBgn0030003	CG2116	BL42512	HMJ02077		NE					
CG11085	FBgn0030408	CG11085	BL42516	HMJ02082		NE					
CG2061	FBgn0027498	CG2061	BL42519	HMJ02085		NE					
CG4937	FBgn0030808	RhoGAP15B	BL42527	HMJ02093		NE					
CG4400	FBgn0030434	CG4400	BL42533	HMJ02100		NE					
CG7122	FBgn0030893	RhoGAP16F	BL42541	HMJ02111		NE					
CG30115	FBgn0050115	GEFmeso	BL42545	HMJ02116		NE					
CG32721	FBgn0027553	NELF-B	BL42547	HMJ02119		NE					
CG4394	FBgn0030748	Traf-like	BL42549	HMJ02121		NE					
CG6506	FBgn0030874	CG6506	BL42552	HMJ02125		NE					
CG33080	FBgn0053080	CG33080	BL42554	HMJ02127		NE					
CG14225	FBgn0031055	et	BL42557	HMJ02213		NE					
CG13316	FBgn0023215	Mnt	BL42558	HMJ02214		NE					
CG1848	FBgn0041203	LIMK1	BL42576	HMJ02235		NE					
CG18734	FBgn0004598	Fur2	BL42577	HMJ02236		NE					
CG9065	FBgn0030610	CG9065	BL42595	HMS02427		NE					
CG3466	FBgn0011576	Cyp4d2	BL42600	HMS02432		NE					
CG32858	FBgn0003447	sn	BL42615	HMS02450		NE					
CG6824	FBgn0003028	ovo	BL42627	HMS02462		NE					
CG14802	FBgn0026873	MED18	BL42634	HMS02470		NE					
CG9900	FBgn0004643	mit(1)15	BL42643	HMS02479		NE					
CG4590	FBgn0027108	inx2	BL42645	HMS02481		NE					
CG2045	FBgn0019929	Ser7	BL42649	HMS02485		NE					
CG18572	FBgn0003189	r	BL42828	HMS02510		NE					
CG32528	FBgn0052528	CG32528	BL42831	HMS02523		NE					
CG12175	FBgn0030502	tth	BL42849	HMS02541		NE					
CG14815	FBgn0023516	Pex5	BL42854	HMS02546		NE					
CG12530	FBgn0010341	Cdc42	BL42861	HMS02553		NE					
CG14421	FBgn0029644	CG14421	BL42865	HMS02558	E	E	NE	NE	E		NE
CG5966	FBgn0029831	CG5966	BL42869	HMS02562		NE					
CG12993	FBgn0030840	p-cup	BL42876	HMS02569		NE					

CG3056	FBgn0024987	ssx	BL42881	HMS02574		NE					
CG2056	FBgn0030051	spirit	BL42882	HMS02575		NE					
CG7766	FBgn0030087	CG7766	BL42890	HMS02583		NE					
CG9164	FBgn0030634	CG9164	BL42899	HMS02592		NE					
CG1532	FBgn0031143	CG1532	BL42900	HMS02593		NE					
CG1786	FBgn0030369	Cyp318a1	BL42904	HMS02597		NE					
CG6847	FBgn0030884	CG6847	BL42908	HMS02601		NE					
CG3044	FBgn0029913	Cht11	BL42927	HMS02620		NE					
CG17333	FBgn0030239	CG17333	BL42933	HMS02626		NE					
CG15296	FBgn0030215	CG15296	BL42946	HMS02639		NE					
CG13365	FBgn0029529	CG13365	BL42951	HMS02644	A	E-L	E-L			E-L	
CG12075	FBgn0030065	CG12075	BL42952	HMS02645		NE					
CG3446	FBgn0029868	CG3446	BL43279	HMC02678		NE					
CG9053	FBgn0264389	opm	BL43280	HMC02679		NE					
CG1474	FBgn0023506	Es2	BL43285	HMS02657		NE					
CG9675	FBgn0030774	spheroide	BL43295	HMS02668		NE					
CG33250	FBgn0065035	AlkB	BL43300	HMS02673		NE					
CG12111	FBgn0030050	CG12111	BL43311	HMS02695		NE					
CG32685	FBgn0052685	ZAP3	BL43317	HMS02701		NE					
CG3977	FBgn0062413	Ctr1A	BL44000	HMS02714		NE					
CG13005	FBgn0030794	CG13005	BL44018	HMS02733		NE					
CG2071	FBgn0011834	Ser6	BL44026	HMS02741		NE					
CG6998	FBgn0011760	ctp	BL44044	HMS02760		NE					
CG3039	FBgn0004646	ogre	BL44048	HMS02764	A	ME	ME			E	
CG15042	FBgn0030937	CG15042	BL44049	HMS02765		NE					
CG2715	FBgn0024980	Syx4	BL44054	HMS02771		NE					
CG4407	FBgn0030431	CG4407	BL44055	HMS02772		NE					
CG43947	FBgn0264598	PsGEF	BL44061	HMS02778		NE					
CG32683	FBgn0052683	CG32683	BL44079	HMS02796		NE					
CG14406	FBgn0030595	CG14406	BL44081	HMS02798		NE					
CG1987	FBgn0030479	Rbp1-like	BL44100	HMS02820		NE					
CG32666	FBgn0052666	Drak	BL44102	HMS02822		NE					
CG44132	FBgn0264981	mamo	BL44103	HMS02823		NE					
CG17829	FBgn0025635	CG17829	BL44104	HMS02824		NE					
CG32808	FBgn0052808	CG32808	BL44270	HMS02812		NE					

CG4122	FBgn0004648	svr	BL44487	HMC02395		NE					
CG2675	FBgn0024994	Csat	BL44488	HMC02402		NE					
CG14796	FBgn0025390	Mur2B	BL44489	HMC02403		NE					
CG1847	FBgn0030345	CG1847	BL44490	HMC02409		NE					
CG4678	FBgn0030778	CG4678	BL44491	HMC02413		NE					
CG1440	FBgn0030038	CG1440	BL44521	HMC02912		NE					
CG4096	FBgn0029791	CG4096	BL44522	HMC02914	MS	MS		S	MS		NE
CG40305	FBgn0044872	FucTC	BL44540	HMC02935		NE					
CG1771	FBgn0004456	mew	BL44553	HMS02849		NE					
CG1404	FBgn0020255	ran	BL44587	HMS02885	A	ME	E			E	
CG17063	FBgn0027107	inx6	BL44663	HMS02883		NE					
CG4766	FBgn0027546	CG4766	BL50605	HMC02404		NE					
CG10555	FBgn0030034	CG10555	BL50606	HMC02408		NE					
CG3024	FBgn0025615	Torsin	BL50620	HMC02987		NE					
CG33517	FBgn0053517	D2R	BL50621	HMC02988		NE					
CG2263	FBgn0030007	CG2263	BL50624	HMC02991		NE					
CG2155	FBgn0003965	v	BL50641	HMC03041		NE					
CG4746	FBgn0029003	mab-21	BL50644	HMC03044		NE					
CG32751	FBgn0052751	CG32751	BL50653	HMC03054		NE					
CG12529	FBgn0004057	Zw	BL50667	HMC03068	A	ME	ME			ME	
CG17336	FBgn0010240	Lcch3	BL50668	HMC03069		NE					
CG4136	FBgn0263511	Vsx1	BL50684	HMC03085		NE					
CG1597	FBgn0030289	CG1597	BL50699	HMC03101		NE					
CG11293	FBgn0034889	CG11293	BL50728	HMS02964		NE					
CG6157	FBgn0015926	dah	BL50733	HMS02969		NE					
CG9802	FBgn0015615	Cap	BL50899	HMJ03116		NE					
CG12723	FBgn0030459	CG12723	BL50917	HMJ21006		NE					
CR32658	FBgn0040859	CR32658	BL50928	HMJ21022		NE					
CG9565	FBgn0031081	Nep3	BL50930	HMJ21024		NE					
CG2861	FBgn0029728	CG2861	BL50931	HMJ21025		NE					
CG32588	FBgn0052588	CG32588	BL50935	HMJ21030		NE					
CG1515	FBgn0260858	Ykt6	BL50937	HMJ21032		NE					
CG4557	FBgn0029912	CG4557	BL50953	HMJ21054		NE					
CG2254	FBgn0029994	CG2254	BL50999	HMJ21112		NE					
CG16989	FBgn0025621	CG16989	BL51017	HMJ21141		NE					

CG6961	FBgn0030959	CG6961	BL51022	HMJ21148		NE					
CG14416	FBgn0040352	CG14416	BL51047	HMJ21181		NE					
CG32538	FBgn0086778	gfA	BL51049	HMJ21183		NE					
CG15736	FBgn0043001	Chrac-16	BL51155	HMC02362		NE					
CG3002	FBgn0030141	Gga	BL51170	HMJ21093		NE					
CG14789	FBgn0027791	O-fut2	BL51392	HMJ21038		NE					
CG11172	FBgn0030505	NFAT	BL51422	HMC02411	(MEPOSSIBLE)	NE					
CG32627	FBgn0052627	NnaD	BL51430	HMC03138		NE					
CG43154	FBgn0262684	CG43154	BL51431	HMC03139		NE					
CG10379	FBgn0015513	mbc	BL51446	HMC03172		NE					
CG32763	FBgn0026702	l(1)G0045	BL51448	HMC03178		NE					
CG10798	FBgn0262656	dm	BL51454	HMC03189	E-L	E-L	NE	MS	E-L		NE
CG32602	FBgn0052602	Muc12Ea	BL51467	HMC03207		NE					
CG1461	FBgn0030558	CG1461	BL51470	HMC03212		NE					
CG11654	FBgn0014455	Ahcy13	BL51477	HMC03222		NE					
CG4317	FBgn0026060	Mipp2	BL51482	HMC03229		NE					
CG15743	FBgn0030465	CG15743	BL51486	HMC03233		NE					
CG3973	FBgn0029881	pigs	BL51490	HMC03241		NE					
CG1889	FBgn0030164	CG1889	BL51512	HMC03288		NE					
CG43689	FBgn0263772	CG43689	BL51513	HMC03290		NE					
CG17596	FBgn0262866	S6kII	BL51694	HMC03140		NE					
CG10742	FBgn0040334	Tsp3A	BL51706	HMC03196		NE					
CG1799	FBgn0003204	ras	BL51717	HMC03250		NE					
CG42346	FBgn0259677	CG42346	BL51719	HMC03255		NE					
CG4318	FBgn0030455	CG4318	BL51720	HMC03257		NE					
CG1791	FBgn0030163	CG1791	BL51727	HMC03271		NE					
CG32702	FBgn0052702	CG32702	BL51736	HMS03167		NE					
CG2685	FBgn0024998	CG2685	BL51750	HMC03301		NE					
CG42797	FBgn0261931	CG42797	BL51767	HMC03322		NE					
CG32772	FBgn0052772	CG32772	BL51768	HMC03323		NE					
CG11734	FBgn0031107	HERC2	BL51773	HMC03328		NE					
CG4094	FBgn0028336	l(1)G0255	BL51779	HMC03334		NE					
CG10932	FBgn0029969	CG10932	BL51785	HMC03340		NE					
CG1885	FBgn0030066	CG1885	BL51786	HMC03341		NE					

CG9220	FBgn0030662	CG9220	BL51787	HMC03343		NE					
CG8909	FBgn0030706	CG8909	BL51788	HMC03344		NE					
CG9653	FBgn0024250	brk	BL51789	HMC03345		NE					
CG9413	FBgn0030574	CG9413	BL51791	HMC03347		NE					
CG9209	FBgn0003969	vap	BL51793	HMC03349		NE					
CG11403	FBgn0026876	CG11403	BL51800	HMC03357		NE					
CG6358	FBgn0004832	Xpac	BL51806	HMC03365		NE					
CG1417	FBgn0003423	slgA	BL51811	HMC03382		NE					
CG10778	FBgn0029980	CG10778	BL51815	HMC03386		NE					
CG4349	FBgn0030449	Fer3HCH	BL51825	HMC03397		NE					
CG11354	FBgn0026411	Lim1	BL51831	HMC03403		NE					
CG6172	FBgn0261930	vnd	BL51833	HMC03405		NE					
CG17440	FBgn0030120	CG17440	BL51843	HMC03416		NE					
CG1795	FBgn0027864	Ogg1	BL51852	HMC03426		NE					
CG8948	FBgn0030685	Graf	BL51853	HMC03427		NE					
CG3415	FBgn0030731	Mfe2	BL51854	HMC03428	A	ME	ME			E	
CG5703	FBgn0030853	CG5703	BL51855	HMC03429		NE					
CG1467	FBgn0031106	Syx16	BL51856	HMC03430		NE					
CG12176	FBgn0030506	Lig4	BL51933	HMC03211		NE					
CG3926	FBgn0014031	Spat	BL51935	HMC03220		NE					
CG16892	FBgn0030122	CG16892	BL51938	HMC03342		NE					
CG4039	FBgn0025815	Mcm6	BL52111	HMC03356		NE					
CG6367	FBgn0030926	psh	BL52877	HMC03615		NE					
CG11418	FBgn0024360	CG11418	BL52881	HMC03619		NE					
CG18155	FBgn0029945	CG18155	BL52884	HMC03622		NE					
CG9676	FBgn0030773	CG9676	BL52901	HMC03641		NE					
CG3125	FBgn0261383	IntS6	BL52904	HMC03644	A	E	E			E	
CG9126	FBgn0045073	Stim	BL52911	HMC03651		NE					
CG4211	FBgn0004227	nonA	BL52933	HMC03675		NE					
CG10598	FBgn0003057	CG10598	BL52948	HMJ21617		NE					
CG12640	FBgn0030202	CG12640	BL52952	HMJ21621	A	E	E			E	
CG5529	FBgn0011758	B-H1	BL52954	HMJ21623		NE					
CG12637	FBgn0030224	CG12637	BL52978	HMJ21665		NE					
CG3656	FBgn0005670	Cyp4d1	BL52979	HMJ21666		NE					
CG5254	FBgn0040383	CG5254	BL52990	HMJ21682		NE					

CG32580	FBgn0052580	Muc14A	BL53011	HMJ21730		NE					
CG10788	FBgn0010295	ng3	BL53026	HMJ21751		NE					
CG1871	FBgn0011586	e(r)	BL53301	HMC03528		NE					
CG17629	FBgn0001314	kl-3	BL53317	HMC03546		NE					
CG3149	FBgn0027564	CG3149	BL53324	HMC03553		NE					
CG12203	FBgn0031021	CG12203	BL53325	HMC03554		NE					
CG2194	FBgn0086450	su(r)	BL53339	HMC03568		NE					
CG4396	FBgn0086675	fne	BL53340	HMC03569		NE					
CG12348	FBgn0003380	Sh	BL53347	HMC03576		NE					
CG3835	FBgn0023507	CG3835	BL53355	HMC03584		NE					
CG1304	FBgn0031141	CG1304	BL53363	HMC03592		NE					
CG1632	FBgn0030027	CG1632	BL53368	HMC03597		NE					
CG6854	FBgn0262707	CTPsyn	BL53378	HMJ02094		NE					
CG12057	FBgn0030098	CG12057	BL53686	HMJ21609	E	E	NE	NE	E		NE
CG32695	FBgn0052695	CG32695	BL53687	HMJ21616		NE					
CG15196	FBgn0030296	CG15196	BL53688	HMJ21648		NE					
CG15201	FBgn0030272	CG15201	BL53689	HMJ21672		NE					
CG9034	FBgn0040931	CG9034	BL53700	HMJ21729		NE					
CG8023	FBgn0035860	eIF4E-3	BL53880	HMJ21195		NE					
CG10706	FBgn0029761	SK	BL53881	HMJ21196	A	ME	ME	S	E	ME	
CG2151	FBgn0020653	Trxr-1	BL53883	HMJ21198		NE					
CG3457	FBgn0024984	CG3457	BL53885	HMJ21203		NE					
CG8944	FBgn0030680	CG8944	BL53889	HMJ21207		NE					
CG14226	FBgn0043903	dome	BL53890	HMJ21208		NE					
CG9916	FBgn0004432	Cyp1	BL53894	HMJ21213		NE					
CG8198	FBgn0026666	l(1)G0136	BL53909	HMJ21239		NE					
CG32654	FBgn0052654	Sec16	BL53917	HMJ21252	A	E-L	E-L			E-L	
CG17885	FBgn0029521	Or1a	BL53926	HMJ21271		NE					
CG2885	FBgn0030200	RabX2	BL53928	HMJ21273		NE					
CG2941	FBgn0029686	CG2941	BL53989	HMJ21393		NE					
CG43313	FBgn0263005	CG43313	BL53990	HMJ21394		NE					
CG1615	FBgn0017561	Ork1	BL53994	HMJ21398		NE					
CG12156	FBgn0029959	Rab39	BL53995	HMJ21399	A	E	ME	S	E	E	
CG32633	FBgn0052633	CG32633	BL54008	HMJ21431		NE					
CG1989	FBgn0026749	Yippee	BL54020	HMJ21446		NE					

CG34015	FBgn0054015	CG34015	BL54031	HMJ21474		NE					
CG14615	FBgn0031184	CG14615	BL54044	HMJ21487		NE					
CG3203	FBgn0029897	RpL17	BL54048	HMS03519		NE					
CG42684	FBgn0261570	CG42684	BL54056	HMS03717		NE					
CG14782	FBgn0025381	rush	BL54057	HMJ21364		NE					
CG10790	FBgn0003086	Pig1	BL54058	HMJ21201		NE					
CG32789	FBgn0260484	HIP	BL54458	HMS03718		NE					
CG1628	FBgn0030218	CG1628	BL54464	HMC03731		NE					
CG8952	FBgn0030688	CG8952	BL54469	HMS03737		NE					
CG8497	FBgn0026374	Rhp	BL54474	HMS03725		NE					
CG14231	FBgn0031060	CG14231	BL54799	HMJ21493		NE					
CG43934	FBgn0264562	Hr4	BL54803	HMJ21497		NE					
CG43374	FBgn0263132	Cht6	BL54823	HMJ21542		NE					
CG12481	FBgn0030542	CG12481	BL54826	HMJ21545		NE					
CG2930	FBgn0028491	CG2930	BL54827	HMJ21546	A	ME	ME	S		ME	
CG32594	FBgn0052594	be	BL54834	HMJ21553		NE					
CG1492	FBgn0030361	CG1492	BL54838	HMJ21557		NE					
CG3021	FBgn0040337	CG3021	BL55144	HMC03742		NE					
CG9998	FBgn0005411	U2af50	BL55153	HMC03810	A	ME	ME			E	
CG17764	FBgn0029751	CG17764	BL55156	HMC03829		NE					
CG6999	FBgn0030085	CG6999	BL55157	HMC03830		NE					
CG6361	FBgn0030925	CG6361	BL55174	HMC03855		NE					
CG3019	FBgn0003638	su(w[a])	BL55175	HMC03856	(ME POSSIBLE)	NE					
CG1641	FBgn0003411	sisA	BL55181	HMC03864		NE					
CG3869	FBgn0029870	Marf	BL55189	HMC03883		NE					
CG4542	FBgn0029906	CG4542	BL55190	HMC03884		NE					
CG34359	FBgn0085388	IP3K2	BL55240	HMC02364		NE					
CG1591	FBgn0029133	REG	BL55248	HMC03935		NE					
CG32533	FBgn0052533	CG32533	BL55255	HMC03942		NE					
CG9009	FBgn0027601	pdgy	BL55272	HMC03959		NE					
CG6531	FBgn0030941	wgn	BL55275	HMC03962		NE					
CG3704	FBgn0040346	CG3704	BL55294	HMC03981		NE					
CG43155	FBgn0262685	CG43155	BL55299	HMC03986		NE					
CG3697	FBgn0002707	mei-9	BL55313	HMC04000		NE					

CG6146	FBgn0004924	Top1	BL55314	HMC04001		NE					
CG12117	FBgn0014032	Sptr	BL55317	HMC04004		NE					
CG3806	FBgn0023512	eIF2B-epsilon	BL55321	HMC04008		NE					
CG17896	FBgn0023537	CG17896	BL55323	HMC04010		NE					
CG2658	FBgn0024992	CG2658	BL55324	HMC04011		NE					
CG14808	FBgn0025391	Scgdelta	BL55325	HMC04012	A	E	E			E	
CG12108	FBgn0030057	Ppt1	BL55331	HMC04018		NE					
CG15738	FBgn0030352	CG15738	BL55332	HMC04019		NE					
CG7010	FBgn0028325	l(1)G0334	BL55345	HMC04032		NE					
CG1677	FBgn0029941	CG1677	BL55355	HMC04042	S	S		S	E		NE
CG8565	FBgn0030697	CG8565	BL55368	HMC04056		NE					
CG1582	FBgn0030246	CG1582	BL55373	HMC04061		NE					
CG1780	FBgn0026415	ldgf4	BL55381	HMC04069		NE					
CG12056	FBgn0030099	CG12056	BL55382	HMC04070		NE					
CG7876	FBgn0031000	Muc18B	BL55394	HMC04082		NE					
CG18809	FBgn0042132	CG18809	BL55399	HMC04087		NE					
CG8544	FBgn0003345	sd	BL55404	HMC04092	ME	ME	NE	MS	E-L		NE
CG2212	FBgn0003656	sws	BL55406	HMC04094		NE					
CG1659	FBgn0025549	unc-119	BL55604	HMC03736		NE					
CG32523	FBgn0052523	CG32523	BL55607	HMC03745		NE					
CG40444	FBgn0001315	kl-5	BL55609	HMC03747		NE					
CG14780	FBgn0025383	CG14780	BL55616	HMC03759		NE					
CG15046	FBgn0030927	CG15046	BL55620	HMC03764		NE					
CG7288	FBgn0030969	CG7288	BL55632	HMC03779		NE					
CG6227	FBgn0030631	CG6227	BL55638	HMC03786		NE					
CG1622	FBgn0030468	CG1622	BL55648	HMC03797		NE					
CG4119	FBgn0028474	CG4119	BL55668	HMC03823	A	E-L	E-L			E-L	
CG2677	FBgn0024996	eIF2B-beta	BL55675	HMC03838		NE					
CG6340	FBgn0030648	CG6340	BL55677	HMC03842		NE					
CG2845	FBgn0003079	phl/raf	BL55679	HMC03854		NE					
CG5877	FBgn0030625	CG5877	BL55690	HMC03904		NE					
CG17170	FBgn0003559	su(f)	BL55693	HMC03907		NE					
CG17168	FBgn0039943	CG17168	BL55703	HMC03926		NE					
CG12311	FBgn0086368	tw	BL55735	HMC03806		NE					
CG15747	FBgn0030474	CG15747	BL55747	HMC03934	A	ME	ME	MS	E	ME	NE

CG3135	FBgn0003390	shf	BL55867	HMC04137		NE					
CG4290	FBgn0025625	Sik2	BL55880	HMC04153		NE					
CG32742	FBgn0028360	l(1)G0148	BL55884	HMC04157		NE					
CG5941	FBgn0029833	MCTS1	BL55920	HMC04207		NE					
CG2979	FBgn0005391	Yp2	BL55931	HMC04219		NE					
CG6186	FBgn0022355	Tsf1	BL55936	HMC04224		NE					
CG4666	FBgn0029838	CG4666	BL55939	HMC04227		NE					
CG15641	FBgn0030643	CG15641	BL55940	HMC04228		NE					
CG6788	FBgn0030880	CG6788	BL55941	HMC04229		NE					
CG2918	FBgn0023529	CG2918	BL55962	HMC04256		NE					
CG32698	FBgn0052698	CG32698	BL56000	HMC04296		NE					
CG15199	FBgn0030270	CG15199	BL56024	HMC04320		NE					
CG15202	FBgn0030271	CG15202	BL56026	HMC04322		NE					
CG6190	FBgn0061469	Ube3a	BL57151	HMC04528		NE					
CG5387	FBgn0027491	Cdk5alpha	BL57290	HMJ21283		NE					
CG1214	FBgn0003295	ru	BL58065	HMJ21921		NE					
CG17922	FBgn0034656	CG17922	BL58072	HMJ21964		NE					
CG12413	FBgn0039588	CG12413	BL58096	HMJ22011		NE					
CG30020	FBgn0050020	CG30020	BL58110	HMJ22046		NE					
CG7962	FBgn0010350	CdsA	BL58118	HMJ22055		NE					
CG13772	FBgn0031866	neuroligin	BL58128	HMJ22077		NE					
CG8532	FBgn0028582	lqf	BL58130	HMJ22079		NE					
CG14886	FBgn0038436	Gyc-89Db	BL58139	HMJ22088		NE					
CG3940	FBgn0037788	CG3940	BL58160	HMJ22111		NE					
CG31673	FBgn0051673	CG31673	BL58161	HMJ22112		NE					
CG11125	FBgn0033174	CG11125	BL58164	HMJ22141		NE					
CG17383	FBgn0039350	jigr1	BL58173	HMJ22150		NE					
CG9913	FBgn0038205	Kif19A	BL58193	HMJ21855		NE					
CG2346	FBgn0000715		BL58197	HMJ22167		NE					
CG18287	FBgn0039679	ppk19	BL58203	HMJ22173		NE					
CG9793	FBgn0037620	ranshi	BL58206	HMJ22176		NE					
CG8598	FBgn0035766	eco	BL58221	HMJ22229		NE					
CG31183	FBgn0051183	CG31183	BL58224	HMJ22232		NE					
CG3134	FBgn0003009	ord	BL58228	HMJ22248		NE					
CG6620	FBgn0024227	ial	BL58308	HMJ22415		NE					

CG5656	FBgn0037083	CG5656	BL58334	HMJ22464		NE					
CG9634	FBgn0027528	CG9634	BL58344	HMJ22475		NE					
CG32810	FBgn0025394	inc	BL58346	HMJ22477		NE					
CG9272	FBgn0032907	CG9272	BL58348	HMJ22479		NE					
CG8994	FBgn0000615		BL58351	HMS04331		NE					
CG12878	FBgn0045862	btz	BL58353	HMS04337		NE					
CG8947	FBgn0250848	26-29-p	BL32887	HMS00675		NE					
CG12876	FBgn0086346	ALiX	BL33417	HMS00298		NE					
CG2982	FBgn0029704	CG2982	BL33596	HMS00680		NE					
CG11491	FBgn0000210	br	BL33641	HMS00042	A	E-L	E-L			E-L	
CG5488	FBgn0004854	B-H2	BL33647	HMS00048		NE					
CG4739	FBgn0040257	Ugt86Dc	BL34095	HMS00954		NE					
CG12237	FBgn0031048	CG12237	BL38343	HMS01810		NE					
CG7103	FBgn0030964	Pvf1	BL39038	HMS01958		NE					
CG32628	FBgn0052628	CG32628	BL44036	HMS02752		NE					
CG9737	FBgn0039758	CG9737	BL52880	HMC03618		NE					

APPENDIX 3: CHAPTER 3 SUPPLEMENTARY TABLES AND FIGURES

Chapter 3: Supplementary tables

Table S3-1: Full genotypes

Fig. 1C	Genotype (driver: HS-GAL4, BL2077)	Includes	
LDS-$(G4C2)_{CTRL}^{GR-GFP}$	*w^{1118}, UAS-LDS-$(G4C2)_{4,9,12}^{GR-GFP}$/w*; GAL4-Hsp70/+;*		
LDS-$(G4C2)_{EXP}^{GR-GFP}$	*w^{1118}/w*; GAL4-Hsp70/+; UAS-LDS-$(G4C2)_{4,42,44}^{GR-GFP}$/+*		
Fig. 1D and Sup. Fig. 1	**Genotype (driver: GMR-GAL4^{YH3})**	**Includes**	**Temp**
LDS-$(G4C2)_{CTRL}^{GR-GFP}$	*w^{1118}, UAS-LDS-$(G4C2)_{4,9,12}^{GR-GFP}$/w^{1118};; GMR-GAL4^{YH3}/+*	UAS-DSRED	26°C
LDS-$(G4C2)_{EXP}^{GR-GFP}$	*w^{1118};; UAS-LDS-$(G4C2)_{4,42,44}^{GR-GFP}$/GMR-GAL4^{YH3}*		26°C
GFP CTRL	*w^{1118};; UAS-GFP.NLS/GMR-GAL4^{YH3}*	BDSC #4776	26°C
Neg CTRL	*w^{1118};; GMR-GAL4^{YH3}/+*		26°C
Fig. 1E	**Genotype (driver: GMR-GAL4^{YH3})**	**Includes**	**Temp**
Positive Control	*w^{1118}/Y; UAS-DSRED/+; GMR-GAL4^{YH3}/+*	UAS-DSRED	26°C
LDS-$(G4C2)_{CTRL}^{GR-GFP}$	*w^{1118}, UAS-LDS-$(G4C2)_{4,9,12}^{GR-GFP}$/Y;; GMR-GAL4^{YH3}/+*		26°C
LDS-$(G4C2)_{EXP}^{GR-GFP}$	*w^{1118}/Y;; UAS-LDS-$(G4C2)_{4,42,44}^{GR-GFP}$/GMR-GAL4^{YH3}*		26°C
Fig. 1F	**Genotype (driver: GMR-GAL4^{YH3})**	**Includes**	**Temp**
DSRED	*w^{1118}/Y; UAS-DSRED/+; GMR-GAL4^{YH3}/+*	UAS-DSRED	26°C
LDS-$(G4C2)_{CTRL}^{GR-GFP}$	*w^{1118}, UAS-LDS-$(G4C2)_{4,9,12}^{GR-GFP}$/Y;; GMR-GAL4^{YH3}/+*		26°C
LDS-$(G4C2)_{EXP}^{GR-GFP}$	*w^{1118}/Y;; UAS-LDS-$(G4C2)_{4,42,44}^{GR-GFP}$/GMR-GAL4^{YH3}*		26°C
Fig. 2A - external eye toxicity	**Genotype (driver: GMR-GAL4^{YH3})**	**Includes**	**Temp**
LDS-$(G4C2)_{EXP}^{GR-GFP}$ w/ eIF4B RNAi	*w^{1118}/Y; UAS-eIF4B RNAi^{HMS04503}/+; UAS-LDS-$(G4C2)_{4,42,44}^{GR-GFP}$, GMR-GAL4^{YH3}/+*	BDSC #57305	26°C
LDS-$(G4C2)_{EXP}^{GR-GFP}$ w/ Control RNAi	*w^{1118}/Y;; UAS-LDS-$(G4C2)_{4,42,44}^{GR-GFP}$, GMR-GAL4^{YH3}/UAS-Luc RNAi^{JF01355}*	BDSC #31603	26°C
LDS-$(G4C2)_{EXP}^{GR-GFP}$ w/ eIF3B RNAi	*w^{1118}/Y;; UAS-LDS-$(G4C2)_{4,42,44}^{GR-GFP}$, GMR-GAL4^{YH3}/UAS-eIF3B RNAi^{HMS00668}*	BDSC #32880	26°C
$(GR)_{36}$ w/ eIF4G1 RNAi	*w^{1118}/y^{1}, sc*, v^{1}; UAS-$(GR)_{36}$/+; GMR-GAL4^{YH3}/UAS-eIF4G1 RNAi^{HMS00762}*	BDSC #33049	24°C
$(GR)_{36}$ w/ Control RNAi	*w^{1118}/y^{1}, v^{1}; UAS-$(GR)_{36}$/+; GMR-GAL4^{YH3}/UAS-Luc RNAi^{JF01355}*	BDSC #31603	24°C
$(GR)_{36}$ w/ eIF4B RNAi	*w^{1118}/y^{1}, sc*, v^{1}; UAS-$(GR)_{36}$/UAS-eIF4B RNAi^{HMS04503}; GMR-GAL4^{YH3}/+*	BDSC #57305	24°C
Fig. 2A - external eye GR-GFP	**Genotype (driver: GMR-GAL4^{YH3})**	**Includes**	**Temp**

LDS-$(G4C2)_{EXP}^{GR-GFP}$ w/ eIF4B RNAi	*w^{1118}/y^{1}, sc*, v^{1}; UAS-eIF4B RNAi^{HMS04503}/+; UAS-LDS-$(G4C2)_{4,42,44}^{GR-GFP}$, GMR-GAL4^{YH3}/+*	BDSC #57305	26°C
LDS-$(G4C2)_{EXP}^{GR-GFP}$ w/ Control RNAi	*w^{1118}/y^{1}, v^{1};; UAS-LDS-$(G4C2)_{4,42,44}^{GR-GFP}$, GMR-GAL4^{YH3}/UAS-Luc RNAi^{JF01355}*	BDSC #31603	26°C
LDS-$(G4C2)_{EXP}^{GR-GFP}$ w/ eIF3B RNAi	*w^{1118}/y^{1}, sc*, v^{1};; UAS-LDS-$(G4C2)_{4,42,44}^{GR-GFP}$, GMR-GAL4^{YH3}/UAS-eIF3B RNAi^{HMS00668}*	BDSC #32880	26°C
Fig. 3A	Genotype (driver: Da-GAL4, III)	Includes	Temp
Control RNAi	*w^{1118}/Y;; UAS-Luc RNAi^{JF01355}/Da-GAL4*	BDSC #31603	26°C
eIF4B RNAi	*w^{1118}/Y; UAS-eIF4B RNAi^{HMS04503}/+; Da-GAL4/+*	BDSC #57305	26°C
eIF4H1 RNAi	*w^{1118}/Y; UAS-eIF4H1 RNAi^{HMS04504}/+; Da-GAL4/+*	BDSC #57306	26°C
Fig. 3B	Genotype (driver: Da-GAL4, III)	Includes	Temp
progeny with eIF4B RNAi	*UAS-eIF4B RNAi^{HMS04503}/+; Da-GAL4/+*	BDSC #57305	26°C
progeny without eIF4B RNAi	*CyO/+; Da-GAL4/+*		26°C
progeny with eIF4H1 RNAi	*UAS-eIF4B RNAi^{HMS04504}/+; Da-GAL4/+*	BDSC #57306	26°C
progeny without eIF4H1 RNAi	*CyO/+; Da-GAL4/+*		26°C
Fig. 4A-B and 5A-B	Genotype (driver: GMR-GAL4^{YH3})	Includes	Temp
LDS-$(G4C2)_{EXP}^{GR-GFP}$ w/ Control RNAi	*w^{1118}/Y;; UAS-LDS-$(G4C2)_{4,42,44}^{GR-GFP}$, GMR-GAL4^{YH3}/UAS-Luc RNAi^{JF01355}*	BDSC #31603	26°C
LDS-$(G4C2)_{EXP}^{GR-GFP}$ w/ eIF4B RNAi	*w^{1118}/Y; UAS-eIF4B RNAi^{HMS04503}/+; UAS-LDS-$(G4C2)_{4,42,44}^{GR-GFP}$, GMR-GAL4^{YH3}/+*	BDSC #57305	26°C
LDS-$(G4C2)_{EXP}^{GR-GFP}$ w/ eIF4H1 RNAi	*w^{1118}/Y; UAS-eIF4H1 RNAi^{HMS04504}/+; UAS-LDS-$(G4C2)_{4,42,44}^{GR-GFP}$, GMR-GAL4^{YH3}/+*	BDSC #57306	26°C
Fig. 4C-D	Genotype (driver: GMR-GAL4^{YH3})	Includes	Temp
$(GR)_{36}$ w/ Control RNAi	*w^{1118}/y^{1}, v^{1}; UAS-$(GR)_{36}$/+; GMR-GAL4^{YH3}/UAS-Luc RNAi^{JF01355}*	BDSC #31603	24°C
$(GR)_{36}$ w/ eIF4B RNAi	*w^{1118}/y^{1}, sc*, v^{1}; UAS-$(GR)_{36}$/UAS-eIF4B RNAi^{HMS04503}; GMR-GAL4^{YH3}/+*	BDSC #57305	24°C
$(GR)_{36}$ w/ eIF4B RNAi	*w^{1118}/y^{1}, sc*, v^{1}; UAS-$(GR)_{36}$/UAS-eIF4B RNAi^{HMS04504}; GMR-GAL4^{YH3}/+*	BDSC #57306	24°C
Fig. 4E-F	Genotype (driver: GMR-GAL4^{YH3})	Includes	Temp
Control RNAi	*w^{1118}/Y;; GMR-GAL4^{YH3}/UAS-Luc RNAi^{JF01355}*	BDSC #31603	26°C
eIF4B RNAi	*w^{1118}/Y; UAS-eIF4B RNAi^{HMS04503}/+; GMR-GAL4^{YH3}/+*	BDSC #57305	26°C
eIF4H1 RNAi	*w^{1118}/Y; UAS-eIF4H1 RNAi^{HMS04504}/+; GMR-GAL4^{YH3}/+*	BDSC #57306	26°C
Fig. 5C-D	Genotype (driver: GMR-GAL4^{1104})	Includes	Temp
DsRed w/ Control RNAi	*w^{1118}/Y; UAS-DsRed, GMR-GAL4/+; UAS-Luc RNAi^{JF01355}/+*	BDSC #31603	26°C
DsRed w/ eIF4B RNAi	*w^{1118}/Y, v^{1}; UAS-DsRed, GMR-GAL4/UAS-eIF4B RNAi^{HMS04503};*	BDSC #57305	26°C
DsRed w/ eIF4B RNAi	*w^{1118}/Y; UAS-DsRed, GMR-GAL4/UAS-eIF4B RNAi^{HMS04504};*	BDSC #57306	26°C

Fig. 5E	Genotype (driver: GMR-GAL4^{1104})	Includes	Temp
LacZ w/ Control RNAi	*w^{1118}/Y; UAS-LacZ, GMR-GAL4/+; UAS-Luc RNAi^{JF01355}/+*	BDSC #31603	26°C
LacZ w/ eIF4B RNAi	*w^{1118}/Y, v^{1}; UAS-LacZ, GMR-GAL4/UAS-eIF4B RNAi^{HMS04503};*	BDSC #57305	26°C
LacZ w/ eIF4B RNAi	*w^{1118}/Y; UAS-LacZ, GMR-GAL4/UAS-eIF4B RNAi^{HMS04504};*	BDSC #57306	26°C
Sup. Fig. 2	**Genotype (driver: GMR-GAL4^{YH3})**	**Includes**	**Temp**
Control RNAi	*w^{1118}/Y;; UAS-LDS-(G4C2)$_{4,42,44}^{GR-GFP}$, GMR-GAL4^{YH3}/UAS-Luc RNAi^{JF01355}*	BDSC #31603	26°C
eIF5B RNAi	*w^{1118}/Y;; UAS-LDS-(G4C2)$_{4,42,44}^{GR-GFP}$, GMR-GAL4^{YH3}/UAS-eIF5B RNAi^{GL01593}*	BDSC #57305	26°C
eIF5 RNAi	*w^{1118}/Y;; UAS-LDS-(G4C2)$_{4,42,44}^{GR-GFP}$, GMR-GAL4^{YH3}/UAS-eIF5 RNAi^{HMS00159}*	BDSC #34841	26°C
eIF2β RNAi	*w^{1118}/Y;; UAS-LDS-(G4C2)$_{4,42,44}^{GR-GFP}$, GMR-GAL4^{YH3}/UAS-eIF2β RNAi^{HMC02396}*	BDSC #53268	26°C
eIF2Bα RNAi	*w^{1118}/Y; UAS-eIF2Bα RNAi^{HMC03768}/+; UAS-LDS-(G4C2)$_{4,42,44}^{GR-GFP}$, GMR-GAL4^{YH3}/+*	BDSC #55624	26°C
eIF3g1 RNAi	*w^{1118}/Y;; UAS-LDS-(G4C2)$_{4,42,44}^{GR-GFP}$, GMR-GAL4^{YH3}/UAS-eIF3g1 RNAi^{GLC01430}*	BDSC #43243	26°C
eEFSec RNAi	*w^{1118}/Y;; UAS-LDS-(G4C2)$_{4,42,44}^{GR-GFP}$, GMR-GAL4^{YH3}/UAS-eIF3g1 RNAi^{GL01178}*	BDSC #42805	26°C
Sup. Fig. 3A	**Genotype (driver: Da-GAL4, III)**	**Includes**	**Temp**
w^{1118}	*w^{1118}/Y;; Da-GAL4/+*		26°C
eIF4B RNAi-2	*w^{1118}/Y; UAS-eIF4B RNAi^{330010}/+; Da-GAL4/+*	VDRC #330010	26°C
eIF4H1 RNAi-2	*w^{1118}/Y; UAS-eIF4H1 RNAi^{108805}/+; Da-GAL4/+*	VDRC #100817	26°C
Sup Fig. 3B-E	**Genotype (driver: GMR-GAL4^{YH3})**	**Includes**	**Temp**
Control RNAi	*w^{1118}/Y;; UAS-LDS-(G4C2)$_{4,42,44}^{GR-GFP}$, GMR-GAL4^{YH3}/UAS-Luc RNAi^{JF01355}*	BDSC #31603	26°C
eIF4B RNAi-2	*w^{1118}/Y; UAS-eIF4B RNAi^{330010}/+; UAS-LDS-(G4C2)$_{4,42,44}^{GR-GFP}$, GMR-GAL4^{YH3}/+*	VDRC #330010	26°C
eIF4H1 RNAi-2	*w^{1118}/Y; UAS-eIF4H1 RNAi^{108805}/+; UAS-LDS-(G4C2)$_{4,42,44}^{GR-GFP}$, GMR-GAL4^{YH3}/+*	VDRC #100817	26°C
Sup. Fig. 3F	**Genotype (driver: GMR-GAL4^{1104})**	**Includes**	**Temp**
LacZ w/ Control	*w^{1118}/Y; UAS-LacZ, GMR-GAL4/UAS-DSRED;*	UAS-DSRED	26°C
LacZ w/ eIF4B RNAi-2	*w^{1118}/Y, v^{1}; UAS-LacZ, GMR-GAL4/UAS-eIF4B RNAi^{330010};*	VDRC #330010	26°C
LacZ w/ eIF4B RNAi-2	*w^{1118}/Y; UAS-LacZ, GMR-GAL4/UAS-eIF4B RNAi^{1088057};*	VDRC #100817	26°C

Table S3-2: Full screen

Color scheme:	Suppressor	Mild Suppressor	No Effect	Mild Enhancer	Enhancer	Lethal Enhancer	not tested

Fly Gene	Human orthologue	BDSC stock #	Genotype of stock	LOF line type	Final Call	LDS-$(G4C2)_{EXP}$		$(GR)_{36}$	Alone	Control (LacZ) expression
						Toxicity	GR-GFP levels	Toxicity	Phenotype	
eIF4B	*EIF4B*	57305	y1 sc* v1; P{TRiP.HMS04503}attP40	RNAi	Candidate RAN-translation factor					
eIF4H1	*EIF4H*	57306	y1 sc* v1; P{TRiP.HMS04504}attP40	RNAi	Candidate RAN-translation factor					
eIF4E3	*EIF4E*	53880	y1 v1; P{TRiP.HMJ21195}attP40	RNAi	Candidate RAN-translation factor					
eIF4E4	*EIF4E*	50951	y1 v1; P{TRiP.HMJ21052}attP40	RNAi	Candidate RAN-translation factor					
eIF4E7	*EIF4E*	33471	P{EP}eIF4E7G1355 w*	mutant	Candidate RAN-translation factor					
eIF5B	*EIF5B*	44418	y1 sc* v1; P{TRiP.GL01593}attP2/TM3,	RNAi	Candidate RAN-translation factor					
eIF5	*EIF5*	34841	y1 sc* v1; P{TRiP.HMS00159}attP2	RNAi	Candidate RAN-translation factor					
eIF2 β	*EIF2S2*	53268	y1 sc* v1; P{TRiP.HMC02396}attP2/TM3,	RNAi	Candidate RAN-translation factor					
eIF3d1 (eIF-3p66)	*EIF3D*	20072	y1 w67c23; P{EPgy2}eIF3d1EY05735/TM3,	mutant	Candidate RAN-translation factor					
eIF4E5	*EIF4E*	66332	y1 sc* v1; P{TRiP.HMC06261}attP40	RNAi	Candidate RAN-translation factor					
eIF3i (eIF3-S2)	*EIF3I*	34978	y1 sc* v1; P{TRiP.HMS01387}attP2	RNAi	Candidate RAN-translation factor					
eIF3K	*EIF3K*	44493	y1 sc* v1; P{TRiP.HMC02415}attP2	RNAi	Potential RAN-translation factor					
eIF2Bγ	*EIF2B3*	41948	y1 sc* v1; P{TRiP.HMS02345}attP40	RNAi	G4C2 Suppressor					
eEF2	*EEF2*	21351	y1 w67c23; P{EPgy2}eEF2EY02807/CyO	mutant	G4C2 Suppressor					
eIF2Bδ	*EIF2B4*	15441	y1 w67c23; P{EPgy2}eIF2BδEY03558	mutant	G4C2 Suppressor					
eEF1 β	*EEF1B2*	16371	y1 w67c23; P{EPgy2}eEF1βEY05513	mutant	G4C2 Suppressor					
eIF4G1	*EIF4G3*	33049	y1 sc* v1; P{TRiP.HMS00762}attP2	RNAi	GR suppressor					
eIF3b (eIF3-S9)	*EIF3B*	32880	y1 sc* v1; P{TRiP.HMS00668}attP2	RNAi	GR Enhancer					
eIF3l	*EIF3L*	50959	y1 v1; P{TRiP.HMJ21061}attP40/CyO	RNAi	GR Enhancer					
eIF4E1	*EIF4E*	34096	y1 sc* v1; P{TRiP.HMS00969}attP2	RNAi	GR Enhancer					
NAT1	*EIF4G2*	32357	y1 sc* v1; P{TRiP.HMS00348}attP2	RNAi	GR Enhancer					
eIF5C	*BZW1*	27248	y1 v1; P{TRiP.JF02556}attP2	RNAi	GR Enhancer					
eIF1	*EIF1B*	57174	y1 sc* v1; P{TRiP.HMC04556}attP40	RNAi	No Effect					
eIF2Bα	*EIF2B1*	55624	y1 sc* v1; P{TRiP.HMC03768}attP40	RNAi	No Effect					
eIF2B β	*EIF2B2*	55675	y1 sc* v1; P{TRiP.HMC03838}attP40	RNAi	No Effect					
eIF2Bε	*EIF2B5*	55321	y1 v1; P{TRiP.HMC04008}attP40	RNAi	No Effect					
eIF2D	*EIF2D*	33995	y1 sc* v1; P{TRiP.HMS00958}attP2	RNAi	No Effect					
eIF3c (eIF3-S8)	*EIF3CL*	16857	y1 w67c23; P{EPgy2}eIF3cEY07713/CyO	mutant	No Effect					
eIF3f1 (eIF3-S5)	*EIF3F*	33980	y1 sc* v1; P{TRiP.HMS00940}attP2	RNAi	No Effect					
eIF3g1 (eIF3-S4)	*EIF3G*	43243	y1 sc* v1; P{TRiP.GLC01430}attP2	RNAi	No Effect					

eIF3h (eIF-3p40)	*EIF3H*	55603	y1 sc* v1; P{TRiP.GL01831}attP2	RNAi	No Effect					
eIF4AIII	*EIF4A3*	32444	y1 sc* v1; P{TRiP.HMS00442}attP2	RNAi	No Effect					
eIF4G2	*EIF4G1, EIF4G3*	42893	y1 sc* v1; P{TRiP.HMS02586}attP40	RNAi	No Effect					
eIF4H2	*EIF4H*	v32191	w1118; P{GD8011}v32191/CyO	RNAi	No Effect					
eEF1α1	*EEF1A2*	33960	y1 sc* v1; P{TRiP.HMS00917}attP2	RNAi	No Effect					
eEF1α2	*EEF1A2*	64659	y1 sc* v1; P{TRiP.HMC05694}attP40	RNAi	No Effect					
eEF1γ	*EEF1G*	31811	w1118; P{EP}eEF1γG16379/TM6C, Sb1	mutant	No Effect					
eEF1δ	*EEF1D*	29605	y1 v1; P{TRiP.JF03284}attP2	RNAi	No Effect					
eEFSec	*EEFSEC*	42805	y1 v1; P{TRiP.GL01178}attP2	RNAi	No Effect					
eRF1	*ETF1*	17265	w1118; P{EP}eRF1EP3195/TM6B, Tb1	mutant	No Effect					
eRF3	*GSPT1*	36703	y1 sc* v1; P{TRiP.HMS01592}attP2	RNAi	No Effect					
eIF4EHP	*EIF4E2*	43990	y1 sc* v1; P{TRiP.HMS02703}attP40	RNAi	No Effect					
eIF1A	*EIF1AY*	29316	y1 v1; P{TRiP.JF02475}attP2	RNAi	Unspecific enhancer					
eIF2α	*EIF2S1*	44449	y1 v1; P{TRiP.GLC01598}attP2/TM3,	RNAi	Unspecific enhancer					
eIF2γ	*EIF2S3*	33401	y1 sc* v1; P{TRiP.HMS00279}attP2	RNAi	Unspecific enhancer					
eIF3α (eIF3-S10)	*EIF3A*	34353	y1 sc* v1; P{TRiP.HMS01342}attP2	RNAi	Unspecific enhancer					
eIF3m	*EIF3M*	32879	y1 sc* v1; P{TRiP.HMS00667}attP2	RNAi	Unspecific enhancer					
eIF4A	*EIF4A1*	33970	y1 sc* v1; P{TRiP.HMS00927}attP2	RNAi	Unspecific enhancer					

Table S3-3: Fibroblast cell lines

Fibroblast cell line #	NINDS/Coriell Code	Mutation	Diagnosis	Age at onset	Age at sampling	Gender	Source
1	ND29178	n/a	healthy	n/a	66	M	Rutgers
2	ND29510	n/a	healthy	n/a	55	F	Rutgers
3	ND34769	n/a	healthy	n/a	68	F	Rutgers
4	ND36320	n/a	healthy	n/a	71	F	Rutgers
5	ND38530	n/a	healthy	n/a	55	M	Rutgers
6	ND40069	*C9orf72: Intermediate*	Parkinsonism	71	75	F	Rutgers
7	ND42496	*C9orf72*	FTD	At Risk	57	M	Rutgers
8	ND42504	*C9orf72*	FTD	At Risk	53	F	Rutgers
9	ND42506	*C9orf72*	FTD	At Risk	46	F	Rutgers

Table S3-4: Patient details

The sample median (minimum, 25th percentile, 75th percentile, and maximum) is given for age at onset, age at death and disease duration, all given in years.

	***C9orf72*-positive**			
	All	**ALS**	**ALS/FTLD**	**FTLD**
Number of cases	66	19	21	26
Gender (male)	38 (57.58%)	7 (36.84%)	12 (57.14%)	19 (73.08%)
Age at onset	61 (41, 55, 67, 79)	56 (41, 49, 61, 69)	58 (50, 54, 65, 74)	66 (44, 57, 70, 79)
Age at death	64 (43, 59, 72, 90)	60 (43, 51, 64, 72)	62 (51, 60, 68, 80)	72 (52, 65, 78, 90)
Disease duration	3.9 (1.0, 2.3, 6.7, 14.5)	2.1 (1.0, 1.5, 3.1, 6.3)	4.8 (1.1, 2.7, 6.7, 10.4)	7.3 (2.4, 5.8, 9.4, 14.5)

	***C9orf72*-negative**			
	All	**ALS**	**ALS/FTLD**	**FTLD**
Number of cases	46	21	9	16
Gender (male)	21 (45.65%)	10 (47.62%)	3 (33.33%)	8 (50.00%)
Age at onset	66 (45, 57, 73, 86)	59 (45, 49, 66, 76)	70 (46, 57, 70, 78)	73 (57, 66, 80, 86)
Age at death	72 (47, 64, 83, 100)	66 (47, 59, 71, 83)	73 (49, 63, 78, 85)	85 (66, 78, 89, 100)
Disease duration	4.6 (0.6, 2.9, 8.6, 21.9)	3.4 (0.9, 2.0, 4.8, 21.5)	2.9 (0.6, 1.8, 7.8, 21.9)	8.5 (3.9, 8.2, 10.1, 20.5)

	Healthy controls
Number of cases	22
Gender (male)	12 (54.54%)
Age at death	79 (57, 64, 89, 99)

Table S3-5: Fly lines

Name	Location	Source	ID #	Full genotype
Gmr-GAL4 (III)	3	Matthew Freeman	n/a	w*;; Gmr-GAL4^{YH3}/TM3,Sb
Gmr-GAL4 (II)	2	BDSC	1104	w*; Gmr-GAL4;
Da-GAL4	3	BDSC	55851	w*;; Da-GAL4
HS-GAL4	3	BDSC	1799	w[*];; P{w[+mC]=GAL4-Hsp70.PB}89-2-1
Control (DSRED)	2	Nancy Bonini	n/a	w[1118]; UAS-DSRED;
LDS-(G4C2)12$^{GR\text{-}GFP}$	3	Nancy Bonini	n/a	w[1118];; UAS-LDS-(G4C2)$_{4,9,12}$[GR-GFP]
LDS-(G4C2)44$^{GR\text{-}GFP}$	3	Nancy Bonini	n/a	w[1118];; UAS-LDS-(G4C2)$_{4,42,44}$[GR-GFP]
Control (w^{1118})	n/a	BDSC	5905	w[1118];;
Control RNAi	3	BDSC	31603	y[1] v[1];; P{y[+t7.7] v[+t1.8]=TRiP.JF01355}attP2
(GR)36	2	BDSC	58692	w[1118]; P{y[+t7.7] w[+mC]=UAS-poly-GR.PO-36}attP40;
eIF4B RNAi	2	BDSC	57305	y1 sc* v1; P{TRiP.HMS04503}attP40;
eIF4B RNAi-2	2	VDRC	330010	w*; P{VSH330010}attP40;
eIF4H1 RNAi	2	BDSC	57306	y1 sc* v1; P{TRiP.HMS04504}attP40;
eIF4H1 RNAi-2	2	VDRC	100817	w*; P{KK108805}VIE-260B;

BDSC = Bloomington *Drosophila* Stock Center
VDRC = Vienna *Drosophila* Resource Center

Table S3-5: Primers

Target	Species	Assay	Forward (5'-3')	Reverse (5'-3')	Reference
LDS-G4C2	*Dmel.*	PCR	ACTCGCTGAGGGTGAACAAG	CGACTCCTGAGTTCCAGAGC	Goodman et al, Nat Neuro, 2019
GFP tag	*Dmel.*	qPCR	ACGTAAACGGCCACAAGTTC	AAGTCGTGCTGCTTCATGTG	Goodman et al, Nat Neuro, 2019
RP49	*Dmel.*	qPCR	TGTCCTTCCAGCTTCAAGATGACCATC	CTTGGGCTTGCGCCATTTGTG	Gabler, M. et al., 2005
eIF4B	*Dmel.*	qPCR	CGCATTGAGCTATCGAATGA	CCAATTTCCGGAATCCCTAT	this paper
eIF4H1	*Dmel.*	qPCR	GGGAAACGGATCAGTTCAAA	CTTCTGGAAACCGTCTCTGC	this paper
EIF4H	*Hsap.*	qPCR	GGTGGCTTTGGATTCAGAAA	CCCTGAAGCCAGAATTGAAG	this paper
EIF4B	*Hsap.*	qPCR	AGCTCAGACACAGAGCAGCA	CTTTCCTTCCTGGTCCTTCC	this paper
RPLP0	*Hsap*	qPCR	TCTACAACCCTGAAGTGCTTGAT	CAATCTGCAGACAGACACTGG	Goodman et al, Nat Neuro, 2019
GAPDH	*Hsap*	qPCR	GTTCGACAGTCAGCCGCATC	GGAATTTGCCATGGGTGGA	Goodman et al, Nat Neuro, 2019

Chapter 3: Supplementary figures and legends

Figure S3-1

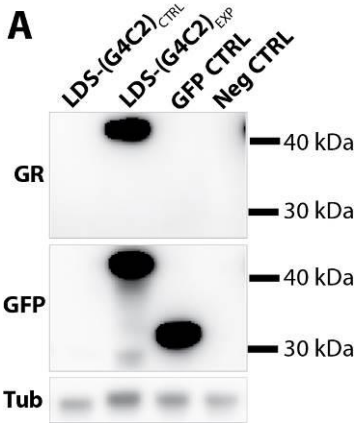

Supplementary Figure S3-1: Extended LDS-G4C2 fly line characterization.

Western immunoblots were used to confirm GR dipeptide is produced and successfully tagged with GFP in expanded G4C2 flies **(Fig. 3-1D)**. Blots were overexposed to see if GR/GFP dipeptide could be detected in control G4C2 flies. Shown is a representative image of the original blot, imaged at > 4X the original exposure. > 10X the original exposure also showed no GR/GFP dipeptide in control G4C2 flies (data not shown). Note that the faint band at a molecular weight below GFP alone in the LDS-$(G4C2)_{EXP}$ lane is a non-specific band that is found in multiple lanes of the complete western immunoblot (see **Supplementary Fig. S3-4** for Uncropped westerns)**.**

Figure S3-2

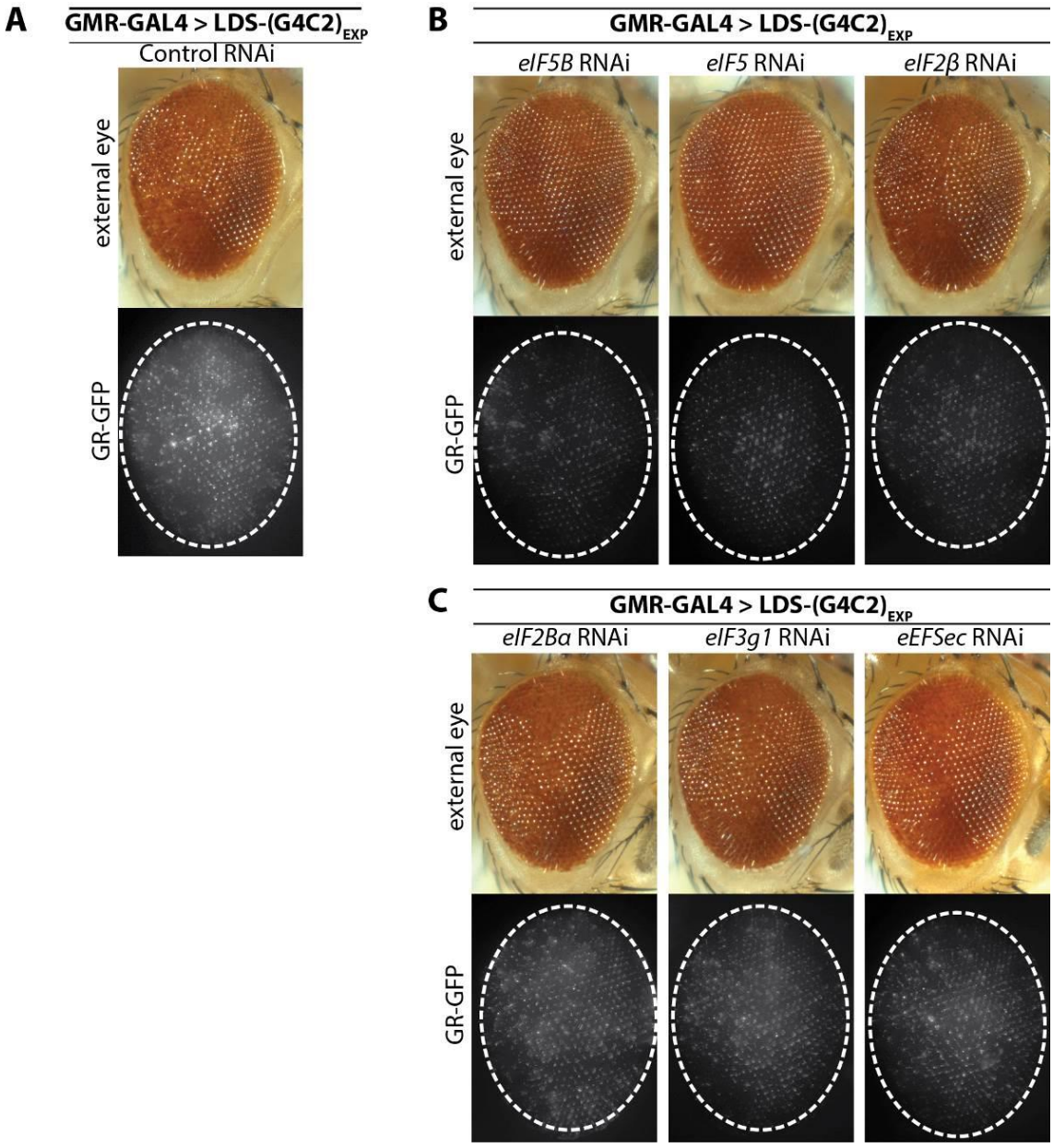
A
GMR-GAL4 > LDS-(G4C2)EXP
Control RNAi
external eye
GR-GFP
B
GMR-GAL4 > LDS-(G4C2)EXP
eIF5B RNAi
eIF5 RNAi
eIF2β RNAi
external eye
GR-GFP
C
GMR-GAL4 > LDS-(G4C2)EXP
eIF2Bα RNAi
eIF3g1 RNAi
eEFSec RNAi
external eye
GR-GFP

Supplementary Figure S3-2: Extended translation factor screen data.

A. External eye and GR-GFP imaging in LDS-$(G4C2)_{EXP}$ animals co-expressing control (*Luc*) RNAi. **B.** Additional examples of candidate RAN-translation factors, showing suppression of toxicity in the external eye and reduced GR-GFP levels. Note, *eIF2β* RNAi only mildly altered toxicity in the external eye. **C.** Examples of RNAi targeting translation factors that did not significantly alter LDS-$(G4C2)_{EXP}$ toxicity nor GR-GFP levels. RNAi lines: control (JF01355), *eIF5B* (GL01593), *eIF5* (HMS00159), *eIF2β* (HMC02396), ***eIF2Bα*** (HMC03768), *eIF3g1* (GLC01430), *eEFSec* (GL01178). For full genotypes see **Supplementary Table S3-1**. Shown: representative images while all RNAi were tested 2+ times for effects on LDS-$(G4C2)_{EXP}$ toxicity and GR-GFP levels.

Figure S3-3

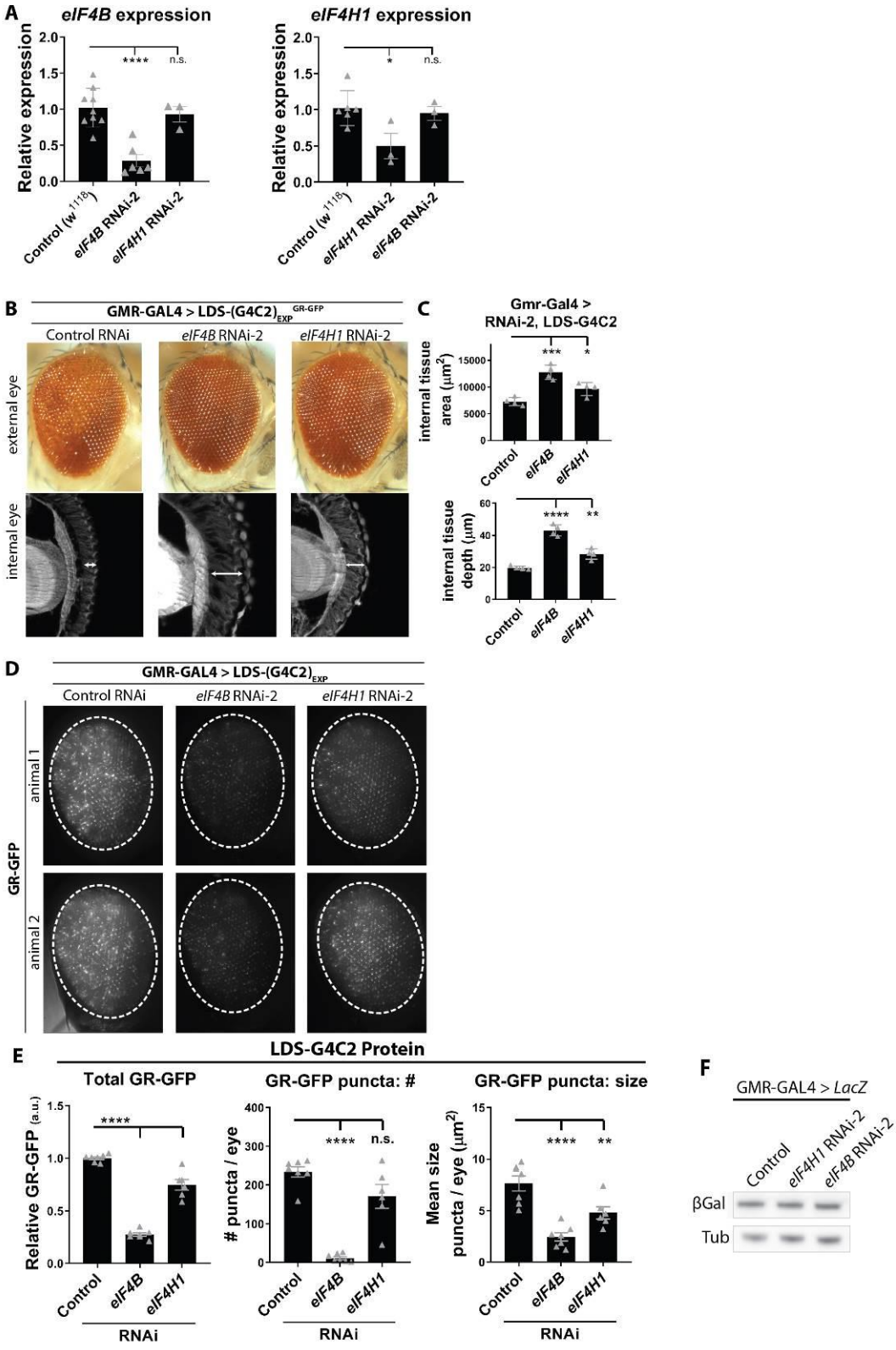
A
eIF4B expression
eIF4H1 expression
Relative expression
Control (w1118)
eIF4B RNAi-2
eIF4H1 RNAi-2
B
GMR-GAL4 > LDS-(G4C2)EXP GR-GFP
Control RNAi
eIF4B RNAi-2
eIF4H1 RNAi-2
external eye
internal eye
C
Gmr-Gal4 > RNAi-2, LDS-G4C2
internal tissue area (μm2)
internal tissue depth (μm)
D
GMR-GAL4 > LDS-(G4C2)EXP
GR-GFP
animal 1
animal 2
E
LDS-G4C2 Protein
Total GR-GFP
GR-GFP puncta: #
GR-GFP puncta: size
Relative GR-GFP (a.u.)
puncta / eye
Mean size puncta / eye (μm2)
RNAi
F
GMR-GAL4 > LacZ
βGal
Tub

Supplementary Figure S3-3: *eIF4B* and *eIF4H1* RNAi-2 data.

eIF4B and *eIF4H1* downregulation in LDS-$(G4C2)_{EXP}$ flies using a second set of RNAi lines show similar results. **A.** RNA levels produced from *eIF4B* or *eIF4H1* were assessed by qPCR in flies ubiquitously expressing RNAi-2 (by Daughterless-GAL4 driver). Shown: individual data points with mean±SD. **B.** Using GMR-GAL4, RNAi-2-mediated depletion of *eIF4B* or *eIF4H1* in LDS-$(G4C2)_{EXP}$ expressing flies results in reduced toxicity in both the external and internal eye: seen externally by recovered pigment and ommatidial structure, seen internally by recovered retinal tissue integrity. **C.** Blinded quantification of internal retina tissue was done by measuring the total surface area of tissue present and by measuring the depth of the tissue at the position of the optic chiasm. n=4 animals per genotype. Shown: individual data points each representing 1 animal, with mean±SD. **D.** Fluorescence imaging in LDS-$(G4C2)_{EXP}$ expressing flies co-expressing *eIF4B* or *eIF4H* RNAi-2 results in reduced GR-GFP levels (GMR-GAL4). **E.** Blinded quantification of GR-GFP signal in LDS-$(G4C2)_{EXP}$ animals relative to signal in control RNAi animals. Note that *eIF4H1* RNAi-2 did not cause a significant reduction in GR-GFP puncta number, likely due to this RNAi only causing a 50% downregulation of *eIF4H1*; it did reduce puncta size and total GR-GFP fluorescence. n=6-7 animals per genotype. Shown: individual data points each representing 1 animal from two independent experiments with mean±SEM. **F.** A representative western immunoblot image for β-Galactosidase in *LacZ* flies co-expressing a control transgene, *eIF4B* RNAi-2, or *eIF4H1* RNAi-2. Uncropped westerns (**Sup. Fig. S3-4).** Statistics: one-way ANOVAs with Tukey's multiple comparison correction, p-values ****<0.0001, ***<0.001, **<0.01, *<0.05, no significance >0.05. RNAi lines: control (JF01355), *eIF4B* RNAi-2 (VSH330010), *eIF4H1* RNAi-2 (KK108805). For full genotypes see **Supplementary Table S3-1**.

Figure S3-4

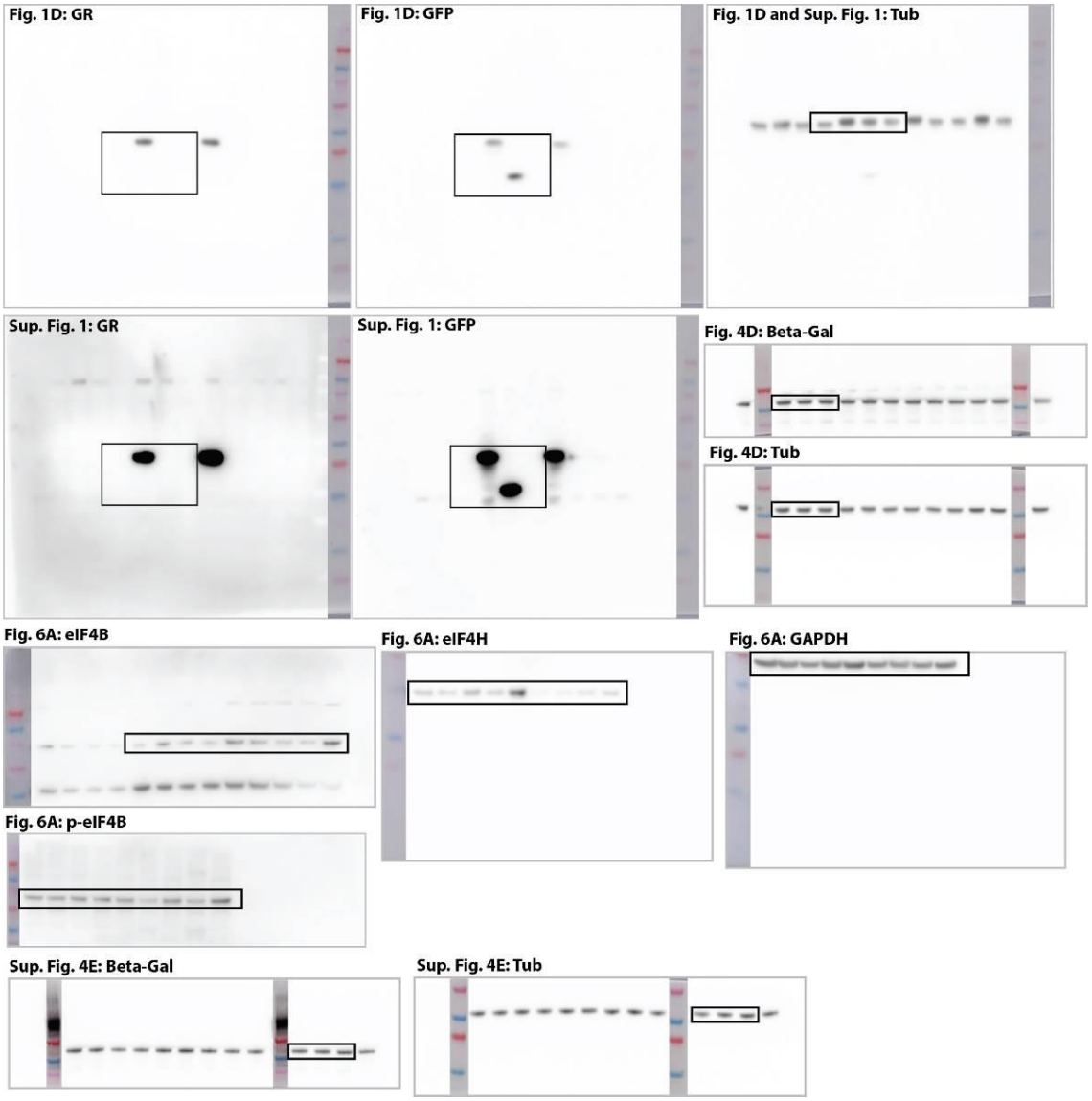

Supplementary Figure S3-4: full Western immunoblot images for Fig. 3-1D, Sup. Fig. S3-1, Fig. 3-4D, Fig. 3-6A and Sup. Fig. S3-4E, including ladder, Novex sharp Protein Standard (Invitrogen #LC5800).

APPENDIX 4: DETAILED PROTOCOLS FOR SELECT EXPERIMENTS

gDNA extraction (flies)

Methods 1: High quality DNA (Puregene Kit)

REAGENTS/MATERIALS

- Gentra Puregene Tissue Kit (Qiagen #158667), prepare stock solutions according to company's instructions
- phenol: chloroform:isoamyl alcohol
- isopropanol
- 70% ethanol (200 proof ethanol + milliQ water)
- pellet/pestle disposable blue microcentrifuge tubes (Kimble # 749520-0000)
- pellet/pestle cordless motor (Kimble # 749540-0000)
- microcentrifuge tubes

PROTOCOL

1. Prep:
    a. Pre-chill 500ul cell lysis buffer per sample on ice for 10 min.
    b. set a heat block to 65°C
    c. set a heat block to 37°C
    d. (optional) pre-chill refrigerated microcentrifuge
2. Collect 15-30 transgenic flies and transfer to a blue tube for use with the plastic disposable pestles. Immediately add 100ul of chilled lysis buffer and grind the tissue using pellet pestles. When completely homogenized, add an additional 200ul of chilled lysis buffer and vortex briefly to mix. Place the tube back on ice until next step.
3. Heat the lysate at 65°C for 30min to inactivate endogenous DNase.
4. Transfer lysates to an ice-bucket containing ice and incubate for 5min.
5. Add 1.5µl of RNase A soln. Mix well by inverting 25X and incubate the lysate at 37°C for 30-60 min.
6. Add 200µl of prechilled lysis buffer and incubate on ice for 1min.
7. Add 180µl of protein precipitation buffer to the RNAase A-treated lysate. Immediately vortex at max speed for 30 sec.
8. Incubate lysate on ice for 10 min.
9. Centrifuge at 20,000 x g for 10 min at 4°C.
    Note: samples tend to still have chunks of stuff within the supernatant. Repeating the protein precipitation steps does not seem to help. Just move forward.
10. Transfer supernatant to a new 1.5ml tube by dumping the solution from 1 tube into the next. Be gentle so as to avoid accidently dislodging the pellet.
11. Add 650µl phenol: chloroform:isoamyl alcohol (be sure to take solution from the bottom of the container as the top is an aqueous layer). Immediately mix by inverting 50X. Incubate at RT 5min.
12. Centrifuge at 16000 x g for 10 min.
13. Transfer upper aqueous layer (~580µl) to a new 1.5ml tube.
14. Add 700µl isopropanol into the tube. Mix the sample by inverting gently 50X.
15. Centrifuge at 16000 x g for 10 min. Remove supernatant by pouring it into a waste container – be sure to keep the tube inverted (!) and dab the edge on

clean paper towel to remove the supernatant. Pellet may be loose so use caution not to lose it during pouring off supernatant.

16. Wash the DNA pellet once with 300µl 70% ethanol by gently adding the EtOH than immediately removing it with the same pipet tip. Pellet may be loose so use caution not to lose it during ethanol removal. Using a tabletop centrifuge, centrifuge the samples briefly to collect residual liquid. Remove it with a pipette.
17. Air dry pellet for 10 min. Add 3µl/animal DNA hydration solution (or TE buffer) to dissolve it. Mix by pipette if necessary to make sure that pellet is fully dissolved.
    a. If necessary, samples can be stored overnight at 4^{o}C to allow them to dissolve completely. Store the genomic DNA at -20^{o}C.
    b. Do not store your isolated DNA in water. DNA is an acid and is best stored under buffered conditions. The standard TE will work. The EDTA concentration can be reduced, however, it is usually diluted to a concentration that does not inhibit the PCR or other downstream reactions.
18. Assess DNA quality
    a. Check the quantity & quality of DNA on the Nanodrop. The A260/280 ratios should be around 1.8 for DNA. Note: A260/230 ratios maybe <2.0 due to phenol contamination. This does not typically affect PCRs.
    b. (optional) Check the quality of genomic DNA on 1.0% agarose TAE gel with a 1kb ladder.
        i. Run for ~30-60 min on a 0.8-1% gel at 100 V. If you see a thick and well-defined band that barely migrates (is genomic DNA and it is extremely heavy to migrate), it is your DNA and it is in good shape. The blurrier it looks, the more degraded your DNA is. If the band has a thick smear it is very degraded. It does not matter if the genomic DNA is totally intact for PCR as long as the smear extends above the expected length of your amplicon and the DNA does not have any PCR inhibitors.

Method 2: Squash Buffer

NOTES

- Good for
    - Rapid genotyping of a fly line
    - Genotyping single animals (e.g. determining if a single, potential recombinant male indeed has the desired genotype)
- Does not work on LDS-G4C2 fly model w/ G4C2 PCR protocol
- May need to reduce amount of supernatant used per PCR reaction to 1µl depending on your PCR reaction

REAGENTS/MATERIALS

- 1M Tris-HCl, pH 8.0
- 0.5M EDTA, pH 8.0
- 5M NaCl

- proteinase K (Roche cat# 12445700, 20mg/ml)
- microcentrifuge tubes
- pellet/pestle disposable blue microcentrifuge tubes (Kimble # 749520-0000)
- pellet/pestle cordless motor (Kimble # 749540-0000)

PROTOCOL

1. Prepare:
    a. Squash Buffer Stock (10 mM Tris-HCl, pH 8.0; 1 mM EDTA; 25 mM NaCl) - can make 50mL in a conical and store long-term at room temperature
    b. Preheat two heat-blocks: one to 37^{o}C, one to 95^{o}C
2. Prepare Working Squash Buffer by adding 5µl proteinase K to 250ul of Squash Buffer Stock (need 30µl per sample).
3. Place 1-2 flies in a pre-labeled, blue microcentrifuge tube. Using disposable pestle and motor, grind the fly for 5-10 sec in 30µl of Working Squash Buffer.
4. Incubate tubes at 37^{o}C for 40min.
5. Incubate tubes at 95^{o}C for 5min to inactivate protease K.
6. Pellet cuticle by centrifuging samples at 12,000xg for 5-10 min.
7. Transfer supernatant to a fresh, prelabeled microcentrifuge tube with a 200µL pipette, making sure to avoid pellet.
8. Store at -20^{o}C.
9. Use 2µl of aqueous supernatant as PCR template for 10µl PCR reaction.

PCR reactions for UAS, GAL4, GS transgenes

TRANSGENE-SPECIFIC REACTIONS

- pUAS transgenes (flanking primers)
    - UAS-(GR)36 parameters
        - annealing temperature: 59 ^{o}C
        - DNA template per reaction: 100ng
        - PCR product: ~520bp by agarose gel
    - Other pUAS transgenes parameters
        - annealing temperature: Run a gradient temperature reaction from 55-52^{o}C on a positive sample to define the best annealing temperature
        - DNA template per reaction: test 100 and 200ng
        - PCR product: ~300bp + the size of the transgene
    - Forward primer: 5'- AGCAACCAAGTAAATCAACTGC -3'
    - Reverse primer: 5'- TTCATCAGTTCCATAGGTTGG -3'
- GAL4 transgenes
    - Parameters

        - annealing temperature: 58 °C
        - DNA template per reaction: 200ng
        - PCR product: ~420bp by agarose gel
    - Forward primer: 5'- GTCTTCTATCGAACAAGCATGCGA -3'
    - Reverse primer: 5'- TGACCTTTGTTACTACTCTCTTCC -3'
- GAL4[geneswitch] transgenes
    - Parameters
        - annealing temperature: 62 °C
        - DNA template per reaction: 100ng
        - PCR product: ~520bp by agarose gel
    - Forward primer: 5'-GGGCTACGAAGTCAAACCCA-3'
    - Reverse primer: 5'-TCTGCCCAGAAGGAAACACC-3'

REAGENTS/MATERIALS

- Fly genomic DNA (*see General protocols: gDNA extraction (flies)*)
- FastStart PCR Master Mix (Roche # 04710436001)
- 6X Gel Loading Dye (New England biolabs #B7021S)
- MilliQ water

SUPPLEMENTARY FILE: PCR reactions for UAS-GAL4 transgenes.xlsx

PROTOCOL

1. Thaw the following at RT
    a. Fly genomic DNA
    b. FastStart PCR Master Mix (Roche # 04710436001)
2. Prepare a master mix using the Supplementary file to automatically calculate the volumes of each reagent to add. Be sure to include a no-template (water only) control and a positive control.

Master Mix Component	**Final concentration**
2X FastStart Master Mix	1X
Forward Primer (3µM)	0.3µM
Reverse Primer (3µM)	0.3µM
Genomic DNA	Volume is based on your samples, typically 1-2µl
MilliQ water (must be room temperature)	Volume is based on your desired end volume, typically 10µl

Notes

- Make sure you have a no-template (water) control and a positive control. If using the plasmid construct as the positive control, only use 5-20ng of purified plasmid per reaction.

3. pipette the correct amount of master mix into desired # of PCR tubes. Typically, 8-9µl of master mix/tube.
4. add genomic DNA to the PCR tubes, being sure to keep track of the order. Typically, 1-2µl of 100ng/µl genomic DNA per tube.
5. Place tubes into a thermocycler. Press firmly down on each tube's lid to make sure they are sealed. Run the following program:

Step	**Temperature**	**Time**	**Number Cycles**
Initial denaturation	95 °C	6 min	1
Denaturation	95 °C	30 sec	35
Primer annealing	varies	30 sec	
Extension	72 °C	1min	
Final Extension	72 °C	7min	1
Cooling	4 °C	Hold	1

6. PCR samples can be stored at -20°C for future use.
7. Run PCR products on a 1% TAE agarose gel
    a. Prepare a 1% TAE agarose gel
        i. prep the agarose gel casting equipment with an appropriate size comb – includes placing the tray in the mount and adding the comb then making sure it's all level with a level
        ii. add desired volume of 1X TAE to a Erlenmeyer flask (for mini gel this is 70ml, for a midi gel this is 200ml)
        iii. add agarose powder to the TAE for a final concentration of 1% (w/v) (for a mini gel this is 0.7g, for a midi gel this is 2g)
        iv. place a kimwipe or paper towel into the mouth of the flask and microwave the agarose until it has COMPLETELY melted. Usually ~3min, swirl flask every minute to mix. At the end, confirm there are no unmelted pieces within the solution – it should have no particles floating in it. microwave more as needed.
        v. add SYBR safe DNA stain to the melted agarose to 1x volume (7µl for mini gel, 20µl for midi gel). Swirl flask gently until stain is well mixed – be sure to avoid creating bubbles
        vi. gently pour the agarose into the prepared gel casting tray making sure to avoid bubbles. If bubbles to form, try to remove them or at

least move them to the sides using a pipette tip. Bubbles around the comb can be a particular problem.

vii. Cover the gel *loosely* with Al foil to avoid light exposure (do not seal it! this is just to protect it from light but you want it to cool as if the foil was absent)

viii. let agarose gel solidify for 45min-90min

b. Prepare samples

i. Thaw an aliquot an appropriate sized DNA ladder

ii. Dilute PCR products into 6X diluted sample buffer and mix thoroughly

1. If running PCR products prepared from high-quality DNA, run ~5µl of PCR product per lane.

2. If running PCR products prepared from Squash Method DNA preps, run 5-10µl of PCR product per lane

c. Run Gel

i. Prepare gel running equipment
   1. Gently remove comb from the solidified gel
   2. Place gel into the electrophoresis tank and add 1x TAE until it covers the top of the gel

ii. Add 5µl of each DNA ladder and 5-10µl of prepared PCR products per lane into the pre-determined lanes, being sure to keep track of which samples are in which lanes

iii. run the gel
   1. put the lid onto the electrophoresis tank paying special attention to the position of the electrodes. The black/negative electrodes at the top and the red/positive electrodes at the bottom.
   2. Plug the electrodes into a power-source, again paying special attention to the position of the electrodes – black-to-black and red-to-red.

iv. run the power supply at 100V for 40-75min until the blue indicator dye is ~2/3 of the way down the gel. DO NOT OVERRUN THE GELS AS THIS REDUCES TO SIGNAL STRENGTH. YOU CAN ALWAYS STOP THE GEL, CHECK IT ON THE UV IMAGER AND RUN IT MORE IF NEEDED TO GET SEPERATION OF BANDS.

d. Image the gel using the UV imager. The Bonini lab imager is significantly better while bands from these reactions should be relatively bright. Also, be prepared to look visually at the gel and to play around with exposure if bands are faint. If needed, you can soak the gel in 1X SYBR Safe DNA stain in TAE buffer for 10min and reimage.

e. Estimate the size of the PCR product(s) based on the DNA ladders.

Repeat-length determination

G4C2 PCR Reaction

NOTES

- Protocols for isolating genomic DNA from flies are in “General Protocols”
- Primers were designed that flank the repeat
    - UAS-G4C2 lines
        - a 350bp PCR product is expected for 49 repeats
        - Forward primer: 5’-GAATTCGAGCTCAGATCTCCCG-3’
        - Reverse primer: 5’-TCTAGAGGATCCGGTACCGAGTCTCGAG-3’
    - UAS-LDS-G4C2 lines
        - a 461bp PCR product is expected for 49 repeats
        - Forward primer: 5'-CTCGCTGAGGGTGAACAAGA-3'
        - Reverse primer: 5'-ACTTGTGGCCGTTTACGTCG-3'

REAGENTS

- Fly genomic DNA (*see General protocols: gDNA extraction (flies)*)
- KAPA HiFi Hotstart Kit (KAPA Biosystems #KK 2501)
- DMSO
- 5M Betaine (Sigma #B0300-1VL, stored at 4°C)
- MilliQ water

SUPPLEMENTARY FILE: G4C2 PCR Reaction (KAPA HiFi Hot-start Kit).xlsx

PROTOCOL

1. Thaw the following at RT
    a. From Kapa HiFi Kit
        i. 5X GC Buffer
        ii. KAPA dNTP mix (10mM)
    b. Working stocks for primers (at 10µM)
    c. Genomic DNA samples
2. (recommended) Update the G4C2 PCR Reaction (KAPA HiFi Hot-start Kit) supplementary file with relevant information and print the excel sheet for use at bench.
3. Prepare a master mix using the Supplementary file to automatically calculate the volumes of each reagent to add. Be sure to include a no-template (water only) control and a positive control.

Master Mix Component	**Final concentration**
5X GC Buffer	1X

KAPA dNTP mix (10mM)	0.3mM
Forward Primer (10uM)	0.3µM
Reverse Primer (10uM)	0.3µM
DMSO	5%
Betaine (5M)	1M
KAPA HiFi Hotstart DNA polymerase (1 U/µl)	0.02 U/1µl rxn
Genomic DNA (200ng)	Volume is based on your samples, typically 2µl
MilliQ water (must be room temperature)	Volume is based on your desired end volume, typically 10µl

Notes:

- It is important that the reaction mix remain at room temperature as DMSO freezes at 4°C. Accordingly, use RT water and let the reaction mix reach RT before adding the enzyme.
- Make sure you have a no-template (water) control and a positive control. If using the plasmid construct as the positive control, only use 20ng of purified plasmid per reaction.

4. pipette the correct amount of master mix into desired # of PCR tubes. Typically, 8µl of master mix/tube.
5. add genomic DNA to the PCR tubes, being sure to keep track of the order. Typically, 2µl of 100ng/µl genomic DNA per tube.
6. Place tubes into a thermocycler. Press firmly down on each tube's lid to make sure they are sealed. Run the following program: in Eppendorf PCR Machine #3 under Lindsey > G4C2 PCR > Kapa hotstart.

Step	**Temperature**	**Time**	**Number Cycles**
Initial denaturation	95 °C	5 min	1
Denaturation	98 °C	20 sec	35
Primer annealing	61 °C	30 sec	

Extension	72 °C	1min	
Final Extension	72 °C	5min	1
Cooling	4 °C	Hold	1

7. PCR samples can be stored at -20°C for future use.

Estimate repeat length: agarose gel

REAGENTS

- KAPA-HiFi PCR products
- 2X diluted sample buffer
    - 20µl of 6X Gel Loading Dye (New England biolabs #B7021S)
    - 6.6µl of 1M Tris-HCL, pH=8.0 to 6.6mM
    - 100µl of 50% glycerol to 5%
    - 873.4µl of MilliQ water to 1ml
- SYBR Safe DNA stain
- 50bp DNA ladder
- 25bp DNA ladder
- 1X TAE buffer
- Standard melting point agarose (Invitrogen #16500500)

PROTOCOL

1. Prepare a 1.5% TAE agarose gel
    a. prep the agarose gel casting equipment with an appropriate size comb – includes placing the tray in the mount and adding the comb then making sure it's all level with a level
    b. add desired volume of 1X TAE to a Erlenmeyer flask (for mini gel this is 70ml, for a midi gel this is 200ml)
    c. add agarose powder to the TAE for a final concentration of 1.5% (w/v) (for a mini gel this is ~1g, for a midi gel this is 3g)
    d. place a kimwipe or paper towel into the mouth of the flask and microwave the agarose until it has COMPLETELY melted. Usually ~3min, swirl flask every minute to mix. At the end, confirm there are no unmelted pieces within the solution – it should have no particles floating in it. microwave more as needed.
    e. add SYBR safe DNA stain to the melted agarose to 1x volume (7µl for mini gel, 20µl for midi gel). Swirl flask gently until stain is well mixed – be sure to avoid creating bubbles
    f. gently pour the agarose into the prepared gel casting tray making sure to avoid bubbles. If bubbles to form, try to remove them or at least move them to the sides using a pipette tip. Bubbles around the comb can be a particular problem.

g. Cover the gel *loosely* with Al foil to avoid light exposure (do not seal it! this is just to protect it from light but you want it to cool as if the foil was absent)
h. let agarose gel solidify for 45min-90min

2. Prepare samples
    a. Thaw an aliquot of 25bp and 50bp DNA ladder
    b. Dilute PCR products into 2X diluted sample buffer and mix thoroughly
        i. If running PCR products prepared from high-quality DNA, run 5-10µl of PCR product per lane. Be sure to save 5µl of PCR product for Bioanalyzer analysis if desired. If you are not running a bioanalyzer, its best to use more PCR product in the gel as the bands are not always bright.
        ii. If running PCR products prepared from Squash Method DNA preps, run 10-20µl of PCR product per lane
3. Run Gel
    a. Prepare gel running equipment
        i. Gently remove comb from the solidified gel
        ii. Place gel into the electrophoresis tank and add 1x TAE until it covers the top of the gel
    b. Add 5µl of each DNA ladder and 10-20µl of prepared PCR products per lane into the pre-determined lanes, being sure to keep track of which samples are in which lanes
    c. run the gel
        i. put the lid onto the electrophoresis tank paying special attention to the position of the electrodes. The black/negative electrodes at the top and the red/positive electrodes at the bottom.
        ii. Plug the electrodes into a power-source, again paying special attention to the position of the electrodes – black-to-black and red-to-red.
    d. run the power supply at 100V for 40-75min until the blue indicator dye is ~2/3 of the way down the gel. DO NOT OVERRUN THE GELS AS THIS REDUCES TO SIGNAL STRENGTH. YOU CAN ALWAYS STOP THE GEL, CHECK IT ON THE UV IMAGER AND RUN IT MORE IF NEEDED TO GET SEPERATION OF BANDS.
4. Image the gel using the UV imager. The Bonini lab imager is significantly better for seeing these PCR products as they can be faint. Other imagers don't always work. Also, be prepared to look visually at the gel and to play around with exposure if bands are faint. If needed, you can soak the gel in 1X SYBR Safe DNA stain in TAE buffer for 10min and reimage.
5. Estimate the size of the PCR product(s) based on the DNA ladders. Calculate the # of repeats present
    a. For UAS-G4C2 lines: [(PCR product length) – (49bp of non-G4C2 sequence)] ÷ 6 = X
    b. For UAS-LDS-G4C2[GA-GFP] lines: [(PCR product length) – (203bp of non-G4C2 sequence)] ÷ 6 = X

c. For UAS-LDS-G4C2[GR-GFP] lines: [(PCR product length) – (205bp of non-G4C2 sequence)] ÷ 6 = X

Calculate repeat length: Bioanalyzer

1. add 1µl of PCR products to 4µl MilliQ water in pre-labeled PCR tubes. Samples can be stored at -20^{o}C until you've accumulated a whole chip's worth of samples. Keep the remaining 4µl of the PCR product for future use. You may need to resubmit samples at a higher concentration.
2. Submit samples to the CHOP DNA core for analysis using the Agilent DNA 1000 chip/protocol.
3. From the PCR product lengths reported by the Bioanalyzer, calculate the # of repeats present
    a. For UAS-G4C2 lines: [(PCR product length) – (49bp of non-G4C2 sequence)] ÷ 6 = X
    b. For UAS-LDS-G4C2[GA-GFP] lines: [(PCR product length) – (203bp of non-G4C2 sequence)] ÷ 6 =
    c. For UAS-LDS-G4C2[GR-GFP] lines: [(PCR product length) – (205bp of non-G4C2 sequence)] ÷ 6 = X

RNA extraction (flies)

Total RNA extraction (Trizol)

NOTES: Typical yield for fly heads with 20min incubation at RT for step 11

Yield	
	total ng/head
mean	531
median	496
min	423
max	721

REAGENTS/MATERIALS

- Tissue
  - Use 5-10 whole larvae or flies per sample
  - Use 20-30 fly heads per sample
- Trizol
- Isopropanol
- 75% ethanol (200 proof ethanol + MilliQ water)
- DEPC-treated water
- RNaseZAP
- Ambion RNase free 1.5 mL microcentrifuge tubes (Thermo Sci # AM12400)
- RNase-free pellet/pestle disposable blue microcentrifuge tubes (Fisher Sci # 12-141-368)
  - Alternative: the standard pellet/pestle disposable blue microcentrifuge tubes (Kimble # 749520-0000) can be used if the bag is maintained for RNA work
- pellet/pestle cordless motor (Kimble # 749540-0000)
- RNaseZap (Thermo Sci # AM9780)
- Filtered pipette tips

PROTOCOL

1. Prepare an RNase-free work space:
   a. Place a clean piece of plastic wrap on counter of your work station
   b. Spray pipettes with RNaseZAP
   c. Obtain filtered pipette tips
   d. In general, it is good practice to spray hands with RNaseZAP after touching non-treated surfaces (like centrifuges) and to exchange gloves periodically, never grabbing them by the fingertips.
2. Using mortar & pestle, homogenize tissue in 100µl Trizol extraction buffer in blue microcentrifuge tubes.
   * if using frozen tissue, keep on dry ice until adding Trizol
3. Add an additional 900µl Trizol and vortex.
4. Repeat for all samples and then incubate at RT for 5min allowing complete dissociation of the nucleoprotein complex (so some samples will have sat longer than 5min. This does not seem to effect results.)
   * homogenate can be stored at -80 C for 1mo. To thaw, place at RT for

5-10min until have equilibrated fully.

5. Add 200µl chloroform to each tube (in the hood)
6. Vortex for 20sec and incubate at RT for 2-3min.
   * With some samples, the cuticle ends up separating into the aqueous portion during this time. If this occurs, re-vortex.
7. Centrifuge for 15min at 15000xg, 4°C. (treat rotor with RNase-Zap before use if not using a RNA-designated centrifuge)
8. Prep: label RNase-free microcentrifuge tubes
9. Immediately, gently remove tubes from centrifuge. Remove upper aqueous phase while avoiding the organic layer or lower red phenol-chloroform phase. Put into fresh tube, pre-labeled with sample name.
   * Usually remove ~450ul and leave ~50ul of aqueous layer so as to avoid the other layers.
10. Add equal volume of 100% isopropanol (or more). Turn tube upside down 40-60X to mix.
    * Usually add ~600-650µl isopropanol
    ** Do not vortex as this breaks RNA strands and can result in degraded sample
11. Incubate RNA in isopropanol
    a. For whole animals: incubation at RT for 20min is sufficient
    b. For fly heads: store samples overnight at -80°C to increase yield (must become frozen for a significant effect)
19. Centrifuge tubes at 12,000xg for 20min. Remove supernatant by pouring it into a waste container – be sure to keep the tube inverted (!) and dab the edge on clean paper towel to remove excess supernatant. Pellet may be loose so use caution not to lose it during pouring off supernatant.
12. Wash pellet by adding 1ml 75% EtOH and turn tubes upside down a couple of times until pellet detaches from side of tube. If pellet does not detach, use a P-20 pipet to gently knock it lose.
13. Centrifuge at 7500xg for 5min (4°C). Remove supernatant by pouring it into a waste container – be sure to keep the tube inverted (!) and dab the edge on clean paper towel to remove excess supernatant. Pellet may be loose so use caution not to lose it during pouring off supernatant.
14. Repeat EtOH wash and centrifugation. Remove supernatant.
15. Centrifuge tubes briefly to collect residual supernatant to the bottom. Carefully pipet off residual EtOH using P20 or P200 pipet. Do not touch the pellets.
16. Dry pellets at room temperature for ~2-3min
17. Add 2µl DEPC-water per whole animal or 0.5µl DEPC-water per head (total 10-50ul) and incubate at RT for 5-10min.
18. Resuspend pellet by pipetting and place on ice.
    * pellets should dissolve completely. Add more DEPC water if necessary.

1. (optional) perform DNase treatment (below). DNase treatment is not needed for Northerns but is good practice for qRT-PCR particularly if primers do not span exons.
2. Assess RNA concentration and quality by nanodrop and by gel (optional).
3. Store samples at -80°C.

DNase Treatment

REAGENTS/MATERIALS

- Turbo DNA free kit (Ambion AM1907)
- Microcentrifuge tubes

PROTOCOL

1. Prepare an RNase-free work space:
    a. Place a clean piece of plastic wrap on counter of your work station
    b. Spray pipettes with RNaseZAP
    c. Obtain filtered pipette tips
    d. In general, it is good practice to spray hands with RNaseZAP after touching non-treated surfaces (like centrifuges) and to exchange gloves periodically, never grabbing them by the fingertips
2. Add 0.1 volume 10X TURBO DNase Buffer and 1ul TURBO DNase to the RNA, and mix gently.
    Tip: You can make a master mix of 10X TURBO DNase Buffer and TURBO DNase.
3. Incubate at 37°C for 20–30 min.
4. Add resuspended DNase Inactivation Reagent (0.1 volume) and mix well.
5. Incubate 2-5 min at room temp, mixing occasionally.
6. Centrifuge at 10,000 x g for 1.5 min and transfer the RNA to a fresh, pre-labeled microcentrifuge tubes tube.
7. Assess RNA concentration and quality (below)

Assessing RNA quality

1. If samples are frozen, thaw them on ice and mix by tapping the side of the tube. (Do not vortex as this can break RNA strands.)
2. Measure concentration by Nanodrop. A260/280 ratio should be around 2.0.
    Note: A260/230 ratios maybe <2.0 due to trizol contamination. This does not seem to affect qRT-PCRs or northerns.

a. Normalize the concentration of the RNA so all samples are the same (typically 200ng/µl)

3. (optional) run samples on a gel
    i. When learning how to get outstanding quality RNA, run ~0.5-1µg/lane of RNA on a 1% Agarose TBE gel (use RNase free water. Ideally DEPC-treated water, but Millipore water should also work).
4. (optional) run samples on a Bioanalyzer to confirm outstanding quality using Agilent RNA 6000 Nano Kit. Please note that this is very sensitive.

qRT-PCR (SYBR Green)

DNA Primer design

IDEAL PRIMERS

- are 19-21bp long
- For RNA expression studies: are exon spanning (so selective for RNA/cDNA in case there's contaminating genomic DNA)
- produce 50-100bp products (can go up to 200bp if necessary)
- are specific to your target gene (are not predicted to produce < 500bp product from an off-target gene)
- are not predicted to form primer-dimers

PROTOCOL

1. Look up gene sequence on Flybase or NCBI. It's nice to use the CDS sequence.
2. Copy sequence into Primer3: http://bioinfo.ut.ee/primer3-0.4.0/.
    a. I usually set product to 50-150bp. If this doesn't return primers than you can go up to 200bp for qPCR
    b. I typically buy 2 exon spanning primer sets to test. And then after checking their melt curves and running them on a gel, I pick the best set for my studies.
3. For RNA expression studies: check if primers are exon spanning
    a. (best approach) input primer sequences into http://projects.insilico.us/SpliceCenter/PrimerCheck.jsp with the gene target.
    b. Check primers against the total gene sequence to see which ones span an exon.
        i. For flies, go to flybase.com and click on "Get genome region"
        ii. For human, use NCBI's website
4. To confirm primer specificity, input primers into https://www.ncbi.nlm.nih.gov/tools/primer-blast/ . Be sure to select the right species.

- Alternative approaches:
    - Look up publication which have done qPCR for your target. They should publish their primer sequences in the methods section.
    - Look up the gene on Applied Biosystem's website and copy their forward and reverse primers for you target that they designed for Taqman. Taqman also uses a probe, which you don't use w/ Sybr Green but the same primers should work for both assays.
        - http://www.thermofisher.com/us/en/home/life-science/pcr/real-time-pcr/real-time-pcr-assays/taqman-gene-expression.html
- If you need to take the reverse complement for the reverse primer -- http://reverse-complement.com/

cDNA preparation

NOTES

- I find it convenient to prepare cDNA in PCR plates to keep them well organized and labeled. However, for small numbers of samples, PCR strips may be better.
- I tend to organize data so the RNA prep is the first tab of an excel worksheet. Then the cDNA prep is the following tab, then a tab for the qRT-PCR plate setup and a final tab for results. Additional qRT-PCR experiments on the same RNA/cDNA preps will be added as additional tabs so everything is together.

REAGENTS/MATERIALS

- Total RNA samples (*see General Protocols: RNA extraction (flies) or Fibroblasts: RNA extraction*)
    - DNase-treated RNA is recommended at all times
    - DNase-treated RNA is required if your primers are not exon spanning
- High-Capacity cDNA Reverse Transcription Kit (Applied Biosystems # 4368814)
- RNaseZap (Thermo Sci # AM9780)
- RNase-free PCR tubes or plates
- RNase-free Microcentrifuge tubes
- Filtered pipette tips
- MilliQ water

SUPPLEMENTARY FILE: cDNA prep.xlsx

PROTOCOL

1. Prepare an RNase-free work space:
    a. Place a clean piece of plastic wrap on counter of your work station
    b. Spray pipettes with RNaseZAP
    c. In general, it is good practice to spray hands with RNaseZAP after touching non-treated surfaces (like centrifuges) and to exchange gloves periodically, never grabbing them by the fingertips.
2. Thaw on ice: RNA samples, 10X RT buffer, 10X RT Random Primers, 25X dNTP mix.
3. (recommended) Update the cDNA prep supplementary file with relevant information: experiment purpose and sample details, # samples, plate template. Print the excel sheet for use at bench.
4. Prepare a master mix using filtered pipette tips
    a. For 10ul/reaction

	Master mix (µl)
10× RT Buffer	1
10× RT Random Primers	1

25× dNTP Mix (100 mM)	0.4
Reverse Transcriptase	0.5
Total RNA (200-400ng)	(up to 7.1µl)
MilliQ water	(to 10µl final volume)

b. For 20ul/reaction

	Master mix (µl)
10× RT Buffer	2
10× RT Random Primers	2
25× dNTP Mix (100 mM)	0.8
Reverse Transcriptase	1
Total RNA (200-400ng)	(up to 14.2µl)
MilliQ water	(to 20µl final volume)

c. Notes:
   i. add the reverse transcriptase last, making sure it stays close to -20°C
   ii. it is vital to mix thoroughly
   iii. Controls:
      1. No template (water) control: add water in place of template RNA, tests if there is contaminants in reagents and if primers can react together (primer dimers)
      2. No Reverse Transcriptase control: add template RNA but no enzyme, tests if there is DNA contamination and if primers amplify DNA

5. Aliquot master mix and RNA samples into a pre-labeled PCR strip or plate using filtered pipette tips.
6. Run cDNA reactions on a thermocycler, making sure the lids are completely closed on samples.

Step	**Temperature**	**Time**
initiation	25 °C	10 min
cDNA reactions	37 °C	120 min
denaturation	85 °C	5min

Cooling	4 °C	Hold

7. (optional) Dilute cDNA 1:10 by adding MilliQ water. Vortex tubes to mix samples thoroughly. Centrifuge to collect samples to bottom of tubes.
    - If target gene is lowly expressed, you may not want to dilute cDNA. In this case, it'll likely be necessary to increase reaction volumes to 20ul so you have enough sample for analysis
8. cDNA can be stored at -20^{o}C for future use. When thawing samples, be rigorous about making sure they are fully mixed. This is a common source of variability during qRT-PCR.

Primer optimization

NOTES

- Variables that we typically change when optimizing new primers
    - Amount of template added
    - Amount of primer added (can go as low as 0.05µM). this typically reduces the presence of primer dimers
- Useful websites for troubleshooting qRT-PCR
    - https://www.slideshare.net/idtdna/understanding-melt-curves-for-improved-sybr-green-assay-analysis-and-troubleshooting
    - https://www.sigmaaldrich.com/technical-documents/articles/biology/troubleshooting.html
    - https://toptipbio.com/calculate-primer-efficiencies/

REAGENTS/MATERIALS

- For RNA expression studies: cDNA prepared from samples expressing the target gene (typically RNA prepared from whole larvae or flies can work while this avoids any variability in tissue-specific expression)
- Forward and Reverse primers for target gene
- Forward and Reverse primers for 1-3 housekeeping gene(s)
- SYBR Green Fast Master Mix (Applied Biosystems # 4385612)
- Microcentrifuge tubes
- Fast optical qRT-PCR plates (384- or 96-well)
- MilliQ water

SUPPLEMENTARY FILE: qRT-PCR primer optimization.xlsx

PROTOCOL

1. If not done yet, resuspend primers in MilliQ water to 100µM and prepare a 1:10 dilution for a 10µM working stock.
    a. Briefly centrifuge tubes containing lypholized primer to pellet.

b. Add the appropriate amount of MilliQ water to make a 100µM Master Stock: multiply the # nmol value by 10. For example: if the nmol value is 38.2, then you will be adding 382µl MilliQ water.
c. Replace caps on tubes and vortex on a medium speed. Vortex the top and the bottom of the tube. Briefly centrifuge to collect solution to the bottom of the tube and incubate for 5-10min to fully resuspend primer.
d. Make a 1:10 dilution for a 10µM working stock by adding 20µl of 100µM primer to 180µl MilliQ water into a pre-labeled microcentrifuge tube. This is what you will use for qRT-PCR reactions.
e. Store the 100µM master stock and the 10µM working stock at -20°C for future use. Thaw on ice.

2. (recommended) Update the qRT-PCR primer optimization supplementary file with relevant information. Print the excel sheet for use at bench.
3. Prepare a master mix and serial dilutions for your samples in a qRT-PCR optical plate. When done, seal the plate with optical film.
    a. Standard 10ul reaction

	µl	Final concentration
SYBR Fast mix (2X)	5	1X
Forw Primer (10uM)	0.5	0.5µM
Rev Primer (10uM)	0.5	0.5µM
template	1-4	Varies
MilliQ water	(to 10µl final volume)	

    b. Notes:
        i. Typical serial dilutions are 1:2 of your template + master mix into a qRT-PCR plate. Run 3-5 dilutions so you can calculate primer efficiency accurately.
        ii. Be sure to include a no template (water) control and a housekeeping gene to make sure the template is good
        iii. Typically we run all reactions in duplicate or triplicate
        iv. Avoid wells on the edge of the qRT-PCR plate, leaving a 2-well barrier, when possible
4. Centrifuge qRT-PCR plate to collect sample to the bottom of the tubes.
5. Run qRT-PCR reactions on a real-time thermocycler
    a. Turn on machine and lobin to ABI software. It maybe necessary to restart the computer and/or the machine.
    b. Go to “Set up” and select “Fast 384-well block”, “comparative CT”, “SYBR Green”, “Fast”. Check the item: include melt curve. Select “standard curve” in experiment properties
    c. Go to define
        i. enter primer (targets) names
        ii. Enter sample names
    d. Go to Assign

i. choose “define and set up standard”
ii. Enter # of point
iii. # replicate wells (Repeats)
iv. Start quantity: 1
v. Select correct serial dilution

e. click next and change reaction volume to 10ul
f. Put qRT-PCR plate into the machine. Be careful there’s nothing will be hit by the plate and the position of the plate is correct). Save and press Run

6. Analyze curves within the software
    a. Run software analysis:
        i. Select the target for this standard curve one by one. Select wells Apply Close
        ii. Go to “Analysis” Standard curve
        iii. Select all needed samples analyze
        iv. Go to “Analysis setting”, “Standard curve setting” to check slopes, which should be ~-3.7.
    b. Look closely at the melt curves for anything abnormal. You want to see 1 strong peak in samples containing template and no peaks in no template controls and no RT controls (if you ran these). Small peaks to the left of the strong peak are typically primer dimers and should be avoided if possible.
    c. Look closely at the amplification curves for anything abnormal. You want the replicate wells to be on top of each other and the serial dilutions to be obvious as you look at the different samples. Curves should be between Ct values of 16 to 30. Typically, anything after 32 is considered noise (no template controls tend to amplify at this point).
    d. Select the best c/DNA dilution for your primers - want a Ct value around 20-22.
    e. Export the data and save it for your records

    Notes:

    - It is appropriate to manually adjust the threshold if the auto-threshold for a primer set is not at the best position. You want the threshold to be within the linear region of the amplification curves and high enough to avoid any noise.
    - By running a couple of wells for a housekeeping gene, you can control for any technical issues not related to the specific primers. For example, if there are no curves in these wells, then there may be something wrong with your c/DNA or your SYBR green master mix.

7. (optional) calculate the primer efficiency in excel using the Ct values for each dilution. See supplementary file qRT-PCR primer optimization.xlsx.
8. (optional) run qRT-PCR products on a 1% TAE agarose gel to confirm that there is 1 PCR product and that it is at the expected size. Primer dimers will show up at the bottom of the well.

qRT-PCR Assays

NOTES

- Useful websites for understanding how to analyze qRT-PCR
  - https://dharmacon.horizondiscovery.com/uploadedfiles/resources/delta-cq-solaris-technote.pdf
  - https://bitesizebio.com/24894/4-easy-steps-to-analyze-your-qpcr-data-using-double-delta-ct-analysis/
  - https://toptipbio.com/delta-delta-ct-pcr/

REAGENTS/MATERIALS

- cDNA prepared from control and experimental samples
- 10µM working stocks of DNA primers *(see primer optimization)*
  - Forward and Reverse primers for target gene(s)
  - Forward and Reverse primers for 1-3 housekeeping gene(s)
- SYBR Green Fast Master Mix (Applied Biosystems # 4385612)
- Microcentrifuge tubes
- Fast optical qRT-PCR plates (384- or 96-well)
- MilliQ water

SUPPLEMENTARY FILE: qRT-PCR.xlsx

PROTOCOL

1. Thaw: primers and cDNA samples on ice. cDNA samples need to be vigorously mixed before use as the samples tend to become heterogonous. Typically, vortex and spin samples 2-3 times before use.
2. (recommended) Update the qRT-PCR supplementary file with relevant information. Print the excel sheet for use at bench.
3. Prepare a master mix for each of your target genes and pipette the master mix then your samples into a qRT-PCR optical plate at the correct volumes. When done, seal the plate with optical film.
   a. Standard 10ul reaction

	µl	Final concentration
SYBR Fast mix (2X)	5	1X
Forw Primer (10uM)	0.5	0.5µM
Rev Primer (10uM)	0.5	0.5µM
cDNA template	1-4	Varies
MilliQ water	(to 10µl final volume)	

   b. Notes:

i. Be sure to include a no template (water) control for each primer set
ii. Typically we run all reactions in duplicate or triplicate
iii. Avoid wells on the edge of the qRT-PCR plate, leaving a 2-well barrier, when possible
iv. Pipette master mixes then cDNA samples: Its best to pipette duplicate or triplicate wells and replicate cDNA samples at the same time to avoid unnecessary variability

4. Centrifuge qRT-PCR plate to collect sample to the bottom of the tubes.
5. While plate spins, setup the experiment on the real-time thermocycler
    a. Turn on machine and login to ABI software. It may be necessary to restart the computer and/or the machine.
    b. Go to "Set up" and select "Fast 384-well block", "comparative CT", "SYBR Green", "Fast". Check the item: include melt curve.
    c. Go to define
        i. enter primer (targets) names
        ii. Enter sample names
    d. Go to Assign
        i. Assign sample names to appropriate wells
        ii. Assign targets to appropriate wells
    e. click next and change reaction volume to 10ul
    f. Put qRT-PCR plate into the machine. Be careful there's nothing will be hit by the plate and the position of the plate is correct). Save and press Run
6. Analyze curves within the software
    a. Look closely at the melt curves for anything abnormal. You want to see 1 strong peak in samples containing template and no peaks in no template controls and no RT controls (if you ran these). Small peaks to the left of the strong peak are typically primer dimers and should be avoided if possible.
    b. Look closely at the amplification curves for anything abnormal. You want the replicate wells to be on top of each other. Curves should be between Ct values of 16 to 30. Typically, anything after 32 is considered noise (no template controls tend to amplify at this point).
    c. (optional) manually adjust the threshold if the auto-threshold for a primer set is not at the best position. You want the threshold to be within the linear region of the amplification curves and high enough to avoid any noise.
    d. Export the data and analyze in excel on your computer
7. Analyze data in excel using the ΔΔCt method
    a. Import the data
    b. Take mean of replicate wells
    c. For each sample, calculate $\Delta Ct = (\text{Mean Ct})_{\text{gene-of-interest}} - (\text{Mean Ct})_{\text{housekeeping gene}}$
        - If using multiple housekeeping genes: $(\text{Mean Ct})_{\text{housekeeping gene}}$ will = average[$(\text{Mean Ct})_{\text{housekeeping gene 1}}$, $(\text{Mean Ct})_{\text{housekeeping gene 2}}$, $(\text{Mean Ct})_{\text{housekeeping gene 3}}$]
    d. Calculate $\Delta\Delta Ct = (\Delta Ct)_{\text{treated}} - (\Delta Ct)_{\text{control}}$
        - Examples of "treated"

- RNAi to gene-of-interest to be compared to control sample (not expressing a RNAi or expressing a control RNAi)
- Animals expressing a disease gene to be compared to control sample (not expressing a disease gene or expressing a control gene)

▪ If you have technical replicate samples (3 samples collected in parallel) then $(\Delta Ct)_{control}$ will = average [$(\Delta Ct)_{control\ 1}$, $(\Delta Ct)_{control\ 2}$, $(\Delta Ct)_{control\ 3}$]

▪ $(\Delta Ct)_{control}$ is the sample that everything is relevant. The ΔΔCt for this sample should be 0: $\Delta\Delta Ct = (\Delta Ct)_{control} - (\Delta Ct)_{control}$. If you are using technical replicate samples, then calculate ΔΔCt the same way you calculate it for the treated samples. This will result in an average ΔΔCt of 0 for the technical replicates while individual points can be above or below 0.

e. Calculate the Fold Change = 2 ^(- ΔΔCt).
   ▪ For control(s) this should equal 1.

f. Report Fold Change as a bar graph, using the average Fold change between technical replicates when applicable.

8. (optional) run qRT-PCR products on a 1% TAE agarose gel to confirm that there is 1 PCR product and that it is at the expected size. Primer dimers will show up at the bottom of the well.

Optimized Primers

	Target	Species	Assay	Forward Primer (5'-3')	Reverse Primer (5'-3')	spans exons	µM primers	cDNA dilution*	Ref.
	Housekeeping genes								
	Actin5C	*Dmel.*	qRT-PCR; ChIP	CGAAGAAGTTGCTGCTCTGGTTGT	GGACGTCCCACAACGATGGGAAG	N	0.5	1:100	[1]
	PGK	*Dmel.*	qRT-PCR; ChIP	ATCACCAGCAACCAGAGAATTG	TGCCAGGGTGTACTGATGTT	N	0.5	1:100	
Main	*RP49 (RpL32)*	*Dmel.*	qRT-PCR	TGTCCTTCCAGCTTCAAGATGACCATC	CTTGGGCTTGCGCATTTGTG	Y	0.5	1:100	[2]
	RpS20	*Dmel.*	qRT-PCR	CCGCATCACCCTGACATCC	TGGTGATGCGAAGGGTCTTG	Y	0.5	1:100	[3]
	βTub56D	*Dmel.*	qRT-PCR	CATCCAAGCTGGTCAGTG	GCCATGCTCATCGAGAT	Y	0.5	1:100	[4]
	βTub56D	*Dmel.*	ChIP	GCAGTTCACCGCTATGTTCA	CACCAGATCGTTCATGTTGC	N	0.5	n/a	[5]

	ACTB	*Hsap.*	qRT-PCR	CATGTACGTTGCTATCCAGGC	CTCCTTAATGTCACGCACGAT	N	0.5	1:100	
Main	*GAPDH*	*Hsap.*	qRT-PCR	GTTCGACAGTCAGCCGCATC	GGAATTTGCCATGGGTGGA	Y	0.5	1:100	
	RPLP0	*Hsap.*	qRT-PCR	TCTACAACCCTGAAGTGCTTGAT	CAATCTGCAGACAGACACTGG	Y	0.5	1:100	[6]
	Intergenic sequences								
	Il171a (2L)	*Dmel.*	ChIP	GTTGGAGAAACTAAGAGCC	CCATACTCAATCGGACC	n/a	0.5	n/a	[7]
	GenBank: AC277990.1	*Hsap.*	ChIP	CCAACTGGGTGCTGCCTAGA	AGGGTGCCCATCACAGATGG	n/a	0.5	n/a	[8]
	Endogenous targets								
dPAF1C	*Atms (dPaf1)*	*Dmel.*	qRT-PCR	CCAAAGCTTCCAAGGGCTAC	CGATAGCGCTGCATACGATG	Y	0.5	1:20	[5]
	Atu (dLeo1)	*Dmel.*	qRT-PCR	ACGGCTGATCGACACTGATA	TGGCTCTCGACTTTATCCCG	Y	0.5	1:20	[5]
	Ctr9	*Dmel.*	qRT-PCR	ATTGCGCACGTTTATGTCGA	GACGGGCCTTAAGTAGCACT	N	0.5	1:20	[5]
	CG3909 (dWdr61)	*Dmel.*	qRT-PCR	AGTTGCGCCACAAACTAAAAGG	GCAATGGTCTGTCCATCGGAA	Y	0.5	1:20	[5]
	CDC73	*Dmel.*	qRT-PCR	AGCGTGAAGACCAACTATCTCA	CGCACGTAGACCGAGTGTT	Y	0.5	1:20	[5]
	Rtf1	*Dmel.*	qRT-PCR	CGGACGCAATCCCTGATCG	CCGTTTGGGGCTTCTTTCG	Y	0.5	1:20	[5]
Stress genes	*Chord*	*Dmel.*	qRT-PCR	TATTTCCCGAGCAGGACAAC	TTGCATTGCTCACATTCACA	Y	0.5	1:40	[9]
	Fkbp59	*Dmel.*	qRT-PCR	GCTCCAAACTACGCTTACGG	TGGTTGGGACTCAAATCCTC	Y	0.5	1:40	[9]
	HSF	*Dmel.*	qRT-PCR	ATCGCTTGATTTGCTGGACC	GAAGCTGGCCATGTTGTTGT	Y	0.5	1:40	[9]
	HSP27	*Dmel.*	qRT-PCR	GGCCACCACAATCAAATGTCAC	CTCCTCGTGCTTCCCCTCTACC	N	0.5	1:40	[3]

	DnaJ-1 (dHSP40)	*Dmel.*	qRT-PCR	GAGATCATC AAGCCCACC ACAAC	CGGGAAACT TAATGTCGA AGGAGAC	N	0.5	1:40	[3]
	HSP68	*Dmel.*	qRT-PCR	GAAGGCACT CAAGGACG CTAAAATG	CTGAACCTT GGGAATAC GAGTG	N	0.5	1:40	[3]
	HSP70	*Dmel.*	qRT-PCR	GGCACCTG CTGGCAAAT T	CGGATAGTG TCGTTGCAC TTGT	N	0.5	1:40	[9]
	HSP83	*Dmel.*	qRT-PCR	GGACAAGG ATGCCAAGA AGAAGAAG	CAGTCGTTG GTCAGGGAT TTGTAG	N	0.5	1:40	[3]
	Stip1	*Dmel.*	qRT-PCR	TGGCCTAAG GGTTACTCA CG	GCATTCGTG GGATCGTAC TT	Y	0.5	1:40	[9]
	Stv	*Dmel.*	qRT-PCR	GTACGCCTA CCTGG CGAGA	CAACTGCAC CTGTGTCAA CC	Y	0.5	1:40	[9]
candidate RANT factors	*eIF2B*	*Dmel.*	qRT-PCR	CGATGGCC AAAAAGAAG AAG	ACCAGGTTG AGCTGTTGT CC	Y	0.5	1:20	
	eIF3i	*Dmel.*	qRT-PCR	GACCATCAT CACAG TCACG	TCCTTGCTC AACTGCATG TC	Y	0.5	1:20	
	eIF4A	*Dmel.*	qRT-PCR	GCAGGAGA ACTGGAAAC TGG	ACATCTCCT GGGTCAGTT GG	Y	0.5	1:100	
	eIF4B	*Dmel.*	qRT-PCR	CGCATTGAG CTATCGAAT GA	CCAATTTCC GGAATCCCT AT	N	0.5	1:20	[10]
	eIF4H1	*Dmel.*	qRT-PCR	GGGAAACG GATCAGTTC AAA	CTTCTGGAA ACCGTCTCT GC	Y	0.5	1:20	[10]
	eIF4H2	*Dmel.*	qRT-PCR	CCACTCGAG GTGGTTTCA AT	ATAGTTGCC GCCTCCATT TA	Y	0.5	1:20	
	eIF5: variants A-G	*Dmel.*	qRT-PCR	GACGCTGTT CGATCACAA GA	CTCGGGGC ATAACACAA ACT	Y	0.5	1:20	
	eIF5B	*Dmel.*	qRT-PCR	GTTCGTTGG AGGCTCTTC TG	CCTCGTGTT CCAACATTG TG	Y	0.5	1:20	
	eIF5C: variants A-G	*Dmel.*	qRT-PCR	TCAAGCAAG AGAAGGGC ATT	TTGTTCGGT GGGAAAAA GTC	Y	0.5	1:20	
	Rpb1	*Dmel.*	qRT-PCR	CGTCAGAC GTTCGAGAA	TGTTGACCC ACACAAGCA	Y	0.5	1:100	

				CAA	AT				
	Rps25	*Dmel.*	qRT-PCR	GTCTCCGAGCGTCTGAAGAT	GCTTGATCAGACCCTTCTCG	Y	0.5	1:100	
C9orf72	*C9: intron 1*, 3' of repeat	*Hsap.*	qRT-PCR, ChIP	CCTGATAGGAGATAACAGGATTCCAC	CGACATCACTGCATTCCAACTGTC	N	0.5	2:5	[11]
	C9: intron 1, 5' of repeat	*Hsap.*	qRT-PCR	GCAAGAGCAGGTGTGGGTTTAG	CCTCAGCGAGTACTGTGAGAGC	N	0.5	2:5	[11]
	C9: Total (V1-3)	*Hsap.*	qRT-PCR	AACTGGAATGGGGATCGCA	CTGATCTTCCATTCTCTCTGTGCC	Y	0.5	2:5	[6]
	C9: variant 1	*Hsap.*	qRT-PCR	CCACGTAAAAGATGACGCTTGATA	TGGGCAAAGAGTCGACATCA	Y	0.5	2:5	[6]
	C9: variant 2	*Hsap.*	qRT-PCR	CGGTGGCGAGTGGATATCTC	TGGGCAAAGAGTCGACATCA	Y	0.5	2:5	[6]
	C9: variant 3	*Hsap.*	qRT-PCR	GCAAGAGCAGGTGTGGGTTT	TGGGCAAAGAGTCGACATCA	Y	0.5	2:5	[6]
RANT factors	*EIF4B*	*Hsap.*	qRT-PCR	AGCTCAGACACAGAGCAGCA	CTTTCCTTCCTGGTCCTTCC	Y	0.5		[10]
	EIF4H	*Hsap.*	qRT-PCR	GGTGGCTTTGGATTCAGAAA	CCCTGAAGCCAGAATTGAAG	Y	0.5		[10]
hPAF1C	*CDC73*	*Hsap.*	qRT-PCR	GGGGCACTGCAATTAGTGTT	CTGCACAAAAACGGCTACAA	Y	0.5	1:20	[5]
	LEO1	*Hsap.*	qRT-PCR	CAAGTGGTCAGATGGAAGCA	TGGGGCTTTGTACACATCAA	Y	0.5	1:20	[5]
	PAF1	*Hsap.*	qRT-PCR	CCACTGAGTTCAACCGTTATGG	TCCTCGGTAAACTGCTGCTTC	Y	0.5	1:20	[5]
	RTF1	*Hsap.*	qRT-PCR	GGTGTCACATGCCCTTCTTT	GTAATCTCAGCGACCCGGTA	Y	0.5	1:20	[5]
	p21	*Hsap.*	Leo1 ChIP	CCAGGAAGGGCGAGGAAA	GGGACCGATCCTAGACGAACTT	N	0.5	n/a	[12]
	SUPT4H1	*Hsap.*	qRT-PCR	TTGCGATGATGAGTCCAGAG	TGGATTTGTAGGCCACTCCT	Y	0.5	1:20	[6]
	UAS transgenes								

LDS-G4C2: 5' LDS	*Dmel.*	qRT-PCR	CGCTGAGGGTGAACAAGAA	CGACTCCTGAGTTCCAGAGC	n/a	0.5	1:100	
LDS-G4C2: 3' GFP tag	*Dmel.*	qRT-PCR	ACGTAAACGGCCACAAGTTC	AAGTCGTGCTGCTTCATGTG	n/a	0.5	1:100	[5]
GFP tag: mCD8	*Dmel.*	qRT-PCR	TATGGCTTCATCCCACAACA	GACTGGCACGACAGAACTGA	n/a	0.5	1:100	
G4C2	*Dmel.*	qRT-PCR; ChIP	AGACTCGGTACCGGATCCTC	GCTCCCATTCATCAGTTCCA	n/a	0.05	1:100	[5]
TDP-43	*Dmel.*	qRT-PCR	TGTCTTCATCCCCAAGCCAT	TGTGCTTAGGTTCGGCATTG	n/a	0.5	1:100	[13]

* cDNA dilution: the final concentration of cDNA added to the qRT-PCR reaction (e.g. 2:5 = 4µl of undiluted cDNA added to a 10µl reaction; 1:100 = 1µl of cDNA that had been diluted 1:10 and added to a 10µl reaction)

REFERENCES

1. Petersen AJ, Rimkus SA, Wassarman DA. ATM kinase inhibition in glial cells activates the innate immune response and causes neurodegeneration in Drosophila. Proc Natl Acad Sci. 2012;109:E656–64.

2. Gabler M, Volkmar M, Weinlich S, Herbst A, Dobberthien P, Sklarss S, et al. Trans-splicing of the mod(mdg4) Complex Locus Is Conserved Between the Distantly Related Species Drosophila melanogaster and D. virilis. Genetics. 2005;169:723–36.

3. Colinet H, Lee SF, Hoffmann A. Temporal expression of heat shock genes during cold stress and recovery from chill coma in adult Drosophila melanogaster. FEBS J. 2010;277:174–85.

4. McGurk L, Bonini NM. Protein interacting with C kinase (PICK1) is a suppressor of spinocerebellar ataxia 3-associated neurodegeneration in Drosophila. Hum Mol Genet. 2012;21:76.

5. Goodman LD, Prudencio M, Kramer NJ, Martinez-Ramirez LF, Srinivasan AR, Lan M, et al. Expanded GGGGCC repeat transcription is mediated by the PAF1 complex in C9orf72-associated FTD. Nature Neuroscience; accepted in principle; 2019.

6. Kramer NJ, Carlomagno Y, Zhang Y-J, Almeida S, Cook CN, Gendron TF, et al. Spt4 selectively regulates the expression of C9orf72 sense and antisense mutant transcripts associated with c9FTD/ALS. Science. 2016;353:708–12.

7. Li Z, Liu M, Zhang L, Zhang W, Gao G, Zhu Z, et al. Detection of intergenic non-coding RNAs expressed in the main developmental stages in Drosophila melanogaster. Nucleic Acids Res. 2009;37:4308–14.

8. Kim N, Sun H-Y, Youn M-Y, Yoo J-Y. IL-1β–specific recruitment of GCN5 histone acetyltransferase induces the release of PAF1 from chromatin for the de-repression of inflammatory response genes. Nucleic Acids Res. 2013;41:4495–506.

9. Mordes DA, Prudencio M, Goodman LD, Klim JR, Moccia R, Limone F, et al. Dipeptide repeat proteins activate a heat shock response found in C9ORF72-ALS/FTLD patients. Acta Neuropathol Commun [Internet]. 2018 [cited 2018 Nov 28];6. Available from: https://www.ncbi.nlm.nih.gov/pmc/articles/PMC6031111/

10. Goodman LD, Prudencio M, Srinivasan AR, Rifai OM, Lee VM-Y, Petrucelli L, et al. eIF4B and eIF4H mediate GR production from expanded G4C2 in a Drosophila model for C9orf72-associated ALS. Acta Neuropathol Commun. 2019;

11. Niblock M, Smith BN, Lee Y-B, Sardone V, Topp S, Troakes C, et al. Retention of hexanucleotide repeat-containing intron in C9orf72 mRNA: implications for the pathogenesis of ALS/FTD. Acta Neuropathol Commun [Internet]. 2016 [cited 2017 Dec 14];4. Available from: https://www.ncbi.nlm.nih.gov/pmc/articles/PMC4766718/

12. Kim TS, Liu CL, Yassour M, Holik J, Friedman N, Buratowski S, et al. RNA polymerase mapping during stress responses reveals widespread nonproductive transcription in yeast. Genome Biol. 2010;11:R75.

13. Chung C-Y, Berson A, Kennerdell JR, Sartoris A, Unger T, Porta S, et al. Aberrant activation of non-coding RNA targets of transcriptional elongation complexes contributes to TDP-43 toxicity. Nat Commun [Internet]. 2018 [cited 2018 Nov 28];9. Available from: https://www.ncbi.nlm.nih.gov/pmc/articles/PMC6199344/

Defining transgene expression

Heat-shock induced expression of UAS transgenes

HS-GAL4 FLY LINES

- BL1799/TM3 (*w[*];;GAL4-Hsp70/TM3,Sb*)
- BL2077/Cy (*w[*];GAL4-Hsp70/Cy;*) - the Cy phenotype is super weak even at 26°C. I recommend used BL1799

PROTOCOL

1. Setup crosses at 21°C. Setup crosses in bottles or if using vials, flip parents into fresh vials after 3d and again after 2d to increase # of progeny
    a. Controls to be run with every set of crosses: BL5905, UAS-mCD8-GFP
2. Collect newly eclosed progeny with the desired genotype and age to 1-2d at 21°C.
    a. It can be convenient to collect males for protein and females for RNA
    b. For every genotype, a minimum of 3 replicate samples are needed (5-10 animals per sample)
3. Heat-shock 1-2d progeny
    a. Turn on water bath to 37°C. Be sure to check the temperature with the same thermometer and to use the same water bath for all samples and all subsequent assays.
    b. Anesthetize animals on a CO2 pad and transfer 5-10 flies to a 1.5ml microcentrifuge tube for each sample. Be sure to label tubes with genotype, experiment date, gender, and any other pertinent information. Immediately, use a small piece of cotton to create a plug that will prevent flies from being above the waters surface during heat shock. It is vital that there are no crevasses that the flies can use to crawl above the waterline. Poke a hole in the top of the tube using a pushpin so there is an air-hole.
    c. Let animals recover for 30-45min from CO2.
    d. Heat shock flies at 37°C for 30 min.
    e. Transfer flies to a 25°C incubator and incubate for *exactly* 3 hours. Any deviations from this time will effect expression of the transgene!
    f. Immediately transfer tubes to dry ice to freeze the flies and then into a -80°C freezer. (can also flash-freeze them with LN2, but I didn't find this necessary as expression data in replicates were consistent.)
4. Isolate RNA and protein as needed for transgene analysis.
    a. Analyze protein expression by western blot (antibody needed)

b. Assays to analyze RNA expression

i. SV40 Northern blots (see General Protocols): use probes targeting the common SV40 terminal tail or probes designed to target your transgene. SV40 can be used for most pUAS transgenes.

ii. qRT-PCR (see General Protocols): use primers designed to target the UAS-G4C2 or UAS-LDS-G4C2 transgenes.

Note on SV40 and qRT-PCR: I have consistent data on DaGS > UAS transgenes showing that SV40 primers do not differentiate the pUAS transgene and Gal4 transgenes as both have SV40 terminal sequences. Importantly, the DaGS only sample had strong SV40 signal.

5. Compare RNA expression levels using Northern blots and SV40 probe or qRT-PCR using primers targeting the transgene

mRNA Northern blots

REAGENTS/MATERIALS

- Total RNA samples (*see General Protocols: RNA extraction (flies)*)
  - DNase treated is recommended at all times
- UltraPure Agarose (Invitrogen #16500-100)
- NorthernMax 10X Denaturing Gel Buffer, stored at 4°C (Thermo Sci #AM8676)
- NorthernMax 10x Running Buffer (MOPS), stored at 4°C (Thermo Sci #AM8671)
- RNA SYBR Green II stain, stored at -20°C (ThermoSci # S7564)
- RNA ladder:
  - 50-1000bp ladder (NEB # N0364S), stored at -80°C
  - 500-9000bp ladder (NEB # N0362S), stored at -80°C
  - Note: Must use their protocol and loading buffer for an accurate ladder
- Whatman 3MM chromatography sheets, 18 x 34cm, thickness: 0.34mm (GE Whatman #3030-221)
- NorthernMax Transfer Buffer, stored at RT (Thermo Sci #AM8672)
- Hybond N+ nylon membrane (GE HealthCare#RPN303B)
- Hybridization buffer (depends on your probe), stored at 4°C
- NorthernMax Formaldehyde loading buffer, stored in -20°C (Thermo Sci # AM8552)
- RNaseZap (Thermo Sci # AM9780)
- Ambion RNase-free 1.5 mL microcentrifuge tubes (Thermo Sci # AM12400)
- 20X SSC buffer
- 20% SDS solution
- filtered pipette tips
- Paper towels
- Plastic wrap

PROTOCOL

Day 1

1. Make RNA denaturing gel
    a. Prep:
        i. Warm to RT: RNA SYBR green (protected from light), an aliquot of NorthernMax 10X Denaturing Gel Buffer (mini gel: 7ml transferred into a 15ml conical; midi gel: 20ml transferred into a 50ml conical)
        ii. Thaw on ice: RNA samples, Formaldehyde loading buffer, RNA ladder + NEB loading buffer
        iii. Warm: a water bath to 58^{o}C, a heat block to 70^{o}C
        iv. Prepare RNase-free workstation and equipment
            1. Spray with RNaseZap: gel tray, gel comb, gel casting box, gel electrophoresis chamber, Erlenmeyer flask (mini: 250ml; midi: 500ml flask), graduated cylinder (mini: 50ml; midi: 250ml). Rinse with MilliQ water twice.
            2. Place plastic wrap on bench
            3. Spray pipettes with RNaseZap
            4. Obtain filtered pipette tips
        v. Setup gel-casting station by securing gel tray between casting plates and adding the comb. This should be setup on a bench covered with plastic wrap to prevent RNase contamination.
    b. Make 1% gel:
        i. Add MilliQ water to the RNase-free Erlenmeyer flask and add agarose (Mini: 0.7g agarose + 68ml water; midi: 2g agarose + 190ml water). Swirl to mix.
            Note: stated volumes of water account for evaporation later.
        ii. Place kimwipe loosely into top of flask to prevent boiling-over during microwaving. Microwave for 1.5-3min until agarose is completely melted. There cannot be any flakes as this will cause blurry bands!
        iii. Place flask into 58^{o}C water bath to reduce temperature (mini: 6.5-7min; midi: 8min – timing is essential for sharp bands while you don't want solution to be > 60^{o}C as formaldehyde will evaporate out at this temperature).
    c. Pour RT Denaturing Gel Buffer into flask containing 58^{o}C, molten agarose. Add RNA SYBR green (mini: 7µl; midi: 20µl). Swirl *gently* (to prevent bubble formation) to mix and immediately pour into gel tray.
    d. Loosely cover gel with aluminum foil to protect it from light. Do not seal! You want it cool without disruptions.
    e. Allow gel to solidify at room temperature for 30-45min.
2. Prepare RNA
    a. Add RNA into RNase-free microcentrifuge tubes. The amount of RNA to be used should be determined empirically for each target you are detecting.

        i. Most human protocols recommended 10-20µg total RNA or 0.5-1µg mRNA.
        ii. For flies, 1-2µg total RNA worked well for highly expressed targets (e.g. transgenes). Can increase to 5-10µg RNA for weaker targets.
    b. Add more than equal volume of Formaldehyde Loading dye into each tube. For example, if you have 5µl of RNA sample, you should add at least 5µl of loading dye. Mix well.
    c. Heat the samples at 70°C for 15min, cool down on ice for 1min.
3. Prepare RNA ladder, following NEB protocol
    a. Combine into a RNase-free microcentrifuge tube: 2µl ssRNA ladder for 1µg, 3µl DEPC water, 5µl provided RNA loading buffer (do not use the same buffer as samples)
    b. Heat at 70°C for 5min.
    c. Chill on ice for 1min
4. Run RNA on the denaturing gel
    a. Make 250ml of 1x Running Buffer: 225ml MilliQ water + 25ml of 10x NorthernMax 10x Running Buffer (MOPS).
    b. Pour a small amount of running buffer onto top of solidified gel within the casting box and *gently* remove comb while gel is still locked into casting box. Remove gel/tray from casting box and transfer to the gel electrophoresis chamber.
    c. Pour remaining running buffer over the top of the gel (effectively cleaning out the wells) until solution is ~1-2mm above gel.
    d. Load prepared RNA samples and ladder into designated lanes.
    e. Run at 100V for 1~1.5h until loading dye is ~1inche from the bottom of the gel.
    f. Image gel using the Bonini lab imager. You should see bands of 18s rRNA (2kb), and RNA size ladder. Note that the top band of the RNA ladder can be very faint and some imagers don't capture it.
5. Setup transfer
    a. Put a piece of plastic wrap onto bench (if not already done) and stack paper towels to ~10cm tall (mini: cut standard towels in half; midi: align 2 stacks of paper towels side-by-side along long side and place 1-2 pieces on top of the stack to traverse the crevice between the two stacks) onto the plastic wrap.

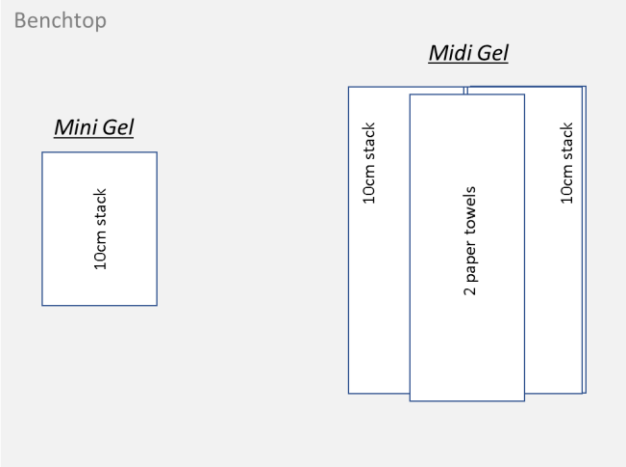

b. Cut 5 pieces of Whatman paper and 1 piece of Hybnd+ membrane to the size of the gel, accounting for wells being removed.
c. Center 3 Whatman papers onto the paper towels.
d. Pour NorthernMax transferring buffer into a container (such as empty pipet tip box for mini gel or a plastic tub for a midi gel). Filling up to ~2cm from the bottom should be enough.
e. Wet 1 piece of Whatman paper with transferring buffer, put onto the stack of paper towels/Whatman papers.
f. Soak membrane in the transferring buffer and cut a notch in the top right corner as a reference. Place on top of the pre-soaked Whatman paper. Roll out any bubbles that may have formed between layers with a 4" blotting roller (ThermoFisher #84747).
g. Cut wells off the top of the gel using a razor and discard. Place the gel on top of the pre-soaked membrane. Roll out any bubbles that may have formed between layers with a blotting roller. Note: it can help to add a little transfer buffer to the membrane using a transfer pipet. Then "roll" the gel over the membrane, effectively squeezing out bubbles.
h. Add a little transfer buffer onto top of gel with a transfer pipet. Pre-soak the last piece of filter paper with transferring buffer and "roll" it onto the top of the gel. Roll out any bubbles that may have formed between layers with a 4" blotting roller.
i. Cut a long piece of filter paper so it is the same width as the gel, this will be the Whatman paper bridge. Put one side of the paper on top of the filter paper/gel and roll our any bubbles. Soak the other end of the paper

bridge in the transfer buffer so it is submerged.

Mini Gel

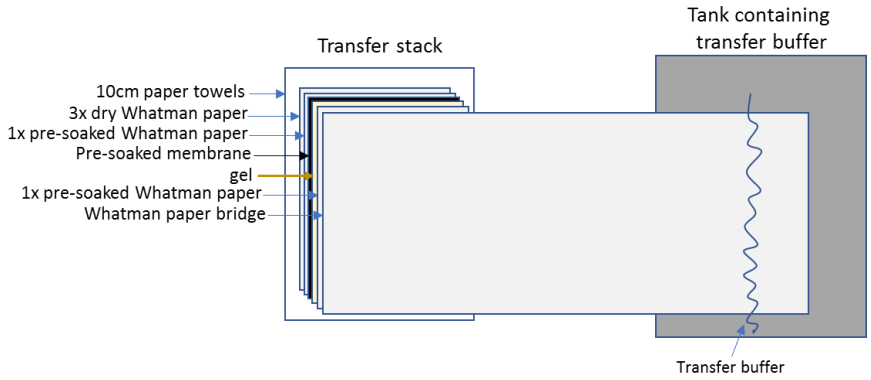

j. Place a gel tray on top of the bridge/transfer stack. Stack glass dissection plates onto the gel tray as a weight (or a textbook or plastic bottle of buffer). Make sure the stack/weights are balanced using a bullseye level so that it won't fall over and the transfer is even.
k. Place plastic wrap loosely over the top of the tank to help reduce evaporation. Be sure it doesn't disrupt the bridge!
l. Transfer until the gel is completely flat. Typically overnight. You cannot over transfer (as long as you don't let it dry out).
m. Clean all tools that came in contact with the transfer buffer thoroughly with distilled water to remove salts.

An alternative way to put the transfer stack together (f-g): (1) place the cut gel upside down onto a piece of Whatmann paper that is bigger than the gel. (2) add a little transfer buffer to the membrane using a transfer pipet. (3) "roll" the pre-soaked membrane upside-down over the gel, effectively squeezing out bubbles. (4) Roll out any bubbles that may have formed between layers with a 4" blotting roller. Then turn the membrane/gel upside-up and place this on top of the filter papers on the paper towels.

Day 2: (written for a mini-gel. Scale volumes up for a midi gel)

1. Crosslinking and Pre-Hybridization
    a. While transferring is ongoing, warm the hybridization buffer to 68°C in one of the Northern incubators.
    b. Carefully remove membrane from the transfer stack, making sure not to touch "top" (the side that was facing the gel where the RNA is located). Place it in a dry plastic tray that is larger than the membrane.
    c. Discard gel, all paper towels, and Whatman papers, and transfer buffer. Clean container thoroughly if it will be reused.
    d. (optional) check the membrane in the gel imager for 18s rRNA signal. Mark the edge of the membrane with a pencil at the position of 18s rRNA (2kb), if visible, and the dark blue and light blue dye indicators (these will not be visible after hybridization). This will help you to later match the gel picture and the position of the gel on the membrane for sizing with the ladder.

e. UV crosslink the RNA onto the membrane in the UV Stratalinker 1800 (Press "AutoCrosslink" (1200u joules x100) and start). Make sure to keep the transferred side facing up. You can keep the membrane in the tray.
f. Gently, transfer the membrane, RNA-side facing inward into a hybridization bottle. Add ~7 ml of pre-warmed hybridization buffer.
g. Pre-hybridize membrane with rotation at 68^{o}C for 30-60min.

Notes:

- The type of hybridization buffer is dependent on the probe.
- It can be convenient to synthesize the probe at this time

2. Hybridize membrane: perform all steps in accordance with EHRS radioactivity safety protocols.
    a. Add the probe the pre-hybridized membrane.
    b. Incubate overnight with rotation at the specified temperature for the probe.

Day 3 (written for a mini-gel. Scale volumes up for a midi gel)

1. Prepare wash buffers
    a. Make 2xSSC/0.1% SDS using MilliQ water.
    b. Make 0.2xSSC/0.1% SDS using MilliQ water.

    Notes

    - Buffers should be relatively fresh. If I'm running a lot of northerns, I'll make 500mL at once and store it at RT.
    - Be careful that the SDS has not precipitated out of solution. If this occurs, warm it in the incubator with the membrane until SDS dissolves.
2. Washing and exposure: perform all steps in accordance with EHRS radioactivity safety protocols.
    a. Perform 3 washes with ~20ml of 2xSSC/0.1% SDS: Add buffer to the membrane/bottle. Close lid. Shake ~5 times. Remove lid and pour buffer directly into drain with warm water running.
    b. Add ~20ml of 2xSSC/0.1% SDS to bottle and rotate for 30min at the hybridization temperature. Let water run in sink during this time.
    c. Perform 3 washes with ~20ml of 0.2xSSC/0.1% SDS: Add buffer to the membrane/bottle. Close lid. Shake ~5 times. Remove lid and pour buffer directly into drain with warm water running.
    d. Add ~20ml of 0.2xSSC/0.1% SDS to bottle and rotate for 60min at the hybridization temperature. Let water run in sink during this time.
3. Prep: blank a phosphor screen by exposing it to a UV lamp for 30min to remove any signal from previous studies.
4. Place membrane into cassette and expose the membrane onto phosphor screen (2h~overnight)
    a. Carefully remove membrane from the bottle with tweezers and transfer it to a hybridization bag cut ~2cm larger than the membrane. Squeeze out any bubbles and seal the hybridization bag.

b. Retrieve phosphor screen and place over membrane, being careful not to slide it around. Close cassette and expose screen for desired exposure time, dependent on the probe.

5. Scan the phosphor screen with a Typhoon imager to get image. Quantify band densities in ImageJ.
6. (optional) reprobe membrane for additional targets
    a. Carefully remove membrane from the cassette and hybridization bag. Transfer it to a glass bottle.
    b. Repeat steps Day 2: 1.g thru Day 3: 6 for the new probe
7. Label membranes/hybridization bag with experiment date, probes used, etc. Store membranes at RT in plastic shielded containers until P32 has fully decayed. You can reprobe membranes after long-term storage.

SV40 probe

NOTES

- It is convenient to probe a membrane with SV40 and then re-probe with 18S for loading. Because SV40 requires 42°C for hybridization, the probe loses binding at 68°C, the temperature required for 18S hybridization.

REAGENTS

- FastStart PCR Master Mix (Sigma # 4710436001)
- DNA Primers
    - forward: 5′-TGTGGTGTGACATAATTGGACA-3′
    - reverse: 5′-AGATGGCATTTCTTCTGAGCA-3′
- vector template: purified plasmid containing a SV40 terminal sequence. For G4C2, I used pUAST-KAN-(G4C2)12 vector.
- MinElute PCR Purification Kit (Qiagen # 28004)
- High Prime DNA Labeling Kit (Sigma # 11585584001)
- 50µCi [P32-α] labeled dCTP (from EHRS)
- UltraHyb Hybridization Buffer (Thermo Sci # AM8670)

PROTOCOL

1. PCR template synthesis and purification
    a. Thaw: FastStart Master Mix, primers, and template vector
    b. Mix the following reagents together in PCR tube

Master Mix Component	**µl**	**Final concentration**
2X FastStart Master Mix	25	1X
Forward Primer (3µM)	5	0.3µM

Reverse Primer (3µM)	5	0.3µM
vector template	(varies)	50ng
MilliQ water	to final volume of 50µl	

c. Run sample on Thermocycler using the following program:

Step	**Temperature**	**Time**	**Number Cycles**
Initial denaturation	95 °C	6 min	1
Denaturation	95 °C	30 sec	30
Primer annealing	58 °C	30 sec	
Extension	72 °C	1min	
Final Extension	72 °C	7min	1
Cooling	4 °C	Hold	1

d. Run 5µl of PCR product on 2% TAE agarose gel using appropriate marker. Expected size = 204bp.
e. Purify PCR product from remaining reaction volume using Qiagen's MinElute PCR Purification Kit – follow the company's protocol. End volume = 10µl. This is your PCR template for probe synthesis.
f. Measure concentration of end PCR template on Nanodrop.
g. PCR templates can be frozen at -20°C for future use.

2. Probe synthesis: perform all steps in accordance with EHRS radioactivity safety protocols.
   a. Thaw: PCR template, materials from High Prime DNA Labeling kit (Reaction mix, dATP, dTTP, dGTP)
   b. In a 1.5ml microcentrifuge tube, mix ~35ng of PCR template in MilliQ water for end volume of 10µl. Denature at 95°C for 10min. Immediately place on ice for 2+ min. (Do not let it cool slowly as it will re-nature.)
   c. Centrifuge sample briefly and add the following to the tube (from High Prime DNA Labeling Kit)
      i. 8µl of High Prime Reaction Mix
      ii. 6µl each of dATP, dTTP, dGTP
      iii. 4µl of 50µCi [P32-α] labeled dCTP
      iv. MilliQ water to an end volume of 40µl
   d. Tap tube to mix thoroughly.
   e. Incubate reaction at 37°C for 60-75min.
   f. Increase temperature on heat block to 99°C and heat sample for 10min to stop synthesis reaction and denature. Immediately place on ice for 2+

min. Probes can be stored at 4°C for ~2wks (until the P32 signal degrades).

5. Hybridization
    a. Pre-hybridize membrane in UltraHyb Hybridization Buffer at 68°C for 30+ min.
    b. Centrifuge probe briefly and add to pre-hybridized membrane. Amount of probe depends on your target and freshness of probe. Use 5-10µl of fresh probe for UAS-G4C2 with 2µg RNA per lane. (Increase the amount of probe based on 2-wk P32 decay rate and amount of RNA.)
    c. Hybridize overnight at 42°C.
    d. Wash hybridized membrane at 42°C
    e. Exposure is usually ~4hrs.

G4C2 probe

NOTES

- It is convenient to probe a membrane with G4C2 and then re-probe with 18S for loading. Because G4C2 requires 50°C for hybridization, the probe binding reduces at 68°C, the temperature required for 18S hybridization.

REAGENTS

- T4 polynucleotide kinase (PNK) Kit, stored in -20°C (NEB # M201S)
- 50µCi [γ-^{32}P] ATP (from EHRS #2P32GATP) (equal to 62.5pmol)
- (G2C4)4 oligo: 5'- GGCCCCGGCCCCGGCCCCGGCCCC -3'
- UltraHyb hybridization Oligo buffer (Thermo Sci # AM8670)

PROTOCOL

1. Thaw T4 PNK buffer and G4C2 probe working stock.
2. Synthesize P32-labeled probe
    a. Mix the following reagents in a microcentrifuge tube:

Component	**µl**	**Final concentration**
10X T4 PNK Buffer	2.5	1X
(G2C4)4 oligo (10µM)	2.5	1µM
MilliQ water	15	--
T4 PNK	1	10units
50µCi [γ-^{32}P] ATP	4	50pmol

Note: add enzyme at the freezer to make sure it stays as close to -20°C as possible

b. Incubate at 37°C for 45-60min.
c. Store at 4°C for 2wks. (calculate amount to add based on 2-wk half-life of P32)

3. Hybridization
    a. Pre-hybridize membrane in UltraHyb Oligo Hybridization Buffer at 68°C for 30+ min.
    b. Centrifuge probe briefly and add to pre-hybridized membrane. Amount of probe depends on your target and freshness of probe. Use 5µl for 1-2µg RNA per lane. (Increase the amount of probe based on P32 decay rate.)
    c. Hybridize overnight at 50°C.
    d. Wash hybridized membrane at 50°C
    e. Exposure is usually ~4hrs.

18S probe (Loading)

REAGENTS

- DNA Primers
    - T7-F Core: 5'- gataatacgactcactatagggaga -3'
    - T7 18S: 5'- AGGGAGCCTGAGAAACGGCTACCACATCTAAGGAAtctccctatagtgagtcgtattatc-3'
    - *Lower case: T7-sequence,* upper case: target gene sequence
- MAXIscript T7 Transcription Kit (Ambion # AM1312)
- 50µCi [P32-α] labeled CTP (from EHRS) *(not dCTP)*
- UltraHyb Hybridization Buffer (Thermo Sci # AM8670)

PROTOCOL

1. Anneal primers
    a. Add T7-4 core and T7-18S primers to a microcentrifuge tube with MilliQ water. Target concentration is 2µM.
    b. Boil 400 ml of water in a large glass beaker on a hotplate.
    c. Incubate the tube of oligonucleotides in the boiling water for 5 minutes.
    d. Turn off the hotplate, leaving the oligonucleotides in the beaker on the hotplate to slowly cool to room temperature.
    e. store at -20°C for future use.
2. Synthesize P32-labeled probe: perform all steps in accordance with EHRS radioactivity safety protocols.
    a. Thaw: Annealed primers, components of the MAXIscript T7 Transcription Kit (Transcription Buffer, CTP, ATP, UTP, GTP)

        Note: Reaction mix tends to form a precipitate. This can be fully dissolved at room temperature with strong vortexing.

    b. Mix the following in a 1.5ml microcentrifuge tube:

i. 2µl Annealed 2µM T7-18S rRNA
ii. 2µl 10X Transcription Buffer (to 1X)
iii. 1µl each of 10mM CTP, ATP, UTP, and GTP

Note: Still add non-P32 labeled CTP to reduce signal strength

iv. 7µl water
v. 2µl T7 enzyme mix

Note: add enzyme at the freezer to make sure it stays as close to -20°C as possible

vi. 3µl of 50µCi [P32-α] labeled CTP

c. Incubate at 37°C for 1 hour.
d. Add 2µl TurboDNase (from kit) and incubate an additional 15min at 37°C.
e. Raise temperature to 95°C and incubate an additional 5min (denaturing).
f. Store at 4°C for 4wks (calculate amount to add based on 2-wk half-life of P32)

3. Hybridization
   a. Pre-hybridize membrane in UltraHyb Hybridization Buffer at 68°C for 30+ min.
   b. Centrifuge probe briefly and add to pre-hybridized membrane. Amount of probe depends on your target and freshness of probe. Use 1µl for 1-2µg RNA per lane. (Increase the amount of probe based on P32 decay rate.)
   c. Hybridize overnight at 68°C.
   d. Wash hybridized membrane at 68°C
   e. Exposure is usually ~2hrs.

Protein extraction (flies)

MATERIALS

- pellet/pestle disposable blue microcentrifuge tubes (Kimble # 749520-0000)
- pellet/pestle cordless motor (Kimble # 749540-0000)

TISSUE PREPARATION

1. For heads
    a. Collect heads as described in *Fly Work*
    b. Heads should be collected into blue microcentrifuge tubes to be used with the disposable pestles
    c. Typically, I prepare 3 replicate samples from 1 cross. Target 5-10 heads per sample. Keep track of the exact # of heads per sample.
    d. Keep frozen heads on dry ice and immediately extract protein using one of the 2 methods below.
2. For whole larvae or adult animals:
    a. transfer 3-5 animals into blue microcentrifuge tubes to be used with the disposable pestles. Keep track of the exact # of animals per tube.
    b. Typically, I prepare 3 replicate samples from 1 cross.
    c. If you are immediately extracting protein, do not let animals sit in the tube long term. Rather, ass the lysis buffer and homogenize the tissue immediately.
    d. Animals can be frozen on dry ice and stored for future use in at -80^{o}C. Keep the tissue frozen until the moment you add the lysis buffer and homogenize the tissue with the disposable pellet as described below.

Method 1: LDS sample buffer

NOTES

- This is the standard protocol in the lab and works well for the majority of targets.
- This protocol works well for heads from the following genotypes
    - Gmr-Gal4> LacZ
    - Gmr-Gal4> TDP-43(37M)

REAGENTS/MATERIALS

- fly tissue (note tissue preparation above)
- NuPAGE LDS sample buffer, 4X (Thermo # NP0008)
- β-mercaptoethanol (β-ME)

PROTOCOL

1. Make 1X sample buffer
    a. 1250µl of 4X LDS sample buffer to 1X
    b. 125µl of B-ME (add in hood) to 2.5%

    c. 3625µl of MilliQ water
    d. Store at -20°C for future use.
2. Prep: pre-warm heat block to 95°C
3. Add the calculated amount of 1X sample buffer to the first sample and immediately homogenize the tissue using a disposable pestle and motor. Transfer the tube to wet ice. Repeat for each subsequent sample. Store samples on ice until done with all samples. Samples must be kept cold from this step forward.
    a. 7ul of 1X sample buffer per head
    b. 10ul of 1X sample buffer per whole animal

    Note: When removing the pestle from the tube it is good practice to lift it just above the solution while the tip is still in the tube and spin it with the motor. This will effectively fling any residual solution of the pestle onto the walls of the tube so it isn't lost. By briefly spinning the sample in the centrifuge, the solution will all be collected to the bottom of the tube.
4. Incubate samples on ice for ~5min
5. Boil samples for 5min at 95°C
6. Centrifuge at RT for 5min, 15,000xg to pellet debris. For whole animals, transfer the supernatant to a fresh pre-labeled microcentrifuge tube and discard the pellet. For heads, there is typically very little debris so this doesn't seem to be necessary.
7. Samples can be frozen at -20°C for future use. thaw on ice and boil them for 2min before loading them into a gel. Typically we load 5µl of sample per lane for a western blot.

Method 2: RIPA lysis

NOTES

- this protocol must be used for assessing DPR levels. Grinding tissue directly into LDS sample buffer produces variable results.
- this protocol works well for heads from the following genotypes
    - Gmr-Gal4> LDS-(G4C2)44[GR-GFP]
    - elavGS> LDS-(G4C2)44[GR-GFP]
    - Gmr-Gal4> (G4C2)n
    - elavGS> (G4C2)n
- this protocol works well for whole adult animals, daGS> (G4C2)n

REAGENTS/MATERIALS

- fly tissue (note tissue preparation above)
- RIPA lysis buffer
    - 10mL of 1M Tris-HCL (pH 7.5) to 50mM
    - 6mL of 5M NaCl to 150mM
    - 2mL NP-40 to 1%
    - 0.42g NaF to 50mM
    - 2mL of 10% SDS to 0.1%
    - 1g Sodium Deoxycholate (DOC) to 0.5%

    - dH2O to 200mL
    - Filter through a 250ml filter system, 0.22µm, PES
    - store at 4°C. Check pH every 6-8mo.
- 5X cOmplete ULTRA Tablets, mini, EASYpack protease inhibitor cocktail (Sigma # 05892970001)
    - 1 tablet dissolved in 1500µl of milliQ water
    - prepare 100µl aliquots
    - store in -20°C. After thawing, precipitate may form and need to be resuspended into solution.
- (optional) 25X PhosSTOP Phosphotase inhibitor cocktail (Sigma # 04906845001)
    - 1 tablet dissolved in 400µl of MilliQ water
    - prepare 25µl aliquots
    - store in -20°C. After thawing, precipitate may form and need to be resuspended into solution.
- 100mM PMSF
    - 0.1742g of PMSF
    - 10mL of isopropanol
    - Filter through a 0.22µm PES filter (Fisher Sci # 09-720-511) using a luer-lock syringe
    - prepare 500µl aliquots
    - store in -20°C. Before use, bring to RT and vortex until precipitate goes back into solution
- 1M DTT
    - 1.5425g of DTT (Dithiothreitol)
    - 10mL MilliQ water
    - Filter through a 0.22µm PES filter (Fisher Sci # 09-720-511) using a Luer-lock syringe
    - prepare 500µl aliquots
    - store in -20°C
        - before use, bring to RT and vortex until precipitate goes back into solution

PROTOCOL

1. Prepare working lysis Buffer: (must be made fresh!)
    a. Calculate the total amount of lysis buffer you will need.
        - For western blot: use 4µl per head or 10µl per whole animal.
        - For dot blot: use 0.2µl per head or 3ul per whole animal.
    b. For every 500µl of working lysis buffer needed, add the following protease and phosphatase inhibitors. Make a minimum of 500µl of working lysis buffer then prepare additional 100µl as needed.
        - 400µL 0.5% RIPA Lysis Buffer Stock
        - 100µL of 5X cOmplete ULTRA protease inhibitor Stock to ~1X
        - 20µL of 25X PhosSTOP Phosphotase inhibitor cocktail Stock to ~1X
        - 5µL of 100mM PMSF to ~1mM
        - 0.5µL of 1M DTT for ~1mM

2. Add the calculated amount of lysis buffer to the first sample and immediately homogenize the tissue using a disposable pestle and motor. Transfer the tube to wet ice. Repeat for each subsequent sample. Store samples on ice until done with all samples. Samples must be kept cold from this step forward.
    Notes:
    - when removing the pestle from the tube it is good practice to lift it just above the solution while the tip is still in the tube and spin it with the motor. This will effectively fling any residual solution of the pestle onto the walls of the tube so it isn't lost. By briefly spinning the sample in the centrifuge, the solution will all be collected to the bottom of the tube.
    - Unused working lysis buffer can be stored at 4^{o}C for use during protein quantification.
3. Incubate samples at 4^{o}C 45min with agitation. (min: 30min, max: 2hr)
    Note: Samples can be frozen at -20^{o}C at this step if needed. Thaw samples on ice.
4. Prep: label new microcentrifuge tubes (standard tubes, not blue tubes).
5. Centrifuge the samples at 4^{o}C for 10min, 15,000xG to pellet debris.
6. Keeping the samples on ice, transfer the supernatant from tubes into pre-labeled microcentrifuge tubes. Discard the pellet.
7. follow *Protein quantification protocol* below if desired. It is best to immediately quantify protein and/or denature samples in LDS sample buffer. However, natured protein lysates can be stored at -20^{o}C if needed. Thaw samples on ice and then perform protein quantification and/or denature samples in LDS sample buffer.

Protein quantification (Bradford)

NOTE: cannot be done on denatured protein (e.g. samples prepared directly into LDS sample buffer.

REAGENTS/MATERIALS

- Bradford Ultra (Expedeon # BFU05L)
- Disposable cuvettes Semi-micro (Fisher Sci # 14-955-128)
- UltraPure BSA, 50mg/ml (Thermo # AM2616)

PROTOCOL

1. Prep:
    a. Thaw: BSA, protein samples on ice that were prepared using RIPA lysis buffer
    b. Pre-warm a heat-block to 95^{o}C
2. Prepare 2mg/ml BSA working stock
    a. 2.8µl of 50mg/ml

b. 67.2µl RIPA lysis buffer

3. Quantify the amount of protein in each sample using Bradford kit
    a. prepare Bradford standards into cuvettes
        - transfer 5 cuvettes into an empty cuvette tray.

          Notes:

          - cuvettes should only be touched on the 2 sides that are frosted!
          - You cannot label the cuvettes so it is important to organize them in a way that is logical and consistent in the tray so you can keep track of which is cuvette contains what. For large numbers of samples, you can write a list of the samples 1-? on a piece of paper and then make sure the cuvettes are in the tray in that order
        - prepare standards as follows, adding the Bradford reagent first then the 2mg/ml BSA working stock

µl Bradford	µl of 2mg/ml BSA	Final concentration (mg/ml)	Final volume (µl)
1500	0.0	0.0	1500
1499	0.75	0.001	1500
1498	2.25	0.003	1500
1494	6.00	0.008	1500
1481	18.75	0.025	1500
1462	37.5	0.050	1500

    b. prepare protein dilutions for each of your samples to be analyzed: add 1495µl of Bradford and then 5µl of protein lysate to one cuvette (1:300 dilution)
    c. Analyze samples on the cuvette-based spectrophotometer
        - Prior to putting the cuvette into the machine, use a piece of parafilm pressed on top of the cuvette as a lid, and turn upside down and back upright 3X to effectively mix the samples. Be sure to move the parafilm to a fresh region between cuvettes. Also be careful not to touch the portion of the cuvettes where the light will shine through to read the absorbance.
        - measure the samples twice using Bradford settings.
        - Save data onto a USB
        - Steps for running the machine
            - Turn it on and pick “Coomassie/Bradford Micro”

- Edit information so have mg/ml units, 4 standards, and correct # of samples, save data to USB and internal memory (put in a USB), test name
- Click “Run standards”
    - Edit each standard so they are the correct value based on the table above (mg/ml column)
- Measure blank by placing the cuvette clear side facing you
- Measure each of the standards
- When done with standards, click “Run Test”
- Run each of the samples
- When done running samples, save data – it should safe to your USB as a txt file

d. In excel, setup a standard curve from your standards. Average the 2 readings from the spectrophotometer per cuvette.
    - You should have an R^2 of > 0.90 (if not, then your standard curve is bad and you need to repeat them.) you will need the formula for the line to calculate protein levels in your samples

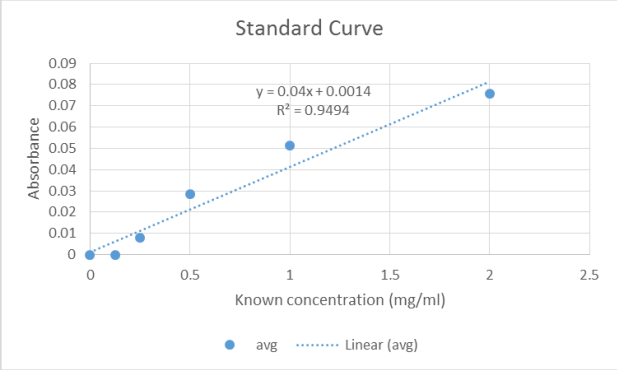

e. Calculate the total mg/ml present in samples using the y = m x + b formula obtained from your standard curve (y = mean absorbance of 2 readings from the spectrophotometer, x = mg/ml). Be sure to compensate for the fact that your samples were diluted 1:300 (by multiplying x by 300)!

4. There are 2 approaches to preparing protein for western blot or dot blot. Follow the one that makes most sense for your experiment
    a. Remove the desired µg of protein per sample and transfer to a fresh, prelabeled microcentrifuge tube. Bring the volumes for all samples up to the same value (≤ 20µl) using leftover RIPA lysis buffer containing inhibitors (if available) or RIPA stock to dilute samples.
        - For western blot:
            - the amount of protein will depend on your target. 10-20µg of protein is typically run on a western blot per lane. Overall, when performing an experiment for the first time it is best to start with 20µg. Also, I’ve seen different results when I ran 10µg vs 20µg protein.

- End volume will depend on the gel's well size. ≤ 20µl is standard.
- If you are running samples on multiple wells in a gel or on multiple gels, scale calculations up so you prepare everything at once.

  - For dot-blot: it is essential to maintain protein at a high concentration, as close to 10µg of protein in 1.6µl of end volume as possible
  - It can be convenient to make multiple aliquots of your protein and freeze them for future use.

b. Normalize the µg/µl of protein between each sample by diluting all of the samples to the lowest value of µg/µl across your samples. Use leftover RIPA lysis buffer containing inhibitors (if available) or RIPA stock to dilute samples.

5. Add 4X LDS sample buffer to 1X (so 6.6µl of 4X LDS sample buffer for 20µl of sample). Mix and spin down samples briefly.
6. Boil at 95^{o}C for 5min.
7. Samples can be frozen at -20^{o}C for future use. thaw on ice and boil them for 2min before loading them into a gel

Western blot

NOTES

- Other people in the lab use a different protein standard. However, these do not include as wide of a range of markers which may be required when cutting a membrane to probe it for 2 immunobands simultaneously. Specifically, for β-gal westerns, this ladder allows you to cut accurately at ~70kDa so you can stain the bottom half with tubulin (at 50kDa) and top half with β-gal (at 110kDa).

REAGENTS/MATERIALS

- Protein samples (see *General Protocols: Protein extraction (Flies)* or *Fibroblasts: Protein extraction*)
  - If using samples prepared with RIPA lysis buffer, you must perform protein quantification (Bradford)
- 1X TBST
  - Prepare 1L from packets (Sigma # T9039)
  - Or make it from 10X TBS stock: 100mL 10X TBS, 900mL MilliQ water, 500µL of Tween-20
- Non-fat milk powder
- Novex Sharp PreStained Protein Standard (Invitrogen # LC5800)
- NuPAGE 4-12% Bis-Tris Protein Gels, 1.5mm, 15-well (Invitrogen #NP0336)
- NuPAGE MES SDS Running Buffer, 20X (Invitrogen #NP0002)
- XCell SureLock Mini-Cell (Invitrogen #EI0001)
- Gel Knife (Invitrogen #EI9010)
- (optional) Buffer Dam for XCell SureLock Mini-Cell (Invitrogen #EI0012)
- (optional) ponceau S (can be reused 10 times)

PROTOCOL

Note: standard protocol for XCell SureLock Mini-Cell can be found in the company's manual: HERE. All images are taken from this protocol.

Day 1

1. Prep
   i. if samples are frozen: thaw samples for 5-10m on ice while you prewarm a heat-block set to 95°C. Re-boil samples for 2-3 minutes to make sure they are completely thawed and that the SDS is dissolved into solution. Typically I do this while I'm setting up the tank (below). After 2-3 minutes at 95°C, samples can sit at RT until loaded into gel.
   ii. Thaw your protein standard. If a precipitate has formed, briefly boil the standard at 95°C for 1-2min until dissolved.
   iii. Make 1X MES running buffer: 50mL of 20X stock + 950mL MilliQ water. Leftover buffer can be stored for future use. Buffer can be reused 3 times as long as loading was clean and no protein samples got into the buffer.

2. Run western using standard 4-12% Bis-Tris premade gels and 1X MES running buffer (for 1L: 50mL 20X MES running buffer, 950mL DI water). Usually run at 120V for ~90min.
    i. Setup a tank (“lower buffer chamber”) with a gel tension wedge and buffer core. If you are running 1 gel, a buffer dam must be positioned where the second gel would have gone.

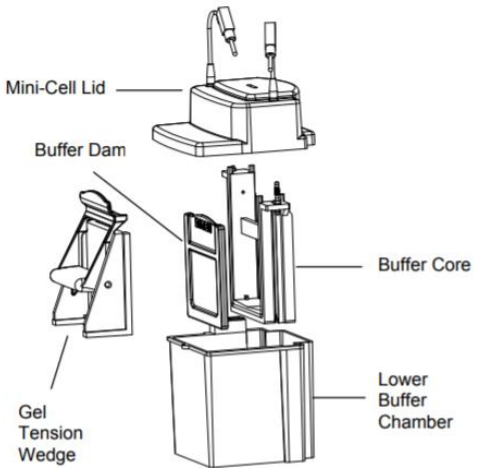

    ii. Obtain a premade gel from the fridge. Open the package and remove the gel. REMOVE THE WHITE STICKER FROM THE BOTTOM OF THE GEL.
    iii. Place the gel along the buffer core in the tank, effectively creating an inner chamber. The comb side of the gel must face the inner chamber. Close the gel tension wedge.

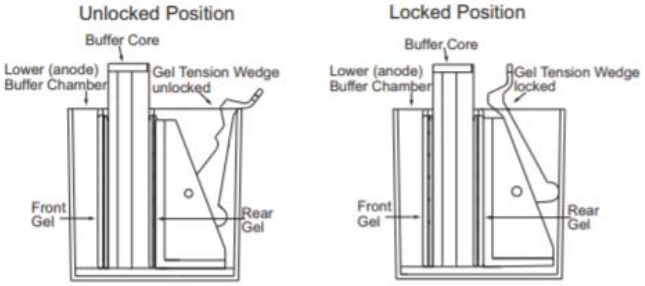

    iv. Pour 1X MES running buffer into the inner chamber, allowing it to run out of the inner chamber and into the outer chamber until the outer chamber is half-way full of buffer (~500mL total).
    v. Gently remove the comb from the gel, making sure to pull it straight up and to not disrupt the gel that makes the lanes.
    vi. Clean out the wells using a P1000 pipette set to 800ul. Draw up buffer from the outer chamber and gently shoot buffer into each of the wells – BE CAREFUL TO WATCH THE SIDES OF THE WELLS AS THEY WILL MOVE IN OLDER GELS AND YOU WILL GENTLY NEED TO REPOSITION THEM INTO THE CORRECT PLACE USING A P10 PIPETTE TIP.
    vii. Using a P10 or P20 load pre-boiled sample into appropriate wells. Load 8µl of protein standard last. Try to avoid the edge wells if you can.
    viii. position the top onto the tank and plug in the cathode and anode wires into a power source – be sure to match red-to-red and black-to-black!

ix. Turn on power source and set to 120V. start power source and a timer for 60m. you will likely run it for closer to 90m but it's good to check the gel periodically. You are done when the blue dye in the samples is at the very bottom of the gel. You can run samples longer as needed to get better separation between larger proteins. It is okay to lose small proteins through the bottom of the gel if you are not interested in them.

3. Prep:
    i. make 5% milk (for 2 gels: 2.5g of dry milk in 50mL TBST; for >2 gels: 5g of dry milk in 100mL TBST). Place on spin plate for the entire time you are transferring the gel (Minimum of 30min).
    ii. Make 1X TBST as needed
4. (optional) Prep: if doing a wet transfer
    i. Make 1X NuPAGE transfer buffer with 20% methanol and 1X reducing agent (for 500mL: 25mL 20X transfer buffer, 100mL Methanol, 500ul NuPAGE Antioxidant (optional), 375mL DI water)
    ii. Soak 6 sponges per gel in transfer buffer for ~30min in a Tupperware container to remove all air bubbles
    iii. cut 1 piece of PVDF membrane per gel
    iv. cut 2 pieces of normal thickness Whatman paper per gel
5. Transfer protein from the gel to a membrane based on the optimized protocol for the target. Importantly, when testing new antibodies, a wet transfer is typically used. Only targets used regularly in the lab (e.g. β-Gal, TDP-43) have been optimized for an iBLOT transfer. I've also had success with GFP.
6. When transfer is done, remove membrane, noting where the protein is located on the membrane. Immediately place the membrane into blocking solution. (DO NOT LET THE MEMBRANE DRY OUT, particularly if you are using PVDF – IT WANTS TO!) Cut the top left corner so we always know the proper orientation.
    i. For 2 membranes, I will cut the top left corner for gel #1 and then cut the 2 top corners and left bottom corner for gel #2 so we can distinguish them.
    ii. (optional) If you want to make sure the transfer was successful or for a loading control, you can stain the membrane with Ponceau S to detect protein. This must be done before the membrane is exposed to TBST. To do this:
        a. Incubate membrane in Ponceau S for 5-20min or until bands can be easily seen (the longer the incubation the darker the bands but you will also have to do more washes to remove background).
        b. Rinse the membrane repeatedly in ddH2O until the background is clean and bands are still visible.
        c. Take a picture of the membrane with your camera phone or on the gel imager with the colorimetric setting.
        d. Wash membrane 3x for 5min in TBST to remove Ponceau S. Continue to blocking step.
7. Incubate the membrane in 5% Non-fat milk/TBST (blocking solution) for 30+ min on a rocker at RT.
8. Incubate the membrane with primary antibody solution (diluted in blocking solution or 3% BSA/0.01% NaAzide/1XTBST) overnight in the cold room on a rocker.
    i. If using % BSA/0.01% NaAzide/1XTBST, rinse milk thoroughly off of the membrane with TBST before putting into primary antibody solution.

Day 2

1. Prep:
    a. put blocking buffer on spinning plate! It needs to spin for a minimum of 20m prior to being used. Make more blocking buffer as needed.
    b. Make sure you have enough TBST for washes. If not, make more.
2. Obtain membranes from cold room. Using a transfer pipette, remove primary antibody and put it into appropriately labeled 50mL conicals for future use.
3. Rinse membrane 3X in TBST and perform 3x 5min washes with TBST at RT on the rocker (higher speed).
4. Pour off TBST and add 16mL blocking buffer. Add HRP-conjugated secondary antibody to the tray at the desired concentration. Incubate on rocker for 2hr.
5. Rinse membrane 3X in TBST. Wash in TBST 4 times for 15 min each on rocker.
    a. Membranes can be left in the last wash for long periods of time.
    b. You can reduce the time of washes for very good antibodies (e.g. 3 x 10min).
6. Prep:
    a. turn on imager so the camera has time to warm up
    b. put blocking buffer on spinning plate if you will be reprobing the same membrane. It needs to spin for a minimum of 20m prior to being used.
7. Image membrane
    a. Prepare ECL Prime reagent (2000ul per membrane total; if membranes are cut, you will use less) by adding reagent B to reagent A at 1:1 ratio and pipetting up and down repeatedly to mix.

        Note: not adding enough ECL is a common factor for variability – particularly obvious when you getting faded signal in portions of the membrane

    b. Lay a piece of parafilm down on flat surface and dot ECL Prime working solution onto the parafilm.
    c. Using forceps to hold membrane, touch corner of membrane to clean tissue repeatedly to remove excess TBST. Lay membrane down flat onto ECL Prime reagent making sure to cover the entire membrane with solution. Incubate for 1.5-2 min.
    d. Quickly remove membrane from ECL Prime Reagent and touch corner to clean tissue to remove excess reagent. Image on Imager.
    i. I usually start with an auto exposure. If the time frame is too long, I then do incremental exposures. BE SURE TO GET A COLORIMETRIC PICTURE OF THE MEMBRANE.
8. Once imaged, rinse membrane 3X in TBST and perform 3x 5min washes with TBST at RT on the rocker (higher speed).
    a. Membranes can be stored in sealed film for future use.
9. If reprobing the same membrane, quench the signal with H2O2 or stripping buffer (protocols below). When done, incubate the membrane in 5% Non-fat milk/TBST (blocking solution) for 30-60min on a rocker. Add desired primary on overnight and repeat Day 2 steps above.

Transfer methods

iBLOT

- iBlot Transfer, nitrocellulose, mini (Fisher Sci # IB301002)
- Blotting roller (ThermoFisher #84747)
- iBlot 1 Dry Blotting system

PROTOCOL

Note: standard protocol for iBlot can be found in the company's manual: HERE.

1. When the gel is done running, gather the materials needed for the iBlot transfer:
    i. From the iBlot kit: Bottom stack, top stack, sponge, 1 piece of whatman paper
    ii. a membrane-sized tray containing DI water
    iii. forceps, gel knife, blotting roller
2. Setup transfer for 1 gel at a time.
    i. Remove the bottom stack from the packaging, keeping it in the transparent plastic tray – only toach the plastic tray. Place it in the iBlot box, so it is within the barriers and in the correct position. (tab should be on the right.)
    ii. Remove the gel from western blot tank/apparatus, crack apart the plates using the gel knife, cut off the bottom portion of the gel. Optional: remove wells.
    iii. Gently lift gel from the bottom (top is too fragile) and place the gel on top of the white nitrocellulose membrane of the bottom stack, using a rolling method to avoid bubbles. Roll out any bubbles with the blotting roller.
    iv. Using forceps, wet the piece of Whatman paper with DI water. Using a rolling method to avoid bubbles, place it on top of the gel. Roll out any bubbles with the blotting roller.
    v. Remove the top stack from the packaging and from the red plastic tray. Carefully place it on top of the whatman paper, using a rolling method to avoid bubbles. Roll out any bubbles with the blotting roller.

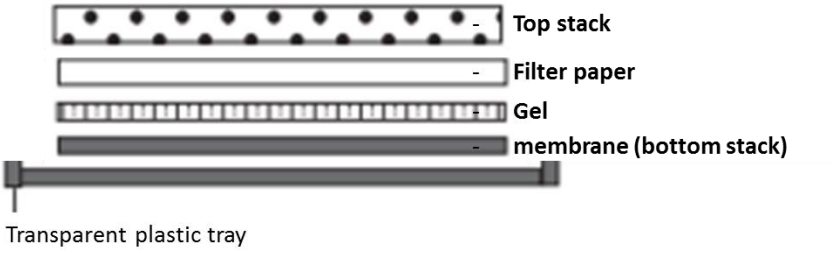

3. Place the sponge into the lid of the iBlot box, making sure that the metal tab is aligned with the metal plate within the bottom of the lid (right side, further point when lid is open).

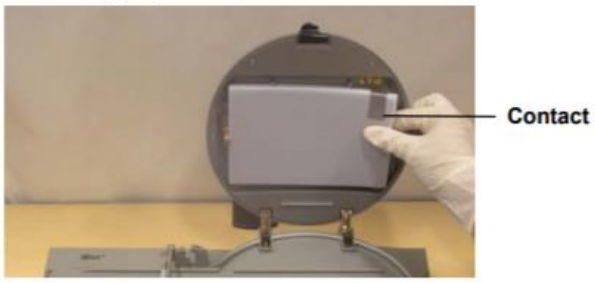

4. Carefully, yet forcefully, close the lid and secure the clasp.
5. Set the desired program and time on the iBlot and clisk start. Set a timer for the same amount of time so you remove the gel quickly once it is done transferring.
6. For 2 gels: remove the first gel and immediately place it into a tray containing blocking buffer. Then setup the second transfer.
7. Continue with Day 1: step 6 of the western protocol

WET

ADDITIONAL REAGENTS/MATERIALS

- XCell II Blot Module (Invitrogen #EI9051)
- Sponge pad for Blotting (Invitrogen #EI9052)
- NuPAGE Transfer Buffer, 20X (Invitrogen #NP0006)
- (optional) NuPAGE Antioxidant (Invitrogen #NP0005)
- Blotting roller (ThermoFisher #84747)
- Methanol
- PVDF membrane
- Whatman 3MM chromatography sheets, 18 x 34cm, thickness: 0.34mm (GE Whatman #3030-221)

PROTOCOL

Note: standard protocol for XCell SureLock Mini-Cell can be found in the company's manual: HERE. All images are taken from this protocol.

1. Prep: 30min before gel is done running
    i. Make 1X NuPAGE transfer buffer with 20% methanol and 1X reducing agent (for 500mL: 25mL 20X transfer buffer, 100mL Methanol, 500ul NuPAGE Antioxidant (optional), 375mL DI water)
    ii. Soak 6 sponges per gel in transfer buffer for ~30min in a Tupperware container to remove all air bubbles
    iii. cut 1 piece of PVDF membrane per gel
    iv. cut 2 pieces of normal thickness Whatman paper per gel
2. When gel is done running, setup transfer using wet transfer apparatus at 30V for 1hr
    i. Gather the materials needed: 1 pre-cut piece of PVDF, 2 pre-cut pieces of whatman paper, forceps, gel knife, blotting roller, 1 membrane-sized tray containing methanol, 1 transfer pipet, new tank with a tension

wedge in place, a top and bottom transfer plate, a empty Tupperware large enough to hold the transfer plates; For each gel, setup a new tank with a gel tension wedge in position. If running 2 gels, you will need 2 separate tanks.

ii. Activate the PVDF membrane in the 100% methanol -- gently shake for 30-60sec in methanol, pour methanol out, do ~3 rapid rinses in dH2O, add transfer buffer. Rotate for ~2-5min until membrane no longer floats (usually the amount of time it takes to setup everything else)

YOU MUST MOVE RELATIVELY QUICKLY ONCE THE PVDF MEMBRANE IS ACTIVATED AS IT TENDS TO QUICKLY DRY OUT WHICH CAN RUIN THE EXPERIMENT.

iii. setup transfer, rolling out bubbles after each layer

FOR EACH GEL, RUN THEM IN SEPARATE TANKS! PUTTING THEM TOGETHER IN THE SAME TANK DOES NOT WORK (DESPITE INVITROGEN'S PROTOCOL SAYING IT CAN BE DONE)

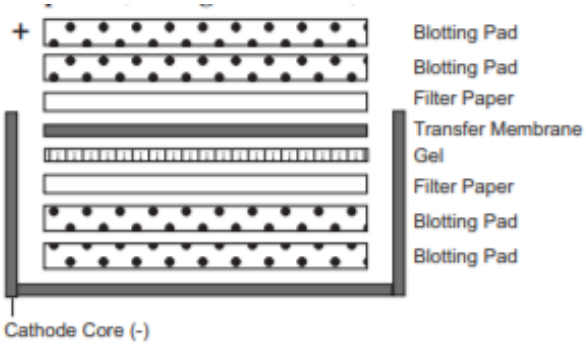

a. place the cathode plate used for transfer in an empty Tupperware container
b. position 2 pre-soaked sponges on top of each other in the bottom of the cathode plate.
c. Using forceps, wet a piece of Whatman paper in transfer buffer and place it on top of the sponge stack. Roll out any bubbles using a blotting roller. Pour 1-2mL of transfer buffer over the top with a transfer pipet.
d. remove gel from apparatus, crack apart the plates using the gel knife, cut off the bottom portion of the gel. Optional: remove wells.
e. Gently lift gel from the bottom (top is too fragile) and place the gel on top of the whatman paper using a rolling method to avoid bubbles. Roll out any bubbles with the blotting roller. Pour 1-2mL of transfer buffer over the top with the transfer pipet.
f. Using forceps, place a piece of activated PVDF membrane on top of the gel using a rolling method to avoid bubbles. Roll out any bubbles with the blotting roller. Pour 1-2mL of transfer buffer over the top with the transfer pipet.
g. Using forceps, wet a piece of Whatman paper with transfer buffer and place it on top of the membrane using a rolling method to

avoid bubbles. Roll out any bubbles with the blotting roller. Pour 1-2mL of transfer buffer over the top with the transfer pipette.

h. place 2+ pre-soaked sponges on top of the whatman paper until there is ~1mm above the top of the cathode plate. Additional sponges maybe needed so there is resistance when you put the anode plate on top of the stack. the tighter the stack the better the transfer.
i. Put the anode plate on top (there should be resistance), lining up the edges of the 2 plates. Squeeze the stack shut (DO NOT LET GO!) and place it into the pre-prepped tank. Clasp the apparatus shut with the tension wedge effectively creating an outer and inner chamber.
j. Repeat for a second gel.

iv. fill the inner cavity with transfer buffer -- only until ~2mm above the stack. fill the outer tank with ~650ml of cold DI water -- ~1cm below the top.
v. position the lid(s) onto the tank(s) and plug in the cathode and anode wires into a power source – be sure to match red-to-red and black-to-black!
vi. Turn on power source and set to 30V. start power source and a timer for 1hr. Both tanks can be plugged into the same power source as long as a constant voltage is used. Be sure to stop then restart the power current if you add a second tank to the same power source if it has already been running. Alternatively use two power sources, 1 for each gel.

3. Continue with Day 1: step 6 of the western protocol

Reprobing methods

NOTES:

- When reprobing a blot, it's important to consider the species of your primary antibodies. If the two antibodies are from the same species (e.g. Rabbit IgG) then they will both be stained with the Rabbit-HRP secondary antibody. Thus they must be a obviously different sizes so you can distinguish the two immunobands.
- It is best to use antibodies from a different species when reprobing. As most of our target use Rabbits to make the antibodies, most of the loading controls I use are mouse-derived antibodies (e.g. Tubulin or GAPDH mouse antibodies) or are directly conjugated with HRP (e.g. Tubulin-HRP).
- I find that using H2O2 over stripping buffer allows me to reprobe the same blot more times with continuing to see strong signal. This method is further preferred when reprobing the same position (e.g. modified H3 versus total H3).
- The stripping time and method may vary between antibodies. When quenching/stripping the membrane, you can re-expose it to ECL and image it again to confirm that you have successfully removed the original signal. You can increase/decrease the time as needed.

- Striping/quenching reduces the ladder strength so make sure you already have a good image of the ladder.

QUENCH HRP (preferred)

REFERENCE: Sennepin AD1, Charpentier S, Normand T, Sarré C, Legrand A, Mollet LM. Multiple reprobing of Western blots after inactivation of peroxidase activity by its substrate, hydrogen peroxide. (Oct 2009) Anal Biochem. 1;393(1):129-31.

REAGENTS

- 30% hydrogen peroxide (H_2O_2) solution
- TBST

PROTOCOL

1. Incubate the membrane in ~5-10mL of H_2O_2 with rotation for 20min. It's best to do this at 37°C. I tend to use the 37°C room across the hall from the Bonini lab and place the membrane/tray on a rotator at a relatively low speed for the machine.
2. Obtain membranes from the 37°C room. Pour off the H_2O_2 and add TBST.
3. Rinse membrane 3X in TBST and perform 3x 5-10min washes with TBST at RT on the rocker (higher speed).
4. Pour off TBST and add blocking buffer. Continue with western blot protocol: Block membrane for 30min at RT. Add primary antibody and incubate overnight at 4°C. Continue with western blot Day 2, step 1.

STRIP

REAGENTS

- Restore Western Blot stripping buffer (ThermoFisher #21059)
- TBST

PROTOCOL

1. Incubate the membrane in ~5-10mL of stripping buffer with rotation for 20min, RT.
2. Pour off the stripping buffer and add TBST.
3. Rinse membrane 3X in TBST and perform 3x 5-10min washes with TBST at RT on the rocker (higher speed).
4. Pour off TBST and add blocking buffer. Continue with western blot protocol: Block membrane for 30min at RT. Add primary antibody and incubate overnight at 4°C. Continue with western blot Day 2, step 1.

Optimized antibodies

Target	Species	Catalog Number	kDa	Dilution	Protein prep	protein/ lane	Transfer method	Ref.
Primary Antibodies								
CDC73/Hyx (*Dmel*.)	Rat	Lis Lab	61	1:3000	LDS	5µl lysate	Wet	[1]
CDC73^{D38E12} (*Hsap*.)	Rabbit	Cell Signaling #8126	61	1:1000	RIPA	20µg	Wet	[3]
eIF4B (*Hsap*.)	Rabbit	Cell Signaling #3592	80	1:1000	RIPA	20µg	Wet	[2]
eIF4B Phospho-Ser422 (*Hsap*.)	Rabbit	Cell Signaling #3591	80	1:1000	RIPA	20µg	Wet	[2]
eIF4H^{D85F2} (*Hsap*.)	Rabbit	Cell Signaling #3469	27	1:1000	RIPA	20µg	Wet	[2]
β-Galactosidase (*Dmel*.)	Rabbit	Promega #Z3781	110	1:2000	LDS	5µl lysate	iBlot: P2, 8min	
GAPDH$^{71.1}$ (*Hsap*.)	Ms IgM	Sigma# G8795	37	1:5000	RIPA	All work	Wet	
GFP^{JL8} (for GR-GFP, *Dmel., Hsap.*)	Ms IgG	Takara# 632380	Varies	1:10000	RIPA	20µg	Wet	[2]
(GR)15 (*Dmel*)	Rabbit	V. Lee Lab #2316	Varies	1:1000	RIPA	20µg	Wet	[2]
Leo1 (*Mmus*., *Hsap.*)	Rabbit	ProteinTech #12281-1-AP	100	1:1000	RIPA	20µg	Wet	[3]
Paf1^{D9G9X} (*Hsap.*)	Rabbit	Cell Signaling #12883	70	1:1000	RIPA	20µg	Wet	[3]
Rtf1 (*Dmel*.)	Rabbit	Lis Lab	88	1:1000	LDS	5µl lysate	Wet	[1]
Rtf1^{D7V3W} (*Hsap.*)	Rabbit	Cell Signaling #14737	60	1:2000	RIPA	20µg	Wet	[3]

TDP-43 (*Dmel.*, *Hsap.*)	Rabbit	ProteinTech #10782-2-AP, Lot# 00009453	43	1:2000	LDS	5µl lysate	iBlot (P0, 7min)	
α-Tubulin (*Dmel.*, *Hsap.*)	Ms IgG	DSHB# AA4.3	55	1:2000	All work	All work	All work	
α-Tubulin^{11H10}-HRP (*Dmel.*, *Hsap.*)	Rabbit	Cell Signaling #9099	55	1:1000	All work	All work	All work	
Secondary antibodies								
Mouse-HRP	Goat	Jackson Labs#115-035-146	Varies	1:5000	All work	All work	All work	
Rabbit-HRP	Goat	Jackson Labs#111-035-144	Varies	1:5000	All work	All work	All work	
Rat-HRP	Goat	Thermo #A10549	Varies	1:5000	All work	All work	All work	

REFERENCES

1. Adelman K, Wei W, Ardehali MB, Werner J, Zhu B, Reinberg D, et al. Drosophila Paf1 Modulates Chromatin Structure at Actively Transcribed Genes. Mol Cell Biol. 2006;26:250–60.

2. Goodman LD, Prudencio M, Srinivasan AR, Rifai OM, Lee VM-Y, Petrucelli L, et al. eIF4B and eIF4H mediate GR production from expanded G4C2 in a Drosophila model for C9orf72-associated ALS. Acta Neuropathol Commun. 2019;

3. Goodman LD, Prudencio M, Kramer NJ, Martinez-Ramirez LF, Srinivasan AR, Lan M, et al. Expanded GGGGCC repeat transcription is mediated by the PAF1 complex in C9orf72-associated FTD. Nature Neuroscience; accepted in principle; 2019.

Behavioral fly assays

RU486-infused food

DISCLAIMER: do not use RU486 if you are pregnant or trying to get pregnant. This is the drug used to induce abortions.

REAGENTS

- RU486 (Mifepristone) powder (Sigma # M8046)
- 200pf Ethanol (newly opened bottle)

PROTOCOL

1. Make RU486 stock and working solution
    a. Make 40mg/ml RU486 stock solution in 100% EtOH. Store in -20^{o}C up to 3mo, covered from light.
    b. Dilute the stock solution to 4 mg/ml working solution in 100% EtOH. Store at 4^{o}deg covered in aluminum to protect it from light.

    NOTE: the 40mg/ml RU486 stock solution can form crystals if old EtOH was used to make it. ALWAYS USE FRESH EtOH. If this occurs, the stock can still be used, you just have to re-dissolve the crystals.

        - Check it ~30min before prepping the dilute working solution. If crystals have formed, incubate the 40mg/ml RU486 stock solution at RT with agitation for ~30min or until it goes into solution.
        - You may need to spin it down to collect all the crystals to the bottom. To do this, spin in a centrifuge at ~3000 x g for ~1min.
2. Make RU486-infused food
    a. Drop 100µl of 4mg/ml working stock to the top of each fly food vial. Concentration depends on how strong of expression you want while typically 50-100µl is used. Use a repeat pipettor for large numbers of vials.
    b. Cover the top of the vials with a piece of cheesecloth and a large rubber band, making sure that the cloth expands past the vials so as to prevent flies from getting into the vials. (For small numbers of vials, you can also just use a cotton plug instead of cheesecloth.)
    c. Rotate vials for 1-3d on a circular rocker
        i. I find I get the most consistent results when I use a slow speed, ~2, on the rocker. When the vials are rotated rapidly, the drug precipitates out of solution and forms clumps in the vials. If this occurs, the food is still usable.
        ii. I check the vials daily to see if the EtOH has fully evaporated. The time it takes seems to depend on the humidity. Once dry, the vials are transferred to the 18^{o}C fly room and can be stored for up to 2wks.

EXPERIMENT DESIGN NOTES

1. For controls, you may want to consider making EtOH only vials (no drug). However, I prefer to use control flies on RU486-infused food as the Gal4[GS]/UAS system seems to have low expression even in the absence of drug.
2. There has been some question in the lab as to the consistency of the RU486 drug's ability to infuse into the food. For short terms experiments, I recommend flipping the flies a minimum of every 2d to help to remove this variable with the logic that the more vials the flies are exposed to the less "noise".
3. For more "immediate" activation of transgene expression it may be necessary to starve the flies overnight before flipping them onto RU486-infused food. It has also been observed that using RU486-infused yeast paste can be ideal for rapid studies.
    a. Starve flies overnight (18-24h) at 25^{o}C in empty vials with a piece of Kimwipe paper wet by water at the bottom.
    b. Transfer starved flies to empty vials with RU486 yeast paste on the wall. Feed flies for 48h at 25^{o}C to induce transgene expression.
4. I recommend flipping the flies every 2d (3d max) onto a fresh RU486-infused vial. The older the flies are, the more vital it is to flip them frequently.

REFERENCES

- Practical Recommendations for the Use of the GeneSwitch Gal4 System to Knock-Down Genes in Drosophila melanogaster. Scialo, F. et al. PLoS One. 2016 Aug 29;11(8):e0161817.
- A conditional tissue-specific transgene expression system using inducible GAL4. Osterwalder, T. et al. Proc Natl Acad Sci U S A. 2001 Oct 23;98(22):12596-601.
- Mitochondrial electron transport chain dysfunction during development does not extend lifespan in Drosophila melanogaster. Rera et al. Mechanisms of Ageing and Development 131 (2010) 156–164.
- The steroid hormone receptor EcR finely modulates Drosophila lifespan during adulthood in a sex-specific manner. Tricoire et al. Mechanisms of Ageing and Development 130 (2009) 547–552.

Lifespans

REAGENTS

- Standard molasses fly food
- RU486-infused food

SUPPLEMENTARY FILE: Lifespan Template.xls

PROTOCOL

1. Setup crosses with DaGS or ElavGS drivers. Raise and maintain progeny at 24^{o}C.
    a. It is good practice to include a negative control of Driver > control transgene (ie. DSRED or BL31603: Luc RNAi). This is a better control than a RU-negative control due to leakiness of the Gal4[geneswitch]/UAS system.
    b. When checking modifiers, it's important to test them for effects alone by expressing the modifier transgene using the driver in the absence of a disease gene.
2. Setup 10 vials of male progeny with the correct genotype/phenotype with 20 animals per vial. Age to 1-2d. It is convenient to use lab tape labeled with the vial identifier and date so you can just transfer this piece of tape to new vials every time you flip the flies.
3. Transfer progeny onto RU486-infused food. Be sure to update the # of animals within the vial if any were dead or lost before putting the animals onto RU so your data is accurate.
4. Transfer the vials to the experimental temperature. I've found that 24^{o}C for DaGS and 29^{o}C for ElavGS produce the most consistent lifespans between experiments.
5. Age flies on RU486-food, flipping every 2d and making sure they are maintained at the same temperature. With every flip, record any animals that have died from natural causes. Censor any animals that escaped or died due to unnatural events: squished during flipping; became wedged between the food and the vial wall in a manner that even a healthy fly would not have been able to survive.
    a. For DaGS: it is essential to record the # of dead flies *every day* until all flies are dead as this is considered a "rapid" lifespan. You still flip every 2d.
    b. It is important to note any dead/censored flies that get transferred into the new vial on the vial so they do not get accidently counted a 2nd time
6. Once all animals have died, update the information in the supplementary file and use this to produce a survival curve and the define any statistical differences between genotypes in GraphPad Prism.

Negative geotaxis

REAGENTS/MATERIALS

- Standard molasses fly food
- RU486-infused food
- Nikon D3200 Camera w/ 2 fully charged batteries
- Marked, empty vials: standard fly vials with lines marked at 1, 3, and 6cm using permanent marker. These vials can be reused so hold onto them!

PROTOCOL

1. Setup crosses with ElavGS. Raise and maintain progeny at 24^{o}C.
    a. It is good practice to include a negative control of Driver > control transgene (ie. DSRED or BL31603: Luc RNAi). This is a better control than a RU-negative control due to leakiness of the Gal4[geneswitch]/UAS system.
    b. When checking modifiers, it's important to test them for effects alone by expressing the modifier transgene using the driver in the absence of a disease gene.
2. Setup 6 vials of desired progeny with the correct genotype/phenotype with 20 animals per vial. Age to 1-2d. It is convenient to use lab tape labeled with the vial identifier and date so you can just transfer this piece of tape to new vials every time you flip the flies. (It is good practice to use males to avoid issues with w+ vs w- on X when comparing multiple RNAi lines from different backgrounds. However females can have stronger climbing deficits.)
3. Transfer progeny onto RU486-infused food. Be sure to update the # of animals within the vial if any were dead or lost before putting the animals onto RU so your data is accurate.
4. Transfer the vials to the experimental temperature. I typically use 24^{o}C.
5. Age flies on RU486-food, flipping every 2d and making sure they are maintained at the same temperature. With every flip, it is important to record any dead or censored animals so you know how many are in each vial.
6. At the desired time point(s), performing climbing assay. THIS MUST BE DONE AT THE SAME TIME EVERY DAY. It is best to perform climbing assays ~10am as this is when the flies are most active. Further, it is convenient to define your time points as days that coincide with flip-days. Last, I like to record the animals using a camera so I can accurately quantify the data later.
    a. Transfer flies from each vial into a marked, empty vial. (I tend to keep the tape with the vial identifier on this vial and then taped above the vial when recording animals for climbing so there is no confusion.)
    b. Let the flies recover for 30min in the incubator set to the experimental temperature. I've found with ElavGS > (G4C2)n animals that they an get hypersensitive to light. To avoid issues in regards to this, I let them recover in a white or yellow rack so they are used to reflective light. Alternatively, traditionally negative geotaxis studies are done in a dark room with a red light.
    c. Prep: setup the camera by sitting it on the lab bench ~ 12" from where the vials will be placed during the assay. Mark a piece of paper with 3 "X"s

evenly spaced apart and tape this to the lab bench where the vials will be. Each vial will then be placed on top of a “X”, ensuring that they are within the visual range of the camera and allowing data from 3 vials to be recorded simultaneously. I also setup an empty fly tray as the backdrop so the flies are against a white background making it easier to see them in the videos.

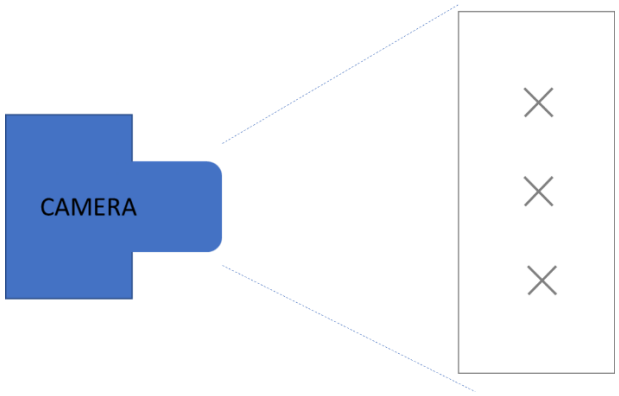

d. Perform round 1 of the climbing assay: place 1 vial on each of the Xs and the tape with the vial identifier on the backdrop above the vial so you know which is which. Set the camera to record. Tap the flies in each vial one at a time down to the bottom of the vial (~3-5 taps). Immediately set the vial down and let the animals recover and climb. Stop recording after ~45-60s. Repeat this for all vials of flies.
e. Let the flies recover for 30min in the incubator set to the experimental temperature.
f. Perform round 2 of the climbing assay as described above.
g. Let the flies recover for 30min in the incubator set to the experimental temperature
h. Perform round 3 of the climbing assay as described above.
i. Once done, anesthetize the flies in each vial one at a time onto a CO2 pad. Record the number of flies present so you have an accurate n. transfer flies into a fresh RU486-infused vial.
j. Place the flies back into the correct incubator set to the experimental temperature until the next time point. Discard the flies when you have recorded data from the last time point.
k. Transfer the video files to your computer for analysis.

7. Analyze the climbing data from the videos, carefully defining the best parameters for your experiment. Typically, I use the 3cm line and record any flies that are unable to climb to this line within 15 or 20sec. For quantification, the final value will be reported as the average % of animals that could climb per vial, using the average from the 3 rounds to compensate for natural variability.

External fly eye imaging

Eye morphology

SUPPLEMENTARY FILE: External Eye Imaging Lab Notebook.xlsx

PROTOCOL

1. Collect flies and age them to desired time point
    a. Collect the progeny with the desired genotype and place them into a new vial. Typically, we image 3-5 flies of the same gender per genotype, thus it's good to collect 4-7 flies in case 1-2 of them get damaged or lost during imaging. Be sure to match the genders and ages of the controls and samples. It is best to collect the progeny at the same time each day in order to ensure they are approximately the same age. By imaging 3 animals, you can then score the samples for quantification in the future.

        Notes

        i. It is best to separate the flies for external eye imaging into different vials than those used for other assays, such as internal sections, as you will be anesthetizing all the flies in the vial during external eye imaging.
        ii. When collecting flies, it's good to visually note any inconsistencies between phenotypes of flies with the same genotype. If there is variation in the external eyes for flies with the same genotypes, gender, and similar age then take 3 images of each different type of eye and note the frequencies of each phenotype to be compared to expected results.
        iii. Typically, we image males for UAS-(G4C2)49 and females for UAS-(GR)36 and UAS-TDP43 (37M). It can be useful to image both sexes for UAS-(G4C2)49 as the milder eye of females promotes the detection of enhancers while the more extreme eye phenotype of males promotes the detection of suppressors.
    b. Age flies for 1 day by placing them back into the incubator from which they came. If you end up imaging them after >1dy, make sure you are consistent between all genotypes, particularly the controls vs samples, for accurate comparisons. Avoid imaging flies >3dyo for typical studies. **Fly Aging**: the flies are 1-2dyo at when imaging as you collected flies when they were 0-1dyo and then aged them by a day making them 1-2dyo. So if you aged them for 2dys then they would be 2-3dyo (another common age to image flies).
2. Imaging the external eyes of *Drosophila*
    a. In the fume hood, pour 1-2 splashes (about 2 mL) of ethyl ether into the bottom of a plastic bottle containing cotton balls in the fume hood. **Make sure you wear gloves during imaging – ether is toxic when in direct**

contact with your skin! Immediately recap the ether bottle so as to prevent evaporation.

b. Turn the microscope on by logging into the computer (Password: drosophila) and opening the LAS program. Gently take the red cover off the microscope and, when prompted, click OK on the computer. The microscope should now move up and down by itself -- if it does not move there is something wrong and you need to contact the person in charge of the APO16! Turn the microscope light on by pressing the switch in the bottom front of the light source.

    Notes

    i. Be sure to switch the light source off when you are not actively imaging to conserve the bulb. This includes if you stop imaging for 30+min with the intention of coming back.
    ii. The microscope and camera should always be on so you should never deal with anything except the computer and the light source.

c. In the fume hood, transfer the flies to be imaged into the white chamber of the pre-prepped ether bottle by flipping them. Immediately place the plastic lid on top of the bottle. Tap the flies to the bottom of the white chamber repeatedly until they remain at the bottom – otherwise they will not all be anesthetized equally. Let the flies incubate for 5-10 minutes in order to anaesthetize them.

    Notes

    i. It is best to turn the microscope on *before* incubating your flies with ether so you can make sure the microscope is functioning normally before anesthetizing precious animals.
    ii. You can use CO_2 to knock out the flies before transferring them to the white chamber if you are uncomfortable flipping them. This also ensures that precious flies won't escape or accidently get crushed.
    iii. Do not incubate animals more than 15min – this starts to dry out the eye tissue while highly degenerative eyes will collapse due to a lack of internal tissue (e.g. YH3 > UAS-(G4C2)49 flies).

d. In the LAS software on the computer, you will need to designate the file in which you want images saved. Under the "Browse" tab, find the folder in which you would like to save your images. Click the folder, and then click "set capture location" – a red dot should appear on your target folder. If you need to create a new folder, name the folder

    Note: It is convenient to name the folders based on the experiment date, in the order YEAR-MONTH-DAY, and a brief description of the experiment. This way, the computer will chronologically organize the folders. Example: "151019 G4C2 TRiP screen".

e. Prepare a slide with double sided tape if you do not already have one.
f. Once the flies are fully anesthetized, gently pour them onto the microscope pad or a paper towel – be sure to check the bottle for any flies stuck in the bottom. Using needle-nose forceps, grab one of the flies <u>by the wings</u> and place it onto the double-sided tape with the animal

facing right (see example slide below). Setup 3-4 flies at a time (if you do more they sit too long and the eyes either move and/or collapse if they are highly degenerative). It is easier to perform this step on a separate dissecting microscope than the APO16 – this also allows you to setup a second set of flies while the first set is being imaged on the APO16, significantly speeding things up (see LARGE-SCALE, RAPID ANALYSIS, below). Reference videos for how to position flies onto double sided tape. Briefly, use a pair of needle-nose forceps to push the fly's abdomen down onto the tape. This should put the eye in a good position for imaging. Keep manipulating the abdomen until the fly's eye is parallel to the plane of the image, not tilted upward or downward. Images have been included below in order to illustrate proper and improper alignments for the fly's eye. If pushing the abdomen no longer causes movement of the head, you can carefully (without touching the eyes) use the tweezers to move fly's head into the correct position and potentially press on the thorax. Do this for each fly one at a time while placing all the flies of the same genotype in a row (see example slide below).

NOTE: there are 3 videos demonstrating this technique that are saved on the APO16 computer: M-external imaging.avi

i. Step 1: position the fly on the slide by grabbing the wings with needle nose forceps and placing the animal on its side, facing right. Be careful not to disrupt the head/eyes.

ii. Step 2: Using the forceps, apply pressure onto the fly's abdomen. It's best to not close the forceps fully, so the abdomen will rupture. If you do not do this, animals may become swollen while imaging and this will cause the eye to move and blurry images.

iii. Step 3: Manipulate the abdomen, head and proboscis with the forceps to get the eye into a level position for imaging, starting with the abdomen. It may be necessary to fold the wing closes to you down over the ruptured tissue so the forceps don't get stuck. Your goal is to get the tissue surrounding the eye to be in the same visual plane. Reference images in *Troubleshooting* for examples. Be careful not to touch the eye with the forceps! Also, if there is debris on the eye (seen as white flakes), it can be gently brushed away with a paint brush or forceps.

Example Slide: Animals are organized with all of one genotype in a column to keep track of samples. Importantly, you cannot place flies to the right on the one you are imaging as this will create a shadow. Animals are organized with all of one genotype in a column to keep track of samples.

Flies are organized on a slide so all of one genotype is in a column, with 3-4 animals per column. Always image from the furthest right column, where there is empty space to the right of the animals, or you will get a shadow.

g. Place the slide with the flies on the microscope pad of the APO16. The large/bottom wheel on the microscope is the coarse focus (zooms in and out of the image) and the small/top wheel is the fine focus (makes the image clearer). Zoom out using the coarse focus and adjust the slide so that the head of your fly is in the image on the computer.
h. Once the fly's head is in the image, slowly zoom in using the coarse focus until it reaches maximum, 115x. You may have to periodically adjust the slide while zooming to ensure that the fly's head stays within the image.
    Note: When you get good at this, you may be able to put the flies in the correct position without zooming in/out. This will significantly save time, while you need to be careful that you are imaging the intended animal. Check this by waving the point of the forceps above the intended animal. You should be able to see the forcepsp in the scope.
i. On the computer, click on the tab that says "Acquire". You will now be performing a z-stack, which takes pictures of the eye with different areas in focus, "different visual planes", and compiles them into a single image with the whole eye in focus.
j. Under the Z-stack tab, click the orange/brown button labeled "Start" once to set the first focus image to be taken. The button should turn black. At this point, adjust the fine focus on the microscope while watching the image on the computer screen so that the center/distal of the eye is just coming into focus. Everything besides the center/distal of the eye should be blurry. Once you are happy with the focus, click the "Start" button again and it should turn orange/brown.

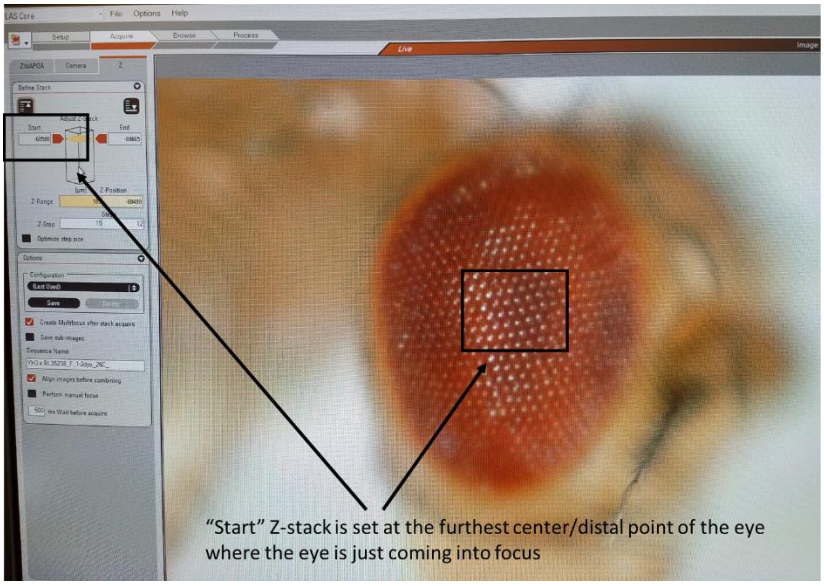

k. Set the "End" focus setting by the same method. Click the orange/brown button labeled "End", which should turn black, and then adjust the fine focus. This time, the center/distal of the eye should be blurry, but the tissue surrounding the external eye should just be in focus. All the tissue on all sides of the eye should be in focus in this visual plane or the eye is tilted (see *Troubleshooting*). Adjust the eye as needed. Once you are happy with the focus and eye position, click the end button and it should once again turn orange/brown.

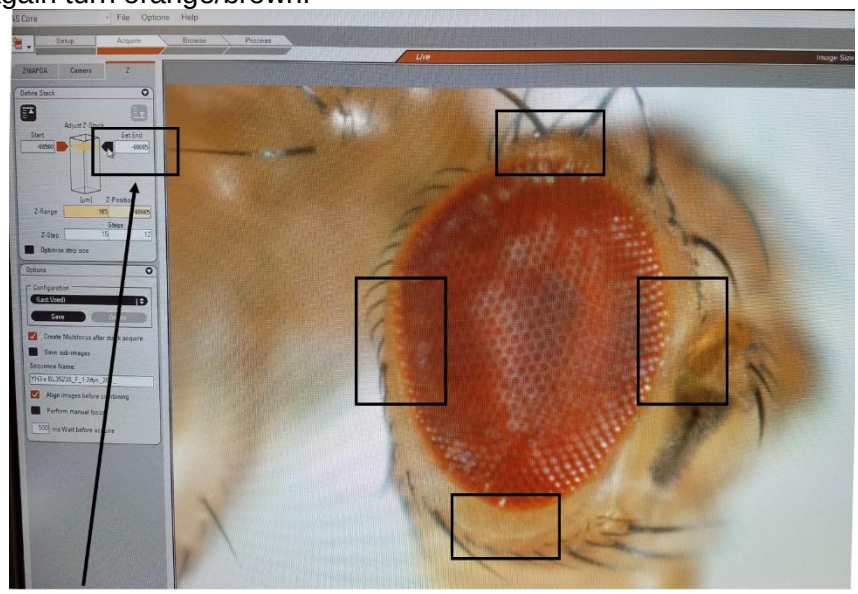

"End" Z-stack is set at the point where the tissue surrounding the eye is just coming into focus. This is also when you can make sure the eye is not tilted as you should be able to see all the surrounding tissue in focus within the same visual plane.

Notes

i. Make sure that the z-step setting is set to 15 steps and the "optimize step size" setting is turned <u>off</u>.

ii. The best images have the background as overexposed and the eye is just below being overexposed. Use the exposure button to detect over/under exposed areas. Go into Acquire and select the "Camera" tab. Click "show under/over exposure" button (which is blue and red). The background should be red indicating it is overexposed while the eye tissue should only have red speckles at bright spots where the ommatidia are reflecting the light.

iii. Preferred settings for external eye images are as follows. The light exposure time will likely change if the light source is moved. The Hue and Sat are not at 0 which creates a slightly bluer image – better for detecting pigment loss as the reds are less robust in the final image.

Exposure: 132ms (varies with light position)

Gain: 2.0x

Saturation: 1.4

Gamma: 0.6

Hue: 180

Sat: 6

l. Under sequence name, enter image name.

Note: It is convenient to keep track of the genotype, age, and gender of the fly here. Example: "FLY LINE x MODIFIER_Sex_age_Temp_" = "49#3.1 x BL31603_M_1-2dyo_26C_". Also, by ending the image name with a "_" the software will automatically add numbers to replicate images so you don't have to change the name for each animal but rather just between genotypes.

m. Place the eyepiece cover (an old pipet tip box) over the eyepieces. Click "Acquire Multifocus" and allow the Z-stack to proceed.

Note**:** At 60% completion, you can move the slide without harming the image (the software is compiling the Z-stacks at this time), so to speed things up you can go ahead and start putting the next animal into position for imaging.

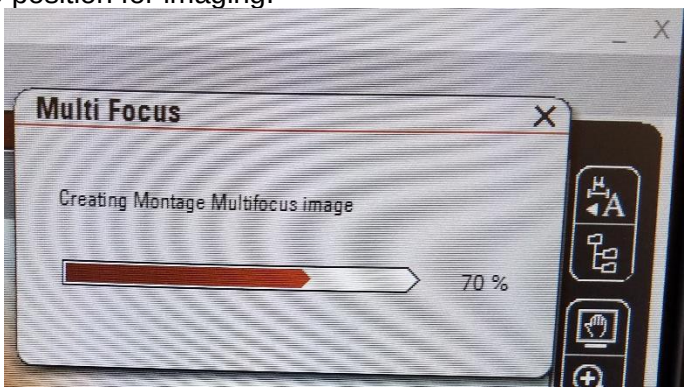

n. When done, close the software (your images will automatically be saved into the selected folder during imaging). Turn of the light source. Gently, place the red cover over the miscroscope while long imaging sessions

may leave the camera (back portion) hot so it may be best not to cover this region up – only covert he eye pieces and main microscope region. You may turn off the computer. DO NOT TURN OFF ANY OTHER SWITCHED -- THE MICROSCOPE OR CAMERA! Remove your images from the computer promptly.

LARGE-SCALE, RAPID ANALYSIS

I typically have 2 slides during one imaging session, 1 slide has flies being imaged on the APO16 while I will be mounting flies onto the second slide under a normal dissection scope. Also, for large scale screens, image 2 flies per genotype, not 3, unless there are inconsistent results. Also, it may be helpful to use the gender differences, particularly for UAS-(G4C2)49, to your advantage. For example, the females of YH3 > UAS-(G4C2)49 tend to have a less severe phenotype than males. So for looking at mild enhancement, females are most useful while males are most useful for looking for suppression. You will be repeating potential hits and that is when you can increase your n.

1. Setup 3 bottles of ether and flip live flies from their vials into the bottles in order – bottle A, bottle B, bottle C. KEEP THE EMPTY VIAL NEXT TO THE CORRESPONDING FLIES AT ALL TIMES UNTIL THE FLIES HAVE BEEN IMAGED SO YOU KEEP TRACK OF WHICH FLIES ARE WHERE.
2. After the flies are anesthetized (~8min), setup the first genotype of flies from bottle A onto slide 1 under a normal dissection scope. Then, start imaging these samples on the APO16. KEEP THE VIAL FOR THESE FLIES NEXT TO THE APO16 SO YOU KNOW WHAT FLIES ARE BEING IMAGED.
3. While they are being imaged, flip a new genotype into the empty bottle A so they will start to be anesthetized and place this bottle behind bottle C, effectively creating a conveyer belt-like system to keep track of everything. MOVE THE CORRESPONDING VIALS SO THEY REMAIN NEXT TO THEIR CORRESPONDING BOTTLE AT ALL TIMES SO YOU KNOW WHICH FLIES ARE IN THE BOTTLE.
4. Start to setup the next genotype of flies from bottle B onto a second slide under the dissection scope, stopping intermittently to image the next fly on slide 1 on the APO16. KEEP THE VIAL FOR THESE FLIES NEXT TO THE DISSECTION SCOPE SO YOU KNOW WHAT FLIES ARE BEING SETUP FOR IMAGING. When all the flies on slide 1 are imaged, I then start to image the flies on slide 2. BE SURE TO RENAME THE NEW SET OF FLIES CORRECTLY IN THE SOFTWARE SO YOU DON'T GET GENOTYPES MIXED UP.
5. As before, I flip the next set of live flies from their vial into the empty bottle B and move the bottles so now bottle C is in the front and B in the back of the conveyer belt-like line – KEEPING THE VIALS NEXT TO THE CORRECT BOTTLES.
6. Repeat this system, setting up the flies from bottle C onto slide 1 while the 2nd set of flies are being imaged on the APO16, stopping intermittently to image the next fly. Repeat until done.

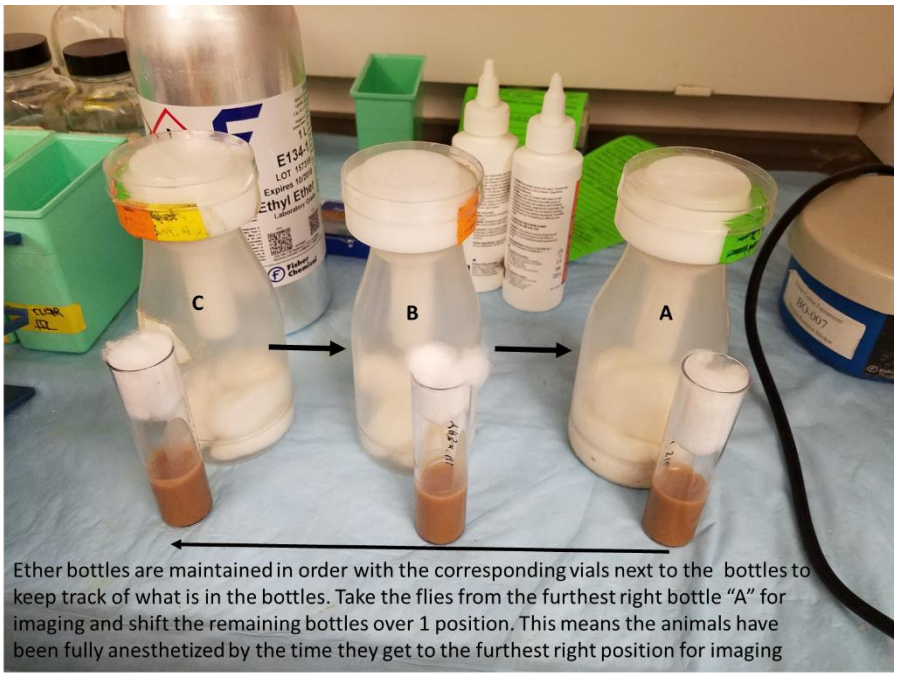

Ether bottles are maintained in order with the corresponding vials next to the bottles to keep track of what is in the bottles. Take the flies from the furthest right bottle "A" for imaging and shift the remaining bottles over 1 position. This means the animals have been fully anesthetized by the time they get to the furthest right position for imaging

Note: some people move slower than others. 3 bottles is standard, but if you are faster, you may find that you need to add a fourth bottle so the flies are effectively anesthetized by the time you get to them. You want the flies to incubate in the ether for ~8min. You may also want to use less bottles if you are imaging more animals per sample than 3 as the flies will be in the ether bottles for longer than 15min. For some genotypes, like (G4C2)49 you cannot keep them in ether for >20min as the eyes will start to collapse.

TROUBLESHOOTING

The APO16 tends to have a problem with the fine focus drifting to the max position over time. You can tell this is happening as the arrow indicating the position of the fine focus drive (the top line on the wheel) will be at the far right edge. When this occurs you need to readjust the position of the fine focus drive.

1. Go into Acquire and select the "Z16APOA" tab. Click "FF" and "C".
2. On the wheel pad, move the wheel position for the fine focus drive back to the left. Move the wheel until the arrow is between the 9:00 and 10:00 position. DO NOT move it all the way to the edge.
3. On the computer, click "MF" and refocus the sample using the arrows on the screen (not the wheel!). This effectively resets the main focus drive position based on the changes you made to the fine focus drive position so you can image.
4. Reclick "FF" and "F" in the software. Continue imaging like normal.

POSITION AND LIGHT SETTINGS

Below are 3 examples of good images. The center of the eye is parallel with the page and in full focus. The top and bottom of the eye are also focused. The eye is

not tilted as is indicated by the tissue surrounding the external eye being in the same visual plane. Further, in these images, it is easy to follow a row of ommatidia across the eye, while the sizes of the ommatida is consistent with the concave nature of the eye. The background is mostly overexposed while the external eye tissue is at the correct exposure.

Correct position and light settings

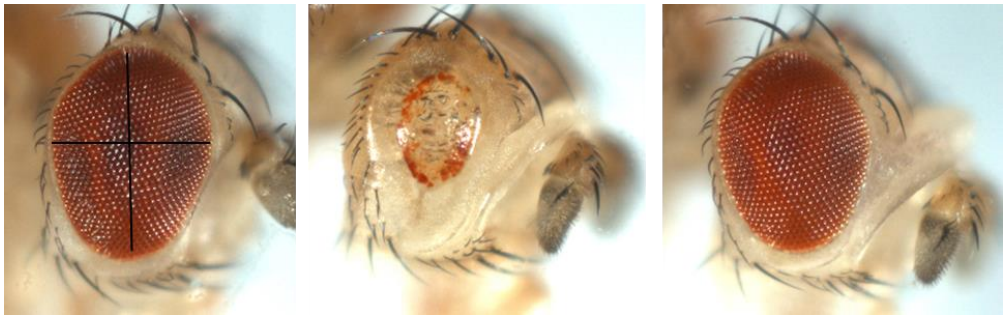

Incorrect position and light settings

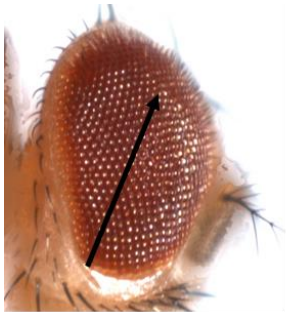

In this image, the eye is dramatically tilted upward and to the right. You can tell as you (1) cannot see all the surrounding tissue and (2) you cannot follow a row of ommatidia across the eye. It is important to manipulate the eye so you can see all of the surrounding tissue around the eye in the same visual plane. This eye needs to be tilted downward and to the left.

In this image, you can see all of the surrounding tissue around, but it is not in the same visual plane as seen by the ommatidia, which become out of focus as you move to the right. The eye is tilted down and to the right. This can easily be fixed by pushing gently upward on the proboscis.

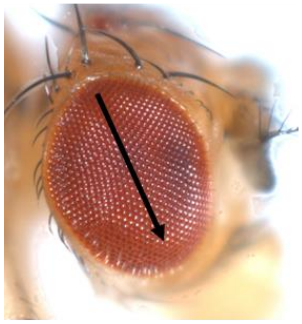

In this image, the bottom of the fly's eye is out of focus while the eye is tilted downward as seen by the surrounding tissue being out of focus when the tissue at the top is in focus. In order to capture a better image, the head should have been adjusted upward by gently pushing up on the proboscis with the forceps, making the surrounding tissue in the same visual plane. This image is also overexposed.

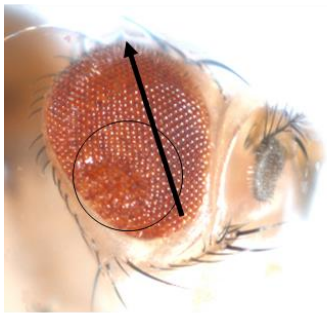

In this image, the top of the fly's eye is out of focus, indicating that it is tilted too far upward. The fly's head should have been tilted downward more so that the full eye was in focus. There is also a dent in the bottom left corner of the fly's eye, which may have occurred if the eye was touched by the forceps. This image is also overexposed.

Eye Morphology Quantification

During my investigations, I performed a large number of modifier crosses to YH3 > (G4C2)49, (GR)36, and TDP-43 flies. From these data, I compiled the below scales to create a scoring method based on the severity of the external eye phenotype.

External eye quantification scale for Gmr-GAL4^{YH3} > (G4C2)49

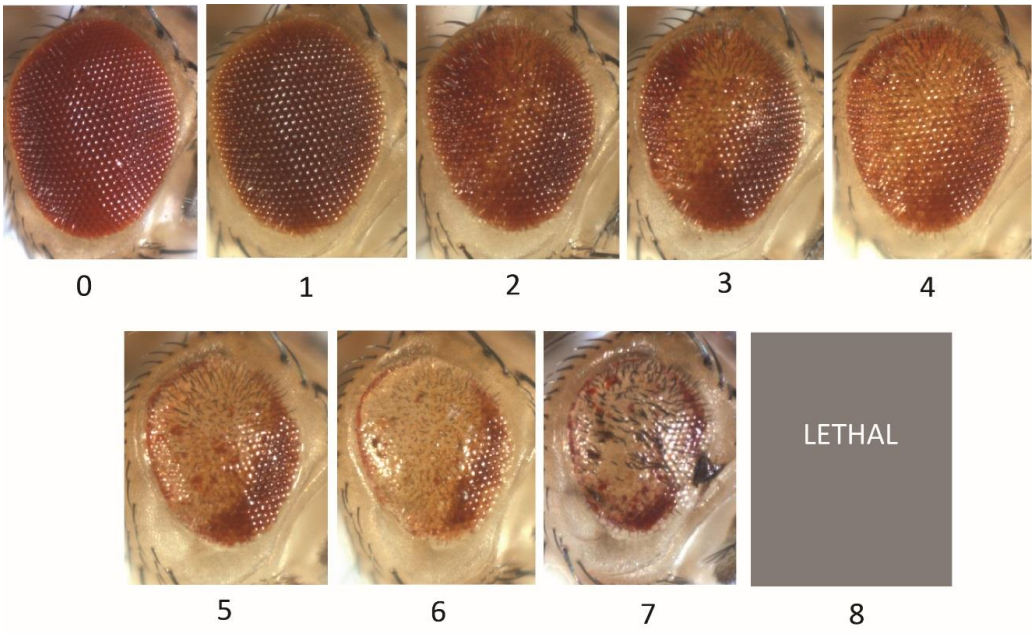

REFERENCE

Kramer NJ, Carlomagno Y, Zhang Y-J, Almeida S, Cook CN, Gendron TF, et al. Spt4 selectively regulates the expression of C9orf72 sense and antisense mutant transcripts associated with c9FTD/ALS. Science. 2016;353:708–12.

External eye quantification scale for Gmr-GAL4^{YH3} > (GR)36

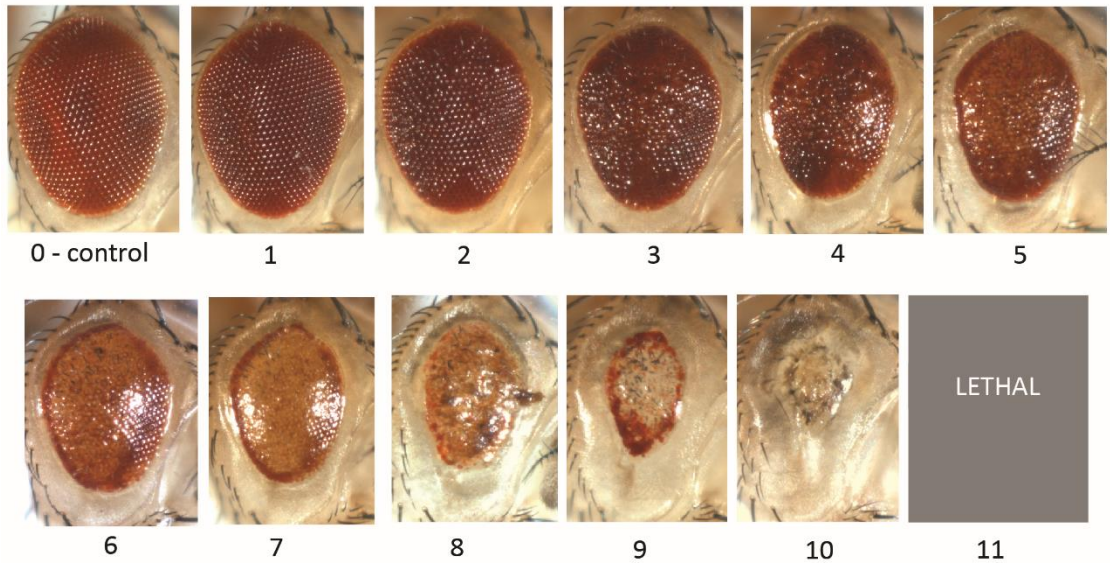

REFERENCE

Mordes DA, Prudencio M, Goodman LD, Klim JR, Moccia R, Limone F, et al. Dipeptide repeat proteins activate a heat shock response found in C9ORF72-ALS/FTLD patients. Acta Neuropathol Commun [Internet]. 2018 [cited 2018 Nov 28];6. Available from: https://www.ncbi.nlm.nih.gov/pmc/articles/PMC6031111/

External eye quantification scale for Gmr-GAL4^{YH3} > TDP-43^{37M}

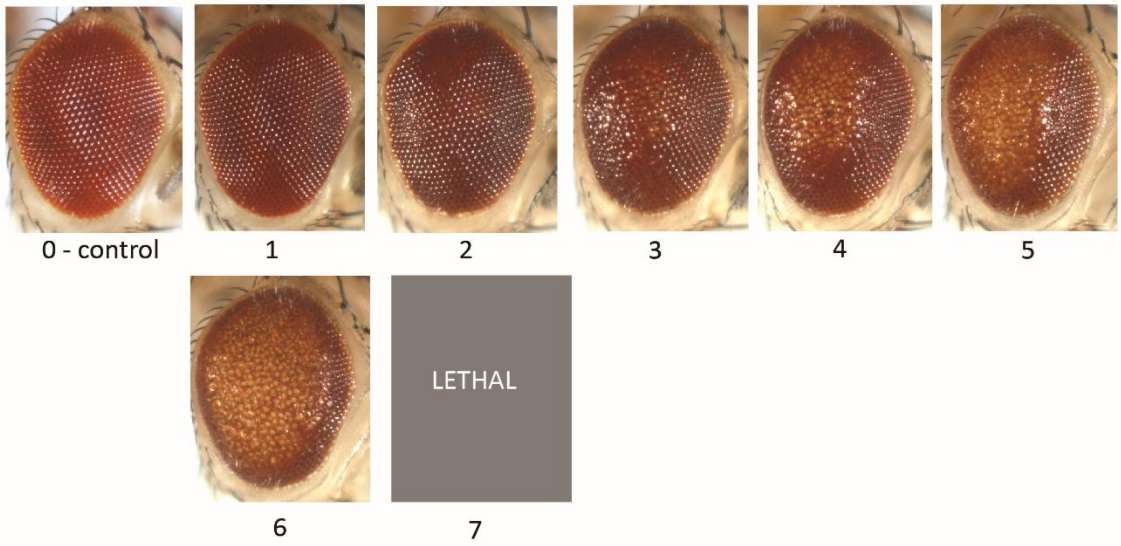

Fluorescence (GFP)

NOTES

- When performing multiple assays on the same cross (external eye imaging for morphology and GFP, plus collecting eyes for internal eye analysis), it is easiest to separate the flies for each assay into different vials.
- Typically, we image females as they are larger and easier to image. Further, females tend to have less of an external eye phenotype so we are able to avoid any loss is signal due to reduced tissue integrity.
- For YH3 > LDS-(G4C2)44$^{GR\text{-}GFP}$ flies, it is essential that you match the *white* gene between crosses and controls (either image all flies with mutant *white* or all flies with wild-type *white*). The *mini-white* gene seems to look the same as *white* mutant flies.
- For modification of extreme degenerative phenotypes, like YH3 > LDS-(G4C2)42$^{GA\text{-}GFP}$#2S, consider if any reduced fluorescence is the result of suppression of toxicity caused by a modifier and thus recovered pigmentation versus actual reduced fluorescence. (this is not a concern with YH3 > LDS-(G4C2)44$^{GR\text{-}GFP}$ flies as pigment loss is relatively weak.)

FLY LINE: Gmr-GAL4^{YH3} (III)

PROTOCOL

1. Collect flies and age them to desired time point (typically 1-2d)
    a. Collect the progeny with the desired genotype and place them into a new vial. Typically, we image 3-4 flies of the same gender per genotype for screening and 6-10 flies for quantification, thus it's good to collect a few extra flies in case 1-2 of them get damaged or lost during imaging. Be sure to match the genders and ages of the controls and samples. It is best to collect the progeny at the same time each day in order to ensure they are approximately the same age. By imaging 3+ animals, you can then score the samples for quantification in the future.

        Note**:** When collecting flies, it's good to visually note any inconsistencies between phenotypes of flies with the same genotype. If there is variation in the external eyes for flies with the same genotypes, gender, and similar age then take 3 images of each different type of eye and note the frequencies of each phenotype to be compared to expected results.

    b. Age flies for 1 day by placing them back into the incubator from which they came. If you end up imaging them after >1dy, make sure you are consistent between all genotypes, particularly the controls vs samples, for accurate comparisons. Avoid imaging flies >3dyo for typical studies.
        Note: It is essential that all flies are the same age. 1-2d vs 2-3d YH3 > LDS-(G4C2)44$^{GR\text{-}GFP}$ flies have different GFP-signal strength depending on their age. I tend to use 1-2d animals.

2. GFP Imaging
    b. Prepare a 10cc or 20cc luer-lock syringe with Vaseline by filling the syringe with Vaseline – pull out the plunger and fill the syringe with Vaseline using a spatula. Replace the plunger and add a 20G needle. Squeeze out the air until you start to get a thin stream of Vaseline. Use a Kimwipe to clean away excess Vaseline. *Very carefully, recap the needle*.
    c. In the microscope room, turn on the Leica DM6000 B microscope by flipping the switch on the main microscope (right side box) and the fluorescence lamp (left side box) on the shelf. The microscope should start making noise as it turns on. After it is fully on, open the primary software on the computer, LAS AF, making sure that the configuration is set to "DefaultDynamicWidefieldTree". Press OK and the system will turn on completely.

        Notes**:**

        i. Be sure to turn the microscope off when you are done!
        ii. Be sure to keep the fluorescence lamp on for a minimum of 30min. Turning it off too soon can damage the bulb.

    d. In the LAS software on the computer, click on the "Experiments" tab and click "new" to start a new experiment. Label the experiment file. Click the "Acquisition" tab and click "z" to turn on Z-stacks. Setup 2 channel imaging with GFP being the first channel then brightfield the second channel. *IT IS IMPORTANT THAT GFP IS IMAGED FIRST AS THE SIGNAL QUENCHES RELATIVELY EASILY.* Typical settings for GFP: 0.1-1s exposure, 1.0 gain. Typical settings for brightfield: 50ms exposure, 1.0 gain. Z-stacks are set to 1um stacks.

        Notes

        i. It is convenient to name the folders based on the experiment date, in the order YEAR-MONTH-DAY, and a brief description of the experiment. This way, the computer will chronologically organize the folders while you know which experiment is which. Example: "151019 G4C2 TRiP screen".
        ii. It is convenient to simply open up a previous experiment. Right click on one of the samples and select "properties". Then click "apply settings". This will automatically set the software's settings to those desired – z-stack, correct exposure, etc. Further, this ensures consistency between different time points for the same experiment as the settings will all be the same between time points. You will still need to manually change the objective, etc on the microscope.
        iii. It is important to record the exact settings you used for each experiment. For example, the exposure time may be different between experiments so you should have recorded exactly what was done. This also means you can recheck that everything is correct as settings may have been changed by other users. This includes settings in the software, but more importantly settings on the microscope (e.g. intensity and field).

e. Prepare the microscope by turning the settings to normal brightfield. Use the 20X objective with a 1x optical zoom.
f. Turn CO_2 tanks on by turning the knob (by the door). Turn on the CO_2 for the dissecting scope next to the fluorescent microscope by unclipping the white clip on the hose so it is going through the CO_2 pad (you should be able to hear it, but don't want it to be too strong as it's a waste of CO_2). Transfer the flies to be imaged onto the white CO_2 pad by flipping the vial so the opening faces the CO_2 pad and tapping the flies onto the pad. The CO_2 should be running just strong enough to keep the flies anesthetized.
g. Once the flies are fully anesthetized, squeeze a thin line of Vaseline onto a clean microscope slide; I usually make the stripe the length of the slide and then save the slide for serial imaging sessions. Reference videos for how to position fly heads into Vaseline for imaging. Briefly, using 2 pairs of needle-nose forceps, decapitate the first animal by squeezing the "shoulders" together with one pair and grabbing the neck with the second pair. Transfer the head to the slide, placing it next to the Vaseline and facing upwards. Flip the head onto one side so the head is being held in place by the Vaseline while one eye is facing upward for imaging. Be careful not to get Vaseline on the eye to be imaged as this will create a blotchy image. Setup 2-5 heads at a time, depending on your speed.
    Notes:
    i. The heads must be imaged within 15min or the cells start to decay, reducing the image quality.
    ii. Try to avoid too much light exposure while setting up the heads by turning the dissection scope light off when you are not actively using it. Also, I let samples sit for ~1-2min before imaging to allow any quenched signal to recover.
h. Step 1: position the fly for decapitation by grabbing it by the "shoulders" with one hand, squeezing gently to make the head "pop-out" and expose the neck. With your dominant hand, grab the "neck" of the fly and tear at an angle (must be at an angle to effectively sever the ganglia and organs).

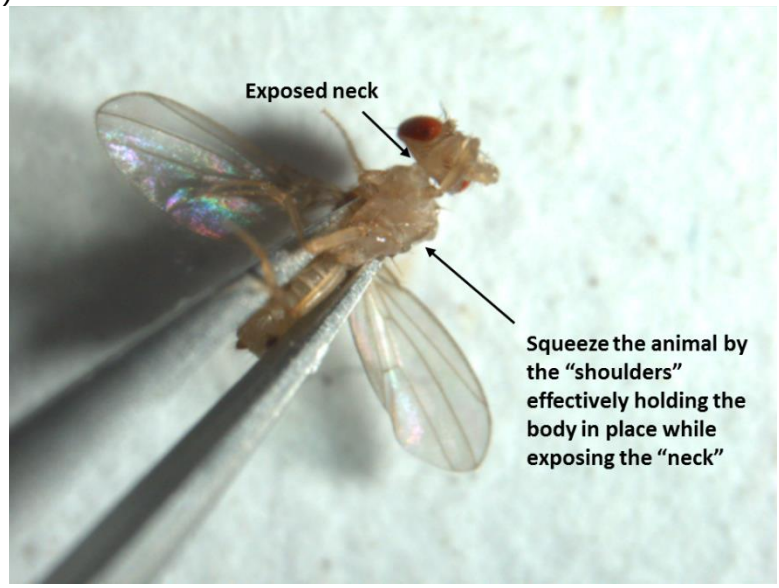

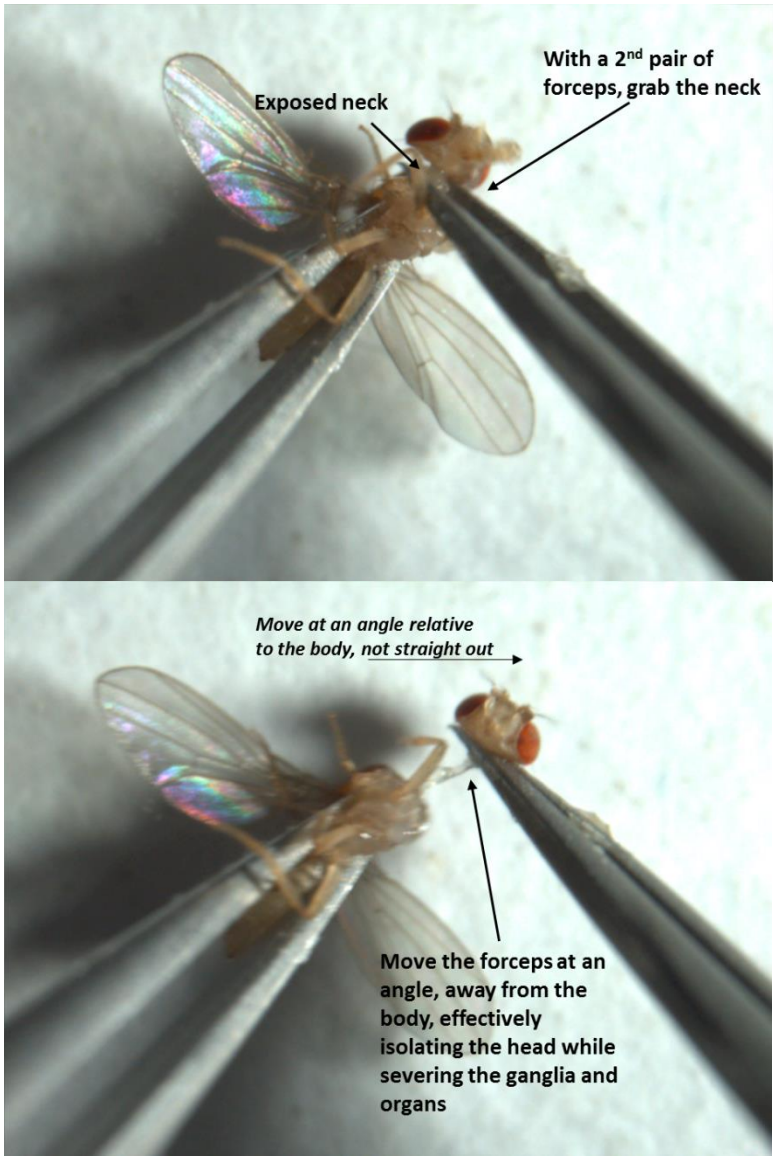
With a 2nd pair of forceps, grab the neck
Exposed neck
Move at an angle relative to the body, not straight out
Move the forceps at an angle, away from the body, effectively isolating the head while severing the ganglia and organs

i. Step 2: Position the isolated head against a ~1-1.5cm line of Vaseline on a clean microscope slide. Sit the head on the slide then move the eye closest to the Vaseline into the Vaseline. Then move the other eye upward effectively positioning the head for imaging on its side.

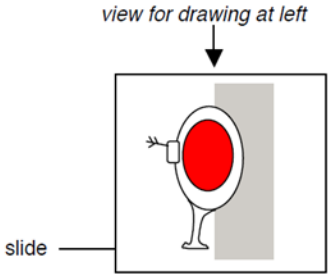

From Derek Lessing's protocol

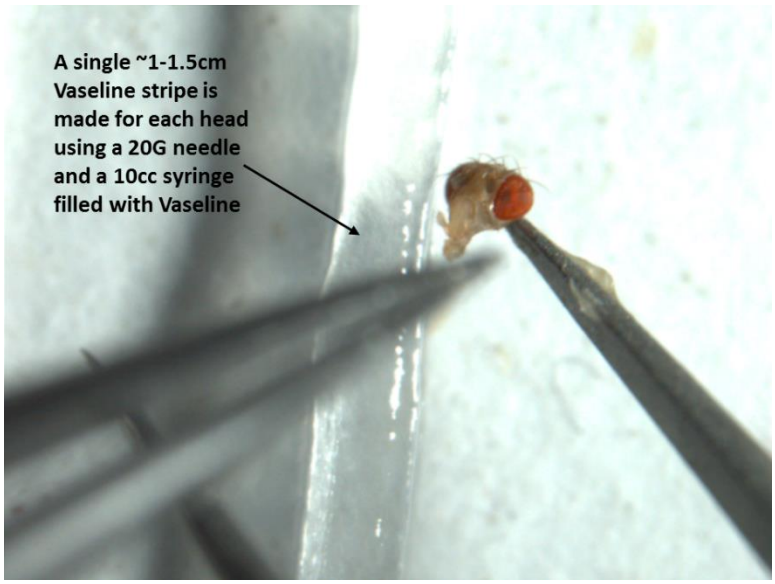

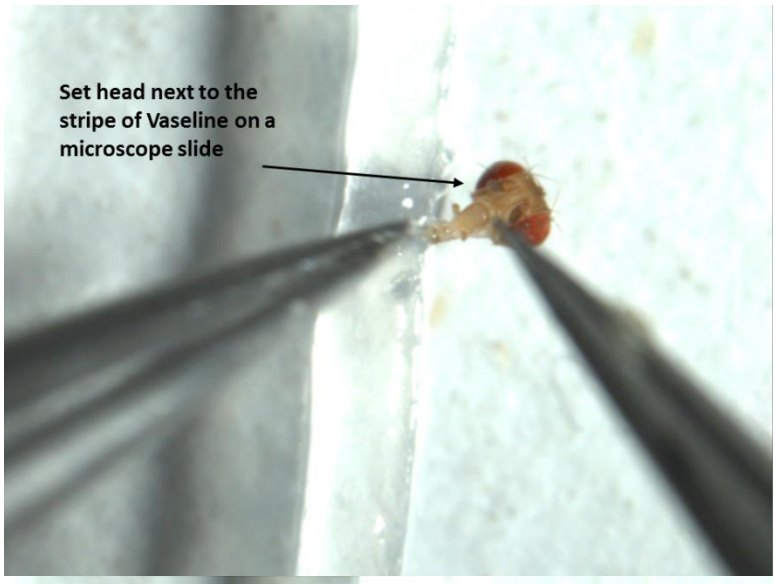
Set head next to the
stripe of Vaseline on a
microscope slide

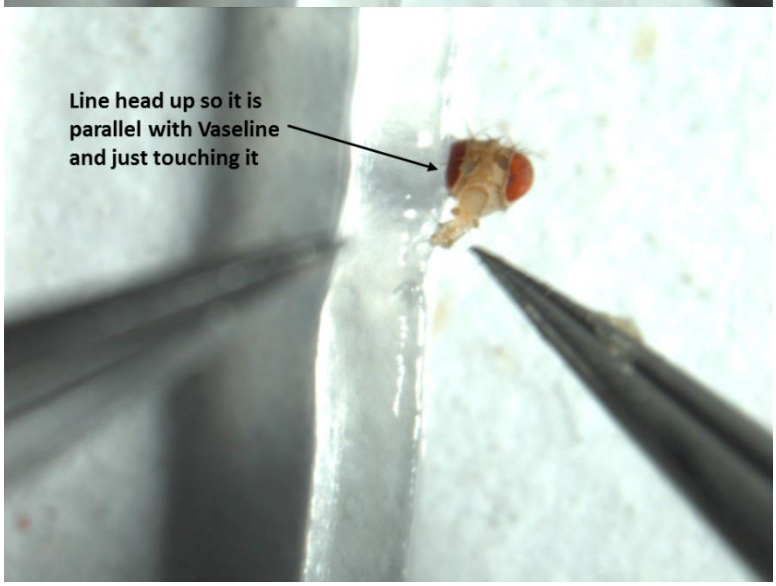
Line head up so it is
parallel with Vaseline
and just touching it

Place forceps under the 2nd eye and gently move the head onto its side with an upward motion, effectively exposing the retinal tissue of the eye to be imaged. Be careful not to get Vaseline on this eye by regularly wiping off the forceps with a Kimwipe

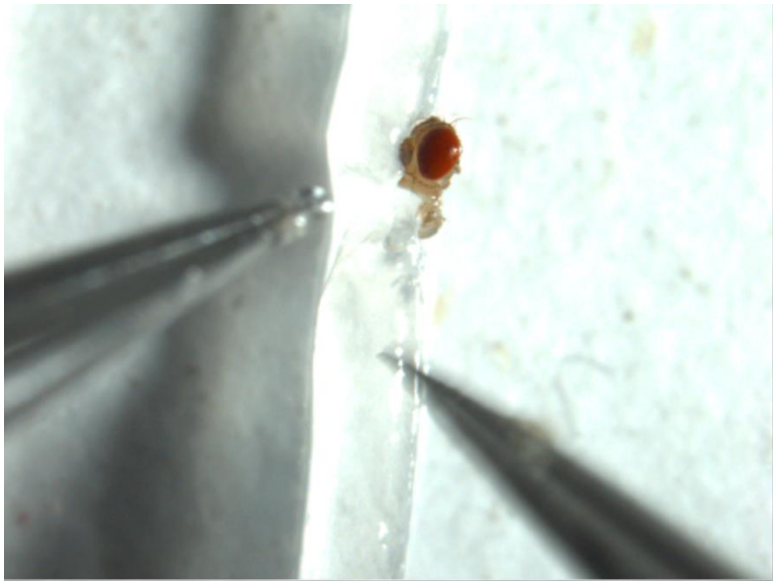

j. Step 3: To ensure that the head remains in position during imaging with immersion oil, wrap a small amount of the Vaseline around the proboscis effectively holding the head in place. Be sure to avoid getting Vaseline on the eye tissue as this will result in blurred images and/or higher background.

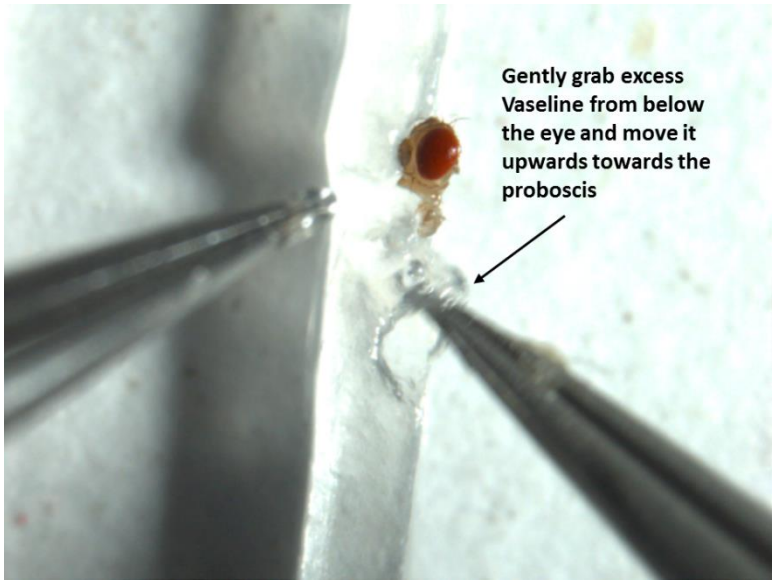

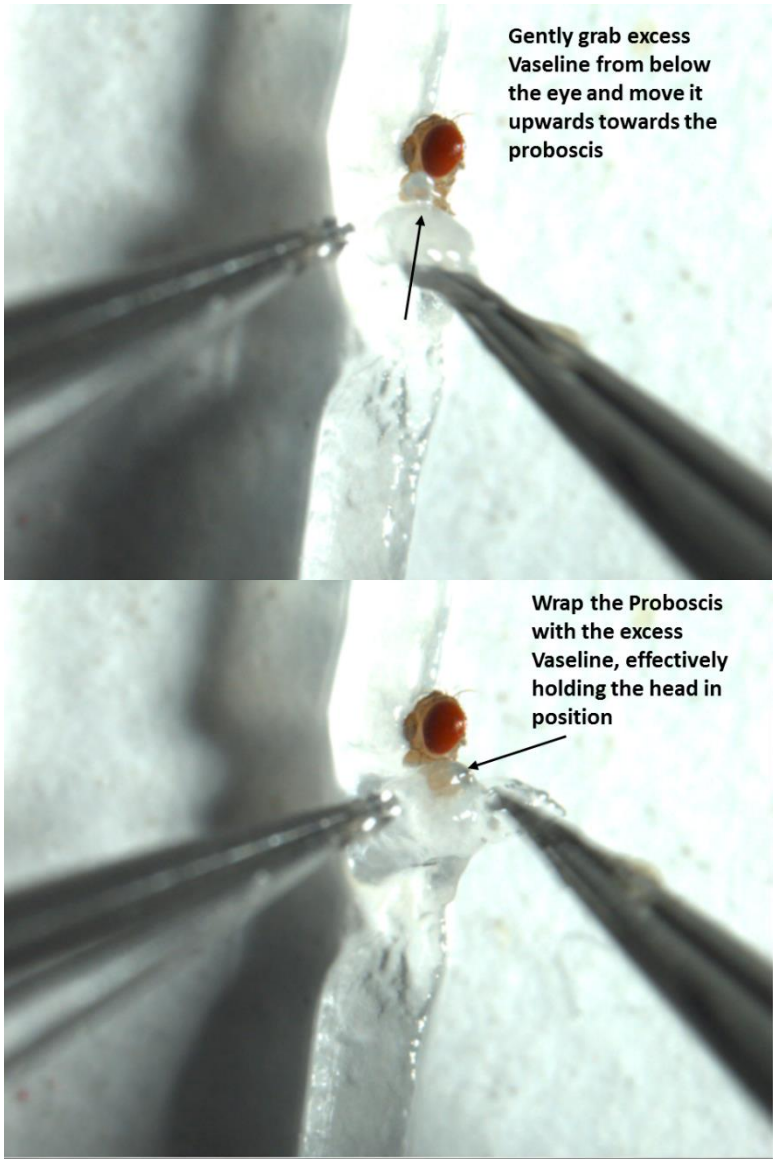
Gently grab excess Vaseline from below the eye and move it upwards towards the proboscis
Wrap the Proboscis with the excess Vaseline, effectively holding the head in position

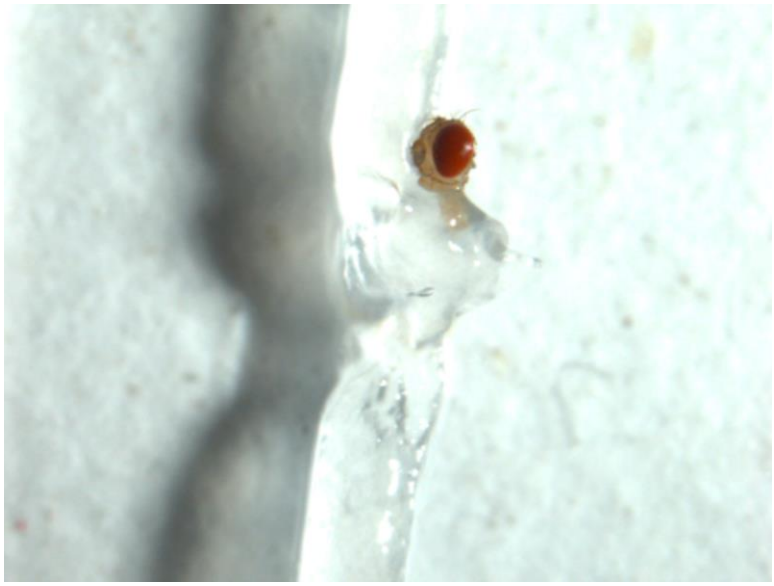

k. Place the slide on the stage of the DM6000 and turn on the brightfeild light. Move the first head into a position close to the light beam so you are relatively in the correct location while looking from the side of the microscope – you can tell as the light will turn darker with slight reddish hue when it is directly above the head. While looking through the eyepiece, slowly move the course focus into position above the eye until you can start to make out the external eye. On the microscope, click "live" set the top and bottom Z-stacks so you capture the entire external eye surface in the image. *To avoid taking pictures when the GFP signal is quenched, let the head sit for 1-2min without being exposed to any light.* Once the fly's head is ready for imaging click "start".
    Note: Normally I image both with the eyepiece and camera open (middle position of the knob on the left of the eyepiece). However, on dimmer samples it may be necessary to adjust the knob so the image is going through only the camera or the eyepiece depending on what you are doing.
l. Rename the image sequence under "Experiments" based on the genotype and any other relevant information.
m. When done, be sure to save the experiment and close the software. Turn off the microscope.

2. Quantify data in ImageJ using the Z-stacked image:
    a. Open images from the .lif file in FIJI (ImageJ)
    b. Create compiled Z-stack: Click Image > stacks > Z project
    c. Measure total fluorescence: https://sciencetechblog.wordpress.com/2011/05/24/measuring-cell-fluorescence-using-imagej/
    d. Measure particle # and size
        i. Click Analyze > set scale: Record scale value (should be 2.7151pixels/micron if images taken with 20X objective lens and 1.25X zoom)
        ii. Click Image > stacks > Z project (should be set to "Max Intensity") > OK (should be a 8-bit, gray-scale image)

iii. Click Image > adjust > threshold
    1. Set threshold 45-255 (settings may change depending on the assay)
    2. Click “Apply” > “X” > “Cancel” on pop-up box that says, “convert stack to Binary”
iv. Click Analyze > Analyze particles
    1. Set size (micron^2) to “0.5-infinity”
    2. Under “Show” click “outlines” – check that the objects outlined are accurate. If foci are being merged into 1 object, increase threshold. If you are missing foci, decrease threshold.
    3. Check: Display results, Clear results, summarize
    4. Click “OK”. It will ask if you want to analyze 2 images. Click No (but doesn’t really matter)
v. Copy Area data to Excel
    1. Report number of objects per eye
    2. Report Mean Area of objects per eye

3. For publication, I use the compiled Z-stack image of the GFP. I then use the lowest stack from the brightfield image to determine where the eye tissue is within the GFP image, drawing a dotted line around the eye tissue. It is also useful to determine if there is increased GFP expression by setting the exposure on the controls to just right below overexposure using the LUT image setting. Then when you image the samples of interest, if the GFP signal is indeed brighter, there will be blue overexposed regions.

Example of final image with LUT setting: LUT allows for detection of increased GFP with mild changes. Combined external eye images from the APO16 with these GFP images allow for analysis of GFP levels in comparison to how toxicity in the eye is changed with modifiers.

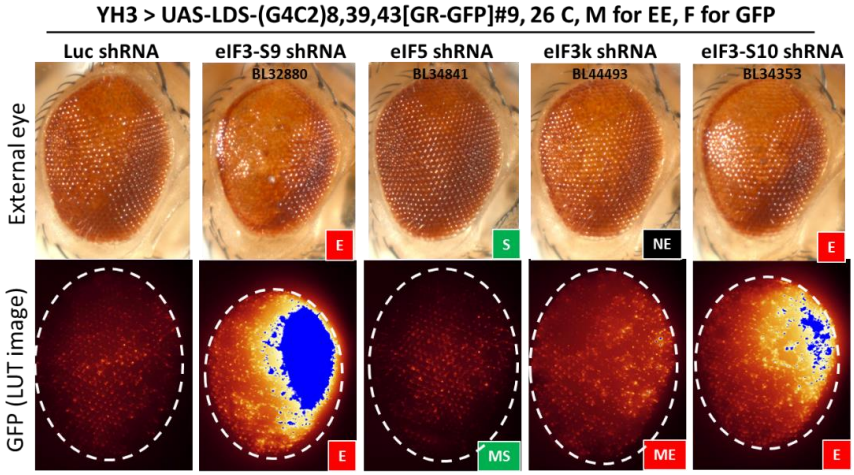

All images taken with a 300ms exposure

Internal fly eye imaging

NOTE: The lab tends to use Cytoseal/Hysto-clear for mounting coverslips onto slides. Herein, I use Permount/xylenes. Permount is significantly easier to handle and is used by pathologists in the clinic! Either will work and the protocol doesn't change overall. Note that Permount can be removed by soaking the slides in xylenes; this can be convenient if something goes wrong during this step. Also, Permount requires xylenes (cannot be used with histoclear).

RECORD KEEPING

The standard way of keeping track of paraffin-embedded tissue is to assign a coded number to each sample. I used "GC###" for G4C2-project while most people use their initials. I maintain an excel sheet summarizing all samples. I recommend recording the following information: Experiment Date, parental flies, genotype, gender, n, temperature, age, days on Bouin's, date of processing, days in EtOH after leaching, date that they were sectioned (n). It is convenient to keep track of dates in case reagents go bad or for any other troubleshooting.

REAGENTS/MATERIALS

- Bouin's Fixative (Sigma # HT10132)
- Salinized Glass Wool (Sigma # 20411)
- Disposable Transfer pipettes
    - Standard: 2.5mL (Thermo Sci # 212)
    - Fine Tip: 1.5mL (Fisher Sci # 13-711-25)
- Leaching buffer:
    - 50ml of 1M Tris, ph8.0 to 50mM (Invitrogen Cat# 15568-025)
    - 8.7g of NaCl to 150mM
    - Water to 1L
- Lid from a 6- or 12-welled tissue culture (TC-) plate
- Permount (Fisher Sci # SP15-100)
- Xylenes (Fisher Sci. # X5S-4)
- 25 x 75mm glass slides (positively charged)
- 22 x 50mm cover slips
- Embedding paraffin, medium (Leica # 3801320)
- Lens paper, cut into ~1.5" x 2" sheets (fisher Sci # 11-996)
- Embedding cassette (Fisher Sci # 15-200-402)
- Embedding rings (EMS # 62350)
- Metal molds (EMS # 62527-16)
- Slide rack (EMS # 62543-06)
- Staining dish (EMS # 62541)
- Microtome blades (Leica # 63065-HP)

PROTOCOL
Day 0

1. Fixing Heads for Paraffin Sections
    a. Collect flies. Typically 6-8 flies/genotype is sufficient.
        i. For Gmr-gal4 studies, it is best to collect 1-3 day old animals as these have reached full maturation
        ii. Females are larger so there is a size advantage to using them. Setting/ checking sectioning orientation is more difficult with males. However, males and females can show differences in transgene expression which can be useful in screening enhancers vs suppressors.
    b. Using forceps, decapitate the animals and put their heads into the pre-labeled microcentrifuge tube containing ~1.0ml Bouin's fixative.
        i. Anesthetize the flies with CO2. With one pair of needle-nose forceps, squeeze a fly at the "shoulders" which causes the head to prop outward revealing the neck. With a second pair of foceps, cut the head off at the neck. Clean up the head prep by removing any crop, foregut or other tissue still attached to the head, being cautious to avoid any damage to the eyes and head.
        ii. Immediately, transfer heads to the Bouin's/tube.
        iii. Collect additional heads
    c. Slowly submerge a bean-sized piece of glass wool into the microcentrifuge tube, allowing air to move around the glass wool. Effectively this submerges the heads into Bouin's and acts as a plug.
        Note: I've found that a looser ball of wool is better. Tighter plugs result in air bubbles forming between the wool and the Bouin's surface.

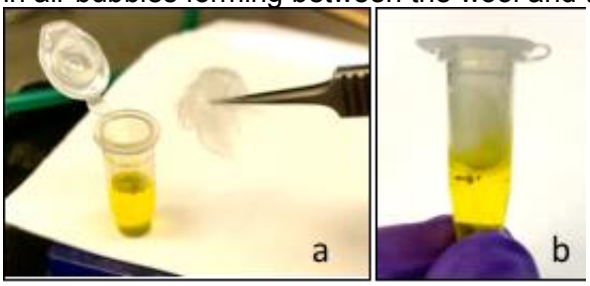

2. Repeat these steps for each genotype until all heads are collected.
3. Incubate tubes at RT for 5d with slow agitation.

    Note: you may need to check the samples after 24h to remove bubbles that form below the plug. To do this, using forceps squish the glass wool to one side and gently push down, effectively squeezing the bubble out from the side of the tube free of the wool.

Day 5

a. Leach samples for paraffin embedding. Note: It is convenient to transfer heads to cassettes and leach them at the end of the day so they are ready to be processed in the morning.
    a. Prep: Collect the following reagents into the fume hood

i. Pre-cut lens paper (1 per sample)
ii. Staining dish filled half-way with leaching buffer
iii. 2 pairs of needle-nose forceps
iv. TC-plate lid
v. pre-labeled plastic cassettes (labeled with pencil!)
vi. a transfer pipettes (both sizes)
vii. a waste container for formaldehyde waste
viii. samples that have been on fixative for 5d.

b. Using forceps, carefully remove the glass wool from your first sample. Using the fine tip transfer pipette, immediately remove all the Bouin's. Using a standard transfer pipette, immediately add ~500-1000µl of leaching buffer. Make sure not to squish or lose any heads. Repeat for all samples.

Note; The heads typically sink to the bottom of the tubes when fixed, but this is not necessary. I have had great images using heads that floated at this stage.

c. Perform 2-3 washes with leaching buffer using the fine tip transfer pipette to remove buffer in the tube and using the standard transfer pipette to add fresh leaching buffer. When on last wash, keep all samples in leaching buffer.

b. Transfer fixed heads to a plastic cassette

a. Position the TC-plate lid so the cell-side is facing you and it is at ~20^{o} angle. Wet a piece of lens paper placed on top it using a standard transfer pipette – just need a few drops to get the paper to stick to the lid.

Notes:

- the angle allows excess buffer to roll to the bottom of the plate when transferring heads to the paper. The edges of the lid help to collect the buffer at the bottom while the ridges for each well create small barriers which are useful for keeping heads in place.
- do not add too much buffer when wetting the lens paper. This can make it difficult later when trying to keep heads in the center of the paper.

b. Using the standard transfer pipette, gently transfer the heads to the center of the pre-wet lens paper on the lid. Fold the lens paper around the heads using forceps, effectively creating a package with them trapped inside. Try to avoid any bubbles forming between or around heads as this will prevent chemical access later.

Notes

- It is vital that the heads are fully enclosed or you will lose them!
- it is important to position the heads so that they do not fall into any creases when the paper is folded as this prevents processing chemicals from accessing the heads.
- It is preferable to separate the heads from each other for better chemical access.
- It is preferable to not align the edges of the lens paper as this will make it more difficult to access the heads within the lens paper later.

c. transfer the heads/lens paper to a pre-labeled embedding cassette. Immediately transfer to the staining dish.

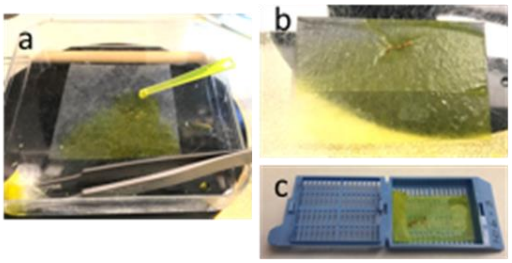

Note: this sample has too much residual Bouin's. it should be clear, not yellow. Also, it's better to avoid lining up edges of the lens paper when folding the paper around the heads. (b did not do this)

d. Repeat steps for all samples, adding more leaching buffer to the staining dish as needed to keep cassettes submerged.

c. Leach samples for 4-10h with agitation at RT.

Notes:

- samples can be stored at 4°C in 70% ethanol for ~5d prior to processing. (This is useful for accumulating multiple samples.)
- I have had success leaching samples overnight in the tubes and then transferring the heads to cassettes the next morning for processing.

Day 6: Embed samples into paraffin

1. Prepare
   a. ethanol (EtOH) and xylene solutions (can be reused ~10 times)
      - 70% EtOH
      - 90% EtOH (it is convenient to simply use 190pf EtOH if available)
      - 95% EtOH
      - 100% EtOH I
      - 100% EtOH II
      - Xylenes I (in fume hood)
      - Xylenes II (in fume hood)
   b. make sure paraffin tanks are on (should be ~61°C) and there is sufficient paraffin in them. Add more paraffin as needed (so ~1.5" deep).
2. Pour leaching buffer out of staining dish containing leached samples and pour in 70% EtOH. Incubate for 30min at RT with agitation.
3. Pour 70% EtOH out of staining dish and pour in 90% EtOH. Incubate for 30min at RT with agitation. Continue 30min incubations with the subsequent EtOH solutions: 95% EtOH → 100% EtOH I → 100% EtOH II.
4. In the fume hood, pour 100% EtOH II out of staining dish and pour in Xylenes I. Incubate for 30min within the fume hood. Continue 30min incubation with Xylenes II.
5. Transfer cassettes to paraffin I tank (closest to fume hood), making sure they are all fully submerged. Incubate for 1h. Note: It is convenient to use the metal cassette-rack that is stored above the paraffin tanks to hold cassettes together.

6. Transfer cassettes to paraffin II tank, making sure to let the paraffin drain between tanks (<1min) and that they are all fully submerged once in the new tank. Incubate for 1h.
7. Remove cassettes from paraffin tank II and let them cool to RT in the fume hood. It can be convenient to cool them on a cardboard fly-vial rack insert, as they tend to stick together or to paper towels.
8. Store cassettes at RT for future use.

Section paraffin-embedded fly heads

1. Block heads

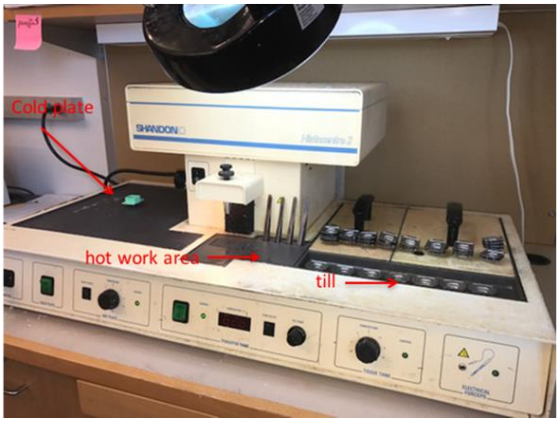

Bonini lab blocking station: Molten paraffin is distributed from a nozzle in the hot work area controlled by a foot pedal located on the floor. The hot work area includes spaces for four forceps kept heated in hot paraffin for manipulating the orientation of the head specimens. The hot work area is used for maintaining molds containing paraffin and for exposing heads from cassettes. The till can be used to pre-warm molds. The cold plate is used to solidify samples and remove molds. (Do not the cold-plate on while blocking heads.)

   a. Prepare
      i. Pre-warm metal molds on the blocking station so they reach ~61°C. (The Bonini lab uses a Shandon Histocentre2 station.) Need 1 per head.
      ii. Pre-label embedding rings with your sample name using pencil (!). Usually we cut 4-10 heads per genotype.
   b. Thoroughly clean excess wax off of 3 molds using a kimwipe. Fill each mold with molten paraffin to the top of the chamber. Maintain these on a ~61°C surface of the blocking station to keep paraffin melted.

There are two parts to the block: a metal mold shapes the area that will contain the head, an embedding ring fits on top of the mold. After completing the blocking step, the metal molds are removed. The "wings" of the metal mold go in the opposite direction as the "wings" of the plastic piece. The proboscis of the head should face one of the wings of the metal mold.

   c. Expose your first cassette containing paraffin-embedded heads to a ~61°C surface of the blocking station, just enough to where the cassette can be opened and the heads/lens paper removed.
   d. Expose the heads/lens paper to a ~61°C surface of the blocking station, just enough to where you can open-up the lens paper and expose the heads. DO NOT FULLY MELT THE HEADS/PARAFFIN AS THIS CAN DISRUPT THE TISSUE'S INTEGRITY. Use pre-warmed needle-nose forceps as needed.

e. Transfer 1 head into each of the prepared molds using pre-warmed forceps to “cut” them out of the wax. The heads should sink at this stage. If a head does not sink it has not been properly embedded and should be discarded.

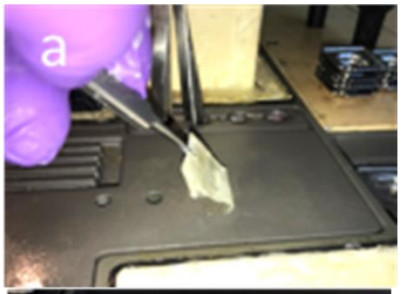

Melt the edges of the lens paper packet just enough to pull the folds open with forceps and expose the heads. It is convenient to warm the folded edges of the paper with targeted exposure to the hot surface while avoiding the area containing the heads. Once the heads are accessible, remove the paper from heat and extract a head by carefully cutting it out of the wax with hot forceps. Place the head in a mold containing molten paraffin and set the orientation as appropriate. Be sure the change forceps frequently so you are always using warmed forceps.

f. Position the head within the mold so the proboscis is facing one of the wings of the mold. Move the head/mold to a RT surface of the blocking station and allow the wax to cool just enough that the head can be held in place. Using prewarmed forceps, flip the head by pushing up on the proboscis so it is sitting on the superior part of the head, with the inferior side facing the surface of the molten paraffin. This creates horizontal sections.

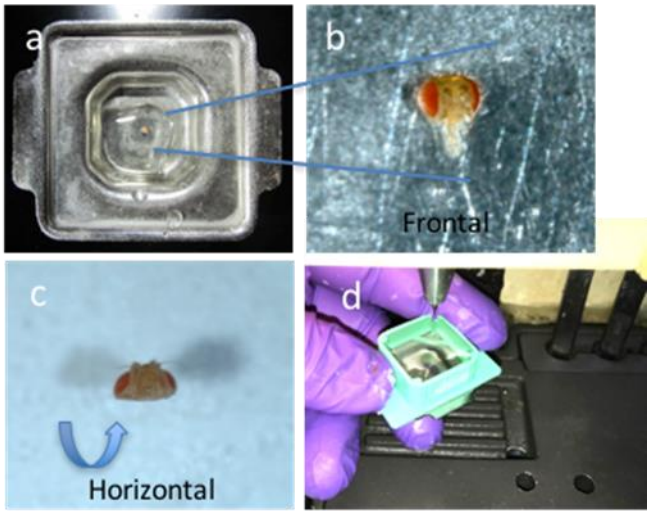

g. Carefully place a pre-labeled embedding ring on top of the mold so the wings of the mold are on opposing side from the wings on the ring. Make sure the edges are sealed together. Fill the ring/mold with molten paraffin to the top of the ring by pouring the paraffin at an edge of the mold (not center where the head is located. IT IS VITAL THAT YOU DO NOT

DISTURB THE HEAD BY LETTING THE FRESH MAX MELT THE COOLED WAX AROUNG THE HEAD!

h. Transfer to the cold-plate of the blocking station while you block additional heads. (do not turn it on, yet.)
i. Repeat blocking of each head for all heads/samples.
j. When done blocking, turn on the cold-plate of the blocking station and incubate samples for ~30min until the molds can be easily separated from the paraffin/ring. (they typically make a popping sound when the seal is broken.) BE SURE TO TURN THE COLD-PLATE OFF WHEN DONE!
k. Blocks can be stored long-term at RT.

2. Trim blocks: Using a sharp razor blade, cut excess wax away from the head within a room-temperature block, creating a small trapezoid around the head that is ~3mm (top edge) x 4mm (bottom edge). Be cautious of the position of the trapezoid in relation to the wings of the mold – the top edge should be perpendicular to the wings and angled-sides should run (relatively) parallel to the wings. Top and bottom edges should be as close to parallel as possible to avoid the ribbon from curling later. Trimmed blocks can be stored long-term at RT.

   Note: it can be convenient to keep the trapezoid a little larger than the final shape to leave room for further trimming the block during sectioning.

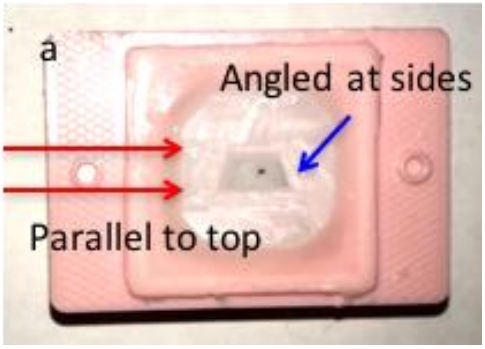

3. Section heads (8µm thickness)

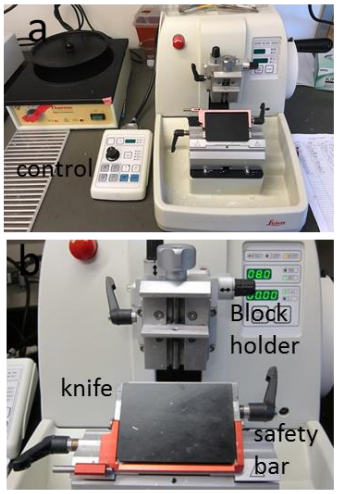

The Leica RM2255 microtome is used to section the paraffin-embedded sample blocks. Left, panel A shows the water-bath, microtome control pad, and microtome. Blocks are clamped into the block holder. Each rotation of the wheel advances the block-holder 8µm towards the knfe, resulting in a tissue slice 8µm thick when a block is being sectioned

   a. Preparation:
      i. Clean excess wax out of the water bath next to the microtome, fill it with water, and pre-warm it to 52°C.

ii. Position a new microtome blade onto the microtome. (One blade can be used to section ~15 heads and then it needs to be replaced.) To insert a new knife, loosen the red handle clamping the knife into the knife holder and use the magnet at the opposite end of the course brush to pull out the old knife. Take a new knife from the pack and insert. Use the handle of a fly brush to press the knife into the correct position and tighten the knife clamp
iii. Fill a small beaker with ice and chill 2-3 pairs of needle-nose forceps.
iv. Pre-label glass slides using pencil (!)
v. Obtain and slide rack, paper towels, and a piece of dark poster-board or napkin.

b. In an ice-bucket full of ice, place the blocks tissue-side down into the ice. Chill blocks for 30+ minutes.

c. With the microtome wheel locked and the blade safety bar in place, position a chilled block into the block holder on the microtome and firmly tightening the knob. The wings of the embedding ring should be on the left/right sides; in other words, The parallel edges of the blocks (top and bottom) should be parallel to the knife. MAKE SURE THE BLOCK HOLDER IS POSITIONED FAR ENOUGH BACK THAT WHEN YOU START THE MICROTOME YOU DON'T CUT THE PORTION CONTAINING THE HEAD OFF OF THE BLOCK!
d. Unlike the wheel and advance the tissue forward to where it is just barely touching the blade (little flakes of paraffin come off of the block).
e. Start the microtome at a low speed (~2), using the control pad. Run the microtome enough to get a sense of whether any adjustments need to be made to the trapezoid shape with the goal of a relatively straight ribbon being formed by the tissue sections. Brush off excess paraffin from the blade using a large paintbrush (move the grain of the brush along the edge of the blade, not against, or you will damage the blades' edge).

Microtome control pad:
- up/down arrows move the block holder forward (up) and backward (down)
- Knob is used to set the speed for the auto-rotation. It needs to be set to "Cont." for continuous to run.
- To start auto-rotation, push both blue buttons simultaneously. To stop, press wither button.

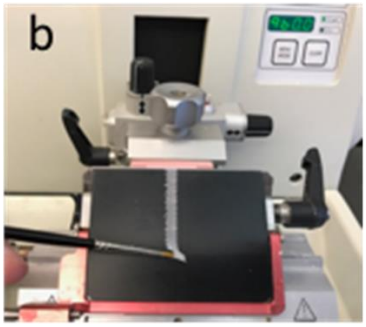

A "ribbon" is formed from subsequent tissue slices. If the trapezoid is not straight, it will curl to the left or right. Re-adjust the top and bottom edges of the trapezoid in early sections before reaching the tissue within the block.

f. Run the microtome on continuous at ~5 until you reach the head tissue. Stop the microtome and discard the ribbon thus-far as this is just wax (no tissue).
g. Run the microtome on continuous at ~2 until you reach the end of the head tissue. When running the microtome, guide the ribbon with small paint brushes, or else it will not stay straight. Stop the microtome when you no longer see red eye tissue.
h. Using 2 small paintbrushes, gently free the last section of the ribbon from the blade and transfer the whole ribbon to a piece of dark napkin; matte side of the ribbon should be facing up. Cut the ribbon into 2-3 smaller sections using a sharp razor-blade.

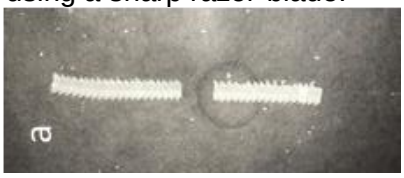

Notes
- I tend to measure the ribbon with a glass slide to see how short to cut the sections
- Be aware that when you cut the ribbon with the blade, the wax can cut stuck onto the napkin. Gently free the ribbon with the small paintbrushes.
- It is convenient to remove sections on the ends of the ribbon that do not contain any red-eye tissue.

i. Transfer each section of the ribbon, one at a time, into the water bath; matte side up. I usually achieve this by using 1 small paintbrush to lift 1 side of the section up and onto the tip of a closed, pre-chilled forcep. It is essential that the forceps be cold or the tissue/paraffin with stick to it! also, it is convenient to use maintain any small droplets of cold water that have formed on the tip of the forceps as this can help “hold” onto the ribbon.

j. Using cold forceps, gently bring the sections together. The edges should interact, so the sections stay together. It is vital that you frequently switch forceps so they stay cold. A good strategy for imaging later is to place the two ribbons next to each other in an antiparallel fashion so the adjacent regions of the ribbons are next to each other on the slide.

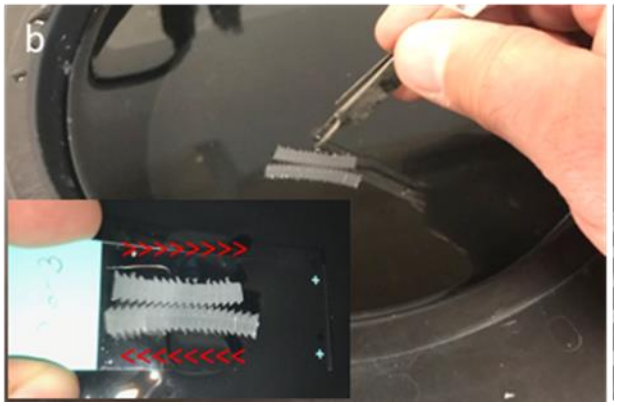

k. Gently transfer the sections onto a pre-labeled glass slide, guiding the sections with a pair of chilled forceps.

l. Tap the slide onto paper towels to remove excess water. Dry slide in a slide rack while you section additional samples.

m. When sectioning is complete, place the wheel of the microtome in the locked position and put the blade guard back up. Turn off the water bath, microtome and clean up paraffin debris.

n. Dry slides at room temperature (overnight or more).

4. Mount coverslips onto slides

a. Preparation

i. Warm an incubator or oven to 60°C

ii. Prep: Collect the following reagents into the fume hood

- 2 slide dishes filled with Xylenes – labeled Xylenes (I) and Xylenes (II). Xylenes can be reused ~10 times when stored in bottles.
- Paper towels
- 22 x 50mm cover slips
- Permount
- A standard transfer pipette

b. Incubate slides/slide rack at 60^{o}C for ~60min. (termed: baking)
c. Allow slides to cool for 30+ min.
d. Transfer slides/slide rack to the slide dish containing Xylenes I. Incubate in the fume hood for 10min.
e. Transfer slides/slide rack to the slide dish containing Xylenes II. Incubate in the fume hood for 10min. DO NOT REMOVE SLIDES/SLIDE RACK FROM THE XYLENES UNTIL THE MOMENT THAT YOU ARE MOUNTING THE COVERSLIP ON EACH INDIVIDUAL SLIDE. Tissue is ruined if it is allowed to dry out at this stage.
f. Mount cover slips onto slides
    i. Align 1-3 coverslips along a paper towel. Using the transfer pipette, add 3 small drops of Permount onto each coverslip so they are evenly distributed length-wise. DO NOT USE EXCESS PERMOUNT. It does not take much! them using a disposable pipet.
    ii. remove 1 slide from the slide rack/xylenes. Wipe away excess xylenes from the back of the slide. Place the slide tissue-side down onto the prepared coverslip. The xylenes should help the permount to evenly distribute across the coverslip.
    iii. Dab the edges of the slides on a piece of paper towel to remove excess solution and the straighten the coverslip. Also, check for any bubbles that maybe in the same position as the tissue. bubbles can be gently squeezed out from between the slide and coverslip using the lead tip of an automatic pencil.
    iv. Place the mounted slide coverslip side up onto a piece of cardboard to dry 1-2d in the fume hood. (It is convenient to use old fly-bottle trays and to angle the slides slightly with paper towels.)
    v. repeat steps i-iv for remaining slides.

2. Image slides on the DM6000 microscope using a 20X dry objective with 1.25 zoom and 588 fluorescence (looking at auto-fluorescence of the tissue). For internal eyes, use anatomical landmarks to define the tissue region for fair comparisons between samples. Typically, I image the tissue when I can see the following landmarks: AL + LH + optic chiasma.

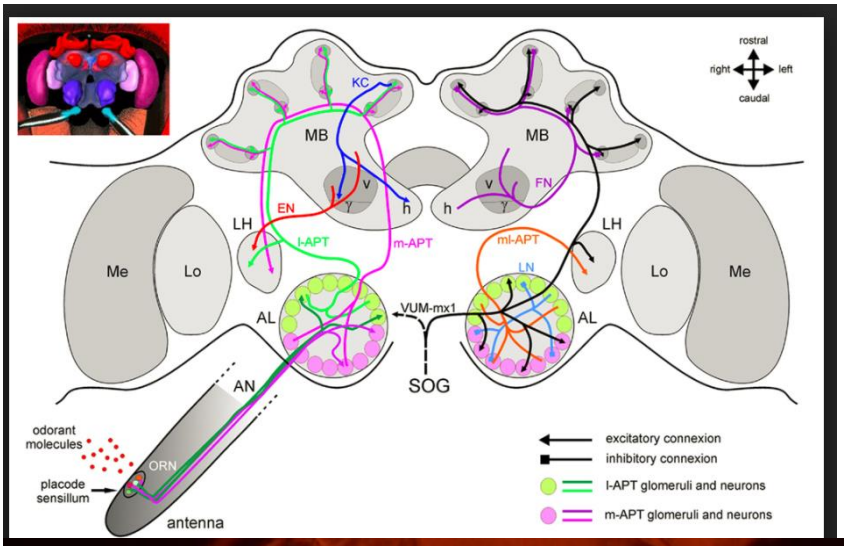

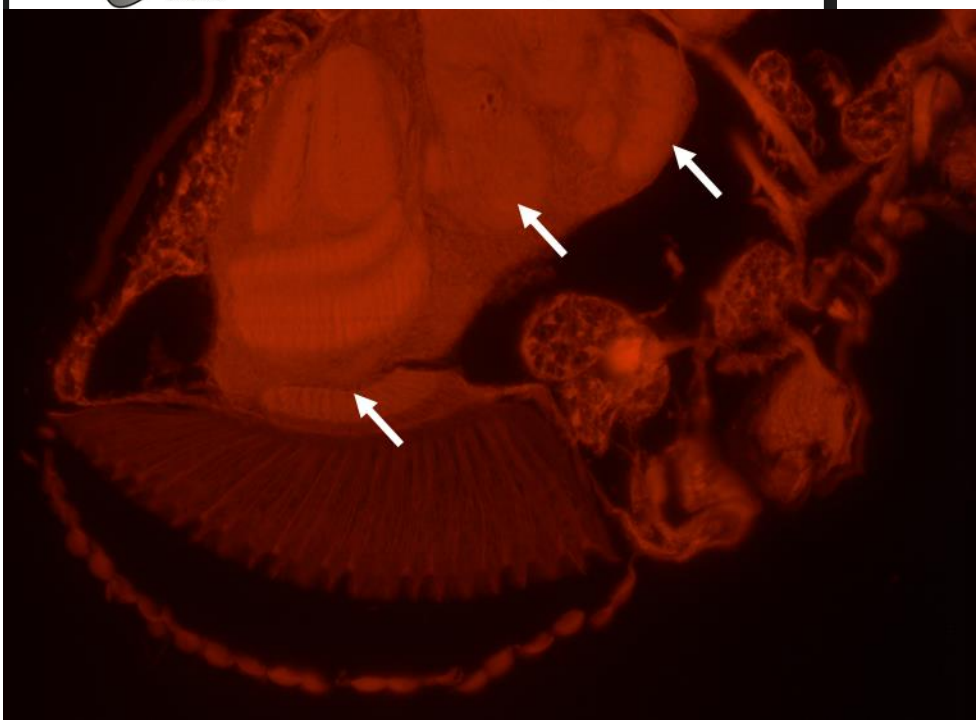

3. Quantify internal eye tissue depth and total surface area in ImageJ.
    a. Open eye images taken on a microscope in Fuji (ImageJ). If you open from the original .lif file, the scale bar will already be set.
    b. (if not using the .lif file) Click “Analyze” > “Set scale”.
    c. Measuring the tissue depth
        i. Using the line tool, draw a line the depth of the eye tissue at the optic chiasm.
        ii. Click “Analyze” > “Measure”
        iii. Copy and paste the length measurement into excel. This is in units you previously set for the scale.
        iv. Example

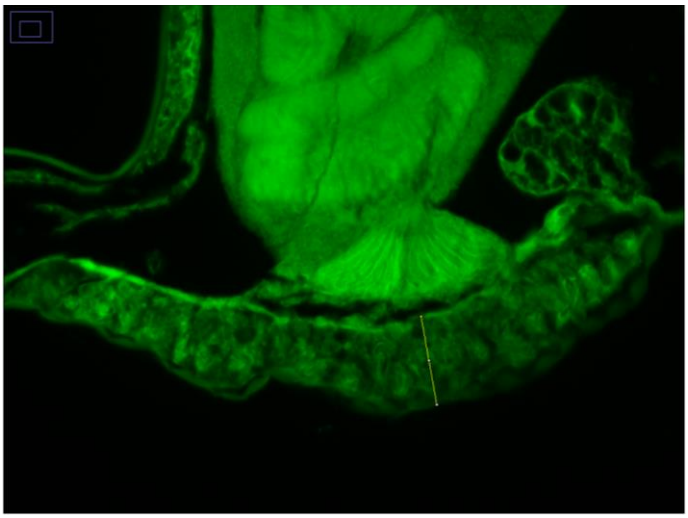

d. Measuring the total surface area of the retina tissue
    i. Using the Freehand selection tool, trace the outer edges of the internal eye tissue. Click “Analyze” > “Measure”. This will give you the Area in the units you previously set for the scale.
    ii. Copy and paste the Area measurement into excel.
    iii. For any pockets in the eye tissue, repeat steps a-b while tracing around these pockets. The area values given should then be subtracted from the total area measurement to give an accurate, final measurement.
    iv. Examples

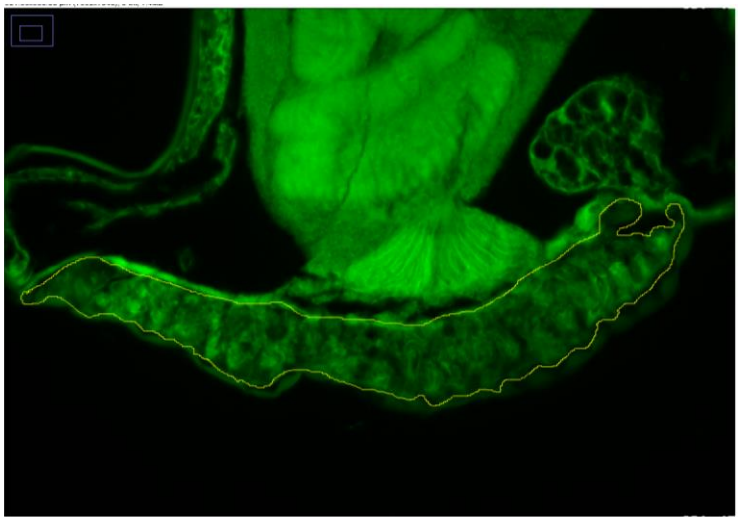

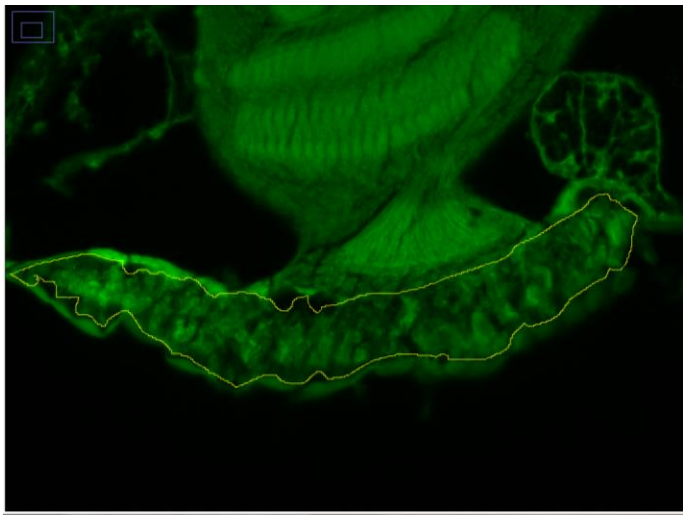

TROUBLESHOOTING

- After much trial and error, we've found that 5d on Bouin's results in the best tissue integrity. 4 and 6d can also produce some good sections while the percent of good sections reduces.
- When cleaning the microtome blade, it is essential to only use upward-strokes with a brush to avoid dulling the knife.
- It is advisable to change to a new knife on the microtome and to track the areas that have previously been used. A sharp knife will alleviate many sectioning problems.

FIBROBLASTS

Thawing, culturing, freezing

REAGENTS/MATERIALS

- DMSO, sterile (Sigma # D2650)
- heat-inactivated, sterile Fetal Bovine Serum (FBS)
- 50X MEM Amino Acids Solution (Invitrogen # 11130051)
- Pen/Strep solution
- DMEM - high glucose 4.5g/L and Sodium Pyruvate
- 0.25% Trypsin-EDTA
- dPBS without Ca/Mg
- 500mL filter system (PES, 0.22µm)
- 50mL filter system (PES, 0.22µm) (Corning # 430320)
- Standard tissue-culture materials

MEDIA

Note: all media must be prepared in the TC-cabinet under sterile conditions.

- Culture media
    - 75mL heat-inactivated, sterile Fetal Bovine Serum (FBS) to 15%
    - 5mL of 50X MEM Amino Acids Solution to 1X
    - 5mL of Pen/Strep solution to 1%
    - 415mL DMEM - high glucose 4.5g/L and Sodium Pyruvate
    - Filter through a 500mL filter system
    - Store at 4^{o}C for up to 2mo. (Alternatively, discard media when it changes colors based on the pH indicator within the DMEM.)

- Freezing media
    - 5mL of DMSO (sterile) to 10%
    - 45mL heat-inactivated, sterile Fetal Bovine Serum (FBS)
    - Filter through a 50mL filter system
    - Store at 4^{o}C for up to 2mo.

PROTOCOL

Notes:
- Cells are maintained in a standard tissue culture incubator with 5% CO_2 and at 37^{o}C.
- the following represents general protocols while adjustments may need to be made for specific lines, etc.
- For all steps, it is vital to maintain sterility, spraying materials and hands regularly with 70% EtOH, etc. All steps must be performed in the tissue culture (TC-) room and when applicable, in the TC-cabinet.
- the following protocol uses TC- flasks while cells can also be grown in TC-dishes if desired.

1. Thaw 1 vial of cells:
    a. Obtain a vial of cells from the LN2 tank and maintain it on dry ice. If necessary, you can do this 1-3d before thawing the cells and store the vial in the -80^{o}C.
    b. Prep: label a T25 (or T75) flask with the cell line name, date, and the passage number on the vial. It is vital that you keep track of the passage number! Note that it doesn't start at "1" for when you start growing the cells – as the cells have already been grown for a number of passages (P) prior to you culturing it. All cells must be discarded once you reach P20-25.
    c. Thaw the vial of cells in a 37^{o}C water bath. When the ice is almost completely gone (~a pea size), transfer the vial to the TC-cabinet after spraying it thoroughly with 70% EtOH to sterilize it.
    d. Immediately, carefully remove the cap from the vial and transfer the cell suspension to the prepared flask. It is vital that this is done relatively quickly.
    e. Transfer the flask to a 37^{o}C incubator overnight to allow the viable cells to adhere to the bottom of the flask. The next morning, remove all of the media and add fresh, pre-warmed culture media to the flask, effectively removing the freezing media and cell debris.
    f. Transfer the flask back to the 37^{o}C incubator and check on the cells every 2-3d. when the cells reach 90-100% confluence, passage them 1:2 for the first passage after thawing. After that you can increase the passage dilution as needed. It is good practice to passage the cells 1-2x before using them for experiments to allow them to fully recover.
2. Passage cells when they reach 90-100% confluence.
    a. Prep: pre-warm Culture media and Trypsin to 37^{o}C; make sure dPBS is at RT.
    b. Remove growth media and wash cells 1x with dPBS. Add just enough trypsin to cover the monolayer of cells (1.5-2mL for a T25 flask; 3mL for a T75 flask). Incubate cells at 37^{o}C for 5-10min.
    c. Prep:
        i. label new flask(s) with the cell line name, passage number, date, and dilution. It is vital to track passage number. Typically 1:5 dilutions are used for healthy fibroblast lines. However, some lines may require 1:2 dilutions to maintain viability. (1:2 = 1 confluent flask can be split into as many as 2 new flasks; 1: = 1 confluent flask can be split into as many as 5 new flasks)
        ii. Add a minimal amount of growth media to the flasks (~3mL for T25; ~10mL for T75). It is important to consider how much of the cell suspension you will be adding later so you don't add too much volume. You want ~4-6mL end volume in a T25 or ~12-15mL end volume in a T75.
    d. When cells have lifted off the flask, add growth media to stop the reaction (~3mL for T25; ~5-7mL for T75). It is best to pipette the media along the cell-side of the flask to wash all cells to the bottom. Pipette up/down ~5x to fully suspend cells. Transfer a defined volume of the cell suspension into the prepared flasks based on the dilution.

e. Discard the old flask in the biomedical waste container. Transfer the new flask(s) to the 37°C incubator. Every 2-3d, check on the cells to make sure they are growing well. Passage again (or use them for experiments) when they reach 90-100% confluence.
   Note: for slow growing line, you may need to change the media every ~5d. To do this by removing ½ of the current growth media and replacing it with new, pre-warmed media.

3. It is vital to maintain a good freezer stock for every cell line. A good rule of thumb is to always replace a thawed vial with a new vial of frozen cells. To freeze cells:
   a. Prep: pre-warm culture media, trypsin, and freezing media to 37°C; make sure dPBS at RT is available; get a ice-bucket full of dry ice.
      Note: it is vital that the freezing media be pre-warmed as it contains DMSO which crystalizes at 4°C.
   b. Remove growth media and wash cells 1x with dPBS. Add just enough trypsin to cover the monolayer of cells (1.5-2mL for a T25 flask; 3mL for a T75 flask). Incubate cells at 37°C for 5-10min.
   c. Prep:
      i. label cryo-vial with the following information: cell line name, date, passage number, # cells (can be an estimate like "½ T75")
      ii. obtain a sterile 50mL conical and label it with the cell line name (particularly important if you are handling multiple cell lines simultaneously)
   d. When cells have lifted off the flask, add growth media to stop the reaction (~3mL for T25; ~5-7mL for T75). Pipette up/down ~5x to fully suspend cells. Transfer cells into the pre-labeled 50mL conical.
   e. Centrifuge the cells/50mL conical for 5min at 15,000 RPM to pellet the cells.
   f. Remove the supernatant and add 1mL of freezing media for each vial. Pipette up/down ~10x to fully suspend cells. Transfer cells into the pre-labeled vial(s). Immediately cap the vial and transfer it to the bucket of dry ice, making sure the vial is fully surrounded by the ice. Immediately transfer the vial to a -80°C freezer overnight.

      Note: Freezing media has DMSO which is toxic to cells. It is vital that all steps where cells are exposed to the freezing media be performed relatively quickly to get them frozen as fast as possible.

   g. In the morning, transfer the vial to the LN2 tank for long-term storage. Optional: you can maintain vials at -80°C for ~1wk to accumulate multiple vials before transferring them to the LN2.

Protein extraction

REAGENTS

- RIPA lysis buffer
    - 10mL of 1M Tris-HCL (pH 7.5) to 50mM
    - 6mL of 5M NaCl to 150mM
    - 2mL NP-40 to 1%
    - 0.42g NaF to 50mM
    - 2mL of 10% SDS to 0.1%
    - 1g Sodium Deoxycholate (DOC) to 0.5%
    - dH2O to 200mL
    - Filter through a 250ml filter system, 0.22µm, PES
    - store at 4^{o}C. Check pH every 6-8mo.
- 5X cOmplete ULTRA Tablets, mini, EASYpack protease inhibitor cocktail (Sigma # 05892970001)
    - 1 tablet dissolved in 1500µl of milliQ water
    - prepare 100µl aliquots
    - store in -20^{o}C. After thawing, precipitate may form and need to be resuspended into solution.
- (optional) 25X PhosSTOP Phosphotase inhibitor cocktail (Sigma # 04906845001)
    - 1 tablet dissolved in 400µl of MilliQ water
    - prepare 25µl aliquots
    - store in -20^{o}C. After thawing, precipitate may form and need to be resuspended into solution.
- 100mM PMSF
    - 0.1742g of PMSF
    - 10mL of isopropanol
    - Filter through a 0.22µm PES filter (Fisher Sci # 09-720-511) using a luer-lock syringe
    - prepare 500µl aliquots
    - store in -20^{o}C. Before use, bring to RT and vortex until precipitate goes back into solution
- 1M DTT
    - 1.5425g of DTT (Dithiothreitol)
    - 10mL MilliQ water
    - Filter through a 0.22µm PES filter (Fisher Sci # 09-720-511) using a Luer-lock syringe
    - prepare 500µl aliquots
    - store in -20^{o}C
        - before use, bring to RT and vortex until precipitate goes back into solution

PROTOCOL

1. Prepare working lysis Buffer: (must be made fresh! Store on ice.)
    a. Calculate the total amount of lysis buffer you will need. Typically, 50µl per well of a 6-welled plate when using cell pellet method (step 2).
    b. For every 500µl of working lysis buffer needed, add the following protease and phosphatase inhibitors. Make a minimum of 500µl of working lysis buffer then prepare additional 100µl as needed.
        - 400µL 0.5% RIPA Lysis Buffer Stock
        - 100µL of 5X cOmplete ULTRA protease inhibitor Stock to ~1X
        - 20µL of 25X PhosSTOP Phosphotase inhibitor cocktail Stock to ~1X
        - 5µL of 100mM PMSF to ~1mM
        - 0.5µL of 1M DTT for ~1mM
2. Lyse cells using one of two methods. (Written for a 6-welled plate. Scale up as needed.)
    a. Prepare a cell pellet
        i. Advantages
            1. can split up cells from the same plate into multiple assays
            2. cell pellet is prepared in a microcentrifuge tube so lysing no protein will be lost when lysis buffer is added
            3. can lyse cells in small volumes
        ii. Disadvantages
            1. Can lose cells during every centrifuge step
            2. slower
        iii. Protocol
            1. Prep: pre-warm Culture media and Trypsin to 37^{o}C; make sure dPBS is at RT.

                Note: it is good practice to use an aliquot of culture media in a sterile conical to prevent contaminating your primary stock of media

            2. Remove growth media and wash cells 1x with dPBS. Add just enough trypsin to cover the monolayer of cells (~0.5mL per well). Incubate cells at 37^{o}C for 5-10min.
            3. Prep: label 15mL conical

                Note: you will need multiple conicals if you are splitting the cells up for different assays.

            4. When cells have lifted off the plate, add growth media to stop the reaction (~1mL), using a P1000 pipet with tip. Pipette up/down ~5x to fully suspend cells. Transfer the cell suspension into the prepared conical(s).
            5. Using a fresh tip on the P1000 pipet, wash the plate while holding it at an angle so any remaining cells will collect to the bottom. Collect all solution into the conical.
            6. Repeat for remaining wells.
            7. Pellet cells by centrifugation at 5000rpm for 5min.
            8. Prep: label 1.5mL microcentrifuge tubes

9. Wash cells 2x to remove media and typsin by removing supernatant, resuspend cells in 3mL of dPBS, and pelleting cells by centrifugation at 5000rpm for 5min.
10. Remove supernatant. Resuspend cells in desired volume of working lysis buffer.
    Note: other cell pellets can be immediately frozen on dry ice for future use (e.g. RNA extraction).
11. Lyse cells for 20-40min at 4°C with agitation/rotation.
12. Prep: label 1.5mL microcentrifuge tubes
13. Pellet cell debris by centrifuging samples at 15,000xg for 10min.
14. Transfer supernatant to the fresh prelabeled microcentrifuge tube.
15. Quantify protein concentration by Bradford.

b. Lyse cells directly on the TC-plate
    i. Advantages
        1. Faster
        2. Can get more protein from a single preparation
    ii. Disadvantage
        1. Requires larger volumes of lysis buffer, resulting in more dilute protein preparations
        2. If you're not good about washing the plate to collect residual lysate, you will lose protein
    iii. Protocol
        1. Prep: label 1.5mL microcentrifuge tubes
        2. Remove growth media and wash cells 2x with dPBS.
        3. Add desired volume of working lysis buffer (typically ~100-150µL per well)
        4. Using cell scrapers, scrape off cells from the bottom of the plate, making sure to get all edges.
        5. Using a P1000 pipet with tip, transfer all solution to the pre-labeled microcentrifuge tube. Note: it will be gunky.
        6. Using a fresh tip on the P1000 pipet, wash the plate with 100-150µL of lysis buffer while holding it at an angle so any remaining solution will collect to the bottom. Collect all solution into the tube. You should get all the gunky stuff – this is the lysed cells.
        7. Repeat for remaining wells.
        8. Lyse cells for 20-40min at 4°C with agitation/rotation.
        9. Prep: label 1.5mL microcentrifuge tubes
        10. Pellet cell debris by centrifuging samples at 15,000xg for 10min.
        11. Transfer supernatant to the fresh prelabeled microcentrifuge tube.
        12. Quantify protein concentration by Bradford.